VOLUME 18 NUMBER 7 JULY 2012
www.nature.com/naturemedicine

nature medicine

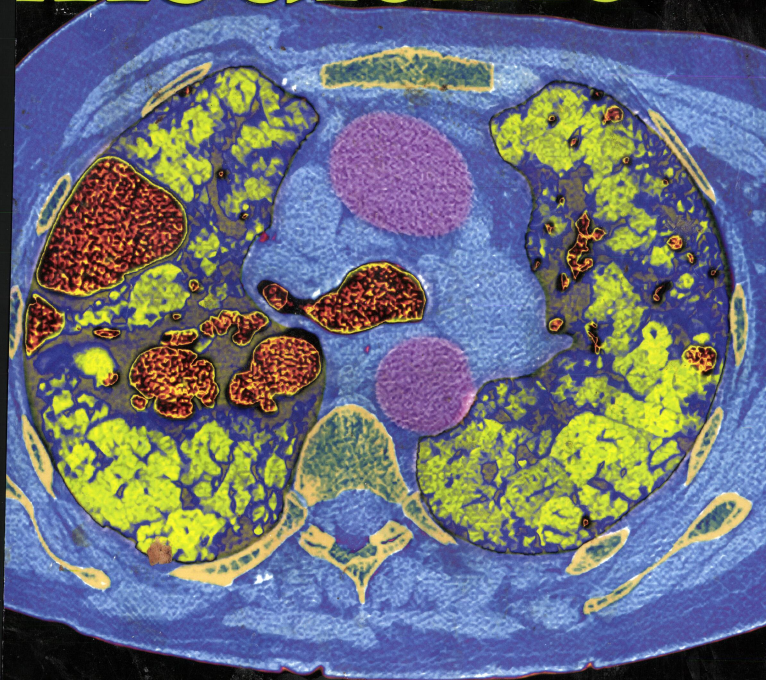

Mechanisms of fibrosis

Spotlight on sepsis

The good side of cholesterol

Simple

FIND ▸ DECIDE ▸ BUY ▸ DISCOVER

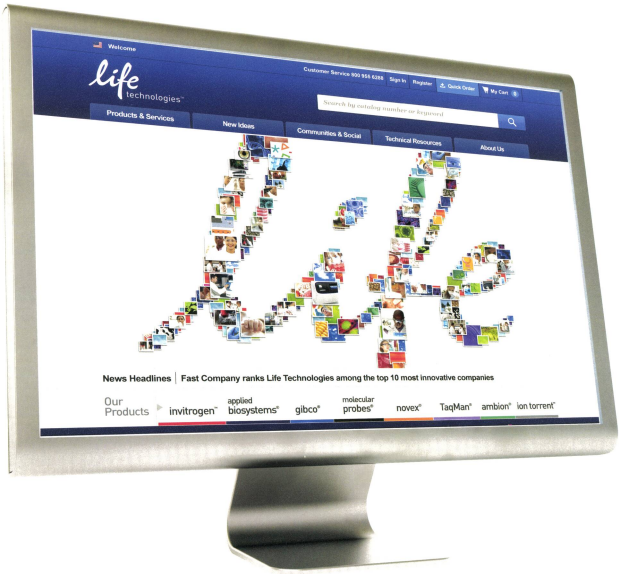

It's easy to get what your research lab needs at

lifetechnologies.com

life technologies

©2012 Life Technologies Corporation. All rights reserved. The trademarks mentioned herein are the property of Life Technologies Corporation or their respective owners. TaqMan® is a registered trademark of Roche Molecular Systems, Inc., used under permission and license. C002537.0512

VOLUME 18 NUMBER 7 JULY 2012

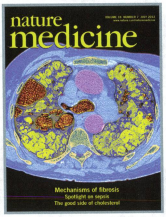

Tissue fibrosis is a costly unmet medical need. In this issue (p. 1028), Wynn and Ramalingam review our current understanding of the mechanistic basis of fibrosis, pointing to future directions for the discovery of new therapies. The cover shows a colored computed tomography scan through the chest of a patient with pulmonary fibrosis, showing the lung tissue in green and the fibrotic areas in orange. Image: Du Cane Medical Imaging LTD/Science Photo Library.

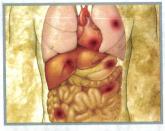

Shock and awe in the sepsis field (p 997)

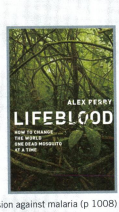

Mission against malaria (p 1008)

nature publishing group

nature medicine

EDITORIAL

989 Learning to share

NEWS

990 'Must-pass' FDA fee renewal jammed with sunscreen and more
991 New adjuvants aim to give whooping cough vaccine a boost
991 Accord could make Canadian generics industry a 'rust bucket'
992 Biobanks look to software solutions to handle data deluge
992 First therapy targeting Parkinson's proteins enters clinical trials
993 Cancer immunotherapy shows promise in multiple tumor types
994 **NEWS IN BRIEF**
996 New class of sleep drugs may offer a safer night's rest
997 **FOCUS ON SEPSIS**
1002 **Q&A:** Phillip Dellinger
1003 **NEWS FEATURE:** To serve and neuroprotect
1007 **OPINION:** Refocus the Recombinant DNA Advisory Committee

BOOK REVIEW

1008 Lifeblood: How to Change the World One Dead Mosquito at a Time
Alex Perry
Reviewed by Mats Wahlgren

NEWS AND VIEWS

1009 **miR-23b is a safeguard against autoimmunity**
Ruozhen Hu & Ryan M O'Connell ▸*see also p 1077*

1011 **Co-opting endogenous microRNAs for therapy**
Christopher E Pearson ▸*see also p 1136*

1013 **To survive radiation injury, remember your aPCs**
John P Chute ▸*see also p 1123*

1014 **NKT cells—an early warning system for HBV infection**
Dale I Godfrey, Adam P Uldrich & Alan G Baxter ▸*see also p 1060*

1016 **Cutting SRC-1 down to size in endometriosis**
Matthew T Dyson & Serdar E Bulun ▸*see also p 1102*

1018 **Primed for inflammation: enthesis-resident T cells**
Rik J Lories & Iain B McInnes ▸*see also p 1069*

1020 **COMMUNITY CORNER: Mining the mechanisms of an HIV vaccine**

Nature Medicine (ISSN 1078-8956) is published monthly by Nature Publishing Group, a trading name of Nature America Inc. located at 75 Varick Street, Fl 9, New York, NY 10013-1917. Periodicals postage paid at New York, NY and additional mailing post offices. **Editorial Office:** 75 Varick Street, Fl 9, New York, NY 10013-1917. Tel: (212) 726 9325, Fax: (212) 683 5751. **Annual subscription rates:** USA/Canada: US$225 (personal), US$4,048 (institution), Canada add 7% GST #140911595RR001; Euro-zone: €287 (personal), €3,214 (institution); Rest of world (excluding China, Japan, Korea): £185 (personal), £2,077 (institution); Japan: Contact NPG Nature Asia-Pacific, Chiyoda Building, 2-37 Ichigayatamachi, Shinjuku-ku, Tokyo 162-0843. Tel: 81 (03) 3267 8751, Fax: 81 (03) 3267 8746. **POSTMASTER:** Send address changes to *Nature Medicine*, Subscriptions Department, 75 Varick Street, 9th Floor, New York, NY 10013-1917. **Authorization to photocopy** material for internal or personal use, or internal or personal use of specific clients, is granted by Nature Publishing Group to libraries and others registered with the Copyright Clearance Center (CCC) Transactional Reporting Service, provided the relevant copyright fee is paid direct to CCC, 222 Rosewood Drive, Danvers, MA 01923, USA. Identification code for *Nature Medicine*: 1078-8956/04. **Back issues:** US$45, Canada add 7% for GST. CPC PUB AGREEMENT #40032744. Printed on acid-free paper by The Sheridan Press, Hanover, PA, USA. Copyright © 2012 Nature Publishing Group. Printed in USA.

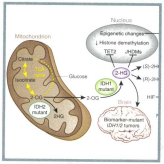

Cancer metabolism in the spotlight (p 1022)

Mechanisms of fibrosis (p 1028)

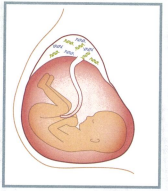

Personalized fetal medicine (p 1041)

BETWEEN BEDSIDE AND BENCH

UNTUNING THE TUMOR METABOLIC MACHINE

1022 **Targeting cancer metabolism: a bedside lesson**
Kivanç Birsoy, David M Sabatini & Richard Possemato

1024 **HIF-α: pro- and antitumorigenic?**
Regina M Young & M Celeste Simon

1026 **RESEARCH HIGHLIGHTS**

REVIEWS

1028 **Mechanisms of fibrosis: therapeutic translation for fibrotic disease**
T A Wynn & T R Ramalingam

1041 **From prenatal genomic diagnosis to fetal personalized medicine: progress and challenges**
D W Bianchi

ARTICLES

1052 **Profiling of residual breast cancers after neoadjuvant chemotherapy identifies DUSP4 deficiency as a mechanism of drug resistance**
J M Balko, R S Cook, D B Vaught, M G Kuba, T W Miller, N E Bhola, M E Sanders, N M Granja-Ingram, J J Smith, I M Meszoely, J Salter, M Dowsett, K Stemke-Hale, A M González-Angulo, G B Mills, J A Pinto, H L Gómez & C L Arteaga

1060 **Hepatitis B virus–induced lipid alterations contribute to natural killer T cell–dependent protective immunity**
S Zeissig, K Murata, L Sweet, J Publicover, Z Hu, A Kaser, E Bosse, J Iqbal, M M Hussain, K Balschun, C Röcken, A Arlt, R Günther, J Hampe, S Schreiber, J L Baron, D B Moody, T J Liang & R S Blumberg ▸*see also p 1014*

1069 **IL-23 induces spondyloarthropathy by acting on ROR-γt$^+$CD3$^+$CD4$^-$CD8$^-$ entheseal resident cells**
J P Sherlock, B Joyce-Shaikh, S P Turner, C-C Chao, M Sathe, J Grein, D Gorman, E P Bowman, T McClanahan, J H Yearley, G Eberl, C D Buckley, R A Kastelein, R H Pierce, D LaFace & D J Cua ▸*see also p 1018*

1077 **The microRNA miR-23b suppresses IL-17–associated autoimmune inflammation by targeting TAB2, TAB3 and IKK-α**
S Zhu, W Pan, X Song, Y Liu, X Shao, Y Tang, D Liang, D He, H Wang, W Liu, Y Shi, J B Harley, N Shen & Y Qian ▸*see also p 1009*

1087 **Silencing microRNA-134 produces neuroprotective and prolonged seizure-suppressive effects**
E M Jimenez-Mateos, T Engel, P Merino-Serrais, R C McKiernan, K Tanaka, G Mouri, T Sano, C O'Tuathaigh, J L Waddington, S Prenter, N Delanty, M A Farrell, D F O'Brien, R M Conroy, R L Stallings, J DeFelipe & D C Henshall

1095 **Matrix IGF-1 maintains bone mass by activation of mTOR in mesenchymal stem cells**
L Xian, X Wu, L Pang, M Lou, C J Rosen, T Qiu, J Crane, F Frassica, L Zhang, J P Rodriguez, X Jia, S Yakar, S Xuan, A Efstratiadis, M Wan & X Cao

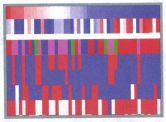

Digital tumor profiling (p 1052)

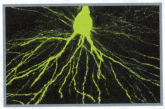

Silencing seizures (p 1087)

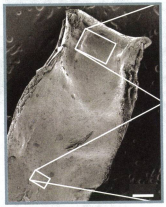

Fast-degrading artery grafts (p 1148)

1102 **A new isoform of steroid receptor coactivator-1 is crucial for pathogenic progression of endometriosis**
S J Han, S M Hawkins, K Begum, S Y Jung, E Kovanci, J Qin, J P Lydon, F J DeMayo & B W O'Malley *see also p 1016*

LETTERS

1112 **Activation of the epithelial Na^+ channel triggers prostaglandin E2 release and production required for embryo implantation**
Y C Ruan, J H Guo, X Liu, R Zhang, L L Tsang, J D Dong, H Chen, M K Yu, X Jiang, X H Zhang, K L Fok, Y W Chung, H Huang, W L Zhou & H C Chan

1118 **Autocrine activation of the MET receptor tyrosine kinase in acute myeloid leukemia**
A Kentsis, C Reed, K L Rice, T Sanda, S J Rodig, E Tholouli, A Christie, P J M Valk, R Delwel, V Ngo, J L Kutok, S E Dahlberg, L A Moreau, R J Byers, J G Christensen, G V Woude, J D Licht, A L Kung, L M Staudt & A T Look

1123 **Pharmacological targeting of the thrombomodulin–activated protein C pathway mitigates radiation toxicity**
H Geiger, S A Pawar, E J Kerschen, K J Nattamai, I Hernandez, H P Liang, J A Fernández, J A Cancelas, M A Ryan, O Kustikova, A Schambach, Q Fu, J Wang, L M Fink, K-U Petersen, D Zhou, J H Griffin, C Baum, H Weiler & M Hauer-Jensen *see also p 1013*

1130 **Therapy of Pelizaeus-Merzbacher disease in mice by feeding a cholesterol-enriched diet**
G Saher, F Rudolphi, K Corthals, T Ruhwedel, K-F Schmidt, S Löwel, P Dibaj, B Barrette, W Möbius & K-A Nave

1136 **Viral delivery of miR-196a ameliorates the SBMA phenotype via the silencing of CELF2**
Y Miyazaki, H Adachi, M Katsuno, M Minamiyama, Y-M Jiang, Z Huang, H Doi, S Matsumoto, N Kondo, M Iida, G Tohnai, F Tanaka, S-i Muramatsu & G Sobue *see also p 1011*

TECHNICAL REPORTS

1142 **Versatile robotic interface to evaluate, enable and train locomotion and balance after neuromotor disorders**
N Dominici, U Keller, H Vallery, L Friedli, R van den Brand, M L Starkey, P Musienko, R Riener & G Courtine

1148 **Fast-degrading elastomer enables rapid remodeling of a cell-free synthetic graft into a neoartery**
W Wu, R A Allen & Y Wang

NATURE MEDICINE CLASSIFIED

See back pages.

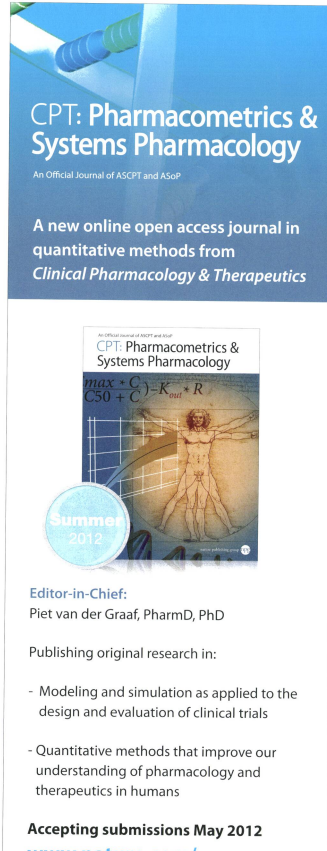
CPT: Pharmacometrics & Systems Pharmacology
An Official Journal of ASCPT and ASoP
A new online open access journal in quantitative methods from Clinical Pharmacology & Therapeutics
CPT: Pharmacometrics & Systems Pharmacology
Summer 2012
Editor-in-Chief:
Piet van der Graaf, PharmD, PhD
Publishing original research in:
- Modeling and simulation as applied to the design and evaluation of clinical trials
- Quantitative methods that improve our understanding of pharmacology and therapeutics in humans
Accepting submissions May 2012
www.nature.com/psp
nature publishing group npg

nature medicine

www.nature.com/naturemedicine

EDITORIAL OFFICE medicine@us.nature.com
75 Varick Street, Fl 9, New York, NY 10013-1917
Tel: (212) 726 9325, Fax: (212) 683 5751
Chief Editor: Juan Carlos López
Senior News Editor: Roxanne Khamsi
News Editor: Elie Dolgin
Editorial Intern, News: Rebecca Hersher
Associate Editors, Reviews and News and Views: Carolina Pola, Meera Swami
Senior Editors, Research Manuscripts: Michael Basson, Eva Chmielnicki, Alison Farrell, Randy Levinson
Associate Editors, Research Manuscripts: Victoria Aranda, Kevin Da Silva
Editor, Technical Reports: Diane Gershon
Copy Editors: Katherine Gora, Heidi Reinholdt
Senior Production Editor: Matt Hansen
Production Editor: Jamel Wooten
Senior Illustrator/Cover Design: Katie Vicari
Illustrator: Marina Corral
Editorial Assistant: Somaliyah Al-Mahdi

MANAGEMENT OFFICES
NPG New York
75 Varick Street, Fl 9, New York, NY 10013-1917
Tel: (212) 726 9200, Fax: (212) 696 9006
Publisher: Melanie Brazil
Executive Editor: Veronique Kiermer
Chief Technology Officer: Howard Ratner
Commercial Director/EVP of Sales: Dean Sanderson
Head of Nature Research & Reviews Marketing: Sara Girard
Marketing Manager: Samantha Savalio
Production Coordinator: Diane Rios
Head of Web Services: Anthony Barrera
Web Production Editor: Eddie Jones

NPG London
The Macmillan Building, 4 Crinan Street, London N1 9XW
Tel: 44 207 833 4000, Fax: 44 207 843 4996
Managing Director: Steven Inchcoombe
Publishing Director: Alison Mitchell
Editor-in-Chief, Nature Publications: Philip Campbell
Director of Web Publishing: Dan Pollock

NPG Nature Asia-Pacific
Chiyoda Building, 2-37 Ichigayatamachi, Shinjuku-ku, Tokyo 162-0843
Tel: 81 3 3267 8751, Fax: 81 3 3267 8750
Regional Managing Director — Asia-Pacific: David Swinbanks
Director — Asia-Pacific: Antoine E. Bocquet
Operations Director: Hiroshi Minemura
Senior Marketing Manager: Sachiyo Ikeda
Asia-Pacific Sales Director: Kate Yoneyama
Asia-Pacific Sales Manager: Ken Mikami

DISPLAY ADVERTISING display@us.nature.com (US/Canada) display@nature.com (Europe) nature@natureasia.com (Asia)
Global Head of Advertising and Sponsorship: Andrew Douglas, Tel: 44 207 843 4975, Fax: 44 207 843 4996
Global Head of Display Advertising and Sponsorship: Gerard Preston, Tel: 44 207 843 4965, Fax: 44 207 843 4749
Asia-Pacific Sales Director: Kate Yoneyama, Tel: 81 3 3267 8765, Fax: 81 3 3267 8752
Display Account Managers:
New England: Sheila Reardon, Tel: (617) 399 4098, Fax: (617) 426 3717
New York/Mid-Atlantic/Southeast: Jim Breault, Tel: (212) 726 9334, Fax: (212) 696 9481
Midwest: Mike Rossi, Tel: (212) 726 9255, Fax: (212) 696 9481
West Coast: George Lui, Tel: (415) 781 3804, Fax: (415) 781 3805
Germany/Switzerland/Austria: Sabine Hugi-Fürst, Tel: 41 52761 3386, Fax: 41 52761 3419
UK/Ireland/Scandinavia/Spain/Portugal: Jhelina Rubio-Hakamson, Tel: 44 207 843 4079, Fax: 44 207 843 4749
France/Belgium/The Netherlands/Luxembourg/Italy/Israel/Other Europe: Nicola Wright, Tel: 44 207 843 4959, Fax: 44 207 843 4749
Asia-Pacific Sales Manager: Ken Mikami, Tel: 81 3 3267 8765, Fax: 81 3 3267 8752
Greater China/Singapore: Gloria To, Tel: 852 2811 7191, Fax: 852 2811 0743

SPONSORSHIP g.preston@nature.com
Global Head of Sponsorship: Gerard Preston, Tel: 44 207 843 4965, Fax: 44 207 843 4749
Business Development Executive: David Bagshaw, Tel: (212) 726 9215, Fax: (212) 696 9591
Business Development Executive: Patrick Murphy, Tel: (617) 475 9216, Fax: (617) 494 4960
Business Development Executive: Reva Silas, Tel: 44 207 843 4977, Fax: 44 207 843 4996
Business Development Manager: Will Piper, Tel: 44 207 014 4181

NATUREJOBS naturejobs@us.nature.com (US/Canada) naturejobs@nature.com (Europe) nature@natureasia.com (Asia)
US Sales Manager: Ken Finnegan, Tel: (212) 726 9248, Fax: (212) 696 9482
European Sales Manager: Dan Churchward, Tel: 44 207 843 4966, Fax: 44 207 843 4596
Asia-Pacific Sales & Business Development Manager: Yuki Fujiwara, Tel: 81 3 3267 8765, Fax: 81 3 3267 8752

SITE LICENSE BUSINESS UNIT
Americas: Tel: (888) 331 6288 institutions@us.nature.com
Asia/Pacific: Tel: 81 3 3267 8769 institutions@natureasia.com
Australia/New Zealand: Tel: 61 3 9825 1160 nature@macmillan.com.au
India: Tel: 91 124 2881054/55 npgindia@nature.com
ROW: Tel: 44 207 843 4759 institutions@nature.com

CUSTOMER SERVICE www.nature.com/help
Senior Global Customer Service Manager: Gerald Coppin
For all print and online assistance, please visit **www.nature.com/help**
Purchase subscriptions:
Americas: *Nature Medicine*, Subscription Dept., 75 Varick Street, Fl 9, New York, NY 10013-1917, USA. Tel: (866) 363 7860, Fax: (212) 334 0879
Europe/ROW: *Nature Medicine*, Subscription Dept., Macmillan Magazines Ltd., Brunel Road, Houndmills, Basingstoke RG21 6XS, United Kingdom. Tel: 44 1256 329 242, Fax: 44 1256 812 358
Asia-Pacific: *Nature Medicine*, NPG Nature Asia-Pacific, Chiyoda Building, 2-37 Ichigayatamachi, Shinjuku-ku, Tokyo 162-0843. Tel: 81 3 3267 8751, Fax: 81 3 3267 8752
India: *Nature Medicine*, NPG India, 3A, 4th Floor, DLF Corporate Park, Gurgaon 122002, India. Tel: 91 124 2881054/55, Fax: 91 124 2881052

REPRINTS reprints@us.nature.com
Nature Medicine, Reprint Department, Nature Publishing Group, 75 Varick Street, Fl 9, New York, NY 10013-1917, USA.
For commercial reprint orders of 600 or more, please contact:
UK Reprints: Tel: 44 1256 302 923, Fax: 44 1256 321 531
US Reprints: Tel: (617) 494 4900, Fax: (617) 494 4960

nature medicine

Learning to share

Biomedical research faces budgetary cuts in the United States and abroad. But although solutions to manage the restricted funds can be found, initiating change may be the greater hurdle.

The US National Institutes of Health (NIH) budget request for the fiscal year (FY) 2013 is ~$30.9 billion, the same amount it received for FY 2012. Yet the NIH maintains that it will continue to increase the number of new, competing research project grants (RPGs) it distributes, awarding 672 more in FY 2013 than in FY 2012 at an average cost of ~$431,000 each. To accomplish this, the NIH needs to find new mechanisms to redistribute funds—mechanisms by which some will lose and some will gain.

To enable continued growth in the number of competing RPGs, the NIH says that it will decrease the value of both competing and noncompeting RPGs (whose funding is contingent on the submission of a progress report) by 1% below FY 2012 amounts and eliminate built-in inflationary increases. Another strategy—which may or may not succeed in generating a sizeable surplus—is to pay greater attention to applications from grantees who already receive more than $1.5 million annually in total funds from the NIH. Those applicants affected by this proposed strategy make up 6% of all extramural NIH-funded principal investigators. A related policy has been in place at the National Institute of General Medical Sciences since 1998.

Some of the strategies for belt tightening in the budget request come from a report issued by the NIH in October 2011 entitled "Ways of Managing NIH Resources" and the responses it generated from the scientific community. The report presented suggestions for tackling a flat—or declining—budget and calculations of the effects on new RPG awards. The four key suggestions of the report included reducing the amount of money per NIH grant by $25,000, restricting the numbers of grants an investigator can hold, capping the total award value held by an investigator and reducing the salaries of principal investigators.

However, none of these four suggestions has been adopted in the 2013 budget request, and the NIH has stated that the greater scrutiny of grant applications from recipients of large amounts of NIH dollars will not constitute a cap on their funding. Interestingly, the report calculated that limiting total per-investigator NIH support to $1 million would free up funds for 2,000 more competing RPGs and that 20% of principal investigators receive 50% of the RPG funds (a figure that has changed little since 1986). These numbers suggest that the NIH could do more—if necessary—with its funds.

Why is the NIH hesitant to impose more substantial changes to its allocation of resources? All researchers are loath to see their funds reduced, and some object to a perceived redistribution of wealth to new and unproven labs at the expense of more experienced investigators. But there is always waste in science, as in any industry, and it's not unreasonable to think that a $25,000 cut per grant across the board—which would sustain growth in the number of competing RPGs—might improve the efficiency of biomedical research. Doing too little to increase funding opportunities risks driving the best young minds away from science and could harm scientific output in the long run.

As it is, there is an imbalance between the number of biomedical trainees and the number of available academic positions in the United States, which may also hinder the recruitment into science of outstanding future principal investigators. On June 14, a report released by the NIH Biomedical Workforce Working Group detailed its recommendations to promote a more sustainable biomedical research workforce in the United States. These suggestions include limiting NIH support to graduate students to six years and using NIH training grants to institutions and individual fellowships to pay for more graduate student and postdoctoral researcher salaries. The report also recommends increasing the salaries and improving the benefits of postdoctoral researchers, doubling the number of awards for postdoctoral researchers transitioning to tenure-track faculty positions and creating new programs to help graduate students identify or investigate career alternatives to research-based pursuits.

Although they are certainly laudable, financial support for these diverse initiatives must come from somewhere. But by making trainees more expensive, Shirley Tilghman, co-chair of the working group, acknowledged that implementing the report's recommendations would probably slow the growth of the biomedical research workforce, perhaps forcing greater efficiency and more productive use of restricted funds. Similar recommendations to the NIH have been made in the past, prior to the doubling of the NIH budget, but they were not implemented. However, given the current economic climate, the NIH may heed this report's suggestions to focus spending and help retain those individuals most likely to succeed in a research-oriented career.

If the FY 2013 NIH budget request is not approved by September 30, the NIH budget would be reduced—perhaps by ~10% as a result of the US Budget Control Act. More severe measures would then presumably be required, although these have yet to be articulated. And regardless of the budgetary outcome, it's clear that the growth of science funding in the United States will be slower than it has been in the recent past. Therefore, it's time to adjust the scientific community's thinking accordingly and recognize the importance of ensuring a continued influx of new, high-quality researchers and of finding equitable funding solutions to sustain scientific advance.

King Abdullah International Medical Research Center

Got Ethics?

We do. Ethics is doing the right thing, even if nobody is watching.

KAIMRC aims to disseminate biomedical ethic concepts into the health care system and community through education and public awareness. In an Islamic matrix of ethics and morality, we strive to set our own trends to formulate policies and guidelines, carry out and coordinate teaching and research, stimulate informed public debate, and provide a resource service for health professionals in our community and beyond. Ethical work behavior is a crucial part of success; all our employees possess a high degree of integrity and an outstanding level of professionalism.

At KAIMRC, a segment in the enormous healthcare system of King Abdulaziz Medical City, we felt the overwhelming sense of obligation towards both the healthcare profession and our institution to launch a Masters Degree program in Biomedical Ethics with the incorporation of Islamic Law. Healthcare professionals who show genuine interest in applying their knowledge and expertise to the ethical aspects of healthcare would be considered for program.

KAIMRC takes pride in its Bioethics Section, as it is home for the UNESCO chair of Saudi Arabia, held by its head Dr. Amin Kashmeery.

"*Whoever works righteousness, man or woman, and has faith, verily, to them will We give a new Life, a life that is good and pure, and We will bestow on such their reward according to the best of their actions.*" - Holy Qur'an, Chapter 16, Verse 97

"*It is better for a leader to make a mistake in forgiving than to make a mistake in punishing.*"- Prophet Mohammed (PBUH)

"*In law a man is guilty when he violates the rights of others. In ethics he is guilty if he only thinks of doing so.*" – Immanuel Kant

"*Ethics is knowing the difference between what you have a right to do and what is right to do.*" – Potter Stewart

cientists Vacancies at King Abdullah nternational Medical Research Center

Today's Question, Tomorrow's Answer

AIMRC provides an opportunity to serve in a dynamic, ulticultural environment with state-of-the-art facilities for mpetent and motivated persons who are willing to dedicate emselves and make a difference in the world of scientific medical search. If you are interested in being involved in demanding and novative projects within one of the leading medical research centers rldwide, then search KAIMRC on Naturejobs.com to find our latest cancies or apply with us by sending your resume to recruitment@kaimrc.ed.sa. Please identify the position that you are applying to in the subject ading of your e mail.

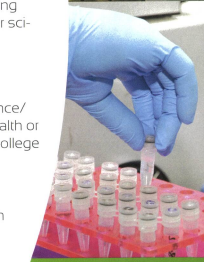

AIMRC Is Looking To Hire The Following:

1. Senior Research Scientist:

Education & Qualifications:

- Doctorate Degree (PhD) in Health Science or in a related discipline from an accredited university(Essential).

Experience:

- Minimum of twelve (12) years of experience in a well recognized research institution, coupled with two (2) years supervisory experience in a senior management position(Essential).

2. Research Scientist:

Education & Qualifications:

- PhD IN Science/Pathology or in a related discipline from an accredited University (Essential).
  Preferably post-doctoral research experience

Experience:

- Eight (8) years working experience in clinical /research institution or Five (5) years experience with one or more publication as Principal Investigator in journal with 12 or more impact factor(Essential).

3. Associate research scientist:

Education & Qualifications:

- Doctorate Degree (PhD) in Health Science or equivalent from an accredited university (Essential).

Experience:

- Completion of Post Doctoral Fellowship (Essential).
- Minimum of three (3) years of experience in a clinical/research institution(Essential).

4. Research Assistant:

Education & Qualifications:

- Master's Degree in Health Science/ Health Management/Public Health or equivalent from an accredited college or university(Essential).

Experience:

- Minimum of four (4) years working experience in clinical research or scientific field(Essential).

5. Research Associate:

Education & Qualifications:

- Master's Degree in Health Science/ Health Management/Public Health or equivalent from an accredited college or university (Essential).

Experience:

- Minimum of seven (7) years of experience in a clinical/research institution(Essential).

For further information
Please visit our website: www.kaimrc.med.sa
To know more about our activities,
the available positions
or our collaboration policies,
Email: researchI@ngha.med.sa

Rest easy:
New orexin-blocking sleeping pills offer safe shuteye

Shock therapy:
A special news focus on sepsis drug development

Stroke of genius:
The quest to develop the first neuroprotective stroke drug

'Must-pass' FDA fee renewal jammed with sunscreen and more

Salmon and sunscreen may seem far removed from the world of cutting-edge drugs and medical devices. Yet both have been, at one time or another, part of the deal-making as the US Congress hashed out the details of the proposed Food and Drug Administration Safety and Innovation Act, currently making its way to the president's desk for final approval. The legislation will renew a version of the Prescription Drug User Fee Act (PDUFA), which requires makers of new therapies to pay fees to support swift completion of the FDA approval process.

On 18 June, the Senate and House of Representatives reconciled their versions of the bill, which policy analysts expect President Barack Obama to sign into law before the end of September, at the latest.

Researchers at the Tufts Center for the Study of Drug Development in Boston credit the law as cutting drug review times in half since its inception in 1992. The government needs to reauthorize a version of PDUFA every five years, and it is considered a must-pass measure because the FDA has become reliant on the money it generates, used to cover employee salaries. In 2010, for example, the more than $550 million in user fees collected by the FDA covered 62% of the agency's costs for drug reviews.

The periodic reauthorization of PDUFA, however, gives special interests a chance to slip in tangentially related rules. "Knowing that this bill is going to pass, they try to put as much in it as they can," says Aaron Kesselheim, who studies health policy at the Brigham and Women's Hospital in Boston.

Indeed, a proposal by Republican Senator Lisa Murkowski of Alaska regarding genetically engineered salmon was introduced at one point, although it floundered and failed to make the final Senate version. It would have required an extensive study of the environmental and economic impacts of genetically modified salmon before it could be considered for FDA approval. Also off the table is a failed proposal to give drugs containing hydrocodone painkillers a more restrictive classification, which would have changed procedures for stocking and prescribing the medication.

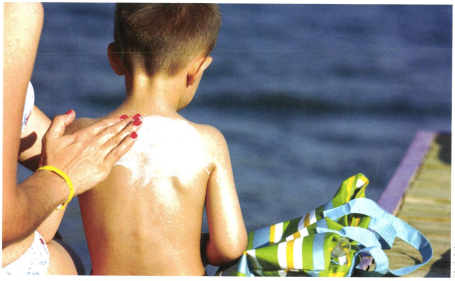

Layer it on: Legislators have tied rules for sunscreen and antibiotics to PDUFA.

Sunscreen remains in the latest version of the legislation, however. Provisional language in the PDUFA-renewing legislation extends by about six months the deadlines for compliance with a law passed last year that forbids sunscreen makers from using the words 'waterproof' or 'sweatproof' on their labeling

Gaining additions

Some people also see the legislation renewing the PDUFA framework as a possible Trojan horse for market protections for industry. As *Nature Medicine* went to press, the Food and Drug Administration Safety and Innovation Act included a provision designed to spur the development of new antibiotics, known as the Generating Antibiotic Incentives Now Act, or the GAIN Act (see *Nat. Med.* **17**, 772, 2011). The GAIN legislation would ensure market exclusivity for new antibiotics for five years to reduce competition from other drugs.

The last time the PDUFA framework was renewed, in 2007, a rule was put in place requiring the FDA to slowly reduce the presence of experts with industry ties who serve on the agency's advisory panels. But meeting that requirement proved difficult, according to Celia Wexler, the Washington, DC representative of the nonpartisan Union of Concerned Scientists, a Cambridge, Massachusetts–based organization that lobbies for evidence-based federal policy. "The FDA was nowhere near reaching that cap this year," she says. The new legislation headed to Obama would remove the cap on the number of experts with conflicts of interest.

The most recent versions of the PDUFA renewal also include rules that will add new responsibilities for the FDA, such as requiring the agency to regularly publish data on demographic subgroups included in studies of all products on which the FDA has oversight. "There hasn't been any transparency about who was included in studies conducted by industry," says Susan Wood, a women's health researcher at George Washington University in Washington, DC and former FDA assistant commissioner of women's health. Additionally, new language in the bill would compel the FDA to study and report drug shortages affecting life-supporting and life-sustaining medications.

There are, of course, updates that do apply to the fees themselves: one change will require makers of generic drugs and biosimilars to pay the same fees already paid by manufacturers of brand-name drugs.

Chase Scheinbaum

New adjuvants aim to give whooping cough vaccine a boost

From 1 January through 9 June of this year, the Washington State Department of Health reported nearly 2,300 cases of pertussis—13 times more than it recorded during those same months in 2011. Public health officials blamed the rash of infections in part on low vaccine uptake in the Northwest, but the existing vaccines against the disease also suffer from serious limitations, prompting scientists around the globe to research better alternatives.

The diphtheria, tetanus and acellular pertussis (DTaP) vaccine given to children in the US and Europe to protect against whooping cough and the related 'Tdap' booster shot both contain purified antigens from the bacterium *Bordetella pertussis*. These products cause fewer adverse reactions than the older whole-cell inoculations that are still in use in the developing world to immunize kids against pertussis, also known as whooping cough. But safety comes at a cost: the existing vaccines provide only up to 85% protection against the disease, compared with up to 95% for some whole-cell formulations. Moreover, when a team led by infectious disease specialist David Witt at Kaiser Permanente Medical Center in San Rafael, California, collected background information about the patients who tested positive for pertussis during a massive 2010 outbreak in California, they found that whooping cough rates were no different in vaccinated versus unvaccinated kids between the ages of 8 and 12 (*Clin. Infect. Dis.*, **60**, 1730–1735, 2012). "It's awfully worrisome," says Witt, as it suggests that protection wanes after several years.

Improvements could be forthcoming. One strategy is to develop better adjuvants, as the current choices, aluminum phosphate or aluminum hydroxide, skew the immune system toward an antibody-driven response—a fact that might limit their effectiveness, explains Scott Halperin, director of the Canadian Center for Vaccinology in Halifax, given that antibodies aren't always effective against pathogens that permeate inside cells, as pertussis does. He had his colleagues have developed a new triple-adjuvant formulation that heightens cell-mediated immune responses, killing infected cells. In a mouse study published last year, they reported that a single dose of their formulation boosted levels of circulating IgG2a antibodies—which are indicative of cell-mediated immunity—to match those produced after the mice received the equivalent of two doses of a commercial infant DTaP vaccine (*Vaccine* **29**, 1595–1604, 2011).

Another approach is to design a vaccine specifically for newborns, who are at the highest risk of dying from pertussis. Vaccines don't typically elicit strong immune responses in young babies, but actual infections do. So, Camille Locht, a microbiologist at the University of Lille–North of France, and his colleagues are developing the first live pertussis vaccine, currently called BPZE1, to be given to babies within the first few days of life. "If we give a single nasal drop in the nose of a one-week-old mouse, just a single administration, the mouse is still protected one year later, which for a mouse is a very long time," Locht explains. And since the bacteria's toxins have been either eliminated or modified, the vaccine should be safe, Locht says.

BPZE1 completed a phase 1 proof-of-concept trial in adults in 2011, but the group is now optimizing the formulation and plans to initiate another phase 1 trial in 2014. The goal "is not to replace the vaccines that we have," Locht says. But, since babies don't get their first DTaP immunizations until they are two months old and aren't usually well shielded until they have received multiple doses, it would be wonderful "to help infants be protected in the most vulnerable time of their life."

Melinda Wenner Moyer

Accord could make Canadian generics industry a 'rust bucket'

A trade agreement in negotiations between Canada and the EU is drawing the ire of generic drugmakers, provincial governments and patient advocates over proposals to extend drug patents by several years in Canada, a move that critics say would delay the arrival of generic medicines to market in that country and inflate healthcare costs.

According to Canada's Department of Foreign Affairs and International Trade, Canada imports C$8.4 billion ($8.2 billion) of pharmaceutical products from the EU annually, making Canada the fifth largest export market for the continent's drugmakers. The sweeping Comprehensive Economic and Trade Agreement (CETA) could add another $2.8 billion to the annual bill, according to a report by health economists Paul Grootendorst, from the University of Toronto, and Aidan Hollis, from the University of Calgary (*J. Generic Med.* **8**, 81–103, 2011). This cost is largely shouldered by the provincial and territorial governments, which pay for healthcare.

CETA—first proposed in 2009 and subsequently leaked in 2010—calls on Canada to beef up its intellectual property rights for pharmaceuticals. The proposed changes would add five years to patents for drugs that are unduly bogged down in the regulatory approval process, lengthen the period of time clinical trial data is kept off-limits for use by generics companies from eight years to ten years (or even longer in the case of pediatric drugs) and grant brand-name companies an appeal process to challenge generics companies on their patent compliance.

"It would elevate or harmonize the intellectual property standards in Canada to those of the EU, which is at the forefront of life sciences research," says Declan Hamill, vice president of legal affairs at Rx&D, an Ottawa-based trade group representing brand-name pharmaceutical companies in Canada. "It might change the way the game is played: you give us longer IP [intellectual property], we'll throw some clinical trials your way," adds Grootendorst.

But critics say that the agreement would largely benefit pharmaceutical companies headquartered in Europe. "We will lose investment and become a rust-bucket kind of industry," says Jim Keon, president of the Toronto-based Canadian Generic Pharmaceutical Association (CGPA), who charges that the intellectual property revisions might prompt its members, most of which are international companies with manufacturing facilities in Canada, to go elsewhere.

The recent analysis by Grootendorst and Hollis—commissioned by the CGPA—found that the plan would give patented drugs an exclusive spot on the market for 3.5 years more, on average, than they currently hold. A counter-analysis by Canadian intellectual property lawyers disputes this, but Grootendorst and Hollis question its methodology.

The Canadian government hopes to wrap up the agreement by the end of this year, the country's International Trade Minister Ed Fast said at an economic conference in Montreal last month.

Hannah Hoag

Biobanks look to software solutions to handle data deluge

Modern biobanks are becoming more than mere warehouses of human biological samples. Nowadays, these repositories of scientific specimens must handle sample intake, collate reams of data and make the resulting information available to the research community in a useful fashion. Shifting from the role of a sample storehouse to an active research engine is no easy task, but powerful informatics technologies are now helping scientists and biobank managers make the transition.

Take, for example, SpecimenTrack, a research management platform unveiled in May at the International Society for Biological and Environmental Repositories meeting in Vancouver, British Columbia. This web-based application, developed by Remedy Informatics near Salt Lake City, Utah, integrates demographic and geographical data relating to specimen donors, along with the output of clinics and laboratories involved in a particular study, all in a simple visual display that allows researchers engaged in multicenter collaborations to analyze the same information wherever they are. "There are other solutions to narrow slices to this kind of work flow, but there's no other that can provide this kind of holistic overview," says Hank Wu, Remedy's director of translational informatics.

Already, SpecimenTrack is being used by ten labs at the Frederick, Maryland, campus of the US National Cancer Institute to consolidate molecular, genetic and clinical data from a number of cancer genome projects.

Bio4D provides another platform for sharing biobank information across multiple laboratories. Created by the India-based software firm Persistent Systems together with the Translational Genomics Research Institute (TGen) in Phoenix, Arizona, Bio4D is currently tasked with tracking samples collected at 40 institutions, following them as they pass between multiple other centers and then feeding back genetic data that help physicians tailor treatments to individual patients. "A solution that allows many different clinical sites, many different biorepositories and various analysis sites to all access the same data, but with proper controls, is extremely valuable," says Tgen cancer geneticist Jonathan Keats, who announced the commercial launch of Bio4D at the Vancouver meeting.

But it's not just the multiple layers of data from disparate sources that biobanks need to keep an eye on. Mistakes creep in often enough at a more basic level of sample management that cannot be solved by fancy software. Last year, for example, in a survey of more than 130 US institutions, researchers found that pathologists mislabeled about one in every 1,000 samples (*Arch. Pathol. Lab. Med.* **135**, 969–974, 2011).

Software sweepstakes

To help with specimen annotation and tracking, a New Jersey start-up called BioTillion is working on a radio-frequency identification tagging system that can electronically label and monitor large collections of samples in ultra-low temperatures—all without even having to open freezer doors. In a similar vein, Dataworks Development, a data management company located near Seattle, has an iPhone app under development that enables scientists to use their mobile devices to scan the barcode of a biological sample or reagent and update the lab's record of supplies so that more can be ordered if they run low. "It works just like in a supermarket," says Rick Michels, vice-president of sales and marketing at Dataworks, who presented a prototype of the app at the Vancouver meeting.

Ideally, the new technologies will both cut mistakes and further what biobanks can do. By their very nature, the latest software products encourage better practice by standardizing how data are recorded and shared. "Biobanks are in a position to coordinate with one another into virtual biobanks that provide larger sample libraries and significant amounts of rare biospecimens," says Wu. And that should help repositories gain economics of scale without actually expanding.

Anna Petherick

First therapy targeting Parkinson's proteins enters clinical trials

Parkinson's disease is driven by the slow and steady death of dopamine-producing neurons—and there's currently little modern medicine can do to stop the process. Dopamine replacement therapies such as levodopa help alleviate some of the more debilitating movement problems, but all the while brain cells continue to die and the neurodegenerative disorder gets worse. That's why the research community was buoyed last month by the announcement that an Austrian company had launched the world's first clinical trail involving a therapy directed against alpha-synuclein, a protein found to be a pathologic hallmark of Parkinson's disease.

"This will have the potential to change the trajectory of the disease, which levodopa does not," says Kuldip Dave, associate director of research programs at the New York–based Michael J. Fox Foundation for Parkinson's Research, which is funding the $1.5 million trial. "If it works, it could be the first disease-modifying therapy in Parkinson's."

The experimental vaccine, from Vienna-based AFFiRiS, contains short peptide fragments designed to trigger the body's antibodies to attack and clear native alpha-synuclein proteins stuck in the cell membrane or spreading between cells. Unpublished experiments performed in collaboration with Eliezer Masliah, a University of California–San Diego (UCSD) neuroscientist, demonstrated that the vaccine, dubbed PD01, reduced the levels of alpha-synuclein in the brain, prevented neuronal loss and led to cognitive improvements in two transgenic mouse models of Parkinson's.

Now, AFFiRiS is testing two different doses of PD01 formulated together with aluminum oxide as an adjuvant in up to 32 people with early Parkinson's disease aged 45 to 65 and following them for a year. In addition to proving that the vaccine is safe, Achim Schneeberger, AFFiRiS's chief medical officer, hopes to see some early signs of efficacy. "We would expect that, given the fact that the dose should be immunogenic in humans, these patients should get an antibody response that could protect them from further decline," he says.

Alpha-beta soup

Immunizing against a neurotoxic protein like alpha-synuclein is not without its risks—as evidenced by the severe brain inflammation experienced by some phase 2 trial participants who received an experimental vaccine called AN-1792 that contained fragments of amyloid-beta, the aberrant protein associated with Alzheimer's disease (see *Nat. Med.* **8**, 199–200, 2002). Worryingly, a team led by Howard Gendelman at the University of Nebraska Medical Center in Omaha has reported that vaccinating mice with a modified fragment of the alpha-synuclein protein can trigger a

Cancer immunotherapy shows promise in multiple tumor types

The approval last year of the immunotherapy drug Yervoy (ipilimumab) in the US and Europe was hailed as a major advance for the treatment of late-stage melanoma. The antibody drug, which promotes broad T cell function by blocking a surface protein called cytotoxic T lymphocyte antigen 4 (CTLA-4), can add years to a person's life, transforming metastatic skin cancer from a death sentence to a manageable condition. However, Yervoy works only in 20–30% of patients who take it, and the drug is often accompanied by severe or even fatal autoimmune side effects. So, the hunt has been on for safer and more broadly applicable immunotherapy strategies, and now a new class of cancer drug that boosts T cells in a more targeted fashion is showing early signs of dramatic success.

At last month's American Society of Clinical Oncology (ASCO) meeting in Chicago, researchers presented phase 1 trial data showing that blocking a protein called programmed death-1 (PD-1) could reduce tumor mass in a variety of cancers. For example, a PD-1–targeting agent from Bristol-Myers Squibb (BMS) called BMS-936558 either eliminated or shrank tumors in 49 of 203 people with advanced skin, kidney or lung cancer. Previous cancer immunotherapies have typically worked in smaller numbers of patients and in fewer types of cancer. The majority of the responses seen with BMS-936558 also lasted longer than one year, scientists reported at ASCO and concurrently in the *New England Journal of Medicine* (doi:10.1056/NEJMoa1200690, 2012).

Down to a T: Yervoy promotes T cell function.

Results like these are unprecedented in the field of cancer immunotherapy, says Kenneth May, a medical oncologist at the Dana-Farber Cancer Institute in Boston who was not involved with any of the current drug trials.

"The exciting part about these anti–PD-1 antibodies is that they're shrinking away large metastatic tumors like lung and kidney that are typically pretty resistant to therapy," he says.

Normally, PD-1, like CTLA-4, works to protect tissues from potentially self-reactive T cells. But in cancer some tumors have "co-opted this system as a mechanism of protecting themselves from immune attack," explains Drew Pardoll, co-director of the Cancer Immunology and Hematopoiesis Program at the Johns Hopkins University School of Medicine in Baltimore.

Pardoll was involved in testing BMS-936558 as well as another BMS antibody directed at the PD-1 ligand (PD-L1) expressed by tumor cells. In a phase 1 trial, 16 of 118 people with skin, kidney or lung cancer treated with the PD-L1–directed agent showed an antitumor response (*N. Engl. J. Med*, doi:10.1056/NEJMoa1200694, 2012).

Better than Yervoy?

Because CTLA-4 binding can occur between T cells and many cells in the body—whereas PD-1's binding partner, PD-L1, is found only on tumor cells—researchers are hopeful that these new immunotherapy drugs will ultimately prove safer and more effective than Yervoy. The experimental antibodies have never been tested head-to-head with Yervoy, but BMS, which is headquartered in New York, is now testing BMS-936558 in combination with Yervoy in about 100 people with advanced melanoma. "It's still early days," says Nils Lonberg, BMS's vice president of biologics discovery. But "they're interesting complementary pathways, so it could be the beginning of an arsenal of immunotherapeutic drugs."

Several other drugmakers, including New Jersey–based Merck, Maryland-based Amplimmune and the Israeli company CureTech, are similarly targeting PD-1 in an effort to fight tumor cells. At ASCO, scientists presented preliminary data showing that Merck's drug, called MK-3475, helped shrink or stabilize solid tumors in four of nine people enrolled in an ongoing phase 1 trial. Meanwhile, South San Francisco–based Genentech has its own PD-L1–specific antibody in early clinical testing. According to Seamus Fernandez, an analyst at Leerink Swann in Boston, these drugs could collectively be worth $2 billion by the end of the decade.

Monica Heger

neuroinflammatory T cell response, leading to the rapid loss of dopamine-producing neurons (*PLoS One* **3**, e1376, 2008). "Rather than fix the disease we actually accelerated it," Gendelman says.

The AFFiRiS scientists haven't specifically checked for the T cell response observed by Gendelman's group. But, at just seven amino acids in length, the peptides in the AFFiRiS product are thought to be too short to elicit any T cell response. Plus, the peptide's amino acid sequence differs from that of native human alpha-synuclein, which should further limit the opportunity for any dangerous autoimmune reactions. "There's no chance it'll have a reactive effect," Masliah says.

Other researchers have tried in the past to develop similar vaccines. A team from the South San Francisco division of Elan Pharmaceuticals, a neuroscience-focused company headquartered in Dublin, together with Masliah's lab previously demonstrated that a vaccine containing full-length alpha-synuclein could halt Parkinson's in a mouse model of the disease (*Neuron* **46**, 857–868, 2005). But more recently the efforts of companies such as Elan have shifted toward engineering antibodies or small-molecule drugs—rather than vaccines—against the protein. Elan scientists and Masliah's group reported on a lead candidate last year (*PLoS One* **6**, e19338, 2011).

"The antibody therapeutics are a well-trodden path," says Elan's chief scientific officer Dale Schenk. The potential for inflammatory reactions like those seen with Elan's AN-1792 is "completely obviated when you give an antibody," he notes. "There is no T cell response. It's not possible."

Other companies developing antibodies and small molecules directed against alpha-synuclein include Washington-based ProteoTech, Pennsylvania-based QR Pharma and Massachusetts-based BioGen Idec. "It's an exciting time," says Biogen's head of translational neurology Ajay Verma, who anticipates his company's antibody to be in clinical trials before the end of the year. "We're really getting close to a tipping point of testing disease-modification therapies."

Elie Dolgin

Biomedical briefing

POLICY

Workforce worksheet

To support a sustainable biomedical workforce, the US National Institutes of Health (NIH) needs to pay postdoctoral researchers more, boost the stature of staff scientists and better prepare graduate students for careers outside academia. Those were some of the conclusions of a draft report presented on 14 June by the NIH's Biomedical Research Workforce Working Group. Another report released at the same time by a separate working group suggested adding a chief diversity position to the committee that advises NIH director Francis Collins. See go.nature.com/SCVuSd for more.

Containment concerns

The US government continues to underestimate the potential for dangerous pathogens escaping from a proposed biosafety level 4 (BSL-4) containment laboratory in Kansas, according to an independent report published on 15 June. A panel convened by the National Research Council concluded that an assessment completed earlier this year by the US Department of Homeland Security (DHS) overestimated the danger posed by tornadoes and earthquakes but underestimated the possibility of a disease being released by human error. Still, developers don't think that those problems merit delaying construction on the $1.14 billion lab, which is slated to replace a half-century-old facility on Plum Island, New York. "If the design is sound and the need is there," says Ron Trewyn, vice president for research at Kansas State University in Manhattan, "then it's time to build the building and do the other things that have been suggested as the building becomes operational."

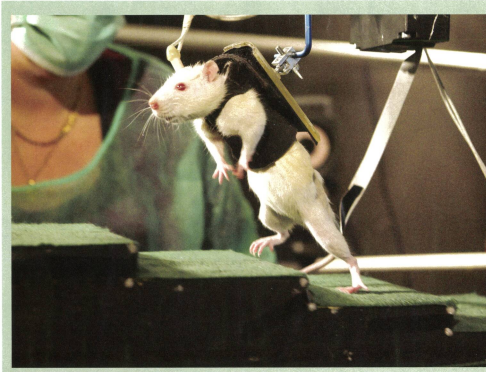

Ecole Polytechnique Fédérale de Lausanne

Robotic rehab aids rat recovery from spinal injury

A combination of neuron-activating chemicals, electrical stimulation and robot-assisted rehabilitation could hold the key to restoring movement after severe spinal injury. A team led by Grégoire Courtine, a neurophysiologist at the Swiss Federal Institute of Technology in Lausanne, administered this rehab regime to paralyzed rats with spinal cord injuries. After several weeks of daily treatment, the rats could walk up small stairs or over obstacles placed in their path, the researchers reported last month in *Science* (**36**, 1182–1185, 2012). Of note, the physical therapy relied on a new kind of robotic interface described on page 1142 of this issue of *Nature Medicine*. "Without the robot, you could not train the rat to regain voluntary control over his paralyzed hind limbs," Courtine says. "This is why we're so eager to try to develop the same interface for humans in the future."

Three's company

The Nuffield Council on Bioethics, an independent advisory body based in London, issued a 100-page report in mid-June that concluded it would be ethical to create embryos containing genetic material from three individuals. The approach swaps in mitochondrial DNA from a third 'parent' to correct for mitochondrial disorders, which affect at least one in 8,500 individuals. Doctors have not yet applied the procedure in the clinic, but the Human Fertilization and Embryology Authority, the UK's regulator on reproductive matters, will decide in April 2013 whether or not to permit its use. Whatever happens, "it will inform the debate in any other country that is looking at a similar issue," says Alison Murdoch, a reproductive biologist at Newcastle University who is licensed to develop mitochondrial DNA transplant techniques.

PEOPLE

Fake out

Andrew Strempler, a pioneer of Canada's online pharmacy trade, could face up to 20 years in prison after US federal authorities arrested and charged him

Drug-resistant tuberculosis takes hold in China

China faces a still-spreading epidemic of drug-resistant tuberculosis, according to the first nationwide study of the disease. The survey, reported last month in the *New England Journal of Medicine* (**366**, 2161–2170, 2012), found that one in ten people treated for tuberculosis in 2007 had a form of the disease that didn't respond to multiple medicines. Worryingly, most of the estimated 110,000 drug-resistant cases in China occurred in people newly diagnosed with tuberculosis, suggesting that drug-resistant bacteria are spreading from person to person rather than just evolving in people who don't respond to first-line treatments. "We need to be looking at everybody, because if you restrict yourself to the so-called 'high risk patients' you're going to miss most of the cases," says Richard Chaisson, director of the Johns Hopkins University Center for Tuberculosis Research in Baltimore who wrote an accompany commentary (*N. Engl. J. Med.* **366**, 2223–2224, 2012).

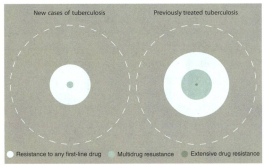

More online

'SMART' biochip for rapid flu diagnosis:
go.nature.com/O4RJbq

Doctors transplant first bioengineered vein:
go.nature.com/UMEpIF

in Miami last month with mail fraud over the sale of potentially fake and otherwise misbranded drugs to American customers. The allegations follow the discovery in August 2006 of fake versions of Lipitor (atorvastatin) and Celebrex (celecoxib), two widely prescribed drugs from New York–based Pfizer. "We will aggressively pursue those who engage in such illicit activity as counterfeit medicines," says the company's chief security officer John Clark. According to a grand jury indictment, Strempler (pictured), the former head of RxNorth.com, sold drugs that he claimed had been packaged in Canada but allegedly originated from the Bahamas.

Associated Press

BUSINESS

Let HER2 rip

Roche's cancer drug franchise has added another weapon in the fight against advanced breast cancer. On 8 June, the Swiss company's South San Francisco–based subsidiary, Genentech, won approval for Perjeta (pertuzumab) for the treatment of metastatic breast tumors in people with high levels of a protein called human epidermal growth factor receptor 2 (HER2), which is elevated in around 20% of all breast cancer cases. Perjeta is designed to be used with Genentech's existing antibody drug Herceptin (trastuzumab), which, like Perjeta, binds HER2, but at a different region of the protein. A combination of the two drugs, together with chemotherapy, boosted progression-free survival by six months compared to Herceptin and chemotherapy alone (*N. Engl. J. Med.* **366**, 109–119, 2012). That added benefit comes at considerable extra cost: Perjeta is priced at close to $6,000 a month, on top of the $4,500 a month cost for Herceptin.

Rare blow

Pfizer's foray into rare diseases suffered a setback last month after the US Food and Drug Administration declined to approve its drug for the treatment of a rare and fatal neurodegenerative disease known as transthyretin familial amyloid polyneuropathy, which affects an estimated 8,000 people worldwide. In a 128-person pivotal trial, participants who took the drug—tafamidis, which helps stabilize the defective transthyretin protein that is associated with the disease—outperformed those receiving placebo on a scale of neurological function, but only when study subjects who dropped out of the study for liver transplants were excluded from the analysis. Agency staffers asked New York–based Pfizer for another efficacy study with a revised endpoint that takes into consideration the high rate of attrition due to organ transplants. European regulators approved the drug, marketed as Vyndaqel, in November 2011.

Corrections

In the June 2012 issue, the article entitled "The vetting process" (*Nat. Med.* **18**, 847–849, 2012) stated that capture myopathy kills up to half of all wildlife brought into captivity. The correct proportion is up to one in ten. The error has been corrected in the PDF and HTML versions of this article.

In the June 2012 issue, the article entitled "The vetting process" (*Nat. Med.* **18**, 847–849, 2012) incorrectly stated that the research techniques designed for freezing, thawing and grafting ovarian tissue for wildlife conservation had helped women give birth to healthy babies after fertility-compromising cancer treatments. These techniques are helping fertility preservation methods but have not been directly applied in human treatments. The error has been corrected in the HTML and PDF versions of the article.

In the March 2012 issue, the article entitled "Korea okays stem cell therapies despite limited peer-review data" (*Nat. Med.* **18**, 329, 2012) incorrectly stated that the Hearticellgram-AMI therapy results related to 80 individuals. In fact, the number is 59, and the difference in left ventricular ejection fraction changes between the treatment and control group was statistically significant. Additionally, the information about this therapy was available through poster presentations, not exclusively through press releases by the Korea Food and Drug Administration, as originally stated. The errors have been corrected in the HTML and PDF versions of the article.

New class of sleep drugs may offer a safer night's rest

Roughly one-fifth of adults in the US experience insomnia, and they'll try everything from counting sheep to popping pills to get some shuteye. Last year, US sleep seekers filled more than 60 million prescriptions for sleep medications and sales topped $1.6 billion, according to the Connecticut-based market research firm IMS Health. But sleeping pills can cause dependence, and their side effects—including falls, confusion and memory problems—can be a nightmare. In some cases, people taking the medications have even started driving cars or binge-eating in their sleep. But a new therapeutic drug class could overcome many of these problems, and the lead compound is now on the verge of regulatory filing.

Reporting at last month's Annual Meeting of the Associated Professional Sleep Societies in Boston, the US drug giant Merck presented data from two phase 3 clinical trials showing that an experimental drug called suvorexant helped people fall asleep faster and stay asleep longer on average than a placebo, without causing serious side effects. Merck plans to file a new drug application with the US Food and Drug Administration (FDA) later this year.

If approved, suvorexant would be the first sleep medication that blocks a neurotransmitter called orexin, which is involved in controlling the body's sleep-wake cycles. In contrast, most popular sleeping pills, including Sanofi's Ambien (zolpidem) and Sunovion Pharmaceuticals' Lunesta (eszopiclone), work by enhancing signaling of a neurotransmitter called gamma-aminobutyric acid (GABA), which quiets activity throughout the brain, including the regions involved in sleep. However, because GABA plays a crucial part in a variety of brain functions, the drugs have a laundry list of potential side effects, which prompted the FDA to add stronger warning labels to some medications in 2007. Some antianxiety pills are also commonly prescribed off label to treat insomnia; however, they come with their own set of concerns, including a 36% increased risk of death, according to one recent estimate (*Can. J. Psychiatry* **55**, 558–567, 2010).

Because orexin signaling happens primarily in the hypothalamus, a key region in regulating sleep, the hope is that blocking this protein will promote sleep without affecting other regions of the brain and causing unwanted effects. As John Renger, site lead of neurosymptomatic disorders at Merck in West Point, Pennsylvania, points out, the process mimics "what goes on naturally in your brain."

"It's a very targeted approach," says David Neubauer, a psychiatrist at the Johns Hopkins Sleep Disorders Center in Baltimore who was not involved in testing suvorexant. "It's not often that you have a compound come along that has a completely new mechanism of action," adds orexin researcher Thomas Scammell, a neurologist in the Harvard Medical School's Division of Sleep Medicine in Boston.

Differentiation protocol

Suvorexant isn't the first orexin blocker to make it to phase 3 trials. A few years back, the Swiss company Actelion Pharmaceuticals collaborated with the UK's GlaxoSmithKline (GSK) to test a drug called almorexant at 90 clinical centers across Australia, Israel and Europe. Almorexant met its main target in the 700-person trial, outperforming placebo with "evidence for differentiation" from Ambien, the companies reported in December 2009. But a little over a year later, they announced plans to halt development of the drug, leaving Merck's suvorexant as the front-runner in the drug class.

Actelion and GSK have not released any details about why they decided to shelve almorexant, although onlookers suspect it was due to off-target effects that triggered a worrisome tolerability profile. According to Renger, Merck saw no major cause for concern among the 2,000 participants enrolled in the company's pivotal three-month trials. The most common complaints associated with suvorexant were headaches and sleepiness, but there were no signs of long-lasting side effects. GSK also has a similar compound called SB-649868 that recently completed phase 2 testing, the results of which have not been released.

According to Gustav Ando, a pharmaceutical analyst with the IHS Healthcare Group in London, Merck's latest results help alleviate some of the nervousness caused by almorexant's failure. Still, he says, "there are quite a lot of question marks out there." In one of Merck's trials, suvorexant failed to reduce the amount of time it took individuals to fall into a continuous sleep. "Regulators are going to be asking why it missed such a critical endpoint," Ando says, especially given that the drug was competing against a placebo rather than another medication.

Cassandra Willyard

Sepracor Inc./PRNewsFoto

Sweet dreams: Looking beyond GABA drugs.

Dreams of riches: The top-selling prescription sleeping pills in the US last year.

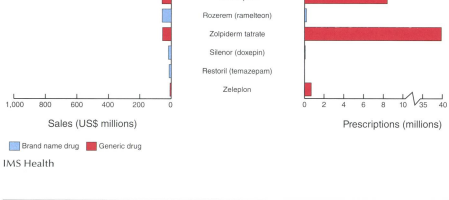

IMS Health

The development of sepsis drugs—like the patients these agents aim to treat—is in desperate need of resuscitation. Last autumn, Eli Lilly pulled the only approved antisepsis drug from global markets, and in May the world found out exactly why: the drug, a recombinant from of activated protein C known as Xigris, proved no better than placebo at preventing death in a global post-marketing trial of 1,700 people at high-risk of septic shock (*N. Engl. J. Med.* **366**, 2055–2064, 2012). Worryingly, critical-care specialists now have no drug therapies they can turn to specifically for the treatment of severe sepsis, a condition that afflicts around 18 million people worldwide each year.

The news isn't all bad, though. Mortality rates from sepsis have been dropping in recent years, thanks to improvements in hospital care and a heightened awareness of the deadly disease. And the drug pipeline is filling once again with new treatment options targeting every stage of the disease process. Nonetheless, severe sepsis still kills around one in four people it affects, and proving that experimental therapies are helpful for treating such a variable disease—one that might best be described as a nonspecific syndrome—remains a major hurdle. In the pages that follow, we highlight how sepsis researchers are working to overcome those challenges, taking aim at every step in drug development and medical practice.

Despite improving hospital care, one in 1,200 Americans will die of severe sepsis this year.

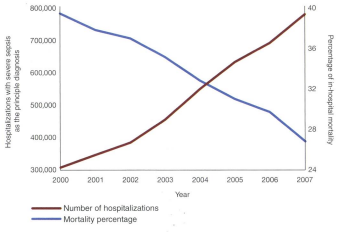

Chest **140**, 1223–1231 (2011).

Most people in the US and Europe have never even heard of sepsis.

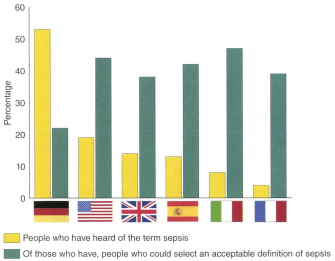

Crit. Care Med. **37**, 167–170 (2009).

Only 2% of hospitalizations are for sepsis, yet they make up 17% of in-hospital deaths in the US.

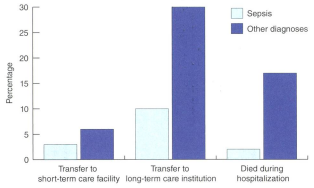

2008 figures from the *NCHS Data Brief* **62** (2011).

Patients hospitalized for sepsis in the US are sicker and stay longer than other inpatients.

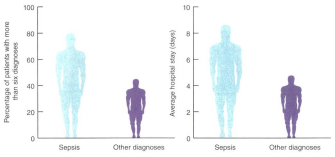

2008 figures from the *NCHS Data Brief* **62** (2011).

Rodent models of sepsis found shockingly lacking

When Kevin Tracey and his colleagues at the Feinstein Institute for Medical Research in Manhasset, New York, set out to test whether they could reverse the cognitive impairments associated with sepsis, they naturally turned to the mouse model of cecal ligation and puncture (CLP). This method of introducing a microbial infection into mice is generally considered the go-to preclinical model in sepsis research. Reporting in May, Tracey's team showed that they could improve memory defects in the CLP model by blocking a protein called high mobility group box-1 (HMGB1), a key mediator of the disease (*Mol. Med.* doi:10.2119/molmed.2012.00195, 2012). But this gain might be a red herring, as rodents remain a poor stand-in for severe sepsis in people. "The mouse models really don't reflect the human condition," says Shaw Warren, an infectious disease specialist at the Massachusetts General Hospital in Boston.

The CLP model was developed more than 30 years ago as a more clinically realistic way to induce sepsis in rodents than previous techniques, which relied mostly on injecting purified bacteria or their toxins into rodents. Using the CLP model—which involves perforating the large intestine to allow fecal material into the peritoneal cavity, thereby triggering the inflammatory immune response typically seen in human sepsis—researchers can tailor the severity of the disease by manipulating the size and timing of the gut breach. But the technique still misses the mark for several reasons.

For one, researchers usually use young, healthy, inbred mice that die fairly quickly after disease onset. "This is very different from the human situation," notes Tracey. "Death and other end points [in humans] develop over weeks and months." The CLP method is also highly prone to experimental error, as factors such as the length of intestine tied off, the size of the needle or the amount of fecal material released can lead to major differences in disease outcome. Peter Ward and his colleagues at the University of Michigan Medical School in Ann Arbor have tried to overcome some of these issues by proposing a set of standardized procedures for inducing sepsis in mice and rats (*Nat. Protoc.* **4**, 31–36, 2009).

Still, variability problems persist. "The unspoken truth is that when identical insults are given to identically aged groups of animals—even from the same litter—we see a variable individual effect," says Mervin Singer, an intensive-care specialist who studies mouse models of sepsis at University College London.

Comorbid curiosity

Some in the field are developing new ways to fine-tune the induction system so that it better mimics the poor health that many sick people are in when they develop sepsis. For example, Robert Star and his colleagues at the US National Institute of Diabetes and Digestive and Kidney Diseases in Bethesda, Maryland, recently stimulated chronic kidney disease in mice before they proceeded with traditional CLP to provoke sepsis. In a study published last year, they showed that the kidney disease worsened the sepsis severity and sepsis-induced organ damage seen in the mice, as evidenced by increased blood levels of HMGB1, vascular endothelial growth factor and other inflammatory cytokines (*Kidney Int.* **80**, 1198–1211, 2011).

"Animal models have to mimic the epidemiologic causes [of sepsis]," Star says. "You have to replicate whatever you have found in humans."

In the end, though, most experts agree that tweaks like these are just minor improvements and that the field really needs to radically redesign animal models of sepsis from the ground up. "Clearly, current animal models seem to be incapable of predicting results in human trials of new agents," says Mitchell Fink, a surgeon at the University of California–Los Angeles. Alas, until they do, few drug developers will be willing to move forward with a drug like Tracey's antibody to HMGB1, despite the promising preclinical results.

Kathleen Raven

Execution of sepsis trials needs an overhaul, experts say

The search for new sepsis drugs continues apace, but now, more than ever, experts say that overlooking the heterogeneous nature of this condition will derail any hopes of proving that these therapies work under the strict scrutiny of a large-scale, randomized clinical trial. "It's exhausting to watch drug companies come out with a compound that they are excited about and then evaluate it in a way that was done in the late 1980s," says Derek Angus, a critical-care specialist at the University of Pittsburgh School of Medicine in Pennsylvania.

The problems begin with study endpoints. In a commentary published late last year, Angus points out that many patients remain hospitalized beyond the 28-day period typically used as the primary clinical endpoint in phase 3 trials (*JAMA* **306**, 2614–2615, 2011). He suggests that trials should focus on a larger window of time and perhaps even shift the focus of drug development in sepsis toward manipulating the patient's immune response further out in time than just a month.

Angus is not alone in calling for this type of rethink. "A number of recent trials have shown that mortality signals are more stable at longer time points—for example, 60 or 90 days," says John Marshall, a critical-care surgeon at St. Michael's Hospital in Toronto. He cites a 2009 study he coauthored that found more steady survival rates three months out in critically ill patients in Australia and Canada (*N. Engl. J. Med.* **360**, 1283–1297, 2009).

Researchers also caution against lumping patients with sepsis into trials without taking into account the fact that causes of the condition vary. Most cases of sepsis are caused by bacteria, but some cases have fungi to blame and some don't have an apparent pathogenic trigger at all. "In the 1980s, we were convinced sepsis was related to infection and infection only," says Paul Walker, chief executive of Spectral Diagnostics, a Toronto-based company developing sepsis-related products. But now, researchers have documented septic shock in individuals following a massive trauma, such as that sustained in a car accident, with no detectable foreign pathogen as the root cause.

Walker's company is currently funding a phase 3 trial in which its diagnostic tool will help identify and stratify study participants according to amount of endotoxin circulating in their system

New biomarkers sought for improving sepsis management and care

For something so deadly, sepsis is surprisingly difficult to characterize. The body's response to a severe blood infection can be virtually identical to its response to other noninfectious triggers such as trauma. And even though approximately one-quarter of all people with severe sepsis eventually die from the disease, it's not easy for physicians to tell who the sickest ones are.

"You'd really like to be able to identify [severe sepsis] before it's obvious," says Mitchell Levy, medical director of the intensive care unit (ICU) at the Rhode Island Hospital in Providence. Right now, he points out, "you have to wait until organs fail until you can really tell how sick someone is."

To overcome this problem, researchers are hunting for new biomarkers that could be used to diagnose the condition earlier and single out individuals who are most likely to benefit from aggressive treatment. To date, however, even the best validated biomarkers can't differentiate sepsis caused by infections from other inflammatory causes and conditions.

Take procalcitronin (PCT), a precursor to a hormone involved in calcium metabolism that Frank Gu, a bioengineer who studies sepsis biomarkers at the University of Waterloo in Ontario, describes as "the champion so far" when it comes to identifying bacterial infections. PCT levels in the blood typically jump 1,000-fold within hours of severe sepsis or septic shock setting in. However, concentrations of the peptide also spike after major trauma, elective surgery, severe burns and even some forms of cancer, which means it might not be specific enough to serve as a diagnostic marker of infection-caused sepsis.

That doesn't mean PCT can't be useful in the critical-care setting, however. In a study published online in May, Czech researchers reported that PCT levels were significantly higher in patients with sepsis infected with Gram-negative bacteria than in patients with either Gram-positive bacterial or fungal infections (*Clin. Exp. Med.* doi:10.1007/s10238-012-0191-8, 2012). This finding suggests that the biomarker could help doctors narrow down appropriate treatment options. Still, most experts in the field agree that a more specific indicator of at-risk patients is needed.

Parsing patients

The 'soluble triggering receptor expressed on myeloid cells', sTREM-1, is one such candidate. In a study published last month, a Korean team measured plasma levels of sTREM-1 in 63 men with severe sepsis and found them to be significantly higher in individuals who ended up dying than in those who survived (*Shock* **37**, 574–578, 2012).

A similar contender is suPAR (short for soluble urokinase-type plasminogen activator receptor). This protein is expressed on the surface of immune cells including neutrophils and macrophages and can differentiate dying patients from those who have both sepsis and pneumonia but will survive (*J. Infect.* **63**, 344–350, 2011). In a 750-person observational trial, Austrian physicians are now evaluating whether measuring levels of suPAR and another biomarker shown to predict mortality in severe sepsis called ST2, a receptor involved in helper T cell responses, can help forecast not only clinical outcome but also infection type and treatment response.

Ultimately, this kind of biomarker combination approach will probably be more effective than any single biomarker would be. A team from the French University Hospital Centers in Nancy and Dijon has developed a 'Bioscore' that pools levels of three biomarkers: PCT, sTREM-1 and a type of glycoprotein expressed on the surface of neutrophils. Reporting in April, the French team showed that the composite metric performed better than each of the individual biomarkers—a finding that they validated in two separate cohorts (*Am. J. Respir. Crit. Care Med.* doi:10.1164/rccm.201201-0037OC, 2012).

The hope now, says Francois Philippart, an immunologist at the Pasteur Institute in Paris who is developing his own combination index, is to move these kinds of analysis out of clinical trials and into routine practice. "If we find an interesting panel of biomarkers, it will be useful for [diagnosing sepsis in] any kind of ICU patient," he says.

Melinda Wenner Moyer

before they receive treatment. The failure to account for patient heterogeneity, Walker says, "has been the major mistake that big pharma has made."

Pinning down the moving target

Other researchers have turned their attention to inherited susceptibility to sepsis. For instance, a team from St. Paul's Hospital in Vancouver, Canada has been analyzing blood samples from patients with sepsis to look for mutations associated with disease risk. In a study published last year, they showed that people with a particular mutation in both copies of the gene encoding interleukin-17A, a cytokine involved in defending against microbial infection, were twice as likely to be infected with Gram-positive bacteria and about 50% more likely to die at 28 days compared to those with other gene variants (*Crit. Care* **15**, R254, 2011).

Given this variance, a single medicine might produce varying results in a clinical trial if all these cases are grouped together—creating a headache for drug developers and regulators alike. "A small subset of patients might really benefit and do so consistently, but this group could get lost in a large megatrial," says infectious disease specialist Steven Opal of the Brown University School of Medicine in Providence, Rhode Island. Some experts point out, for example, that patients with sepsis fare better if their illness stems from pneumonia in the lungs rather than from an infection in the abdomen. Pulling this group out into a separate trial could give a clearer picture of a particular drug's efficacy.

At the end of the day, however, Opal still thinks the traditional, catch-all approach might be best. "I personally like megatrials, as they are a good measure of effectiveness under real-world conditions," he says. Still, he concedes that there's plenty of room for improvement. One idea floated by experts at a two-day conference held in May at the US National Institutes of Health in Bethesda, Maryland, was to create a number of so-called 'Centers of Excellence'—institutions that are familiar with the problems associated with clinical trials in sepsis and could help raise the standard of current trial design and execution.

Angus would welcome such a move. "We would be better off spending our time enrolling a lot more patients into far larger randomized trials and getting to a much more robust answer much sooner," he says. "We still fundamentally believe in the idea that randomized trials help us make inferences of causality, but the vast majority of patients who get severe sepsis are never enrolled in clinical trials."

Roxanne Khamsi

Trial failure prompts soul-searching for critical-care specialists

In late May, researchers delivered the final analysis of the boldly named PROWESS-SHOCK trial. Despite the study's gallant moniker, though, the antisepsis drug Xigris (activated protein C) showed little prowess—and the results came as no shock, as Eli Lilly, the Indiana-based drugmaker behind the medicine, had already withdrawn Xigris from worldwide markets in October 2011. At the end of the day, global sales of Xigris came in at only $104 million in 2010, the last full year the agent was in use. But the PROWESS-SHOCK study continues to be a point of contention in the sepsis field as researchers dispute whether the results of randomized trials in the sepsis arena can fully be trusted.

"The outcome of [PROWESS-SHOCK] was not only bad for Lilly and activated protein C, but it was really bad for the entire field," says Steven Opal, an infectious disease specialist at the Brown University School of Medicine in Providence, Rhode Island.

For one thing, says Derek Angus, a critical-care physician at the University of Pittsburgh in Pennsylvania who sat on the data and safety monitoring board for the PROWESS-SHOCK trial, the whole Xigris story is "a bit of a faith shaker around how much of a house of sand are we building here" with clinical trials for sepsis. "The whole potential fickleness of this is quite disconcerting," he says.

Lilly's decision to pull Xigris came nearly a decade after US and European regulators approved the drug off the back of the first phase 3 PROWESS trial. That 1,700-person study was stopped early, in June 2000, because Xigris's results seemed so amazing: a reduction in 28-day mortality from 31% in the placebo group to 25% in Xigris-treated individuals (*N. Engl. J. Med.* **344**, 699–709, 2001). Yet subsequent findings proved disappointing. Additional trials requested by the US Food and Drug Administration (FDA), one in less ill adults and another in children with severe sepsis, did not show a benefit for Xigris (*N. Engl. J. Med.* **353**, 1332–1341, 2005; *Lancet* **369**, 836–843, 2007), and, like PROWESS, both studies were stopped prematurely—in these cases, however, for futility, rather than efficacy, reasons.

The PROWESS-SHOCK trial came about at the behest of the European Medicines Agency, which requested another large study of Xigris after numerous critics pointed out aspects of the original PROWESS design and implementation that may have helped yield a favorable result. For example, organizers changed the enrollment criteria halfway through the PROWESS trial to include more participants at high risk of death. Upon retesting, Xigris ultimately failed to reduce mortality in patients with septic shock in the PROWESS-SHOCK trial, a finding that has cast further doubt on the integrity of the first study.

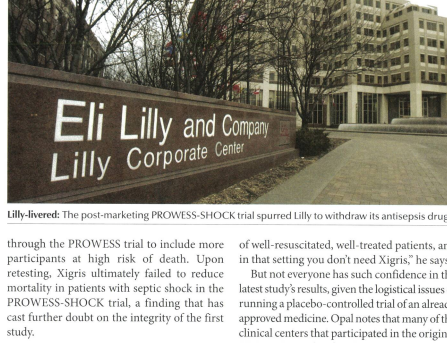

Damon Cummings / Associated Press

Lilly-livered: The post-marketing PROWESS-SHOCK trial spurred Lilly to withdraw its antisepsis drug.

Which trial results do you believe?

Some researchers now think both trials were valid but came to different conclusions simply because of improvements in general sepsis management over the past decade that improved the survival rate of the control group and thereby diminished the comparative influence of the drug. Researchers involved in PROWESS-SHOCK had originally expected a 28-day survival rate in the placebo group below 70%, as was seen in PROWESS. But what they eventually saw was a rate of 76%. "When you have a moving target of placebo mortality and improvements in the standard of care, that adds additional challenges to running these types of studies, which are already very complicated and difficult," notes Jonathan Janes, medical director for acute care with Lilly.

Against that backdrop, PROWESS-SHOCK may have been underpowered to detect a significant benefit for Xigris. "This is a study that's negative for Xigris but positive for critical-care medicine," says Marco Ranieri, an anesthesiologist and intensive-care physician at the University of Turin in Italy. Or, perhaps, Xigris is now superfluous given the state of modern medicine, notes Taylor Thompson, director of the medical intensive care unit at the Massachusetts General Hospital in Boston who, together with Ranieri, led the PROWESS-SHOCK trial. "What we've got is a clinical trial of well-resuscitated, well-treated patients, and in that setting you don't need Xigris," he says.

But not everyone has such confidence in the latest study's results, given the logistical issues of running a placebo-controlled trial of an already approved medicine. Opal notes that many of the clinical centers that participated in the original PROWESS trial refused to take part in the follow-up, and he suspects that those sites that did enroll individuals in PROWESS-SHOCK—and were thus willing to give a placebo—might have been prejudiced, subconsciously or otherwise, against the drug from the get-go. "If you take the better places out of the globe and you exclude them from the study, it's possible that you've biased the study for failure rather than success," he says.

Guido Bertolini, a clinical epidemiologist who specializes in intensive care at the Mario Negri Institute for Pharmacological Research in Bergamo, Italy, also worries about the "dangerous precedent" that such a trial poses. "The idea to look for a confirmatory trial on efficacy without withdrawing the drug from the market is unbelievable from an ethical perspective," he says.

Not to worry, argues Thompson. "Reading the tea leaves from the FDA, my guess is that they'll never do this again," he says. "They'll ask for two trials" before granting approval for antisepsis drugs.

That may help mitigate some concerns. But, given the cost and uncertainty of such trials, the need for large-scale replication could have a chilling effect on the whole field. "It's going to take the financial incentive that was mildly present in the past to do these sepsis trials out of the equation," Opal says.

Elie Dolgin

After Xigris, researchers look to new targets to combat sepsis

Experimental drug therapies for sepsis have not fared well recently. In January 2011, Japan's Eisai announced that it would delay seeking regulatory approval for the company's anti–Toll-like receptor 4 compound after the drug, known as eritoran, failed to show any benefit in a pivotal 2,000-person trial. And Eli Lilly famously pulled Xigris (activated protein C) from the market in October following the negative results of the 1,700-person PROWESS-SHOCK trial. With the withdrawal of Xigris, critical-care physicians now have no drugs specifically approved to treat severe sepsis. But, after all the latest hard knocks to an already downtrodden field, scientists are picking themselves back up and tackling new approaches. They're studying new drugs and drug targets and focusing their efforts on how to better identify the most at-risk patients with sepsis and design more insightful clinical trials.

"There's this notion of despair among some people now. They say it's too complicated and nothing will ever work," says Steven LaRosa, an infectious disease physician at the Texas A&M Health Science Center in College Station who was involved in testing both Eisai's and Lilly's failed products. "But that's the wrong mindset. We absolutely are chipping away at sepsis. I think that if we just get more sophisticated at how we do these trials, there will be therapies." And those therapies could be lucrative. According to Santosh Mishra, an analyst with London-Based GlobalData, the worldwide sepsis market was valued at $5 billion in 2010 and is expected to grow by 50% over the next five years. "Significant unmet need is present," he says, "which suggests that there is considerable market share for new entrants to capture in the future."

The difficulty of designing effective sepsis drugs revolves around the complex—and not fully understood—pathophysiology of sepsis. The condition can begin with an infection anywhere in the body and proceed to sepsis when microbes move into the bloodstream and ramp up the innate immune system. A diverse array of immune cells, inflammatory modulators and cytokines are activated or released into the blood. Many of these encourage inflammation or blood clotting, and each represents a potential drug target. At the same time, the adaptive immune system, a second and more specific line of defense, begins to falter, becoming less effective at ridding the body of the pathogen or protecting against future infections.

Therapies currently in the pipeline target each step in this disease progression (see 'Antiseptic swipes'). Starting from the beginning, some companies are developing drugs or devices to remove pathogens from the bloodstream or directly target their ill effects. Toraymyxin, for example, is an antibiotic-coated filter from Toronto-based Spectral Diagnostics currently being tested in 600 people suffering from septic shock across the US, Canada and France. "We are on track with all our predictions for our trial," says Paul Walker, chief executive of Spectral. In an earlier phase 2 study, the perfusion system helped lower 28-day mortality rates from 53% to 32% when added to standard care (*JAMA* **301**, 2445–2452, 2009).

Another strategy blocks the pathogens' so-called superantigens, toxins produced by bacteria that can activate as much as 20% of the body's T cells at once and may be responsible for launching the sepsis-causing immune reaction in the first place. The Israeli company Atox Bio has one such superantigen antagonist, which mimics part of the T cell co-receptor CD28, currently in phase 2 development.

Immune challenge

Other drugs in the pipeline aim to dampen the body's innate immune response after sepsis or after septic shock has kicked in. These include ART-123, a recombinant form of the anticoagulant protein thrombomodulin from Japan's Asahi Kasei Pharma currently in phase 3 testing in the US, and talactoferrin alfa, an immunomodulatory lactoferrin from Germany's Agennix that sits in limbo after the company halted a late-stage trial in response to interim data showing that more participants were dying in the treatment arm of the study than in the placebo arm.

Many in the field are also eagerly awaiting the results of a 300-person trial testing AstraZeneca's CytoFab, an antibody directed against tumor necrosis factor-alpha (TNF-α), a prime mediator of inflammation. Previous experimental TNF-α–targeting monoclonal antibodies have failed to show an effect on mortality rates in patients with sepsis. Yet experts predict that CytoFab will fare better because it contains many different antibody fragments, which could lead to a more complete blockage of the cytokine's function. In a 70-person dose-escalation trial published in February, study subjects who received multiple doses of CytoFab had near-undetectable levels of TNF-α in their blood serum within two hours of starting the drug treatment, and they experienced only mild side effects (*Crit. Care* **16**, R31, 2012).

A final set of sepsis drugs are directed at boosting the adaptive immune system response to restore the body's ability to fight the disease. Such drugs—which include interleukin modulators, immunoadjuvants and other ways of controlling T and B cell function—are not as far along in clinical development, but their importance is beginning to be underscored by basic research.

"We don't have a magic drug yet," says Shaw Warren, an infectious disease specialist at the Massachusetts General Hospital in Boston. "But we've learned a lot. The field is regrouping now, and people are looking for a new direction."

Sarah C P Williams

Antiseptic swipes: Drugs and devices in clinical development for combating sepsis.

Approach	Drug	Company	Mechanism	Phase
Targeting pathogens and their products	Toraymyxin	Spectral Diagnostics	Antibiotic-coated hemoperfusion column	3
	AB103	Atox Bio	Blocks bacterial superantigens	2
	Alkaline phosphatase	AM-Pharma	Detoxifies bacterial products	2
Dampening innate immune and inflammatory responses	ART-123	Asahi Kahei Pharma	Recombinant thrombomodulin	3[a]
	Bicizar	BioGenius	C1-esterase inhibitor blocks complement activation	3[b]
	Talactoferrin alfa	Agennix	Recombinant human lactoferrin	2/3[c]
	CytoFab	Astra-Zeneca	Polyclonal TNF-α–specific antibody fragment	2
	Actos (pioglitazone)	Takeda Pharmaceuticals[d]	Activates peroxisome proliferator-activated receptor gamma	1
	SRT2379	GlaxoSmithKline	Sirtuin-1 activator	1

[a]ART-123 is approved in Japan and in phase 3 testing in the US. [b]Bicizar is in clinical testing only in Russia. [c]Trial halted in February pending a company review of the data. [d]Although the trial includes a Takeda drug, the company is not involved in the study.

Phillip Dellinger

Straight talk with… **Phillip Dellinger**

Phillip Dellinger has seen his fair share of people go into septic shock. As head of the division of critical-care medicine and director of the medical and surgical intensive care unit (ICU) at Cooper University Hospital in Camden, New Jersey, Dellinger ensures that doctors follow best practice when treating sepsis. But his influence on sepsis protocols goes far beyond the US Northeast. In 2002, Dellinger, along with Graham Ramsay of Anglia Ruskin University in Chelmsford, UK, and Mitchell Levy of Brown University's Alpert Medical School in Providence, Rhode Island, proposed both the concept and the plan for the Surviving Sepsis Campaign, a massive international effort aimed at improving the treatment of severe sepsis and reducing the high rate of mortality associated with the condition.

Ten years on, the Surviving Sepsis Campaign has successfully developed a series of best-practice criteria—the International Guidelines on the Management of Severe Sepsis and Septic Shock, which are currently being revised under Dellinger's leadership—as well as engaged physicians and the general public around the world in a broad educational program to warn about the threat posed by the disease. The campaign has also engendered controversy—notably, accusations that the initiative served as little more than a marketing tool for Eli Lilly, the manufacturer of Xigris (drotrecogin alfa), which was the only approved therapy specifically for the treatment of sepsis over the past decade. But Dellinger stands by the campaign's records, and he argues that it has helped saved countless numbers of people from a deadly disease. He spoke with **Roxanne Khamsi** about the struggle to catalyze change in the sepsis field.

What is the history of the Surviving Sepsis Campaign?

The campaign began in 2002, and it was originally administered by the Society of Critical Care Medicine, the European Society of Intensive Care Medicine and the International Sepsis Forum. It subsequently created the first set of guidelines in 2004 and began a performance improvement program internationally.

What goals have you set?

We targeted a very ambitious goal of 25% reduction in mortality within five years. We've come pretty close to it. Between January 2005 and March 2008 we saw a 19% relative reduction in mortality in 165 hospitals across the world.

In the absence of a drug that turns things around, what explains this improvement?

What we have is more awareness, earlier identification and more rapid administration of antibiotics and more fluids being administered. And I think it's likely that those are the sepsis-specific things that have made a difference. Our ventilatory support is better across the board; nutrition is better.

How was the campaign's former support from Lilly and other drugmakers perceived?

Notable academics were concerned about the industry funding, even with the transparency and lack of industry involvement [in creating the guidelines]. But the 2008 guidelines were published without industry funding, and the forthcoming 2012 guidelines will be, too. The goal recently was to totally strip the Surviving Sepsis Campaign from any association with industry funding, which has now been done. Now we are funded by the Gordon and Betty Moore Foundation.

The campaign's new sepsis guidelines are expected this fall. How do they compare with the 2008 guidelines?

We've had major changes in our vasopressor recommendations and our fluid recommendations. We've added a nutrition section and changed our glycemic control section. The updates are all clinical-trial based.

How does sepsis treatment differ globally?

The primary differences would be that in some places colloids, such as albumin [used in fluid management], would be less available. Additionally, clinics differ in the ability to transduce catheters in the vascular system to obtain pressures or measure flows. Activated protein C would have been a good example while it was on the market; it was [mostly] available in more developed areas. Another thing that varies is where the patients are treated, and that is based on how many ICU beds are in a hospital.

What do academic researchers fail to appreciate about sepsis?

That there's not just one fix for the cells' inability to utilize oxygen in the case when there is cellular dysoxia [altered oxygen use] in sepsis.

And what are the things that pharma fails to grasp about sepsis?

That there needs to be a better approach to the experimental design of studies. I think that patient selection has not been adequate. Patients have been enrolled in clinical trials based on clinical syndromes, and step 1 is to identify a biomarker that is present in severe sepsis. Then get a drug or technology that targets that molecule, and then measure the presence of that molecule in the blood of the patient with severe sepsis before you give the drug.

Is there any prospect that the campaign might nurture that approach?

We currently don't work with pharma because we currently are not involved with clinical trials.

Is that something that might change?

I don't think there are any plans to get involved with clinical trial design. We just spent four or five years doing away with any liaison with industry because of the guidelines, so there would be hesitation in going back in the other direction.

Matt Hansen

Drugs designed to protect or rescue neurons from damage wrought by stroke have repeatedly failed in clinical trials, prompting a mass flight of pharmaceutical companies from the field. A small Canadian startup is bucking the trend—and it hopes that monkey data will help the field evolve. **Elie Dolgin** reports.

The telltale signs appear suddenly. Words come out jumbled, a side of the face droops down or vision blurs. The symptoms are familiar because stroke is, after all, the second leading cause of death and the most common cause of acquired adult disability worldwide[1]. Yet even in the world's most advanced hospitals, the only approved therapy for this devastating insult to the brain is a clot-buster called tissue plasminogen activator, or tPA, that does little to stop the damage in the choked-off areas of the brain once the cascade of cell death starts to spread.

More than 100 drugs thought to protect neurons against injury have previously failed in human trials, despite showing efficacy in rodent models of stroke. There was a glimmer of hope for the neurological community when, in May 2005, the British pharmaceutical giant AstraZeneca announced the results of a 1,700-person trial showing that the company's neuroprotective drug, called Cerovive (NXY-059), improved patient scores by 20% on a common scale for measuring disability after stroke as compared with placebo[2]. Finally, a drug had arrived that showed potential for helping stroke victims get back on their feet, upping their chances of returning to work and running independent lives.

The trial met its primary clinical endpoint. But, in a harbinger of disappointment down the road, Cerovive—a free radical scavenger thought to shield neurons from the oxidative stress that mediates brain cell damage—did no better than placebo when doctors measured other factors such as consciousness, language, visual-field loss and motor strength.

One person following the Cerovive results with great interest was Michael Tymianski. "It was not a huge benefit," he says. "But you know who had a great drug? NoNO." Tymianski, director of the neuroprotection laboratory at the Toronto Western Hospital Research Institute, had cofounded NoNO in 2003 to help develop a neuroprotective compound called NA-1, a cell-permeable peptide that blocks the formation of a free radical in the brain called nitric oxide (NO)—hence the company's name, 'no NO'. The drug was on the cusp of entering phase 1 safety testing when the Cerovive results came out, and Tymianski reckoned that his Toronto-based biotechnology company would be well positioned to follow AstraZeneca's lead to big pharma funding and eventual market approval. By 2006, the research firm Datamonitor was already forecasting annual sales for AstraZeneca of up to $1 billion within five years of Cerovive's approval, and Tymianski was confident that NA-1 had an even better therapeutic profile.

But then the bomb dropped on Cerovive and, in effect, on every other drugmaker developing neuroprotective drugs for stroke. In October 2006, AstraZeneca released the findings of a second major trial, this time involving 3,200 participants, which found that Cerovive had no effect whatsoever on disability scores or neurologic outcomes[3].

On the heels of so many failed trials, the Cerovive disappointment was the last nail in the coffin for neuroprotectants: every major pharmaceutical company subsequently curtailed its programs in this area, and the situation hasn't improved since. "Stroke has been a no man's land since AstraZeneca's failure," says Harry Tracy, publisher of NI Research, a California-based monthly review of the neurotherapeutic field.

In spite of the commercial and scientific hurdles, NoNO has stuck with its dogged pursuit of neuroprotection—and onlookers say it could be revitalizing commercial interest along the way. "The field [of neuroprotection] has been close to moribund," says Sean Savitz, a neurologist at the University of Texas Medical School in Houston. "This agent that Tymianski has developed, I'm hoping, is going to revive the field and spark new interest."

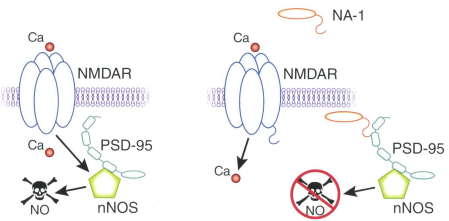

Adapted from *Science* **298**, 846–850 (2002).

The glutamate that binds: In the absence of NoNO's NA-1 (left), a protein called postsynaptic density-95 (PSD-95) tethers the calcium (Ca)-dependent enzyme neuronal nitric oxide synthase (nNOS) to the mouths of *N*-methyl-D-aspartate receptor (NMDAR) channels, triggering the production of nitric oxide (NO). NA-1 mediates the neurotoxic consequences of NO by dissociating the NMDAR–PSD-95 complex (right).

To NoNO avail

The search for NA-1 began, like with most drugs, in a lab dish. In 1999, Tymianski and his colleagues first demonstrated, using antisense oligonucleotides in cultured brain cells, that they could prevent the formation of neuron-killing nitric oxide by suppressing the production of a protein called postsynaptic density-95 (PSD-95), which helps bring neurotoxic signaling molecules to the *N*-methyl-D-aspartate receptor (NMDAR), a type of ion channel on the surface of neurons that contributes to neuronal death after stroke[4].

Three years later, Tymianski, in collaboration with Michael Salter, a neuroscientist at the Hospital for Sick Children in Toronto, then created a peptide drug—which later became known as NA-1—that could achieve the same effect in rats, leading to reduced tissue death in the rodents' brains and improved neurologic function[5]. Subsequent rodent experiments performed jointly with Andrew Tasker, a behavioral neuroscientist at the University of Prince Edward Island in Charlottetown, showed that treatment with NA-1 led to durable improvements in a variety of behavioral tests[6]. "It was such a long-lasting effect," Tasker says. "That a single injection a short time after the stroke would still be providing neuroprotection in a rat model two months out was really something."

> **"The field of neuroprotection has been close to moribund. This agent is going to revive the field and spark new interest."**

Many drug companies had previously tested compounds that block NMDAR in clinical trials. But, because this glutamate receptor also has a crucial role in wakefulness and breathing, these agents had to be tested at such low doses that they failed to show a protective effect on the brain. The success of NA-1 lay in the strategy of targeting PSD-95 rather than NMDAR itself, thereby warding off the glutamate receptor's ill effects without impeding normal synaptic activity (see 'The glutamate that binds'). "You inhibit the pathological processes while leaving the normal function intact," Salter explains.

Tymianski, Salter, Tasker and three other scientists involved in the project soon spun off NoNO. And in September 2006, in collaboration with Arbor Vita Corporation, a small California-based biotech that owned a patent portfolio covering proteins with a type of structural domain found in PSD-95, they launched their first human clinical trial in 62 healthy volunteers. (NoNO bought all of Arbor Vita's rights to the compound last year for an undisclosed sum of money, and the former partner is no longer involved in the drug's development.)

With the collapse of Cerovive, however, a cloud hung over neuroprotectants, and Tymianski realized that he would have to go back into the laboratory to convince the world—and himself—of NA-1's therapeutic worth. He enlisted neurosurgery resident Douglas Cook and lab manager Lucy Teves, and together they started working on a new monkey model of stroke. "We felt that if we could produce evidence in brains that are very similar to human brains, then we'd get closer to answering the question of whether or not neuroprotection was possible and whether or not it could be made practical," Tymianski says. "Without that kind of data we wouldn't stand a chance of moving this work further in humans."

Tymianski wasn't alone in his logic. In 1999, following a slew of failed trials, the world's leading stroke researchers convened in Orlando, Florida for a meeting known as the Stroke Therapy Academic Industry Roundtable (STAIR) that culminated in a series of best-practice guidelines for developing neuroprotective drugs. Among other proposals, the committee members, led by Marc Fisher of the University of Massachusetts Medical School in Worcester, recommended that drugs showing promise in rodents should subsequently be tested in primates before moving into large clinical trials with humans[7]. "I've really come to the conclusion that primate modeling makes sense after rodent modeling is used as an initial screening," says Fisher, now editor of the journal *Stroke*.

AstraZeneca had actually followed the STAIR criteria and tested Cerovive in a nonhuman primate model—the marmoset monkey—and the drug still failed. However, primate species vary widely in their brain anatomy and physiology, and these differences could explain why not all primate findings have translated to humans. Like rodents, marmosets and other New World monkeys

have smooth brains that lack the highly folded and convoluted structures found in the human cerebral cortex. In contrast, the brains of macaques and other Old World monkeys show the more elaborate 'gyrencephalic' organization, and so some experts believe that inducing stroke in their brains might serve as a better model for the human condition. That's why three years ago the STAIR panel updated its guidelines to explicitly encourage research in higher-order primates such as macaques[8].

That idea that macaques and other Old World monkeys provide a better stroke model is still unproven. There are no studies to date showing that gross brain structure predicts responsiveness to neuroprotection. Plus, in the absence of any positive phase 3 human studies, it's impossible to say whether efficacy in higher primates can foretell success in people. But Tymianski is betting that it will. With support from the Canadian Stroke Network and the Heart and Stroke Foundation of Ontario, his team has spent the last five years perfecting their induction of stroke syndromes in cynomolgus macaques, with promising results to show for the work.

"The STAIR criteria are a hypothesis that has never been tested," says Gregory del Zoppo, a stroke researcher at the University of Washington School of Medicine in Seattle who has worked extensively with baboon models in the past. "We have few groups using primates nowadays and few other than Michael [Tymianski] who are actually using these in a format that might be clinically appropriate. So, there's a lot riding on his work."

No brain, no gain

In the past, many stroke researchers working with monkey models have permanently removed an eye to gain access to and clamp down on the middle cerebral artery (MCA), one of the three major paired arteries that supply blood to the cerebrum and the site of most strokes in humans. This can induce an ischemic stroke, but it leaves the animals without binocular vision, which can compromise the reliability of behavioral tests of neurologic function. So, Tymianski's team opted to surgically open up the cranium and then apply a titanium clip at various sites along the MCA to induce strokes of varying severity. Then, to assess outcomes, the researchers performed magnetic resonance imaging (MRI) and ran primate versions of well-accepted diagnostic and behavioral tests of stroke severity. "We worked hard to create a model that mimics the clinical scenario of acute ischemic stroke in humans," explains Cook, now a clinical fellow at the Stanford University School of Medicine in California.

After validating the model, the researchers gave the monkeys NA-1 or placebo intravenously. Reporting earlier this year in *Nature*, they showed that the treatment reduced the amount of dead tissue seen in brain scans and preserved neuronal cell function, as measured by gene arrays and behavioral tests, even when the drug was administered up to three hours after the onset of stroke[9]. "It's probably the best preclinical paper that I've ever seen," says Fisher, who has worked with Tymianski's team to test NA-1 in rats[10] but was not involved in the monkey study. Savitz agrees: "I've never seen such a comprehensive assessment of a [neuroprotective] drug done in primate studies before."

"Mike [Tymianski] has got to be commended for sticking with something now for ten or fifteen years and being very meticulous and scientific about maximizing what we know," says neurologist Alastair Buchan, head of the Medical Science Division at the University of Oxford, UK. "He's kept his focus, he's kept the line of inquiry going, and that's to his everlasting credit."

At the same time, though, new research suggests that the Tymianski's compound might have room for improvement. A team led by Kristian Strømgaard, a chemical biologist at the University of Copenhagen, created a new kind of two-pronged peptide that has a 1,000-times-higher affinity for PSD-95 relative to NoNO's agent. Strømgaard and his colleagues tested the compound in a mouse model of stroke, and, reporting in February, they showed that the peptide dimer reduced the volume of brain damage by 40% compared to either NA-1 or placebo[11]. "That NA-1 can go into phase 2 really demonstrates the promise for this target," says Strømgaard. "But because it's a relatively weak inhibitor, you potentially need to give a very high dose, which could be a limiting factor that our dimeric compound might overcome. However, so far NA-1 is really showing great promise."

Stroke of insight

NA-1 isn't the only potential neuroprotectant now backed by macaque data. In recent years, the oxygen-carrying molecule hemoglobin[12], an antiplatelet agent[13], an inhibitor of a key DNA repair protein[14], an immunosuppressive drug called tacrolimus[15] and human mesenchymal stem cells[16] have all been shown to exert neuroprotective activity when given following the onset of stroke to various cynomolgus macaque models. However, most of these agents have less monkey data to show for themselves and none have yet entered clinical trials.

One approach with promising macaque data that may soon enter human testing comes from the Oregon Health & Science University (OHSU) in Portland. Over the past few years, a team there led by Mary Stenzel-Poore and Rena Bahjat developed a preconditioning regimen that seems to protect rhesus macaques from strokes even before they happen. In a study published last year, the researchers gave the monkeys either a saline solution or targeted strands of nucleic

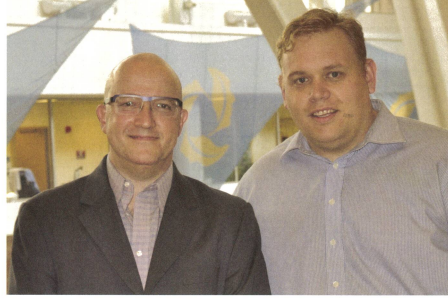

Janet Lunn

Primate movers: Michael Tymianski (left) and Douglas Cook (right) tested NA-1 in a monkey model.

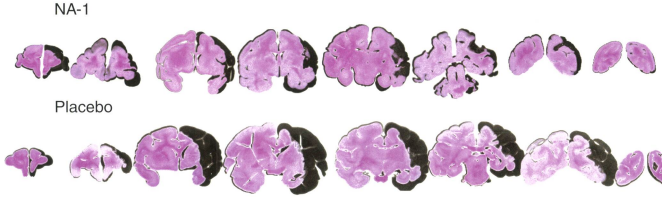

Nature 483, 213–217 (2012).

Slices of life: Serial brain sections taken 30 days after the onset of stroke from cynomulgus macaques; shaded areas denote cell death.

acid three days before inducing strokes in the macaques. After the ischemic injury, they showed that the monkeys that received the prophylactic treatment—a synthetic string of DNA that mimics a bacterial sequence and activates Toll-like receptor 9, a key player in innate immunity—had smaller areas of dead brain tissue and better motor function than the control animals[17].

"I could see differences in the animals in the function of their arms, their hands, their legs," says Bahjat. "With this model, you can really pinpoint the deficit, and that will be important to discerning if something is efficacious from a drug development standpoint." Now, Bahjat says that her group has generated "even more impressive efficacy data" with a similar agent that she hopes to advance into clinical studies for people at high risk of stroke, such as those undergoing coronary bypass surgery, carotid stenting or brain aneurysm repair, a procedure in which a small catheter is threaded from the groin into the blood vessels of the brain, often knocking off small plaques that can trigger tiny strokes.

"It'll be like putting a helmet on when you get on a skateboard," says Stenzel-Poore, senior associate dean for research in the OHSU School of Medicine. "You're still going to fall, but you'll be protecting your head." They plan to initiate toxicology and pharmacokinetics studies next year and launch human trials in 2014.

Meanwhile, NoNO is looking for funding or partners to advance the company's drug into larger trials. The company recently announced the results of 185-person, phase 2 trial involving individuals at risk of developing small strokes while undergoing surgery to repair either burst or intact brain aneurysms. Reporting at the International Stroke Meeting in New Orleans in February, NoNO showed that study subjects taking the drug suffered around half the number of mini strokes compared to those who received placebo. In a promising sign that the drug was halting more than just the damage inflicted by the corrective procedure, NA-1 "seemed to be particularly effective in people who had a ruptured aneurysm, versus people who did not," says Michael Hill, director of the stroke unit at Foothills Medical Centre in Calgary, Alberta, who led the trial. Now, the company plans to advance the drug for the treatment of strokes suffered as a result of the internal bleeding that stems from burst aneurysms, which occur in around 30,000 Americans annually, as well as for combating acute ischemic stroke, which accounts for around 85% of the nearly 800,000 cases of stroke in the US each year.

"I'm living proof that this drug was a success."

Millie Nelles is one person who will be rooting for NoNO to succeed. On 6 September 2008, three days before her sixtieth birthday, Nelles, an accounting clerk at a placement agency in Calgary, became the first person to ever receive NA-1 as part of the recently reported trial, known as ENACT, short for 'Evaluating Neuroprotection in Aneurysm Coiling Therapy'. She had already experienced a mild stroke and undergone surgery to correct the complications of a debilitating nerve disorder called trigeminal neuralgia when her doctors discovered a new neurological issue—an irregular aneurysm—and Nelles didn't think her brain could handle another assault.

Before the trial, she even recorded audio cassettes and wrote letters for her two daughters in case she didn't survive the aneurysm repair surgery. But in the end, she didn't suffer a single stroke, according to the MRI scans, even though the majority of people undergoing the same procedure typically show signs of small strokes. "I'm living proof that this drug was a success," says Nelles, who learned just two months ago that she had received the active drug rather than the placebo. "I honestly and strongly believe that that NA drug saved my life. I don't think I could have taken another stroke."

Tymianski hopes the drug can make a similar impact in other people's lives, too. "The whole point of this odyssey for us is to get a fundamental scientific discovery to the point that it helps people," he says. He's partway there. Now he just has to do what no one developing neuroprotectants has ever done before: demonstrate efficacy in a phase 3 trial.

Elie Dolgin is a news editor with* Nature Medicine *in Cambridge, Massachusetts.

1. World Health Organization. The 10 leading causes of death by broad income group <http://www.who.int/mediacentre/factsheets/fs310/en/index.html> (2008).
2. Lees, K.R. *et al. N. Engl. J. Med.* **354**, 588–600 (2006).
3. Shuaib, A. *et al. N. Engl. J. Med.* **357**, 562–571 (2007).
4. Sattler, R. *et al. Science* **284**, 1845–1848 (1999).
5. Aarts, M. *et al. Science* **298**, 846–850 (2002).
6. Sun, H.S. *et al. Stroke* **39**, 2544–2553 (2008).
7. Stroke Therapy Academic Industry Roundtable (STAIR). *Stroke* **30**, 2752–2758 (1999).
8. Fisher, M. *et al. Stroke* **40**, 2244–2250 (2009).
9. Cook, D.J., Teves, L. & Tymianski, M. *Nature* **483**, 213–217 (2012).
10. Bråtane B.T. *et al. Stroke* **42**, 3265–3270 (2011).
11. Bach, A. *et al. Proc. Natl. Acad. Sci. USA* **109**, 3317–3322 (2012).
12. Kawaguchi, A.T. *et al. J. Pharmacol. Exp. Ther.* **332**, 429–436 (2010).
13. Umemura, K. *et al. J. Nucl. Med.* **46**, 1931–1936 (2005).
14. Matsuura, S. *et al. Brain Res.* **1410**, 122–131 (2011).
15. Furuichi, Y., Maeda, M., Matsuoka, N., Mutoh, S. & Yanagihara, T. *Exp. Neurol.* **204**, 138–146 (2007).
16. Li, J. *et al. Brain Res.* **1334**, 65–72 (2010).
17. Bahjat, F.R. *et. al. J. Cereb. Blood Flow Metab.* **31**, 1229–1242 (2011).

Refocus the Recombinant DNA Advisory Committee

Xandra O Breakefield

Xandra Breakefield

The Recombinant DNA Advisory Committee, formed in 1974, was originally charged with advising on potential risks of recombinant technology and took on review of clinical gene therapy protocols in the late 1980s. But as gene therapy has made headway with safety, it's time to shift the committee's mission toward broader ethical and technical issues linked to the field.

As in the development of any new class of therapeutics, there were many challenges and concerns when the field of gene therapy emerged. To this end, the director of the US National Institutes of Health (NIH) formed the Recombinant DNA Advisory Committee (RAC) in 1974 to provide a forum for public discussion of emerging methodologies within this field and to advise the NIH director on issues concerning risks to public safety. And, since its inception in 1996, the American Society of Gene & Cell Therapy (ASGCT) and its members have worked with the RAC to improve the efficacy and reduce any risks associated with gene transfer in clinical protocols.

Over time, the gene and cell therapy community has evolved in technical sophistication with increasing numbers of trials (over 1,000 clinical trials internationally), and it has reached the stage of commercialized products for several diseases. In recent years, investigators have reported clear benefit in clinical trials using gene and cell therapies for a number of diseases, including hereditary blindness, immune deficiencies and Parkinson's disease. But the RAC continues to use the same formula for review of individual, committee-selected clinical protocols. All proposed clinical trials that used NIH funding in their development must be submitted in full, and the RAC selects about 20% a year for detailed on-site review.

> "As it stands, the RAC clinical review process is basically duplicative of that of regulatory agencies."

In the opinion of many highly regarded experts who are members of ASGCT, the current *modus operandi* of the RAC is not optimal. In the years since the first gene therapy trials were performed, the US Food and Drug Administration (FDA), the Office for Human Research Protections, institutional review boards and institutional biosafety committees have become very experienced and knowledgeable and are fully competent to carry out critical regulatory review of study protocols within the gene and cell therapy field. In addition, reviews of past performance and consideration of safeguards have been put in place since RAC reviews began, such as data safety and monitoring boards for early phase trials, with adverse events reported immediately to the FDA. The current mandate of the RAC adds another layer of nonregulatory review to protocols, thereby increasing time and expense. As it stands, the RAC clinical review process is basically duplicative of that of regulatory agencies, with the difference being that it is carried out in an open forum with representatives from the public. The RAC also comments on the sufficiency of preclinical data and requests new preclinical data to be generated in some cases. As there is no real coordination between the RAC and the FDA on this, investigators are sometimes in 'double jeopardy' trying to serve two masters with differing opinions.

Given these circumstances, in March 2012, the ASGCT board of directors, with the advice of an internal panel of experts, voted to recommend that this system be streamlined. Specifically, the president at the time, Jude Samulski, director of the Gene Therapy Center at the University of North Carolina–Chapel Hill, and I, as president-elect, sent a letter to the NIH in which we recommended that "the RAC would terminate review of individual clinical protocols and would instead identify new areas of research that require a public forum for discussion and review." This position reflects our mission—similar to that of the new NIH National Center for Advancing Translational Sciences—to facilitate the development of effective treatments and bring them to patients as efficiently as possible.

Rather than have the RAC duplicate the efforts of regulatory agencies, a more effective use of resources would be to use its convening power and collective wisdom to facilitate workshops for new investigators entering the field and to discuss common operating procedures, as well as ethical and regulatory issues. The RAC should continue—as it has done so well in the past—to organize focused, in-depth symposia with experts and lay people on newly arising and problematic issues in the field. Such issues would include new vector designs and their associated biosafety risks; the societal aspects of expanded treatment indications such as prenatal therapy; the use of gene delivery for athletic enhancement; and the evaluation of safety issues.

In 2010, for example, together with the European Network for the Advancement of Clinical Gene Transfer and Therapy (CliniGene), the RAC held a public symposium in Bethesda, Maryland, to discuss oncogenic events due to genome-integrating vectors and how to reduce them. In addition, public discussion is urgently needed on the use of a common vector for multiple indications, for instance, ocular gene transfer across diseases of different etiologies when there are only a few patients of each specific subtype and funding and resources are not available for repeated in-depth toxicology studies for each subtype. To ensure that 'no patient is left behind' and 'no disease is too small', the field needs a clear consensus on how best to bring successful approaches to all patients who stand to benefit from these therapies.

Early public concerns about potential negative societal outcomes of gene therapy—such as contamination of the germ line or generation of new pathologic agents—have been allayed by the absence of such events in nearly two decades of clinical trials. In fact, the ASGCT perceives that the public is becoming more concerned that large public investment in biomedical research has been slow to lead to improved treatments for illness. We would therefore welcome a decision by NIH director Francis Collins to initiate an external review of the RAC to modify its operating procedures and bring it into alignment with the current era of rapid advances in gene and cell therapy.

Xandra O. Breakefield is president of the American Society of Gene & Cell Therapy and professor of neurology at the Harvard Medical School in Boston, Massachusetts, USA.

BOOK REVIEW

Mission against malaria

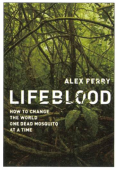

Lifeblood: How to Change the World One Dead Mosquito at a Time

Alex Perry

PublicAffairs, 2011
256 pp., hardcover, $25.99
ISBN: 1610390865

Reviewed by Mats Wahlgren

Lifeblood focuses on the efforts of entrepreneur and multimillionaire Ray Chambers, the Special Envoy for Malaria of the Secretary General of the United Nations, to help eradicate malaria in Africa by aiding in the distribution of insecticide-impregnated bed nets through his non-governmental organization Malaria No More (MNM). Alex Perry, *Time* magazine's Africa bureau chief, reports on his travels with Chambers and writes about malaria, which has haunted Africa for at least 10,000 years. Perry discusses how malaria affects business and society, and much of the book is a perspective on the politics of present-day Africa. *Lifeblood* is worthwhile reading for those individuals involved in the fields of health, research, economics, trade and aid, as well as for people who wish to learn about these topics.

The prevalence of malaria is currently down 25% from the beginning of the twenty-first century. Since 2008, it has been on an even greater decline in the wake of Chambers's efforts with MNM, which works with partners such as the governments of developing countries and the World Health Organization (WHO) to share best practices, skills and tools other than bed nets to tackle malaria. The funding for the bed nets comes from various sources, including the Global Fund to Fight AIDS, Tuberculosis and Malaria, the governments of developed and developing countries and the WHO. Remarkably little is known by the general public of Chambers's involvement and campaign, which had facilitated the distribution of nearly 300 million nets by December 2010. In areas where these nets were used, malaria rates fell, and Chambers now aims to end all malaria-related deaths by 2015.

Perry describes how Chambers is fighting malaria by using his knowledge of politics and business. Perry relates how Chambers in 2006 began to understand the dire consequences of malaria and wanted to "fix it," coming up with business concepts that he hoped would save a million children a year. Perry describes how Chambers made his fortune by initially buying into nursing homes and then later during the 1980s by using financial leverage techniques. Perry relates how Chambers also uses his economic leveraging technique—getting more from less—in 'fixing' malaria. Chambers's approach has three pillars: political leadership, business leadership and the use of the media; this book is therefore an integral part of the strategy. Chambers approached the political-leadership aspect by using his extensive network and by arranging malaria summits in which all the global players involved in the eradication effort meet with world leaders.

Chambers and Perry argue that malaria eradication efforts must now use methods from the business world, including accountability and goal setting. However, Perry does not tell readers enough about previous attempts at malaria eradication, and he makes it clear he is not fond of traditional aid methods, which he claims are often patronizing. However, it should be remembered that traditional aid methods have helped eradicate smallpox and have also drastically reduced the number of cases of measles and tetanus, facts that argue that there are several ways to alleviate the burden of a disease. Africa has changed over the last 20 years, and the situation is more promising than ever, with economic growth (as determined by the gross domestic product) of more than 5% per year in many parts of Africa and with stronger political leadership in many countries. In addition, the African Union has taken on political and health-related responsibilities today that it did not previously.

One interesting portion of the book is dedicated to the history and the current situation of malaria. This portion relates some of the basic findings of malaria epidemiology and the research data on which the impregnated bed net initiative is based. However, this part of the book would have been more effective had further polishing of the text been done, as some stated facts are wrong: chloroquine, a drug currently used to treat malaria, is not a synthetic version of quinine, and malaria was not present in every country of the world at the end of World War II, both of which Perry claims.

Perry seems to believe that we already have the tools needed for malaria eradication. His opinion about the scientists involved in malaria research is that they work in this field "because that was where the money was." However, I am concerned that these views are naive and may mislead decision makers to cut funding to applied or basic malaria research. In fact, it is important to develop new tools for malaria elimination to subsequently eradicate malaria; we must find new ways to fight the parasite. There is no paradox in focusing on both elimination and research, as interest and funding for one will not compete with those for the other. Original, new approaches must be developed, and a deeper understanding of the basic biology of malaria is needed as long as it persists and there is no vaccine. Impregnated bed nets are important, but the presence of nets means that mosquitoes that bite during the daytime are naturally selected for, and malaria parasites are developing resistance to the drugs that are currently used.

Chambers's strategy involves focusing on the seven African nations where malaria most affects the population. He elicits help from religious leaders and politicians and raises money in unorthodox ways. He is currently transferring the bed-net effort to African heads with the help of the newly created organization African Leaders Malaria Alliance, an intergovernmental organization that is dedicated to ending malaria deaths. The continued efforts of Chambers and his partners are laudable, and the publication of this well-written book will certainly achieve its goal of making these efforts more widely known.

Mats Wahlgren is at the Karolinska Institutet, Stockholm, Sweden.
e-mail: mats.wahlgren@ki.se

COMPETING FINANCIAL INTERESTS
The author declares competing financial interests: details are available in the online version of the paper.

MiR-23b is a safeguard against autoimmunity

Ruozhen Hu & Ryan M O'Connell

MicroRNAs (miRNAs) have emerged as crucial mediators of human disease, but their roles in autoimmunity have only recently been appreciated. A new study using mouse and human tissues from various interleukin-17 (IL-17)-related autoimmune disorders now shows that miRNA-23b is a central regulator of inflammation in resident tissue cells during autoimmunity (pages 1077–1086).

Mammalian miRNAs are small, single-stranded RNAs that are encoded by the genome, and recently, their roles in gene regulation have been an intense area of investigation in the context of human disease[1]. At the molecular level, miRNAs repress gene expression post-transcriptionally by directing the RNA-induced silencing complex to specific mRNAs containing cognate miRNA binding sites in their 3′ untranslated regions, which has been shown to have major physiological consequences[2,3]. Although aberrant miRNA expression has been linked to human cancers for about a decade[4], their involvement in autoimmune diseases has only been shown recently, with a handful of studies identifying roles during tissue inflammation for specific miRNAs that are expressed by cells of the immune system[5–7].

In this issue of *Nature Medicine*, Zhu *et al.*[8] take the next step in this field by discovering that the expression of miRNA-23b (miR-23b) is commonly reduced in resident tissue cells isolated from both mice and humans with distinct autoimmune conditions. Notably, they also identify a potent anti-inflammatory role for miR-23b, which is achieved through the inhibition of nuclear factor of κ light polypeptide gene enhancer in B cells 1 (NF-κB), and show that this process is blocked by IL-17 through its repression of miR-23b expression during autoimmunity.

Although autoimmunity is broken down into specific clinical subtypes depending on the type of tissue being targeted by anti-self antigen immune responses (such as multiple sclerosis in the central nervous system, systemic lupus erythematosus in the kidneys or rheumatoid arthritis in the joints—all of which were assessed in the present study), there are many common features that are shared by these disorders. For instance, the overproduction of specific inflammatory cytokines, including tumor necrosis factor α (TNF-α), IL-6 or IL-17, and the recruitment of specialized inflammatory cells to the damaged tissues, such as T helper type 17 (T_H17) cells and granulocytes, are often observed in a variety of clinically distinct conditions[9]. This suggests

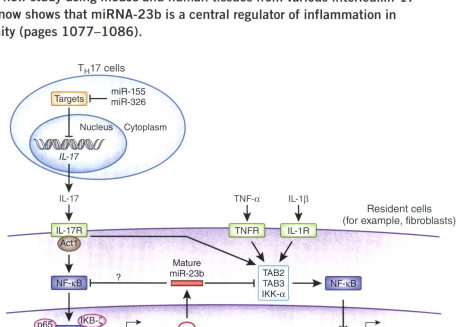

Figure 1 MiR-23b limits tissue inflammation, and its expression is repressed by IL-17 during autoimmunity. MiR-23b is expressed in tissue-resident cells and inhibits NF-κB through direct repression of several upstream signaling mediators, including Tab2, Tab3 and IKK-α. During autoimmunity, T_H17 cells develop and produce IL-17 through a process involving miR-155 and miR-326. After binding its receptor, which is expressed on the surface of tissue-resident cells, IL-17 represses expression of miR-23b through a mechanism involving Act1 signaling and multiple NF-κB family members. As a result of reduced miR-23b expression, activation of NF-κB is increased in response to cytokines, leading to the expression of proinflammatory genes and to tissue damage during various autoimmune disorders. TNFR, TNF receptor.

Ruozhen Hu and Ryan M. O'Connell are at the Division of Microbiology and Immunology, Department of Pathology, University of Utah, Salt Lake City, Utah, USA.
e-mail: ryan.oconnell@path.utah.edu

that perhaps most autoimmune diseases have common proinflammatory regulatory mechanisms and that the development of broad-spectrum therapeutics may be possible. This hypothesis motivated Zhu *et al.*[8] to examine miRNA expression profiles in tissues from a variety of autoimmune conditions that are associated with IL-17 expression, using both mouse models and lesions from human patients in an effort to identify individual miRNAs that are commonly dysregulated in diseased compared to healthy tissues. This approach revealed a small number of miRNAs that were altered in tissue-resident cells. Among these, miR-23b showed the strongest and most consistent difference in expression between healthy and diseased tissue: miR-23b was repressed in tissues taken from patients or in mouse models with different types of autoimmunity, including multiple sclerosis, systemic lupus erythematosus, rheumatoid arthritis and experimental autoimmune encephalomyelitis.

Using transgenic mice and established autoimmune disease models, the authors examined the consequences of altering miR-23b expression. MiR-23b showed anti-inflammatory properties by directly repressing specific proteins. These proteins included TGF-β activated kinase 1/MAP3K7 binding protein 2 (Tab2), Tab3 and inhibitor of nuclear factor κ-B kinase subunit α (IKK-α), which all promote activation of the proinflammatory transcription factor NF-κB[10]. Notably, the cytokine IL-17, which is produced during autoimmunity, including in those disorders analyzed by the authors, repressed miR-23b expression after binding its receptor expressed on tissue-resident cells such as fibroblasts or primary kidney cells. Taken together, these data support a model in which IL-17 reduces miR-23b expression in tissue cells during autoimmunity, allowing for hyper-activation of NF-κB and further tissue damage resulting from elevated and prolonged inflammation (**Fig. 1**).

The inflammatory response must be carefully managed to ensure timely and robust responses against pathogens and during wound healing, however, it must be appropriately resolved to prevent unwanted tissue damage[11]. The current study points to miR-23b as a key player in achieving this balance through its influence on the NF-κB pathway in tissue-resident cells. NF-κB is a crucial driver of inflammation, and regulation of the NF-κB pathway by miRNAs has evolved as an essential regulatory mechanism to modulate the magnitude and duration of the inflammatory response[12]. This is true in immune cells, as has been shown for miR-146a[13], and is now shown in tissue-resident cells through the functions of miR-23b[8].

It is becoming clear that miRNAs are involved in many different aspects of tissue inflammation by acting in both immune cells, which initiate antigen-specific responses and produce initial inflammatory cytokines, and resident tissue cells, which amplify the inflammatory response through such mechanisms as chemokine production to recruit granulocytes. For example, miR-124 is downregulated in resident microglia in the brain, leading to their activation during experimental autoimmune encephalomyelitis[7], whereas miR-155 and miR-326 are expressed in T_H17 cells, promoting their development and function during tissue inflammation[5,6]. Together with the current observation that miR-23b suppresses inflammation during autoimmune pathogenesis, these findings indicate that autoimmune inflammation is temporally and spatially regulated by miRNAs at distinct and wide-ranging steps in the inflammatory process. These include the activation of antigen-presenting cells (for example, miR-124 (ref. 7)), antigen receptor signaling (miR-181a[14]), cellular differentiation (miR-155 (ref. 6) and miR-326 (ref. 5)), cytokine production (miR-29 (ref. 15)) and signaling events downstream of cytokine receptors (miR-23b[8]). Consequently, one can imagine a therapeutic approach that targets individual miRNAs to block a specific stage in this process or that modulates multiple miRNAs simultaneously in an effort to achieve a more potent effect on tissue inflammation.

Many key questions about miR-23b are still unanswered. For example, how is miR-23b expression regulated by IL-17 receptor (IL-17R) signaling? The authors provide some evidence that miR-23b is controlled at the level of transcription by specific NF-κB family members and that this regulation is dependent on the IL-17R–specific signaling mediator TRAF3 interacting protein 2 (Act1). However, a better understanding of the mechanism will require additional interrogation to clarify distinct aspects of this process. Included in this investigation should be a more extensive analysis of cofactors and epigenetic events that are involved in the repression of the miR-23b locus. It is also possible that processing of primary miR-23b into its mature form is regulated post-transcriptionally by IL-17R signaling. A better comprehension of these mechanisms will provide crucial insights that could be used therapeutically to influence miR-23b expression in people suffering from chronic inflammation.

It will also be important to determine whether miR-23b (either the mature miRNA sequence itself or crucial *cis* regulatory elements that manage its expression) is mutated in individuals that are predisposed to autoimmunity. This will be an interesting area of future inquiry and should provide mechanistic insight in addition to diagnostic value. The influence of miR-23b on other types of inflammatory diseases involving NF-κB, such as sepsis, cancer, neurodegenerative disorders and inflammatory hematopoiesis, should also be explored[9,16].

Autoimmunity is a stubborn and expanding problem for the biomedical community, and improved approaches to combat these debilitating conditions are clearly needed. The targeting of miRNAs to treat mammalian diseases has shown much promise in both preclinical models of various diseases and human clinical trials, with inhibition of miR-122 as a treatment for combating hepatitis C infections serving as a prototype[17]. As we continue to identify and understand the functions of the distinct miRNAs that are involved in pathological tissue inflammation, such as miR-23b, strategic manipulation of these regulatory RNAs using next-generation therapeutic approaches could perhaps be used to effectively mitigate the symptoms of human autoimmune diseases.

COMPETING FINANCIAL INTERESTS
The authors declare no competing financial interests.

1. Filipowicz, W., Bhattacharyya, S.N. & Sonenberg, N. *Nat. Rev. Genet.* **9**, 102–114 (2008).
2. Mendell, J.T. & Olson, E.N. *Cell* **148**, 1172–1187 (2012).
3. O'Connell, R.M. & Baltimore, D. *Curr. Top. Dev. Biol.* **99**, 145–174 (2012).
4. Calin, G.A. & Croce, C.M. *Nat. Rev. Cancer* **6**, 857–866 (2006).
5. Du, C. *et al. Nat. Immunol.* **10**, 1252–1259 (2009).
6. O'Connell, R.M. *et al. Immunity* **33**, 607–619 (2010).
7. Ponomarev, E.D., Veremeyko, T., Barteneva, N., Krichevsky, A.M. & Weiner, H.L. *Nat. Med.* **17**, 64–70 (2011).
8. Zhu, S. *et al. Nat. Med.* **18**, 1077–1086 (2012).
9. Hemdan, N.Y. *et al. Autoimmun. Rev.* **9**, 785–792 (2010).
10. Hayden, M.S. & Ghosh, S. *Genes Dev.* **26**, 203–234 (2012).
11. Medzhitov, R. *Cell* **140**, 771–776 (2010).
12. Boldin, M.P. & Baltimore, D. *Immunol. Rev.* **246**, 205–220 (2012).
13. Taganov, K.D., Boldin, M.P., Chang, K.J. & Baltimore, D. *Proc. Natl. Acad. Sci. USA* **103**, 12481–12486 (2006).
14. Li, Q.J. *et al. Cell* **129**, 147–161 (2007).
15. Ma, F. *et al. Nat. Immunol.* **12**, 861–869 (2011).
16. Boldin, M.P. *et al. J. Exp. Med.* **208**, 1189–1201 (2011).
17. Jopling, C.L. *Viruses* **2**, 1382–1393 (2010).

Co-opting endogenous microRNAs for therapy

Christopher E Pearson

A recent study highlights the potential of therapeutically modulating the endogenous miRNA pathway in a mouse model of spinal and bulbar muscular atrophy (SBMA). The overexpression of a naturally occurring miRNA led to the downregulation of the mutant androgen receptor transcript as well as the polyglutamine-containing protein it encodes, both of which may contribute to pathogenesis in SBMA (pages 1136–1141).

Over 40 neurological, neurodegenerative and neuromuscular diseases are associated with expanded DNA-encoded repeats[1]. SBMA was the first disease found to be caused by an expanded repeat within a gene, that encoding the androgen receptor, just over 20 years ago. CAG expansions in the gene encoding androgen receptor lead to a gain of function in the mutant androgen receptor, resulting in a neurodegenerative neuromuscular disease[1]. Many of the repeat diseases have an expanded polyglutamine-encoding CAG tract within the disease gene.

In this issue of *Nature Medicine*, Miyazaki *et al.*[2] show that a serious neurodegenerative and neuromuscular disease can be treated by modulating the organism's natural biology via a specific miRNA. Initially, they observed that five miRNAs (miR-196a, miR-196b, miR-496, miR-323-3p and miR-29b) were upregulated in the spinal cords of SBMA transgenic mice (mice carrying an androgen receptor transgene with an expanded CAG repeat) and individuals with SBMA. By overexpressing one of these miRNAs, miR-196a, the authors downregulated both the mutant CAG-expanded androgen receptor transcript and the mutant protein in SBMA mice, leading to improved neurology (as assessed by rotarod challenge, cage activity and ambulation), body weight and survival. This notable broad-spectrum improvement in the disease phenotype is probably due to the mode of delivery of the therapeutic miR-196a using a recombinant adeno-associated virus (AAV) vector. The AAV vector was efficiently transported via the blood from skeletal muscle to the brain and the motor neurons of the spinal cord.

Miyazaki *et al.*[2] also characterized a mechanism that provides a link between miR-196a and the amounts of the mutant androgen receptor transcript and protein. This effect seems to be mediated by CELF2, an RNA-binding protein known to bind AU-rich sequences[3]. CELF2 is a multifunctional protein that participates in the regulation of mRNA stability and RNA editing, splicing and translation[3–5]. Using a bioinformatic analysis, the authors predicted that miR-196a would bind the CELF2 mRNA, thus downregulating the amounts of the CELF2 transcript and its translated protein. This interpretation was supported by their observations of higher miR-196a and lower CELF2 mRNA levels in the thoracic spinal cords from individuals with SBMA compared with those from nonaffected control subjects.

The authors also supported their regulatory link *in vivo* by showing that the introduction of AAV expressing miR-196a led to a decrease the amounts of the CELF2 transcript and protein in SBMA mice expressing a mutant androgen receptor (**Fig. 1**). Miyazaki *et al.*[2] found that miR-196a–mediated knockdown of CELF2 decreased the stability of the androgen receptor transcript, thus decreasing the amounts of androgen receptor protein. Conversely, overexpression of CELF2 increased the amounts of androgen receptor mRNA and protein. Together, these data suggested that CELF2 could directly regulate the androgen receptor mRNA. Using a mutational analysis, the authors identified a short CUG repeat–containing region of the androgen receptor transcript, upstream of the CAG repeat tract, that is required for the CELF2-mediated stabilization of the androgen receptor transcript. The amounts of the mutant androgen receptor transcript could be regulated by the RNA-binding protein CELF2, which presumably was stabilized by binding of CELF2 to the short CUG tract in the androgen receptor transcript. This also led to altered levels of the toxic polyglutamine-expanded proteins and an improved neurological phenotype (**Fig. 1**). A direct demonstration of an interaction between CELF2 or other RNA-regulating proteins with the androgen receptor transcript would have further supported the regulatory model proposed by Miyazaki *et al.*[2].

Presumably, the decrease in androgen receptor protein upon CELF2 knockdown results from lowered amounts of the androgen receptor transcript. However, in addition to stabilizing the androgen receptor transcript, as proposed by the authors, CELF2 may also regulate androgen receptor translation. Of note, CELF2 has been reported to have a stabilizing effect on the cyclooxygenase-2 (*COX-2*) mRNA as well as an inhibitory effect on the translation and production of the COX-2 protein[5].

It is unclear exactly why the expression of the five miRNAs identified by Miyazaki *et al.*[2] is upregulated in the presence of the mutated androgen receptor–encoding gene. Considering the beneficial effect of over-expressing miR-196a, one might imagine that this could be a futile attempt by the cell to protect itself against the dysregulated physiology that results from the SBMA repeat expansion in the DNA, RNA and/or protein. Alternatively, the aberrant expression of these miRNAs may be part of the pathogenesis associated with CAG repeat expansion. Notably, miR-29b, one of the miRNAs upregulated in this study, has been shown to be downregulated in myotonic dystrophy type 1 (ref. 6) and upregulated in the brains of individuals with amyotrophic lateral sclerosis[7]. It is also possible that these SBMA- and myotonic dystrophy type 1–associated miRNAs have both beneficial and deleterious functions (antagonistic pleiotropy), as recently found for miRNA-34 (ref. 8).

The novelty of this study by Miyazaki *et al.*[2] is its approach: targeting an organism's natural miRNA system to downregulate a disease-linked transcript. The endogenous miRNA machinery can be co-opted to suppress genes of interest. Previous studies have demonstrated the therapeutic potential of RNAi for treating Huntington's disease and other repeat diseases through the exogenous expression of designed siRNAs, shRNAs and artificial miRNAs[9]. An advantage of such an avenue of therapeutic modulation is that it harnesses the natural physiology and specificity of the cell's miRNA system to regulate the amounts of the mutant transcript. This method ensures specificity for the androgen receptor transcript and hopefully reduces the potentially deleterious unknown off-target effects of artificial synthetic RNAi or antisense approaches[10].

Christopher E. Pearson is in the Program of Genetics and Genome Biology, The Hospital for Sick Children, Toronto, Ontario, Canada, and the Department of Molecular Genetics, University of Toronto, Toronto, Ontario, Canada.
e-mail: cepearson.sickkids@gmail.com

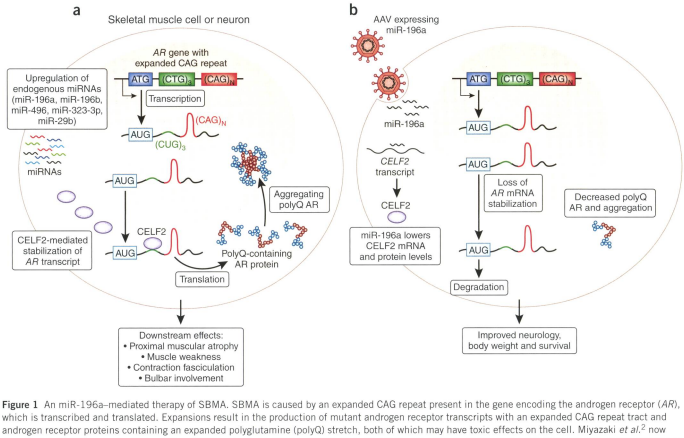

Katie Vicari

Figure 1 An miR-196a–mediated therapy of SBMA. SBMA is caused by an expanded CAG repeat present in the gene encoding the androgen receptor (*AR*), which is transcribed and translated. Expansions result in the production of mutant androgen receptor transcripts with an expanded CAG repeat tract and androgen receptor proteins containing an expanded polyglutamine (polyQ) stretch, both of which may have toxic effects on the cell. Miyazaki *et al.*[2] now show that miR-196a, along with four other miRNAs, is upregulated in SBMA. They find that miR-196a destabilizes the *CELF2* transcript, which encodes an RNA-binding protein, CELF2, that normally stabilizes the androgen receptor transcript, presumably by binding to a short CUG tract upstream of the CAG repeat in the androgen receptor transcript. Thus, administration of AAV overexpressing miR-196a targets CELF2, leading to the degradation of the androgen receptor transcript and reduced translation of the androgen receptor protein, and improves the phenotype of transgenic mice modeling SBMA.

Might the therapeutic use of miR-196a be applied to other diseases? Interestingly, miR-196a has been reported to be upregulated in a wide variety of cancers in which it may have potentially deleterious and suppressive effects[11], and it has also been reported to be involved in differentiation and in the development of the immune system. miR-196a has already been proposed as a therapeutic target for such cancers and immune-mediated conditions[11]. Another interesting question is whether CELF2 can affect the levels of other CUG repeat–containing transcripts. A first place to look might be the myotonic dystrophies types 1 and 2, which are associated with toxic RNAs containing expanded CUG repeat– and CCUG repeat–containing transcripts[1] that may serve as binding sites for CELF2. If CELF2 normally stabilizes the mutant myotonic dystrophy transcripts, then one might expect that regulation of CELF2 by miR-196a could modulate the disease phenotypes associated with these transcripts. Recent evidence suggests that CELF2 is upregulated in the brains of patients with myotonic dystrophy and in mouse models (M. Gomes-Pereira (INSERM, Université Paris Descartes, Hôpital Necker Enfants Malades), personal communication). If the cell were capable of modulating CELF2 levels in a protective manner, it might be downregulated in the presence of a highly expanded CUG transcript. Transgenic mice expressing CUG RNA repeats are a tool to test the benefits of miR-196a upregulation in myotonic dystrophy. It is noteworthy that a CUG-based mechanism is being used in SBMA, a disease commonly thought of as a CAG-based disease. The demonstration that modulating the miRNA pathway can regulate one repeat disease suggests that such miRNA-mediated approaches might be applicable to others.

A strength of the study by Miyazaki *et al.*[2] is that it reveals neurological improvements in an appropriate mouse model of a neurodegenerative disease by modulating the endogenous miRNA pathway that strikes close to the root cause for disease. Unlike previous attempts to treat SBMA, which aimed at altering the activity, nuclear aggregation or degradation of the mutant androgen receptor or further downstream events such as modifying the dysregulated transcriptome in SMBA mice (reviewed in ref. 12), the current study gets closer to the initiating cause of SBMA by targeting both the mutant transcript and protein. This focused attack on the expanded mutant transcript should also cover any potential toxic pathogenic entities that may arise from the toxic transcript, as recently suggested[3].

COMPETING FINANCIAL INTERESTS
The author declares no competing financial interests.

1. Pearson, C.E. *PLoS Genet.* **7**, e1002018 (2011).
2. Miyazaki, Y. *et al. Nat. Med.* **18**, 1136–1141 (2012)
3. Ladd, A.N., Charlet-Beurgerand, C. & Cooper, T. *Mol. Cell Biol.* **21**, 1285–1296 (2001).
4. Anant, S. *et al. J. Biol. Chem.* **276**, 47338–47351 (2001).
5. Mukhopadhyay, D., Houchen, C.W., Kennedy, S., Dieckgraefe, B.K. & Anant, S. *Mol. Cell* **11**, 113–126 (2003).
6. Perbellini, R. *et al. Neuromuscul. Disord.* **21**, 81–88 (2011).
7. Shioya, M. *et al. Neuropathol. Appl. Neurobiol.* **36**, 320–330 (2010).
8. Liu, N. *et al. Nature* **482**, 519–523 (2012).
9. Johnson, C.D. *Hum. Mol. Genet.* **19** R1, R98–R102 (2010).
10. McBride, J.L. *et al. Proc. Natl. Acad. Sci. USA* **105**, 5868–5873 (2008).
11. Chen, C., Zhang, Y., Zhang, L., Weakley, S.M. & Yao, Q. *J. Cell. Mol. Med.* **15**, 14–23 (2011).
12. Katsuno, M. *et al. Arch. Neurol.* **69**, 436–440 (2012).

To survive radiation injury, remember your aPCs

John P Chute

Acute exposure to ionizing radiation can cause lethality via severe damage to the hematopoietic system. A new study shows that infusion of the anticoagulants thrombomodulin or activated protein C reduces radiation toxicities and improves survival (pages 1123–1129).

Acute exposure to ionizing radiation can cause irreparable damage to multiple organ systems, particularly those with highly proliferative cells, such as the hematopoietic system, the skin and the gastrointestinal system[1]. Considered from the historical perspective of the atomic bombings of Hiroshima and Nagasaki[2] or the Chernobyl nuclear reactor accident[3], the effects of acute radiation exposure on humans can be so devastating that the contemplation of rational therapies to minimize these effects can seem futile. Nonetheless, in the decade following 9/11, there is a high ongoing threat of terrorism with radiological or improvised nuclear devices[4]. Furthermore, the events in Fukushima, Japan, in 2011 highlighted that even the threat of radiation fallout can have paralyzing effects on a worldwide scale. Therefore, there has been a renewed interest in developing effective mitigators of acute radiation injury.

Despite an extensive understanding of the effects of ionizing radiation on the hematopoietic system and decades of research to identify mitigators of radiation-induced hematopoietic injury[5,6], there is currently only one validated therapeutic for this syndrome, granulocyte colony-stimulating factor (GCSF)[7]. In this issue of *Nature Medicine*, Geiger *et al.*[8] describe a new mechanism, involving the thrombomodulin–activated protein C (aPC) pathway, that regulates the survival of mice following radiation injury (**Fig. 1**).

Using retroviral insertional mutagenesis, these authors found that thrombomodulin was overexpressed in bone marrow progenitor cells after radiation exposure. They then showed that systemic infusion of recombinant thrombomodulin into mice after high-dose total body irradiation (TBI) mitigated radiation-induced hematopoietic toxicity and significantly improved survival[8]. Similarly, thrombomodulin-deficient mice had a significantly higher mortality rate after TBI compared to control irradiated mice, suggesting that thrombomodulin might have a necessary role in regulating the hematopoietic response to irradiation. The results of Geiger *et al.*[8] are surprising considering that thrombomodulin is a receptor whose known principal activity is as an antifibrinolytic and anticoagulant protein[9]. Thrombomodulin mediates these effects via binding of the procoagulant thrombin, activation of the thrombin-activatable fibrinolysis inhibitor (TAFI) and conversion of plasma zymogen protein C into aPC, a natural anticoagulant[8–10]. aPC inhibits coagulation through its proteolytic activity against the procoagulants factors V and VIII and also mediates anti-inflammatory and prosurvival effects on endothelial cells, neurons and macrophages by binding to the endothelial protein C receptor, protease-activated receptors 1–3 and integrins[11,12].

One of the principal sequelae of the hematopoietic failure that follows radiation injury is thrombocytopenia, which can cause life-threatening bleeding complications. Therefore, one of the fascinating questions raised by the study of Geiger *et al.*[8] is how thrombomodulin, an anticoagulant, mediates radioprotection in mice following acute radiation injury. The authors tried to address this question by testing whether systemic infusion of aPC, which is activated by thrombomodulin, could also provide radioprotection. Interestingly, systemic infusion of aPC or E149-aPC, a recombinant variant with anticoagulant activity, had an equal ability to infusion of thromomodulin at radioprotecting mice, whereas the 5A-aPC variant, which lacks anticoagulant activity, had no beneficial effect. These results suggest that the radioprotective action of aPC is unrelated to its anti-inflammatory and cytoprotective effects and raise the possibility that aPC confers radioprotection through mechanisms that are yet to be discovered.

The beneficial effects of thrombomodulin and aPC in irradiated mice raise another important question: what are the cellular targets of thrombomodulin and aPC in the hematopoietic system? Does thrombomodulin or aPC act directly on hematopoietic stem cells (HSCs) to confer radioprotection or perhaps act indirectly via effects on the HSC niche? Geiger *et al.*[8] found that the overexpression of thrombomodulin in bone marrow hematopoietic progenitor cells (HPCs) conferred no

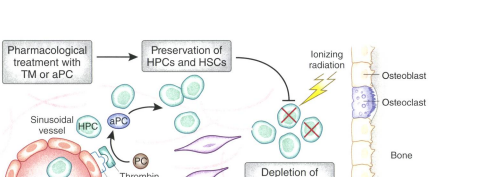

Figure 1 Thrombomodulin and aPC can mitigate radiation-induced toxicity. The bone marrow microenvironment, including HSCs, HPCs, stromal cells such as fibroblasts and vascular endothelial cells, is shown. Geiger *et al.*[8] now suggest a mechanism through which the thrombomodulin (TM)-aPC pathway can protect against radiation-induced hematopoietic injury. Thrombomodulin expressed on the surface of stromal cells and endothelial cells in the bone marrow microenvironment activates protein C (PC) to aPC. aPC can then stimulate the recovery of HSCs and HPCs after radiation damage. Therapeutic administration of thrombomodulin or aPC can augment these effects occurring in the bone marrow niche. ECM, extracellular matrix.

John P. Chute is in the Division of Cellular Therapy, Duke University Medical Center, Durham, North Carolina, USA.
e-mail: john.chute@duke.edu

radioprotection compared to control HPCs *in vitro*, suggesting that cells other than HPCs were involved in mediating protection. Furthermore, thrombomodulin-deficient mice transplanted with wild-type bone marrow cells showed a significant increase in their 30-day mortality compared to wild-type recipient mice, suggesting that the expression of thrombomodulin on cells in the bone marrow microenvironment was important for hematopoietic recovery after TBI. As thrombomodulin is expressed by bone marrow endothelial cells and stromal cells, a plausible hypothesis is that the HSC response to irradiation is dependent on regulation by the thrombomodulin-aPC axis and under the control of the HSC niche. This hypothesis would be consistent with recent reports that suggested that bone marrow endothelial cells positive for vascular endothelial growth factor receptor 2 or vascular endothelial cadherin-based vascular remodeling in the bone marrow are necessary in allowing normal hematopoietic regeneration to occur[13–15]. In future experiments, cell-specific deletion of thrombomodulin or aPC in HSC niche cells should allow the determination of which HSC niche cells are responsible for protecting the hematopoietic system via this mechanism.

The work of Geiger *et al.*[8] has clear clinical implications. First, the development of mitigators for radiation-induced hematopoietic failure should be a top public health priority, as few treatments exist that can improve hematological recovery in victims of acute radiation injury[7]. In light of the Fukushima crisis and the ongoing threat of terrorism using radiological or nuclear materials, an acute radiation disaster that could affect large human populations remains a real possibility. As recombinant human aPC (Xigris, Eli Lilly) was approved by the US Food and Drug Administration for the treatment of severe sepsis in 2001 (although it was removed from the market in 2011 after failing to improve mortality compared to placebo in randomized clinical trials), it may be feasible to test recombinant aPC for its therapeutic utility in radiation-induced hematopoietic failure in humans.

Second, and perhaps more importantly, the cellular mechanisms that regulate the hematopoietic response to acute radiation exposure are likely to be relevant to the hematopoietic response that occurs following other myelosuppressive injuries such as chemotherapy or conditioning before stem cell transplantation. Further studies to delineate the precise mechanisms through which thrombomodulin and aPC mediate the repair and regeneration of HPCs after radiation exposure may provide an important avenue toward the development of therapies to minimize myelosuppression in patients receiving chemotherapy or radiotherapy for cancer.

COMPETING FINANCIAL INTERESTS
The author declares no competing financial interests.

1. Mettler, F.A. & Voelz, G.L. *N. Engl. J. Med.* **346**, 1554–1561 (2002).
2. Oughterson, A.W. & Warren, S. *Medical Effects of the Atomic Bomb in Japan.* (McGraw-Hill, New York, 1956).
3. Baranov, A. *et al. N. Engl. J. Med.* **321**, 205–212 (1989).
4. Allison, G. Report of the Commission on the Prevention of Weapons of Mass Destruction, Proliferation and Terrorism. <http://belfercenter.ksg.harvard.edu/publication/18786/world_at_risk.html> (2009; accessed 13 June 2012).
5. Wasielenko, J.K. *et al. Ann. Intern. Med.* **140**, 1037–1051 (2004).
6. Dainiak, N. *Exp. Hematol.* **30**, 513–528 (2002).
7. Coleman, C.N. *et al. Ann. Emerg. Med.* **53**, 213–222 (2009).
8. Geiger, H. *et al. Nat. Med.* **18**, 1123–1129 (2012).
9. Wang, W., Nagashima, M., Schneider, M., Morser, J. & Nesheim, M. *J. Biol. Chem.* **275**, 22942–22947 (2000).
10. Esmon, N.L., Owen, W. & Esmon, C. *J. Biol. Chem.* **257**, 859–864 (1982).
11. Mosnier, L.O., Zlokovic, B. & Griffin, J. *Blood* **109**, 3161–3172 (2007).
12. Weiler, H. *Cnt. Care Med.* **38**, S18–S25 (2010).
13. Hooper, A.T. *et al. Cell Stem Cell* **4**, 263–274 (2009).
14. Salter, A.B. *et al. Blood* **113**, 2104–2107 (2009).
15. Butler, J.M. *et al. Cell Stem Cell* **6**, 251–264 (2010).

NKT cells—an early warning system for HBV infection

Dale I Godfrey, Adam P Uldrich & Alan G Baxter

Whereas the adaptive immune response is essential for control and clearance of hepatitis B virus infection, the importance of the early innate immune response is controversial and the players involved are poorly defined. A new study shows that activation of natural killer T cells by infected hepatocytes is crucial for the early control of this disease (pages 1060–1068).

Hepatitis B virus (HBV) claims an estimated 1 million lives every year. Most healthy adults mount an effective immune response that can clear HBV; however, many, especially young children, are vulnerable to chronic infection, which can lead to liver cirrhosis and cancer[1,2]. Existing vaccines prevent HBV infection, but current therapies fail to clear chronic disease. The adaptive immune system mounts a multipronged immune response against HBV, but its effectiveness seems to be influenced by the quality of the earlier innate immune response that begins within hours of infection[1,2]. In this issue of *Nature Medicine*, Zeissig *et al.*[3] identify a new mechanism by which innate-like lymphocytes known as natural killer T (NKT) cells can rapidly detect and respond to hepatocytes that have been infected by HBV, dramatically enhancing downstream adaptive antiviral responses (**Fig. 1**).

The immune system has two major strategies for defense against microorganisms. Innate immunity is generally triggered by pattern recognition receptors that detect conserved structural components of pathogens. Within minutes this mobilizes inflammatory, phagocytic and cytotoxic cells, such as neutrophils, macrophages and NK cells. In contrast, adaptive immunity depends on ligation of randomly generated antigen receptors (T cell receptors (TCRs) or surface immunoglobulin) expressed on T cells and B cells. An effective adaptive response requires clonal expansion of rare, antigen-specific T cells and B cells—a process that takes at least several days. HBV clearance is primarily mediated by cytotoxic ($CD8^+$) T cells specific for viral peptides presented by class I major histocompatibility complex (MHC) molecules on the surface of hepatocytes (**Fig. 1**). It results in apoptosis of infected cells, limiting viral replication. Antibodies are also generated by antigen-specific effector B cells (plasma cells),

Dale I. Godfrey and Adam P. Uldrich are in the Department of Microbiology & Immunology, University of Melbourne, Parkville, Victoria, Australia. Alan G. Baxter is at the Comparative Genomics Centre, James Cook University, Townsville, Queensland, Australia.
e-mail: godfrey@unimelb.edu.au

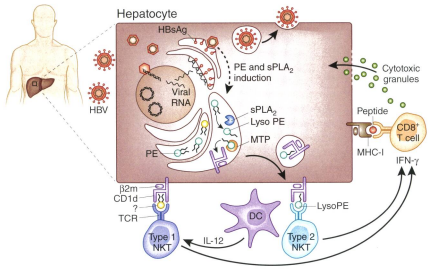

Katie Vicari

Figure 1 Activation of NKT cells by HBV-infected hepatocytes primes the adaptive immune response and promotes viral clearance. Hepatitis B virus infection of hepatocytes results in upregulation of endogenous PE and the secretory phospholipase ($sPLA_2$) enzymes. $sPLA_2$ enzymes are induced by the small HBsAg by unknown mechanisms and convert PE to lysoPE. MTP then transfers the lysoPE into the antigen-binding groove of CD1d for presentation to, and activation of, type 2 NKT cells. IL-12 production associated with this response contributes to the activation of type 1 NKT cells that may also respond to other HBV-induced phospholipid antigens as yet unknown (indicated with a question mark). After activation, both NKT cell types produce interferon-γ (IFN-γ), which supports adaptive antiviral responses and hepatocyte killing by HBV-specific, MHC class I–restricted, $CD8^+$ T cells. β2m, β2 microglobulin; DC, dendritic cell.

particularly against viral surface antigens (HBsAg), limiting viral spread[1,2].

NKT cells are a subset of T lymphocytes that bridge the gap between innate and adaptive immunity. These cells express TCRs but, unlike conventional T cells, recognize lipid-based antigens presented by the MHC-like molecule, CD1d[4]. Upon activation, NKT cells rapidly produce a broad spectrum of cytokines, activating other immune cells and consequently playing a key part in early responses to infection, cancer and transplants, as well as in allergy and autoimmunity[5]. There are two broad categories of NKT cells: type 1 'invariant' NKT cells, which are defined by their invariant TCR-α chain (Vα24-Jα18 in humans; Vα14-Jα18 in mice) and their ability to recognize the synthetic glycolipid antigen α-galactosylceramide (α-GalCer); and type 2 'noninvariant' NKT cells, which neither express the type 1–associated invariant TCR-α chain nor recognize α-GalCer. Instead, type 2 NKT cells express a range of TCRs and bind a variety of lipid antigens, including glycolipids and phospholipids[4].

As HBV does not directly infect mouse hepatocytes, Zeissig *et al.*[3] used a mouse model of HBV involving adenovirus-mediated transfer of replication-competent HBV genome and showed that both type 1 and type 2 liver NKT cells become activated and produce IFN-γ in response to HBV replication *in vivo*. Furthermore, mice lacking NKT cells had persistently higher amounts of HBsAg and HBV DNA in the serum, lower antibody titers and chronic low-grade hepatitis, indicating that NKT cells contributed to effective adaptive immunity and HBV clearance. This builds on an earlier study demonstrating a role for type 2 NKT cells in immunity to HBV[6]. Using *in vitro* coculture of type 1 and type 2 NKT cell lines with infected hepatocytes, the authors dissected the interplay between HBV and host NKT cells[3]. These cells were directly activated by infected hepatocytes in a process dependent on microsomal triglyceride transfer protein (MTP) chaperoning lipids into the CD1d antigen-binding groove[7].

As MTP is primarily involved in lipid transport in the endoplasmic reticulum (ER) and HBV acquires ER lipids for its envelope, the authors investigated the role of ER-derived lipids as antigens in this system. They found that ER-derived phospholipid fractions from HBV-infected hepatocytes activated both type 1 and type 2 NKT cells[3]. Moreover, they showed that the self phospholipid antigens phosphatidylethanolamine (PE) and lysophosphatidylethanolamine (lysoPE), were increased in HBV-infected hepatocytes and, when presented by CD1d, the latter could activate some type 2 NKT cells but not type 1 NKT cells. The endogenous generation of lysoPE from PE, which involves cleavage of one of the two fatty acid acyl chains, was mediated by a subset of secretory phospholipase ($sPLA_2$) enzymes that are upregulated in response to the small HBsAg. Expression of HBsAg in hepatocytes was sufficient to induce CD1d-dependent NKT cell activation (**Fig. 1**).

Whereas the mechanism underlying type 1 NKT cell activation is less clear in the Zeissig *et al.*[3] study, these cells are also required for effective HBV control. Their activation *in vivo* was largely interleukin-12 (IL-12) dependent, but *in vitro* they also responded to unidentified hepatocyte phospholipid antigens induced by HBV infection[3], suggesting that their activation may be both IL-12 and self-antigen dependent (**Fig. 1**). The endogenous ligand, β-glucosylceramide, which in combination with IL-12 activates type 1 NKT cells after bacterial infections[8], seems unlikely to be responsible in this case because it is not a phospholipid. A recently defined type 1 NKT cell antigen, plasmalogen-lysoPE, which is structurally very similar to lysoPE[9], may be worthy of further investigation.

HBV infection of hepatocytes triggered the upregulation and presentation of an endogenous 'danger' signal in the form of the self-lipid antigen, which directly activates type 2 NKT cells[3]. Either simultaneously or sequentially, type 1 NKT cells are activated in an IL-12–dependent manner, but the process potentially involves recognition of other, as yet undefined, self-antigens induced by HBV infection. This combined response serves as an early warning system that initiates an effective adaptive immune response. Although their activation requirements are clearly distinct, it remains to be determined whether type 1 and type 2 NKT cells perform distinct effector functions in resolving HBV infection. HBV immunity was impaired in mice lacking type 1, but not type 2, NKT cells, but this may simply reflect a reduction in the total number of NKT cells.

Although this study is largely focused on mouse models, the relevance of these new findings to human biology is supported by the crucial observation that human hepatocytes exposed to HBV *in vitro* could activate human NKT cell lines in a CD1d-dependent fashion[3]. NKT cells may therefore have a similar role in promoting immunity to HBV infection in humans. Although NKT cells are less abundant in human liver compared to mouse liver, type 1 NKT cell numbers have been shown to be reduced in the blood of individuals with chronic HBV infection compared to healthy controls, which then significantly increased after antiviral therapy[10], consistent with a role in HBV clearance in humans.

The findings by Zeissig *et al.*[3] suggest potential therapeutic approaches to the prevention and treatment of chronic HBV infection. It will be important to determine whether a defect in

NKT cell numbers, activity or both is linked to chronic viral hepatitis. Moreover, NKT cells may be a good target for immunotherapy. In support of this, activation of type 1 NKT cells can eliminate HBV[11] and enhance adaptive T cell immunity to HBsAg in mice[11,12]. Although a clinical trial in which patients chronically infected with HBV were treated with systemic intravenous injection of the type 1 NKT cell antigen, α-GalCer, failed to show significant protective effect[13], more targeted strategies such as combining α-GalCer with HBV vaccines should be considered for further testing. This approach has proven to be very powerful in mouse models of virus infection[14]. A caveat that should be considered with NKT cell–based immunotherapy is the potential risk that an aggressive inflammatory immune response in the liver of patients with HBV may trigger fulminant hepatic failure. The use of antigens such as lysoPE to specifically target type 2 NKT cells may also prove to be a safer approach to NKT cell–based immunotherapy.

NKT cells can control the character and vigor of immune responses. They therefore provide a valuable target for modulation of immunity to HBV and other infections. This study, together with those describing NKT cell activation by β-glucosylceramide in bacterial infections[8], introduces a new paradigm of immune modulation in which self-lipid antigens serve as endogenous 'danger' signals by binding to CD1d and activating NKT cells.

COMPETING FINANCIAL INTERESTS
The authors declare no competing financial interests.

1. Huang, L.M., Lu, C.Y. & Chen, D.S. *Curr. Opin. Immunol.* **23**, 237–243 (2011).
2. Guidotti, L.G. & Chisari, F.V. *Annu. Rev. Pathol.* **1**, 23–61 (2006).
3. Zeissig, S. *et al. Nat. Med.* 18, 1060–1068 (2012).
4. Godfrey, D.I., MacDonald, H.R., Kronenberg, M., Smyth, M.J. & Van Kaer, L. *Nat. Rev. Immunol.* **4**, 231–237 (2004).
5. Godfrey, D.I. & Kronenberg, M. *J. Clin. Invest.* **114**, 1379–1388 (2004).
6. Baron, J.L. *et al. Immunity* **16**, 583–594 (2002).
7. Dougan, S.K. *et al. J. Exp. Med.* **202**, 529–539 (2005).
8. Brennan, P.J. *et al. Nat. Immunol.* **12**, 1202–1211 (2011).
9. Facciotti, F. *et al. Nat. Immunol.* **13**, 474–480 (2012).
10. Jiang, X. *et al. PLoS ONE* **6**, e28871 (2011).
11. Kakimi, K., Guidotti, L.G., Koezuka, Y. & Chisari, F.V. *J. Exp. Med.* **192**, 921–930 (2000).
12. Ito, H. *et al. Int. Immunol.* **20**, 869–879 (2008).
13. Woltman, A.M. *et al. Antivir. Ther.* **14**, 809–818 (2009).
14. Cerundolo, V., Silk, J.D., Masri, S.H. & Salio, M. *Nat. Rev. Immunol.* **9**, 28–38 (2009).

Cutting SRC-1 down to size in endometriosis

Matthew T Dyson & Serdar E Bulun

Endometriosis occurs when estrogen-sensitive endometrial cells that are shed to distal sites manage to attach and survive in a foreign, inflammatory environment. A new study reports a unique interaction between a cleaved form of steroid receptor coactivator 1 (SRC-1) and caspase 8 that blocks apoptosis in endometriotic cells, allowing them to survive (pages 1102–1111).

Endometriosis afflicts millions of women worldwide causing severe menstrual pain, chronic pelvic pain and infertility during what should be their peak years of health[1]. Menstruation is the key trigger for this disease, and although uninterrupted menstrual cycles seem to increase the risk for the endometriosis, it is not understood why only a subset of women develop the disease. When we have asked our patients with endometriosis about menstruation-related symptoms during their teenage years, the vast majority reported debilitating menstrual cramps when they were teenagers that worsened during the following years—thus the disease's symptoms seem to manifest almost immediately after menarche. This consistent feature of endometriosis suggests that these women were predisposed to developing endometriosis from early on in life.

Like menstruation, endometriosis occurs exclusively in primates[2], suggesting that our understanding of this disease's etiology is stunted by the older question of what evolutionary burden drove primates to menstruate when other mammals do not. In placental mammals, sex steroids and cytokines remodel the endometrium to provide a controlled environment that protects and nourishes the embryo while tempering the maternal immunological and inflammatory responses against the embryo itself. Primates uniquely initiate this process before conception, as the periodic shedding and regeneration of endometrial tissue is prerequisite for the deep placental invasion of its stroma and blood vessels. But repetitive menstruation also has an undesired side effect: the retrograde flushing of endometrial tissue and blood onto the pelvic peritoneum, which was proposed by Sampson over 90 years ago to drive the pathogenesis of endometriosis[3]. This theory has upheld well, and currently the definitive method for diagnosing endometriosis is the laproscopic detection of endometrium-like tissue at inflamed ectopic sites, mostly in the pelvic peritoneal cavity[4]. Importantly, these transplanted cells are characterized by molecular and epigenetic defects that allow them to survive in response to estrogen outside the uterus[2].

In most women with endometriosis and pelvic pain, the disease is limited to sparse, small implants on peritoneal surfaces, suggesting that enhanced cell survival rather than unchecked proliferation is the key biological property of endometriotic cells. Consistent with this, endometriotic cells are highly resistant to apoptosis and survive in an inflammatory environment where cytokines such as tumor necrosis factor (TNF) would prompt apoptosis in normal endometrial cells[5]. It is in this context that a study in this issue of *Nature Medicine* by Han *et al.*[6] addresses a fundamental question in endometriosis: what molecular event links aberrant TNF action and steroid signaling to prolonged cell survival?

To address this question, the authors investigated how the steroid receptor coactivators (SRCs) affect endometriosis, given that they mediate the effects of steroid hormone receptors such as the estrogen receptor and that estrogen signaling fuels this disease. By comparing mouse models and human samples of endometriosis, Han *et al.*[6] deduced that SRC-1 expression was crucial for disease progression, but the amounts of SRC-1 protein at its expected molecular weight were unexpectedly reduced in the diseased cells. Furthermore, their mouse model showed similar expression of the *SRC-1* mRNA in both healthy and diseased tissues.

Matthew T. Dyson and Serdar E. Bulun are in the Department of Obstetrics and Gynecology at Feinberg School of Medicine, Feinberg School of Medicine at Northwestern University, Chicago, Illinois, USA.
e-mail: sbulun@nmh.org

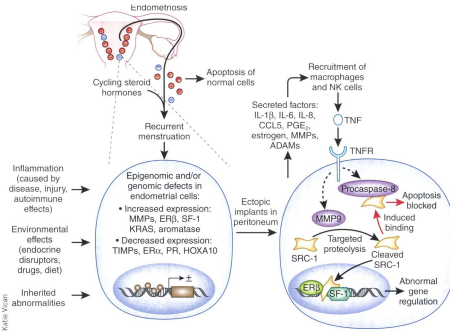

Figure 1 SRC-1 in the etiology of endometriosis. Menstruation follows the withdrawal of steroid hormones ending the luteal phase, during which time endometrial tissue is often unintentionally shed into the pelvic peritoneum. Most of these endometrial cells apoptose; however, defects (either pre-existing or acquired) in some cells can alter the expression of key genes affecting steroid signaling and the TNF response that predisposes them to driving endometriosis. Han *et al.*[6] now show that in endometriosis TNF-activated MMP9 cleaves SRC-1 to generate a truncated SRC-1 isoform, which is distributed to the nucleus and cytoplasm. The truncated SRC-1 retains its ability to interact with nuclear receptors, but it can also bind procaspase-8, potently blocking the ability of TNF and other signals to induce apoptosis. ADAM, a disintegrin and metalloproteinase; CCL5, chemokine (C-C motif) ligand 5; ERα, estrogen receptor-α; HOXA10, homeobox A10; IL-1β, interleukin-1β; NK, natural killer; PGE_2, prostaglandin E_2; PR, progesterone receptor; SF-1, steroidogenic factor 1.

These observations were explained when the authors found that SRC-1 can be proteolytically cleaved in diseased cells by matrix metalloproteinase-9 (MMP9) into a previously unknown shorter SRC-1 isoform, which distributes to the cytoplasm as well as the nucleus. Remarkably, the short isoform retained its ability to interact with nuclear receptors but could also bind and inhibit procaspase-8, thereby blocking apoptosis (**Fig. 1**). More importantly, the authors found that the SRC-1 cleavage process is activated by TNF[6]. Thus, endometriotic cells can survive TNF-induced apoptosis more effectively than healthy cells by processing SRC-1 into a shorter isoform that blocks the execution phase of apoptosis.

The characterization of a TNF–MMP9–SRC-1 axis in endometriosis by Han *et al.*[6] mechanistically connects well-established markers of endometriosis with the progression of the disease, but what initiates this axis is unknown. The heritable component of endometriosis is likely to be epigenetic[2], and the members of this newly identified TNF–MMP9–SRC-1 pathway provide a targeted list of candidates for an epigenetically mediated mechanism of endometriosis pathogenesis. The most attractive of these is MMP9, which along with upstream MMPs and regulatory tissue inhibitors (TIMPs) is crucial for remodeling the endometrium in response to steroid hormones both before and during implantation[7]. In the endometrium, steroid hormones and epigenetic mechanisms coordinate the expression of the MMPs and TIMPs during development and during each menstrual cycle[7,8]. Moreover, aberrant DNA methylation of the genes encoding these proteins has been associated with disease, and hypomethylation of the genes encoding MMPs occurs frequently in cancers, where their increased expression enhances tumor progression and invasion[9]. Epigenetic defects and increased estrogen in endometrial cells that trigger MMP activity could jumpstart the proteolysis of SRC-1, thereby creating more effective seeds for endometriosis. It is striking that in rodent and nonhuman primate models, if a sufficient amount of endometrial tissue is transplanted to the peritoneum, endometriosis can develop, despite these models having low or absent levels of spontaneous endometriosis[10]. This suggests that a small population of endometrial cells is predisposed to causing the disease and that perhaps women prone to endometriosis harbor a larger population of these disease-predisposing cells.

The findings of Han *et al.*[6] provide new insights into how the TNF pathway is conscripted to enhance endometriotic cell survival, but they leave researchers with several questions. Principally, how widespread is this phenomenon regarding the other SRC members and with respect to other tissues? The TNF–MMP9–SRC-1 signaling axis is likely to function in tissues where steroid signaling and inflammation are present and could potentially block apoptosis in cancers in which progression is also correlated with TNF and MMP expression. This pathway may be particularly important in breast cancer, where tumors expressing SRC-1 possess a more aggressive and dedifferentiated phenotype[11]. Regarding the proteolysis of the SRC family members, the MMP9 cleavage site of SRC-1 is well conserved from mice to humans, and Han *et al.*[6] note that SRC-2 and SRC-3 might be similarly processed. O'Malley and others have firmly established that SRCs function as 'pleiotropic rheostats' that coordinate nuclear receptor activity[12]; however, similar mechanisms for the other SRCs would be groundbreaking, expanding the role of SRCs into truly multifunctional proteins. It is now vital to explore how truncated SRC isoforms affect nuclear receptor function and distribution, especially given the cytoplasmic localization of the shorter isoform observed by Han *et al.*[6]. The expression of estrogen and progesterone receptors are profoundly altered in endometriosis, and the redistribution of SRC isoforms with respect to their binding across the genome or their functions in the cytoplasm could affect the sensitivity of diseased tissues to steroid hormones.

The potential treatment options for endometriosis that the discovery of the TNF–MMP9–SRC-1 axis points toward are equally exciting. Recently, TNF inhibitors (infliximab and etanercept) have been used to treat endometriosis in nonhuman primate and rodent models, suggesting that focused work in this area will be fruitful[13]. Similarly, MMP9 inhibitors currently being developed to treat invasive cancer[14] may also prove effective for endometriosis. Han *et al.*[6] suggest that the cleaved SRC-1 isoform is unique to endometriosis, raising the possibility that the detection of the short SRC-1 isoform could be used in endometriosis diagnosis. Looking ahead, the treatment options for endometriosis could improve as the TNF–MMP9–SRC-1 pathway is further dissected, but more importantly the work presented here sheds important light on how some of the therapies currently in testing operate and new insights for how to improve them.

COMPETING FINANCIAL INTERESTS
The authors declare no competing financial interests.

1. Nnoaham, K.E. *et al. Fertil. Steril.* **96**, 366–373 (2011).
2. Buluin, S.E. *N. Engl. J. Med.* **360**, 268–279 (2009).
3. Sampson, J.A. *Am. J. Obstet. Gynecol.* **14**, 422–469 (1927).
4. Giudice, L.C. *N. Engl. J. Med.* **362**, 2389–2398 (2010).
5. Nasu, K., Yuge, A., Tsuno, A., Nishida, M. & Narahara, H. *Histol. Histopathol.* **24**, 1181–1192 (2009).
6. Han, S.J. *et al. Nat. Med.* **18**, 1102–1111 (2012).
7. Gaide Chevronnay, H.P. *et al. Biochim. Biophys. Acta* **1824**, 146–156 (2012).
8. Stilley, J.A., Woods-Marshall, R., Sutovsky, M., Sutovsky, P. & Sharpe-Timms, K.L. *Biol. Reprod.* **80**, 649–656 (2009).
9. Hansen, K.D. *et al. Nat. Genet.* **43**, 768–775 (2011).
10. Braundmeier, A.G. & Fazleabas, A.T. *Mol. Hum. Reprod.* **15**, 577–586 (2009).
11. McBryan, J. *et al. Cancer Res.* **72**, 548–559 (2012).
12. York, B. & O'Malley, B.W. *J. Biol. Chem.* **285**, 38743–38750 (2010).
13. Islimye, M. *et al. Eur. J. Obstet. Gynecol. Reprod. Biol.* **159**, 184–189 (2011).
14. Giraudo, E., Inoue, M. & Hanahan, D. *J. Clin. Invest.* **114**, 623–633 (2004).

Primed for inflammation: enthesis-resident T cells

Rik J Lories & Iain B McInnes

The enthesis is the region at the junction between tendon and bone and has been suggested to be a key target in spondyloarthritic diseases. This zone is now shown to contain a unique population of resident T cells, which, when activated by the cytokine interleukin-23 (IL-23), can promote pathogenesis that is characteristic of spondyloarthritis (pages 1069–1076).

First recognized in ancient Egypt, few musculoskeletal diseases have as notable a phenotype as the postural deficit arising from advanced ankylosing spondylitis. Formerly known as Bechterew's disease, ankylosing spondylitis is the prototypic and most common form of spondyloarthritis. Spondyloarthritis has a prevalence of 1–2% worldwide (affecting 2.4 million people in the United States alone) and causes high levels of disability and a reduced quality of life in those afflicted, as well as a substantial socioeconomic burden[1].

Despite the recognition of an association between the human leukocyte antigen B27 (HLA-B27) and this disease over three decades ago, our understanding of the pathogenesis of ankylosing spondylitis is remarkably limited. The factors that initiate disease processes, the reason why specific sites in the skeleton are affected and the complex relationship between inflammation and new tissue formation have been extensively studied but are still not well defined. Recent genome-wide studies in people with ankylosing spondylitis have identified several disease-associated loci, particularly the IL-23 receptor (IL-23R)[2]. This receptor is of particular interest because it has also previously been associated with other spondyloarthritis-associated disorders such as Crohn's disease and psoriasis[3,4].

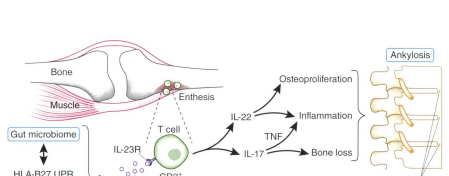

Katie Vicari

Figure 1 IL-23 and entheseal-resident T cells in the pathogenesis of spondyloarthritis. Various pathways may lead to elevated IL-23 expression, and Sherlock *et al.*[7] now show that IL-23 can activate resident T cells within the enthesis, the region in which tendons and ligaments insert into bone. These activated T cells can then promote local inflammation and bone remodeling through a variety of effector mediators, including IL-17 and IL-22. The net result of these actions is the typical ankylosed appearance of the spine. TNF, tumor necrosis factor; UPR, unfolded protein response.

Ankylosing spondylitis comprises inflammation and progressive ankylosis of sacroiliac joints and the spine and is frequently accompanied by oligoarthritis and inflammation of the enthesis, the anatomical zone in which tendons and ligaments insert into bone (entheositis). Extra-articular features of the disease include involvement of the eye (uveitis) and, more rarely, cardiac structures. Elegant imaging and comparative anatomy studies have suggested that the enthesis may actually be the initiating site for musculoskeletal inflammation in ankylosing spondylitis[5,6], although in established disease, entheositis is typically accompanied by synovitis and osteitis. The enthesis is a layered anatomical interface formed by tendon fibers, uncalcified fibrocartilage, mineralized fibrocartilage and bone that provides a functional unit to translate and dissipate the forces generated by muscles onto bone. It has not previously been considered a site of resident immune surveillance.

Although the IL-23 pathway has been implicated in the pathogenesis of spondyloarthritis, it was previously unclear how it promotes entheositis. In this issue of *Nature Medicine*, Sherlock *et al.*[7] identify a previously undescribed lineage of T cells in the enthesis that is responsive to IL-23. They then show that IL-23–mediated stimulation of these lymphocytes leads to the development of entheseal inflammation and local bone remodeling in a mouse model (**Fig. 1**). This work provides an elegant and intriguing cellular link between tissue-specific pathology and systemic cytokine

Rik J. Lories is in the Department of Development and Regeneration, KU Leuven, Leuven, Belgium. Iain B. McInnes is in the College of Medicine, Veterinary Medicine and Life Sciences, University of Glasgow, Glasgow, UK.
e-mail: rik.lories@med.kuleuven.be or iain.mcinnes@glasgow.ac.uk

expression, which could potentially be initiated at distant sites such as the gut.

Using mice that express IL-23R tagged with a fluorescent label, the authors identified a population of $CD3^+CD4^-CD8^-IL\text{-}23R^+$, RAR-related orphan receptor γt ($ROR\text{-}\gamma t$)$^+$ T cells in the enthesis of mice[7]. This finding was unexpected and challenges earlier concepts of entheseal biology. Moreover, using minicircle DNA technology to systemically overexpress IL-23 in mice, they showed that IL-23 overexpression was sufficient to elicit enthesitis and joint disease with histological and bone remodeling features that were reminiscent of ankylosing spondylitis. This pathology was dependent on the presence of $CD3^+CD4^-CD8^-IL\text{-}23R^+ROR\text{-}\gamma t^+$ T cells (as disease was absent in *Rag2*$^{-/-}$ mice that lacked functional B and T cells) but did not require T helper type 17 (T_H17) cells (as depletion of $CD4^+$ T cells did not modify the disease state). In subsequent experiments, Sherlock *et al.*[7] showed that IL-23 promoted the expression of IL-17 and IL-22 in $CD3^+CD4^-CD8^-IL\text{-}23R^+ROR\text{-}\gamma t^+$ entheseal T cells. They found that although IL-17 and IL-22 both participated in disease together, IL-22 was the dominant effector cytokine, particularly in driving bone remodeling (**Fig. 1**). The authors were also able to detect inflammatory changes in the aortic root but not in the gut, liver or kidneys, and, curiously, they observed psoriatiform lesions in the mice overexpressing IL-23.

It is currently under debate[1] whether ankylosing spondylitis is a true autoimmune disease, which would reflect its strong association with HLA-B27 and the presumed role of a conventional peptide presentation and T cell activation cascade, or whether it is an autoinflammatory condition[8]. The entheseal $CD3^+CD4^-CD8^-IL\text{-}23R^+ROR\text{-}\gamma t^+$ T cells and their mode of activation described by Sherlock *et al.*[7] do not provide a definitive resolution to this issue, at least in terms of whether there is a clear contribution from the innate or acquired effector arm of the immune response. The phenotype of the entheseal T cells is reminiscent of the $CD3^+CD4^-CD8^-$ T cell lineages that have been observed in other inflammatory diseases. They do not seem to show natural killer cell markers, although whether they express homologs of killer immunoglobulin-like receptors that can recognize HLA-B27 homodimers should be explored, as this would offer a potential regulatory link between HLA-B27 and entheseal T cell activation. Interestingly, the entheseal-resident T cells have the transcription factor promyelocytic leukemia zinc finger, which confers a capacity for rapid cytokine induction after cellular activation[9]. These cells might therefore be considered to be 'innate-like' T cells that can act as sensors of damage and environmental stress.

It is possible that chronic minimal damage at the enthesis is a normal feature that arises from biomechanical stress. The appropriate recognition and monitoring of such events could be key in maintaining tissue homeostasis and could perhaps be mediated by low amounts of IL-22 and signal transducer and activator of transcription 3–mediated expression of Wnt and bone morphogenetic proteins and, thus, by osteoblast function. Excessive microtrauma or an aberrant sensing of tissue stress may alter the threshold for entheseal $CD3^+CD4^-CD8^-IL\text{-}23R^+ROR\text{-}\gamma t^+$ T cell activation and provoke inflammation. Another biochemical property of HLA-B27 leads to misfolding of the protein in the endoplasmic reticulum, whereby the unfolded protein response may be activated[10]. In myeloid cells, this stress response can lead to the release of IL-23 (ref. 11), and therefore the effect of the unfolded protein response on $CD3^+CD4^-CD8^-IL\text{-}23R^+ROR\text{-}\gamma t^+$ T cell function is worthy of future investigation.

This work also raises many other key questions. What is the origin of IL-23 in the disease state? An attractive hypothesis is that IL-23 is released from distant immune cell populations in the gut and, perhaps, the lung, as IL-23 concentrations are elevated in some individuals with ankylosing spondylitis[12]. The links between gut inflammation (such as in Crohn's disease), the gastrointestinal microbiome (or specific pathogens, for example, *Klebsiella*), local and systemic IL-23 release and the consequent skeletal disease manifestations in spondyloarthritis deserves renewed scrutiny in light of the data of Sherlock *et al.*[7]. Similarly, the functional impact (and directionality) of disease-associated IL-23R polymorphisms in ankylosing spondylitis requires better characterization. Given the wide distribution of innate cell lineages that express IL-23R[13], particularly in the gut, it is not clear why the relatively limited tissue distribution of the entheseal T cells would have emerged; this could suggest that additional regulatory loops operate in the enthesis and in mucosal tissues.

The model reported by Sherlock *et al.*[7] should also be useful in elucidating the molecular pathways that subserve new bone formation and inflammation and will allow dissection of these pathways to establish whether or not they are mutually dependent. Finally, we should recall that the mouse model system used by Sherlock *et al.*[7] does not fully recapitulate the human disease state in which HLA-B27 is clearly a crucial molecular determinant of pathology. By corollary, confirmatory studies in humans with spondyloarthritis will be essential.

Substantial unmet clinical needs remain in the treatment of ankylosing spondylitis and across the spondyloarthritis spectrum. Current therapeutics comprise nonsteroidal anti-inflammatory drugs and early intervention with inhibitors of tumor necrosis factor. The latter group of drugs has resulted in substantial improvements in the clinical symptoms and quality of life of people with spondyloarthritis but has not yet convincingly retarded the progression of disease at the level of bone structure. Therefore, new therapies for these diseases are urgently required. These therapies will probably arise from the elucidation of new pathogenetic pathways, which could then identify targets for intervention. There have been a limited number of clinical trials targeting the IL-23–IL-17 axis in spondyloarthritis, and such approaches have shown modest clinical benefits; these trials have focused mainly on strategies that neutralize IL-17. The data of Sherlock *et al.*[7] suggest that IL-23 mediates broader effects, operating beyond IL-17, and therefore the therapeutic utility of agents that block IL-23 or its receptor may be worthy of early exploration.

COMPETING FINANCIAL INTERESTS
The authors declare competing financial interests: details are available at http://www.nature.com/doifinder/10.1038/nm.2854.

1. Dougados, M. & Baeten, D. *Lancet* **377**, 2127–2137 (2011).
2. Thomas, G.P. & Brown, M.A. *Immunol. Rev.* **233**, 162–180 (2010).
3. Ranman, P. *et al. J. Rheumatol.* **36**, 137–140 (2009).
4. Duerr, R.H. *et al. Science* **314**, 1461–1463 (2006).
5. McGonagle, D. *et al. Ann. Rheum. Dis.* **61**, 534–537 (2002).
6. Benjamin, M. *et al. Arthritis Rheum.* **56**, 224–233 (2007).
7. Sherlock, J.P. *et al. Nat. Med.* **18**, 1069–1076 (2012)
8. May, E. *et al. J. Immunol.* **170**, 1099–1105 (2003).
9. Alonzo, E.S. & Sant'Angelo, D.B. *Curr. Opin. Immunol.* **23**, 220–227 (2011).
10. Colbert, R.A., DeLay, M.L., Klenk, E.I. & Layh-Schmitt, G. *Immunol. Rev.* **233**, 181–202 (2010).
11. Goodall, J.C. *et al. Proc. Natl. Acad. Sci. USA* **107**, 17698–17703 (2010).
12. Ciccia, F. *et al. Arthritis Rheum.* **60**, 955–965 (2009).
13. Cua, D.J. & Tato, C.M. *Nat. Rev. Immunol.* **10**, 479–489 (2010).

Mining the mechanisms of an HIV vaccine

Despite the existence of antiretroviral drugs that can combat HIV, it is thought that the development of an effective vaccine will be required to control the spread of this deadly virus. In 2009, the results from a phase 3 trial (RV144) of a vaccine consisting of a combination of a canarypox vector expressing HIV-1 immunogens and a recombinant HIV-1 envelope protein offered some hope, as the vaccine showed modest efficacy in preventing HIV-1 infection (31.2%) in a Thai population. Barton Haynes *et al.*[1] have now performed a case-control analysis to investigate the immune correlates of protection provided by this vaccine. They found that IgG antibody binding of the variable regions 1 and 2 (V1 and V2) of the HIV-1 envelope (Env) glycoprotein 120 inversely correlated with the rate of HIV-1 infection, and plasma IgA antibody binding to Env directly correlated with the rate of infection. We asked three experts to comment on how these results affect our understanding of immune-mediated protection from HIV and how they might be used to design future vaccine strategies against this virus.

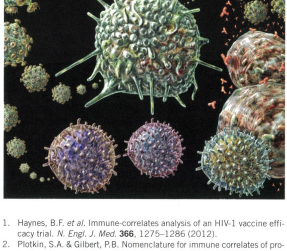

Ronald Kuhlney / Photo Researchers, Inc.

Stanley A Plotkin

In view of the initial opposition by distinguished scientists to the trial, RV144 was a triumph of hope over skepticism, if I may paraphrase Samuel Johnson. Not only did it show some level of efficacy against acquisition of HIV, but also it gave us clues regarding the mechanistic correlates of protection against HIV[2]. As the correlate identified was a non-neutralizing antibody[1], the trial showed that protection against viruses is not always mediated by neutralizing antibodies, or for that matter by cellular immune responses, despite the ability of the latter to control replication after

> "The trial showed that protection against viruses is not always mediated by neutralizing antibodies, or for that matter by cellular immune responses."

acquisition of a virus. Undoubtedly, the entry of viruses into cells is often complex, involving multiple receptors[3], and the identified utility of antibodies against the V1–V2 loops of HIV glycoprotein does not exclude the possible additional value in designing future vaccine strategies that elicit broadly neutralizing antibodies against other parts of the glycoprotein that mediate attachment and entry or that can stimulate effector CD8$^+$ T

Harriet L Robinson

Efficacy trial results have generated seismic shifts on the path to an HIV vaccine. In 2003, antibody elicited by gp120, which mediates binding of HIV to cells, failed to protect against viral acquisition. In 2007, cytotoxic T cells, which recognize and kill infected cells, also failed to protect. And then, in 2009, in the RV144 trial conducted in Thailand, the first protection, albeit modest, was achieved by a vaccine that had been scorned for its potential to elicit protective immune responses[6,7].

> "Further identification of targets, coupled with passive transfers of mixtures of monoclonal antibodies that bind these targets, are now needed."

Now, a collaborative report involving 43 authors identifies two vaccine-elicited correlates of risk for RV144 participants[1]. The first, IgG directed against a scaffolded V1–V2 region of the HIV envelope (Env), correlated inversely with risk of infection; whereas the second, monomeric Env-specific IgA, correlated directly with risk of infection. The V1–V2-targeting IgG did not have

1. Haynes, B.F. *et al.* Immune-correlates analysis of an HIV-1 vaccine efficacy trial. *N. Engl. J. Med.* **366**, 1275–1286 (2012).
2. Plotkin, S.A. & Gilbert, P.B. Nomenclature for immune correlates of protection after vaccination. *Clin. Infect. Dis.* **54**, 1615–1617 (2012).
3. Grove, J. & Marsh, M. The cell biology of receptor-mediated virus entry. *J. Cell Biol.* **195**, 1071–1082 (2011).
4. Walker, L.M. & Burton, D.R. Rational antibody-based HIV-1 vaccine design: current approaches and future directions. *Curr. Opin. Immunol.* **22**, 358–366 (2010).
5. Hansen, S.G. *et al.* Profound early control of highly pathogenic SIV by an effector memory T-cell vaccine. *Nature* **473**, 523–527 (2011).
6. Rerks-Ngarm, S. *et al.* Vaccination with ALVAC and AIDSVAX to prevent HIV-1 infection in Thailand. *N. Engl. J. Med.* **361**, 2209–2220 (2009).
7. Burton, D.R. *et al.* Public health. A sound rationale needed for phase III HIV-1 vaccine trials. *Science* **303**, 316 (2004).
8. Burton, D.R. *et al.* Limited or no protection by weakly or nonneutralizing antibodies against vaginal SHIV challenge of macaques compared with a strongly neutralizing antibody. *Proc. Natl. Acad. Sci. USA* **108**, 11181–11186 (2011).
9. Doria-Rose, N.A. *et al.* HIV-1 neutralization coverage is improved by combining monoclonal antibodies that target independent epitopes. *J. Virol.* **86**, 3393–3397 (2012).
10. Gilbert, P.B. *et al.* Correlation between immunologic responses to a recombinant glycoprotein 120 vaccine and incidence of HIV-1 infection in a phase 3 HIV-1 preventive vaccine trial. *J. Infect. Dis.* **191**, 666–677 (2005).
11. Rerks-Ngarm, S. *et al.* Vaccination with ALVAC and AIDSVAX to prevent HIV-1 infection in Thailand. *N. Engl. J. Med.* **361**, 2209–2220 (2009).

cells capable of killing the earliest infected cells[4,5].

Host protection against the acquisition of a virus can thus be influenced by multiple factors, some of which were illustrated in RV144. For example, efficacy seemed to be lower in higher-risk vaccinees, illustrating the importance of challenge dose and frequency of exposure, and efficacy waned with time, emphasizing the need for durable effector functions in a vaccine that is designed to protect over years of viral exposure. The as yet unexplained interference by plasma IgA antibodies in the efficacy of the vaccine tested in RV144 (ref. 1), whether due to these antibodies themselves or whether they act as a surrogate for some other immune marker, illustrates the complexity of protection. Notably, vaccination with the HIV envelope glycoprotein gp120 alone in the past did not elicit protective responses, and it is becoming imperative to define the mechanisms by which heterologous prime-boost regimens are more immunogenic than homologous boosts. Nevertheless, the way is now open to improve antibody responses to multiple portions of this HIV glycoprotein through new constructs, additional vaccine doses or better adjuvants.

Emeritus Professor of Pediatrics, University of Pennsylvania, Philadelphia, Pennsylvania, USA, and Vaxconsult, Doylestown, Pennsylvania, USA.

COMPETING FINANCIAL INTERESTS
The author declares competing financial interests: details are available at http://www.nature.com/doifinder/10.1038/nm.2858.

neutralizing activity and thus implied that non-neutralizing IgG was mediating prevention of acquisition, a new and fresh concept for HIV vaccine development.

Interestingly, the IgA correlate identified by these authors corroborates the IgG correlate if one hypothesizes that monomeric serum IgA was competing for binding with non-neutralizing, yet protective, IgG. IgG and IgA have distinct Fc regions that bind to different Fc receptors and immune molecules, such as complement proteins, to mediate the recognition of opsonized particles, lysis of cells and degranulation of effector immune cells. Thus, the correlation with reduced risk of infection for binding of IgG, but not monomeric IgA, suggests that protective non-neutralizing activities were being mediated by interactions of the Fcγ region of bound IgG, but not the Fcα region of bound IgA, with physiological effectors.

Not all targets for the binding of non-neutralizing IgG are protective. Currently, two targets have shown some protective activity against HIV: the scaffolded V1–V2 region in the RV144 vaccine trial and the conserved immunodominant region of the gp41 subunit of Env[8]. A trend for the protective potential of the latter was shown in preclinical passive-transfer studies. Further identification of targets, coupled with passive transfers of mixtures of monoclonal antibodies that bind these targets[9], are now needed to test whether non-neutralizing activities of IgG can be moved from a correlate of risk to a correlate for protection for HIV vaccines.

Chief Scientific Officer, GeoVax, Smyrna, Georgia, USA.

COMPETING FINANCIAL INTERESTS
The author declares competing financial interests: details are available at http://www.nature.com/doifinder/10.1038/nm.2858.

Miles P Davenport

A follow-up study of the RV144 HIV vaccine trial has suggested that antibody binding to the virus may protect against infection[1]. As the authors note, the statistical approach was designed to generate hypotheses, not rigorously demonstrate association, and this study is more about finding a correlate of risk of infection rather than a clear cause of protection. The results imply that HIV-binding antibodies may reduce the risk of HIV infection, perhaps through new mechanisms such as antibody-dependent cell-mediated cytotoxicity. Although serum concentrations of HIV-binding IgG antibodies were associated with decreased infection by the virus, HIV-specific serum IgA antibodies (usually associated with mucosal immunity) seemed to negate this protection. This observation is reminiscent of the results of the original trial of an HIV gp120 immunogen (one of the components of this vaccine), where high levels of antibody may have been protective but the impact of this on overall protection was negated by the fact that low levels of antibody may have increased infection in immunized individuals[10].

"Skeptics of large HIV vaccine trials may remain unconvinced, as doubts remain over the original trial's marginally significant (and modest) protection."

Skeptics of large HIV vaccine trials may remain unconvinced, as doubts remain over the original trial's marginally significant (and modest) protection (31% efficacy, $P = 0.04$), which was only seen with a 'modified intention-to-treat' statistical analysis[11]. However, advocates of HIV vaccine trials may suggest that this study provides robust support for the partial efficacy observed in the RV144 trial and that the next step is to find HIV vaccines that induce high IgG and low IgA antibody responses. It is important to remember that the immunized individuals did not receive the alternative of either an IgA-inducing vaccine or an IgG-inducing vaccine. They all received the same vaccine and responded in different ways. Therefore, the IgA effect might result from IgA 'blocking' of IgG binding, or, alternatively, a propensity to produce IgA-biased responses may be a marker of mucosal immune activation. Understanding the antiviral mechanisms of IgG-binding antibodies and the host factors that led to high IgA levels may be a helpful first step in both validating the results of this analysis and moving the HIV vaccine field forward.

Professor of Medicine, Centre for Vascular Research, Faculty of Medicine, University of New South Wales, Sydney, New South Wales, Australia.

COMPETING FINANCIAL INTERESTS
The author declares no competing financial interests.

Untuning the tumor metabolic machine

Several decades of scientific observations followed by years of basic and now clinical research support the notion that the metabolic power of tumor cells can provide the long-desired Achilles' heel of cancer. Yet many questions remain as to what defines the true metabolic makeup of a tumor and whether well-known factors and pathways involved in metabolic signaling act as tumor suppressors or oncogenes. In 'Bedside to Bench', Kıvanç Birsoy, David M. Sabatini and Richard Possemato discuss how retrospective studies of diabetic individuals with pancreatic cancer treated with the antidiabetic drug metformin point to a possible anticancer effect for this drug. Further research will need to discern whether this drug acts at the organismal level or by directly targeting the power plant of tumor cells. In 'Bench to Bedside', Regina M. Young and M. Celeste Simon peruse the complex function of a key metabolic factor that mediates the cell's response to low oxygen levels, often found in tumors. This hypoxia-inducible factor (HIF) comes in two flavors, which can be either tumor promoting or tumor suppressive, depending on the type of cancer. Because of this, the therapeutic use of HIF inhibitors must proceed with caution. Further defining the relationship between metabolic regulation of HIF and tumor progression may open up new diagnostic tools and treatments.

■ BEDSIDE TO BENCH

Targeting cancer metabolism: a bedside lesson

Kıvanç Birsoy, David M Sabatini & Richard Possemato

The decades-old observation that most tumors have an elevated glucose consumption rate compared to normal tissues has received renewed attention in the laboratory as scientists have come to appreciate that altered cancer metabolism is a hallmark of the transformed state[1]. Metabolic enzymes act as tumor suppressors, such as the Krebs cycle enzymes fumarate hydratase and succinate dehydrogenase, which are mutated in hereditary leiomyomatiosis and renal cell cancer and in hereditary paraganglioma and pheochromocytoma, respectively[2]. But mutations can also confer oncogenic capacity to metabolic enzymes, such as isocitrate dehydrogenase 1 (IDH1) or IDH2, driving subtypes of brain cancer and acute myeloid leukemia[3].

Unexpectedly, essential metabolic pathways, such as the serine biosynthetic pathway, are activated by gene amplification or epigenetic changes in estrogen receptor–negative breast cancer, and, surprisingly, essential metabolites such as glycine are highly consumed in rapidly proliferating cancer cells[4,5]. Finally, well-established cancer-relevant pathways, such as the RAS/AKT and mTOR (mammalian target of rapamycin) cascades, and transcription factors, including *c-myc* and HIF, can exert substantial influence over glucose uptake, glycolysis, glutaminolysis, fatty acid oxidation and respiration[6].

The increased glucose consumption of tumors has long been exploited by clinicians through monitoring tumor uptake of a fluorine radioisotope of glucose by positron emission tomography (FDG-PET). This technique has been used to stage cancer, identify metastatic sites and monitor treatment effectiveness. Furthermore, the initial degree of FDG-PET positivity has been correlated to overall patient outcome across cancer types, and can vary by cancer subtype[7]. However, a full characterization of the metabolic phenotype of cancer is still in its initial stages, and recent basic research findings have not yet been translated in the clinic. Yet, traditional chemotherapeutics such as fluorouracil, methotrexate and gemcitabine indeed inhibit metabolic enzymes, indicating that targeting cancer metabolism has clinical potential.

Therapies targeting cancer metabolism typically target either the metabolic state of the organism—such as through caloric restriction[8], ketogenic diets[9] and modulation of circulating nutrient levels through enzymes such as asparaginase[10]—or target the altered metabolism of the tumor itself—such as with 2-deoxyglucose, a glucose mimetic and hexokinase-competitive inhibitor, and 3-bromopyruvic acid, a putative glycolytic inhibitor, in addition to those mentioned above[11]. With the exception of asparaginase, a drug approved for childhood acute lymphoblastic leukemia for decades, the other approaches have shown promise in limiting tumor growth in animal models but have considerable hurdles to overcome before becoming approved therapies.

Surprisingly, several recent retrospective studies have shown in a wide variety of cancer types the substantial antitumor effects of the US Food and Drug Administration–approved antidiabetic drug metformin[12,13]. For example, a retrospective study of diabetic individuals with pancreatic cancer, of whom 117 had received metformin and 185 had not, analyzed the correlation of metformin use with survival and showed an increase in 2-year survival from 15.4% in the control group to 30.1% in the group taking metformin[12]. These studies demonstrate that targeting energy sensing and use may be a viable anticancer strategy and provide basic researchers with some clues for improving upon such strategies, including a potential role of metformin in directly targeting the mitochondria of cancer cells[14].

Centuries before biguanides, such as metformin, became routinely prescribed for diabetes, the French lilac *Galega officinalis* was known to contain an agent that reduced the frequent urination associated with this disease (**Fig. 1**)[15]. It was only in the 1920s that the active ingredient in the French lilac, guanidine, was isolated, nucleating the biguanide class of drugs. Much of the basic research on biguanides since then has focused on their ability to suppress liver gluconeogenesis, which is believed to occur through activation

Kıvanç Birsoy, David M. Sabatini and Richard Possemato are at the Whitehead Institute for Biomedical Research, Cambridge, Massachusetts, USA, the Department of Biology, Massachusetts Institute of Technology (MIT), Cambridge, Massachusetts, USA, the Howard Hughes Medical Institute, MIT, Cambridge, Massachusetts, USA, the Broad Institute, Cambridge, Massachusetts, USA, and The David H. Koch Institute for Integrative Cancer Research at MIT, Cambridge, Massachusetts, USA.
e-mail: posse@wi.mit.edu

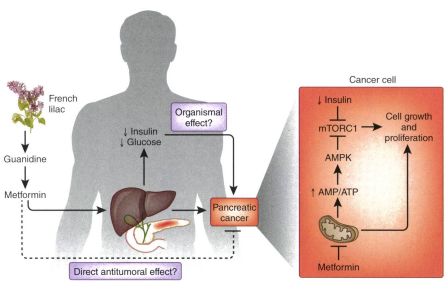

Kelly Vogel

Figure 1 Potential effects of metformin on tumor growth. Metformin is of the biguanide class of compounds, modeled after guanidine derivatives first isolated from the French lilac *G. officinalis*. This drug has a well-established role in suppressing hepatic gluconeogenesis, thereby ameliorating hyperglycemia in individuals with type 2 diabetes, but new studies are beginning to unearth a role for metformin in suppressing cancer progression. It is still unclear whether this is by direct action of the drug on the cancer cells themselves or through an indirect effect on organismal metabolism.

of hepatic AMP-activated protein kinase (AMPK) signaling[16], as biguanides achieve elevated levels in the liver compared to other tissues due to the specific expression of the OCT1 transporter in this organ.

AMPK is itself involved in a cancer-relevant signaling pathway as a downstream target of the STK11 tumor suppressor (also known as LKB1), which is inactivated in Peutz-Jaegers syndrome, a disease characterized by hamartomatous polyps of the intestine as well as an overall increased cancer risk[17]. Interestingly, most inherited syndromes characterized by hamartomatous polyps impinge upon upstream inhibitors of the mTOR complex 1 (mTORC1) pathway[18], including tuberous sclerosis (involving *TSC1* or *TSC2* mutation), the PTEN-hamartoma tumor syndromes (mutation in *PTEN*), neurofibromatosis (mutation in *NF1* or *NF2*) and perhaps also Birt-Hogg-Dubé syndrome (mutation in *FLCN*). mTORC1, a major intracellular nutrient sensor, regulates various cellular processes including protein synthesis, autophagy and ribosomal biogenesis that collectively affect cell growth, and mTORC1 activation has been suggested as a common link for diseases of this type.

Therefore, there is substantial evidence that activation of AMPK by metformin could exert an antitumor effect through modulating the AMPK/mTOR pathways. However, metformin fails to activate AMPK directly using *in vitro* kinase assays[19]. As such, the prevailing view is that this drug class indirectly acts on AMPK by causing an elevated cellular AMP/ATP ratio, which activates the AMPK pathway. Indeed, several recent studies showed metformin to inhibit mitochondrial oxidative phosphorylation[14], a major ATP source in most cells, which would explain its ability to activate AMPK.

Understanding how the organismal and cell-autonomous effects of biguanides translate into an anticancer effect will be important for using these drugs as chemotherapeutics; however, there are several potential mechanisms explaining the anticancer effects of metformin. One potential indirect mechanism is the modulation of circulating insulin levels, as many tumors are driven by insulin receptor signaling, and such tumors can be sensitive to metformin treatment[20]. But, in the retrospective study by Sadeghi *et al.*[12], metformin exerts an antitumor effect on pancreatic cancer regardless of concomitant insulin treatment. As such, the organismal effects of metformin on insulin signaling, as well as other potential organismal effects, will require further evaluation.

In support of a direct effect on mitochondrial oxidative phosphorylation in cancer cells, metformin has been shown to inhibit cancer cell proliferation *in vitro* and *in vivo* in numerous studies. However, it does so *in vitro* only at high doses that might not be achievable *in vivo* in a tumor, arguing that the observed *in vivo* effect is actually indirect. Furthermore, the glycolytic nature of tumors argues against the efficacy of a mitochondrial inhibitor, as cancer cells might derive most of their energy from glycolysis. Nevertheless, recent studies have shown that substantial mitochondrial glucose oxidation occurs in glioblastoma models *in vivo* and *in vitro*[21]. Whereas the importance of mitochondrial glucose oxidation to the tumor has yet to be fully investigated, its suppression may be linked to increased reactive oxygen species production, a loss of mitochondrial membrane potential, energy crisis due to ATP depletion, decreased citric acid cycle function or activation of the AMPK pathway directly in the tumor. Therefore, a thorough analysis of the metabolic state of tumors in animal models or in patients with cancer treated with metformin will be necessary for understanding whether metformin has a direct effect on cancer cells and whether this effect underlies the observed clinical response.

It is unclear whether the efficacy of metformin will be limited to individuals with both diabetes and cancer. Ongoing prospective studies using metformin in nondiabetics will elucidate whether the anticancer effects of metformin also occur in individuals with normal glucose homeostasis. Regardless, the current successes in the clinic are a signal to investigators that mitochondrial inhibition, be it in the liver or the tumor, may inhibit tumor growth and should provide guidance for future laboratory research.

COMPETING FINANCIAL INTERESTS
The authors declare no competing financial interests.

1. Ward, P.S. & Thompson, C.B. *Cancer Cell* **21**, 297–308 (2012).
2. Eng, C., Kiuru, M., Fernandez, M.J. & Aaltonen, L.A. *Nat. Rev. Cancer* **3**, 193–202 (2003).
3. Dang, L., Jin, S. & Su, S.M. *Trends Mol. Med.* **16**, 387–397 (2010).
4. Possemato, R. *et al. Nature* **476**, 346–350 (2011).
5. Jain, M. *et al. Science* **336**, 1040–1044 (2012).
6. DeBerardinis, R.J., Lum, J.J., Hatzivassiliou, G. & Thompson, C.B. *Cell Metab.* **7**, 11–20 (2008).
7. Sanli, Y. *et al. Ann. Nucl. Med.* **26**, 345–350 (2012).
8. Kalaany, N.Y. & Sabatini, D.M. *Nature* **458**, 725–731 (2009).
9. Seyfried, B.T., Kiebish, M., Marsh, J. & Mukherjee, P. *J. Cancer Res. Ther.* **5** Suppl 1, S7–S15 (2009).
10. Broome, J.D. *Cancer Treat. Rep.* **65** Suppl 4, 111–114 (1981).
11. Pelicano, H., Martin, D.S., Xu, R.H. & Huang, P. *Oncogene* **25**, 4633–4646 (2006).
12. Sadeghi, N., Abbruzzese, J.L., Yeung, S.C., Hassan, M. & Li, D. *Clin. Cancer Res.* **18**, 2905–2912 (2012).
13. Decensi, A. *et al. Cancer Prev. Res. (Phila.)* **3**, 1451–1461 (2010).
14. Buzzai, M. *et al. Cancer Res.* **67**, 6745–6752 (2007).
15. Bailey, C.J. & Turner, R.C. *N. Engl. J. Med.* **334**, 574–579 (1996).
16. Zhou, G. *et al. J. Clin. Invest.* **108**, 1167–1174 (2001).
17. Shaw, R.J. *et al. Proc. Natl. Acad. Sci. USA* **101**, 3329–3335 (2004).
18. Clark, R.A. & Pavlis, M. *J. Invest. Dermatol.* **129**, 529–531 (2009).
19. Hawley, S.A., Gadalla, A.E., Olsen, G.S. & Hardie, D.G. *Diabetes* **51**, 2420–2425 (2002).
20. Schneider, M.B. *et al. Gastroenterology* **120**, 1263–1270 (2001).
21. Marin-Valencia, I. *et al. Cell Metab.* **15**, 827–837 (2012).

■ BENCH TO BEDSIDE

HIF-α: pro- and antitumorigenic?

Regina M Young & M Celeste Simon

Solid tumors contain regions of oxygen (O_2) and nutrient limitation resulting from their structurally and functionally abnormal vasculature and the rapid proliferation of cancer cells. The major transcriptional response to hypoxia is mediated by hypoxia-inducible factors (HIFs), which stimulate the expression of hundreds of genes that promote cellular adaptation to low O_2. Some of the HIF target genes regulate processes involved in tumorigenesis, such as increased glucose uptake and glycolysis, angiogenesis, invasion, metastasis and radiation resistance. Furthermore, a number of common oncogenic drivers, such as mTORC1 and Ras, enhance HIF activity.

HIFs function as heterodimers, composed of stable β-subunits and O_2-sensitive α-subunits, which accumulate upon O_2 deprivation. In normal O_2 conditions, HIF-αs are modified by metabolically regulated prolyl hydroxylases (PHDs), leading to physical interactions between HIF-α subunits and the von Hippel-Lindau (VHL)-associated E3 ubiquitin ligase, resulting in rapid HIF-α turnover. Two well-characterized isoforms of the α-subunit, HIF-1α and HIF-2α, have both overlapping functions as well as divergent and even antagonistic roles in hypoxic responses[1]. High HIF-1α and HIF-2α protein amounts in diagnostic tumor biopsies are correlated with poor prognosis in cancers of the bladder, brain, breast, colon, cervix, endometrium, head and neck, lung, ovary, pancreas, prostrate, rectum and stomach[2]. These studies strongly support the development of pharmacological HIF inhibitors for cancer treatment.

Two recent studies, however, suggest that HIFs are not universally tumor promoting[3,4]. In clear-cell renal carcinoma, the most common form of kidney cancer, the *VHL* tumor suppressor gene is often inactivated, leading to constitutive expression HIF-1α, HIF-2α or both. Considerable evidence shows a primary role for HIF-2α in promoting VHL-deficient renal cancers[1]; moreover, *EPAS1* (encoding HIF-2α) polymorphisms are linked to renal carcinoma[5]. However, loss of chromosome 14q, which spans the *HIF1A* locus, is a frequent event in clear cell carcinoma and a poor diagnostic indicator[3]. Furthermore, *HIF1A*—but not neighboring genes—is subject to focal deletions. These data suggest that *VHL* mutations lead to the initial activation of both oncogenic HIF-2α and tumor-suppressive HIF-1α, but subsequent loss of HIF-1α activity through 14q deletion or *HIF1A* truncations leads to a more aggressive form of VHL-deficient renal cell carcinoma[3]. The divergent effects of HIF-1α and HIF-2α seen on renal cell carcinoma have been linked to their opposing effects on c-Myc transcriptional activity; HIF-2α promotes hypoxic cell cycle progression, whereas HIF-1α antagonizes c-Myc–mediated cell cycle progression[1].

HIF-1α also seems to have a tumor suppressive role in gliomas with mutations in isocitrate dehydrogenases 1 and 2 (encoded by *IDH1* and *IDH2*)[4]. These enzymes, which catalyze the conversion of isocitrate to 2-oxoglutarate (2-OG , also known as α-ketoglutarate), are frequently mutated in lower-grade gliomas (more than 70%, grades 2 and 3) and less often in glioblastomas, leukemias and chondrosacrcomas. Mutations in *IDH1* and *IDH2* are confined to the active site and result in the production of a neomorphic metabolite 2-hydroxyglutarate (2HG)—normally found in scarce amounts—through the NADPH-dependent reduction of 2-OG to the *R* enantiomer of 2HG (ref. 6) (**Fig. 1**). This oncometabolite is thought to promote tumorigenesis by influencing several dioxygenases that use 2-OG as a substrate, which include the HIF PHDs[7].

Three papers in a recent issue of *Nature* explore in more detail how the buildup of 2HG resulting from *IDH1/2* mutations contributes to glioma[4,8,9]. Two studies provide further support for the role of *IDH1/2* mutations, and the consequential accumulation of 2HG, in aberrant methylation[8,9]. In the first study, Lu *et al.*[8] show

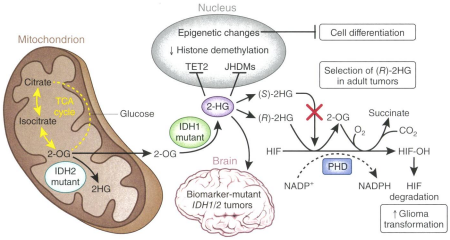

Figure 1 A model for how 2HG promotes glioma transformation. Tumors bearing mutations in *IDH1/2* accumulate high amounts of the metabolite (*R*)-2HG. The role of this oncometabolite in cellular transformation may be linked to its ability to substitute for 2-OG as a cosubstrate for HIF PHDs with the production of succinate through a 2-OG intermediate. High levels of cellular 2HG are hypothesized to drive the hydroxylation of HIF-α, leading to decreased HIF expression and increased glioma transformation. This reaction is specific to the (*R*)-2HG enantiomer, which may explain the selection for (*R*)-2HG as opposed to (*S*)-2HG in adult tumors. In addition, the buildup of 2HG in *IDH1*- and *IDH2*- mutated cells has been linked to epigenetic changes through the inhibition of TET2 and JHDMs. Finally, increased levels of 2HG can be detected noninvasively by magnetic resonance spectroscopy (MRS). Detection of 2HG by MRS has important prognostic value, as *IDH1*- and *IDH2*-mutated tumors are associated with improved survival in glioma-bearing patients.

Regina M. Young and M. Celeste Simon are at the Abramson Family Cancer Research Institute, University of Pennsylvania, Philadelphia, Pennsylvania, USA. Regina M. Young is also in the Department of Cancer Biology, Perelman School of Medicine, University of Pennsylvania, Philadelphia, Pennsylvania, USA. M. Celeste Simon is also at the Howard Hughes Medical Institute, Perelman School of Medicine, University of Pennsylvania, Philadelphia, Pennsylvania, USA.
e-mail: celeste2@mail.med.upenn.edu

that cell-permeable 2HG blocks the *in vitro* differentiation of fibroblast-like cells to adipocytes and increases repressive histone methylation[8]. Furthermore, this block in adipocyte differentiation can be mimicked by siRNA-mediated repression of KDM4C, a histone H3 lysine 9–specific Jumonji-C domain histone demethylase (JHDM). Whereas Turcan *et al.*[9] found that the introduction of mutated *IDH1* into human primary astrocytes progressively remodeled the methylome to mirror the CpG island methylator phenotype observed in low grade gliomas. In contrast, Koivunen *et al.*[4] exploited the fact that 2HG accumulates in an enantiomer-specific manner in *IDH* mutant brain tumors to explain how transformation occurs[4].

Consistent with previous studies, 2HG accumulation inhibits 2-OG–dependent enzymes *in vitro*, including the tet methyl cytosine hydroxylases (TETs), JMJD2D histone demethylases and HIF PHDs. But the *S* enantiomer of 2HG is a more potent inhibitor than the *R* enantiomer for these enzymes[4]. In fact, at tumor-relevant concentrations, (*R*)-2HG was not an effective inhibitor of PHD; instead, it promoted PHD activity while sparing other 2-OG–dependent enzymes. Koivenen *et al.*[4] monitored the *in vitro* hydroxylation of HIF by PHD2 and observed the production of 2-OG and succinate when catalytically active PHD2 was incubated with (*R*)-2HG and HIF-1α polypeptide (**Fig. 1**). Furthermore, modeling studies predict that binding of (*S*)-2HG to PHD2 would not allow O_2 to enter the active site and therefore would block HIF degradation. Collectively, these results suggest that (*R*)-2HG—but not (*S*)-2HG—can substitute for 2-OG as a cosubstrate in the hydroxylation of HIF-1α and HIF-2α and, in this manner, promote their degradation.

What is the *in vivo* relevance of this phenotype? In midpassage immortalized human astrocytes expressing wild-type or mutant $IDH1^{R132H}$ (the most common IDH1 mutation in gliomas), HIF-1α and HIF-2α amounts were shown to decrease upon expression of mutant IDH relative to the wild-type enzyme, and HIF-1α abundance decreased in mutant IDH1–expressing oligodendroglioma and HCT116 cell lines. In addition, the HIF-responsive gene expression signature in proneural tumors with *IDH1* mutations was attenuated relative to *IDH* wild-type lesions. Finally, downregulation of HIF-1α or overexpression of PHD2 promoted growth of human immortalized astrocytes in soft agar. Conversely, decreased amounts of PHD2 inhibited astrocyte proliferation.

Accumulation of (*R*)-2HG therefore leads to reduced HIF-1α expression and pathogenesis of *IDH1*-mutated gliomas. This finding is not inconsistent with (*R*)-2HG also affecting other 2-OG–dependent enzymes, such as TET2 and JHDMs, but it might explain the selection for (*R*)-2HG as opposed to (*S*)-2HG in human adult tumors. Interestingly, Li *et al.*[10] have previously shown that HIF-2α is preferentially expressed in glioma stem cells, and high HIF-2α mRNA levels are associated with poor survival of individuals with glioma. In GSCs, both HIF-1α and HIF-2α were observed to promote self-renewal, proliferation and survival. Although the results from Li *et al.*[10] and Koivunen *et al.*[4] seem contradictory, they may indicate that distinct neural populations—low-grade *IDH1*-mutated gliomas and GSCs—respond differently to alterations in HIF activity. However, it would be interesting to know whether downregulation of HIF-2α inhibits the soft-agar growth of *IDH1*-mutated immortalized astrocytes.

Whether HIF is tumor promoting or inhibitory is complex. In some tumor types, the pro- or antitumorigeneic effects of HIF-α are isoform specific; for example, in VHL-deficient renal cell carcinoma, HIF-2α is tumor promoting and HIF-1α is tumor inhibitory[3]. This is partially because HIF-1α and HIF-2α can regulate unique downstream targets and interact with important oncogenes and tumor suppressors, such as MYC and p53, in an isoform-specific manner[1]. In addition, inappropriate levels of HIF activity may be an important determinant in tumor growth. For example, whereas HIF-2α overexpression contributes to the progression of non–small-cell lung cancer, inhibition of HIF-2α can, paradoxically, promote growth of the same tumor type[11]. Consequently, any discussion of using pharmacological inhibitors of the HIF-PHD pathway as a potential therapeutic strategy must be laced with caution.

When and how to employ HIF inhibitors in the treatment of cancer is under intense investigation; however, the accumulation of 2HG upstream of decreased HIF accumulation in *IDH1/2*-mutated cells opens up the potential for new diagnostic tools in the clinical evaluation of individuals with brain tumors. A recent study of patients with glioma undergoing magnetic resonance imaging revealed that this noninvasive test, routinely used in the clinic, can reliably detect the presence or absence of 2HG within brains[12]. This information has prognostic value because *IDH1/2*-mutated tumors are associated with improved patient survival among those harboring gliomas. In addition, it is possible that 2HG levels can be followed over time to monitor glioma progression, detect recurrent disease and evaluate patient response to chemotherapy.

Human genetic mutations can reprogram metabolism to promote tumor formation and progression. Notably, there are many examples where genetic alterations in metabolic pathways affect HIF-α activity and downstream cellular transformation[1,4,7]. A deeper understanding of the intersections between tumor-potentiating genetic mutations and their metabolic consequences promises new advances in cancer therapy.

COMPETING FINANCIAL INTERESTS
The authors declare no competing financial interests.

1. Keith, B., Johnson, R.S. & Simon, M.C. *Nat. Rev. Cancer* **12**, 9–22 (2012).
2. Semenza, G.L. *Cell* **148**, 399–408 (2012).
3. Shen, C. *et al. Cancer Discov.* **1**, 222–235 (2011).
4. Koivunen, P. *et al. Nature* **483**, 484–488 (2012).
5. Purdue, M.P. *et al. Nat. Genet.* **43**, 60–65 (2011).
6. Dang, L. *et al. Nature* **462**, 739–744 (2009).
7. DeBerardinis, R.J. & Thompson, C.B. *Cell* **148**, 1132–1144 (2012).
8. Lu, C. *et al. Nature* **483**, 474–478 (2012).
9. Turcan, S. *et al. Nature* **483**, 479–483 (2012).
10. Li, Z. *et al. Cancer Cell* **15**, 501–513 (2009).
11. Mazumdar, J. *et al. Proc. Natl. Acad. Sci. USA* **107**, 14182–14187 (2010).
12. Choi, C. *et al. Nat. Med.* **18**, 624–629 (2012).

■ CANCER

Notch plays the skin field

A recent report (*Cell* **149**,1207–1220) uncovers a role for the stromal compartment in skin carcinogenesis.

Skin cancer often appears in the form of field cancerization, a constellation of alterations in the epithelial and mesenchymal tissues that surround a tumorigenic lesion, and is likely to emerge from broad exposure to carcinogens such as sunlight. However, it was not known whether stromal changes could drive this widespread transformation process.

Bing Hu *et al.* investigated the contribution of the stroma to tumorigenesis in mice by inactivating the tumor-suppressive Notch signaling pathway in mesenchymal cells. Interestingly, when they aged, these mice developed spontaneous, multifocal squamous carcinomas of diverse cellular origin, which were infiltrated by inflammatory cells. The formation of these lesions could be prevented by anti-inflammatory drug treatment.

In further studies, the authors confirmed that mouse and human skin fibroblasts with dysfunctional Notch signaling could foster the neoplastic transformation of epithelial cells by a mechanism that involved increased transcriptional activation by AP-1 factors.

Importantly, the stroma surrounding human preneoplastic skin lesions showed similar alterations in Notch signaling to those in the authors' mouse model, and these changes could be induced by exposure to ultraviolet A radiation. These new results expand the protumorigenic role of the stroma that has previously been observed in other tissues such as the mammary gland and draw attention to the role of mesenchymal components as cancer drivers.—*VA*

■ IMMUNOLOGY

Unexpected effects

Foxp3 is a transcription factor that has a key role in the differentiation and function of regulatory T (T_{reg}) cells. Two recent studies report that a commonly used reporter *Foxp3* gene has unexpected effects in different mouse genetic backgrounds (*Immunity* **36**, 717–730; *Immunity* **36**, 731–741).

The *Foxp3*^{tm2Ayr} allele encodes Foxp3 joined to EGFP, allowing tracking of Foxp3-expressing T_{reg} cells *in vivo*. Jaime Darce *et al.* found that this allele reduced the severity of disease when expressed in a mouse model of inflammatory arthritis (the K/BxN model), but made the disease worse when expressed in a nonobese diabetes (NOD) mouse model. These effects seemed to be due to the increased binding of Foxp3-EGFP to insulin regulatory factor 4 (IRF4) and lowered binding to hypoxia-inducible factor 1α (HIF-1α), resulting in increased transcription of IRF4-regulated genes in T_{reg} cells and altered T_{reg} cell responses. The changes in T_{reg} cell responses may have differential effects on autoimmune diseases, depending on the underlying type of immunity, which may be different in diabetes and arthritis.

Similarly, Matthew Bettini *et al.* also observed acceleration of diabetes when *Foxp3*^{tm2Ayr} was expressed in a NOD model as well as impaired development of natural T_{reg} cells in the thymus and of induced T_{reg} cells in the periphery. They found that Foxp3-EGFP showed decreased binding to the histone acetyltransferase Tip60, histone deacetylase 7 and the transcription factor Eos. These changes altered the T_{reg} transcriptome, resulting in deficient T_{reg} cell responses.

These two studies show that the preservation of Foxp3 interactions with other regulatory proteins is necessary for the correct transcriptional program to be enacted in T_{reg} cells. Further investigations will be needed to examine whether disruption of interactions between Foxp3 and its binding partners may have affected the results of previous studies that used the *Foxp3*^{tm2Ayr} allele.—*MS*

MICROBIOLOGY

Friendly fungi

There's more than bacteria to the intestinal flora. According to a report in *Science* (336, 1314–1317), the gut contains indigenous fungi that interact with the immune system and may influence the course of bowel disease.

Previous studies had hinted at the existence of fungi in the gut flora. Following that lead, Iliyan Iliev *et al.* looked for fungal genetic material in the gut of mice and found evidence for the existence of over 100 different species.

As many fungal species interact with the innate immune receptor dectin-1, the team went on to study mice lacking this receptor to see whether they were differentially susceptible to inflammatory disease. In a model of chemically induced colitis, mice deficient for dectin-1 had worse disease, probably owing to an inability to keep the indigenous fungi in check.

These observations may be also relevant to humans, as the researchers identified a polymorphism in the gene for dectin-1 that is associated with a severe form of ulcerative colitis.—*JCL*

David M. Phillips / Photo Researchers, Inc.

■ CANCER

p53 functions under scrutiny

p53 has been thought to act as tumor suppressor by arresting the cell cycle and inducing apoptosis and senescence after stress. A new study in mice shows that other activities involving metabolic regulation and antioxidant function may be key in preventing cancer and that the different p53 responses are controlled by epigenetic modifications (*Cell* **149**, 1269–1283).

Tongyuan Li *et al.* mutated three different DNA acetylation sites in the *Tp53* gene

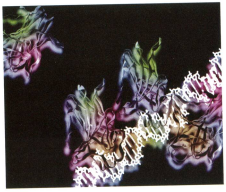

Kenneth Eward / BioGrafx / Photo Researchers, Inc.

that are involved in controlling the apoptotic, cell cycle arrest and senescence functions of p53. Cells and tissues from mice expressing this mutated p53 showed that the mutations abrogated these cellular functions in response to DNA damage, but, surprisingly, the animals were protected from lymphoma development. The expression of genes involved in modulating mitochondrial respiration and limiting glycolysis and oxidative damage were still induced by p53 in these mice, suggesting that p53 may prevent tumorigenesis by regulating metabolism.

Other, as yet unknown, p53 functions may be also involved in cancer suppression, and future research should aim to elucidate the exact antitumor effect of p53-mediated metabolic and antioxidant functions before new therapeutic approaches can be designed to modulate these tumor suppressor pathways.—*CP*

■ METABOLIC DISORDERS

A route to leanness

A population of hypothalamic neurons expressing the Agouti-related peptide (AgRP) has been shown to be important in the induction of feeding. Although the hormones leptin and insulin act on these neurons, knocking out either leptin or insulin signaling in AgRP neurons does not seem to affect energy homeostasis. Now, Hongxia Ren *et al.* show that disabling both these pathways in mice by knocking out a central transcriptional mediator, FoxO1, in AgRP neurons can improve metabolism, resulting in lean mice that eat less (*Cell* **149**, 1314–1326).

The researchers then performed microarray analyses of the AgRP hypothalamic neurons with or without FoxO1 and found that the G-coupled protein receptor Gpr17 was downregulated in FoxO1-deficient neurons. In cell culture studies, they found that FoxO1 directly bound the *Gpr17* gene and increased its expression. When they administered Gpr17 agonists into the brain ventricles of mice, this increased feeding. A Gpr17 antagonist decreased feeding, suggesting that targeting this pathway could be used to treat obesity in humans.—*EC*

■ INFECTIOUS DISEASES

Turning the tide against TB

Multidrug-resistant tuberculosis, accounting for nearly 5% of cases, is difficult and expensive to treat. A recent clinical trial reports positive results for a new drug, delamanid, in people with this form of tuberculosis (*N. Engl. J. Med.* **366**, 2151–2160).

Delamanid, an inhibitor of mycolic acid synthesis, has previously been shown to have antituberculosis activity in both *in vitro* and *in vivo* preclinical studies. Gler *et al.* tested delamanid at two doses in a randomized, placebo-controlled trial. A total of 321 patients with multidrug-resistant tuberculosis were treated with delamanid, as compared to 160 patients treated with placebo, with all patients receiving a background drug regimen. After 2 months of treatment, the two delamanid-treated groups had a higher proportion of sputum cultures that were negative for mycobacterial growth. However, a dose response was not observed. The drug seemed to be well tolerated, although it was associated with an effect on cardiac electrical activity—QT interval prolongation.

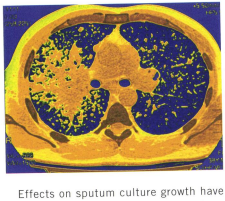

James Cavallini / Photo Researchers, Inc.

Effects on sputum culture growth have previously been associated with long-term outcomes of tuberculosis treatments, but longer clinical trials of delamanid will be needed. In addition, it will be important to determine how delamanid can be used most effectively in combination with other antituberculosis agents.—*MB*

Written by Victoria Aranda, Michael Basson, Eva Chmielnicki, Juan Carlos López, Carolina Pola and Meera Swami.

New from NPG

The mutational landscape of lethal castration-resistant prostate cancer
Grasso, C.S. *et al. Nature* doi:10.1038/nature11125 (20 May).

Exome sequencing identifies recurrent *SPOP*, *FOXA1* and *MED12* mutations in prostate cancer
Barbieri, C.E. *et al. Nat. Genet.* **44**, 685–689 (2012).

Two studies use exome sequencing to investigate the genetic basis of prostate cancer. Barbieri *et al.* identify recurrent mutations in multiple genes in prostate cancer, showing that *SPOP* contains the most frequent recurrent mutations. Grasso *et al.* define mutations in castration-resistant prostate cancer, suggesting a mechanism through which these cancers become resistant to antiandrogen therapy.

F-box protein FBXL19–mediated ubiquitination and degradation of the receptor for IL-33 limits pulmonary inflammation
Zhao, J. *et al. Nat. Immunol.* doi:10.1038/ni.2341 (3 June).

The cytokine IL-33 is important in lung inflammatory conditions such as asthma. The interaction between IL-33 and its receptor ST2L is shown to be regulated by an intracellular protein FBXL19, which binds and degrades ST2L. Therapeutic modulation of this axis might be one way to reduce lung inflammation.

Autism spectrum disorder susceptibility gene *TAOK2* affects basal dendrite formation in the neocortex
Calderon de Anda, F. *et al. Nat. Neurosci.* doi:10.1038/nn.3141 (10 June).

The authors find that the gene encoding thousand-and-one amino acid 3 kinase (TAOK2), which has been associated with susceptibility to autism spectrum disorders, is essential for dendrite morphogenesis. They also define a pathway involving TAOK2, neuropilin 1, semaphorin 3A and JNK that regulates the development of basal dendrites in the cortex.

Structural basis of evasion of cellular adaptive immunity by HIV-1 Nef
Jia, X. *et al. Nat. Struct. Mol. Biol.* doi:10.1038/nsmb.2328 (17 June).

The authors characterize the structure of a complex of the HIV-1 restriction factor Nef, the class I major histocompatibility complex and a subunit of the clathrin adaptor protein complex 1. This allowed them to show how Nef can modulate host membrane trafficking, enabling HIV-1 to evade the adaptive immune system.

REVIEW

nature medicine

Mechanisms of fibrosis: therapeutic translation for fibrotic disease

Thomas A Wynn & Thirumalai R Ramalingam

Fibrosis is a pathological feature of most chronic inflammatory diseases. Fibrosis, or scarring, is defined by the accumulation of excess extracellular matrix components. If highly progressive, the fibrotic process eventually leads to organ malfunction and death. Fibrosis affects nearly every tissue in the body. Here we discuss how key components of the innate and adaptive immune response contribute to the pathogenesis of fibrosis. We also describe how cell-intrinsic changes in important structural cells can perpetuate the fibrotic response by regulating the differentiation, recruitment, proliferation and activation of extracellular matrix–producing myofibroblasts. Finally, we highlight some of the key mechanisms and pathways of fibrosis that are being targeted as potential therapies for a variety of important human diseases.

Fibrosis is the final, common pathological outcome of many chronic inflammatory diseases. Although collagen deposition is an indispensable and, typically, reversible part of wound healing, normal tissue repair can evolve into a progressively irreversible fibrotic response if the tissue injury is severe or repetitive or if the wound-healing response itself becomes dysregulated. Fibrosis is defined by the excessive accumulation of fibrous connective tissue (components of the extracellular matrix (ECM) such as collagen and fibronectin) in and around inflamed or damaged tissue, which can lead to permanent scarring, organ malfunction and, ultimately, death, as seen in end-stage liver disease, kidney disease, idiopathic pulmonary fibrosis (IPF) and heart failure[1,2]. Fibrosis is also a major pathological feature of many chronic autoimmune diseases, including scleroderma, rheumatoid arthritis, Crohn's disease, ulcerative colitis, myelofibrosis and systemic lupus erythematosus. Fibrosis also influences tumor invasion and metastasis, chronic graft rejection and the pathogenesis of many progressive myopathies. Although fibrogenesis is becoming increasingly recognized as a major cause of morbidity and mortality in most chronic inflammatory diseases, there are few—if any—treatment strategies available that specifically target the pathogenesis of fibrosis.

Many distinct triggers can contribute to the development of progressive fibrotic disease. Examples include, to name just a few, inherited genetic disorders; persistent infections; recurrent exposure to toxins, irritants or smoke; chronic autoimmune inflammation; minor human leukocyte antigen mismatches in transplants; myocardial infarction; high serum cholesterol; obesity; and poorly controlled diabetes and hypertension[3]. Regardless of the initiating events, a feature common to all fibrotic diseases is the activation of ECM-producing myofibroblasts, which are the key mediators of fibrotic tissue remodeling[4,5]. For example, the left-ventricular hypertrophy that accompanies chronic hypertension is caused by an abnormal accumulation of collagen and other ECM components in the extracellular space. This reactive and progressive interstitial fibrosis contributes to myocardial stiffness and, ultimately, ventricular dysfunction, and it is believed to result from the persistent activation of cardiac myofibroblasts. Liver cirrhosis caused by chronic hepatitis C virus (HCV) infection, alcohol abuse or nonalcoholic steatohepatitis (NASH) is similarly induced by activated myofibroblasts[1]. In the liver, excessive collagen deposition distorts normal tissue architecture, leading to hepatocellular dysfunction and increased hepatic resistance to blood flow, which cause hepatic insufficiency and portal hypertension. Because ECM-secreting myofibroblasts are central to the pathogenesis of all fibrotic diseases, fibrosis research has focused on elucidating the molecular and immunological mechanisms that initiate, maintain and terminate the differentiation of quiescent fibroblasts into actively proliferating, ECM-producing myofibroblasts.

It is now clear that many elements of the innate and adaptive immune response participate in the differentiation and activation of fibroblasts (**Fig. 1**). In this Review, we describe some of the important mechanisms that contribute to the progression of fibrosis. We also present experimental findings from several different model systems, with the goal of identifying common pathways of fibrosis that could be targeted to facilitate the development of broadly effective antifibrotic drugs. Finally, we discuss some of the major obstacles in antifibrotic-drug development and highlight a few of the important pathways of fibrogenesis that have progressed to clinical testing.

Innate immunity and fibrosis

Acute inflammatory reactions play an important part in triggering fibrosis in many different organ systems. For example, in bleomycin-induced pulmonary fibrosis and carbon tetrachloride–induced liver

Immunopathogenesis Section, Program in Barrier Immunity and Repair, Laboratory of Parasitic Diseases, National Institute of Allergy and Infectious Diseases, National Institutes of Health, Bethesda, Maryland, USA. Correspondence should be addressed to T.A.W. (twynn@niaid.nih.gov).

Published online 6 July 2012; doi:10.1038/nm.2807

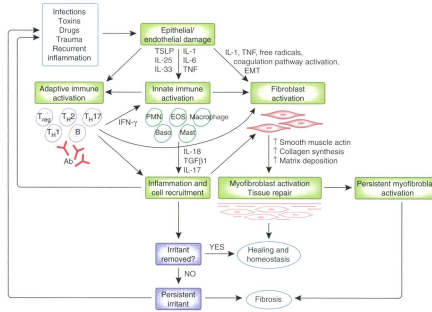

Figure 1 Overview of wound repair and fibrosis. Epithelial and/or endothelial damage caused by various insults triggers complex interconnected wound-healing programs to quickly restore homeostasis. The coagulation pathway, which functions to stem blood loss, is triggered first, followed by acute inflammation and activation of innate immune mediators such as resident macrophages, neutrophils and dendritic cells. Epithelial and innate immune cell–derived cytokines subsequently influence the activation of the adaptive immune response. The tissue damage can also directly activate the adaptive immune response. Inflammatory and immune mediators (cytokines, chemokines and free radicals) attempt to eliminate the inciting factor while activating the resident quiescent fibroblasts into myofibroblasts that orchestrate angiogenesis and production of ECM components. Failure to adequately contain or eliminate the inciting factors can exacerbate the inflammatory response and lead to a chronic wound-healing response, with continued tissue damage, repair and regeneration, ultimately resulting in fibrosis. TSLP, thymic stromal lymphopoietin; Ab, antibody; PMN, polymorphonuclear leukocyte; EOS, eosinophil; Baso, basophil; Mast, mast cell.

fibrosis, brief exposure to these drugs causes epithelial-cell apoptosis and hepatocyte necrosis, respectively, activating an inflammatory wound-healing response that can lead to a temporary excess in deposition of ECM components in the affected tissues[6,7]. Low-grade but persistent inflammation is also thought to contribute to the progression of fibrosis in cardiovascular disease and hypertension. Indeed, in many fibrotic disorders, a persistent inflammatory trigger is crucial to the activation of the wound-healing program that leads to fibrosis. Consequently, removal of the inflammatory trigger is the most straightforward way to halt the progression of tissue remodeling and allow the normal tissue architecture to be restored after injury, as has been observed in individuals with chronic hepatitis B infection who are treated with entecavir, a highly effective oral antiviral drug. This may be easy to accomplish when the tissue-damaging mechanism is known, but in many fibrotic disorders, the tissue-damaging irritant is either unknown or cannot be easily eliminated. In this case, researchers have focused on pinpointing the innate and adaptive mechanisms that control inflammation, with the goal of identifying key mediators that could be targeted to attenuate fibrosis.

Innate wound-healing mechanisms initiate the fibrotic response. The coagulation response is the first wound-healing mechanism activated after injury. When the endothelium is damaged, circulating platelets are activated upon encountering exposed collagen and von Willebrand factor in the subendothelial layer[8]. Coagulation factor II (prothrombin) is also proteolytically cleaved to form thrombin. Thrombin, in turn, functions as a serine protease that converts soluble fibrinogen into insoluble strands of fibrin, which helps platelets clump together to form the fibrin clot that ensures quick hemostasis. Activated platelets also release growth factors such as platelet-derived growth factor (PDGF), a potent chemoattractant for inflammatory cells, and transforming growth factor-β1 (TGF-β1), which stimulates ECM synthesis by local fibroblasts[9]. Consequently, any prolonged disturbance in the coagulation cascade can lead to fibrosis[10]. For example, a recent study demonstrated that activated coagulation factor X (FXa) contributes to fibrosis after acute lung injury by inducing myofibroblast differentiation[11]. The authors showed that bleomycin-induced pulmonary fibrosis could be inhibited in mice when FXa was neutralized. The coagulation response is also believed to be a major driver in the pathogenesis of liver fibrosis. In addition to its role in the coagulation cascade, thrombin can directly promote fibrosis by inducing production of chemokine (C-C motif) ligand 2 (CCL2) and by signaling through protease-activated receptors expressed on liver fibroblasts (hepatic stellate cells)[12]. In support of this hypothesis, antagonists of protease-activated receptor 1 and anticoagulant drugs have each been shown to protect against experimental liver fibrosis in mice[13,14]. However, although the coagulation cascade can be an important initiator of fibrosis, deficiencies in the clotting pathway have also been shown to contribute to fibrosis. Procoagulant deficiencies are common in patients with cirrhosis and portal hypertension. Here, obliterative lesions in the portal and hepatic veins develop in response to microthrombi, which cause tissue ischemia, endothelial-cell death and fibrosis through parenchymal extinction[15]. Together, these findings illustrate how disturbances in the coagulation cascade can substantially contribute to the development of progressive fibrotic disease.

Inflammatory myeloid cells have a role in fibrosis. In addition to activating the coagulation cascade, platelets and damaged epithelial and endothelial cells release a variety of chemotactic factors that recruit inflammatory monocytes and neutrophils to the site of tissue damage (**Fig. 2**). These circulating myeloid cells respond to a gradient of CCL2 and are recruited to damaged tissues, where they differentiate into macrophages that phagocytose the fibrin clot and cellular debris. ECM fragments, including hyaluronan, have also been shown to be important drivers of fibrosis by stimulating chemokine and proinflammatory cytokine production by inflammatory monocytes and macrophages[16]. Neutrophils are also recruited quickly after injury and participate in removal of tissue debris and the killing of invading bacteria. Although the recruitment of inflammatory monocytes and neutrophils at the site of tissue injury is important for the wound-healing process, these cells also secrete a variety of

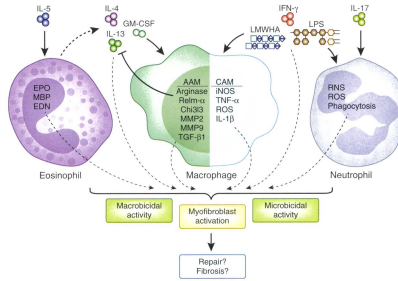

Figure 2 Innate immune cells in fibrosis. The macrophage is the prototypical innate immune cell involved in chronic inflammation and fibrosis. Macrophages are generated from blood monocytes that differentiate into macrophages as they enter tissues or, in some cases, from the local proliferation of tissue-resident macrophages. Depending on their etiology, macrophages are activated by a variety of triggers. IFN-γ and/or Toll-like receptor ligands such as lipopolysaccharide (LPS) and low molecular weight hyaluronic acid (LMWHA) lead to classical activation, which is characterized by the production of reactive oxygen and nitrogen species; IL-4, IL-13 and granulocyte-macrophage colony–stimulating factor (GM-CSF) mediate alternative activation, leading to the production of polyamines and L-proline by L-arginine catabolism. Certain triggers (such as extracellular bacteria and tissue damage) also elicit persistent or recurrent neutrophil infiltration mediated by IL-17 and other neutrophil-recruiting and/or neutrophil-activating signals that can substantially augment the microbicidal and tissue-damaging activities by free radicals. Likewise, helminth antigens and allergens mediate infiltration of eosinophils that assist in parasite killing that can result in substantial collateral damage to host tissues if not tightly confined inside fibrotic granulomata. EPO, erythropoietin; MBP, myelin basic protein; EDN, eosinophil-derived neurotoxin; AAM, alternatively activated macrophage; MMP2, metalloproteinase-2; MMP9, metalloproteinase-9; CAM, classically activated macrophage; iNOS, inducible nitric oxide synthase; ROS, reactive oxygen species; RNS, reactive nitrogen species.

toxic mediators, including reactive oxygen and nitrogen species that are harmful to the surrounding tissues. Consequently, if the inflammatory macrophages and neutrophils are not quickly eliminated, they can further exacerbate the tissue-damaging inflammatory response that leads to scarring. Indeed, proper wound healing can occur only after these inflammatory cells are controlled, as demonstrated by a recent study in which early macrophage depletion was shown to substantially reduce the development of liver fibrosis in mice[17]. Other studies have identified a similar profibrotic role for neutrophils in bleomycin- and hypersensitivity pneumonitis–induced pulmonary fibrosis in mice, and possibly in IPF[18]. It has also been suggested that liver dendritic cells have a role in the development of liver fibrosis, by promoting inflammation and activating hepatic stellate cells[19]. Thus, limiting the proinflammatory activity of innate myeloid-lineage cells might prove highly beneficial in a variety of chronic inflammatory and fibrotic diseases.

Innate inflammatory mediators regulate fibrosis. Various growth factors and cytokines secreted by innate inflammatory cells (including macrophages, neutrophils, mast cells and eosinophils) have emerged as potential targets for antifibrotic therapy. Tumor necrosis factor-α (TNF-α) and interleukin-1β (IL-1β), in particular, have been identified as important targets in a variety of fibrotic diseases[20]. Mice that overexpress TNF-α or IL-1β in the lung develop highly progressive pulmonary fibrosis[21,22]. Studies have also shown an essential role for TNF-α in the development of silica- and bleomycin-induced pulmonary fibrosis in mice[23,24]. In support of these experimental findings, patients with idiopathic or systemic sclerosis–associated pulmonary fibrosis have high levels of TNF-α[25]. TNF-α has also been shown to play a crucial part in radiation-induced fibrosis, Crohn's disease–induced intestinal fibrosis, CCL4- and cholestasis-induced liver fibrosis and NASH[26–28]. Consequently, clinical trials have recently been initiated to evaluate whether TNF pathway inhibitors such as etanercept or infliximab could be beneficial for the treatment of pulmonary fibrosis and other fibrotic diseases[29]. Similarly to the TNF-α studies, other studies have documented profibrotic activity for IL-1β and NALP3/ASC inflammasome signaling in macrophages[30]. Pulmonary fibrosis induced by bleomycin and silica, liver fibrosis in hypercholesterolemic mice, renal interstitial fibrosis resulting from unilateral ureteric obstruction and cardiovascular fibrosis after myocardial infarction are all reduced in IL-1β–deficient mice[31–33]. Like TNF-α, IL-1β is a potent proinflammatory mediator that exacerbates parenchymal-cell injury. It also induces epithelial-mesenchymal transition (EMT) and myofibroblast activation through a TGF-β1–mediated mechanism[34], confirming that it functions as a potent upstream driver of fibrosis. IL-1β and TNF-α also increase expression of IL-6, which shows autocrine growth-factor activity in fibroblasts. IL-6 is an important mediator of fibrosis in diffuse systemic sclerosis, liver fibrosis after CCL4 exposure and fibrosis in chronic cardiac allograft rejection[35,36]. Thus, many innate proinflammatory cytokines have crucial roles in the pathogenesis of fibrosis.

TGF-β1 has both anti-inflammatory and profibrotic activity. Macrophages that appear early in the wound-healing response are also major producers of TGF-β, which is, indisputably, one of the key drivers of fibrosis. TGF-β production correlates with the progression of liver, lung, kidney, skin and cardiac fibrosis, and inhibition of the TGF-β1 signaling pathway has been shown to reduce the development of fibrosis in many experimental models. In addition to its role as a profibrotic cytokine that can directly induce the differentiation of fibroblasts into collagen-secreting myofibroblasts, TGF-β1 is now widely described as a multifunctional cytokine with broad modulatory activities that affect numerous important biological pathways. These include pathways involved in the regulation of embryogenesis, immunity, carcinogenesis, cell proliferation and migration, wound healing, inflammation and fibrosis, among others[37]. Studies have suggested that the cellular source of TGF-β1 dictates its activity, with TGF-β1 derived from macrophages generally showing wound-healing and profibrotic activity and TGF-β1 secreted from $CD4^+$ T regulatory cells (T_{reg} cells) functioning as an anti-inflammatory and antifibrotic mediator[38]. Mice that are deficient in TGF-β1 develop numerous autoimmune disorders and are more susceptible to cancer.

Therefore, it remains unclear whether antagonism of the TGF-β1 signaling pathway will prove beneficial in humans, as patients with progressive fibrosis are likely to require prolonged antifibrotic therapy.

Alternatively activated M2 macrophages suppress fibrosis. A unique functional subset of macrophages, called M2 or alternatively activated macrophages, has also been implicated in the pathogenesis of fibrosis[39]. Gordon and his colleagues first noted that macrophages activated with IL-4 (or IL-13) develop an alternative activation state that is distinct from that of classically activated macrophages (M1) induced by interferon-γ (IFN-γ)[40]. *In vitro* and *in vivo* studies in mice have shown that this phenotype is characterized by elevated expression of the mannose receptor (CD206), chitinase-3–like protein-3 (Chi3l3, also known as Ym1), resistin-like molecule-α (Relm-α, also known as FIZZ-1), major histocompatibility complex class II antigens and the enzyme arginase-1 (Arg1). Expression of Arg1 by M2 cells is of particular interest because this enzyme controls L-proline production, which is required for collagen synthesis by activated myofibroblasts[41]. M2 cells have also been implicated in the development of T helper type 2 (T_H2) effector responses, production of fibrogenic cytokines, suppression of M1 responses and recruitment of fibrocytes[42,43]. Because they are commonly observed during the peak of the profibrotic immune response, M2 macrophages have been hypothesized to be important inducers of wound healing and fibrosis. However, mechanistic studies conducted with $LysM^{Cre}IL\text{-}4R\alpha^{-/flox}$ mice, in which Cre-mediated recombination results in deletion of the IL-4Rα chain in the myeloid cell lineage, including in M2 cells, have demonstrated that M2 macrophages are not required for the development of T_H2 responses or liver fibrosis following infection with *Schistosoma mansoni*[44]. In fact, related studies done in mice with a conditional Arg1 deficiency suggested that Arg1-expressing M2 cells are required for the suppression and resolution of fibrosis[45]. These later experiments suggested that M2 cells compete with T_H2 cells and fibroblasts for L-arginine, which is required for the production of polyamines and L-proline, which regulate cell growth and collagen synthesis, respectively. The inhibitory activity of M2 cells is also consistent with studies showing them to be important inducers of T_{reg} cells[46], which have also been implicated in the suppression of fibrosis. Thus, rather than promoting fibrosis, M2 cells seem to exploit multiple mechanisms to inhibit ECM synthesis by myofibroblasts. Given this modified view of the role of M2 macrophages, it will be important to investigate whether M2 cells have a similar inhibitory role in other models of fibrosis.

These findings suggest that M2 cells could be exploited to ameliorate fibrotic disease. Indeed, drugs that modulate the activation status of macrophages could emerge as a general therapeutic strategy to treat fibrosis. For example, peroxisome proliferator–activated receptor-α (PPAR-α) and PPAR-γ are induced in inflammatory macrophages, and endogenous and synthetic ligands that engage these receptors have been shown to inhibit the development of fibrosis by inducing the differentiation of alternatively activated macrophages that decrease proinflammatory cytokine production by M1 cells[47,48]. PPAR ligands also directly inhibit fibroblast activation induced by TGF-β1 (ref. 49). In support of these observations, PPAR-α and PPAR-γ activators have proven efficacious in a variety of experimental models of fibrosis, including hypertension-induced cardiac fibrosis, bile duct ligation–induced liver fibrosis, unilateral ureteral obstruction–induced renal interstitial fibrosis and bleomycin-induced pulmonary fibrosis[50–53]. The M2 macrophages that develop spontaneously during helminth infection have also been shown to reduce inflammation and slow the progression of liver fibrosis[44,45]. Thus, the conditional IL-4Rα– and Arg1-deficient mice described above will be important tools to further investigate the therapeutic potential of M2 cells in fibrotic disease.

Other innate myeloid-lineage cells have roles in fibrosis. Although it is widely recognized that monocytes, macrophages and neutrophils have important roles in the progression and resolution of fibrosis[39], other myeloid-lineage cells (such as mast cells, eosinophils and basophils) have also been implicated in the pathogenesis of fibrosis in multiple organ systems and are viewed as potential therapeutic targets. For example, studies in mice have identified mast cells as inducers of systemic sclerosis, renal fibrosis after kidney transplantation and left-ventricular fibrosis in hypertensive hearts. Mechanistic studies in rats have suggested that mast cells promote fibrosis by recruiting inflammatory leukocytes and by producing profibrotic mediators[54]. Eosinophils seem to function in a similar fashion and are considered to be important sources of TGF-β1 and IL-13 (refs. 55,56). Although eosinophils have been most commonly associated with the development of pulmonary fibrosis[57], increased numbers of eosinophils have also been linked with the activation of myofibroblasts in skin and liver fibrosis as well as idiopathic retroperitoneal fibrosis[55,58]. Bronchoalveolar-lavage eosinophilia has also been identified as a predictive biomarker of progressive lung disease in IPF and pulmonary fibrosis associated with collagen vascular disorder[59]. Finally, although basophils have a less clear role in the development of fibrosis than the other myeloid-cell populations, they have been implicated in the pathogenesis of myelofibrosis and are frequently found in greater numbers in patients with interstitial lung disease[60]. Basophils are also thought to be an important source of type 2 cytokines, suggesting that they might serve as important drivers of IL-4– and/or IL-13–dependent fibrosis.

Adaptive immunity and fibrosis

T_H17-type immunity is proinflammatory and profibrotic. $CD4^+$ T cells are divided into unique subsets on the basis of the cytokines they secrete and their distinct functional abilities (**Fig. 3**). The $CD4^+$ T_H17 cell subset that expresses the proinflammatory cytokine IL-17A is emerging as an important driver of fibrosis. IL-17A expression has been implicated in the pathogenesis of pulmonary fibrosis[61], chronic allograft rejection[62], fibrosis in orthotopic lung transplantation[63], myocardial fibrosis[64] and hepatitis-induced hepatic fibrosis[65]. In many cases, IL-17A expression is associated with persistent neutrophilia[66], and it has been suggested that exaggerated neutrophil recruitment contributes to the development of tissue damage and fibrosis by inducing apoptosis in vascular endothelial cells[67]. Neutrophil recruitment is also an important predictor of early mortality in IPF patients[68]. Mechanistic studies investigating the IL-17 pathway of fibrosis in mice have identified the proinflammatory cytokines IL-1β and IL-23 as important upstream initiators of profibrotic T_H17 responses[61,69]. A link between IL-17A and TGF-β1 has also been identified[61]. In addition to its role in promoting neutrophilic inflammation, IL-17A has been shown to directly induce expression of matrix metalloproteinase-1 in primary human cardiac fibroblasts[70], suggesting that IL-17A promotes fibrosis by both exacerbating the upstream inflammatory response and regulating the downstream activation of fibroblasts. Together, these data identify the IL-1β–IL-17A–TGF-β1 cytokine axis as an important pathway in inflammation-driven fibrosis.

T_H2-type immunity is a potent driver of progressive fibrosis. Numerous studies have suggested that the type 2 cytokine response is a key driver of progressive fibrosis[71]. T_H2 responses are defined

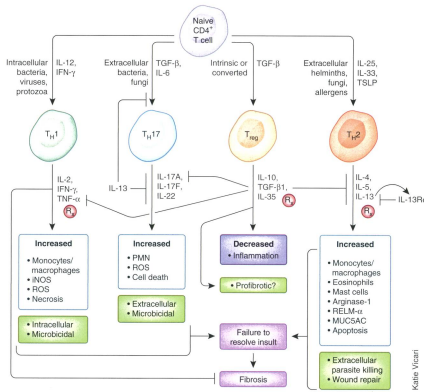

Figure 3 Adaptive immune pathways in fibrosis. Naive CD4$^+$ T cells differentiate into various distinct functional lineages driven by cues produced by injured epithelial cells and activated antigen presenting cells (dendritic cells and macrophages). Intracellular infections trigger IL-12–driven T_H1 responses that produce IFN-γ, which activates microbicidal and cytotoxic activities that aid in pathogen clearance. Extracellular bacteria and certain fungi can lead to inflammasome activation and IL-6 production and can, in the presence of TGF-β1, drive T_H17 differentiation. IL-17 from T_H17 cells helps recruit neutrophils to clear the infection and exacerbates inflammation. Infection with extracellular, tissue-dwelling helminth parasites drives T_H2 differentiation, with IL-4, IL-25, IL-33 and thymic stromal lymphopoietin (TSLP) from innate and epithelial sources guiding the differentiation of CD4$^+$ T_H2 cells. IL-13, when not competed for by the higher-affinity decoy receptor IL-13Rα2, binds its signaling receptor IL-13Rα1, leading to alternative activation of macrophages as well as epithelial apoptosis and myofibroblast activation. T_{reg} cells are crucial in limiting the magnitude of T_H cell responses and thereby ensure proper regulation of the wound-healing response. There is also a great deal of cross-regulation among T_H cell subsets. For example, IL-13 suppresses T_H17 differentiation, whereas IFN-γ can suppress IL-13–induced fibrosis by inducing classical macrophage activation and suppressing IL-13 and TGF-β1–induced collagen synthesis in myofibroblasts. R_x, pathways being targeted for therapy, either preclinically or in clinical trials; iNOS, inducible nitric oxide synthase; ROS, reactive oxygen species; PMN, polymorphonuclear leukocyte; MUC5AC, mucin-5AC.

by the production of IL-4, IL-5 and IL-13 (ref. 72), and although all three have been linked to the development of fibrosis[55,73,74], IL-13 has emerged as a dominant mediator of fibrotic tissue remodeling in several experimental and natural models of fibrosis[74]. IL-13 production has been implicated in the development of fibrosis in chronic asthma[75], IPF[76], models of experimental lung fibrosis[77], systemic sclerosis[78], atopic dermatitis–induced skin fibrosis[79], radiation-induced fibrosis[80], fibrosis associated with ulcerative colitis[81] and liver fibrosis resulting from persistent infections and NASH[82,83]. Mechanistically, IL-13 has been hypothesized to induce fibrosis by stimulating the production and activation of TGF-β[84]. However, other studies have suggested that IL-13 can promote fibrosis independently of TGF-β[85,86] by directly activating the synthetic and proliferative properties of fibroblasts, epithelial cells and smooth-muscle cells[87,88]. Consequently, unlike IL-17A—which seems to promote fibrosis indirectly by inducing tissue damage and inflammation—IL-13 and TGF-β show direct fibrotic activity. T_H2 cells that produce IL-13 and T_{reg} cells that express TGF-β are also known to inhibit T_H17 responses[89], suggesting dual roles for IL-13 and TGF-β in the wound-healing response, as both cytokines suppress inflammation while promoting fibrosis. The profibrotic activity of IL-13 is controlled by the abundance of the IL-13Rα1 signaling receptor and IL-13Rα2 decoy receptor expressed on important target cells such as myofibroblasts[90,91]. When decoy receptor expression is low or absent, IL-13–dependent fibrosis is exacerbated[92]. However, mice deficient in IL-13Rα2 are more resistant to IL-1β– and IL-17–driven inflammation, probably because of the enhanced IL-13 activity[89], suggesting that IL-13Rα2 functions as a key regulator of both T_H17-mediated inflammation and T_H2-driven fibrosis[93].

T_H1-type immunity shows antifibrotic activity. Numerous studies have suggested that T_H1 effector T cells, defined by their production of IFN-γ, have antifibrotic activity[94–96]. IFN-γ–producing natural killer and natural killer T cells have also been shown to have similar roles[97,98]. Mechanistically, IFN-γ is believed to inhibit fibrosis, at least in part, by antagonizing the profibrotic activity of TGF-β1. IFN-γ inhibits the TGF-β–induced phosphorylation of the signal transducer Smad3 and subsequent activation of TGF-β–responsive genes[99]. IFN-γ also acts through a pathway dependent on Janus-associated kinase (Jak1) and the transcription factor Stat1 and induces expression of Smad7, which can prevent the interaction of Smad3 with the TGF-β receptor, thus further attenuating TGF-β–induced signaling. IFN-γ also directly inhibits fibroblast proliferation, TGF-β1–induced expression of the genes encoding procollagen I and procollagen III, and collagen synthesis in activated myofibroblasts[100]. IFN-γ also prevents the T_H2 cytokine–induced differentiation of CD14$^+$ peripheral blood monocytes into fibroblast-like cells called fibrocytes, which are believed to participate in the development of fibrosis in many organ systems[101]. Finally, by virtue of its ability to stimulate IFN-γ production in T_H1 and natural killer cells, IL-12 has shown similar antifibrotic activity *in vivo* in mice[71,102]. But despite an abundance of *in vitro* and *in vivo* evidence supporting an antifibrotic role for T_H1-type immunity, clinical studies investigating the therapeutic potential of IFN-γ in the treatment of IPF, systemic sclerosis and other fibrotic disorders have so far been mostly disappointing[103].

T_{reg} cells either suppress or promote fibrosis. T_{reg} cells are induced in a variety of fibrotic diseases, but their role in tissue fibrogenesis is less clear than that of some of the other subsets of T_H cells.

Foxp3-expressing T_{reg} cells are important producers of immunosuppressive cytokines that control T_{reg} cell function, such as IL-10 and TGF-β1. Thus, one might predict that if T_{reg} cells were present in sufficient numbers, they would inhibit progressive fibrotic disease by negatively regulating the inflammatory response that drives ECM deposition. Indeed, several groups exploring the mechanisms of fibrosis have documented a suppressive role for T_{reg} cells in tissue fibrogenesis. T_{reg} cells have been linked to the amelioration of fibrosis in IPF[104], dystrophic mouse muscle[105], cardiovascular disease[106], chronic graft-versus-host disease–induced lupus nephritis[107] and chronic HCV- and HIV-induced liver fibrosis[108]. One study has suggested that T_{reg} cells protect mice from fibrosis by secreting IL-10 (ref. 38). However, T_{reg} cells are also an important source of TGF-β1, with at least a few studies demonstrating that TGF-β–producing T_{reg} cells induce rather than inhibit fibrosis[109,110]. Therefore, it remains uncertain whether T_{reg} cells can be effectively exploited to ameliorate progressive fibrotic disease. It is unclear why T_{reg} cells would have antifibrotic activity in some situations and profibrotic activity in others, but the development and recruitment of T_{reg} cells relative to other effector T cell populations is likely to have a decisive role. It also seems plausible that T_{reg} cells could suppress T_H17- and T_H2-driven fibrosis but exacerbate TGF-β1–dependent fibrosis.

Intrinsic, autocrine and epigenetic mechanisms regulate fibrosis

Mechanical modifications to the ECM and cell-intrinsic changes in fibroblasts and epithelial cells have also been shown to contribute to the progression of fibrosis by maintaining the activation of key fibrogenic pathways.

Mechanisms that perpetuate myofibroblast activation. The Wnt–β-catenin signaling pathway, which regulates cell growth and is intimately involved in tumorigenesis, is constitutively activated in alveolar epithelial type II (ATII) cells in mouse models of pulmonary fibrosis and in patients diagnosed with IPF and chronic obstructive pulmonary disease[111]. Activation of Wnt–β-catenin signaling has also been reported in kidney, liver, skin and cardiac fibrosis[112,113]. Mechanistically, Wnt-1–inducible signaling protein 1 (WISP-1) has been shown in mice to increase the proliferation of ATII cells, promote EMT in the lung and kidney and mediate TGF-β1–driven renal fibrosis[114] (**Fig. 4**). WISP-1 also increases the synthesis of ECM components in mouse and human lung fibroblasts and regulates activation of hepatic stellate cells in the liver[115]. Blocking studies demonstrated that bleomycin-induced pulmonary fibrosis is highly dependent on the Wnt-1 pathway[116]. Thus, Wnt signaling has emerged as a potential therapeutic target for IPF and several other chronic fibrotic disorders.

As tissues become more fibrotic, the increased tissue stiffness and decreased elasticity result in mechanical stress, which has been shown to exacerbate tissue injury and perpetuate the activation of local fibroblasts expressing α-smooth muscle actin (α-SMA)[117]. Two recent *in vitro* studies in mouse and porcine cells have suggested that mechanical stress contributes to aberrant wound healing and fibrosis by inducing EMT in alveolar type II epithelial cells via a mechanism driven by TGF-β1, Wnt–β-catenin and hyaluronan[118,119]. Fibroblasts that are activated as a result of increased tissue or substrate stiffness also seem to maintain their activated phenotype when returned to healthy 'soft' tissues[120], suggesting that mechanical sensing by fibroblasts can permanently alter their behavior in favor of a fibrotic phenotype. Indeed, it has been suggested that the differentiation of fibroblasts into ECM-producing myofibroblasts is controlled by the combined actions of IL-1β, TGF-β1 and mechanical tension[121]. Increased compression, shear forces and hydrostatic pressures associated with portal hypertension and vascular remodeling can also perpetuate myofibroblast activation.

Epigenetic modifications in fibroblasts also contribute to the pathogenesis of fibrosis by stably altering the activation status of myofibroblasts. A recent genome-wide methylation scan of fibroblasts revealed several DNA methylation modifications that were unique to collagen-secreting myofibroblasts obtained from fibrotic mouse kidneys[122]. One of the modifications contributed to the epigenetic silencing of *Rasal1* (encoding a suppressor of the Ras oncoprotein), which increased Ras activity and led to spontaneous, growth factor–independent proliferation of fibroblasts. These findings were important because they suggested that intrinsic changes in fibroblasts could lead to the uncontrolled expansion of myofibroblasts seen in some cancers. They also provided a new molecular explanation for the sustained and heritable activation of fibroblasts that is often seen in IPF and other highly progressive fibrotic diseases. On the basis of these observations, it may be predicted that the targeted repression of known antifibrotic genes by hypermethylation could contribute to the development of fibrosis, as was recently documented in IPF[123]. DNA methyltransferase inhibitors were found to reverse epigenetic modifications and protect mice from pulmonary fibrosis[124]. Therefore, because epigenetic modifications seem to be reversible, they could emerge as important targets for antifibrotic therapy.

Endoplasmic reticulum stress and the unfolded protein response. Intrinsic mechanisms that contribute to cell death have also been hypothesized to regulate the progression of fibrosis. Endoplasmic reticulum (ER) stress leading to apoptosis of key structural cells, such as epithelial cells, endothelial cells and hepatocytes, is believed to be an important driver of fibrosis. For example, excess accumulation of unfolded or misfolded proteins in the ER activates cellular stress pathways. The stress response, in turn, activates a complex counter-response, which is typically protective for the cell. However, if the counter-response is delayed, inadequate or associated with substantial mitochondrial dysfunction, it can lead to apoptosis and sustained activation of the wound-healing response. Hepatocyte apoptosis driven by ER stress is believed to play a major part in the pathogenesis of liver fibrosis in NASH[125]. ER stress leading to apoptosis in alveolar epithelial cells is also thought to have a key role in sporadic IPF[126,127]. Therefore, a better understanding of the mechanisms that induce ER stress or lead to its resolution could reveal new strategies to prevent or treat progressive fibrotic disease.

Telomere shortening in mesenchymal cells promotes injury leading to fibrosis. Telomere shortening has been hypothesized to be an important contributor to the development of adult-onset and familial forms of pulmonary fibrosis[128,129]. Indeed, circulating peripheral leukocytes with shortened telomeres are found in a large percentage of sporadic, familial and idiopathic cases of pulmonary fibrosis. This shortening has been attributed to mutations in the gene encoding telomerase reverse transcriptase (TERT), an enzyme crucial to the maintenance of telomere length in adult stem cells[130–132]. Alveolar type 2 cells and lung-resident mesenchymal stem cells express telomerase, and mutations in this enzyme have been shown to contribute to their premature death, resulting in decreased lung regeneration after injury. Telomerase-null mice also show compromised lung alveolar integrity and decreased myofibroblast differentiation as a result of telomere shortening[133,134]. Profibrotic mediators, such as

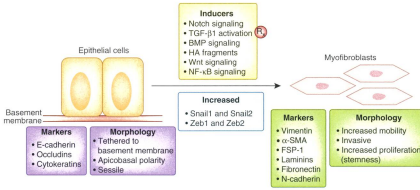

Figure 4 EMT in fibrosis. In mouse models of renal and hepatic fibrosis, up to 40% of α-SMA–positive, collagen-secreting myofibroblasts have been shown to arise from the differentiation of local epithelial progenitors via EMT. Repression of the transcription factors Snail1, Snail2, Zeb1 and Zeb2 are important for the maintenance of epithelial morphology. Several factors that are upregulated in the context of inflammation, including nuclear factor-κB (NF-κB), TGF-β1, bone morphogenetic proteins (BMPs), Wnt and Notch signaling proteins, can activate the Snail-Zeb pathway, leading to mesenchymal differentiation in these cells. R_x, pathways being targeted for therapy, either preclinically or in clinical trials; HA, hyaluronic acid; FSP-1, fibroblast-specific protein-1.

TGF-β1 and reactive oxygen intermediates, also participate in telomere shortening[135,136], suggesting that a vicious cycle of profibrotic-mediator production, impaired telomerase activity and increased senescence of stem cells and/or AT2 cells contributes to the pathogenesis of fibrosis. Nevertheless, studies with TERT-deficient mice have raised questions about whether TERT has only a protective role in fibrosis, as telomerase activity was found to be necessary for development of bleomycin-induced pulmonary fibrosis in mice[137].

MicroRNAs regulate fibroblast growth and activation. MicroRNAs (miRNAs) include a broad class of small evolutionarily conserved noncoding RNAs that have important roles in a variety of pathophysiological processes by blocking translation or promoting degradation of complementary target mRNAs. Although unique subsets of miRNAs have been identified in various fibrotic diseases, a much smaller subset of miRNAs have emerged as key regulators of the fibrotic process. For example, miR-21 is expressed in the lungs of individuals with IPF, and mice treated with miR-21 antisense probes were protected from bleomycin-induced pulmonary fibrosis[138] and cardiac fibrosis induced by pressure overload[139]. Mechanistically, miR-21 is thought to promote fibrosis by regulating TGF-β1 and MAP kinase signaling in activated myofibroblasts[138,139]. miR-21 suppresses several tumor suppressor genes, suggesting that *MIR21* may also function as an oncogene. miR-21 also operates as an anti-apoptotic factor in tumor cells[140]. Aberrant expression of miR-21 or other key miRNAs in fibroblasts could, therefore, contribute to their survival and/or differentiation into pathogenic ECM-producing myofibroblasts. Nevertheless, a recent study with miR-21–null mice has raised questions about the overall importance of miR-21 in pathological cardiac remodeling[141]. In rat and mouse studies, miR-192, miR-216a and miR-217 have, like miR-21, been identified as key triggers of fibrosis driven by TGF-β and Smad3 (refs. 142,143). miR-29 has also been identified in human and mouse studies as a potential therapeutic target in systemic sclerosis, liver fibrosis and cardiac fibrosis[144–146]. miR-29 seems to promote fibrosis in human cells by directly regulating type I collagen expression[147]. Other miRNAs are constitutively expressed in healthy tissues but are downregulated as fibrosis develops, suggesting that they might have a protective antifibrotic role such as that shown recently for the miRNA let-7d in IPF[148]. Decreases in miR-133 and miR-30 have also been linked to increased activity of connective tissue growth factor (CTGF), which resulted in increased myocardial matrix remodeling[149]. Downregulation of miRNA-150 and miRNA-194 in hepatic stellate cells has been hypothesized to contribute to stellate cell activation and increased ECM production in the liver[150]. Finally, expression of miR-200a has been shown to prevent renal fibrogenesis by repressing TGF-β2 expression[151]. Thus, identifying specific miRNAs that inhibit important fibrogenic pathways or promote tissue healing or regeneration could prove highly beneficial in the treatment of fibrosis[148]. Indeed, the targeting of specific miRNAs with small-molecule inhibitors or miRNA mimics could be a general strategy to treat fibrotic disease.

Key fibrogenic pathways for therapeutic targeting

Mechanistic studies of tissue fibrogenesis have revealed a variety of potential therapeutic approaches to combating progressive fibrotic disease. Some of the unique strategies and targets that have progressed to the clinical-trial phase are discussed briefly in the following sections.

Myofibroblasts and the TGF-β pathway. Because activated myofibroblasts are the key pathogenic cells in all fibrotic diseases, a number of experimental antifibrotic strategies are attempting to target activation, proliferation and/or recruitment of fibroblasts (**Box 1** and **Table 1**). Pirfenidone, marketed under the names Esbriet and Pirespa, is the first targeted antifibrotic drug to be approved for the treatment of IPF in Europe and Japan[152]. Although its exact mechanism of action remains unclear, pirfenidone is believed to attenuate fibroblast proliferation and the production by activated myofibroblasts of fibrosis-associated mediators and ECM components. Pirfenidone has also shown efficacy in preclinical models of liver fibrosis, renal fibrosis, hypertrophic cardiomyopathy and radiation-induced fibrosis, suggesting that it may have broad antifibrotic activity. Therapeutic antibodies to TGF-β1 (ref. 153), a key cytokine involved in the activation of myofibroblasts; CTGF, a matrix-associated, heparin-binding protein that mirrors the profibrotic activity of TGF-β on fibroblasts; and integrin $\alpha_v\beta_6$, which is responsible for the activation of constitutively expressed latent TGF-β[154], are also being investigated for their antifibrotic activity. A humanized monoclonal antibody to $\alpha_v\beta_6$ developed by Stromedix and Biogen Idec is being investigated as a treatment for interstitial fibrosis and tubular atrophy in kidney-transplant recipients and as a therapy for IPF[155]. Genzyme (owned by Sanofi-Aventis) is also exploring a humanized pan–TGF-β inhibitor (fresolimumab) as a treatment for patients with early-stage diffuse systemic sclerosis, focal segmental glomerulosclerosis, IPF and myelofibrosis[156,157], and antibodies and antisense drugs targeting CTGF are being investigated in IPF and scar-revision surgery[158]. Antagonists of the lysophosphatidic acid-1 receptor, a growth factor that induces CTGF and TGF-β1 expression, are being considered as treatments for kidney fibrosis, IPF and systemic sclerosis[159,160]. Bone morphogenetic protein-7 has also been identified as a potential therapeutic agent for chronic

BOX 1 Myofibroblasts

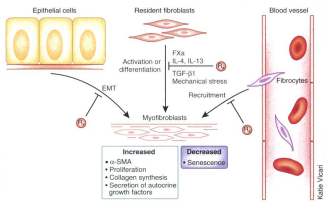

During equilibrium, tissue-resident fibroblasts are in a quiescent state, although they are metabolically active and biomechanically support the form and function of the organ they are present in. To repair, regenerate and restore homeostasis after injury, these tissue-resident fibroblasts are activated and transform into myofibroblasts, contractile cells expressing α-SMA and myosin bundles. Myofibroblasts secrete copious amounts of ECM and are vital players in the granulation tissue of the wound, aiding in contracture and closure and orchestrating many aspects of the healing response. Aberrations in the wound-healing program or in other pathological states can summon and sustain myofibroblasts, and several studies have shown that they are an important source of collagens in active fibrotic areas. But evidence is accumulating that, in a variety of tissues, a substantial portion of these profibrotic cells could also arise from regenerating epithelial or endothelial cells or from epithelial stem cell progenitors via EMT or endothelial-mesenchymal transition (EndMT). In some instances, circulating CD34$^+$ bone marrow–derived progenitor cells, termed fibrocytes, have also been shown to be recruited in a CCL2-dependent manner, contributing to the myofibroblast pool at the site of wound repair and fibrosis. Myofibroblast activation, proliferation and survival are mediated by a variety of secreted, soluble and physical factors in the milieu, such as cytokines (IL-1, TNF, TGF-β1 and IL-13), growth factors (CTGF and PDGF) and matrix factors (hyaluronan fragments, mechanical stress and/or stiffness). During normal wound healing, myofibroblasts undergo apoptosis after re-epithelialization of the wound—but the rogue myofibroblasts encountered in fibrotic loci are known to be resistant to programmed cell death. Pathways that elicit and recruit high numbers of myofibroblasts and those that engender resistance to apoptosis are active areas of fibrosis research (see illustration). R_x, pathways being targeted for therapy, either preclinically or in clinical trials.

renal injury because it can counteract TGF-β1–induced EMT[161]. An antagonist of the endothelin receptor, which promotes myofibroblast contraction and migration, is being explored in cardiovascular disease and IPF[162]. A humanized monoclonal antibody targeting lysyl oxidase–like-2, an enzyme that catalyzes the cross-linking of collagen, is being explored by Gilead Sciences as a treatment for cardiac fibrosis, IPF and liver fibrosis[163]. Other matrix assembly proteins, such as prolyl hydroxylases, are being investigated preclinically for antifibrotic activity[164]. Bortezomib, a proteasomal inhibitor approved by the US Food and Drug Administration, inhibits TGF-β1 signaling *in vitro* and has been shown to protect mice from bleomycin-induced skin and lung fibrosis[165]. It also induces apoptosis of hepatic stellate cells[166]. Consequently, bortezomib may prove efficacious for diseases in which TGF-β1, ER stress and activated myofibroblasts have been identified as key pathogenic mediators. Studies are also under way to examine whether a serine/threonine protein kinase inhibitor reduces the number of circulating fibrocytes in individuals with IPF[167]. Because ECM-producing myofibroblasts are the final common pathogenic cell in all fibrotic diseases, any therapy that successfully ablates their activity could have broad antifibrotic activity.

Proinflammatory pathways. Targeting key inflammatory pathways might also prove beneficial in the treatment of fibrosis. Because TNF-α has emerged as a key driver of fibrosis in many experimental studies, clinical trials have been initiated to examine whether inhibitors of the TNF-α pathway could be used to treat IPF and other scarring disorders[29]. Although the small-molecule tyrosine kinase inhibitor imatinib mesylate (Gleevec), which inhibits signaling of PDGF receptor and vascular endothelial growth factor receptor, did not affect survival or lung function in patients with IPF[168], ongoing trials are investigating its potential as a treatment for nephrogenic systemic fibrosis[169]. Boehringer Ingelheim also has ongoing clinical studies with another investigational tyrosine kinase inhibitor, BIBF 1120, which showed promise in slowing lung-function decline in patients with IPF[170]. Inhibitors of Jaks, a family of intracellular, nonreceptor tyrosine kinases that transduce cytokine-mediated signals via the Jak-Stat pathway, are also being investigated for their therapeutic activity in liver fibrosis and myelofibrosis[171]. Finally, given that recent studies have directly linked IL-17A with TGF-β1 (ref. 61), therapeutic antibodies that disrupt IL-17 signaling might also prove beneficial for the treatment of fibrosis. Targeting upstream proinflammatory pathways would probably be required in situations in which sustained inflammation is a major driving force in the development of fibrosis. However, it is important to point out that although IFN-γ is a well-known antifibrotic cytokine, IFN-γ1b showed little efficacy in the treatment of IPF or chronic HCV-induced liver fibrosis[172,173]. Numerous anti-inflammatory drugs, including corticosteroids, immunomodulatory agents and cytotoxic drugs, have also been tested and found to have little to no therapeutic benefit in IPF or other fibrotic diseases, so it remains uncertain whether the newer class of 'anti-inflammatory' drugs will ultimately prove beneficial for fibrosis.

The profibrotic type 2 immune response. The T_H2-associated cytokine IL-13 has emerged as a key driver of infection and allergen-driven fibrosis[74,82,84]. IL-13 and its receptors have also been detected at high levels in the lungs and blood of patients with IPF[76,174]. On the basis of these results, Novartis has initiated clinical studies to determine whether humanized IL-13–specific monoclonal antibodies could be used to treat IPF. Sanofi is also exploring the role of type 2 cytokines in IPF using an antibody that targets both IL-4 and IL-13. Support for the potential utility of an IL-13 blocker comes from a recent study in which lebrikizumab, a humanized monoclonal antibody to IL-13 developed by Genentech, was shown to be effective in a subset of adults with poorly controlled asthma[175]. Patients showing the greatest improvement in lung function after lebrikizumab therapy had high pretreatment levels of serum periostin, an

Table 1 Antifibrotic strategies between bench and clinic

Category	Name	Target/mechanism	Class	Target disease	Manufacturer	Phase
Growth factors	Pirfenidone	TGF-β activity, inflammation	Small molecule	IPF, hepatic and renal fibroses, hypertrophic cardiomyopathy	InterMune	Clinic[a]
	GC1008	TGF-β1	Monoclonal antibody	Myelofibrosis, systemic sclerosis	Genzyme	1
	LY2382770	TGF-β1	Monoclonal antibody	Diabetic glomerulosclerosis	Eli Lilly and Company	2
	FG-3019	CTGF	Monoclonal antibody, antisense	IPF, scar-revision surgery	FibroGen	1/2
	PRM-151	SAP (pentraxin 2)	Recombinant protein	IPF, post-surgical scarring	Promedior	1/2
ECM	GS-6624	Lysyl oxidase-like-2	Monoclonal antibody, small molecule	Cardiac fibrosis, IPF	Gilead Sciences	1/2
	STX-100	Integrin $\alpha_v\beta_6$	Monoclonal antibody	IPF, renal fibrosis	Stromedix	1
Intracellular enzymes	Sivelestat	Neutrophil elastase	Small molecule	Acute lung injury, chronic obstructive pulmonary disease, IPF	Ono Pharmaceutical	1
	FG-4592	Hypoxia-inducible factor prolyl hydroxylase	Small molecule	Chronic kidney disease	FibroGen	2
	Bortezomib	26S proteasome	Small molecule	Pulmonary and dermal fibrosis	Millennium	Clinic[b]
	Imatinib	PDGFR tyrosine kinase	Small molecule	Nephrogenic systemic fibrosis	Novartis	2
	Sirolimus	Mammalian target of rapamycin (mTOR)	Small molecule	Renal fibrosis, IPF	Pfizer	3/4[c]
	BIBF 1120[d]	Angiokinases	Small molecule	IPF	Boehringer Ingelheim	2
	INCB018424	Jak2	Small molecule	Myelofibrosis	Sanofi-Aventis	1/2
	CC-930	JNK	Small molecule	IPF	Celgene	2
Immunomodulators/ Inflammatory modulators	Etanercept	TNF-α	TNF receptor 2–IgG1 fusion protein	IPF	Pfizer	2
	QAX576	IL-13	Monoclonal antibody	IPF, eosinophilic esophagitis, asthma	Novartis	2
	Anakinra	IL-1	Recombinant protein	Arthrofibrosis	Amgen/Biovitrum	Clinic[e]
	CNTO-888	CCL2	Monoclonal antibody	IPF, fibrocyte reduction	Janssen	2
	Thalidomide	Anti-inflammatory, proapoptotic?	Small molecule	IPF	Celgene	2
	Azathioprine	Cytotoxic, immunosuppressive	Small molecule	IPF	Multiple	3
	Aviptadil	Vasoactive intestinal polypeptide analog	Synthetic peptide	Pulmonary arterial hypertension, IPF	mondoBIOTECH	1
Antioxidants	*N*-acetylcysteine	Oxidative stress	Small molecule	IPF, hepatic fibrosis	Multiple	3
Coagulation pathway	PAR1 antagonists	Thrombin and FXa signaling	Small molecule	IPF, hepatic fibrosis	Multiple	Preclinical
Others	Losartan	Angiotensin II receptor signaling	Small molecule	Hepatic, pulmonary and cardiac fibroses	Multiple	Clinic[f]
	Bosentan	Dual endothelin receptor antagonism	Small molecule	Dermal fibrosis, IPF	Actelion	3

[a]Approved for IPF in EU and Japan. [b]Approved for multiple myeloma. [c]Combination therapy with immunosuppressants. [d]Inhibits the receptor tyrosine kinases VEGFR, PDGFR and FGFR. [e]Approved for rheumatoid arthritis. [f]Approved for hypertension.

Several steps in cell growth, inflammation, and immune activation have become targets for antifibrotic intervention. Key targets that are now being tested in preclinical models or in phase 2 or phase 3 clinical trials are included.

IL-13–induced protein[176]. Thus, it will be interesting to determine whether this circulating biomarker could be used to identify individuals with IL-13–dependent fibrosis who might also benefit from anti–IL-13 therapy. Because a growing number of chronic fibrotic diseases are characterized by the excess production of IL-13 and/or increased expression of IL-13–inducible genes, many individuals with fibrosis might benefit from the neutralization of IL-13.

Myeloid cells and T_{reg} cells. Numerous studies have suggested that macrophages have stage-specific roles in fibrosis[2]. Macrophages show profibrotic activity in the early phases of the wound-healing response by producing inflammatory mediators that can exacerbate tissue injury, such as IL-1β, TNF-α and reactive oxygen and nitrogen species. They also produce profibrotic mediators such as TGF-β1. But in the later stages of the wound-healing response, a subset of macrophages converts into a suppressive phenotype that expresses a variety of anti-inflammatory mediators, such as IL-10, Arg1, programmed death ligand-2 and Relm-α, which promote wound healing and direct the resolution of the inflammatory response[46]. Given the central role that macrophages have in fibrosis, a number of experimental antifibrotic strategies are being designed to regulate the activation and/or recruitment of distinct myeloid-cell populations. For example, Johnson & Johnson is conducting a phase 1 study in individuals with IPF of a human monoclonal antibody to CCL2 (also known as MCP-1), which is involved in the recruitment of inflammatory monocytes[177]. Researchers at Promedior are investigating the protective effects of recombinant human serum amyloid P (SAP; also known as pentraxin 2) in IPF and post-surgical scarring in patients treated for glaucoma[178]. Their preclinical studies have suggested that SAP reduces inflammation and fibrosis by inducing the production of IL-10 in 'proresolution' macrophages[179]. Ono Pharmaceutical is examining whether a competitive inhibitor of human neutrophil elastase would

be beneficial in the treatment of pulmonary fibrosis and idiopathic interstitial pneumonia. Inhibitors of histone deacetylases, enzymes that regulate gene transcription, have been hypothesized to prevent cardiac fibrosis by inducing T_{reg} cells and reducing numbers of fibrocytes[180]. Finally, ImmuneWorks is examining whether T_{reg} cells could be induced to treat IPF. It has been suggested that IPF is an autoimmune disease driven by an immune response against collagen type V[181]. ImmuneWorks investigators are examining whether an orally administered antigen will induce oral tolerance by expanding a population of collagen type V–specific T_{reg} cells[104]. Thus, therapies that modulate the activation and/or recruitment of T_{reg} cells or distinct macrophage populations could emerge as viable treatments for fibrotic disease. These strategies are particularly attractive because they are based on alteration of the character of the immune response rather than simple disruption of it, which could have a more durable antifibrotic effect.

Conclusions and future directions

There are many distinct immunological and molecular mechanisms that can contribute to the progression of fibrotic disease. Dysregulated innate and adaptive immune responses are major contributors to fibrosis. However, cell-intrinsic modifications in fibroblasts and other structural cells can also contribute to fibrosis and should be considered in the design and testing of new antifibrotic therapies. Because fibrosis is often characterized by the activation of several profibrotic pathways, a multipronged approach will probably be needed to slow the progression of fibrosis. Therapeutics that target key epigenetic modifications or miRNAs could emerge as viable strategies because they regulate large families of genes rather than a single target. However, a more integrated antifibrotic strategy that simultaneously targets important inflammatory mediators, profibrotic cytokines and epigenetic and cell and/or tissue intrinsic changes will probably emerge as the most successful way to treat this highly complex and difficult-to-manage pathology. Thus, we need to begin devising and testing strategies that incorporate combination therapies. One of the major obstacles slowing the development of antifibrotic drugs is the lack of disease-specific biomarkers that can be used to identify patients who might benefit from a specific therapy. Therefore, it will be important to incorporate genetic and biological phenotyping in the clinical staging of patients diagnosed with fibrosis, so that more homogenous patient populations can be selected for specific trials. It will also be important to design clinical trials with well-defined clinical endpoints and to develop techniques that can quickly, noninvasively and accurately evaluate the efficacy of new antifibrotic therapies. Examples of such techniques are the 6-minute walk test, measurements of forced vital capacity and patient-recorded outcomes (such as dyspnea and quality-of-life changes) used in some IPF trials. New and improved preclinical models that more closely replicate fibrotic diseases in humans are also needed, as was recently demonstrated in a mouse model of liver cirrhosis[92]. Studies are increasingly suggesting that, although fibrosis is often linked with a strong inflammatory response initially, there are specific mediators and pathways contributing to the pathogenesis of fibrosis that are distinct from the mechanisms driving inflammation. Thus, to design effective therapeutics for fibrotic disease, we need to begin viewing fibrosis as a pathological process distinct from inflammation. Further, because inflammatory mediators are intimately involved in wound repair and regulate both the initiation and resolution of fibrosis, we need to figure out how to harness the beneficial aspects of inflammation so that fibrosis can be slowed or reversed and normal tissue regenerated, which is the ultimate goal of all fibrosis research.

ACKNOWLEDGMENTS

We would like to sincerely thank the past and present members of our laboratory for their guidance, comments and support. The Wynn laboratory is supported by the intramural research program of the US National Institutes of Health, National Institute of Allergy and Infectious Diseases and has benefited from cooperative research-and-development agreements with Pfizer, MedImmune, Amgen, Regeneron, Centocor and Genentech.

COMPETING FINANCIAL INTERESTS

The authors declare competing financial interests: details are available in the online version of the paper.

Published online at http://www.nature.com/doifinder/10.1038/nm.2807.
Reprints and permissions information is available online at http://www.nature.com/reprints/index.html.

1. Bataller, R. & Brenner, D.A. Liver fibrosis. *J. Clin. Invest.* **115**, 209–218 (2005).
2. Wynn, T.A. Integrating mechanisms of pulmonary fibrosis. *J. Exp. Med.* **208**, 1339–1350 (2011).
3. Wynn, T.A. Cellular and molecular mechanisms of fibrosis. *J. Pathol.* **214**, 199–210 (2008).
4. Gabbiani, G. The myofibroblast in wound healing and fibrocontractive diseases. *J. Pathol.* **200**, 500–503 (2003).
5. Kalluri, R. & Zeisberg, M. Fibroblasts in cancer. *Nat. Rev. Cancer* **6**, 392–401 (2006).
6. Fujii, T. *et al.* Mouse model of carbon tetrachloride–induced liver fibrosis: histopathological changes and expression of CD133 and epidermal growth factor. *BMC Gastroenterol.* **10**, 79 (2010).
7. Chen, J. & Stubbe, J. Bleomycins: towards better therapeutics. *Nat. Rev. Cancer* **5**, 102–112 (2005).
8. Esmon, C.T. The interactions between inflammation and coagulation. *Br. J. Haematol.* **131**, 417–430 (2005).
9. Barrientos, S., Stojadinovic, O., Golinko, M.S., Brem, H. & Tomic-Canic, M. Growth factors and cytokines in wound healing. *Wound Repair Regen.* **16**, 585–601 (2008).
10. Chambers, R.C. Procoagulant signalling mechanisms in lung inflammation and fibrosis: novel opportunities for pharmacological intervention? *Br. J. Pharmacol.* **153**, S367–S378 (2008).
11. Scotton, C.J. *et al.* Increased local expression of coagulation factor X contributes to the fibrotic response in human and murine lung injury. *J. Clin. Invest.* **119**, 2550–2563 (2009).
12. Coughlin, S.R. Thrombin signalling and protease-activated receptors. *Nature* **407**, 258–264 (2000).
13. Fiorucci, S. *et al.* PAR1 antagonism protects against experimental liver fibrosis. Role of proteinase receptors in stellate cell activation. *Hepatology* **39**, 365–375 (2004).
14. Anstee, Q.M. *et al.* Coagulation status modulates murine hepatic fibrogenesis: implications for the development of novel therapies. *J. Thromb. Haemost.* **6**, 1336–1343 (2008).
15. Wanless, I.R. *et al.* Hepatic and portal vein thrombosis in cirrhosis: possible role in development of parenchymal extinction and portal hypertension. *Hepatology* **21**, 1238–1247 (1995).
16. Li, Y. *et al.* Severe lung fibrosis requires an invasive fibroblast phenotype regulated by hyaluronan and CD44. *J. Exp. Med.* **208**, 1459–1471 (2011).
17. Duffield, J.S. *et al.* Selective depletion of macrophages reveals distinct, opposing roles during liver injury and repair. *J. Clin. Invest.* **115**, 56–65 (2005).
18. Pardo, A. *et al.* Increase of lung neutrophils in hypersensitivity pneumonitis is associated with lung fibrosis. *Am. J. Respir. Crit. Care Med.* **161**, 1698–1704 (2000).
19. Connolly, M.K. *et al.* In liver fibrosis, dendritic cells govern hepatic inflammation in mice via TNF-α. *J. Clin. Invest.* **119**, 3213–3225 (2009).
20. Zhang, Y., Lee, T.C., Guillemin, B., Yu, M.C. & Rom, W.N. Enhanced IL-1β and tumor necrosis factor-α release and messenger RNA expression in macrophages from idiopathic pulmonary fibrosis or after asbestos exposure. *J. Immunol.* **150**, 4188–4196 (1993).
21. Miyazaki, Y. *et al.* Expression of a tumor necrosis factor-α transgene in murine lung causes lymphocytic and fibrosing alveolitis. A mouse model of progressive pulmonary fibrosis. *J. Clin. Invest.* **96**, 250–259 (1995).
22. Kolb, M., Margetts, P.J., Anthony, D.C., Pitossi, F. & Gauldie, J. Transient expression of IL-1β induces acute lung injury and chronic repair leading to pulmonary fibrosis. *J. Clin. Invest.* **107**, 1529–1536 (2001).
23. Piguet, P.F., Collart, M.A., Grau, G.E., Sappino, A.P. & Vassalli, P. Requirement of tumour necrosis factor for development of silica-induced pulmonary fibrosis. *Nature* **344**, 245–247 (1990).
24. Piguet, P.F., Collart, M.A., Grau, G.E., Kapanci, Y. & Vassalli, P. Tumor necrosis factor/cachectin plays a key role in bleomycin-induced pneumopathy and fibrosis. *J. Exp. Med.* **170**, 655–663 (1989).
25. Piguet, P.F., Ribaux, C., Karpuz, V., Grau, G.E. & Kapanci, Y. Expression and localization of tumor necrosis factor-α and its mRNA in idiopathic pulmonary fibrosis. *Am. J. Pathol.* **143**, 651–655 (1993).
26. Bahcecioglu, I.H. *et al.* Hepatoprotective effect of infliximab, an anti–TNF-α agent, on carbon tetrachloride–induced hepatic fibrosis. *Inflammation* **31**, 215–221 (2008).

27. Nawroth, I. *et al.* Intraperitoneal administration of chitosan/DsiRNA nanoparticles targeting TNF-α prevents radiation-induced fibrosis. *Radiother. Oncol.* **97**, 143–148 (2010).
28. Tomita, K. *et al.* Tumour necrosis factor-α signalling through activation of Kupffer cells plays an essential role in liver fibrosis of non-alcoholic steatohepatitis in mice. *Gut* **55**, 415–424 (2006).
29. Raghu, G. *et al.* Treatment of idiopathic pulmonary fibrosis with etanercept: an exploratory, placebo-controlled trial. *Am. J. Respir. Crit. Care Med.* **178**, 948–955 (2008).
30. Gasse, P. *et al.* IL-1R1/MyD88 signaling and the inflammasome are essential in pulmonary inflammation and fibrosis in mice. *J. Clin. Invest.* **117**, 3786–3799 (2007).
31. Bujak, M. & Frangogiannis, N.G. The role of IL-1 in the pathogenesis of heart disease. *Arch. Immunol. Ther. Exp. (Warsz.)* **57**, 165–176 (2009).
32. Jones, L.K. *et al.* IL-1RI deficiency ameliorates early experimental renal interstitial fibrosis. *Nephrol. Dial. Transplant.* **24**, 3024–3032 (2009).
33. Kamari, Y. *et al.* Lack of interleukin-1α or interleukin-1β inhibits transformation of steatosis to steatohepatitis and liver fibrosis in hypercholesterolemic mice. *J. Hepatol.* **55**, 1086–1094 (2011).
34. Fan, J.M. *et al.* Interleukin-1 induces tubular epithelial-myofibroblast transdifferentiation through a transforming growth factor-β1–dependent mechanism *in vitro*. *Am. J. Kidney Dis.* **37**, 820–831 (2001).
35. Diaz, J.A. *et al.* Critical role for IL-6 in hypertrophy and fibrosis in chronic cardiac allograft rejection. *Am. J. Transplant.* **9**, 1773–1783 (2009).
36. Natsume, M. *et al.* Attenuated liver fibrosis and depressed serum albumin levels in carbon tetrachloride–treated IL-6–deficient mice. *J. Leukoc. Biol.* **66**, 601–608 (1999).
37. Verrecchia, F. & Mauviel, A. Transforming growth factor-β and fibrosis. *World J. Gastroenterol.* **13**, 3056–3062 (2007).
38. Kitani, A. *et al.* Transforming growth factor (TGF)-β1–producing regulatory T cells induce Smad-mediated interleukin-10 secretion that facilitates coordinated immunoregulatory activity and amelioration of TGF-β1–mediated fibrosis. *J. Exp. Med.* **198**, 1179–1188 (2003).
39. Wynn, T.A. & Barron, L. Macrophages: master regulators of inflammation and fibrosis. *Semin. Liver Dis.* **30**, 245–257 (2010).
40. Gordon, S. & Taylor, P.R. Monocyte and macrophage heterogeneity. *Nat. Rev. Immunol.* **5**, 953–964 (2005).
41. Hesse, M. *et al.* Differential regulation of nitric oxide synthase-2 and arginase-1 by type 1/type 2 cytokines *in vivo*: granulomatous pathology is shaped by the pattern of l-arginine metabolism. *J. Immunol.* **167**, 6533–6544 (2001).
42. Song, E. *et al.* Influence of alternatively and classically activated macrophages on fibrogenic activities of human fibroblasts. *Cell. Immunol.* **204**, 19–28 (2000).
43. Sun, L. *et al.* New concepts of IL-10–induced lung fibrosis: fibrocyte recruitment and M2 activation in a CCL2/CCR2 axis. *Am. J. Physiol. Lung Cell Mol. Physiol.* **300**, L341–L353 (2011).
44. Herbert, D.R. *et al.* Alternative macrophage activation is essential for survival during schistosomiasis and downmodulates T helper 1 responses and immunopathology. *Immunity* **20**, 623–635 (2004).
45. Pesce, J.T. *et al.* Arginase-1–expressing macrophages suppress $T_{H}2$ cytokine-driven inflammation and fibrosis. *PLoS Pathog.* **5**, e1000371 (2009).
46. Murray, P.J. & Wynn, T.A. Protective and pathogenic functions of macrophage subsets. *Nat. Rev. Immunol.* **11**, 723–737 (2011).
47. Ricote, M., Li, A.C., Willson, T.M., Kelly, C.J. & Glass, C.K. The peroxisome proliferator–activated receptor-γ is a negative regulator of macrophage activation. *Nature* **391**, 79–82 (1998).
48. Odegaard, J.I. *et al.* Macrophage-specific PPAR-γ controls alternative activation and improves insulin resistance. *Nature* **447**, 1116–1120 (2007).
49. Kulkarni, A.A. *et al.* PPAR-γ ligands repress TGF-β–induced myofibroblast differentiation by targeting the PI3K/Akt pathway: implications for therapy of fibrosis. *PLoS ONE* **6**, e15909 (2011).
50. Iglarz, M. *et al.* Peroxisome proliferator-activated receptor-α and receptor-γ activators prevent cardiac fibrosis in mineralocorticoid-dependent hypertension. *Hypertension* **42**, 737–743 (2003).
51. Yang, L., Scimpson, A.A., Chen, L., Wallace Harrington, W. & Rockey, D.C. Effectiveness of the PPAR-γ agonist, GW570, in liver fibrosis. *Inflamm. Res.* **59**, 1061–1071 (2010).
52. Kawai, T. *et al.* PPAR-γ agonist attenuates renal interstitial fibrosis and inflammation through reduction of TGF-β. *Lab. Invest.* **89**, 47–58 (2009).
53. Aoki, Y. *et al.* Pioglitazone, a peroxisome proliferator–activated receptor-γ ligand, suppresses bleomycin-induced acute lung injury and fibrosis. *Respiration* **77**, 311–319 (2009).
54. Levick, S.P. *et al.* Cardiac mast cells mediate left ventricular fibrosis in the hypertensive rat heart. *Hypertension* **53**, 1041–1047 (2009).
55. Reiman, R.M. *et al.* Interleukin-5 (IL-5) augments the progression of liver fibrosis by regulating IL-13 activity. *Infect. Immun.* **74**, 1471–1479 (2006).
56. Minshall, E.M. *et al.* Eosinophil-associated TGF-β1 mRNA expression and airways fibrosis in bronchial asthma. *Am. J. Respir. Cell Mol. Biol.* **17**, 326–333 (1997).
57. Humbles, A.A. *et al.* A critical role for eosinophils in allergic airways remodeling. *Science* **305**, 1776–1779 (2004).
58. Levi-Schaffer, F. *et al.* Human eosinophils regulate human lung- and skin-derived fibroblast properties *in vitro*: a role for transforming growth factor-β (TGF-β). *Proc. Natl. Acad. Sci. USA* **96**, 9660–9665 (1999).
59. Peterson, M.W., Monick, M. & Hunninghake, G.W. Prognostic role of eosinophils in pulmonary fibrosis. *Chest* **92**, 51–56 (1987).
60. Gilbert, H.S. Myelofibrosis revisited: characterization and classification of myelofibrosis in the setting of myeloproliferative disease. *Prog. Clin. Biol. Res.* **154**, 3–17 (1984).
61. Wilson, M.S. *et al.* Bleomycin and IL-1β–mediated pulmonary fibrosis is IL-17A dependent. *J. Exp. Med.* **207**, 535–552 (2010).
62. Faust, S.M. *et al.* Role of T cell TGF-β signaling and IL-17 in allograft acceptance and fibrosis associated with chronic rejection. *J. Immunol.* **183**, 7297–7306 (2009).
63. Fan, L. *et al.* Neutralizing IL-17 prevents obliterative bronchiolitis in murine orthotopic lung transplantation. *Am. J. Transplant.* **11**, 911–922 (2011).
64. Feng, W. *et al.* IL-17 induces myocardial fibrosis and enhances RANKL/OPG and MMP/TIMP signaling in isoproterenol-induced heart failure. *Exp. Mol. Pathol.* **87**, 212–218 (2009).
65. Wang, L., Chen, S.J. & Xu, K.S. IL-17 expression is correlated with hepatitis B–related liver diseases and fibrosis. *Int. J. Mol. Med.* **27**, 385–392 (2011).
66. Laan, M. *et al.* Neutrophil recruitment by human IL-17 via CXC chemokine release in the airways. *J. Immunol.* **162**, 2347–2352 (1999).
67. Zhu, F. *et al.* IL-17 induces apoptosis of vascular endothelial cells—a potential mechanism for human acute coronary syndrome. *Clin. Immunol.* **141**, 152–160 (2011).
68. Kinder, B.W. *et al.* Baseline BAL neutrophilia predicts early mortality in idiopathic pulmonary fibrosis. *Chest* **133**, 226–232 (2008).
69. Gasse, P. *et al.* IL-1 and IL-23 mediate early IL-17A production in pulmonary inflammation leading to late fibrosis. *PLoS ONE* **6**, e23185 (2011).
70. Cortez, D.M. *et al.* IL-17 stimulates MMP-1 expression in primary human cardiac fibroblasts via p38 MAPK- and ERK1/2-dependent C/EBP-β, NF-κB and AP-1 activation. *Am. J. Physiol. Heart Circ. Physiol.* **293**, H3356–H3365 (2007).
71. Wynn, T.A. *et al.* An IL-12–based vaccination method for preventing fibrosis induced by schistosome infection. *Nature* **376**, 594–596 (1995).
72. Wynn, T.A. Fibrotic disease and the $T_{H}1/T_{H}2$ paradigm. *Nat. Rev. Immunol.* **4**, 583–594 (2004).
73. Ong, C., Wong, C., Roberts, C.R., Teh, H.S. & Jirik, F.R. Anti-IL-4 treatment prevents dermal collagen deposition in the tight-skin mouse model of scleroderma. *Eur. J. Immunol.* **28**, 2619–2629 (1998).
74. Chiaramonte, M.G., Donaldson, D.D., Cheever, A.W. & Wynn, T.A. An IL-13 inhibitor blocks the development of hepatic fibrosis during a T helper type 2–dominated inflammatory response. *J. Clin. Invest.* **104**, 777–785 (1999).
75. Yang, G. *et al.* Anti–IL-13 monoclonal antibody inhibits airway hyper-responsiveness, inflammation and airway remodeling. *Cytokine* **28**, 224–232 (2004).
76. Murray, L.A. *et al.* Hyper-responsiveness of IPF/UIP fibroblasts: interplay between TGF-β1, IL-13 and CCL2. *Int. J. Biochem. Cell Biol.* **40**, 2174–2182 (2008).
77. Kolodsick, J.E. *et al.* Protection from fluorescein isothiocyanate–induced fibrosis in IL-13–deficient, but not IL-4–deficient, mice results from impaired collagen synthesis by fibroblasts. *J. Immunol.* **172**, 4068–4076 (2004).
78. Fuschiotti, P. Role of IL-13 in systemic sclerosis. *Cytokine* **56**, 544–549 (2011).
79. Oh, M.H. *et al.* IL-13 induces skin fibrosis in atopic dermatitis by thymic stromal lymphopoietin. *J. Immunol.* **186**, 7232–7242 (2011).
80. Han, G., Zhang, H., Xie, C.H. & Zhou, Y.F. $T_{H}2$-like immune response in radiation-induced lung fibrosis. *Oncol. Rep.* **26**, 383–388 (2011).
81. Heller, F., Fuss, I.J., Nieuwenhuis, E.E., Blumberg, R.S. & Strober, W. Oxazolone colitis, a $T_{H}2$ colitis model resembling ulcerative colitis, is mediated by IL-13–producing NKT cells. *Immunity* **17**, 629–638 (2002).
82. Weng, H.L. *et al.* The etiology of liver damage imparts cytokines transforming growth factor-β1 or interleukin-13 as driving forces in fibrogenesis. *Hepatology* **50**, 230–243 (2009).
83. Shimamura, T. *et al.* Novel role of IL-13 in fibrosis induced by nonalcoholic steatohepatitis and its amelioration by IL-13R–directed cytotoxin in a rat model. *J. Immunol.* **181**, 4656–4665 (2008).
84. Lee, C.G. *et al.* Interleukin-13 induces tissue fibrosis by selectively stimulating and activating transforming growth factor-β1. *J. Exp. Med.* **194**, 809–822 (2001).
85. Liu, Y. *et al.* IL-13 induces connective tissue growth factor in rat hepatic stellate cells via TGF-β–independent Smad signaling. *J. Immunol.* **187**, 2814–2823 (2011).
86. Kavratne, M. *et al.* IL-13 activates a mechanism of tissue fibrosis that is completely TGF-β independent. *J. Immunol.* **173**, 4020–4029 (2004).
87. Lanone, S., D.A. *et al.* Direct effects of interleukin-13 on epithelial cells cause airway hyperreactivity and mucus overproduction in asthma. *Nat. Med.* **8**, 885–889 (2002).
88. Lee, J.H. *et al.* Interleukin-13 induces dramatically different transcriptional programs in three human airway cell types. *Am. J. Respir. Cell Mol. Biol.* **25**, 474–485 (2001).
89. Wilson, M.S. *et al.* Colitis and intestinal inflammation in *IL10*$^{-/-}$ mice results from IL-13Rα2–mediated attenuation of IL-13 activity. *Gastroenterology* **140**, 254–264 *e2* (2011).
90. Ramalingam, T.R. *et al.* Unique functions of the type II interleukin-4 receptor identified in mice lacking the interleukin-13 receptor-α1 chain. *Nat. Immunol.* **9**, 25–33 (2008).
91. Chiaramonte, M.G. *et al.* Regulation and function of the interleukin-13 receptor-α2 during a T helper cell type 2–dominant immune response. *J. Exp. Med.* **197**, 687–701 (2003).

92. Mentink-Kane, M.M. *et al.* Accelerated and progressive and lethal liver fibrosis in mice that lack interleukin (IL)-10, IL-12p40, and IL-13Rα2. *Gastroenterology* **141**, 2200–2209 (2011).
93. Mentink-Kane, M.M. & Wynn, T.A. Opposing roles for IL-13 and IL-13 receptor-α2 in health and disease. *Immunol. Rev.* **202**, 191–202 (2004).
94. Baroni, G.S. *et al.* Interferon-γ decreases hepatic stellate cell activation and extracellular matrix deposition in rat liver fibrosis. *Hepatology* **23**, 1189–1199 (1996).
95. Giri, S.N., Hyde, D.M. & Marafino, B.J. Jr. Ameliorating effect of murine interferon-γ on bleomycin-induced lung collagen fibrosis in mice. *Biochem. Med. Metab. Biol.* **36**, 194–197 (1986).
96. Oldroyd, S.D., Thomas, G.L., Gabbiani, G. & El Nahas, A.M. Interferon-γ inhibits experimental renal fibrosis. *Kidney Int.* **56**, 2116–2127 (1999).
97. Kim, J.H. *et al.* Natural killer T (NKT) cells attenuate bleomycin-induced pulmonary fibrosis by producing interferon-γ. *Am. J. Pathol.* **167**, 1231–1241 (2005).
98. Jeong, W.I., Park, O. & Gao, B. Abrogation of the antifibrotic effects of natural killer cells/interferon-γ contributes to alcohol acceleration of liver fibrosis. *Gastroenterology* **134**, 248–258 (2008).
99. Ulloa, L., Doody, J. & Massague, J. Inhibition of transforming growth factor-β/SMAD signalling by the interferon-γ/STAT pathway. *Nature* **397**, 710–713 (1999).
100. Gurujeyalakshmi, G. & Giri, S.N. Molecular mechanisms of antifibrotic effect of interferon-γ in bleomycin mouse model of lung fibrosis: downregulation of TGF-β and procollagen I and III gene expression. *Exp. Lung Res.* **21**, 791–808 (1995).
101. Shao, D.D., Suresh, R., Vakil, V., Gomer, R.H. & Pilling, D. Pivotal advance: T_H1 cytokines inhibit, and T_H2 cytokines promote fibrocyte differentiation. *J. Leukoc. Biol.* **83**, 1323–1333 (2008).
102. Keane, M.P., Belperio, J.A., Burdick, M.D. & Strieter, R.M. IL-12 attenuates bleomycin-induced pulmonary fibrosis. *Am. J. Physiol. Lung Cell Mol. Physiol.* **281**, L92–L97 (2001).
103. King, T.E. Jr. *et al.* Effect of interferon-γ-1b on survival in patients with idiopathic pulmonary fibrosis (INSPIRE): a multicentre, randomised, placebo-controlled trial. *Lancet* **374**, 222–228 (2009).
104. Kotsianidis, I. *et al.* Global impairment of $CD4^+CD25^+FOXP3^+$ regulatory T cells in idiopathic pulmonary fibrosis. *Am. J. Respir. Crit. Care Med.* **179**, 1121–1130 (2009).
105. Vetrone, S.A. *et al.* Osteopontin promotes fibrosis in dystrophic mouse muscle by modulating immune cell subsets and intramuscular TGF-β. *J. Clin. Invest.* **119**, 1583–1594 (2009).
106. Kanellakis, P., Dinh, T.N., Agrotis, A. & Bobik, A. $CD4^+CD25^+Foxp3^+$ regulatory T cells suppress cardiac fibrosis in the hypertensive heart. *J. Hypertens.* **29**, 1820–1828 (2011).
107. Zhang, J.L. *et al.* CD3 mAb treatment ameliorated the severity of the cGVHD-induced lupus nephritis in mice by upregulation of $Foxp3^+$ regulatory T cells in the target tissue: kidney. *Transpl. Immunol.* **24**, 17–25 (2010).
108. Claassen, M.A., de Knegt, R.J., Tilanus, H.W., Janssen, H.L. & Boonstra, A. Abundant numbers of regulatory T cells localize to the liver of chronic hepatitis C–infected patients and limit the extent of fibrosis. *J. Hepatol.* **52**, 315–321 (2010).
109. Estes, J.D. *et al.* Simian immunodeficiency virus-induced lymphatic tissue fibrosis is mediated by transforming growth factor-β1–positive regulatory T cells and begins in early infection. *J. Infect. Dis.* **195**, 551–561 (2007).
110. Liu, F. *et al.* $CD4^+CD25^+Foxp3^+$ regulatory T cells depletion may attenuate the development of silica-induced lung fibrosis in mice. *PLoS ONE* **5**, e15404 (2010).
111. Baarsma, H.A. *et al.* Activation of Wnt/β-catenin signaling in pulmonary fibroblasts by TGF-β is increased in chronic obstructive pulmonary disease. *PLoS ONE* **6**, e25450 (2011).
112. Wei, J. *et al.* Canonical Wnt signaling induces skin fibrosis and subcutaneous lipoatrophy: a novel mouse model for scleroderma? *Arthritis Rheum.* **63**, 1707–1717 (2011).
113. Surendran, K., Schiavi, S. & Hruska, K.A. Wnt-dependent β-catenin signaling is activated after unilateral ureteral obstruction, and recombinant secreted frizzled-related protein 4 alters the progression of renal fibrosis. *J. Am. Soc. Nephrol.* **16**, 2373–2384 (2005).
114. Wang, D., Dai, C., Li, Y. & Liu, Y. Canonical Wnt/β-catenin signaling mediates transforming growth factor-β1–driven podocyte injury and proteinuria. *Kidney Int.* **80**, 1159–1169 (2011).
115. Jiang, F., Parsons, C.J. & Stefanovic, B. Gene-expression profile of quiescent and activated rat hepatic stellate cells implicates Wnt signaling pathway in activation. *J. Hepatol.* **45**, 401–409 (2006).
116. Königshoff, M. *et al.* WNT1-inducible signaling protein-1 mediates pulmonary fibrosis in mice and is upregulated in humans with idiopathic pulmonary fibrosis. *J. Clin. Invest.* **119**, 772–787 (2009).
117. Hinz, B., Celetta, G., Tomasek, J.J., Gabbiani, G. & Chaponnier, C. α-smooth muscle actin expression upregulates fibroblast contractile activity. *Mol. Biol. Cell* **12**, 2730–2741 (2001).
118. Heise, R.L., Stober, V., Cheluvaraju, C., Hollingsworth, J.W. & Garantziotis, S. Mechanical stretch induces epithelial-mesenchymal transition in alveolar epithelia via hyaluronan activation of innate immunity. *J. Biol. Chem.* **286**, 17435–17444 (2011).
119. Chen, J.H., Chen, W.L., Sider, K.L., Yip, C.Y. & Simmons, C.A. β-catenin mediates mechanically regulated, transforming growth factor-β1–induced myofibroblast differentiation of aortic valve interstitial cells. *Arterioscler. Thromb. Vasc. Biol.* **31**, 590–597 (2011).
120. Balestrini, J.L., Chaudhry, S., Sarrazy, V., Koehler, A. & Hinz, B. The mechanical memory of lung myofibroblasts. *Integr. Biol.* **4**, 410–421 (2012).
121. Hinz, B. Tissue stiffness, latent TGF-β1 activation, and mechanical signal transduction: implications for the pathogenesis and treatment of fibrosis. *Curr. Rheumatol. Rep.* **11**, 120–126 (2009).
122. Bechtel, W. *et al.* Methylation determines fibroblast activation and fibrogenesis in the kidney. *Nat. Med.* **16**, 544–550 (2010).
123. Coward, W.R., Watts, K., Feghali-Bostwick, C.A., Jenkins, G. & Pang, L. Repression of IP-10 by interactions between histone deacetylation and hypermethylation in idiopathic pulmonary fibrosis. *Mol. Cell Biol.* **30**, 2874–2886 (2010).
124. Sanders, Y.Y. *et al. Thy-1* promoter hypermethylation: a novel epigenetic pathogenic mechanism in pulmonary fibrosis. *Am. J. Respir. Cell Mol. Biol.* **39**, 610–618 (2008).
125. Malhi, H. & Gores, G.J. Molecular mechanisms of lipotoxicity in nonalcoholic fatty liver disease. *Semin. Liver Dis.* **28**, 360–369 (2008).
126. Korfei, M. *et al.* Epithelial endoplasmic reticulum stress and apoptosis in sporadic idiopathic pulmonary fibrosis. *Am. J. Respir. Crit. Care Med.* **178**, 838–846 (2008).
127. Lawson, W.E. *et al.* Endoplasmic reticulum stress in alveolar epithelial cells is prominent in IPF: association with altered surfactant protein processing and herpesvirus infection. *Am. J. Physiol. Lung Cell Mol. Physiol.* **294**, L1119–L1126 (2008).
128. Calado, R.T. & Young, N.S. Telomere diseases. *N. Engl. J. Med.* **361**, 2353–2365 (2009).
129. Tsakiri, K.D. *et al.* Adult-onset pulmonary fibrosis caused by mutations in telomerase. *Proc. Natl. Acad. Sci. USA* **104**, 7552–7557 (2007).
130. Cronkhite, J.T. *et al.* Telomere shortening in familial and sporadic pulmonary fibrosis. *Am. J. Respir. Crit. Care Med.* **178**, 729–737 (2008).
131. Alder, J.K. *et al.* Short telomeres are a risk factor for idiopathic pulmonary fibrosis. *Proc. Natl. Acad. Sci. USA* **105**, 13051–13056 (2008).
132. Armanios, M.Y. *et al.* Telomerase mutations in families with idiopathic pulmonary fibrosis. *N. Engl. J. Med.* **356**, 1317–1326 (2007).
133. Lee, J. *et al.* Lung alveolar integrity is compromised by telomere shortening in telomerase-null mice. *Am. J. Physiol. Lung Cell Mol. Physiol.* **296**, L57–L70 (2009).
134. Liu, T. *et al.* Telomerase regulation of myofibroblast differentiation. *Am. J. Respir. Cell Mol. Biol.* **34**, 625–633 (2006).
135. Li, H., Xu, D., Li, J., Berndt, M.C. & Liu, J.P. Transforming growth factor-β suppresses human telomerase reverse transcriptase (hTERT) by Smad3 interactions with c-Myc and the hTERT gene. *J. Biol. Chem.* **281**, 25588–25600 (2006).
136. Proctor, C.J. & Kirkwood, T.B. Modelling telomere shortening and the role of oxidative stress. *Mech. Ageing Dev.* **123**, 351–363 (2002).
137. Liu, T. *et al.* Telomerase activity is required for bleomycin-induced pulmonary fibrosis in mice. *J. Clin. Invest.* **117**, 3800–3809 (2007).
138. Liu, G. *et al.* miR-21 mediates fibrogenic activation of pulmonary fibroblasts and lung fibrosis. *J. Exp. Med.* **207**, 1589–1597 (2010).
139. Thum, T. *et al.* MicroRNA-21 contributes to myocardial disease by stimulating MAP kinase signalling in fibroblasts. *Nature* **456**, 980–984 (2008).
140. Chan, J.A., Krichevsky, A.M. & Kosik, K.S. MicroRNA-21 is an antiapoptotic factor in human glioblastoma cells. *Cancer Res.* **65**, 6029–6033 (2005).
141. Patrick, D.M. *et al.* Stress-dependent cardiac remodeling occurs in the absence of microRNA-21 in mice. *J. Clin. Invest.* **120**, 3912–3916 (2010).
142. Chung, A.C., Huang, X.R., Meng, X. & Lan, H.Y. miR-192 mediates TGF-β/Smad3-driven renal fibrosis. *J. Am. Soc. Nephrol.* **21**, 1317–1325 (2010).
143. Kato, M. *et al.* TGF-β activates Akt kinase through a microRNA-dependent amplifying circuit targeting PTEN. *Nat. Cell Biol.* **11**, 881–889 (2009).
144. Maurer, B. *et al.* microRNA-29, a key regulator of collagen expression in systemic sclerosis. *Arthritis Rheum.* **62**, 1733–1743 (2010).
145. Roderburg, C. *et al.* Micro-RNA profiling reveals a role for miR-29 in human and murine liver fibrosis. *Hepatology* **53**, 209–218 (2011).
146. van Rooij, E. *et al.* Dysregulation of microRNAs after myocardial infarction reveals a role of miR-29 in cardiac fibrosis. *Proc. Natl. Acad. Sci. USA* **105**, 13027–13032 (2008).
147. Ogawa, T. *et al.* Suppression of type I collagen production by microRNA-29b in cultured human stellate cells. *Biochem. Biophys. Res. Commun.* **391**, 316–321 (2010).
148. Pandit, K.V. *et al.* Inhibition and role of let-7d in idiopathic pulmonary fibrosis. *Am. J. Respir. Crit. Care Med.* **182**, 220–229 (2010).
149. Duisters, R.F. *et al.* miR-133 and miR-30 regulate connective tissue growth factor: implications for a role of microRNAs in myocardial matrix remodeling. *Circ. Res.* **104**, 170–178 (2009).
150. Venugopal, S.K. *et al.* Liver fibrosis causes downregulation of miRNA-150 and miRNA-194 in hepatic stellate cells, and their overexpression causes decreased stellate cell activation. *Am. J. Physiol. Gastrointest. Liver Physiol.* **298**, G101–G106 (2010).
151. Wang, B. *et al.* miR-200a Prevents renal fibrogenesis through repression of TGF-β2 expression. *Diabetes* **60**, 280–287 (2011).
152. Richeldi, L. & du Bois, R.M. Pirfenidone in idiopathic pulmonary fibrosis: the CAPACITY program. *Expert Rev. Respir. Med.* **5**, 473–481 (2011).
153. Nakanishi, H., Sugiura, T., Streisand, J.B., Lonning, S.M. & Roberts, J.D. Jr. TGF-β–neutralizing antibodies improve pulmonary alveologenesis and vasculogenesis in the injured newborn lung. *Am. J. Physiol. Lung Cell Mol. Physiol.* **293**, L151–L161 (2007).

154. Munger, J.S. *et al.* The integrin $\alpha_v\beta_6$ binds and activates latent TGF-β1: a mechanism for regulating pulmonary inflammation and fibrosis. *Cell* **96**, 319–328 (1999).
155. Hahm, K. *et al.* $\alpha_v\beta_6$ integrin regulates renal fibrosis and inflammation in Alport mouse. *Am. J. Pathol.* **170**, 110–125 (2007).
156. Hemavathy, K. & Wang, J.C. Epigenetic modifications: new therapeutic targets in primary myelofibrosis. *Curr. Stem Cell Res. Ther.* **4**, 281–286 (2009).
157. Tedstone, J.L., Richards, S.M., Garman, R.D. & Ruzek, M.C. Ultrasound imaging accurately detects skin thickening in a mouse scleroderma model. *Ultrasound Med. Biol.* **34**, 1239–1247 (2008).
158. Kono, M. *et al.* Plasma CCN2 (connective tissue growth factor; CTGF) is a potential biomarker in idiopathic pulmonary fibrosis (IPF). *Clin. Chim. Acta* **412**, 2211–2215 (2011).
159. Pradere, J.P. *et al.* LPA1 receptor activation promotes renal interstitial fibrosis. *J. Am. Soc. Nephrol.* **18**, 3110–3118 (2007).
160. Tager, A.M. *et al.* The lysophosphatidic acid receptor LPA1 links pulmonary fibrosis to lung injury by mediating fibroblast recruitment and vascular leak. *Nat. Med.* **14**, 45–54 (2008).
161. Zeisberg, M. *et al.* BMP-7 counteracts TGF-β1–induced epithelial-to-mesenchymal transition and reverses chronic renal injury. *Nat. Med.* **9**, 964–968 (2003).
162. Sidharta, P.N., van Giersbergen, P.L., Halabi, A. & Dingemanse, J. Macitentan: entry-into-humans study with a new endothelin receptor antagonist. *Eur. J. Clin. Pharmacol.* **67**, 977–984 (2011).
163. Barry-Hamilton, V. *et al.* Allosteric inhibition of lysyl oxidase-like-2 impedes the development of a pathologic microenvironment. *Nat. Med.* **16**, 1009–1017 (2010).
164. Myllyharju, J. Prolyl 4-hydroxylases, key enzymes in the synthesis of collagens and regulation of the response to hypoxia, and their roles as treatment targets. *Ann. Med.* **40**, 402–417 (2008).
165. Fineschi, S. *et al. In vivo* investigations on antifibrotic potential of proteasome inhibition in lung and skin fibrosis. *Am. J. Respir. Cell Mol. Biol.* **39**, 458–465 (2008).
166. Anan, A. *et al.* Proteasome inhibition induces hepatic stellate cell apoptosis. *Hepatology* **43**, 335–344 (2006).
167. Kralovics, R. *et al.* A gain-of-function mutation of *JAK2* in myeloproliferative disorders. *N. Engl. J. Med.* **352**, 1779–1790 (2005).
168. Daniels, C.E. *et al.* Imatinib treatment for idiopathic pulmonary fibrosis: randomized placebo-controlled trial results. *Am. J. Respir. Crit. Care Med.* **181**, 604–610 (2010).
169. Kay, J. & High, W.A. Imatinib mesylate treatment of nephrogenic systemic fibrosis. *Arthritis Rheum.* **58**, 2543–2548 (2008).
170. Richeldi, L. *et al.* Efficacy of a tyrosine kinase inhibitor in idiopathic pulmonary fibrosis. *N. Engl. J. Med.* **365**, 1079–1087 (2011).
171. Verstovsek, S. Therapeutic potential of Janus-activated kinase-2 inhibitors for the management of myelofibrosis. *Clin. Cancer Res.* **16**, 1988–1996 (2010).
172. Pockros, P.J. *et al.* Final results of a double-blind, placebo-controlled trial of the antifibrotic efficacy of interferon-γ1b in chronic hepatitis C patients with advanced fibrosis or cirrhosis. *Hepatology* **45**, 569–578 (2007).
173. Noble, P.W., Richeldi, L. & Kaminski, N. End of an ERA: lessons from negative clinical trials in idiopathic pulmonary fibrosis. *Am. J. Respir. Crit. Care Med.* **184**, 4–5 (2011).
174. Park, S.W. *et al.* Interleukin-13 and its receptors in idiopathic interstitial pneumonia: clinical implications for lung function. *J. Korean Med. Sci.* **24**, 614–620 (2009).
175. Corren, J. *et al.* Lebrikizumab treatment in adults with asthma. *N. Engl. J. Med.* **365**, 1088–1098 (2011).
176. Kraft, M. Asthma phenotypes and interleukin-13—moving closer to personalized medicine. *N. Engl. J. Med.* **365**, 1141–1144 (2011).
177. Ekert, J.E. *et al.* Chemokine (C-C motif) ligand-2 mediates direct and indirect fibrotic responses in human and murine cultured fibrocytes. *Fibrogenesis Tissue Repair* **4**, 23 (2011).
178. Duffield, J.S. & Lupher, M.L. Jr. PRM-151 (recombinant human serum amyloid P/pentraxin 2) for the treatment of fibrosis. *Drug News Perspect.* **23**, 305–315 (2010).
179. Castaño, A.P. *et al.* Serum amyloid P inhibits fibrosis through FcγR-dependent monocyte-macrophage regulation *in vivo*. *Sci. Transl. Med.* **1**, 5ra13 (2009).
180. McKinsey, T.A. Therapeutic potential for HDAC inhibitors in the heart. *Annu. Rev. Pharmacol. Toxicol.* **52**, 303–319 (2012).
181. Dart, M.L. *et al.* Interleukin-17–dependent autoimmunity to collagen type V in atherosclerosis. *Circ. Res.* **107**, 1106–1116 (2010).

REVIEW

nature medicine

From prenatal genomic diagnosis to fetal personalized medicine: progress and challenges

Diana W Bianchi

Thus far, the focus of personalized medicine has been the prevention and treatment of conditions that affect adults. Although advances in genetic technology have been applied more frequently to prenatal diagnosis than to fetal treatment, genetic and genomic information is beginning to influence pregnancy management. Recent developments in sequencing the fetal genome combined with progress in understanding fetal physiology using gene expression arrays indicate that we could have the technical capabilities to apply an individualized medicine approach to the fetus. Here I review recent advances in prenatal genetic diagnostics, the challenges associated with these new technologies and how the information derived from them can be used to advance fetal care. Historically, the goal of prenatal diagnosis has been to provide an informed choice to prospective parents. We are now at a point where that goal can and should be expanded to incorporate genetic, genomic and transcriptomic data to develop new approaches to fetal treatment.

The goal of personalized medicine is to optimize health and develop individualized therapy for disease by combining a person's genetic and genomic data with information about their lifestyle and exposures. So far, personalized medicine has focused on the prevention and treatment of conditions affecting adults, such as cancer and cardiovascular disease[1]. Remarkably, few studies have addressed the therapeutic implications of recent advances in genetic technologies for the fetus. This is surprising, as progress in prenatal diagnosis[2] has led to widespread antenatal screening programs that have been successfully reproduced throughout the developed world. One could argue that a personalized medicine approach would have maximal benefit over the course of an individual's lifetime if it began in the womb or at birth. However, a major limitation of applying advanced genetic and genomic techniques in the prenatal setting is that genomic variation can be identified for which the clinical implications are not known. But as knowledge of the fetus and fetal development progresses by sequencing fetal DNA and RNA, new treatment opportunities will emerge. Now is the time to acknowledge the scientific progress that has taken place in the area of prenatal genomic medicine and consider the practical and ethical considerations raised by these technologies. Furthermore, the strong interest in and acceptance of direct-to-consumer genetic testing by many pregnant women[3–5] effectively mandates that multidisciplinary specialists should consider and discuss these issues before a 'parallel universe' populated by commercial interests is fully established outside of the traditional health care system.

Importantly, advances in prenatal diagnosis that allow for a more detailed analysis of fetal genetics and genomics provide some of the data necessary for a personalized approach to fetal medicine. I first discuss these technological advances and provide examples of how they have provided a greater understanding of the genetic basis of specific fetal disorders (**Table 1**). In the prenatal setting, pure fetal material may be obtained invasively through amniocentesis or chorionic villus sampling or noninvasively through maternal blood. The invasive diagnostic techniques are generally safe and accurate, although they need to be performed by obstetricians with specific expertise, and they carry with them a small but measurable chance of miscarriage. There is expanding interest in noninvasive techniques of fetal assessment using cell-free DNA and RNA molecules that circulate in the maternal blood. Maternal venipuncture has no associated risk of fetal loss; however, maternal blood contains a mixture of both fetal and maternal nucleic acids, which increases the downstream analytic complexity.

Transcriptomic analyses are also beginning to be applied to prenatal diagnosis; these analyses can provide a dynamic view of fetal and placental development. I discuss advances in this area and how such approaches might be used to find new biomarkers for fetal diseases or provide insights into the functional pathways involved in a particular disorder. I also discuss the practical and ethical challenges facing the field of fetal diagnostics, including how these new technologies should be incorporated into clinical practice, as well as how to move forward to translate these insights to provide new therapeutic strategies for fetal disease and achieve the goal of fetal personalized medicine.

The Mother Infant Research Institute at Tufts Medical Center and the Division of Genetics, Department of Pediatrics, Floating Hospital for Children, Boston, Massachusetts, USA. Correspondence should be addressed to D.W.B. (dbianchi@tuftsmedicalcenter.org).

Published online 6 July 2012; doi:10.1038/nm.2829

Table 1 Overview of advances in molecular testing that affect fetal diagnostics and treatment

Genetic material analyzed	Type of testing	Consequences
Chromosomal DNA	Chromosome microarray analysis	Detection of submicroscopic fetal chromosome abnormalities. Detection of copy number variation in the genome.
Cell-free DNA in maternal blood	Real-time PCR amplification; massively parallel sequencing	Noninvasive prenatal diagnosis of fetal sex, RhD genotype, aneuploidy, other submicroscopic chromosome abnormalities and single-gene disorders.
Cell-free RNA in amniotic fluid	Gene expression microarray analysis; comparative transcriptomic analyses between normal and affected individuals	Improved knowledge of fetal functional development in health and in disease states. Development of new biomarkers. Identification of new therapeutic targets.
RNA in maternal blood	Gene expression microarray analysis; comparative transcriptomic analyses between normal and affected individuals; quantitative miRNA analysis	Improved knowledge of fetal functional development in health and in disease states. Development of new biomarkers. Identification of new therapeutic targets.
RNA in placenta	Gene expression microarray analysis; comparative transcriptomic analyses between normal and affected individuals	Improved knowledge of fetal functional development in health and in disease states. Development of new biomarkers. Identification of new therapeutic targets.
RNA in cord blood	Gene expression microarray analysis; comparative transcriptomic analyses between normal and affected individuals	Improved knowledge of fetal functional development in health and in disease states. Development of new biomarkers. Identification of new therapeutic targets.

Advances in invasive diagnosis by fetal cytogenomics

Cytogenetic diagnosis is in a transition from the microscopic analysis of chromosomes in metaphase to the analysis of DNA within chromosomes using microarrays (**Fig. 1**). In the postnatal setting, a chromosomal microarray analysis is now considered to be the first-tier cytogenetic diagnostic test for individuals with congenital anomalies, intellectual disability or both[6]. Even before the International Standard Cytogenomic Array (ISCA) Consortium (https://www.isca consortium.org/) published their evidence-based summary of 33 studies involving over 21,000 children and adults in 2010 (ref. 6), there was a demand for applying this technology prenatally. Therefore, in 2007 the *Eunice Kennedy Shriver* National Institute of Child Health and Human Development (NICHD) funded a clinical trial comparing the accuracy of microarrays to that of standard cytogenetic analyses (NCT01279733).

Microarrays offer advantages over conventional karyotyping. The advantages of microarray testing over the current standard, metaphase karyotyping, include a higher sensitivity to detect chromosome deletions, duplications and unbalanced rearrangements and a shorter turnaround time. This shorter time is because the DNA isolation procedures can be automated, and there is no need to culture the fetal cells. Whereas metaphase analyses using banding techniques can identify chromosome deletions and duplications in the range of 5–10 Mb, the higher resolution provided by microarrays can detect changes as small as 50–100 kb[7]. The disadvantages of microarrays include their inability to detect a balanced chromosome rearrangement or a triploid karyotype. The design of the array is crucial. Oligonucleotide and bacterial artificial chromosome arrays provide less coverage of the genome but are specifically designed to identify known chromosomal aberrations that are associated with clinically significant disease. Whole-genome arrays provide sequence information without complete knowledge of the long-term prognostic implications of all of the variants detected. Such sequence information, however, may be permanently archived and used as a reference source to advance our knowledge of the health of individuals and populations, human development and disease.

The challenge of assessing clinical meaning from microarray results. A major concern regarding the widespread application of chromosome microarray technology to low-risk pregnancies is the possibility of detecting copy number variants (CNVs) that have unknown clinical consequences. This is a problem because the phenotype of the fetus cannot be completely assessed while in the womb, so it can be difficult to determine the functional consequences of these genetic changes. When an indeterminate CNV is detected, several factors increase the probability of its pathogenicity. These include being absent in the parents (*de novo*), having a size of larger than 1 Mb, being a deletion rather than a duplication or involving a gene-rich area of the genome. A final consideration is whether there is a similar phenotype that involves genes within the same pathway[7]. When a *de novo* CNV is found in the fetus, publicly available references can be consulted to interpret its clinical implications, such as the database of Genotypes and Phenotypes (dbGAP) (http://www.ncbi.nlm.nih.gov/gap)[8] or the Database of Chromosomal Imbalance and Phenotype in Humans using Ensembl Resources (DECIPHER) (http://decipher.sanger.ac.uk/)[9]. However, most clinicians do not have adequate training to perform such interpretations of CNVs.

Combining karyotype and microarray analyses to maximize information. In the prenatal setting, there is uncertainty as to whether it is better to use an array that only detects findings of known clinical meaning or one that has the greatest possible resolution[10]. Despite this uncertainty, a consensus exists with regard to the essential need for counseling before and after testing as well as the clinical scenarios in which microarrays are a useful adjunct to metaphase karyotyping. For example, in the settings of miscarriage[11] and stillbirth[12,13], in which tissue culture frequently fails, the quality of the chromosome preparation is suboptimal or both, microarrays have been shown to improve the detection of genomic alterations in the fetus. Similarly, the addition of a microarray analysis when there is a fetal structural anomaly and a normal metaphase karyotype results in the detection of 1–16% additional clinically relevant chromosome abnormalities[14–21]. The lower end of the range reflects the use of lower density arrays[14–18], and the higher percentages are derived from the studies that used whole-genome platforms[19–21]. The use of microarrays has shown that up to 25% of apparently balanced translocations analyzed by metaphase karyotyping are in fact unbalanced and contain substantial aberrations in regions of the genome known to encode for essential genes.

A recent retrospective study performed in Israel compared antenatal karyotyping to microarrays; both options were routinely offered to couples undergoing invasive procedures[22]. This study illustrated the potential added value of a microarray analysis in a prenatal context. Of the 269 fetuses examined, 254 had a normal metaphase karyotype and 15 had abnormal metaphase findings of

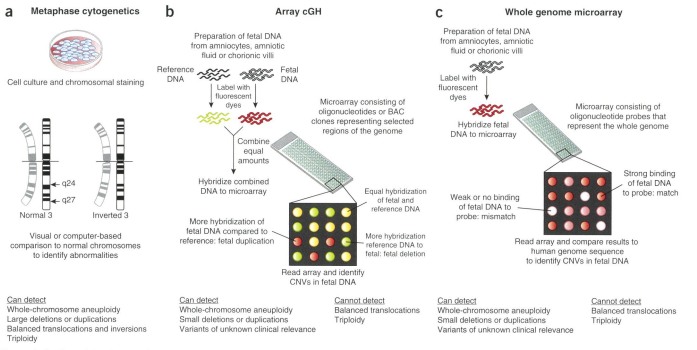
a
Metaphase cytogenetics
Cell culture and chromosomal staining
q24
q27
Normal 3
Inverted 3
Visual or computer-based comparison to normal chromosomes to identify abnormalities
Can detect
Whole-chromosome aneuploidy
Large deletions or duplications
Balanced translocations and inversions
Triploidy
b
Array cGH
Preparation of fetal DNA from amniocytes, amniotic fluid or chorionic villi
Reference DNA
Fetal DNA
Label with fluorescent dyes
Combine equal amounts
Hybridize combined DNA to microarray
Microarray consisting of oligonucleotides or BAC clones representing selected regions of the genome
Equal hybridization of fetal and reference DNA
More hybridization of fetal DNA compared to reference: fetal duplication
More hybridization reference DNA to fetal: fetal deletion
Read array and identify CNVs in fetal DNA
Can detect
Whole-chromosome aneuploidy
Small deletions or duplications
Variants of unknown clinical relevance
Cannot detect
Balanced translocations
Triploidy
c
Whole genome microarray
Preparation of fetal DNA from amniocytes, amniotic fluid or chorionic villi
Label with fluorescent dyes
Hybridize fetal DNA to microarray
Microarray consisting of oligonucleotide probes that represent the whole genome
Strong binding of fetal DNA to probe: match
Weak or no binding of fetal DNA to probe: mismatch
Read array and compare results to human genome sequence to identify CNVs in fetal DNA
Can detect
Whole-chromosome aneuploidy
Small deletions or duplications
Variants of unknown clinical relevance
Cannot detect
Balanced translocations
Triploidy

Figure 1 Outline of the three major current techniques for analyzing fetal chromosomes. (**a**) Fetal cells are cultured and analyzed during cell division in metaphase. Chromosomes are analyzed under the microscope for the presence of dark and light staining bands. The staining patterns are compared with normal reference standards. Only relatively large deviations from normal (~5–10 Mb) can be detected. (**b**,**c**) The DNA within the fetal chromosomes, rather than the fetal chromosome itself, is compared to reference genomes. The DNA can be isolated from fetal cells or cell-free amniotic fluid with or without prior cell culture. In array comparative genomic hybridization (cGH) (**b**), patient and reference DNA samples are labeled with competing fluorescent dyes and hybridized to an array that contains DNA probes. Each probe is known to map to a specific region of the human genome. When the array is read, areas of mismatch appear as red or green. Special software converts the signal to indicate the affected area of the genome. In the method shown in **c**, only the patient's DNA is hybridized to an array that contains oligonucleotides (~60 bp) with coverage across the human genome. Areas of mismatch between the patient's DNA and the reference sequence are identified as CNVs. BAC, bacterial artificial chromosome.

unknown clinical meaning. In the former group, 36 out of 254 fetuses had an abnormal microarray result, and 33 of these 36 fetuses were found to have benign CNVs. The remaining three fetuses had *de novo* duplications (two of them also had sonographic abnormalities). All three of the women carrying these fetuses opted for termination. The overall risk of having an unbalanced genomic finding after a normal karyotype was 1 in 84, or 1.1%. The microarray results were normal in 11 of the 15 fetuses (73.3%) with an abnormal metaphase finding; all of these pregnancies were continued. In four fetuses, unbalanced abnormalities in the karyotype were confirmed by a microarray analysis; the women chose to terminate their pregnancies in these instances. In the entire study, clinically relevant genetic or genomic changes that had not been previously detected were found in 18 out of 269 (6.5%, or 1 in 15) fetuses. Thus, the addition of genomic data allowed the physicians to better define the expected prognosis for the child, which substantially influenced subsequent pregnancy management and parental decisions.

Advances in noninvasive prenatal diagnosis

The clinical experience with microarrays illustrates the immediate impact that rapid advances in technology can have on clinical care, even before the completion of a prospective blinded trial. The same phenomenon occurred with the noninvasive diagnosis of fetal sex and the Rhesus D blood group (RhD) using circulating nucleic acids. In 1997, Lo and his colleagues first found that cell-free fetal DNA circulates in maternal plasma and serum by showing that gene sequences that are unique to the fetus could be amplified from maternal plasma[23]. Maternal blood contains a mixture of maternal and fetal (predominantly placental[24–30]) cell-free nucleic acids. Therefore, fetal DNA can be isolated from maternal blood and analyzed noninvasively (**Fig. 2**).

Noninvasive diagnosis of RhD. By the early 1990s, the gene sequence for RhD (*RHD*) was known, and the prenatal diagnosis of fetal Rhesus blood groups had moved from the serotyping of fetal blood to the genotyping of amniocytes or villi[31]. An immediate clinical application for cell-free fetal DNA in maternal blood was envisioned for the noninvasive diagnosis of fetal blood type. In an initial feasibility study, fetal *RHD* genotype was accurately predicted by PCR amplification of cell-free DNA isolated from peripheral blood samples in 55 of 57 RhD$^-$ pregnant women[32]. The definitive fetal genotype was determined by amplification of *RHD* in the amniotic fluid or by serology at birth. There were two false-negative calls in first-trimester samples, which were presumed to be the result of a low concentration of fetal DNA in maternal plasma early in gestation. As early as 2001, after appropriate preclinical validation studies, the International Blood Group Reference Laboratory in the UK transitioned this test to prenatal care[33].

Similar large-scale clinical studies were performed in France and The Netherlands[34] that identified the major challenges associated with noninvasive testing. False-negative results were generally caused by a lack of fetal DNA in the sample, either for biological (too early in gestation) or technical (poor extraction) reasons[34]. More recent studies have incorporated secondary PCRs using sex determining region Y (*SRY*), a Y chromosome sequence used as a marker of male fetal DNA, *RASSF1A*, a marker of differentially methylated placental

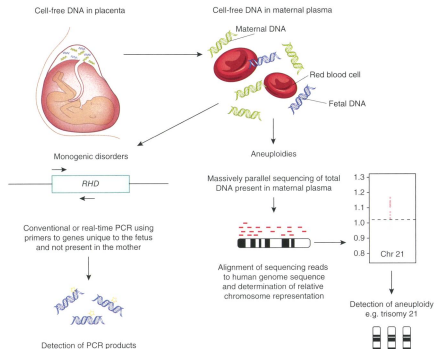
Cell-free DNA in placenta
Cell-free DNA in maternal plasma
Maternal DNA
Red blood cell
Fetal DNA
Monogenic disorders
Aneuploidies
RHD
Massively parallel sequencing of total DNA present in maternal plasma
1.3
1.2
1.1
1.0
0.9
0.8
Chr 21
Conventional or real-time PCR using primers to genes unique to the fetus and not present in the mother
Alignment of sequencing reads to human genome sequence and determination of relative chromosome representation
Detection of aneuploidy e.g. trisomy 21
Detection of PCR products corresponding to fetal-specific genes such as RHD

Figure 2 Cell-free DNA analysis to diagnose fetal disorders. Cell-free DNA from maternal plasma is a mixture of maternal and fetal DNA. When testing is being performed for the diagnosis of the presence or absence of a uniquely fetal gene, the relatively low-cost method of real-time quantitative PCR can be used (left). Primers and probes that map uniquely to the fetal genome can be used to amplify the gene of interest to allow, for example, the detection of the *RHD* gene. For diagnosing aneuploidies such as Down's syndrome, the total cell-free DNA in maternal plasma is sequenced (right). The DNA is fragmented and analyzed in 36-bp lengths known as reads. These 36-bp reads are aligned against the human genome sequence and counted. The amount of DNA in chromosomes of interest, for example, those involved in common fetal aneuploidies such as those of chromosomes 13, 18 and 21, is normalized against the DNA from other chromosomes to determine the relative number of reads present in a given sample. The lower right image shows an increased number of sequences derived from chromosome (chr) 21 (in red) plotted against what should normally be present, indicated by the dashed line slightly above 1.0. This result is consistent with a fetus that has trisomy 21.

DNA, or other paternal genetic markers as internal controls to verify that fetal DNA is present in the sample[35]. In general, instances of false positives are caused by the fact that the majority of RhD^- individuals of African ancestry have one of two *RHD* variants, the *RHD* pseudogene or the *RHD-CE-D*^{s} hybrid sequence[36]. Once these variants were identified, primer and probe combinations were developed to either specifically recognize or entirely avoid the problem of false-positive amplification. Noninvasive prenatal testing (NIPT) of *RHD* has recently been implemented on a routine national basis in Denmark[37]. Prior to this policy change, all RhD^- pregnant women received RhD immunoglobulin. In the Danish study, routine noninvasive prenatal testing meant that 862 women (37.2% of the total) could avoid unnecessary exposure to this blood product. NIPT has advanced antenatal care by limiting RhD prophylaxis to only those women who carry an RhD^+ fetus. In addition, noninvasive fetal blood group tests are available for the blood groups C, c, E and KEL[35,36].

Noninvasive diagnosis of sex-linked disorders. Similarly, PCR amplification of cell-free DNA in maternal blood has been used as a noninvasive alternative to cytogenetic diagnosis after an invasive procedure to determine fetal sex. Such diagnostic tests are recommended when knowledge of fetal sex is needed for the management of X-linked conditions or of ambiguous genitalia detected by sonogram. Furthermore, knowledge of fetal sex helps determine which women need to take steroids to prevent the masculinization of a female fetus that is at risk for congenital adrenal hyperplasia. The widespread availability of this technology over the internet and in pharmacies in the United States, however, raises substantial ethical concerns[4]. To determine the analytic and clinical validity of diagnosing fetal sex, a recent meta-analysis of 80 discrete datasets from 57 studies and 6,541 singleton fetuses showed that the overall diagnostic performance of noninvasive testing was high (with a 95.4% sensitivity and a 98.1% specificity) when maternal blood samples were obtained after 7 weeks of gestation[38]. The variables that had the biggest effect on test performance were gestational age and DNA amplification methodology. Currently in the United States, noninvasive fetal DNA testing is not available at point of care, and this testing is not approved by the Clinical Laboratory Improvement Amendments (CLIA) or reimbursed by insurers, despite the results of this meta-analysis[38]. In contrast, in the UK, this approach has already been incorporated into prenatal care and has led to a reduction in invasive prenatal diagnostic procedures for sex-linked disorders[39].

Noninvasive prenatal testing for fetal aneuploidies. Antenatal recognition of fetuses with trisomy 21 is a major goal of all screening programs in the developed world[40]. Whereas NIPT of fetal sex and *RHD* genotype can be performed using the relatively straightforward technique of real-time PCR, identification of fetal trisomy 21 using maternal plasma is much more complicated because there are no unique fetal gene sequences to be detected. Multiple attempts over the past two decades have used intact fetal cells in maternal blood[41,42], cell-free DNA[43] or cell-free RNA[44,45] to noninvasively diagnose Down's syndrome. The subsequent development of digital PCR techniques led to the ability to quantify the amount of nucleic acids in a maternal sample by counting amplifications from single molecules. Digital PCR has been applied to the molecular detection of aneuploidy using cell-free RNA[46] or DNA[47].

Although some of the early studies achieved success on a small scale, the arrival of massively parallel sequencing techniques and instrumentation substantially changed the landscape for this type of research. In 2008, two independent reports published 2 months apart each showed that fetal aneuploidy could be accurately diagnosed using DNA isolated from maternal plasma samples by mapping and aligning short sequence tags to a reference human genome, followed by counting and bioinformatics analyses[48,49].

Subsequently, progress has been rapid. Since January 2011, at least ten independent large-scale clinical trials involving NIPT of trisomies 21, 18 and 13 have been published[50–59]. Three of these studies

were prospective[54–56]. So far, all of them were performed with study subjects that were at a high risk for fetal aneuploidy and incorporated a case-control study design in which an independent third party matched known euploid fetuses with fetuses that had a variety of chromosomal abnormalities. The teams that performed the sample processing, sequencing and bioinformatics analyses were blinded. All of the studies achieved similar, near-perfect rates of detection of trisomy 21, including in two sets of twins (in which at least one was affected)[52], three cases of mosaic trisomy 21 (ref. 56) and several cases caused by an unbalanced translocation[56,60]. All of the studies had very low false-positive rates (<1%). The various studies, however, differed in their bioinformatics analytical approaches. In some of them, the number of sequence tags on the chromosome of interest was normalized to the number of tags on all chromosomes in the particular sequencing run (the *z*-score)[49–51,53–55]. In other studies[52,56], a normalized chromosome value (NCV) was used to calculate the ratio of the number of counts on the chromosome of interest (for example, 21) in a specific sample to the number of counts on a reference chromosome or a chromosome set derived from an unaffected group of samples. The NCV is a fixed ratio that removes variation within and between sequencing runs. A third approach incorporates information on the fraction of fetal DNA present in the sample to calculate an individual risk of trisomy[59].

By late 2011, NIPT of trisomy 21 by sequencing of maternal plasma DNA began to be offered on a clinical and commercial basis in the United States and China at approximate costs ranging from $475 to $1,900, depending on the patient's insurance. This development prompted a rapid response statement to be issued by the International Society for Prenatal Diagnosis[61], which cautioned that before routine population screening for fetal Down's syndrome is introduced, additional trials are needed, particularly in low-risk populations. Despite these concerns, noninvasive testing using massively parallel sequencing of maternal plasma DNA is now a clinical reality. As of April 2012, over 25,000 clinical tests have been performed in China and several thousand have been performed in the United States (http:// www.genomeweb.com/mdx/non-invasive-t21-testing-space-abuzz-firms-jockey-share-1b-market-battle-over-ip).

Compared with the antenatal diagnosis of Down's syndrome, the diagnosis of other commonly occurring fetal aneuploidies, such as trisomies 13 and 18, is more challenging because the accuracy of aneuploidy detection is affected by the GC base content of an individual chromosome. Whereas chromosome 21 has a midrange percentage of GC content, chromosomes 18 and 13 have a lower percentage, which increases the coefficient of variation in the sequencing reactions of these chromosomes[48,53]. Specific quantitative correction of the GC content bias in the sequencing data using modified *z*-score equations has resulted in improved sensitivity and specificity in the detection of trisomies 13 and 18 (ref. 53). The NCV analytic method was sensitive enough to detect a case of mosaic trisomy 9, an 11q21-23 deletion, partial trisomy of 6q12-16.3 and several sex chromosome abnormalities[52,56], suggesting this method may have expanded clinical utility as compared to the *z*-score.

Insights into fetal cell-free DNA from a noninvasive diagnosis. Crucially, the noninvasive sequencing studies have provided basic information regarding the biology of the fetal cell-free DNA in maternal plasma. The majority of the total (mainly maternal) circulating cell-free DNA derives from apoptotic hematopoietic cells[62], with a peak fragment size of about 162–169 bp[48,63,64]. In the circulation, the DNA double helix is wound around a nucleosome, and a 20-bp fragment links the nucleosome to its core particle. Fetal DNA, which derives from the placenta[24–30], is present in shorter fragments that predominantly, but not exclusively, measure around 143 bp[63–65]. The sizes of the maternal DNA and fetal DNA differ because in the fetal DNA, the 20-bp linker fragment has been cleaved from the nucleosome[48,63]. The median amount of circulating cell-free fetal DNA in maternal plasma is 10%[23,63,66]. Single nucleotide polymorphism (SNP) analyses reveal that the entire fetal genome is represented in maternal plasma and that the relative proportions of maternal and fetal sequence are constant[63]. This implies that it is theoretically possible to noninvasively screen maternal blood for both fetal DNA copy number variation and single-gene disorders. In two proof-of-concept studies of cell-free DNA analysis using blood samples from women carrying fetuses with known diagnoses, Peters *et al.*[67] found the presence of a familial 4.2-Mb deletion in chromosome 12p inherited by the fetus, and Lo *et al.*[63] showed that a fetus carried the paternal (but not the maternal) mutation for β-thalassemia.

Prenatal detection of aneuploidy using maternal plasma DNA is effective because the diagnosis relies on counting sequence tags and mapping them to the clinically relevant chromosomes. NIPD of single-gene disorders, many of which are inherited as autosomal or X-linked recessive conditions, is fundamentally even more complex because of the fact that the mother and fetus share the same mutation. In preliminary studies, a digital relative mutation dosage method has been used to deduce whether the mutant or the wild-type allele is overrepresented in the maternal plasma DNA[68–70]. This method can be applied in autosomal or X-linked recessive conditions in which a pregnant woman carries a heterozygous gene mutation. If a woman's fetus is homozygous for either the wild-type or mutant allele, there is an underrepresentation or overrepresentation of the mutant allele in her plasma DNA. Digital PCR amplification, followed by counting and statistical analyses, determines whether an allelic imbalance is present. In small research studies, this has facilitated accurate diagnoses of hemoglobin β (*HBB)* mutations that cause hemoglobin E disease[68], β-thalassemia[68] or sickle cell anemia[69], as well as of *F8* and *F9* mutations that cause hemophilia[70]. In one instance of a fetus that was at risk for β-thalassemia, a proof-of-concept whole-genome sequencing study was performed using maternal plasma DNA[63], and the fetal genome was successfully inferred from SNP genotyping data of parental and chorionic villus samples. In the future, targeted sequencing approaches may be applied to noninvasively diagnose groups of single-gene disorders for which the fetus is at risk based on the ethnic background of the parents.

Advances in analyzing the fetal transcriptome

The dynamic nature of fetal developmental processes, coupled with a need to distinguish normal from abnormal physiology (especially when a fetus appears normal on sonographic examination), has led to an interest in exploring the fetal transcriptome. Unlike fetal DNA, which is released into maternal plasma in consistently increasing amounts as gestation advances[71], fetal RNA levels are more variable and reflect differential expression as a function of development[72]. The finding that fetal Y-chromosome–specific mRNA sequences could remain intact in the maternal circulation despite the presence of circulating RNases did not occur until 2000 (ref. 73). Later work showed that fetal mRNA fragments were relatively stable in the maternal plasma[74,75], probably because this mRNA circulates within apoptotic bodies that are protected from further degradation.

Interestingly, transcripts that originate from the placenta are more easily detected in maternal plasma[76], whereas transcripts that originate

in the fetus are more easily found in maternal whole blood[77]. In one study, a gene expression microarray analysis was used to compare transcripts found in maternal whole blood at term immediately before and 24–36 hours after delivery with newborn umbilical cord blood to identify circulating fetal biomarkers[77]. Sequences that were statistically significantly upregulated in both antepartum maternal blood and newborn blood, but not in maternal postpartum blood, were identified as possible fetal transcripts. This work showed that the majority of the circulating fetal transcripts in third-trimester maternal blood were related to visual or central nervous system development, sense of smell and the ability to mount an inflammatory response. The identification that these particular systems were actively developing at this stage made sense according to what was already known about third-trimester fetal physiology. What was new, however, was the knowledge regarding the relative proportions of the actively expressed transcripts, such as the 10% of transcripts that are devoted to development of the immune response. This study also identified specific genes that are normally expressed by the fetus before delivery at term and suggested the possibility that a multiplex, RT-PCR–based assay could be developed to track physiological gene expression[78]. Such an assay could then possibly be used to track abnormal patterns of gene expression and identify fetuses or infants that might be at risk for developmental delays.

Another area of current research is the investigation of placental microRNAs (miRNAs) in maternal plasma[79–84]. MiRNAs are small (~19–25 nt) single-stranded noncoding RNA molecules that repress protein translation by binding to the 3′ untranslated regions of their target mRNAs. Because they are remarkably stable in plasma, miRNAs are under evaluation as pregnancy-specific biomarkers in conditions such as preeclampsia[80] and fetal growth restriction[81]. Thus far, approximately 40 placenta-specific miRNAs have been identified, although none are presently used in clinical assays[82–84]. MiRNAs are exported from syncytiotrophoblasts by exosomes[79], which are circulating microparticles that may have a role in intercellular communication. Circulating miRNAs may therefore have a functional role in fetomaternal communication or the development of immune tolerance.

Transcriptomic analysis of fetal abnormalities. Discovery-driven fetal research using maternal blood is limited because the majority of the circulating transcripts are maternal in origin. Larrabee *et al.*[85] hypothesized that amniotic fluid supernatant might be a useful source of pure fetal gene expression information that would provide new data on human development. In an initial proof-of-concept study, they analyzed cell-free fetal RNA in amniotic fluid samples from pregnant women in the second or third trimester undergoing amnioreduction for twin-to-twin transfusion syndrome (TTTS) or hydrops fetalis[85]. The results showed that fetal gene expression is dynamic and is influenced by gestational age and gender. For example, the genes encoding surfactant proteins A2, B and C, tracheobronchial, gastric and salivary mucin and statherin (a protein involved in both salivary secretion and ossification) were all upregulated as a function of gestational age. Conversely, keratin gene transcript expression decreased with gestational age, which probably reflects the decreased contact between keratin-producing cells and amniotic fluid as the fetal skin matures. Specific transcripts that were upregulated secondary to disease, such as the water transporter aquaporin 1 (*AQP1*) in TTTS, were also identified in this study. The authors suggested that *AQP1* may have a role in TTTS by affecting water movement from the amniotic cavity across the placenta and into the fetal circulation.

The amniotic fluid transcriptome was further studied in fetuses with trisomies 21 (ref. 86) and 18 (ref. 87) and was compared to the transcriptome of euploid fetuses that were matched for sex and gestational age. In both aneuploidies, hundreds of statistically significantly differentially regulated genes were found; however, only a handful mapped to the chromosome of interest (for example, 21 or 18). This provided strong evidence to suggest that the pathology in fetuses with aneuploidy is the result largely of complex downstream processes and not simply a gene dosage effect caused by the extra chromosome. Subsequent functional and pathway analyses suggested that each aneuploidy has a unique and characteristic transcriptome.

In the fetuses with Down's syndrome, oxidative stress, ion transport and G protein signaling were the major functional abnormalities. Whereas oxidative stress response genes have been previously examined in adults with Down's syndrome[88], this study was the first to show that fetuses with Down's syndrome can also be affected by oxidative stress and its intermediate consequences, such as cell stress responses and ion transport. Furthermore, this study was the first, using the Connectivity Map database[89], to identify compounds that might reverse the molecular phenotype of Down's syndrome and be considered as potential therapies that can be administered antenatally. Primary cultures of amniocytes[90,91] and trophoblasts[92] have also been used as a source of mRNA to further study human autosomal trisomy. Although there is always the possibility that the cell culture induces artifactual changes in gene expression, these studies concluded that the Down's syndrome phenotype derives partly from overexpressed genes on chromosome 21 and partly by secondary genome-wide transcriptional dysregulation. Interestingly, in trophoblasts, the changes in the expression of genes involved in the ubiquitin cycle were one of the greatest discriminators of trisomy 21 and euploid placentas[90]. This finding implies that epigenetic mechanisms that affect post-transcriptional modification by ubiquitination may also play a part in the Down's syndrome phenotype.

In the fetuses with trisomy 18, significant downregulation of genes involved in adrenal development was identified[87], which could explain both the low concentrations of maternal serum estriols and the prenatal and postnatal growth restriction observed in affected fetuses and infants. A functional analysis also highlighted differential regulation of pathways related to cardiovascular disease, which is not surprising given that congenital heart disease is a major problem in affected fetuses. In particular, Rho-associated kinase 1 (*ROCK1*), a gene located on chromosome 18, was significantly upregulated in fetuses with trisomy 18. Prior to this study, *ROCK1* was not known to be associated with trisomy 18, illustrating one of the benefits of using transcriptomic analyses to discover genes involved in fetal disease. *ROCK1* has a key role in the regulation of endocardial cell differentiation and migration in early heart development. In addition, it is one of only six genes that are dysregulated in both trisomies 18 and 21 compared to euploid controls[87].

In addition to the amniotic fluid transcriptome of fetuses with aneuploidies, the normal amniotic fluid transcriptome has also been analyzed in euploid fetuses[93]. Four hundred seventy six well-annotated genes were identified as being expressed in 12 second trimester amniotic fluid samples. Of the 23 transcripts that mapped to specific organs, six were highly expressed in fetal brain. Other transcripts originated in fetal lung, skin, thyroid, pancreas, blood, liver and placenta. A new finding from this study was the identification of the mammalian target of rapamycin (mTOR), a central regulator of cell growth, as part of a key developmental pathway in fetuses. This study showed that the amniotic fluid core transcriptome could provide information on the development of a number of different organ systems in real time from living human fetuses.

Analysis of the transcriptome in common complications of pregnancy. Subsequent translational investigations have focused on the presence of specific placental transcripts in maternal blood that can serve as biomarkers for various complications of pregnancy[94–98]. For example, the upregulation of the human chorionic gonadotropin β subunit, human placental lactogen and corticotrophin-releasing hormone transcripts were shown to be potential biomarkers in the blood of women who developed preeclampsia[99]. In a large study of placentas from 37 preeclamptic and 57 normal pregnancies, genome-wide transcriptional profiling identified 455 differentially expressed genes between preeclampsia and normal pregnancy[100]. New and previously described genes relating to the pathophysiology of preeclampsia were identified. The most significantly dysregulated canonical pathway identified was tryptophan metabolism. *KYNU*, which was upregulated in preeclampsia, encodes kynureninase, an enzyme that is key in tryptophan metabolism. This enzyme metabolizes L-kynurenine, which suppresses T cell proliferation and natural killer cells, adding to previous information that immune tolerance to foreign antigens plays a part in the pathogenesis of preeclampsia. Other cell signaling and metabolic pathways that were dysregulated in the preeclamptic placentas included linoleic, fatty acid and arachidonic metabolism, notch signaling, endoplasmic reticulum stress and oxidative stress mediated by nuclear respiratory factor 2. Notably, some differentially regulated genes are involved in the production of hydrogen peroxides and the elimination of lipid peroxidation products. These differences may be among the factors that activate the maternal endothelium and result in atherosclerotic-like lesions that trigger systemic inflammation in preeclampsia.

The placental transcriptome is also being used to understand key fetal biological processes such as intrauterine growth restriction (IUGR), in which the growth of the fetus is substantially reduced compared to normal, healthy fetuses. In one study, the analysis of differentially regulated genes in growth-restricted fetuses suggested that the affected placentas have an upregulation of inflammation that is mediated by chemokine and cytokine signaling pathways[101]. Importantly, none of the genes known to be imprinted in the placenta were differentially expressed between the normal placentas and those with IUGR, suggesting that epigenetic modification has a minor role in the pathogenesis of IUGR and that perhaps future therapies for this condition should be directed toward decreasing inflammation. Furthermore, hydroxysteroid (11-β) dehydrogenase 1 was upregulated in the IUGR placentas. This enzyme has a role in the regeneration of cortisol from cortisone, which enhances the effect of glucocorticoids on the production of pulmonary surfactant. This may explain why growth-restricted newborns often have substantially accelerated lung maturation for their gestational age.

In an investigation of umbilical cord blood from premature neonates with fetal inflammatory response syndrome, a gene expression analysis of leukocyte mRNA showed an enrichment of biological pathways related to antigen presentation and processing, B cell receptor and phosphatidylinositol signaling and cell adhesion and metabolism compared to neonates without evidence of inflammation[102]. The transcriptomic studies showed that despite age-related differences in the fetal and adult immune systems, they had many similar responses to infection and inflammation. Among the many genes that were shown to be upregulated in fetal inflammatory response syndrome were ones that are known to play a part in leukocyte adhesion, leukotriene synthesis and chemotaxis.

The All Our Babies Cohort Study[103], currently enrolling subjects in Alberta, Canada, is taking a fetal personalized medicine approach to understanding preterm birth by prospectively collecting maternal blood RNA and examining environmental factors. All of these investigations use comparative microarray analyses to identify new biomarkers and potential avenues for intervention.

Advancing from diagnosis to personalized prenatal medicine

Challenges for prenatal diagnostics. It should be clear from the preceding paragraphs that the technical advances in prenatal diagnosis that have occurred in the last 5 years have greatly exceeded their translation into clinical practice. The major considerations that affect their incorporation into routine obstetric care include education, cost and ethical issues (**Table 2**).

A crucial aspect of this incorporation will be education, as there is no question that improvement in the genomic literacy[104] of health care providers is a fundamental requirement in all fields of medicine. This is especially true in obstetrics and gynecology because of the widespread availability of direct-to-consumer prenatal testing and intense patient interest in the well being of their fetuses. Should any of the direct-to-consumer tests reveal an abnormal fetal finding, it will ultimately be the obstetrician who will have the responsibility for follow-up management. Therefore, obstetricians in particular need frequent and comprehensive educational updates regarding the practical implications of advances in genetics and genomics. Although in many instances the new genetic tests perform better than the old ones, it is currently unknown how these new tests will be incorporated into prenatal care. With regard to cytogenetic analyses, it is cost

Table 2 Emerging challenges for prenatal diagnosis and fetal personalized medicine

Prenatal diagnosis	Fetal personalized medicine
Practical issues	Improve annotation of genes to show information about their function and expression in a fetal context
Need for professional standards and guidelines	Integration of the transcriptome with proteome, metabolome and epigenetic information
Advanced training and education for providers	Determine if (and what) animal models are useful in which to evaluate treatment(s)
Need to decide what is optimal and what is feasible	Decide whether existing drugs can be repurposed or new drugs need to be developed
Resource allocation	Need to show safety and absence of teratogenicity when developing drug trials for pregnant women and fetuses
Confidentiality of information obtained	Substantial costs involved in developing large-scale clinical trials for potentially rare diseases
Technological issues	Resource allocation
Reduce cost and duplication of services	Confidentiality of information obtained
Improve efficiency	
Determine clinical meaning of copy number variants detected by chromosome microarrays	
Ethical issues	
Direct-to-consumer genetic testing	
Possibility of detecting mistaken paternity and incest	
Possibility of coercion to have DNA testing	
Fewer opportunities for reflection and counseling	
Devaluation of affected individuals with trisomy	
Role of industry in promoting research	

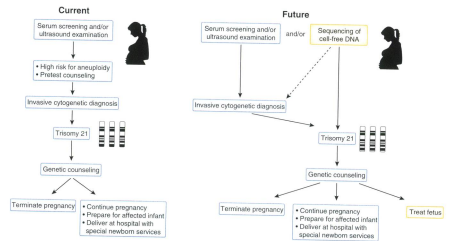

Figure 3 A potential future diagnostic and treatment strategy for Down's syndrome. A comparison of the current two-tiered approach for the noninvasive diagnosis of fetal trisomy 21 with no fetal treatment options and a possible future approach in which sequencing of maternal plasma DNA may eliminate the need for invasive testing. Furthermore, advances in study of the fetal transcriptome may identify new treatments that could be administered to the pregnant woman as soon as the diagnosis is made.

prohibitive to offer both classical cytogenetic analyses and microarray analyses to all pregnant women undergoing invasive procedures. The average cost for a metaphase karyotype is currently $750 (ranging from $250 to $1,000), and the average cost for a microarray study is $1,500 (ranging from $750 to $3,000). The results of the prospective blinded NICHD trial of prenatal cytogenetic diagnosis by array-based copy number analysis, including data on approximately 4,400 pregnancies, were presented orally at the annual Society for Maternal Fetal Medicine meeting in February 2012 and indicated that karyotyping and microarray analysis were equally accurate in the detection of aneuploidy[105]. In fetuses with apparently normal metaphase karyotypes sampled for advanced maternal age or abnormal serum screens, chromosome microarray studies detected 1.7% additional clinically relevant abnormalities. In fetuses with sonographic abnormalities and normal cytogenetic studies, this figure rose to 5.8%. These data prompted the investigators to recommend that microarray investigations transition to a first-line diagnostic test in the antenatal setting.

For prenatal diagnosis of Down's syndrome, the current standard of care involves a two-tiered approach (for example, serum screening and nuchal translucency measurement, followed by an offer of invasive procedures such as amniocentesis or chorionic villus sampling to screen women who tested positive) (**Fig. 3**). If NIPT of Down's syndrome achieves diagnostic accuracy, the cost of testing could be offset by a reduction or elimination of these invasive procedures. Using population-based data from Victoria, Australia, Susman *et al.*[106] investigated the impact of changing from the current screening algorithms to a one-stage noninvasive approach. Their results showed that there would be an 84% reduction in the number of invasive procedures, with an additional 7% of cases of Down's syndrome being detected, albeit with an accompanying reduction in the number of other abnormalities detected. Additional testing will require an increased commitment to pretesting counseling services that will affect the overall cost to the health care system[107]. Although these added costs have not yet been systematically addressed in very many studies, in one report, the costs of noninvasive prenatal diagnosis of fetal sex for X-linked conditions did not differ from invasive prenatal diagnosis[108]. As the number of laboratory tests increases, the cost of testing is also expected to decrease.

Although NIPT of Down's syndrome has greater sensitivity and specificity compared with the serum screening algorithms that are currently used in the clinic, the expenses associated with DNA sequencing, bioinformatic analysis and data storage are considerable. Current research is therefore focused on reducing the cost and improving the efficiency of NIPT. Recent approaches have included the enrichment of fetal DNA concentrations by fragment size selection[65,66], targeted sequencing of regions from specific chromosomes of clinical interest[57–59,109], the possible use of antibodies to histone H1 to bind and remove circulating maternal DNA[63], immunoprecipitation of methylated DNA sequences followed by real-time PCR amplification[110] and the use of highly heterozygous SNPs to calculate haplotype ratios between the maternally and paternally inherited genes in maternal plasma, thereby inferring information about the fetal karyotype[111].

The personalized approach to fetal diagnosis raises several ethical concerns[112]. With chromosome microarray studies, the detection of CNVs of unknown clinical meaning or variants that have known effects but incomplete penetrance raises parental anxiety, as well as the possibility of termination of a clinically unaffected fetus[112]. Furthermore, chromosome microarrays can readily detect mistaken paternity and incest, which are issues that are not usually discussed during pretesting counseling sessions[113]. With regard to NIPT of aneuploidy, there are multiple issues[114], including how consent for the test should be obtained[115]. The current multistep approach to Down's syndrome screening allows several opportunities for reflection that will be lost if replaced by a single blood test[116]. There is also the potential for coercion to take the test by providers, peers or insurers. A proof-of-principle study[63] showed that it is already feasible to noninvasively obtain information on the entire fetal genome, raising practical and ethical questions with regard to what to do with information that is not relevant in infancy, for example, predisposition to an adult-onset condition. In addition, in contrast to the prior introduction of new laboratory tests by academic laboratories, tests associated with the sequencing of fetal DNA are being developed mainly by industry[112]. It is unknown how intellectual property rights will affect the implementation of these tests and their costs. There are already several patent infringement lawsuits under consideration in the United States.

Challenges for developing new therapies for fetal diseases and pregnancy disorders. As presented here, the discovery-driven approach that is associated with analysis of the transcriptome has facilitated the identification of many genes that seem to have key roles in both normal and abnormal fetal and placental development. A substantial challenge that already exists is acquiring age-appropriate annotation of gene expression (**Table 2**). Most of the publicly available databases provide gene expression information that is annotated only for adult humans. For example, *natriuretic peptide receptor A (NPR1)*, a gene that is significantly upregulated in all normal full-term infants, is functionally annotated as being associated with congestive heart failure.

Whereas that may be true for adults, in infants, this transcript is probably upregulated as a result of the normal physiological diuresis that occurs after delivery. Another challenge will be the integration of massive amounts of data from other types of investigations, such as analyses of the fetal proteome and metabolome along with an improved understanding of epigenetic influences, with the information on the fetal genome and transcriptome presented here. There is a need to learn more about physiological fetal functional gene expression, for example, what genes must be expressed at different stages of gestation for normal fetal maturation? As key genes in fetal development are identified, more focused and cost-effective platforms can be created to measure or monitor specific fetal organ system function[117]. Such platforms could provide new information that would supplement fetal sonographic studies that currently detect anatomic, but not functional, abnormalities.

With regard to the discovery and evaluation of new fetal treatments, there will be a need to identify appropriate animal models with similar placentation to humans. Even if new therapeutics show promise in animal models, there will be a need to demonstrate their safety and an absence of accompanying teratogenicity in pregnant women and their fetuses. Some of the diseases discussed here are rare; it is unknown whether any organization will wish to invest the substantial costs involved in implementing large-scale clinical trials to test the therapy. The development of new treatments, whether the result of repurposing existing drugs or of developing new ones, is a logical extension of the transcriptomic studies discussed here. As an example, a potential future vision of how the transcriptome might change prenatal diagnosis and treatment of Down's syndrome is given in **Figure 3**.

Outlook

Prenatal genetic diagnostic technology is advancing at an astonishingly rapid pace. Of the 117 references cited in this paper, 53 (45%) of them have been published in the past 2 years. Professional education and guidelines for incorporating new genetic tests into current practice are urgently needed. High-level economic analyses are also required to assess the benefits and limitations of current compared to future approaches. Government organizations, such as the United States Food and Drug Administration, need to be more proactively involved to ensure the quality and safety of the tests. Multidisciplinary research teams consisting of basic and translational scientists, clinicians, ethicists and parents should be formed to consider many of the issues raised here. Time is of the essence because the commercial sector has already made some of these tests, such as fetal sex and determination of paternity, directly available to pregnant women.

In parallel, relatively recent developments in the ability to sequence the fetal genome, both directly from fetal tissue and indirectly from maternal blood, as well as progress in understanding normal and abnormal fetal physiology using gene expression arrays, provide evidence that we could have the technical capabilities to apply a personalized medicine approach to the fetus. Increasing amounts of fetal genetic and genomic information are now available, and that information has already influenced subsequent pregnancy management, such as decreasing the need for invasive cytogenetic procedures or the administration of steroids or blood products to pregnant women. Although we still have a way to go before new fetal therapeutics can be identified and translated to clinical care, preliminary data indicate that translational approaches based on genomic and transcriptomic information are feasible and that the fetal transcriptome contains crucial new information about fetal development and physiology that can be repeatedly mined.

For the past 30 years, the goal of prenatal diagnosis has been to provide an informed choice to prospective parents. That paradigm is now shifting. We are now at a point where that goal can and should be expanded to incorporate genetic and genomic data to pave the way for a personalized approach to fetal treatment.

ACKNOWLEDGMENTS

The author would like to thank D. Walt, E. Norwitz, J. Maron and L. Hui for their critical reading of the manuscript and their suggestions. In addition, she is grateful for the administrative support provided by R. Forman. The author's time and effort in writing this manuscript was partially supported by the US National Institutes of Health grant HD42053-09.

COMPETING FINANCIAL INTERESTS

The author declares competing financial interests: details are available in the online version of the paper.

Published online at http://www.nature.com/doifinder/10.1038/nm.2829.
Reprints and permissions information is available online at http://www.nature.com/reprints/index.html.

1. Khoury, M.J. *et al.* The scientific foundation for personal genomics: recommendations from an NIH-CDC multidisciplinary workshop. *Genet. Med.* **11**, 559–567 (2009).
2. Ferguson-Smith, M.A. & Bianchi, D.W. Prenatal diagnosis: past, present, and future. *Prenat. Diagn.* **30**, 601–604 (2010).
3. Wolfberg, A.J. Genes on the web-direct-to-consumer marketing of genetic testing. *N. Engl. J. Med.* **355**, 543–545 (2006).
4. Bianchi, D.W. At-home fetal DNA gender testing: *caveat emptor*. *Obstet. Gynecol.* **107**, 216–218 (2006).
5. Hawkins, A.K. & Ho, A. Genetic counseling and the ethical issues around direct to consumer genetic testing. *J. Genet. Counsel.* **21**, 367–373 (2012).
6. Miller, D.T. *et al.* Consensus statement: chromosomal microarray is a first-tier clinical diagnostic test for individuals with developmental disabilities or congenital anomalies. *Am. J. Hum. Genet.* **86**, 749–764 (2010).
7. Friedman, J.M. High-resolution array genomic hybridization in prenatal diagnosis. *Prenat. Diagn.* **29**, 20–28 (2009).
8. Mailman, M.D. *et al.* The NCBI dbGAP database of genotypes and phenotypes. *Nat. Genet.* **39**, 1181–1186 (2007).
9. Firth, H.V. *et al.* DECIPHER: Database of Chromosomal Imbalance and Phenotype in Humans Using Ensembl Resources. *Am. J. Hum. Genet.* **84**, 524–533 (2009).
10. Anonymous. ACOG Committee Opinion No. 446: array comparative genomic hybridization in prenatal diagnosis. *Obstet. Gynecol.* **114**, 1161–1163 (2009).
11. Schaeffer, A.J. *et al.* Comparative genomic hybridization-array analysis enhances the detection of aneuploidies and submicroscopic imbalances in spontaneous miscarriages. *Am. J. Hum. Genet.* **74**, 1168–1174 (2004).
12. Raca, G. *et al.* Array-based comparative genomic hybridization (aCGH) in the genetic evaluation of stillbirth. *Am. J. Med. Genet. A* **149A**, 2437–2443 (2009).
13. Harris, R.A. *et al.* Genome-wide array-based copy number profiling in human placentas from unexplained stillbirths. *Prenat. Diagn.* **31**, 932–944 (2011).
14. Shaffer, L.G. *et al.* Comparison of microarray-based detection rates for cytogenetic abnormalities in prenatal and neonatal specimens. *Prenat. Diagn.* **28**, 789–795 (2008).
15. Coppinger, J. *et al.* Whole-genome microarray analysis in prenatal specimens identifies clinically significant chromosome alterations without increase in results of unclear significance compared to targeted microarray. *Prenat. Diagn.* **29**, 1156–1166 (2009).
16. Van den Veyver, I.B. *et al.* Clinical use of array comparative genomic hybridization (aCGH) for prenatal diagnosis in 300 cases. *Prenat. Diagn.* **29**, 29–39 (2009).
17. Park, J.H. *et al.* Application of a target array comparative genomic hybridization to prenatal diagnosis. *BMC Med. Genet.* **11**, 102 (2010).
18. Kleeman, L. *et al.* Use of array comparative genomic hybridization for prenatal diagnosis of fetuses with sonographic anomalies and normal metaphase karyotype. *Prenat. Diagn.* **29**, 1213–1217 (2009).
19. Tyreman, M. *et al.* High resolution array analysis: diagnosing pregnancies with abnormal ultrasound findings. *J. Med. Genet.* **46**, 531–541 (2009).
20. Faas, B.H. *et al.* Identification of clinically significant, submicroscopic chromosome alterations and UPD in fetuses with ultrasound anomalies using genome-wide 250k SNP array analysis. *J. Med. Genet.* **47**, 586–594 (2010).
21. D'Amours, G. *et al.* Whole-genome array CGH identifies pathogenic copy number variations in fetuses with major malformations and a normal karyotype. *Clin. Genet.* **81**, 128–141 (2012).
22. Maya, I. *et al.* Diagnostic utility of array-based comparative genomic hybridization (aCGH) in a prenatal setting. *Prenat. Diagn.* **30**, 1131–1137 (2010).
23. Lo, Y.M. *et al.* Presence of fetal DNA in maternal plasma and serum. *Lancet* **350**, 485–487 (1997).

24. Tjoa, M.L., Cindrova-Davies, T., Spasic-Boskovic, O., Bianchi, D.W. & Burton, G.J. Trophoblastic oxidative stress and the release of cell-free feto-placental DNA. *Am. J. Pathol.* **169**, 400–404 (2006).
25. Alberry, M. *et al.* Free fetal DNA in maternal plasma in anembryonic pregnancies: confirmation that the origin is the trophoblast. *Prenat. Diagn.* **27**, 415–418 (2007).
26. Bischoff, F.Z., Lewis, D.E. & Simpson, J.L. Cell-free fetal DNA in maternal blood: kinetics, source and structure. *Hum. Reprod. Update* **11**, 59–67 (2005).
27. Masuzaki, H. *et al.* Detection of cell free placental DNA in maternal plasma: direct evidence from three cases of confined placental mosaicism. *J. Med. Genet.* **41**, 289–292 (2004).
28. Sekizawa, A. *et al.* Evaluation of bidirectional transfer of plasma DNA through placenta. *Hum. Genet.* **113**, 307–310 (2003).
29. Chim, S.S. *et al.* Detection of the placental epigenetic signature of the *maspin* gene in maternal plasma. *Proc. Natl. Acad. Sci. USA* **102**, 14753–14758 (2005).
30. Chan, K.C. *et al.* Hypermethylated *RASSF1A* in maternal plasma: a universal fetal DNA marker that improves the reliability of noninvasive prenatal diagnosis. *Clin. Chem.* **52**, 2211–2218 (2006).
31. Bennett, P.R. *et al.* Prenatal determination of fetal RhD type by DNA amplification. *N. Engl. J. Med.* **329**, 607–610 (1993).
32. Lo, Y.M. *et al.* Prenatal diagnosis of fetal RhD status by molecular analysis of maternal plasma. *N. Engl. J. Med.* **339**, 1734–1738 (1998).
33. Finning, K.M., Martin, P.G., Soothill, P.W. & Avent, N.D. Prediction of fetal D status from maternal plasma: introduction of a new noninvasive fetal RHD genotyping service. *Transfusion* **42**, 1079–1085 (2002).
34. Bianchi, D.W., Avent, N.D., Costa, J.M. & van der Schoot, E.M. Noninvasive prenatal diagnosis of fetal Rhesus D: ready for prime(r) time. *Obstet. Gynecol.* **106**, 841–844 (2005).
35. Scheffer, P.G., van der Schoot, C.E., Page-Christiaens, G.C. & de Haas, M. Noninvasive fetal blood group genotyping of the Rhesus D, c, E and cK in alloimmunised pregnant women: evaluation of a 7-year clinical experience. *BJOG* **118**, 1340–1348 (2011).
36. Daniels, G., Finning, K. & Martin, P. Noninvasive fetal blood grouping: present and future. *Clin. Lab. Med.* **30**, 431–442 (2010).
37. Clausen, F.B. *et al.* Report of the first nationally implemented clinical routine screening for fetal RHD in D- pregnant women to ascertain the requirements for antenatal D prophylaxis. *Transfusion* **52**, 752–758 (2012).
38. Devaney, S.A., Palomaki, G.E., Scott, J.A. & Bianchi, D.W. Noninvasive fetal sex determination using cell-free fetal DNA. *J. Am. Med. Assoc.* **306**, 627–636 (2011).
39. Hill, M. *et al.* Non-invasive prenatal determination of fetal sex: translating research into clinical practice. *Clin. Genet.* **80**, 68–75 (2011).
40. ACOG Committee on Practice Bulletins. ACOG practice bulletin no. 77: screening for fetal chromosomal abnormalities. *Obstet. Gynecol.* **109**, 217–227 (2007).
41. Bianchi, D.W. *et al.* Fetal gender and aneuploidy detection using fetal cells in maternal blood: analysis of NIFTY I data. National Institute of Child Health and Development Fetal Cell Isolation Study. *Prenat. Diagn.* **22**, 609–615 (2002).
42. Bianchi, D.W. & Hanson, F.W. Sharpening the tools: a summary of a National Institutes of Health workshop on new technologies for detection of fetal cells in maternal blood for early prenatal diagnosis. *J. Matern. Fetal Neonatal Med.* **19**, 199–207 (2006).
43. Lo, Y.M. Noninvasive prenatal detection of fetal chromosomal aneuploidies by maternal plasma nucleic acid analysis: a review of the current state of the art. *BJOG* **116**, 152–157 (2009).
44. Lo, Y.M. *et al.* Plasma placental RNA allelic ratio permits noninvasive prenatal chromosomal aneuploidy detection. *Nat. Med.* **13**, 218–223 (2007).
45. Tsui, N.B. *et al.* Synergy of total and *PLAC4* RNA concentration and measurement of the RNA single-nucleotide polymorphism allelic ratio for the noninvasive prenatal detection of trisomy 21. *Clin. Chem.* **56**, 73–81 (2010).
46. Lo, Y.M. *et al.* Digital PCR for the molecular detection of fetal chromosomal aneuploidy. *Proc. Natl. Acad. Sci. USA* **104**, 13116–13121 (2007).
47. Fan, H.C. & Quake, S.R. Detection of aneuploidy with digital polymerase chain reaction. *Anal. Chem.* **79**, 7576–7579 (2007).
48. Fan, H.C., Blumenfeld, Y.J., Chitkara, U., Hudgins, L. & Quake, S.R. Noninvasive diagnosis of fetal aneuploidy by shotgun sequencing DNA from maternal blood. *Proc. Natl. Acad. Sci. USA* **105**, 16266–16271 (2008).
49. Chiu, R.W. *et al.* Noninvasive prenatal diagnosis of fetal chromosomal aneuploidy by massively parallel genomic sequencing of DNA in maternal plasma. *Proc. Natl. Acad. Sci. USA* **105**, 20458–20463 (2008).
50. Chiu, R.W. *et al.* Non-invasive prenatal assessment of trisomy 21 by multiplexed maternal plasma DNA sequencing: large scale validity study. *Br. Med. J.* **342**, c7401 (2011).
51. Ehrich, M. *et al.* Noninvasive detection of fetal trisomy 21 by sequencing of DNA in maternal blood: a study in a clinical setting. *Am. J. Obstet. Gynecol.* **204**, 205.e1–11 (2011).
52. Sehnert, A.J. *et al.* Optimal detection of fetal chromosomal abnormalities by massively parallel sequencing of cell-free fetal DNA from maternal blood. *Clin. Chem.* **57**, 1042–1049 (2011).
53. Chen, E.Z. *et al.* Noninvasive prenatal diagnosis of fetal trisomy 18 and trisomy 13 by maternal plasma DNA sequencing. *PLoS ONE* **6**, e21791 (2011).
54. Palomaki, G.E. *et al.* DNA sequencing of maternal plasma to detect Down syndrome: an international clinical validation study. *Genet. Med.* **13**, 913–920 (2011).
55. Palomaki, G.E. *et al.* DNA sequencing of maternal plasma reliably identifies trisomy 18 and trisomy 13 as well as Down syndrome: an international collaborative study. *Genet. Med.* **14**, 296–305 (2012).
56. Bianchi, D.W. *et al.* Genome-wide fetal aneuploidy detection by maternal plasma DNA sequencing. *Obstet. Gynecol.* **119**, 890–901 (2012).
57. Sparks, A.B. *et al.* Selective analysis of cell-free DNA in maternal blood for evaluation of fetal trisomy. *Prenat. Diagn.* **32**, 3–9 (2012).
58. Ashoor, G., Syngelaki, A., Wagner, M., Birdir, C. & Nicolaides, K.H. Chromosome-selective sequencing of maternal plasma cell-free DNA for first-trimester detection of trisomy 21 and trisomy 18. *Am. J. Obstet. Gynecol.* **206**, 322.e1–5 (2012).
59. Sparks, A.B., Struble, C.A., Wang, E.T., Song, K. & Oliphant, A. Non-invasive prenatal detection and selective analysis of cell-free DNA obtained from maternal blood: evaluation for trisomy 21 and trisomy 18. *Am. J. Obstet. Gynecol.* **206**, 319.e1–9 (2012).
60. Lun, F.M. *et al.* Noninvasive prenatal diagnosis of a case of Down syndrome due to Robertsonian translocation by massively parallel sequencing of maternal plasma DNA. *Clin. Chem.* **57**, 917–919 (2011).
61. Benn, P. *et al.* Prenatal detection of Down syndrome using massively parallel sequencing (MPS): a rapid response statement from a committee on behalf of the Board of the International Society for Prenatal Diagnosis, 24 October 2011. *Prenat. Diagn.* **32**, 1–2 (2012).
62. Lui, Y.Y. *et al.* Predominant hematopoietic origin of cell-free DNA in plasma and serum after sex-mismatched bone marrow transplantation. *Clin. Chem.* **48**, 421–427 (2002).
63. Lo, Y.M. *et al.* Maternal plasma DNA sequencing reveals the genome-wide genetic and mutational profile of the fetus. *Sci. Transl. Med.* **2**, 61ra91 (2010).
64. Fan, H.C. *et al.* Analysis of the size distributions of fetal and maternal cell-free DNA by paired-end sequencing. *Clin. Chem.* **56**, 1279–1286 (2010).
65. Chan, K.C. *et al.* Size distributions of maternal and fetal DNA in maternal plasma. *Clin. Chem.* **50**, 88–92 (2004).
66. Lun, F.M. *et al.* Microfluidics digital PCR reveals a higher than expected fraction of fetal DNA in maternal plasma. *Clin. Chem.* **54**, 1664–1672 (2008).
67. Peters, D. *et al.* Noninvasive prenatal diagnosis of a fetal microdeletion syndrome. *N. Engl. J. Med.* **365**, 1847–1848 (2011).
68. Lun, F.M. *et al.* Noninvasive prenatal diagnosis of monogenic diseases by digital size selection and relative mutation dosage on DNA in maternal plasma. *Proc. Natl. Acad. Sci. USA* **105**, 19920–19925 (2008).
69. Barrett, A.N., McDonnell, T.C., Chan, K.C. & Chitty, L.S. Digital PCR analysis of maternal plasma for noninvasive detection of sickle cell anemia. *Clin. Chem.* (2012).
70. Tsui, N.B. *et al.* Noninvasive prenatal diagnosis of hemophilia by microfluidics digital PCR analysis of maternal plasma DNA. *Blood* **117**, 3684–3691 (2011).
71. Lo, Y.M. *et al.* Quantitative analysis of fetal DNA in maternal plasma and serum: implications for noninvasive prenatal diagnosis. *Am. J. Hum. Genet.* **62**, 768–775 (1998).
72. Chiu, R.W. *et al.* Time profile of appearance and disappearance of circulating placenta-derived mRNA in maternal plasma. *Clin. Chem.* **52**, 313–316 (2006).
73. Poon, L.L., Leung, T.N., Lau, T.K. & Lo, Y.M. Presence of fetal RNA in maternal plasma. *Clin. Chem.* **46**, 1832–1834 (2000).
74. Tsui, N.B., Ng, E.K. & Lo, Y.M. Stability of endogenous and added RNA in blood specimens, serum, and plasma. *Clin. Chem.* **48**, 1647–1653 (2002).
75. Ng, E.K. *et al.* mRNA of placental origin is readily detectable in maternal plasma. *Proc. Natl. Acad. Sci. USA* **100**, 4748–4753 (2003).
76. Heung, M.M. *et al.* Placenta-derived fetal specific mRNA is more readily detectable in maternal plasma than in whole blood. *PLoS ONE* **4**, e5858 (2009).
77. Maron, J.L. *et al.* Gene expression analysis in pregnant women and their infants identifies unique fetal biomarkers that circulate in maternal blood. *J. Clin. Invest.* **117**, 3007–3019 (2007).
78. Bianchi, D.W., Maron, J.L. & Johnson, K.L. Insights into fetal and neonatal development through analysis of cell-free RNA in body fluids. *Early Hum. Dev.* **86**, 747–752 (2010).
79. Luo, S.S. *et al.* Human villous trophoblasts express and secrete placenta-specific microRNAs into maternal circulation via exosomes. *Biol. Reprod.* **81**, 717–729 (2009).
80. Pineles, B.L. *et al.* Distinct subsets of microRNAs are expressed differentially in the human placentas of patients with preeclampsia. *Am. J. Obstet. Gynecol.* **196**, 261.e1–6 (2007).
81. Mouillet, J.F. *et al.* The levels of hypoxia-regulated microRNAs in plasma of pregnant women with fetal growth restriction. *Placenta* **31**, 781–784 (2010).
82. Chim, S.S. *et al.* Detection and characterization of placental microRNAs in maternal plasma. *Clin. Chem.* **54**, 482–490 (2008).
83. Miura, K. *et al.* Identification of pregnancy-associated microRNAs in maternal plasma. *Clin. Chem.* **56**, 1767–1771 (2010).
84. Kotlabova, K., Doucha, J. & Hromadnikova, I. Placental-specific microRNA in maternal circulation-identification of appropriate pregnancy-associated microRNAs with diagnostic potential. *J. Reprod. Immunol.* **89**, 185–191 (2011).
85. Larrabee, P.B. *et al.* Global gene expression analysis of the living human fetus using cell-free messenger RNA in amniotic fluid. *J. Am. Med. Assoc.* **293**, 836–842 (2005).
86. Slonim, D.K. *et al.* Functional genomic analysis of amniotic fluid cell-free mRNA suggests that oxidative stress is significant in Down syndrome fetuses. *Proc. Natl. Acad. Sci. USA* **106**, 9425–9429 (2009).

87. Koide, K. *et al.* Transcriptomic analysis of cell-free fetal RNA suggests a specific molecular phenotype in trisomy 18. *Hum. Genet.* **129**, 295–305 (2011).
88. Zana, M., Janka, Z. & Kalman, J. Oxidative stress: a bridge between Down's syndrome and Alzheimer's disease. *Neurobiol. Aging* **28**, 648–676 (2007).
89. Lamb, J. *et al.* The Connectivity Map: using gene-expression signatures to connect small molecules, genes, and disease. *Science* **313**, 1929–1935 (2006).
90. FitzPatrick, D.R. *et al.* Transcriptome analysis of human autosomal trisomy. *Hum. Mol. Genet.* **11**, 3249–3256 (2002).
91. Chung, I.H. *et al.* Gene expression analysis of cultured amniotic fluid cell with Down syndrome by DNA microarray. *J. Korean Med. Sci.* **20**, 82–87 (2005).
92. Rozovski, U. *et al.* Genome-wide expression analysis of cultured trophoblast with trisomy 21 karyotype. *Hum. Reprod.* **22**, 2538–2545 (2007).
93. Hui, L. *et al.* The amniotic fluid transcriptome: a source of novel information about human fetal development. *Obstet. Gynecol.* **119**, 111–118 (2012).
94. Tsui, N.B. *et al.* Systematic micro-array based identification of placental mRNA in maternal plasma: towards non-invasive prenatal gene expression profiling. *J. Med. Genet.* **41**, 461–467 (2004).
95. Purwosunu, Y. *et al.* Cell-free mRNA concentrations of *CRH*, *PLAC1*, and *selectin-P* are increased in the plasma of pregnant women with preeclampsia. *Prenat. Diagn.* **27**, 772–777 (2007).
96. Okazaki, S. *et al.* Placenta-derived, cellular messenger RNA expression in the maternal blood of preeclamptic women. *Obstet. Gynecol.* **110**, 1130–1136 (2007).
97. Miura, K. *et al.* The possibility of microarray-based analysis using cell-free placental mRNA in maternal plasma. *Prenat. Diagn.* **30**, 849–861 (2010).
98. Miura, K. *et al.* Increased levels of cell-free placenta mRNA in a subgroup of placenta previa that needs hysterectomy. *Prenat. Diagn.* **28**, 805–809 (2008).
99. Ng, E.K. *et al.* The concentration of circulating corticotrophin-releasing hormone mRNA in maternal plasma is increased in preeclampsia. *Clin. Chem.* **49**, 727–731 (2003).
100. Løset, M. *et al.* A transcriptional profile of the decidua in preeclampsia. *Am. J. Obstet. Gynecol.* **204**, 84.e1–27 (2011).
101. Sitras, V., Paulssen, R., Leirvik, J., Vartun, A. & Acharya, G. Placental gene expression profile in intrauterine growth restriction due to placental insufficiency. *Reprod. Sci.* **16**, 701–711 (2009).
102. Madsen-Bouterse, S.A. *et al.* The transcriptome of the fetal inflammatory response syndrome. *Am. J. Reprod. Immunol.* **63**, 73–92 (2010).
103. Gracie, S.K. *et al.* All Our Babies Cohort Study: recruitment of a cohort to predict women at risk of preterm birth through the examination of gene expression profiles and the environment. *BMC Pregnancy Childbirth* **10**, 87 (2010).
104. Guttmacher, A.E. *et al.* Educating health-care professionals about genetics and genomics. *Nat. Rev. Genet.* **8**, 151–157 (2007).
105. Wapner, R. A multicenter, prospective, masked comparison of chromosomal microarray with standard karyotyping for routine and high risk prenatal diagnosis. *Am. J. Obstet. Gynecol.* **206**, S2 (2012).
106. Susman, M.R. *et al.* Using population-based data to predict the impact of introducing noninvasive prenatal diagnosis for Down syndrome. *Genet. Med.* **12**, 298–303 (2010).
107. Benn, P.A. & Chapman, A.R. Practical and ethical considerations of noninvasive prenatal diagnosis. *J. Am. Med. Assoc.* **301**, 2154–2156 (2009).
108. Hill, M. *et al.* Incremental cost of non-invasive prenatal diagnosis versus invasive prenatal diagnosis of fetal sex in England. *Prenat. Diagn.* **31**, 267–273 (2011).
109. Liao, G.J. *et al.* Targeted massively parallel sequencing of maternal plasma DNA permits efficient and unbiased detection of fetal alleles. *Clin. Chem.* **57**, 92–101 (2011).
110. Papageorgiou, E.A. *et al.* Fetal-specific DNA methylation ratio permits noninvasive prenatal diagnosis of trisomy 21. *Nat. Med.* **17**, 510–513 (2011).
111. Ghanta, S. *et al.* Non-invasive prenatal detection of trisomy 21 using tandem single nucleotide polymorphisms. *PLoS ONE* **5**, e13184 (2010).
112. Benn, P.A. & Chapman, A.R. Ethical challenges in providing noninvasive prenatal diagnosis. *Curr. Opin. Obstet. Gynecol.* **22**, 128–134 (2010).
113. Beaudet, A.L. Ethical issues raised by common copy number variants and single nucleotide polymorphisms of certain and uncertain significance in general medical practice. *Genome Med.* **2**, 42 (2010).
114. Greely, H.T. Get ready for the flood of fetal gene screening. *Nature* **469**, 289–291 (2011).
115. Deans, Z. & Newson, A.J. Should non-invasiveness change informed consent procedures for prenatal diagnosis? *Health Care Anal.* **19**, 122–132 (2011).
116. Hall, A., Bostanci, A. & Wright, C.F. Non-invasive prenatal diagnosis using cell-free fetal DNA technology: applications and implications. *Public Health Genomics* **13**, 246–255 (2010).
117. Massingham, L.J. *et al.* Proof of concept study to assess fetal gene expression in amniotic fluid by nanoarray PCR. *J. Mol. Diagn.* **13**, 565–570 (2011).

nature medicine

Profiling of residual breast cancers after neoadjuvant chemotherapy identifies DUSP4 deficiency as a mechanism of drug resistance

Justin M Balko[1], Rebecca S Cook[2,3], David B Vaught[2], María G Kuba[4], Todd W Miller[2,3], Neil E Bhola[1], Melinda E Sanders[3,4], Nara M Granja-Ingram[4], J Joshua Smith[5], Ingrid M Meszoely[3,5], Janine Salter[6,7], Mitch Dowsett[6,7], Katherine Stemke-Hale[8], Ana M González-Angulo[8,9], Gordon B Mills[8], Joseph A Pinto[10], Henry L Gómez[11] & Carlos L Arteaga[1–3]

Neoadjuvant chemotherapy (NAC) induces a pathological complete response (pCR) in ~30% of patients with breast cancer. However, many patients have residual cancer after chemotherapy, which correlates with a higher risk of metastatic recurrence and poorer outcome than those who achieve a pCR. We hypothesized that molecular profiling of tumors after NAC would identify genes associated with drug resistance. Digital transcript counting was used to profile surgically resected breast cancers after NAC. Low concentrations of dual specificity protein phosphatase 4 (DUSP4), an ERK phosphatase, correlated with high post-NAC tumor cell proliferation and with basal-like breast cancer (BLBC) status. BLBC had higher DUSP4 promoter methylation and gene expression patterns of Ras-ERK pathway activation relative to other breast cancer subtypes. DUSP4 overexpression increased chemotherapy-induced apoptosis, whereas DUSP4 depletion dampened the response to chemotherapy. Reduced DUSP4 expression in primary tumors after NAC was associated with treatment-refractory high Ki-67 scores and shorter recurrence-free survival. Finally, inhibition of mitogen-activated protein kinase kinase (MEK) synergized with docetaxel treatment in BLBC xenografts. Thus, DUSP4 downregulation activates the Ras-ERK pathway in BLBC, resulting in an attenuated response to anti-cancer chemotherapy.

Chemotherapy is the standard treatment for patients with triple negative breast cancers (TNBCs), which are estrogen-receptor protein (ER), progesterone-receptor protein (PR) and human epidermal growth factor receptor 2 (HER2) negative. Although NAC is effective in reducing the size of the primary tumor before surgery, residual disease after NAC is common and is associated with higher risk of metastatic recurrence compared to patients achieving a pCR. A growing amount of evidence shows that chemotherapeutic agents spare cancer-initiating or stem-like cells[1–4]. Thus, we hypothesized that molecular profiling of treatment-refractory tumor cells may reveal alterations that are associated with drug resistance, metastatic recurrence and disease progression.

Here we used NanoString analyses[5] to interrogate gene expression patterns in 49 residual breast tumors after NAC to identify causal effectors of drug resistance. We quantified the levels of 355 transcripts and evaluated them for association with Ki-67 immunohistochemistry (IHC) score in tumors after NAC. From this analysis, we identified *DUSP4*, a negative regulator of extracellular-regulated kinase (ERK) activity, as a potential mediator of resistance to chemotherapy and a tumor suppressor in BLBC. We further characterized the role of DUSP4 in BLBC through analyses of microarray data and *in vitro* and *in vivo* studies. We also provide evidence that loss of DUSP4 may underlie Ras-ERK pathway activation in BLBC, which can be targeted clinically with inhibitors of MEK.

RESULTS

We performed NanoString gene expression profiling on 49 formalin-fixed paraffin-embedded (FFPE) archival tissues from breast cancers resected after NAC (**Fig. 1a** and **Supplementary Table 1**). Because high tumor cell proliferation after NAC, as measured by Ki-67 IHC score, correlates with long-term outcome[6,7], we used this biomarker as a surrogate endpoint for the effects of therapy. This cohort was enriched with TNBC specimens, where chemotherapy is the standard of care. The Ki-67 score ranged from 2.44–99.03% (**Fig. 1b**) and was

[1]Department of Medicine, Vanderbilt-Ingram Comprehensive Cancer Center, Vanderbilt University, Nashville, Tennessee, USA. [2]Department of Cancer Biology, Vanderbilt-Ingram Comprehensive Cancer Center, Vanderbilt University, Nashville, Tennessee, USA. [3]Breast Cancer Research Program, Vanderbilt-Ingram Comprehensive Cancer Center, Vanderbilt University, Nashville, Tennessee, USA. [4]Department of Pathology, Vanderbilt-Ingram Comprehensive Cancer Center, Vanderbilt University, Nashville, Tennessee, USA. [5]Department of Surgery, Vanderbilt-Ingram Comprehensive Cancer Center, Vanderbilt University, Nashville, Tennessee, USA. [6]Breakthrough Breast Cancer Centre, Institute of Cancer Research, Royal Marsden Hospital, London, UK. [7]Academic Department of Biochemistry, Royal Marsden Hospital, London, UK. [8]Department of Systems Biology, University of Texas, M.D. Anderson Cancer Center, Houston, Texas, USA. [9]Department of Breast Medical Oncology, University of Texas, M.D. Anderson Cancer Center, Houston, Texas, USA. [10]División de Investigación, Oncosalud, Lima, Perú. [11]Instituto Nacional de Enfermedades Neoplásicas, Lima, Perú. Correspondence should be addressed to C.L.A. (carlos.arteaga@vanderbilt.edu).

Received 7 April 2011; accepted 18 April 2012; published online 10 June 2012; doi:10.1038/nm.2795

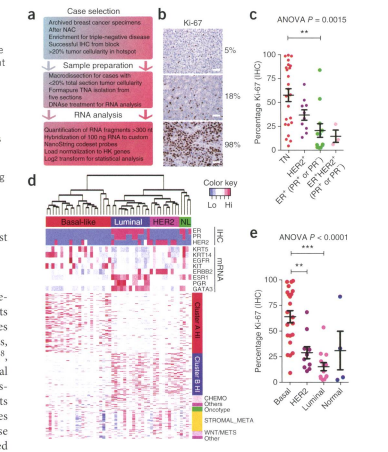

Figure 1 Ki-67–associated gene expression in chemotherapy-refractory breast cancers. (**a**) Scheme for the analysis of gene expression patterns in tumor-sparse FFPE tissues. HK genes, housekeeper genes. (**b**) Representative IHC of breast cancers after NAC with low, intermediate and high Ki-67 scores. Scale bars, 50 μm. (**c**) Association of pretreatment receptor status with Ki-67 score after chemotherapy. $P = 0.0015$ by analysis of variance (ANOVA) followed by Bonferroni *post-hoc t* test correction. $^{**}P < 0.01$. TN, triple negative. Data are mean ± s.e.m. (**d**) Heatmap depicting the gene expression patterns in 49 tumors after NAC assayed by NanoString digital RNA transcript counting. Clinical (HER2, ER, PR) and molecular parameters are annotated for the samples (*x* axis), and gene signature or metagene membership is annotated for the genes (*y* axis). Red indicates high expression, and blue indicates low expression. NL, normal-like (**e**) Ki-67 score after NAC is plotted according to molecular subtype. $P < 0.0001$ by ANOVA followed by Bonferroni *post-hoc t* test correction, $^{**}P < 0.01$, $^{***}P < 0.001$.

associated with hormone receptors and HER2 status, with the highest positivity present in the TNBC samples (**Fig. 1c**).

Gene expression profiling in archival tissues after NAC

Because of limitations in the number of genes that can be simultaneously assayed by NanoString, we assembled a priority list of transcripts to quantify. We interrogated the literature to identify gene signatures that are associated with high-grade, chemotherapy-resistant tumors, including the 21-gene Recurrence Score (Oncotype DX) signature[8], an 18-gene chemo-resistance signature (CHEMO)[9], a 50-gene stromal metagene signature (STROMAL_META)[10] and a 13-gene wingless-related MMTV integration site (Wnt) pathway signature that predicts metastatic behavior (WNT/METS)[11]. We also analyzed other genes known to be involved in breast cancer that were not included in these signatures (**Supplementary Table 2**). Additionally, we incorporated class discovery approaches into the analysis (see Online Methods). Briefly, we subjected ER$^-$ breast tumors from the European Organisation for Research and Treatment of Cancer (EORTC) 10994 study that did not achieve a complete response to NAC[10] to hierarchical clustering to identify the two most biologically distinct groups of tumors (**Supplementary Fig. 1a**). We hypothesized that these tumor and patient groups may correspond to Ki-67^{hi} and Ki-67^{lo} phenotypes after NAC. We tested the 354 microarray probe sets (244 unique genes, hereafter referred as the CLUSTER signature) differentiating these two classes for overlap with the Molecular Signatures Database (http://www.broadinstitute.org/; c2 curated), and we found them to be enriched for genes indicative of Ras activation, breast cancer 1 (BRCA1) deficiency (cluster A) and ER activation (cluster B) (**Supplementary Fig. 1b**). These genes clustered a panel of 50 breast cancer cell lines according to molecular subtype (**Supplementary Fig. 1c**), and we combined this panel with the previously published signatures to form a target set comprising 355 unique transcripts.

We profiled the RNA extracted from the 49 tumor blocks (**Supplementary Fig. 2a**–**e**) in duplicate using NanoString. The inter-replicate correlations ranged from 0.9985 to ~1.0 (**Supplementary Fig. 2f**). The seven control genes, selected from existing microdissected tumor microarray data as having low interpatient variability, were well correlated, suggesting that they were appropriate normalization factors (**Supplementary Fig. 2g**). We excluded 10 of the 355 transcripts because of poor signal-to-noise ratios. The normalized data and sample annotations are shown in **Supplementary Tables 3** and **4**. As an internal control, digital transcript counts for *ESR1* (encoding ER), *PGR* (encoding PR) and *ERBB2* (encoding HER2) were highly associated with clinical ER, PR and HER2 status (**Supplementary Fig. 3a**–**f**). Ki-67 score in the tumors after NAC was also highly correlated with expression of *MKI67* (Pearson's $r = 0.7$, $P < 0.0001$) (**Supplementary Fig. 3g**). These findings show the integrity of the acquired gene expression data.

Ki-67 score after NAC varies with molecular subtype

Molecular subtype is a strong prognostic variable in breast cancer and should be considered when performing gene expression profiling of breast tumors[6,7,12,13]. To determine the molecular subtype of the 49 tumors, we used unsupervised hierarchical clustering of the expression data, which produced four distinct clusters (**Fig. 1d**). The gene expression patterns of known basal and luminal markers differentiated between the two most prominent clusters (basal-like and luminal, $n = 22$ and 13, respectively); the third cluster contained the majority of the HER2-overexpressing tumors ($n = 10$). The fourth cluster contained both basal and luminal markers, and we designated it as the 'normal-like' cluster ($n = 4$).

Similar to hormone receptors (ER and PR) and HER2 status (**Fig. 1c**), we found a strong association between molecular subtype and Ki-67 score after NAC, which was the highest in the BLBCs (**Fig. 1e**). However, Ki-67 scores after NAC had high intra-subtype variability, particularly in BLBC, reflecting the heterogeneity of the basal-like subtype.

Gene sets associated with Ki-67 scores in treated tumors

We next applied the CLUSTER signature, described above, to the 49 breast tumors. We hypothesized that the collective expression of these genes may be associated with Ki-67 scores after NAC. Indeed, the CLUSTER signature (**Supplementary Table 2**) was highly correlated with Ki-67 score after NAC, as well as with the grade, mitotic index and

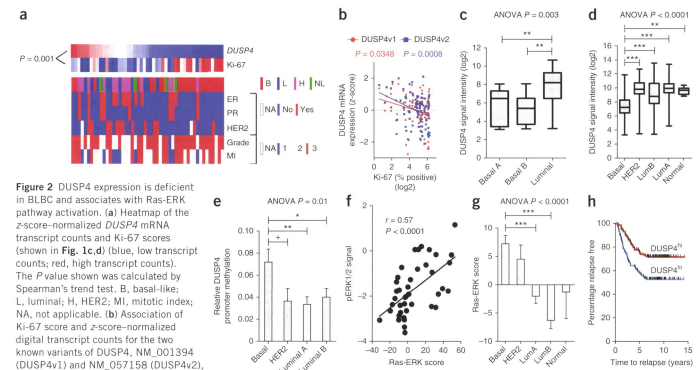

Figure 2 DUSP4 expression is deficient in BLBC and associates with Ras-ERK pathway activation. (**a**) Heatmap of the *z*-score–normalized *DUSP4* mRNA transcript counts and Ki-67 scores (shown in **Fig. 1c,d**) (blue, low transcript counts; red, high transcript counts). The *P* value shown was calculated by Spearman's trend test. B, basal-like; L, luminal; H, HER2; MI, mitotic index; NA, not applicable. (**b**) Association of Ki-67 score and *z*-score–normalized digital transcript counts for the two known variants of DUSP4, NM_001394 (DUSP4v1) and NM_057158 (DUSP4v2), assayed by NanoString in 89 primary TNBCs treated with NAC. The *P* values shown were calculated by Pearson's trend test. (**c**) Association of molecular subtype (as previously reported[20]) with *DUSP4* gene expression (Affymetrix probe set 204014_at) in the ICBP-50 panel of breast cancer cell lines. $P = 0.003$ by ANOVA followed by Bonferroni *post-hoc t* test correction. $^{**}P < 0.01$. (**d**) Association of molecular subtype and *DUSP4* gene expression (204014 _at) in 230 breast tumors from the MAQC-II study[21]. $P < 0.0001$ by ANOVA followed by Bonferroni *post-hoc t* test correction. $^{**}P < 0.01$, $^{***}P < 0.001$. LumA, luminal A; LumB, luminal B. (**e**) Association of *DUSP4* promoter methylation data with reported molecular subtype[22] in 138 annotated breast tumors. $P = 0.01$ by ANOVA followed by Bonferroni *post-hoc t* test correction. $^{*}P < 0.1$, $^{*}P < 0.05$, $^{**}P < 0.01$. (**f**) Association of the Ras-ERK pathway score[24] (Online Methods) with pERK1/2 signal, as measured by RPPA in 42 of 50 cell lines in the ICBP-50 panel. The *P* value shown was calculated using Pearson's trend test. (**g**) Association of the Ras-ERK pathway score for 230 breast tumors of patients in the MAQC-II study[21] with molecular subtype, as determined by PAM50 analysis. $P < 0.0001$ by ANOVA followed by Bonferroni *post-hoc t* test correction. $^{***}P < 0.001$. (**h**) Kaplan-Meier analysis of 286 breast tumors (Gene Expression Omnibus accession GSE2034)[25] dichotomized at the median *DUSP4* (204014_at) expression. Data in **e** and **g** are mean ± s.e.m.

molecular subtype of the tumors (**Supplementary Fig. 4a–e**). Three of the four preselected signatures (from CHEMO[9], WNT/METS[11] and Oncotype DX[8]) were also associated with Ki-67 score after NAC (**Supplementary Fig. 5**). Both the STROMAL_META signature and the CHEMO signature were previously reported to predict resistance to chemotherapy[9,10]. Paradoxically, the signature scores for CHEMO and WNT/WETS here were inversely correlated with a high Ki-67 score (we observed the lowest chemotherapy resistance scores for the tumors with the highest expression of Ki-67). This finding suggests two possibilities: (i) many gene signatures predicting sensitivity to chemotherapy are driven primarily by proliferation-related genes, as highly proliferative tumors are often responsive to this type of treatment and/or (ii) gene expression profiling of the tumors after NAC produces different information than profiling before NAC. The Oncotype DX algorithm maintained a strong predictive capacity in tumors after NAC, presumably because it is heavily weighted to proliferation-associated genes (**Supplementary Fig. 5d**). Although Ki-67 score after NAC prognosticates patient outcome but not necessarily chemoresistance, it is intuitive that those cells that retain high proliferation despite treatment will probably be resistant to chemotherapeutic agents.

Ras-ERK pathway activation in breast tumors after NAC

To identify targetable pathways in chemotherapy-refractory cancer cells, we tested genes that significantly correlated with a high Ki-67 score ($P < 0.05$) for overlap with the Molecular Signatures Database. To limit the identification of signatures associated with the subtypes of breast cancer (basal or luminal and clinical ER or HER2 status), we restricted the analysis to the 22 BLBC tumors, thereby focusing on pathways and gene sets that may be activated in tumors with high Ki-67 scores specifically within BLBC. Two of the 20 enriched gene sets represented genes downregulated by the activated proto-oncogene KRAS, a member of the Ras protein family (**Supplementary Table 5**)[14,15]. The expression of these genes was inversely correlated with Ki-67 score after NAC, suggesting that activation of KRAS is associated with high tumor cell proliferation after treatment. This was surprising to us, as mutations in *KRAS* are rare in human breast tumors[16,17], and sequencing of *KRAS* codon 12 in the BLBCs from this cohort did not identify any mutations (data not shown). Thus, the gene signatures observed in BLBCs expressing a high Ki-67 score that associate with Ras-ERK pathway activation probably occur through mechanisms other than *KRAS* mutations.

DUSP4 loss associates with BLBC and Ras-ERK activation

Consistent with activation of the Ras-ERK pathway, low expression of *DUSP4*, a negative regulator of ERK1 and ERK2, had the strongest correlation with high Ki-67 score ($P = 0.001$; **Fig. 2a**). Low *DUSP4* expression also correlated with BLBC subtype but retained its inverse association with Ki-67 score when considering only basal-like tumors (Spearman's $r = -0.64$, $P = 0.001$). To confirm this finding, we examined *DUSP4* expression as measured by NanoString in a second cohort

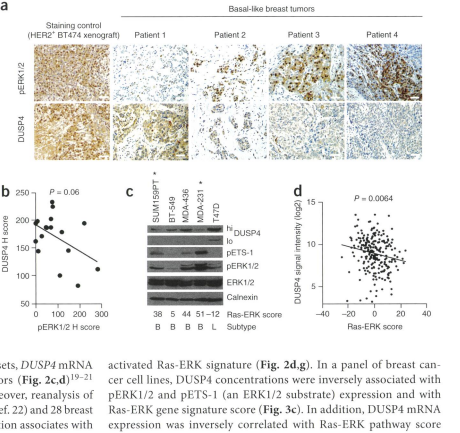

Figure 3 DUSP4 expression is inversely associated with Ras-ERK pathway activation. (**a**) Four representative BLBC sections stained by IHC for pERK1/2 and DUSP4. A HER2 gene-amplified BT-474 xenograft (pERK1/2^{hi}, *DUSP4*^{hi}) was included as a control. Scale bars, 50 μm. (**b**) Association of DUSP4 and pERK1/2 H scores (nuclear and cytoplasmic; see Online Methods for an explanation of H scores). The *P* value shown was calculated by Pearson's trend test. (**c**) Immunoblot analysis of breast cancer cell lines harvested at subconfluence under normal growth conditions. The Ras-ERK score from **Figure 2e** is noted below. B, basal-like; L, luminal. Asterisks indicate cell lines with a known activating Ras and/or Raf mutation. (**d**) Association of the Ras-ERK pathway score and *DUSP4* gene expression (204014_at). The *P* value shown was calculated by Pearson's trend test.

of 89 TNBCs after NAC (**Fig. 2b**). Probes specific for each of the known DUSP4 transcript variants (NM_001394 and NM_057158 (ref. 18)) correlated significantly with the Ki-67 score after NAC ($P = 0.0348$ and $P = 0.0008$, respectively). In existing microarray datasets, *DUSP4* mRNA levels were lowest in BLBC cell lines and tumors (**Fig. 2c,d**)[19–21] despite their high intra-subtype variability. Moreover, reanalysis of two recent methylation studies in cohorts of 138 (ref. 22) and 28 breast cancers[23] showed that *DUSP4* promoter methylation associates with BLBC (**Fig. 2e** and **Supplementary Fig. 6**).

We next examined the relationship between *DUSP4* expression and a Ras-ERK pathway activation gene signature[24]. First, we confirmed that a published gene expression-based Ras-ERK pathway activation score correlated with the amount of phosphorylation at Thr202 and Tyr204 in ERK1 and Thr185 and Tyr187 of ERK2 respectively (pERK1/2$^{T202/Y204}$) determined by reverse-phase protein arrays (RPPA) in the Integrative Cancer Biology Program (ICBP)-50 breast cancer cell line panel (Pearson's $r = 0.57$, $P < 0.0001$; **Fig. 2f**). The signature also correlated with basal-like and HER2$^+$ primary tumors but not with the luminal A and B subtypes (**Fig. 2g**; $n = 230$)[21]. HER2 strongly activates Ras-ERK signaling, potentially explaining the association with this molecular subtype. Moreover, in a dataset of 286 breast cancers from patients who did not receive adjuvant therapy[25], low *DUSP4* expression predicted shorter recurrence-free survival time ($P = 0.0004$, hazard ratio = 1.99, Cox proportional hazard univariate $P = 0.0005$; **Fig. 2h**). Notably, *DUSP4* mRNA expression retained its significance after adjusting for molecular subtype in a multivariate analysis (Cox proportional hazard $P = 0.002$). These data suggest that low DUSP4 expression in resected tumors is a potential biomarker for a high likelihood of residual micrometastatic disease and tumor recurrence that is independent of molecular subtype.

DUSP4 loss associates with high ERK activity in BLBC

IHC staining for DUSP4 and pERK1/2$^{T202/Y204}$ in 17 BLBCs after NAC revealed an inverse correlation between pERK1/2 and DUSP4 (**Fig. 3a,b**), suggesting that DUSP4 deficiency associates with Ras-ERK pathway activation in chemotherapy-refractory BLBC. Sections from a *HER2*-gene–amplified BT-474 xenograft stained high for both DUSP4 and pERK1/2 (**Fig. 3a**), consistent with the observation that HER2-overexpressing tumors have high mRNA expression and an activated Ras-ERK signature (**Fig. 2d,g**). In a panel of breast cancer cell lines, DUSP4 concentrations were inversely associated with pERK1/2 and pETS-1 (an ERK1/2 substrate) expression and with Ras-ERK gene signature score (**Fig. 3c**). In addition, DUSP4 mRNA expression was inversely correlated with Ras-ERK pathway score ($P = 0.0064$) in a series of 230 primary breast cancers (**Fig. 3d**).

DUSP4 expression modulates ERK activity in BLBC

We next tested the effect of restoring DUSP4 expression in BLBC cell lines. Reconstitution of DUSP4 inhibited the phosphorylation of ERK1/2 and downstream effectors ETS-1 and ELK-1, members of the ETS oncogene family (**Fig. 4a**). In contrast, these effectors were activated after transduction with constitutively active MEK1. DUSP4 overexpression reduced the viability of MDA-231 and BT-549 cells but had little effect on MDA-436 cells (**Fig. 4b**).

To study the effects of loss of DUSP4, we transfected breast cancer cells with siRNA targeting DUSP4 (siDUSP4) (**Fig. 4c,d**). Treatment with either of two siDUSP4 sequences had variable effects on ERK phosphorylation but consistently induced activation and expression of the ERK effector ETS-1 in three out of three basal-like cell lines (MDA-231, BT-549 and MDA-436). We speculate that ETS-1 activation may be a better marker of ERK activity in the nucleus, where DUSP4 localizes, than total cellular phosphorylation of ERK.

Knockdown of DUSP4 attenuates response to chemotherapy

We next examined whether DUSP4 loss exerts a chemoprotective effect in breast epithelial cells. SiRNA knockdown of DUSP4 increased the half-maximal inhibitory concentration (IC_{50}) of docetaxel, enhanced MEK-dependent cell proliferation and protected against docetaxel-induced apoptosis in MCF-10A immortalized human mammary epithelial cells (**Supplementary Fig. 7a–d**). We obtained similar results in MDA-231 and MCF-7 breast cancer cells transfected with siDUSP4 (**Supplementary Fig. 7e,f**). To confirm the specificity of this result to DUSP4, we transduced MDA-231 cells with wild-type DUSP4 or with a synonymous DUSP4 mutant that is resistant to siRNA-mediated degradation (**Supplementary Fig. 7g–i**). Transduction with the

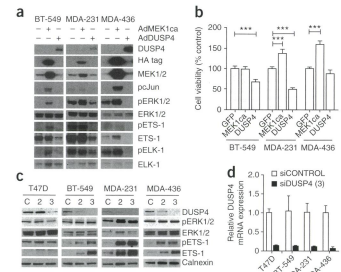

Figure 4 DUSP4 regulates MAPK signaling and cell viability. (**a**) Immunoblot analysis for MAPK pathway activation after adenoviral transduction with GFP, constitutively active MEK1 (AdMEK1ca), or DUSP4 (AdDUSP4). HA, hemagglutinin. (**b**) Sulfarhodamine B (SRB) viability analysis of the cells in **a** 72 h after transduction. Student's *t* test, $***P < 0.001$. (**c**) Immunoblot analysis of breast cancer cell lines transiently transfected for 72 h with one of two sequences of siRNA targeting DUSP4 (siDUSP4, 2 or 3) or a nontargeting siRNA control (siCONTROL, C). (**d**) Quantitative RT-PCR analysis of DUSP4 mRNA expression, normalized to glyceraldehyde 3-phosphate dehydrogenase (GAPDH), 48 h after siRNA transfection with the siDUSP4 construct 3 described in **c**). Data in **b** and **d** are mean ± s.d.

siRNA-resistant DUSP4 mutant but not with wild-type DUSP4 partially abrogated the effect of siDUSP4 on docetaxel-induced caspase 3 and 7 cleavage in MDA-231 cells (**Supplementary Fig. 7j**). Collectively, these results suggest that DUSP4 loss protects breast cancer cells from chemotherapy-induced apoptosis.

DUSP4 loss after NAC correlates with poor patient outcome

Our *in vitro* studies suggested a role for DUSP4 in dampening the response to chemotherapy. To further support a chemoprotective effect of DUSP4 loss, at least one of two scenarios must occur: (i) pre-treatment concentrations of DUSP4 must predict clinical response to NAC, or (ii) cells expressing low amounts of *DUSP4* must be enriched after NAC. In the EORTC 10994 (ref. 10) and MAQC-II breast cancer studies[21], after adjusting for molecular subtype, *DUSP4* expression before treatment was not associated with pathological complete response (pCR) (data not shown), thus arguing against the first possibility. We next asked whether *DUSP4* expression was reduced in the residual tumors following NAC. We assayed the pretreatment biopsies from 15 patients in our cohort for Ki-67 score and *DUSP4* expression and compared these results to those from the residual tumor after NAC. Patients that lost DUSP4 expression also had an increase in the tumor Ki-67 score after NAC. Of note, these patients had a shorter recurrence-free survival (**Fig. 5a,b**). We confirmed the association of loss of DUSP4 expression with poor clinical response to NAC in two other published cohorts (**Fig. 5c**). In one of these studies, 32 breast tumors were sampled before and after four cycles of NAC with epirubicin and cyclophosphamide, which was followed by four cycles of docetaxel[26]. All patients with expression data at both time points had residual disease after therapy. Patients with a substantial volumetric response by ultrasonography showed increased DUSP4 expression after NAC, whereas patients with a poor response to NAC lost or maintained low DUSP4 expression. A similar finding was made by a second study comprised of 15 patients who were treated with four cycles of docetaxel and capecitabine. Data from tumors sampled at baseline and at surgery were analyzed. Patients were categorized as responders or non-responders based on the change in tumor size by clinical exam and pathological response[27]. Thus, the combined analyses of these three studies suggest a causal association between DUSP4 deficiency and a lower response to anti-cancer chemotherapy.

Inhibition of MEK improves chemotherapy-induced apoptosis

Given the role of DUSP4 in negative regulation of ERK1 and ERK2, we hypothesized that low expression of DUSP4 may be partly responsible for Ras-ERK pathway dependency and may be a potential biomarker for response to MEK inhibition. In support of this notion, we found that *DUSP4* mRNA expression correlated inversely with sensitivity to the MEK inhibitors CI-1040 and U0126 across 17 BLBC cell lines, particularly when we excluded cell lines with

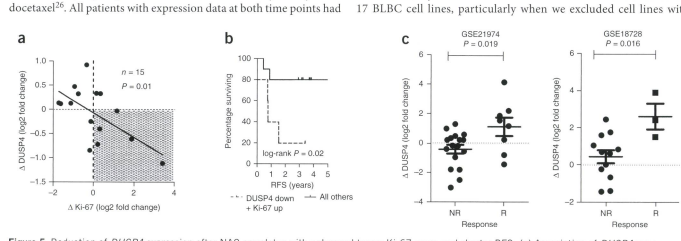

Figure 5 Reduction of *DUSP4* expression after NAC correlates with enhanced tumor Ki-67 score and shorter RFS. (**a**) Association of *DUSP4* gene expression and Ki-67 score in 15 breast tumors (paired diagnostic biopsies and surgical specimens after NAC). The *P* value shown was calculated by Pearson's trend test. (**b**) Kaplan-Meier survival analysis of the population from the thatched area in **a** (loss of DUSP4 (DUSP down) and gain of Ki-67 score (Ki-67 up)) compared to all other tumors. (**c**) Association of the change in *DUSP4* gene expression from paired breast tumors before and after NAC with response to NAC in two published studies[26,27]. A two-tailed *t* test was used to test for differences between patients who had a substantial tumor response (R) to NAC and those that did not (NR).

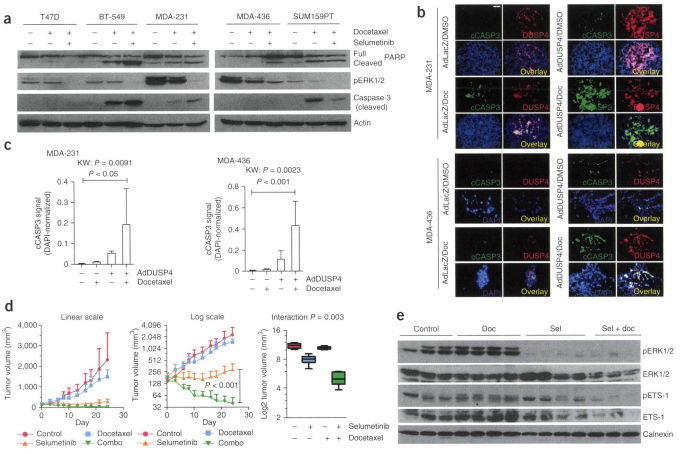

Figure 6 Pharmacological or genetic inhibition of MEK improves chemotherapy-induced apoptosis *in vitro* and *in vivo*. (**a**) Immunoblot analysis of breast cancer cell lines treated for 6 h with docetaxel or DMSO in normal growth medium, followed by drug washout and treatment with DMSO or selumetinib for 72 h. (**b**) Immunofluorescence for cleaved caspase 3 and DUSP4 in MDA-231 and MDA-436 cells transduced with adenovirus encoding *DUSP4* (AdDUSP4) or *LacZ* (AdLacZ, control) followed by 24 h of docetaxel (Doc) or DMSO treatment. DUSP4 is shown in red, cleaved caspase 3 (cCASP3) is shown in green, and DAPI is shown in blue. The overlay (yellow) is shown in the lower right quadrant of each group. Scale bar, 50 μm. (**c**) Quantification of the immunofluorescence in **b**. FITC (cleaved caspase 3) signals were normalized to DAPI and are shown as mean ± s.d. ($n = 5$). The Kruskal-Wallis (nonparametric ANOVA equivalent; KW) test was used to test for differences among the groups, with a Dunn's post-test to compare individual groups. (**d**) Tumor growth curves of MDA-231 xenografts randomized to treatment with selumetinib, docetaxel, the combination of both (combo) or vehicle control ($n = 9$ per arm). The results are shown on the linear scale (left) and the log2 scale (center) to visualize the differences in smaller tumors. Boxplot of final tumor volumes (day 24, right). The treatment interaction was tested by two-way ANOVA. Data are mean ± range. (**e**) Immunoblot analysis of xenografts harvested after 3 d of treatment, 1 h after the last dose of selumetinib (Sel).

loss of phosphatase and tensin homolog (PTEN) (**Supplementary Fig. 8**). Thus, we next determined whether MEK inhibition with AZD6244 (selumetinib) enhances docetaxel-induced apoptosis in breast cancer cells. Selumetinib was anti-proliferative in BLBC cells and antagonized the effects of docetaxel (data not shown), as has been observed by others[28]. However, three out of four BLBC cell lines treated with sequenced selumetinib after docetaxel treatment showed higher levels of cleaved caspase 3 and cleaved poly-(ADP-ribose) polymerase (PARP) compared to lines treated with docetaxel alone (**Fig. 6a**). Similar to selumetinib, transduction of DUSP4 also enhanced docetaxel-induced apoptosis in MDA-231 and MDA-436 cells (**Fig. 6b,c**).

To confirm these findings *in vivo*, we established MDA-231 xenografts in athymic mice and randomized them to treatment with docetaxel or vehicle, each with or without selumetinib. Treatment with selumetinib alone arrested the growth of MDA-231 xenografts, whereas treatment with docetaxel alone transiently delayed tumor growth. In contrast, we found marked tumor regression in the combination treatment arm (**Fig. 6d**). There was significant interaction effect ($P = 0.003$) between selumetinib and docetaxel in the effect on tumor size, suggesting therapeutic synergy. Immunoblot analyses of tumor lysates harvested after 3 days of treatment confirmed downregulation of pERK1/2 and ETS-1 in xenografts treated with selumetinib alone or in combination with docetaxel (**Fig. 6e**). These data provide further evidence that activation of the Ras-MAPK pathway can dampen the response to anti-cancer chemotherapy *in vivo* and support clinical trials combining these agents in DUSP4-deficient BLBC.

DISCUSSION

Archival FFPE tissues are a large source of primary tumor material that can be used for the identification of molecular markers that are associated with cancer behavior and patient outcome. Recent advances in cancer stem cell biology and tumor cell drug resistance have suggested the importance of molecularly profiling tumors after *in vivo* drug selection of treatment-refractory cancer cell subpopulations[6,29–31]. However, tumors after treatment are often paucicellular and include substantial necrotic and non-tumor cell contamination.

Thus, accurate profiling in these specimens can be challenging. Using macrodissection coupled with digital expression analyses in treatment-refractory breast tumors after NAC, we report here a discovery-based methodology that may be useful in identifying mechanisms of drug resistance. Because patients with residual tumors after NAC, particularly those with high residual cell proliferation, have a higher probability of early metastatic recurrence and death than those who achieve a pCR, we hypothesize that the gene expression profile in these refractory cancers should mirror the expression profile of the residual micrometastases[6,7]. Exploring these profiles may enable the discovery of molecular alterations driving tumor recurrence, paving the way for rational adjuvant therapies targeting micrometastases.

Gene expression profiling of specimens after NAC resulted in several key findings. First, the Ki-67 score after NAC was highly related to the molecular and clinical subtype of breast cancer. To our knowledge, this association has not been previously shown. Second, in line with the hypothesis that residual tumors with high Ki-67 scores after chemotherapy harbor biomarkers and causal effectors of drug resistance, we identified loss of the phosphatase DUSP4 as a targetable mediator of drug resistance.

DUSP4 deregulation has been observed in lung cancer cell lines and primary tumors, and epigenetic silencing of DUSP4 has been noted in glioblastomas[32–34]. A previous study showed DUSP4 copy number loss by fluorescence *in situ* hybridization in breast cancers[35]. Thus, copy number loss may also influence *DUSP4* expression, resulting in a loss of negative feedback mechanisms to Ras-ERK pathway activation and a dependence on this pathway for tumor cell proliferation and survival. Supporting this notion, we found that *DUSP4* mRNA expression correlated inversely with sensitivity to the MEK inhibitors CI-1040 and U0126 in BLBC cell lines, particularly when excluding PTEN-null cell lines. PTEN loss increases phosphoinositide-3-kinase (PI3K) pathway activation, potentially providing MEK-independent growth and survival signals. Thus, we predict that *DUSP4* expression (coupled with PTEN status) is a testable biomarker for sensitivity to MEK inhibitors in patients with BLBC. Furthermore, as *DUSP4* expression was reduced in breast tumors that responded poorly to NAC, we propose that patients with residual disease after NAC may benefit from adjuvant therapy with an inhibitor of MEK.

In HEK293 cells, overexpression of DUSP4 also results in chemoresistance through repression of apoptosis mediated by mitogen-activated protein kinase 8 (JNK)[36]. However, these data contrast with other data supporting a breast-cancer–promoting role for JNK[37–39]. JNK and ERK1/2 pathway crosstalk mediates an epithelial-mesenchymal transition phenotype in breast cancer[39], which is a hallmark of chemotherapy-resistant, tumor-initiating cancer cells[3,40]. Future studies will be needed to elucidate the contributions of JNK and ERK in promoting stem-like behavior in DUSP4-deficient breast cancer cells.

In summary, molecular profiling of chemotherapy-resistant breast cancers after NAC identified loss of the MAPK phosphatase DUSP4 and activation of the Ras-ERK pathway in BLBC. We propose that further molecular profiling of tumor samples after NAC will yield other actionable molecular targets that can be used to eliminate drug-resistant subpopulations of breast cancer cells.

METHODS

Methods and any associated references are available in the online version of the paper.

Note: Supplementary information is available in the online version of the paper.

ACKNOWLEDGMENTS

We would like to thank E. Penni Black (University of Kentucky), who provided the AdMEK1ca adenoviral construct. The authors would also like to thank P.D. Smith and AstraZeneca for supplying selumetinib utilized in the *in vivo* experiments. This work was supported by Breast Cancer Specialized Program of Research Excellence (SPORE) grant P50CA98131, Vanderbilt-Ingram Cancer Center Support grant P30CA68485, a grant from the Breast Cancer Research Foundation, the American Cancer Society Clinical Research Professorship grant CRP-07-234 and the Lee Jeans Translational Breast Cancer Research Program (to C.L.A.). G.B.M. was supported by the SU2C Dream Team award, PO1CA099031 and the Komen Promise grant KG 081694. J.S. and M.D. were funded by the Breakthrough Breast Cancer and the Royal Marsden National Institutes of Health Research Biomedical Research Centre.

AUTHOR CONTRIBUTIONS

J.M.B. designed and performed the experiments, and authored the manuscript. R.S.C. provided expert guidance on *in vivo* models and performed immunofluorescence. M.G.K., N.M.G.-I. and M.E.S. provided pathology support and performed IHC staining and scoring. D.B.V., T.W.M. and N.E.B. provided scientific advice. K.S.-H., A.M.G.-A. and G.B.M. performed RPPA analysis. J.S., M.D., J.A.P. and H.L.G. provided post-NAC patient tumor samples. J.J.S. and I.M.M. identified the Vanderbilt cohort and managed the clinical database, including performing retrospective chart review. M.E.S. and I.M.M. functioned as honest brokers to maintain patient privacy. C.L.A. provided scientific direction, established collaborations, prepared the manuscript with J.M.B. and allocated funding for the work. All the authors participated in the preparation of the manuscript.

COMPETING FINANCIAL INTERESTS

The authors declare competing financial interests: details are available in the online version of the paper.

Published online at http://www.nature.com/doifinder/10.1038/nm.2795.
Reprints and permissions information is available online at http://www.nature.com/reprints/index.html.

1. Levina, V., Marrangoni, A.M., DeMarco, R., Gorelik, E. & Lokshin, A.E. Drug-selected human lung cancer stem cells: cytokine network, tumorigenic and metastatic properties. *PLoS ONE* **3**, e3077 (2008).
2. Morel, A.P. *et al.* Generation of breast cancer stem cells through epithelial-mesenchymal transition. *PLoS ONE* **3**, e2888 (2008).
3. Creighton, C.J. *et al.* Residual breast cancers after conventional therapy display mesenchymal as well as tumor-initiating features. *Proc. Natl. Acad. Sci. USA* **106**, 13820–13825 (2009).
4. Calcagno, A.M. *et al.* Prolonged drug selection of breast cancer cells and enrichment of cancer stem cell characteristics. *J. Natl. Cancer Inst.* **102**, 1637–1652 (2010).
5. Geiss, G.K. *et al.* Direct multiplexed measurement of gene expression with color-coded probe pairs. *Nat. Biotechnol.* **26**, 317–325 (2008).
6. Guarneri, V. *et al.* A prognostic model based on nodal status and Ki-67 predicts the risk of recurrence and death in breast cancer patients with residual disease after preoperative chemotherapy. *Ann. Oncol.* **20**, 1193–1198 (2009).
7. Jones, R.L. *et al.* The prognostic significance of Ki67 before and after neoadjuvant chemotherapy in breast cancer. *Breast Cancer Res. Treat.* **116**, 53–68 (2009).
8. Paik, S. *et al.* A multigene assay to predict recurrence of tamoxifen-treated, node-negative breast cancer. *N. Engl. J. Med.* **351**, 2817–2826 (2004).
9. Hess, K.R. *et al.* Pharmacogenomic predictor of sensitivity to preoperative chemotherapy with paclitaxel and fluorouracil, doxorubicin, and cyclophosphamide in breast cancer. *J. Clin. Oncol.* **24**, 4236–4244 (2006).
10. Farmer, P. *et al.* A stroma-related gene signature predicts resistance to neoadjuvant chemotherapy in breast cancer. *Nat. Med.* **15**, 68–74 (2009).
11. DiMeo, T.A. *et al.* A novel lung metastasis signature links Wnt signaling with cancer cell self-renewal and epithelial-mesenchymal transition in basal-like breast cancer. *Cancer Res.* **69**, 5364–5373 (2009).
12. Cheang, M.C. *et al.* Ki67 index, HER2 status, and prognosis of patients with luminal B breast cancer. *J. Natl. Cancer Inst.* **101**, 736–750 (2009).
13. Parker, J.S. *et al.* Supervised risk predictor of breast cancer based on intrinsic subtypes. *J. Clin. Oncol.* **27**, 1160–1167 (2009).
14. Sweet-Cordero, A. *et al.* An oncogenic KRAS2 expression signature identified by cross-species gene-expression analysis. *Nat. Genet.* **37**, 48–55 (2005).
15. Chiaradonna, F. *et al.* Ras-dependent carbon metabolism and transformation in mouse fibroblasts. *Oncogene* **25**, 5391–5404 (2006).
16. Sánchez-Munoz, A. *et al.* Lack of evidence for KRAS oncogenic mutations in triple-negative breast cancer. *BMC Cancer* **10**, 136 (2010).
17. Forbes, S.A. *et al.* The Catalogue of Somatic Mutations in Cancer (COSMIC). *Curr. Protoc. Hum. Genet.* Chapter 10 Unit 10.11 (2008).

18. Cadalbert, L.C. *et al.* Differential regulation of MAP kinase activation by a novel splice variant of human MAP kinase phosphatase-2. *Cell. Signal.* **22**, 357–365 (2010).
19. Mirzoeva, O.K. *et al.* Basal subtype and MAPK/ERK kinase (MEK)-phosphoinositide 3-kinase feedback signaling determine susceptibility of breast cancer cells to MEK inhibition. *Cancer Res.* **69**, 565–572 (2009).
20. Neve, R.M. *et al.* A collection of breast cancer cell lines for the study of functionally distinct cancer subtypes. *Cancer Cell* **10**, 515–527 (2006).
21. Popovici, V. *et al.* Effect of training-sample size and classification difficulty on the accuracy of genomic predictors. *Breast Cancer Res.* **12**, R5 (2010).
22. Holm, K. *et al.* Molecular subtypes of breast cancer are associated with characteristic DNA methylation patterns. *Breast Cancer Res.* **12**, R36 (2010).
23. Bediaga, N.G. *et al.* DNA methylation epigenotypes in breast cancer molecular subtypes. *Breast Cancer Res.* **12**, R77 (2010).
24. Pratilas, C.A. *et al.* (V600E)BRAF is associated with disabled feedback inhibition of RAF-MEK signaling and elevated transcriptional output of the pathway. *Proc. Natl. Acad. Sci. USA* **106**, 4519–4524 (2009).
25. Wang, Y. *et al.* Gene-expression profiles to predict distant metastasis of lymph-node-negative primary breast cancer. *Lancet* **365**, 671–679 (2005).
26. Stickeler, E. *et al.* Basal-like molecular subtype and HER4 up-regulation and response to neoadjuvant chemotherapy in breast cancer. *Oncol. Rep.* **26**, 1037–1045 (2011).
27. Korde, L.A. *et al.* Gene expression pathway analysis to predict response to neoadjuvant docetaxel and capecitabine for breast cancer. *Breast Cancer Res. Treat.* **119**, 685–699 (2010).
28. Yacoub, A. *et al.* Sequence dependent exposure of mammary carcinoma cells to Taxotere and the MEK1/2 inhibitor U0126 causes enhanced cell killing *in vitro*. *Cancer Biol. Ther.* **2**, 670–676 (2003).
29. Dowsett, M. *et al.* Short-term changes in Ki-67 during neoadjuvant treatment of primary breast cancer with anastrozole or tamoxifen alone or combined correlate with recurrence-free survival. *Clin. Cancer Res.* **11**, 951s–958s (2005).
30. Dowsett, M. *et al.* Prognostic value of Ki67 expression after short-term presurgical endocrine therapy for primary breast cancer. *J. Natl. Cancer Inst.* **99**, 167–170 (2007).
31. Miller, W.R. *et al.* Gene expression profiles differentiating between breast cancers clinically responsive or resistant to letrozole. *J. Clin. Oncol.* **27**, 1382–1387 (2009).
32. Britson, J.S., Barton, F., Balko, J.M. & Black, E.P. Deregulation of DUSP activity in EGFR-mutant lung cancer cell lines contributes to sustained ERK1/2 signaling. *Biochem. Biophys. Res. Commun.* **390**, 849–854 (2009).
33. Chitale, D. *et al.* An integrated genomic analysis of lung cancer reveals loss of DUSP4 in EGFR-mutant tumors. *Oncogene* **28**, 2773–2783 (2009).
34. Waha, A. *et al.* Epigenetic downregulation of mitogen-activated protein kinase phosphatase MKP-2 relieves its growth suppressive activity in glioma cells. *Cancer Res.* **70**, 1689–1699 (2010).
35. Armes, J.E. *et al.* Candidate tumor-suppressor genes on chromosome arm 8p in early-onset and high-grade breast cancers. *Oncogene* **23**, 5697–5702 (2004).
36. Cadalbert, L., Sloss, C.M., Cameron, P. & Plevin, R. Conditional expression of MAP kinase phosphatase-2 protects against genotoxic stress-induced apoptosis by binding and selective dephosphorylation of nuclear activated c-jun N-terminal kinase. *Cell. Signal.* **17**, 1254–1264 (2005).
37. Brumby, A.M. *et al.* Identification of novel Ras-cooperating oncogenes in *Drosophila melanogaster*: a RhoGEF/Rho-family/JNK pathway is a central driver of tumorigenesis. *Genetics* 105–125 (2011).
38. Kan, Z. *et al.* Diverse somatic mutation patterns and pathway alterations in human cancers. *Nature* **466**, 869–873 (2010).
39. Wang, J. *et al.* Sustained c-Jun-NH_2-kinase activity promotes epithelial-mesenchymal transition, invasion, and survival of breast cancer cells by regulating extracellular signal-regulated kinase activation. *Mol. Cancer Res.* **8**, 266–277 (2010).
40. Creighton, C.J., Chang, J.C. & Rosen, J.M. Epithelial-mesenchymal transition (EMT) in tumor-initiating cells and its clinical implications in breast cancer. *J. Mammary Gland Biol. Neoplasia* **15**, 253–260 (2010).

nature medicine

Hepatitis B virus–induced lipid alterations contribute to natural killer T cell–dependent protective immunity

Sebastian Zeissig[1,2], Kazumoto Murata[3], Lindsay Sweet[4], Jean Publicover[5], Zongyi Hu[3], Arthur Kaser[1,9], Esther Bosse[2], Jahangir Iqbal[6], M Mahmood Hussain[6,7], Katharina Balschun[8], Christoph Röcken[8], Alexander Arlt[2], Rainer Günther[2], Jochen Hampe[2], Stefan Schreiber[2], Jody L Baron[5], D Branch Moody[4], T Jake Liang[3,10] & Richard S Blumberg[1,10]

In most adult humans, hepatitis B is a self-limiting disease leading to life-long protective immunity, which is the consequence of a robust adaptive immune response occurring weeks after hepatitis B virus (HBV) infection. Notably, HBV-specific T cells can be detected shortly after infection, but the mechanisms underlying this early immune priming and its consequences for subsequent control of viral replication are poorly understood. Using primary human and mouse hepatocytes and mouse models of transgenic and adenoviral HBV expression, we show that HBV-expressing hepatocytes produce endoplasmic reticulum (ER)-associated endogenous antigenic lipids including lysophospholipids that are generated by HBV-induced secretory phospholipases and that lead to activation of natural killer T (NKT) cells. The absence of NKT cells or CD1d or a defect in ER-associated transfer of lipids onto CD1d results in diminished HBV-specific T and B cell responses and delayed viral control in mice. NKT cells may therefore contribute to control of HBV infection through sensing of HBV-induced modified self-lipids.

Conventional T and B cells have a crucial role in HBV infection[1–5]. In contrast, the contribution of cells at the interface between innate and adaptive immunity, such as NKT cells, remains controversial[6]. NKT cells respond in a T cell receptor (TCR)-restricted manner to lipid antigens presented by CD1d on professional and nonprofessional antigen-presenting cells and show pronounced cytokine secretion within hours of cognate antigen recognition, which enables broad effects on activation of other innate (NK) and adaptive (T and B) immune cells[7,8]. Given the central role of NKT cells in both direct and indirect modulation of the immune system, NKT cells have been shown to be crucial in the defense against a variety of microbial pathogens[8].

Analysis of liver gene expression in chimpanzees 2 weeks after HBV infection has shown evidence for a lack of induction of immune-related genes, suggesting that HBV acts a stealth virus that escapes innate immune responses during early infection[9]. However, studies in HBV-infected humans and chimpanzees have demonstrated the presence of HBV-specific T and B cells within weeks of infection, consistent with successful priming of an adaptive immune response[1,10,11]. These observations suggest that HBV might be susceptible to recognition by the immune system directly after infection. Accordingly, recent studies in animal models of *Hepadnaviridae* infection and in HBV-infected humans have shown activation of NKT cells at very early time points following infection[10–12]. Thus, infection of woodchucks with woodchuck hepatitis virus led to hepatic NKT cell infiltration within 48 h, which correlated with interferon-γ (IFN-γ) secretion and temporary suppression of viral replication[12]. These findings are consistent with the observation that pharmacological stimulation of invariant NKT (iNKT) cells, a subset of NKT cells defined by expression of the Vα14-Jα18 TCR in mice and Vα24-Jα18 TCR in humans, leads to rapid IFN-γ–dependent inhibition of viral replication in transgenic mice expressing replication-competent HBV genomes[13]. Similarly, a study of humans during the incubation phase of HBV infection showed increased levels of peripheral NK cells consistent with innate immune activation early after HBV infection[11]. Most notably, a recent report on two humans with HBV demonstrated very early activation of peripheral natural T cells, a population of cells that phenotypically resemble classical NKT cells. Natural T cell activation preceded activation of NK and conventional T cells and was associated with subsequent control of HBV infection[10]. These studies demonstrate a correlation between viral control and NKT cell activation. To investigate whether NKT cells are an important checkpoint that contributes to control of HBV infection, we studied various *in vitro* and *in vivo* models of HBV infection.

[1]Division of Gastroenterology, Hepatology, and Endoscopy, Brigham and Women's Hospital, Harvard Medical School, Boston, Massachusetts, USA. [2]Department of Internal Medicine I, University Medical Center Schleswig-Holstein, Christian-Albrechts-University, Kiel, Germany. [3]Liver Diseases Branch, National Institute of Diabetes and Digestive and Kidney Diseases, US National Institutes of Health, Bethesda, Maryland, USA. [4]Division of Rheumatology, Immunology and Allergy, Brigham and Women's Hospital and Harvard Medical School, Boston, Massachusetts USA. [5]Department of Medicine, Liver Center, University of California–San Francisco, San Francisco, California, USA. [6]Department of Cell Biology, State University of New York Downstate Medical Center, Brooklyn, New York, USA. [7]Department of Pediatrics, State University of New York Downstate Medical Center, Brooklyn, New York, USA. [8]Department of Pathology, University Medical Center Schleswig-Holstein, Campus Kiel, Christian-Albrechts-University, Kiel, Germany. [9]Present address: Division of Gastroenterology and Hepatology, Addenbrooke's Hospital, School of Clinical Medicine, University of Cambridge, Cambridge, UK. [10]These authors contributed equally to this work. Correspondence should be addressed to R.S.B. (rblumberg@partners.org) or T.J.L. (jliang@nih.gov).

Received 15 February; accepted 24 April; published online 17 June 2012; doi:10.1038/nm.2811

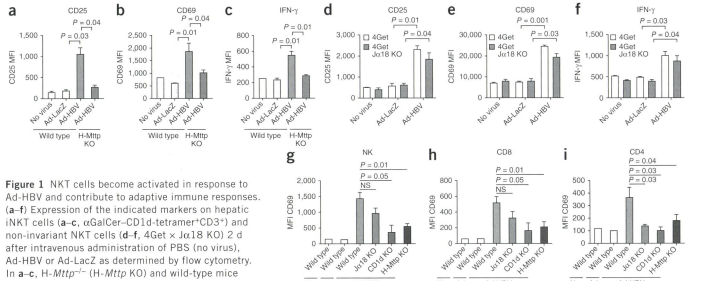

Figure 1 NKT cells become activated in response to Ad-HBV and contribute to adaptive immune responses. (**a**–**f**) Expression of the indicated markers on hepatic iNKT cells (**a**–**c**, αGalCer–CD1d-tetramer$^+$CD3$^+$) and non-invariant NKT cells (**d**–**f**, 4Get × Jα18 KO) 2 d after intravenous administration of PBS (no virus), Ad-HBV or Ad-LacZ as determined by flow cytometry. In **a**–**c**, H-*Mttp*$^{-/-}$ (H-*Mttp* KO) and wild-type mice are shown. (**g**–**i**) NK (CD3$^-$NK1.1$^+$) and conventional (αGalCer–CD1d-tetramer$^-$) CD8$^+$ and CD4$^+$ T cell activation 5 d after virus injection as described above. Shown is the mean fluorescence intensity (MFI). For all panels, data are means ± s.e.m. of 4–6 mice per group. Results are representative of three independent experiments.

RESULTS

Early activation of NKT cells in response to Ad-HBV

To study NKT cell responses, we investigated a mouse model that overcomes the nonpermissiveness of mouse hepatocytes to HBV through adenoviral delivery of a replication-competent HBV genome under the control of its endogenous promoters[14–16]. Injection of 1×10^9 HBV-expressing adenoviral particles (Ad-HBV), a dose shown by us (**Supplementary Fig. 1a**) and others[16] to induce an immune response against HBV but not the adenoviral carrier, led to HBV replication (**Supplementary Fig. 1b**) followed by a rapid drop in hepatic HBV DNA and serum HBV surface antigen (HBsAg) that preceded hepatitis (**Supplementary Fig. 1b,c**). A control adenovirus expressing β-galactosidase (Ad-LacZ) did not lead to hepatitis, confirming HBV-dependent inflammation (**Supplementary Fig. 1a**)[14–16]. As Ad-HBV infection in mice resembles the course of natural HBV infection in humans[17], we further studied NKT cell responses in this model.

Notably, the entire population of liver but not splenic iNKT cells showed activation and IFN-γ secretion as early as 1 d after Ad-HBV but not Ad-LacZ administration and thus before histological inflammation and the rise in serum alanine aminotransferase (ALT) levels (**Fig. 1a**–**c** and **Supplementary Fig. 2**). Similar to iNKT cells, hepatic but not splenic noninvariant NKT cells, an NKT cell population expressing a rather diverse set of TCRs that were detected by a reporter model developed for these studies (see **Supplementary Data** and **Supplementary Fig. 3**), showed pronounced activation and IFN-γ secretion in response to Ad-HBV (**Fig. 1d**–**f** and **Supplementary Fig. 4**). In contrast, activation of NK and T cells was not observed until 3 d after Ad-HBV challenge (**Fig. 1g**–**i** and data not shown) and thus followed activation of NKT cells, similar to observations in patients with HBV[10].

NKT cells contribute to the immune response against HBV

To investigate whether NKT cells contribute to innate and adaptive immune responses against HBV, we analyzed activation of liver mononuclear cells (LMNCs) in response to Ad-HBV in mice lacking invariant NKT cells (Jα18-deficient mice) or all NKT cells (CD1d-deficient mice). In wild-type mice, hepatic NK, CD4$^+$ and CD8$^+$ T cells showed strong activation and IFN-γ secretion in response to infection with Ad-HBV, but not Ad-LacZ (**Fig. 1g**–**i** and data not shown). In contrast, CD1d-deficient mice showed significantly diminished NK, CD4$^+$ and CD8$^+$ T cell activation, whereas Jα18 deficiency predominantly affected CD4$^+$ T cell activation (**Fig. 1g**–**i**). Viral transduction of hepatocytes was similar in all mouse strains (**Supplementary Fig. 5**).

NKT-dependent activation was also observed for HBV-specific CD8$^+$ T cell responses among liver mononuclear cells (LMNCs) against envelope (HBsAg, S, amino acids 190–197; VWLSVIWM) and HBV core (HBcAg, C, amino acids 93–100; MGLKFRQL) antigens analyzed *ex vivo* but not in response to phytohemagglutinin (**Fig. 2a** and **Supplementary Fig. 6a,b**). Analysis of LMNC responses to pools of peptides spanning the entire HBV envelope[18] revealed pronounced defects in the magnitude but not diversity of HBV-specific CD8$^+$ T cell responses in HBV envelope–transgenic × *Rag1*$^{-/-}$ × CD1d-deficient mice (HBVEnv *Rag1*$^{-/-}$ CD1d-deficient mice) that received, by adoptive transfer, wild-type splenocytes (**Fig. 2b** and **Supplementary Fig. 6c**). The adaptive immune defects extended to B cells, as levels of HBsAg-specific antibodies were lower in Ad-HBV–challenged CD1d-deficient and Jα18-deficient mice compared to wild-type mice(**Fig. 2c**) and in HBVEnv *Rag1*$^{-/-}$ CD1d-deficient mice compared to HBVEnv *Rag1*$^{-/-}$ mice (**Fig. 2d**), resulting in lack of sustained HBsAg clearance from serum (**Fig. 2e**). These data show that NKT cells contribute to activation of NK, T and B cells in different HBV mouse models.

In accordance with a central role of NKT cells in HBV-induced hepatitis[19,20], CD1d-deficient and Jα18-deficient mice showed reduced peak levels of serum ALT (**Fig. 2f**), liver IFN-γ (**Fig. 2g**) and hepatic immune cell infiltration (data not shown). However, CD1d-deficient and Jα18-deficient mice developed chronic low-grade inflammation that persisted at least to day 30 (**Fig. 2f**,**h**), the end of the observation period. This was associated with delayed clearance of serum HBsAg (**Fig. 2i**) and serum and liver HBV DNA

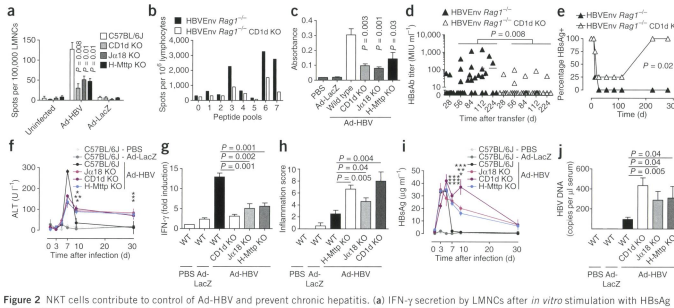

Figure 2 NKT cells contribute to control of Ad-HBV and prevent chronic hepatitis. (**a**) IFN-γ secretion by LMNCs after *in vitro* stimulation with HBsAg S190–197 peptide (VWLSVIWM) 14 d after injection of the indicated viruses. (**b**) IFN-γ–secreting cells as detected by enzyme-linked immunospot (ELISPOT) among LMNCs obtained 8 d after wild-type splenocyte transfer into HBV envelope × Rag1$^{-/-}$ (HBVEnv *Rag1*$^{-/-}$) and HBVEnv *Rag1*$^{-/-}$ CD1d-deficient mice (C57BL/6 background) and re-stimulation in the presence of the indicated HBV envelope peptide pools. (**c**) Anti-HBsAg level in wild-type mice 30 days after injection of the indicated viruses. (**d**,**e**) HBsAg-specific antibody (HBsAb) titers (**d**) and percentage of HBsAg-positive mice (**e**) at the indicated time after transfer of wild-type splenocytes into the indicated HBsAg-transgenic mouse strains. MIU, milli–international units. (**f**–**j**) Serum ALT (**f**), IFN-γ mRNA in liver tissue as determined by qPCR (**g**, day 5 after virus injection), histological grading of liver inflammation[24] (**h**, day 30 after virus injection), serum HBsAg (**i**) and serum HBV DNA (**j**, day 7 after virus injection). In **f** and **i**, significance levels as indicated by asterisks (*$P < 0.05$, **$P < 0.01$, ***$P < 0.001$) reflect from top to bottom Jα18 KO, CD1d KO, H-*Mttp* KO versus control wild-type mice at each relevant time point. Mean ± s.e.m. is shown in all panels (6–8 mice per group). Results are representative of two independent experiments.

(**Fig. 2j** and **Supplementary Fig. 7d**,**e**), consistent with defects in viral control leading to chronic inflammation. Consistent with a crucial role of CD8$^+$ T cells in the antiviral response against HBV[1], NKT cells were necessary but not sufficient for viral control, as *Tap1*$^{-/-}$ mice lacking CD8$^+$ T cells also showed severe defects in HBV clearance (**Supplementary Fig. 7**). These results show that NKT cells contribute to the initiation of antiviral immune responses against HBV and to viral control and prevention of chronic viral replication in the Ad-HBV model.

HBV-infected human and mouse hepatocytes activate NKT cells

To identify the cell type responsible for NKT cell activation upon Ad-HBV challenge, we studied activation of NKT cell hybridomas in response to T cell–depleted liver and spleen mononuclear cells and primary hepatocytes obtained from Ad-HBV–infected mice. Ad-HBV–transduced hepatocytes but not T cell–depleted mononuclear cells induced activation of NKT cells (**Fig. 3a**, **Supplementary Fig. 8a** and data not shown). We observed similar activation of NKT cells upon *in vitro* exposure of primary hepatocytes to Ad-HBV (**Supplementary Fig. 8b**; for purity and transduction of primary hepatocytes see **Supplementary Fig. 9**).

NKT activation by Ad-HBV–infected hepatocytes was CD1d restricted (**Fig. 3b**) and limited to NKT cells, as demonstrated by unaffected major histocompatibility complex (MHC) class I presentation and CD8$^+$ T cell activation (**Fig. 3c**). Activation was specific for a subset of invariant (24.7 cell line) and noninvariant (14S.6 cell line) mouse NKT cell hybridomas (**Fig. 3a**) and could also be demonstrated with human primary hepatocytes infected with Ad-HBV or a primary (nonadenoviral) HBV isolate (**Fig. 3d**,**e**). These data reveal an unanticipated role of hepatocytes in HBV-dependent NKT cell activation.

NKT cell activation is dependent on lipid transfer

Microsomal triglyceride transfer protein (MTP) is an ER-resident protein that transfers endogenous phospholipids onto CD1d and is crucial for CD1d function[21–25]. To delineate the role of hepatocyte MTP and CD1d in Ad-HBV infection, we generated mice with hepatocyte-specific deletion of *Mttp*, which codes for MTP (H-*Mttp*$^{-/-}$[26], **Supplementary Fig. 10a**). MTP deficiency led to severe defects in the presentation of endogenous and exogenous lipid antigens that were specific for hepatocytes and limited to CD1d (**Supplementary Fig. 10b**–**e**).

Consistent with a key role of MTP in HBV-induced and CD1d-restricted antigen presentation, primary hepatocytes from H-*Mttp*$^{-/-}$ mice showed impaired activation of NKT cells in response to Ad-HBV *in vitro* (**Fig. 3f**,**g** and **Supplementary Fig. 10**). We made similar observations upon chemical inhibition of MTP (**Supplementary Fig. 11**) and in human hepatocytes infected with a primary HBV isolate (**Fig. 3e**). These results were confirmed by *in vivo* experiments, in which NKT cells from Ad-HBV–challenged H-*Mttp*$^{-/-}$ mice showed reduced activation and impaired IFN-γ secretion (**Fig. 1a**–**c**). Accordingly, NKT cell–dependent activation of NK cells and HBV-specific T and B cells was impaired in H-*Mttp*$^{-/-}$ mice (**Fig. 1g**–**i**, **Fig. 2a**,**c** and **Supplementary Fig. 6a**). H-*Mttp*$^{-/-}$ mice showed diminished acute hepatitis, delayed viral control and chronic low-grade inflammation upon Ad-HBV challenge (**Fig. 2** and **Supplementary Fig. 7**). These data confirm that hepatocytes are the antigen-presenting cells responsible for NKT cell activation and show that this effect is dependent upon hepatocyte expression of MTP and CD1d.

Alterations in hepatocyte lipids upon Ad-HBV infection

Ad-HBV–induced NKT cell activation was not the consequence of altered CD1d expression or trafficking (**Supplementary Fig. 12a**,**b**).

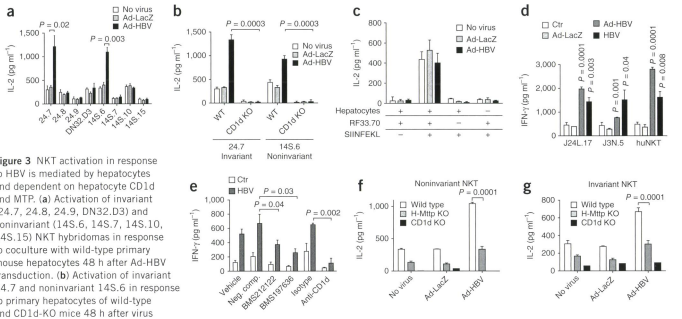

Figure 3 NKT activation in response to HBV is mediated by hepatocytes and dependent on hepatocyte CD1d and MTP. (**a**) Activation of invariant (24.7, 24.8, 24.9, DN32.D3) and noninvariant (14S.6, 14S.7, 14S.10, 14S.15) NKT hybridomas in response to coculture with wild-type primary mouse hepatocytes 48 h after Ad-HBV transduction. (**b**) Activation of invariant 24.7 and noninvariant 14S.6 in response to primary hepatocytes of wild-type and CD1d-KO mice 48 h after virus administration. Viral transduction was similar in hepatocytes from both strains (see **Supplementary Fig. 9**). (**c**) Activation of the MHC class I–restricted T cell hybridoma RF33.70 in response to SIINFEKL (1 μg ml^{-1}) presented by primary hepatocytes 48 h post infection. (**d**) Activation of human iNKT cell clones J24L.17 and J3N.5 and Jα24Vβ11-positive human iNKT cells (huNKT) expanded from peripheral blood in response to human hepatocytes infected with Ad-LacZ, Ad-HBV, or a primary HBV isolate. (**e**) IFN-γ secretion by J24L.17 NKT cells, as determined 72 h after HBV infection of primary human hepatocytes and 48 h after treatment with CD1d-blocking antibodies and MTP inhibitors (BMS212122, BMS197636) or a structurally related negative compound. (**f**,**g**) Activation of noninvariant 14S.6 (**f**) and invariant 24.7 (**g**) by primary hepatocytes from the indicated mouse strains 48 h after infection with the indicated viruses or vehicle. Cytokine secretion in **a**–**g** was determined by ELISA 24 h after coculture. Mean ± s.e.m. of triplicate cultures are shown. Results are representative of three independent experiments.

Similarly, iNKT cell activation by hepatocytes loaded with the exogenous model lipid α-galactosylceramide (αGalCer) was not affected by Ad-HBV (**Supplementary Fig. 12c**). Given that nucleocapsid-free subviral HBsAg particles, which are produced at considerably higher numbers compared to complete HBV virions[27], bud at ER and Golgi membranes[28] and selectively recruit ER lipids for their envelopes[29], we investigated whether HBV-induced NKT activation is the consequence of alterations in endogenous ER-acquired CD1d lipids. We studied activation of NKT hybridomas in response to plate-bound CD1d loaded with lipids obtained from Ad-HBV–infected primary mouse hepatocytes. We found that even uninfected primary hepatocytes contained antigenic CD1d lipids that were enriched in microsomal ER preparations (**Supplementary Fig. 13a**–**e**). However, microsomes from Ad-HBV– but not Ad-LacZ–transduced hepatocytes showed significantly increased activation of invariant and noninvariant NKT cell hybridomas (**Fig. 4a**,**b**) compared to microsomes from uninfected hepatocytes. Microsomal lipids obtained from CD1d-deficient and H-*Mttp*$^{-/-}$ hepatocytes showed similar NKT cell activation (**Supplementary Fig. 13f** and data not shown), indicating that antigenic lipids were unable to be loaded onto (H-*Mttp*$^{-/-}$) or presented by (CD1d-deficient mice) CD1d. Accordingly, purified MTP enhanced presentation of immunogenic Ad-HBV–dependent lipids (**Fig. 4c**).

Only a subset of NKT cell hybridomas recognized Ad-HBV–infected hepatocytes (**Fig. 3a**). Given that the TCRαβ repertoire of these hybridomas is unlikely to reflect that of liver NKT cells *in vivo*[30], we investigated the response of primary liver-derived NKT cells to hepatocyte microsomal lipids. A significant population of sorted noninvariant liver NKT cells recognized Ad-HBV–induced alterations in microsomal lipids, as determined by upregulation of CD69 expression (**Fig. 4d**,**e**). CD69 upregulation was less pronounced for sorted iNKT cells, suggesting that iNKT cell responses to Ad-HBV are either restricted to a subpopulation of these cells or that iNKT cells are broadly but less strongly activated by Ad-HBV (**Fig. 4d**,**e**). In conclusion, exposure to Ad-HBV is associated with increased antigenicity of ER lipids, which are recognized by NKT cells.

Ad-HBV induces antigenic lysophosphatidylethanolamine

To characterize Ad-HBV–dependent lipid alterations, we separated microsomal lipids obtained from hepatocytes according to solubility[31]. Ad-HBV–induced stimulatory fractions for noninvariant and invariant NKT cells were both recovered in phospholipid-enriched methanol eluents, but subfractionation indicated that the two NKT cell subtypes were activated by different lipids (**Fig. 4f**,**g**). To characterize the particular lipids induced by Ad-HBV and stimulatory for NKT cells, we screened methanol fractions by HPLC mass spectrometry (HPLC-MS). Previous reports demonstrated selective recruitment of ER lipids by HBV subviral particles and underrepresentation of phosphatidylethanolamine (PE) species in the HBV envelope[29]. Comparison of chromatograms corresponding to the mass and collisional spectra of diacyl PE showed strong enrichment of PE and lysophosphatidylethanolamine (lysoPE) after Ad-HBV exposure (**Supplementary Fig. 14**). Lysophospholipids have recently been shown to be antigenic endogenous CD1d ligands in human cells *in vitro*[32,33]. Therefore, we rescreened stimulatory fractions at masses corresponding to monoacyl PE species with C16, C18:2, C18:1 and C18 monacyl forms and found in all cases that these lipids were upregulated after Ad-HBV administration *in vivo* (**Fig. 5a**). Thus, there is an overlap among the types of lipids upregulated in response to Ad-HBV and lysophosopholipids that can stimulate NKT cells.

To further test initial conclusions derived from complex cellular lipid mixtures generated *in vivo*, we tested activation of mouse NKT

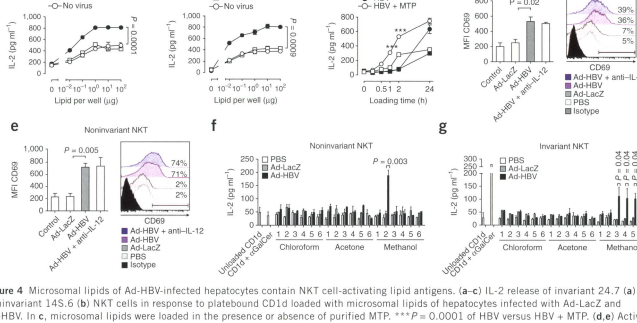

Figure 4 Microsomal lipids of Ad-HBV-infected hepatocytes contain NKT cell-activating lipid antigens. (**a**–**c**) IL-2 release of invariant 24.7 (**a**) and noninvariant 14S.6 (**b**) NKT cells in response to platebound CD1d loaded with microsomal lipids of hepatocytes infected with Ad-LacZ and Ad-HBV. In **c**, microsomal lipids were loaded in the presence or absence of purified MTP. ***$P = 0.0001$ of HBV versus HBV + MTP. (**d**,**e**) Activation of primary invariant (**d**) and noninvariant (**e**) NKT cells in response to plate-bound CD1d presenting microsomal lipids obtained from hepatocytes transduced with the indicated viruses. Invariant and noninvariant NKT cells were as sorted GFP$^+$ αGalCer–CD1d-tetramer$^+$ 4Get (**d**) and GFP$^+$ 4Get × Jα18 KO liver mononuclear cells (**e**), respectively. Flow cytometric analysis of CD69 (MFI, left; histogram, right) gated on GFP$^+$CD3$^+$ cells is shown. Numbers in histograms indicate the percentage of cells that shift in expression of CD69 compared to microsomal lipids of uninfected cells (PBS). IL-12 neutralization demonstrates absence of indirect cytokine-mediated NKT cell activation as expected in an antigen-presenting cell–free assay. (**f**,**g**) Activation of noninvariant 14S.6 (**f**) and invariant 24.7 (**g**) NKT cells in response to plate-bound CD1d presenting chloroform-, acetone- or methanol-soluble lipids obtained 2 d after infection with Ad-LacZ and Ad-HBV. IL-2 secretion was determined by ELISA. Mean ± s.e.m. of triplicate cultures is shown. Results are representative of two (**d**,**e**) or three (**a**–**c**,**f**,**g**) independent experiments.

hybridomas in response to various purified phospholipids *in vitro*. 14S.6, a noninvariant NKT cell hybridoma that responded to Ad-HBV (**Fig. 3a**), showed activation in response to lysoPE and lysophosphatidylcholine (lysoPC) species containing hydrocarbon chains with lengths of 16 and 18 carbons (**Fig. 5b**). As hepatocyte lysoPE but not lysoPC abundance was increased in response to Ad-HBV (**Supplementary Fig. 14**), only lysoPE is implicated in the response to Ad-HBV. NKT cell activation by lysoPE was, among hybridomas, specific for 14S.6 and not observed with other iNKT hybridomas (24.7, 24.8, 24.9 or DN32.D3) or noninvariant NKT hybridomas (14S.7, 14S.10 or 14S.15; **Fig. 5b** and data not shown). Lyso-PE–induced NKT activation required plate-bound CD1d (data not shown), and purified MTP facilitated lysoPE presentation (**Fig. 5c**). These results extended to primary NKT cells, as >50% of sorted noninvariant liver NKT cells obtained from IL-4–IRES-GFP–enhanced transcript (4Get) × Jα18-deficient mice liver NKT cells showed upregulation of CD69 expression in response to lysoPE but not PE (**Fig. 5d**). Noninvariant NKT cell activation was not limited to cells expressing Vβ14, the TCRβ chain shared by the noninvariant NKT hybridoma (14S.6) that recognized lysoPE (**Fig. 5d**). This suggests that lysoPE broadly activates noninvariant NKT cells in the liver and further reiterates the limited overlap between currently available NKT hybridomas and primary NKT cells *in vivo*. In contrast, iNKT cells did not show activation in response to lysoPE (**Fig. 5d**).

NKT cell activation is dependent on secretory phospholipases

Secretory phospholipase A_2 (sPLA$_2$) enzymes contribute to the generation of lysophospholipids recognized by NKT cells and are active within secretory compartments[33,34]. We therefore investigated the role of sPLA$_2$ in Ad-HBV–dependent NKT cell activation. Chemical inhibitors of sPLA$_2$ but not cytoplasmic PLA$_2$ (cPLA$_2$) prevented HBV-dependent activation of noninvariant NKT cells without affecting MHC class I presentation (**Fig. 5e** and **Supplementary Fig. 15a**–**g**). sPLA$_2$ inhibitors also did not affect iNKT cells, in accordance with the lack of lysoPE-dependent iNKT activation (**Fig. 5f**).

As Ad-HBV–transduction of hepatocytes leads to increased abundance of PE (**Supplementary Fig. 14b**), the substrate for PLA$_2$-mediated production of lysoPE, we investigated hepatocyte gene expression of sPLA$_2$ (gene names listed in **Fig. 5g**), cPLA$_2$ (*Pla2g4a*) and calcium-independent PLA$_2$ (iPLA$_2$, *Pla2g6a*) enzymes. Ad-HBV led to rapid and selective upregulation of sPLA$_2$ enzymes *Pla2g2c* and *Pla2g5* but not other sPLA$_2$, cPLA$_2$ and iPLA$_2$ enzymes *in vivo* (**Fig. 5g** and **Supplementary Fig. 16a**). These results are in accordance with increased hepatic PLA$_2$ group II and V expression in patients with viral hepatitis[35,36]. Primary mouse hepatocytes also showed Ad-HBV–induced *Pla2g2c* upregulation, confirming hepatocyte-specific effects and demonstrating that sPLA$_2$ regulation is not secondary to hepatic inflammation but a direct consequence of exposure to Ad-HBV (**Supplementary Fig. 16b**). Primary human hepatocytes exposed to Ad-HBV or a primary HBV isolate also showed upregulation of sPLA$_2$, specifically of *PLA2G2A* (**Fig. 5h**). As lysoPE activates transcription of *PLA2G2A*[37], it most likely supports its own production through a positive-feedback loop involving sPLA$_2$. Thus, HBV leads to upregulation of sPLA$_2$ group II in mouse and human hepatocytes. Specific subgroups of sPLA$_2$ differ between humans and mice

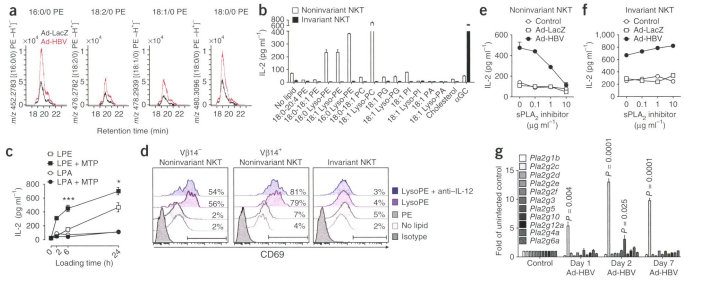

Figure 5 HBV-mediated activation of noninvariant NKT cells is dependent on lysophospholipids and sPLA$_2$. (**a**) Methanol fraction 2 of lipid extracts of microsomes obtained from Ad-HBV and Ad-LacZ-infected hepatocytes as analyzed by MS. Ion chromatograms corresponding in mass to the indicated lyso-PE species are shown. (**b**) IL-2 secretion of noninvariant 14S.6 and invariant 24.7 NKT cells in response to lipids presented by plate-bound CD1d is shown. PA, phosphatidic acid; PG, phosphatidylglycerol; PI, phosphatidylinositol. The dash separates the carbon chain length for both carbon chains in case of diacylated lipids. (**c**) IL-2 secretion by the 14S.6 noninvariant NKT cell hybridoma in response to lysophosphatidylethanolamine (LPE) and lysophosphatidic acid (LPA) presented by plate-bound CD1d and loaded in the presence or absence of purified MTP. $^{***}P = 0.005$, $^{*}P = 0.04$ of LPE versus LPE + MTP. (**d**) Activation of primary noninvariant (left, middle) and iNKT (right) cells in response to plate-bound CD1d presenting the indicated lipids. NKT cells were obtained as sorted invariant GFP$^+$ αGalCer–CD1d-tetramer$^+$ 4Get (right) and noninvariant GFP$^+$ 4Get × Jα18-KO liver NKT cells (left, middle). Flow cytometric analysis of CD69 gated on GFP$^+$ CD3$^+$ cells is shown. (**e**,**f**) Invariant 24.7 and noninvariant 14S.6 NKT cell responses to primary hepatocytes infected as indicated and treated with the sPLA$_2$ inhibitor c(2NapA)LS(2NapA)R before addition of NKT cells. (**g**) Expression of PLA$_2$ transcripts in mouse liver tissue after *in vivo* exposure to Ad-HBV. (**h**) Analysis of PLA$_2$ RNA expression in primary human hepatocytes 24 h after *in vitro* infection. Mean ± s.e.m. of triplicate cultures are shown. ND, not detectable. (**i**,**j**) IL-2 release by NKT cells in response to primary hepatocytes infected with the indicated viruses before transfection with siRNAs as indicated and coculture with NKT cells. Results are representative of two (**a**,**d**) or three (**b**,**c**,**e**–**j**) independent experiments. All data are expressed as means ± s.e.m.

in accordance with differences in the genomic organization of sPLA$_2$ loci (*PLA2G2C* is a pseudogene in humans[38]; *Pla2g2a* is inactivated by a frameshift in C57BL/6J mice).

Consistent with a crucial role for sPLA$_2$ in HBV-dependent generation of lysophospholipids as major antigens recognized by noninvariant NKT cells, siRNA directed against *Pla2g2c* and *Pla2g5* (**Supplementary Fig. 17a**) but not the genes encoding other sPLA$_2$, cPLA$_2$ and iPLA$_2$ enzymes prevented Ad-HBV–induced activation of noninvariant NKT but not invariant NKT cells or MHC class I–restricted T cells (**Fig. 5i,j** and **Supplementary Fig. 17b** and data not shown).

HBsAg contributes to NKT cell activation

To investigate the requisite HBV element for NKT cell activation, we inactivated individual HBV open reading frames and studied the effects on NKT activation. Although all viral mutants showed similar transduction rates (**Supplementary Figs. 5** and **9**), only deletion of the small HBsAg (HBsAg S$^-$), which is required for viral secretion, led to impaired activation of noninvariant NKT cells (**Fig. 6a**). We observed a similar but nonsignificant trend for iNKT cells (**Fig. 6b**). Ad-HBV S$^-$ led to impaired hepatocyte sPLA$_2$ upregulation and impaired activation of noninvariant NKT cells by microsomal hepatocyte lipids (**Fig. 6c** and **Supplementary Fig. 16c**).

To extend these findings, we examined mice transgenically expressing HBsAg[19]. HBsAg-transgenic mouse hepatocytes led to CD1d-dependent activation of noninvariant and invariant NKT cell hybridomas but not MHC class I–restricted T cell hybridomas (**Fig. 6d**–**f**). In addition, microsomal lipids of HBsAg-transgenic hepatocytes activated NKT cells (**Fig. 6g,h**). *In vivo* administration of Ad-HBV S$^-$ resulted in prolonged chronic necroinflammation and delayed viral control in association with sustained viral replication and impaired hepatic IFN-γ induction (**Supplementary Fig. 18**). These studies show that the small HBsAg contributes to Ad-HBV–mediated activation of NKT cells, which is in accordance with a temporal association between HBsAg expression and early NKT cell activation in human HBV infection[10].

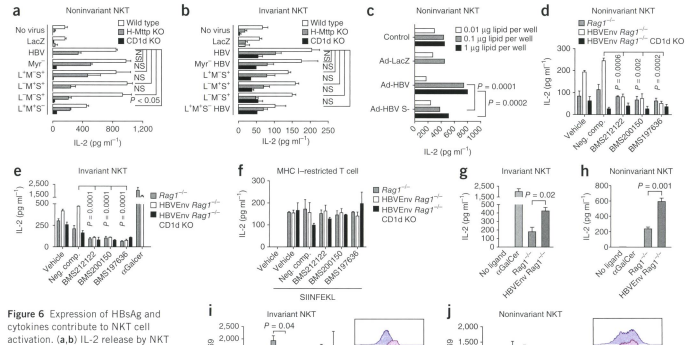

Figure 6 Expression of HBsAg and cytokines contribute to NKT cell activation. (**a**,**b**) IL-2 release by NKT cells in response to primary hepatocytes infected *in vitro* with the indicated Ad-HBV mutants deficient in the large (L^-), middle (M^-), and small (S^-) HBsAg or carrying a point mutation in the myristylation site of the large HBsAg (Myr^-), which were cocultured 24 h after infection with noninvariant (14S.6, **a**) and invariant (24.7, **b**) NKT cell hybridomas. NS, not statistically significant. (**c**) NKT cell IL-2 release in response to microsomal lipids of primary hepatocytes obtained 48 h after infection with the indicated viruses and presented by plate-bound CD1d to the noninvariant NKT cell hybridoma 14S.6. (**d**–**f**) NKT cell IL-2 release in response to primary hepatocytes of the indicated mouse strains treated with MTP inhibitors or 9-fluorenyl carboxylic acid as a negative control compound for 48 h. Hepatocytes were cocultured with noninvariant 14S.6 NKT cells (**d**), invariant 24.7 NKT cells (**e**) or MHC class I–restricted RF33.70 T cells (**f**). (**g**,**h**) NKT cell IL-2 release in response to microsomal lipids of the indicated mouse strains loaded onto plate-bound CD1d. Presentation to invariant 24.7 (**g**) and noninvariant 14S.6 (**h**) is shown. IL-2 secretion by T cell hybridomas in **a**–**h** was determined by ELISA. (**i**,**j**) Expression of CD69 as determined by flow cytometric analysis of GFP^+ αGalCer–CD1d-tetramer$^+$ CD3$^+$ invariant NKT cells (**i**) and GFP^+ αGalCer–CD1d-tetramer$^-$ CD3$^+$ noninvariant NKT cells obtained from 4Get mice injected with the indicated viruses, LPS (indirect NKT cell activation) or αGalCer (direct iNKT cell activation) in the presence or absence of antibody-mediated IL-12 neutralization. Liver mononuclear cells were obtained 6 h (αGalCer) and 24 h (viruses, LPS) after stimulation. (**j**). Representative histograms and dot plots are shown. Bar graphs show mean ± s.e.m. Results are representative of two (**d**–**j**) or three (**a**–**c**) independent experiments.

iNKT cell activation *in vivo* is cytokine dependent

Primary liver iNKT cells were not activated by lysoPE (**Fig. 5d**) and showed less robust activation in response to Ad-HBV microsomal lipids (**Fig. 4d**). We therefore investigated whether cytokine-mediated indirect activation contributes to Ad-HBV–induced iNKT cell activation *in vivo*. Indeed, neutralization of interleukin-12 (IL-12), a cytokine essential for indirect NKT cell activation[39–41], largely prevented CD69 upregulation and IFN-γ secretion by iNKT cells but had negligible effects on noninvariant NKT cells (**Fig. 6i,j** and **Supplementary Fig. 19**). These results suggest that noninvariant NKT cells are directly activated upon Ad-HBV exposure by CD1d-restricted presentation of lysoPE and other uncharacterized hepatocyte antigens. This, in turn, may lead to cytokine-dependent activation of iNKT cells, presumably through activation of liver dendritic cells and macrophages[39,40]. Notably, IL-12–mediated indirect activation of liver iNKT cells requires hepatocyte MTP (**Fig. 1a–c**), suggesting that cytokine-dependent iNKT activation is downstream of CD1d-restricted activation of noninvariant NKT cells and NKT-dependent dendritic cell maturation[42,43].

DISCUSSION

The findings presented here show that immune responses provided by NKT cells contribute not only to HBV-induced hepatitis[19] but also to viral control. Although HBV-induced NKT cell activation is associated with acute hepatitis, NKT cells contribute considerably to the emergence of antiviral B and T cell immunity. In the absence of this NKT cell response, adaptive immunity and viral control are diminished and chronic, low-grade hepatitis ensues. We show that the cell type responsible for orchestrating these HBV-induced responses is previously unappreciated and, notably, the infected hepatocyte itself and not a professional antigen-presenting cell. Within the hepatocyte, HBV induces the production of ER lipids, including lysophospholipids derived from PE through the action of HBV-induced secretory phospholipases. CD1d-restricted presentation of lysophospholipids leads to direct activation of noninvariant NKT cells and subsequent IL-12–mediated indirect iNKT cell activation, confirming that both direct and indirect mechanisms contribute to NKT cell activation *in vivo*[39,40].

The generation of antigenic lipids is partially dependent on the presence of the HBV surface antigen, the principal HBV structural

component responsible for assembling PC-rich particles in the ER, and possibly results from an imbalanced lipid milieu within the ER[29]. As such, the hepatocyte uses secretory phospholipases, MTP and CD1d to sense the presence of HBV and alert NKT cells through the display of modified self-lipids on the cell surface of the hepatocyte to trigger an adaptive immune response.

Our findings of an NKT cell response soon after HBV exposure are in accordance with other recent observations in humans and animal models of HBV[10–12] and suggest that NKT cells are part of an early, important sensing system that activates the immune response, leading to effective priming of HBV-specific adaptive immune cells that are required for viral clearance. Our data suggest that although HBV acts as a stealth virus during a prolonged phase preceding viral control[9], it is susceptible to a distinct type of immune recognition directly following infection, which is important for subsequent immune clearance. Further studies in HBV-infected humans are required to confirm a central role of NKT cells in human HBV infection.

METHODS

Methods and any associated references are available in the online version of the paper.

Note: Supplementary information is available in the online version of the paper.

ACKNOWLEDGMENTS

This work was supported by US National Institutes of Health (NIH) grants DK51362, DK44319, DK53056, DK88199, the Harvard Digestive Diseases Center DK034854 (to R.S.B.); the Deutsche Forschungsgemeinschaft (Ze 814/1-1, Ze 814/4-1), a Marie Curie International Reintegration Grant within the 7th European Community Framework Programme (256363) and the Crohn's and Colitis Foundation of America (to S.Z.); the Crohn's and Colitis Foundation of America, Austrian Science Fund, and Max Kade Foundation (to A.K.); NIH AR048632, AI049313 and the Burroughs Wellcome Fund for Translational Research (to D.B.M.); DK46900 (to M.M.H.); the NIH Intramural Research Program (K.M., Z.H. and T.J.L.); NIH grants AI068090, DK026743 and the Burroughs Wellcome Fund (to J.L.B.); and the A.P. Gianinni Foundation (to J.P.). We thank D.E. Cohen, E. Scapa and S.K. Dougan for insightful discussions.

AUTHOR CONTRIBUTIONS

S.Z. designed, performed and analyzed experiments and prepared the manuscript with R.S.B. and T.J.L.; K.M. and Z.H. generated adenoviruses and adenoviral mutants and contributed to Ad-HBV studies; L.S. and D.B.M. designed, performed and analyzed LC-MS experiments together with S.Z.; J.P. and J.L.B. designed, performed and analyzed studies with HBV-Env mice; A.K. generated $H\text{-}Mttp^{-/-}$ mice and contributed to their characterization; K.B. and C.R. performed histopathological analyses; M.M.H. and J.L. obtained purified MTP; E.B. performed PLA$_2$ inhibitor and siRNA studies; R.G. obtained primary HBV isolates; A.A. and J.H. contributed to human hepatocyte studies; S.S. contributed to supervision of the studies; T.J.L. and R.S.B. supervised the studies.

COMPETING FINANCIAL INTERESTS

The authors declare no competing financial interests.

Published online at http://www.nature.com/doifinder/10.1038/nm.2811. Reprints and permissions information is available online at http://www.nature.com/reprints/index.html.

1. Thimme, R. *et al.* CD8$^+$ T cells mediate viral clearance and disease pathogenesis during acute hepatitis B virus infection. *J. Virol.* **77**, 68–76 (2003).
2. Yeo, W. *et al.* Hepatitis B virus reactivation in lymphoma patients with prior resolved hepatitis B undergoing anticancer therapy with or without rituximab. *J. Clin. Oncol.* **27**, 605–611 (2009).
3. Esteve, M. *et al.* Chronic hepatitis B reactivation following infliximab therapy in Crohn's disease patients: need for primary prophylaxis. *Gut* **53**, 1363–1365 (2004).
4. Calabrese, L.H., Zein, N.N. & Vassilopoulos, D. Hepatitis B virus (HBV) reactivation with immunosuppressive therapy in rheumatic diseases: assessment and preventive strategies. *Ann. Rheum. Dis.* **65**, 983–989 (2006).
5. Thio, C.L. *et al.* HIV-1, hepatitis B virus, and risk of liver-related mortality in the Multicenter Cohort Study (MACS). *Lancet* **360**, 1921–1926 (2002).
6. Guidotti, L.G. & Chisari, F.V. Immunobiology and pathogenesis of viral hepatitis. *Annu. Rev. Pathol.* **1**, 23–61 (2006).
7. Bendelac, A., Savage, P.B. & Teyton, L. The biology of NKT cells. *Annu. Rev. Immunol.* **25**, 297–336 (2007).
8. Tupin, E., Kinjo, Y. & Kronenberg, M. The unique role of natural killer T cells in the response to microorganisms. *Nat. Rev. Microbiol.* **5**, 405–417 (2007).
9. Wieland, S., Thimme, R., Purcell, R.H. & Chisari, F.V. Genomic analysis of the host response to hepatitis B virus infection. *Proc. Natl. Acad. Sci. USA* **101**, 6669–6674 (2004).
10. Fisicaro, P. *et al.* Early kinetics of innate and adaptive immune responses during hepatitis B virus infection. *Gut* **58**, 974–982 (2009).
11. Webster, G.J. *et al.* Incubation phase of acute hepatitis B in man: dynamic of cellular immune mechanisms. *Hepatology* **32**, 1117–1124 (2000).
12. Guy, C.S., Mulrooney-Cousins, P.M., Churchill, N.D. & Michalak, T.I. Intrahepatic expression of genes affiliated with innate and adaptive immune responses immediately after invasion and during acute infection with woodchuck hepadnavirus. *J. Virol.* **82**, 8579–8591 (2008).
13. Kakimi, K., Guidotti, L.G., Koezuka, Y. & Chisari, F.V. Natural killer T cell activation inhibits hepatitis B virus replication in vivo. *J. Exp. Med.* **192**, 921–930 (2000).
14. Isogawa, M., Kakimi, K., Kamamoto, H., Protzer, U. & Chisari, F.V. Differential dynamics of the peripheral and intrahepatic cytotoxic T lymphocyte response to hepatitis B surface antigen. *Virology* **333**, 293–300 (2005).
15. Sprinzl, M.F., Oberwinkler, H., Schaller, H. & Protzer, U. Transfer of hepatitis B virus genome by adenovirus vectors into cultured cells and mice: crossing the species barrier. *J. Virol.* **75**, 5108–5118 (2001).
16. von Freyend, M.J. *et al.* Sequential control of hepatitis B virus in a mouse model of acute, self-resolving hepatitis B. *J. Viral Hepat.* **18**, 216–226 (2011).
17. Guidotti, L.G. *et al.* Viral clearance without destruction of infected cells during acute HBV infection. *Science* **284**, 825–829 (1999).
18. Publicover, J. *et al.* IL-21 is pivotal in determining age-dependent effectiveness of immune responses in a mouse model of human hepatitis B. *J. Clin. Invest.* **121**, 1154–1162 (2011).
19. Baron, J.L. *et al.* Activation of a nonclassical NKT cell subset in a transgenic mouse model of hepatitis B virus infection. *Immunity* **16**, 583–594 (2002).
20. Vilarinho, S., Ogasawara, K., Nishimura, S., Lanier, L.L. & Baron, J.L. Blockade of NKG2D on NKT cells prevents hepatitis and the acute immune response to hepatitis B virus. *Proc. Natl. Acad. Sci. USA* **104**, 18187–18192 (2007).
21. Brozovic, S. *et al.* CD1d function is regulated by microsomal triglyceride transfer protein. *Nat. Med.* **10**, 535–539 (2004).
22. Dougan, S.K., Rava, P., Hussain, M.M. & Blumberg, R.S. MTP regulated by an alternate promoter is essential for NKT cell development. *J. Exp. Med.* **204**, 533–545 (2007).
23. Dougan, S.K. *et al.* Microsomal triglyceride transfer protein lipidation and control of CD1d on antigen-presenting cells. *J. Exp. Med.* **202**, 529–539 (2005).
24. Kaser, A. *et al.* Microsomal triglyceride transfer protein regulates endogenous and exogenous antigen presentation by group 1 CD1 molecules. *Eur. J. Immunol.* **38**, 2351–2359 (2008).
25. Zeissig, S. *et al.* Primary deficiency of microsomal triglyceride transfer protein in human abetalipoproteinemia is associated with loss of CD1 function. *J. Clin. Invest.* **120**, 2889–2899 (2010).
26. Khatun, I. *et al.* Phospholipid transfer activity of microsomal triglyceride transfer protein produces apolipoprotein B and receptor-associated hepatosteatosis while maintaining low plasma lipids in mice. *Hepatology* **55**, 1356–1368 (2012).
27. Ganem, D. & Prince, A.M. Hepatitis B virus infection—natural history and clinical consequences. *N. Engl. J. Med.* **350**, 1118–1129 (2004).
28. Patient, R., Hourioux, C. & Roingeard, P. Morphogenesis of hepatitis B virus and its subviral envelope particles. *Cell. Microbiol.* **11**, 1561–1570 (2009).
29. Satoh, O., Umeda, M., Imai, H., Tunoo, H. & Inoue, K. Lipid composition of hepatitis B virus surface antigen particles and the particle-producing human hepatoma cell lines. *J. Lipid Res.* **31**, 1293–1300 (1990).
30. Arrenberg, P., Halder, R., Dai, Y., Maricic, I. & Kumar, V. Oligoclonality and innate-like features in the TCR repertoire of type II NKT cells reactive to a beta-linked self-glycolipid. *Proc. Natl. Acad. Sci. USA* **107**, 10984–10989 (2010).
31. Gumperz, J.E. *et al.* Murine CD1d-restricted T cell recognition of cellular lipids. *Immunity* **12**, 211–221 (2000).
32. Cox, D. *et al.* Determination of cellular lipids bound to human CD1d molecules. *PLoS ONE* **4**, e5325 (2009).
33. Fox, L.M. *et al.* Recognition of lyso-phospholipids by human natural killer T lymphocytes. *PLoS Biol.* **7**, e1000228 (2009).
34. Ni, Z., Okeley, N.M., Smart, B.P. & Gelb, M.H. Intracellular actions of group IIA secreted phospholipase A2 and group IVA cytosolic phospholipase A2 contribute to arachidonic acid release and prostaglandin production in rat gastric mucosal cells and transfected human embryonic kidney cells. *J. Biol. Chem.* **281**, 16245–16255 (2006).
35. Ito, M. *et al.* Distribution of type V secretory phospholipase A2 expression in human hepatocytes damaged by liver disease. *J. Gastroenterol. Hepatol.* **19**, 1140–1149 (2004).
36. Masuda, S., Murakami, M., Ishikawa, Y., Ishii, T. & Kudo, I. Diverse cellular localizations of secretory phospholipase A2 enzymes in several human tissues. *Biochim. Biophys. Acta* **1736**, 200–210 (2005).

37. Kuwata, H., Yamamoto, S., Takekura, A., Murakami, M. & Kudo, I. Group IIA secretory phospholipase A2 is a unique 12/15-lipoxygenase-regulated gene in cytokine-stimulated rat fibroblastic 3Y1 cells. *Biochim. Biophys. Acta* **1686**, 15–23 (2004).
38. Tischfield, J.A. *et al.* Low-molecular-weight, calcium-dependent phospholipase A2 genes are linked and map to homologous chromosome regions in mouse and human. *Genomics* **32**, 328–333 (1996).
39. Brigl, M., Bry, L., Kent, S.C., Gumperz, J.E. & Brenner, M.B. Mechanism of CD1d-restricted natural killer T cell activation during microbial infection. *Nat. Immunol.* **4**, 1230–1237 (2003).
40. Brigl, M. *et al.* Innate and cytokine-driven signals, rather than microbial antigens, dominate in natural killer T cell activation during microbial infection. *J. Exp. Med.* **208**, 1163–1177 (2011).
41. Nagarajan, N.A. & Kronenberg, M. Invariant NKT cells amplify the innate immune response to lipopolysaccharide. *J. Immunol.* **178**, 2706–2713 (2007).
42. Fujii, S., Liu, K., Smith, C., Bonito, A.J. & Steinman, R.M. The linkage of innate to adaptive immunity via maturing dendritic cells *in vivo* requires CD40 ligation in addition to antigen presentation and CD80/86 costimulation. *J. Exp. Med.* **199**, 1607–1618 (2004).
43. Fujii, S., Shimizu, K., Smith, C., Bonifaz, L. & Steinman, R.M. Activation of natural killer T cells by α-galactosylceramide rapidly induces the full maturation of dendritic cells *in vivo* and thereby acts as an adjuvant for combined CD4 and CD8 T cell immunity to a coadministered protein. *J. Exp. Med.* **198**, 267–279 (2003).
44. Ishak, K. *et al.* Histological grading and staging of chronic hepatitis. *J. Hepatol.* **22**, 696–699 (1995).

nature medicine

IL-23 induces spondyloarthropathy by acting on ROR-γt$^+$ CD3$^+$CD4$^-$CD8$^-$ entheseal resident T cells

Jonathan P Sherlock[1–3,5], Barbara Joyce-Shaikh[1,5], Scott P Turner[1], Cheng-Chi Chao[1], Manjiri Sathe[1], Jeff Grein[1], Daniel M Gorman[1], Edward P Bowman[1], Terrill K McClanahan[1], Jennifer H Yearley[1], Gérard Eberl[4], Christopher D Buckley[3], Robert A Kastelein[1], Robert H Pierce[1], Drake M LaFace[1,5] & Daniel J Cua[1,5]

The spondyloarthropathies are a group of rheumatic diseases that are associated with inflammation at anatomically distal sites, particularly the tendon-bone attachments (entheses) and the aortic root. Serum concentrations of interleukin-23 (IL-23) are elevated and polymorphisms in the IL-23 receptor are associated with ankyosing spondylitis, however, it remains unclear whether IL-23 acts locally at the enthesis or distally on circulating cell populations. We show here that IL-23 is essential in enthesitis and acts on previously unidentified IL-23 receptor (IL-23R)$^+$, RAR-related orphan receptor γt (ROR-γt)$^+$CD3$^+$CD4$^-$CD8$^-$, stem cell antigen 1 (Sca1)$^+$ entheseal resident T cells. These cells allow entheses to respond to IL-23 *in vitro*—in the absence of further cellular recruitment—and to elaborate inflammatory mediators including IL-6, IL-17, IL-22 and chemokine (C-X-C motif) ligand 1 (CXCL1). Notably, the *in vivo* expression of IL-23 is sufficient to phenocopy the human disease, with the specific and characteristic development of enthesitis and entheseal new bone formation in the initial complete absence of synovitis. As in the human condition, inflammation also develops *in vivo* at the aortic root and valve, which are structurally similar to entheses. The presence of these entheseal resident cells and their production of IL-22, which activates signal transducer and activator of transcription 3 (STAT3)-dependent osteoblast-mediated bone remodeling, explains why dysregulation of IL-23 results in inflammation at this precise anatomical site.

The spondyloarthropathies are a complex group of rheumatic diseases that are characterized by articular inflammation, erosion and new bone formation at peripheral and axial sites. Unlike rheumatoid arthritis, no therapies have been shown to be strongly disease modifying in the prototypical spondyloarthropathy, ankylosing spondylitis[1,2]. Although tumor necrosis factor (TNF) antagonism reduces the symptoms and spinal inflammation in ankylosing spondylitis[3,4], ultimately, new bone growth continues.

The primary articular site of inflammation in spondyloarthropathy has been proposed to be the enthesis[5], an anatomic region at the junction of tendon to bone, rather than the synovium. Although TNF overexpression in rodents has been used to model arthritis, these rodents develop a synovial-associated pathology with pannus formation that is more reminiscent of rheumatoid arthritis than spondyloarthropathy[6]. Despite the profound impact of TNF inhibition on the signs and symptoms of spondyloarthropathy, thus far, the evidence of its ability to affect the structural progression of the disorder is much weaker. Together, these findings suggest that pathways other than TNF are crucial in the development of the disease. It was noted recently that polymorphisms in the receptor for IL-23 are associated not only with ankylosing spondylitis but also with other associated conditions, such as psoriatic arthritis and inflammatory bowel disease[7–9]. Moreover, IL-23 is active at mucosal surfaces and is produced by the gut[10], suggesting that the intestinal mucosa could be a key site of IL-23 production in spondyloarthropathy, which is known to be associated with bowel inflammation secondary to autoimmune or infective processes. Indeed, intestinal inflammation and rheumatic pathology are closely linked[11]. Moreover human leukocyte antigen B27 (HLA-B27), which is present in up to 90% of patients with ankylosing spondylitis, has a tendency to misfold, and this misfolding results in the production of IL-23 (ref. 12). Moreover, IL-23 is also produced in response to the endoplasmic reticulum stress response that is triggered by *Chlamydia trachomatis*, a bacterium that is associated with the reactive arthritis subtype of spondyloarthropathy[13]. Taken together, these observations suggest that overproduction of, or heightened sensitivity to, IL-23 may be central to the pathogenesis of spondyloarthropathy. Indeed, serum concentrations of IL-23 are elevated in patients with ankylosing spondylitis[14–17].

It remains unclear how elevated IL-23 production is associated with inflammation specifically at the enthesis. It is now known that not only T helper type 17 (T_H17) cells but also a wide range of other immune cells can respond to IL-23 (ref. 18). Biopsies of entheseal lesions are extremely limited but show the presence of both macrophages and lymphocytes at this site[19–23]. Whether these entheseal cell populations can respond to IL-23 and, indeed, whether IL-23 acts locally at the enthesis or distally on circulating populations is unknown.

We show here that IL-23 promotes highly specific entheseal inflammation by acting on a previously unidentified population of CD3$^+$CD4$^-$CD8$^-$ entheseal resident lymphocytes and also

[1]Merck Research Laboratories, Palo Alto, California, USA. [2]University of Oxford, Trinity College, Oxford, UK. [3]University of Birmingham, Birmingham, UK. [4]Institut Pasteur, Paris, France. [5]These authors contributed equally to this work. Correspondence should be addressed to D.J.C. (daniel.cua@merck.com).

Received 14 November 2011; accepted 27 April 2012; published online 1 July 2012; doi:10.1038/nm.2817

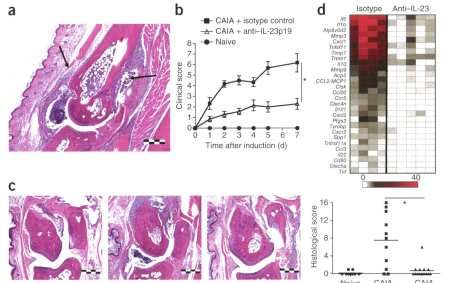

Figure 1 Entheseal inflammation in a passive transfer model of collagen-antibody–induced arthritis (CAIA) is dependent on IL-23. (**a**) Paw histology 7 d after type II–collagen–specific antibody transfer in B10.RIII male mice. Arrows indicate entheseal inflammation. Scale bar, 500 μm. The stain used was H&E. (**b**) Clinical scores of mice with CAIA in the presence of neutralizing antibody to IL-23p19 (anti–IL-23p19) and isotype control antibodies. $^*P = 0.025$ by Mann Whitney test. The graph shows the means and s.e.m., with seven mice per group. (**c**) Histology performed on the same treatment groups in **b** at day 7 after antibody transfer and histological enthesitis score. Scale bars, 500 μm. The stain used was H&E. $^*P = 0.0023$ by Mann Whitney test. (**d**) Molecular profiling by quantitative PCR on individual mice from the same treatment groups. The colored bar shows the fold upregulation of gene expression in comparison to naive mice. Data are representative of three independent experiments.

that expression of this cytokine alone, in the absence of any other inflammatory signal, is sufficient to reproduce the classical systemic features of spondyloarthropathy.

RESULTS

IL-23 drives enthesitis *in vivo*

We sought to investigate the role of IL-23 in joint inflammation. The arthritis model induced by type II–collagen–specific antibodies is characterized by broad articular inflammation and synovitis, however, we noted that on day 7 after passive immunization, B10.RIII mice also developed severe enthesitis. Indeed, this enthesitis was prominent before progression to the well-defined destructive arthritis of the articular surfaces (**Fig. 1a**).

Neutralization with an antibody to the IL-23 subunit p19 (IL-23p19) given at disease induction not only reduced clinical disease scores (**Fig. 1b**) but also reduced histological entheseal inflammation (**Fig. 1c**). This reduction was associated with the downregulation of several inflammatory mediators, such as *Il6* and *Il1b*, and genes known to be involved in erosion of bone and tissue, such as *Rankl*, *Ctsk* and matrix metalloproteinases (**Fig. 1d**). Chemokines, including those encoded by *Cxcl1* and *Cxcl2*, are likewise downregulated. The entheseal inflammation observed is consistent with the presence of type II collagen in entheseal fibrocartilage[24–32], with its specific localization in fibrocartilage but not in the tendon proper[28,32], and the ability of immunization with type II collagen to induce an ossifying enthesopathy in rats[33]. We thus sought to investigate the role of IL-23 in enthesitis.

Entheses contain an IL-23R$^+$ resident cell

Although the association between SNPs in the IL-23R and clinical spondyloarthropathy is now well established, the key site of action of

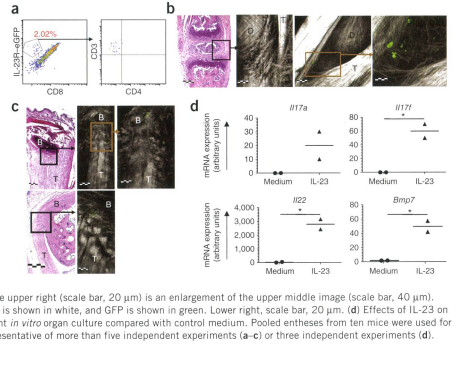

Figure 2 Entheses contain an IL-23R$^+$ resident cell population. (**a**) Flow cytometry of entheseal cell suspensions from naive IL-23R–eGFP reporter mice. The initial plot (left) was gated on CD45$^+$ entheseal cells, the second plot (right) was gated on GFP$^+$ cells. (**b**) Multiphoton microscopy of naive, intact axial tissue from IL-23R–eGFP reporter mice. A representative H&E section (left, scale bar, 200 μm) is included to show the anatomical site of the multiphoton image (center left, scale bar, 50 μm). Fine entheseal fibers are visible in relation to the longitudinal tendon (T) and intervertebral disc (D). Collagen is shown in white, and GFP is shown in green. The center right image (scale bar, 50 μm) shows another example, with an enlarged image shown on the right (scale bar, 20 μm). (**c**) Multiphoton microscopy of Achilles' tendon and entheses from an intact heal from naive IL-23R–eGFP mice. A posterior view (top) and lateral view (bottom) are shown, with representative H&E sections (upper left, scale bar, 200 μm; lower left, scale bar, 100 μm) showing the anatomical locations. The image on the upper right (scale bar, 20 μm) is an enlargement of the upper middle image (scale bar, 40 μm). T, Achilles' tendon; B, bone (calcaneum). Collagen is shown in white, and GFP is shown in green. Lower right, scale bar, 20 μm. (**d**) Effects of IL-23 on gene expression in Achilles' entheses after overnight *in vitro* organ culture compared with control medium. Pooled entheses from ten mice were used for each data point. $^*P < 0.01$ by *t* test. Data are representative of more than five independent experiments (**a**–**c**) or three independent experiments (**d**).

IL-23 in spondyloarthropathy has remained elusive. IL-23–responsive cells are located at sites such as mucosal surfaces, where they are crucial in the maintenance of tissue homeostasis and barrier function[18]. Entheses show histological features of continual tissue damage and repair[34], and we hypothesized that entheses themselves contain IL-23R$^+$ cells that are capable of responding locally to IL-23 and inducing inflammation and remodeling. We used IL-23R–eGFP reporter mice to investigate the presence of such cells.

An evaluation of CD45$^+$ entheseal cells from naive mice using flow cytometry revealed that the IL-23R–eGFP$^+$ fraction expresses CD3 but is double negative (DN) for CD4 and CD8 (**Fig. 2a**). To show the exact anatomical location of these cells, we performed multiphoton

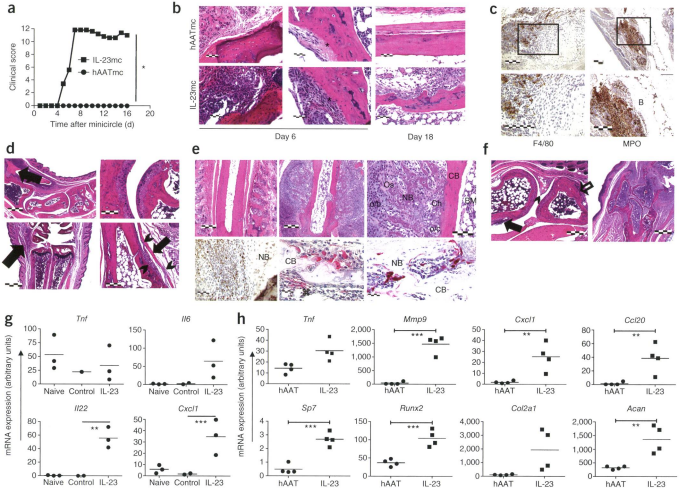

Figure 3 Systemic IL-23 expression *in vivo* induces highly specific entheseal inflammation. (**a**) Clinical paw swelling scores in B10.RIII mice treated with 3 μg IL-23mc or human α1 anti-trypsin control minicircle (hAATmc). $^*P < 0.001$ by Mann Whitney test. (**b**) Two examples of entheseal histology at day 6 after IL-23mc or control hAATmc treatment (scale bars, 40 μm) and histology of periosteal disease and osteoblast expansion at day 18 after treatment (scale bars, 50 μm) in B10.RIII mice. The asterisks indicate the entheseal tendon-bone interface. (**c**) Immunoperoxidase staining of the entheseal infiltrate for MPO and F4/80 after 18 days of *in vivo* IL-23 expression. Bone (B) is marked, and the counterstain used was hematoxylin. The bottom row of images shows magnified views of the boxed areas in the upper images. Scale bars, 200 μm. (**d**) Entheseal histology at day 35 after treatment (upper left, scale bar, 500 μm), with new entheseal bone formation indicated (arrow). To the right is a magnified view of the normal articular surface at 35 d after treatment (upper right, scale bar, 100 μm). Early enthesitis of carpal entheses (arrow) at day 8 after treatment (lower left, scale bar, 500 μm). The specificity of IL-23–induced enthesitis at day 8 after treatment is shown in relation to the tendon approaching and connecting to the bone (arrowheads) compared to the intervening tendon (arrow) (lower right, scale bar, 500 μm). (**e**) Periosteal bone formation 18 d after IL-23mc administration (upper middle, scale bar, 400 μm) compared with control hAATmc treatment (upper left, scale bar, 400 μm). The image on the upper right is a magnified view (scale bar, 50 μm) showing the relation of chondrocyte-rich cartilage (Ch), new bone (NB), osteoid (Os), osteoblasts (o/b) and osteoclasts (o/c) to cortical bone (CB) and bone marrow (BM). The image on the lower left shows a Ki-67 immunoperoxidase stain of proliferating cells with a hematoxylin counterstain (scale bar, 50 μm), the image in the lower middle shows osteoblasts stained for alkaline phosphatase, and the image on the lower right shows osteoclasts stained for tartrate-resistant alkaline phosphatase (scale bars, 20 μm). (**f**) Enthesitis (open arrow) and periostitis (filled arrow) at day 35 after treatment (left, scale bar, 500 μm) showing continuity of the enthesis and synovium (arrowhead), with erosive disease at day 67 after treatment (right, scale bar, 800 μm). Data are representative of three similar experiments (**a**–**f**). (**g**) Molecular profiling of microdissected entheses after 5 d of systemic expression of IL-23 compared to treatment with control (albumin) minicircle or to naive tissue. $^{**}P = 0.01$, $^{***}P = 0.006$ by *t* test. Each data point represents pooled Achilles' entheses from four B10.RIII mice. (**h**) Molecular profiling of microdissected Achilles' entheses after 4 weeks of IL-23 expression *in vivo* compared to hAAT control treatment. Each data point shows one of four repeats of the results from 14 Achilles' entheses from seven mice; the bar indicates the mean. $^*P < 0.05$, $^{**}P < 0.006$, $^{***}P < 0.001$ by *t* test.

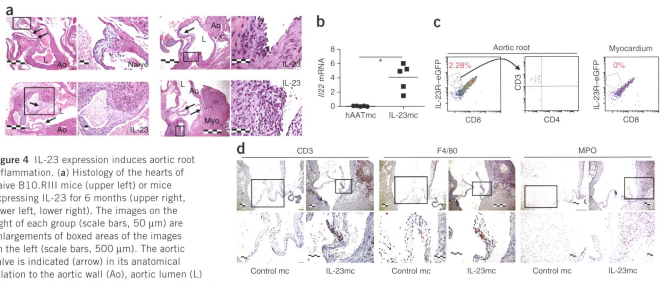

Figure 4 IL-23 expression induces aortic root inflammation. (**a**) Histology of the hearts of naive B10.RIII mice (upper left) or mice expressing IL-23 for 6 months (upper right, lower left, lower right). The images on the right of each group (scale bars, 50 μm) are enlargements of boxed areas of the images on the left (scale bars, 500 μm). The aortic valve is indicated (arrow) in its anatomical relation to the aortic wall (Ao), aortic lumen (L) and myocardium (Myo). Data are representative of three independent experiments. (**b**) Molecular profiling of the aortic root after treatment with IL-23mc or control hAATmc. Each data point represents one of five separate isolated aortic roots. $^*P = 0.0013$ by *t* test. (**c**) Flow cytometric evaluation of cell suspensions prepared from the aortic root and valve or the myocardium of naive IL-23R–eGFP reporter mice. The initial plot (left) was gated on CD45$^+$ cells. (**d**) Immunohistochemical staining of aortic roots 2 months after administration of IL-23mc or control (mutated, inactive IL-23) minicircle (control mc). Data are representative of the stained hearts of more than five mice. The images in the bottom row (scale bars, 50 μm) are magnified views of the boxed areas in the images in the top row (scale bars, 100 μm).

microscopy on intact, live, unmanipulated tissue from naive mice. We found that IL-23R–eGFP$^+$ cells are located at the entheseal interface between the tendon and bone at both axial (**Fig. 2b**) and peripheral (**Fig. 2c**) articular locations and that these cells are absent from the tendon proper.

To confirm the direct responsiveness of entheses to IL-23 in the absence of further cellular infiltration, we cultured entheseal tissue by incubation at an air-liquid interface. Entheses in culture respond to IL-23 by upregulating expression of *Il17a, Il17f, Il22* and bone morphogenic protein 7 (*Bmp7*) (**Fig. 2d**).

IL-23 alone is sufficient to drive enthesitis *in vivo*

Given the presence of IL-23R$^+$ entheseal resident cells, we next investigated the effects of the expression of IL-23 on entheses *in vivo*. Because IL-23 transgenic mice die at a young age[35], we used minicircle DNA technology[36] to express IL-23 in the hepatocytes of mice. Hydrodynamic delivery of an IL-23 minicircle (IL-23mc) into the tail veins of mice resulted in long-term expression of IL-23 and elevated serum IL-23 concentration for 100 d, with a titratable dose response (**Supplementary Fig. 1**).

After systemic expression of IL-23 resulting from the administration of IL-23mc, B10.RIII mice developed severe paw swelling (**Fig. 3a**), with the severity of the swelling correlating with the dose of IL-23mc (**Supplementary Fig. 1**). At the highest dose, mice developed clinical disease 5 d after administration, with the maximal disease score being attained by day 7–10 after administration (**Fig. 3a**). Despite this rheumatic pathology in B10.RIII mice, there was no histopathological disease in the gut, liver and kidney of the mice, even at 100 d after administration (data not shown). An examination of early disease showed that the inflammatory pathology is focused on the entheses and periosteum, with severe entheseal inflammation developing at 6 d after induction of IL-23 expression and expansion of periosteal osteoblasts developing by day 18 (**Fig. 3b**). The entheseal infiltrate is composed of F4/80$^+$ macrophages and myeloperoxidase (MPO)$^+$ neutrophils (**Fig. 3c**). A histological analysis after 35 d of IL-23 exposure revealed the highly specific presence of enthesitis in the entheses of both the front and back paws and, crucially, such enthesitis was present in the absence of synovial joint destruction at this time point (**Fig. 3d**).

An examination of the articular structures in the mice showed the presence of new entheseal bone after 18 d of elevated systemic IL-23 expression (**Fig. 3e**). We also found formation of cartilage, osteoid and new bone at the periosteum, along with osteoblasts and chondrocytes, and Ki-67 staining demonstrating active proliferation at this site. Moreover, we found multinucleate osteoclasts to be eroding the cortical bone, showing both the anabolic and catabolic bone changes that are characteristic of spondyloarthropathy (**Fig. 3e**). Although early disease is characterized by specific entheseal inflammation, at later time points, synovitis with destruction of the articular surfaces is evident in association with florid enthesitis (**Fig. 3f**). *Ex vivo* molecular profiling of microdissected entheseal tissue showed the induction of *Il6*, *Il22* and *Cxcl1* by day 5 of IL-23 expression compared to naive mice and those receiving a control minicircle (**Fig. 3g**). After 4 weeks of IL-23 expression *in vivo*, the upregulation of genes involved in the recruitment of neutrophils (*Cxcl1*) and the induction of a bone remodeling program were evident in entheses isolated *ex vivo* (**Fig. 3h**), as evidenced by upregulation of *Col2a* and *Acan* and induction of *Runx2* and *Sp7*, genes that regulate the differentiation of osteoblasts and chondrocytes. The upregulation of *Ccl20* at this time point shows the potential for the inflamed enthesis to recruit additional IL-23–responsive cells. Despite their upregulation, IL-23–driven disease is not substantially ameliorated by the neutralization of TNF, IL-6 or receptor activator of nuclear factor κB ligand (RANKL) (**Supplementary Fig. 2**).

Examination of the spines of the treated mice revealed the presence of axial enthesitis at the sites of attachment of the spinal ligaments to bone and sacroiliitis (**Supplementary Fig. 3**) after *in vivo* IL-23 exposure. Psoriasis was also present in mice expressing IL-23 (**Supplementary Fig. 3**).

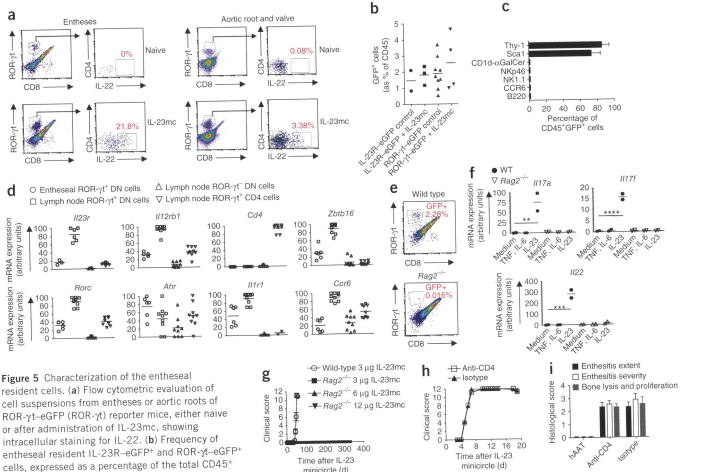

Figure 5 Characterization of the entheseal resident cells. (**a**) Flow cytometric evaluation of cell suspensions from entheses or aortic roots of ROR-γt–eGFP (ROR-γt) reporter mice, either naive or after administration of IL-23mc, showing intracellular staining for IL-22. (**b**) Frequency of entheseal resident IL-23R–eGFP$^+$ and ROR-γt–eGFP$^+$ cells, expressed as a percentage of the total CD45$^+$ cells. Each dot represents one experiment with pooled entheses from two mice. (**c**) Immunophenotype of ROR-γt–eGFP$^+$ cells from naive mice, expressed as a percentage of the total CD45$^+$GFP$^+$ entheseal cells. Data are pooled from three independent experiments. Bars show the mean and s.e.m. CD1d-αGalCer, α-galactosylceramide–loaded CD1d tetramer. (**d**) Molecular profiling of sorted naive ROR-γt$^+$ entheseal CD4$^-$CD8$^-$ (DN) T cells compared with populations of lymph node cells. Data are pooled from three independent experiments. Each data point represents a PCR analysis performed on 20–30 sorted cells, with the maximum expression normalized to 100. The bars represent the mean. (**e**) Flow cytometric analysis of dissociated entheseal cells from ROR-γt–eGFP reporter mice on a wild-type or *Rag2*$^{-/-}$ background. Each plot represents pooled samples from three mice. Data are representative of two independent experiments. (**f**) Inflammatory cytokine expression in isolated wild-type (WT) or *Rag2*$^{-/-}$ entheses cultured *in vitro* overnight with TNF and IL-6 or with IL-23. Each dot represents peripheral paw entheses pooled from ten mice. Data are representative of three independent experiments. $^{**}P < 0.05$, $^{***}P < 0.01$, $^{****}P < 0.005$ by *t* test. (**g**) Clinical paw swelling scores of wild-type or *Rag2*$^{-/-}$ C57BL/6 mice treated with IL-23mc. Wild-type mice were euthanized after maximal disease induction. (**h**) Clinical paw swelling score of B10.RIII mice treated with IL-23mc in the presence of depleting antibody to CD4 (anti-CD4) or isotype control antibody. $P = 0.90$ by Mann Whitney test for comparison of the terminal scores. (**i**) Histological enthesitis score in mice treated with control hAATmc or IL-23mc in the presence of either depleting antibody to CD4 or isotype control antibody from day –1. Data are representative of three independent experiments and are shown as mean with s.e.m. (**g**–**i**).

IL-23R$^+$CD4$^-$CD8$^-$T cells reside in the aortic root

Spondyloarthropathy in humans is associated with inflammation of the aortic root and proximal aorta, leading to aortic valve insufficiency[37]. We therefore examined the hearts of mice expressing IL-23 *in vivo*, and we found that in contrast to naive mice, mice overexpressing IL-23 developed inflammation of the attachment site of the aorta valve to the aortic wall (**Fig. 4a**). A range of lesions were present that showed early inflammation of the point of valve insertion, increased inflammation of this insertion site and extensive inflammation of the aortic root without inflammation of the myocardium. A molecular analysis showed the induction of *Il22* expression in the aortic root after IL-23 exposure *in vivo* compared to mice treated with a control minicircle (**Fig. 4b**).

The aortic valve and peripheral entheses are known to have histological similarities, including the presence of cartilage and chondrocytes where the valve joins the aorta proper and where the valve moves and flexes like an entheses. We hypothesized that the aortic valve and root might contain similar cells to peripheral entheses. Indeed, a flow cytometric analysis showed the presence of IL-23R$^+$CD4$^-$CD8$^-$ T cells in the aortic root and valve but not in the myocardium (**Fig. 4c**), which is consistent with the histological evidence of pathology at this site after IL-23mc administration. Overexpression of IL-23 resulted in a dense infiltrate of T cells, macrophages and neutrophils in the aortic root (**Fig. 4d**).

IL-23 promotes IL-17 and IL-22 expression by entheseal cells

Because ROR-γt is a key transcription factor in IL-23–responsive cells[38], we sought to determine whether our cell population of interest expresses this transcription factor. We therefore prepared cell

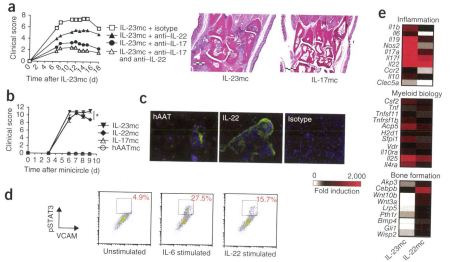

Figure 6 IL-22 induces a bone remodeling program. (**a**) Clinical paw swelling score during IL-23mc–induced disease in B10.RIII mice in the presence of a neutralizing antibody to IL-22, a neutralizing antibody to IL-17 or both antibodies (left). Data points represent the mean of six mice. Shown are the histology of the paws of the mice 18 d after administration of IL-23mc or IL-17mc (middle and right images, scale bars, 500 μm). (**b**) Clinical score after administration of minicircles encoding a range of inflammatory cytokines. *$P = 0.20$ by Mann Whitney test. Data points show the mean of five mice per group. (**c**) Immunofluorescent microscopy of phosphorylated STAT3 (pSTAT3) in paws to show the effects of prior exposure to IL-22 or control (hAAT). Isotype staining is shown, with pSTAT3 in green and DAPI in blue. (**d**) Assessment of pSTAT3 by flow cytometry of the osteoblast cell line CRL-12424 without stimulation or after stimulation with IL-6 or IL-22. (**e**) Molecular profiling of gene expression in paws 20 d after administration of IL-22mc or IL-23mc. The colored bar shows the fold upregulation in comparison to mice treated with control minicircle. Data are representative of three (**a**–**c**) or two (**d**,**e**) independent experiments.

suspensions from entheses and aortic roots of ROR-γt–eGFP reporter mice and identified the presence of ROR-γt$^+$ entheseal T cells, which are also double negative for CD4 and CD8 (**Fig. 5a**,**b**).

We next examined the effects of IL-23–mediated activation of these cells *in vivo*. We treated mice with IL-23mc, and we isolated their entheseal cells 8 d after the onset of clinical disease and examined them for cytokine expression. ROR-γt$^+$CD4$^-$CD8$^-$ entheseal T cells from mice with systemic IL-23 expression, but not those from naive mice, expressed intracellular IL-22 protein when treated *ex vivo* with phorbol myristate acetate and ionomycin (**Fig. 5a**). An examination of the resident cells of the aortic root of the IL-23mc–treated mice revealed that the ROR-γt$^+$CD4$^-$CD8$^-$ cells also produced IL-22 after exposure to IL-23 *in vivo* (**Fig. 5a**). Pooled results from multiple experiments revealed that IL-23R$^+$ and ROR-γt$^+$ entheseal resident cells were present at a frequency on the order of 2% of the entheseal CD45$^+$ hematopoietic cells (**Fig. 5b**). The IL-23R$^+$ and ROR-γt$^+$ cells express thymus cell antigen 1 (Thy-1) and Sca1 but not natural cytotoxicity triggering receptor 1 (NKp46) or killer cell lectin-like receptor subfamily B member 1C (NK1.1), and they do not bind α-galactosylceramide–loaded CD1d tetramers (**Fig. 5c**). To further characterize these cells, we performed molecular profiling of sorted entheseal resident ROR-γt–eGFP$^+$CD4$^-$CD8$^-$ T cells, and we compared these cells with ROR-γt–eGFP$^+$ and ROR-γt–eGFP$^-$CD4$^-$CD8$^-$ T cells and ROR-γt–eGFP$^+$CD4$^+$ cells from the inguinal lymph nodes (**Fig. 5d**). The expected distribution of the expression of *Il23r*, *Il12rb1* and *Rorc* in the ROR-γt$^+$ cells and of *Cd4* in the CD4$^+$ cells confirmed the purity of the cell sorting. This analysis reveals that the ROR-γt$^+$CD4$^-$CD8$^-$ T cells express *Il1r1* and *Ahr*, which is consistent with findings in other IL-23–responsive cell types. We show that these CD4$^-$CD8$^-$ T cells also express *Zbtb16*, which encodes the PLZF transcription factor that allows cells to respond immediately to cytokines. Consistent with their tissue resident status, the entheseal ROR-γt$^+$CD4$^-$CD8$^-$ T cells do not express *Ccr6*.

Enthesitis requires a *Rag*-dependent cell but not T_H17 cells

We next sought to confirm the role of the entheseal resident CD4$^-$CD8$^-$ T cell population by examination of *Rag2*$^{-/-}$ mice. Crossing ROR-γt–eGFP C57BL/6 reporter mice with *Rag2*$^{-/-}$ mice confirmed that, in contrast to the ROR-γt–eGFP$^+$ entheseal resident cells we found in wild-type mice, *Rag2*$^{-/-}$ mice do not have this cell population (**Fig. 5e**). The presence of CD4$^-$CD8$^-$ T cells is required for entheseal responsiveness to IL-23, as *Rag2*$^{-/-}$ entheses do not upregulate cytokines in response to *in vitro* stimulation with IL-23, whereas wild-type entheses upregulate *Il17a*, *Il17f* and *Il22* after this treatment (**Fig. 5f**). Development of entheseal inflammation is similarly abrogated *in vivo* in C57BL/6 *Rag2*$^{-/-}$ mice, which do not develop disease despite confirmed high expression of IL-23 serum protein for 1 year after injection of IL-23mc, whereas C57BL/6 wild-type mice develop disease by 45–50 d after exposure (**Fig. 5g**). These *Rag2*$^{-/-}$ mice expressing IL-23 have normal paw histology (data not shown).

As T_H17 cells are crucial in many IL-23–dependent inflammatory disorders, we sought to investigate the role of these cells in IL-23–driven enthesitis. We depleted T_H17 cells in wild-type B10.RIII mice with an antibody specific to CD4 and found that this did not alter the course of clinical disease after administration of IL-23mc (**Fig. 5h**). Moreover, the histological enthesitis score was not reduced by depletion of CD4$^+$ cells (**Fig. 5i**). We confirmed depletion by the antibodies to CD4 by showing an absence of CD4$^+$ cells in the lymph nodes (**Supplementary Fig. 4**). Moreover, we found that CD4$^+$ cells are not present in the enthesis during clinical disease at day 10 after IL-23mc administration (**Supplementary Fig. 4**). These findings confirm that disease is independent of T_H17 cells, which is consistent with the key role of the local resident IL-23R$^+$ entheseal cell population in mediating disease.

IL-22 promotes entheseal and periosteal bone formation

IL-23 is an immunomodulatory cytokine, the effects of which are mediated by downstream cytokines such as IL-17 and IL-22. Indeed, we found that entheseal resident cells produce IL-17 (**Supplementary Fig. 5a**) and IL-22 (**Fig. 5a**) after *in vivo* stimulation with IL-23. To assess the role of these cytokines, we administered neutralizing antibodies to IL-17, neutralizing antibodies to IL-22 or both antibodies after inducing IL-23–mediated enthesitis in B10.RIII mice by IL-23mc administration. Inhibition of IL-17 or IL-22 resulted in decreased clinical paw swelling scores, particularly when the two antibodies were administered together (**Fig. 6a**). Overexpression of IL-17 using minicircle technology, however, did not lead to clinical or histological pathology (**Fig. 6a**,**b**).

We next tested whether IL-22 could act on bone cells and mediate the osteoproliferative effects observed after expression of IL-23. To examine the effects of IL-22 on entheseal bone growth, we induced systemic expression of IL-22 in B10.RIII mice using a minicircle DNA vector specific for IL-22 and, as for IL-23, this resulted in clinically evident paw swelling (**Fig. 6b**). Immunofluorescence revealed increased phosphorylation of STAT3 that was localized to the bone (**Fig. 6c**). Osteoblasts are central to the formation of new bone, and, using the osteoblast cell line CRL-12424, we found that IL-22 can induce phosphorylation of STAT3 in these cells (**Fig. 6d**). Although *in vivo* expression of IL-23 is more effective than expression of IL-22 in upregulating inflammatory genes in the paws of mice, IL-22 more effectively induces genes that regulate bone formation, specifically those that encode Wnt family members, bone morphogenic proteins and alkaline phosphatase (**Fig. 6e**). Taken together, these results suggest that the osteoproliferative component of disease is mediated by IL-22.

DISCUSSION

Although certain diseases are associated with clear evidence of autoreactivity, other inflammatory conditions can result from mutations that cause elevated cytokine signaling[39]. Despite the strong and robust association of HLA-B27 with ankylosing spondylitis[12], no reproducible evidence for an antigen-specific response in this disease has emerged. Indeed, spondyloarthropathy in HLA-B27 transgenic rodents is not associated with the activation of CD8 T cells[40] and is independent of these lymphocytes[40,41]. The precise anatomical pattern of pathology seems inconsistent with a pattern determined only by antigen reactivity[42].

Recent findings have converged on the cytokine IL-23 as a key factor in spondyloarthropathy. HLA-B27 can misfold, triggering a cellular stress response resulting in the production of IL-23 (ref. 12), and polymorphisms in IL-23R are associated with ankylosing spondylitis and its associated conditions[8,9,43]. It remains unclear how such elevated IL-23 production can result in the distinct pattern of inflammatory involvement observed in spondyloarthropathy.

We show here that the anatomical sites that are inflamed in spondyloarthropathy are primed to rapidly react to IL-23 by the presence of a previously unidentified population of IL-23R$^+$ resident cells that express the PLZF transcription factor, which is known to confer an immediate, 'innate-like' responsiveness[44]. *In vivo* exposure to IL-23 is sufficient to induce highly specific entheseal inflammation in the absence of T_H17 cells and with rapid kinetics. The enthesis is therefore a functional IL-23–responsive anatomic site that, like the gut and lung, which contain innate IL-23–responsive cells[18], is primed to respond immediately to IL-23.

CD4$^-$CD8$^-$ T cells are also central to the lupus-like disease seen in MRL/*lpr* mice[45], and IL-23R controls the expansion and elaboration of IL-17 by CD4$^-$CD8$^-$ T cells in wild-type mice during infection[46], where at early stages they contribute more to IL-17 production than do conventional T_H17 cells[47]. CD4$^-$CD8$^-$ T cells are also found in humans with lupus[48] and have been associated with Behcet's disease[49,50] and systemic sclerosis[51]. Together with our finding of their central role in IL-23–mediated spondyloarthropathy, this shows the key role of these double-negative cells more broadly in the rheumatic inflammation of connective tissue.

Our experimental model of systemic IL-23 overexpression is relevant to the spondyloarthropathies, as these diseases are accompanied by elevated concentrations of serum IL-23 (refs. 14–17). The relationship between intestinal inflammatory disease and rheumatic symptoms[11] suggests that circulating gut-derived IL-23 may be responsible for the rheumatic inflammation. Indeed, ankylosing spondylitis is associated with elevated expression of IL-23 in the intestine[15].

We propose that the various systemic manifestations of spondyloarthropathy represent a fundamental unity: genetically, the various subtypes share common susceptibility genes, and they are intimately interrelated clinically; immunologically, they have dysregulated IL-23 biology in common. We suggest that neutralization of IL-23 pathway targets, including IL-17 and IL-22, may ameliorate disease pathology at the various anatomical sites that are inflamed in spondyloarthropathy and that these are promising targets for the treatment of ankylosing spondylitis.

METHODS

Methods and any associated references are available in the online version of the paper.

Note: Supplementary information is available in the online version of the paper.

ACKNOWLEDGMENTS

We are grateful for the assistance of S. Jungers for flow cytometric sorting. We also thank P. Bowness, H. Gaston, A. van der Merwe and A. Cooke for helpful comments on this study. This research was funded by and conducted within Merck Research Laboratories. We thank Z.-Y. Chen (Departments of Pediatrics and Genetics, Stanford University School of Medicine) for the minicircle vector plasmid.

AUTHOR CONTRIBUTIONS

J.P.S. identified the role of IL-23 in entheositis, designed and performed the experiments to investigate IL-23 induction of rheumatic lesions, developed the methodology to isolate, culture and analyze entheseal cells and prepared the manuscript. B.J.-S. identified the role of IL-22 in entheseal disease and designed and performed IL-22 signaling and antibody blocking studies, as well as studies using antibodies against collagen to induce arthritis. S.P.T. directed and performed the multiphoton microscopy and assisted with flow cytometry. C.-C.C., E.P.B. and C.D.B. provided expert advice about murine arthritis models. M.S., J.G. and T.K.M. provided the gene expression data. D.M.G. produced, validated and provided all gene expression minicircle constructs. J.H.Y. and R.H.P. directed histological studies and analyses and developed an enthesitis scoring system. G.E. provided ROR-γt–eGFP reporter mice and discussed key experimental designs. R.A.K. provided expert advice to enable the IL-23 minicircle project. D.M.L. supervised the project and performed the hydrodynamic injections. D.J.C. directed the project, oversaw the experimental design, data analysis and research direction and prepared the manuscript.

COMPETING FINANCIAL INTERESTS

The authors declare competing financial interests: details are available in the online version of the paper.

Published online at http://www.nature.com/doifinder/10.1038/nm.2817.
Reprints and permissions information is available online at http://www.nature.com/reprints/index.html.

1. Lories, R.J., de Vlam, K. & Luyten, F.P. Are current available therapies disease-modifying in spondyloarthritis? *Best Pract. Res. Clin. Rheumatol.* **24**, 625–635 (2010).
2. Maksymowych, W.P. Disease modification in ankylosing spondylitis. *Nat. Rev. Rheumatol.* **6**, 75–81 (2010).
3. Lambert, R.G. *et al.* Adalimumab significantly reduces both spinal and sacroiliac joint inflammation in patients with ankylosing spondylitis: a multicenter, randomized, double-blind, placebo-controlled study. *Arthritis Rheum.* **56**, 4005–4014 (2007).
4. van der Heijde, D. *et al.* Assessment of radiographic progression in the spines of patients with ankylosing spondylitis treated with adalimumab for up to 2 years. *Arthritis Res. Ther.* **11**, R127 (2009).
5. McGonagle, D., Gibbon, W. & Emery, P. Classification of inflammatory arthritis by enthesitis. *Lancet* **352**, 1137–1140 (1998).
6. Keffer, J. *et al.* Transgenic mice expressing human tumour necrosis factor: a predictive genetic model of arthritis. *EMBO J.* **10**, 4025–4031 (1991).
7. Rahman, P. *et al.* Association of interleukin 23 receptor variants with psoriatic arthritis. *J. Rheumatol.* **36**, 137–140 (2009).
8. Burton, P.R. *et al.* Association scan of 14,500 nonsynonymous SNPs in four diseases identifies autoimmunity variants. *Nat. Genet.* **39**, 1329–1337 (2007).
9. Duerr, R.H. *et al.* A genome-wide association study identifies *IL23R* as an inflammatory bowel disease gene. *Science* **314**, 1461–1463 (2006).

10. Becker, C. *et al.* Constitutive p40 promoter activation and IL-23 production in the terminal ileum mediated by dendritic cells. *J. Clin. Invest.* **112**, 693–706 (2003).
11. Mielants, H. *et al.* The evolution of spondyloarthropathies in relation to gut histology. III. Relation between gut and joint. *J. Rheumatol.* **22**, 2279–2284 (1995).
12. Colbert, R.A., DeLay, M.L., Klenk, E.I. & Layh-Schmitt, G. From HLA-B27 to spondyloarthritis: a journey through the ER. *Immunol. Rev.* **233**, 181–202 (2010).
13. Goodall, J.C. *et al.* Endoplasmic reticulum stress-induced transcription factor, CHOP, is crucial for dendritic cell IL-23 expression. *Proc. Natl. Acad. Sci. USA* **107**, 17698–17703 (2010).
14. Mei, Y. *et al.* Increased serum IL-17 and IL-23 in the patient with ankylosing spondylitis. *Clin. Rheumatol.* **30**, 269–273 (2011).
15. Ciccia, F. *et al.* Overexpression of interleukin-23, but not interleukin-17, as an immunologic signature of subclinical intestinal inflammation in ankylosing spondylitis. *Arthritis Rheum.* **60**, 955–965 (2009).
16. Wang, X., Lin, Z., Wei, Q., Jiang, Y. & Gu, J. Expression of IL-23 and IL-17 and effect of IL-23 on IL-17 production in ankylosing spondylitis. *Rheumatol. Int.* **29**, 1343–1347 (2009).
17. Melis, L. *et al.* Systemic levels of IL-23 are strongly associated with disease activity in rheumatoid arthritis but not spondyloarthritis. *Ann. Rheum. Dis.* **69**, 618–623 (2010).
18. Cua, D.J. & Tato, C.M. Innate IL-17–producing cells: the sentinels of the immune system. *Nat. Rev. Immunol.* **10**, 479–489 (2010).
19. Appel, H. *et al.* Immunohistologic analysis of zygapophyseal joints in patients with ankylosing spondylitis. *Arthritis Rheum.* **54**, 2845–2851 (2006).
20. Appel, H. *et al.* Correlation of histopathological findings and magnetic resonance imaging in the spine of patients with ankylosing spondylitis. *Arthritis Res. Ther.* **8**, R143 (2006).
21. Kruithof, E., *et al.* Synovial histopathology of psoriatic arthritis, both oligo- and polyarticular, resembles spondyloarthropathy more than it does rheumatoid arthritis. *Arthritis Res. Ther.* **7**, R569–R580 (2005).
22. McGonagle, D. *et al.* Histological assessment of the early enthesitis lesion in spondyloarthropathy. *Ann. Rheum. Dis.* **61**, 534–537 (2002).
23. Bollow, M. *et al.* Quantitative analyses of sacroiliac biopsies in spondyloarthropathies: T cells and macrophages predominate in early and active sacroiliitis- cellularity correlates with the degree of enhancement detected by magnetic resonance imaging. *Ann. Rheum. Dis.* **59**, 135–140 (2000).
24. Fukuta, S., Oyama, M., Kavalkovich, K., Fu, F.H. & Nyibizi, C., Identification of types II. IX and X collagens at the insertion site of the bovine achilles tendon. *Matrix Biol.* **17**, 65–73 (1998).
25. Gao, J., Messner, K., Ralphs, J.R. & Benjamin, M. An immunohistochemical study of enthesis development in the medial collateral ligament of the rat knee joint. *Anat. Embryol. (Berl.)* **194**, 399–406 (1996).
26. Niyibizi, C., Sagarrigo Visconti, C., Gibson, G. & Kavalkovich, K. Identification and immunolocalization of type X collagen at the ligament-bone interface. *Biochem. Biophys. Res. Commun.* **222**, 584–589 (1996).
27. Sagarriga Visconti, C., Kavalkovich, K., Wu, J. & Niyibizi, C. Biochemical analysis of collagens at the ligament-bone interface reveals presence of cartilage-specific collagens. *Arch. Biochem. Biophys.* **328**, 135–142 (1996).
28. Kumagai, J., Sarkar, K., Uhthoff, H.K., Okawara, Y. & Ooshima, A. Immunohistochemical distribution of type I, II and III collagens in the rabbit supraspinatus tendon insertion. *J. Anat.* **185**, 279–284 (1994).
29. Ralphs, J.R. & Benjamin, M. The joint capsule: structure, composition, ageing and disease. *J. Anat.* **184**, 503–509 (1994).
30. Rufai, A., Benjamin, M. & Ralphs, J.R. Development and ageing of phenotypically distinct fibrocartilages associated with the rat Achilles tendon. *Anat. Embryol. (Berl.)* **186**, 611–618 (1992).
31. Ralphs, J.R., Tyers, R.N. & Benjamin, M. Development of functionally distinct fibrocartilages at two sites in the quadriceps tendon of the rat: the suprapatella and the attachment to the patella. *Anat. Embryol. (Berl.)* **185**, 181–187 (1992).
32. Waggett, A.D., Ralphs, J.R., Kwan, A.P., Woodnutt, D. & Benjamin, M. Characterization of collagens and proteoglycans at the insertion of the human Achilles tendon. *Matrix Biol.* **16**, 457–470 (1998).
33. Gillet, P. *et al.* Studies on type II collagen induced arthritis in rats: an experimental model of peripheral and axial ossifying enthesopathy. *J. Rheumatol.* **16**, 721–728 (1989).
34. Benjamin, M. *et al.* Microdamage and altered vascularity at the enthesis-bone interface provides an anatomic explanation for bone involvement in the HLA-B27–associated spondylarthritides and allied disorders. *Arthritis Rheum.* **56**, 224–233 (2007).
35. Wiekowski, M.T. *et al.* Ubiquitous transgenic expression of the IL-23 subunit p19 induces multiorgan inflammation, runting, infertility, and premature death. *J. Immunol.* **166**, 7563–7570 (2001).
36. Chen, Z.Y., He, C.Y., Ehrhardt, A. & Kay, M.A. Minicircle DNA vectors devoid of bacterial DNA result in persistent and high-level transgene expression *in vivo*. *Mol. Ther.* **8**, 495–500 (2003).
37. Palazzi, C., Salvarani, C., D'Angelo, S. & Olivieri, I. Aortitis and periaortitis in ankylosing spondylitis. *Joint Bone Spine* **78**, 451–455 (2011).
38. Ivanov, I.I. *et al.* The orphan nuclear receptor RORγt directs the differentiation program of proinflammatory IL-17$^+$ T helper cells. *Cell* **126**, 1121–1133 (2006).
39. Grateau, G. & Duruoz, M.T. Autoinflammatory conditions: when to suspect? How to treat? *Best Pract. Res. Clin. Rheumatol.* **24**, 401–411 (2010).
40. May, E. *et al.* CD8 αβ T cells are not essential to the pathogenesis of arthritis or colitis in HLA-B27 transgenic rats. *J. Immunol.* **170**, 1099–1105 (2003).
41. Taurog, J.D. *et al.* Spondylarthritis in HLA-B27/human β2-microglobulin-transgenic rats is not prevented by lack of CD8. *Arthritis Rheum.* **60**, 1977–1984 (2009).
42. McGonagle, D. *et al.* Characteristic magnetic resonance imaging entheseal changes of knee synovitis in spondylarthropathy. *Arthritis Rheum.* **41**, 694–700 (1998).
43. Rahman, P. *et al.* Association of interleukin-23 receptor variants with ankylosing spondylitis. *Arthritis Rheum.* **58**, 1020–1025 (2008).
44. Alonzo, E.S. & Sant'Angelo, D.B. Development of PLZF-expressing innate T cells. *Curr. Opin. Immunol.* **23**, 220–227 (2011).
45. Wofsy, D., Hardy, R.R. & Seaman, W.E. The proliferating cells in autoimmune MRL/lpr mice lack L3T4, an antigen on "helper" T cells that is involved in the response to class II major histocompatibility antigens. *J. Immunol.* **132**, 2686–2689 (1984).
46. Riol-Blanco, L. *et al.* IL-23 receptor regulates unconventional IL-17-producing T cells that control bacterial infections. *J. Immunol.* **184**, 1710–1720 (2010).
47. Cowley, S.C., Meierovics, A.I., Frelinger, J.A., Iwakura, Y. & Elkins, K.L. Lung CD4$^-$CD8$^-$ double-negative T cells are prominent producers of IL-17A and IFN-γ during primary respiratory murine infection with *Francisella tularensis* live vaccine strain. *J. Immunol.* **184**, 5791–5801 (2010).
48. Crispín, J.C. *et al.* Expanded double negative T cells in patients with systemic lupus erythematosus produce IL-17 and infiltrate the kidneys. *J. Immunol.* **181**, 8761–8766 (2008).
49. Ling, E., Shubinsky, G. & Press, J. Increased proportion of CD3$^+$CD4$^-$CD8$^-$ double-negative T cells in peripheral blood of children with Behcet's disease. *Autoimmun. Rev.* **6**, 237–240 (2007).
50. Venzor, J., Hua, Q., Bressler, R.B., Miranda, C.H. & Huston, D.P. Behcet's-like syndrome associated with idiopathic CD4$^+$ T-lymphocytopenia, opportunistic infections, and a large population of TCRαβ$^+$ CD4$^-$ CD8$^-$ T cells. *Am. J. Med. Sci.* **313**, 236–238 (1997).
51. Sakamoto, A. *et al.* T cell receptor Vβ repertoire of double-negative αVβ T cells in patients with systemic sclerosis. *Arthritis Rheum.* **35**, 944–948 (1992).

nature medicine

The microRNA miR-23b suppresses IL-17-associated autoimmune inflammation by targeting TAB2, TAB3 and IKK-α

Shu Zhu[1,8], Wen Pan[1,8], Xinyang Song[1], Yan Liu[1], Xinrui Shao[1], Yuanjia Tang[2], Dong Liang[3], Dongyi He[4], Honglin Wang[5], Wenjun Liu[6], Yufang Shi[1], John B Harley[3,7], Nan Shen[1–3] & Youcun Qian[1]

Inflammatory cytokines such as interleukin-17 (IL-17) promote inflammatory autoimmune diseases. Although several microRNAs (miRNAs) have been shown to regulate autoimmune pathogenesis by affecting lymphocyte development and function, the role of miRNAs in resident cells present in inflammatory lesions remains unclear. Here we show that miR-23b is downregulated in inflammatory lesions of humans with lupus or rheumatoid arthritis, as well as in the mouse models of lupus, rheumatoid arthritis or multiple sclerosis. IL-17 downregulates miR-23b expression in human fibroblast-like synoviocytes, mouse primary kidney cells and astrocytes and is essential for the downregulation of miR-23b during autoimmune pathogenesis. In turn, miR-23b suppresses IL-17–, tumor necrosis factor α (TNF-α)– or IL-1β–induced NF-κB activation and inflammatory cytokine expression by targeting TGF-β–activated kinase 1/MAP3K7 binding protein 2 (TAB2), TAB3 and inhibitor of nuclear factor κ-B kinase subunit α (IKK-α) and, consequently, represses autoimmune inflammation. Thus, IL-17 contributes to autoimmune pathogenesis by suppressing miR-23b expression in radio-resident cells and promoting proinflammatory cytokine expression.

Abnormal inflammatory responses promote tissue damage in autoimmune diseases, including rheumatoid arthritis, multiple sclerosis and systemic lupus erythematosus (SLE)[1–3]. Most of our understanding of the pathogenesis of autoimmune diseases comes from investigations of the relevant mouse models, such as collagen-induced arthritis (CIA), experimental autoimmune encephalomyelitis (EAE) and the autoimmune-prone MRL/*lpr* mouse strain[4]. Expression of proinflammatory cytokines, including TNF-α, IL-1β and IL-17, has been shown to be elevated in patients with rheumatoid arthritis, multiple sclerosis or SLE, and these cytokines contribute to the pathogenesis of autoimmune diseases[5–8]. The use of blocking antibodies that inhibit the functions of these cytokines is beneficial in several preclinical models and in patients with autoimmune diseases[9–12], suggesting shared signaling pathways and common inflammatory components in the pathogenesis of seemingly disparate autoimmune diseases.

MiRNAs have been shown to have a central role in the development and regulation of the immune system[13–24]. Several miRNAs, including miR-155, miR-146a and miR-326, affect the functions of T and B cells, thereby modulating autoimmune pathogenesis[13–16,23]. However, the function of miRNAs in local resident cells, such as fibroblast-like synoviocytes (FLSs) and kidney cells, during autoimmune pathogenesis is unclear. IL-17 can promote secretion of proinflammatory cytokines by local resident cells in autoimmune diseases, but it remains unclear whether IL-17 regulates miRNAs to contribute to disease pathogenesis. Here, using comparative miRNA profilings of local inflammatory lesions of humans or mice with autoimmune disease, we identified miR-23b as a commonly downregulated miRNA in patients with rheumatoid arthritis or SLE and in the mouse models of CIA, MRL/*lpr* and EAE. IL-17 is responsible for downregulating miR-23b. MiR-23b suppresses the pathogenesis of multiple autoimmune diseases by targeting proinflammatory cytokine-mediated signaling. Thus, miR-23b may be a new common target for inflammatory autoimmune diseases.

RESULTS

MiR-23b is downregulated in autoimmune disease

miRNA screening studies performed to date have focused on individual autoimmune diseases and mainly on peripheral blood cells[25–30]. To determine whether there are commonly regulated miRNAs in the inflammatory lesions of different autoimmune diseases, we performed comparative miRNA screenings of affected tissues of humans with rheumatoid arthritis or SLE, as well as of the relevant mouse models, including CIA for rheumatoid arthritis, MRL/*lpr* for SLE and EAE for multiple sclerosis, using human or mouse miRNA arrays (**Fig. 1a** and

[1]The Key Laboratory of Stem Cell Biology, Institute of Health Sciences, Shanghai Institutes for Biological Sciences, Chinese Academy of Sciences and Shanghai Jiao Tong University School of Medicine, Shanghai, China. [2]Shanghai Institute of Rheumatology, Shanghai Renji Hospital, Shanghai Jiaotong University School of Medicine, Shanghai, China. [3]Division of Rheumatology and the Center for Autoimmune Genomics and Etiology (CAGE), Cincinnati Children's Hospital Medical Center, Cincinnati, Ohio, USA. [4]Guanghua Rheumatology Hospital, Shanghai, China. [5]Shanghai Institute of Immunology, Institute of Medical Sciences, Shanghai Jiao Tong University School of Medicine, Shanghai, China. [6]Department of Biochemistry and Medical Genetics, University of Manitoba, Winnipeg, Manitoba, Canada. [7]US Department of Veterans Affairs Medical Center, Cincinnati, Ohio, USA. [8]These authors contributed equally to this work. Correspondence should be addressed to Y.Q. (ycqian@sibs.ac.cn) or N.S. (nanshensibs@gmail.com).

Received 15 December 2011; accepted 25 April 2012; published online 3 June 2012; doi:10.1038/nm.2815

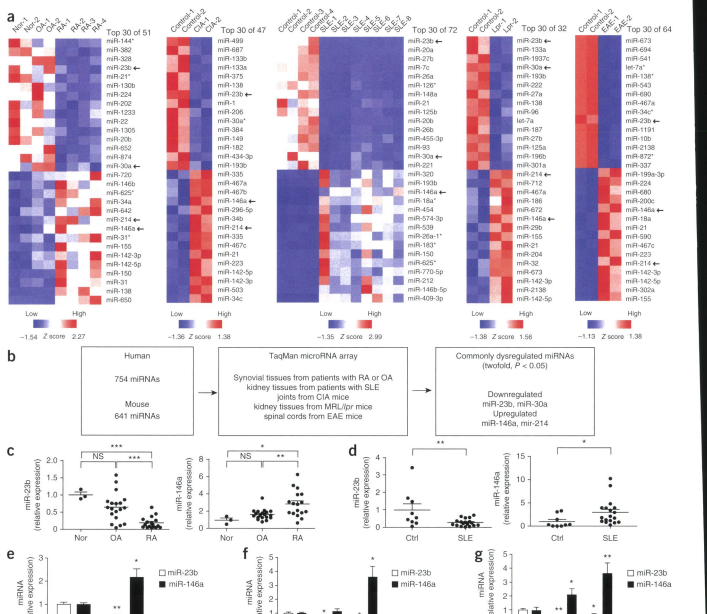

Figure 1 MiR-23b expression is downregulated in inflammatory lesions in autoimmune disease. (**a**) Screening of miRNAs differentially expressed in inflammatory tissue from human autoimmune diseases and the related mouse models. Shown are heatmaps of the 15 most upregulated and 15 most downregulated miRNAs in synovia from four individuals with rheumatoid arthritis (RA) (RA-1–RA-4) compared to two individuals with osteoarthritis (OA) (OA-1 and OA-2) and two healthy controls (Nor-1 and Nor-2); of two samples from CIA mice (CIA-1 and CIA-2) compared to two samples from naive control mice (control-1 and control-2); of renal biopsy samples from eight individuals with SLE (SLE-1–SLE-8) compared to tumor-adjacent tissues from four individuals with kidney cancer (control-1–control-4); of two samples from MRL/*lpr* mice (Lpr-1 and Lpr-2) compared to two samples from control mice (control-1 and control-2); and of two samples from EAE mice (EAE-1 and EAE-2) compared to two samples from naive control mice (control-1 and control-2). The mouse samples represent pooled tissues from 3–6 mice. All miRNAs with a reliable value (Ct < 30) and a significant difference between the tissues of autoimmune diseases and their respective controls (twofold, $P < 0.05$) are listed in **Supplementary Table 3**. (**b**) Scheme showing the screening procedure for the commonly dysregulated miRNAs that are indicated by arrows in **a** or are colored red in **Supplementary Table 3**. (**c**,**d**) qPCR validation of miR-23b expression and miR-146a as a positive control in synovia from 17 individuals with rheumatoid arthritis, 19 individuals with osteoarthritis or 3 healthy controls (nor) (**Supplementary Table 1**) (**c**) or in renal biopsy samples from 18 individuals with SLE or tumor-adjacent kidney tissues of 9 individuals with kidney cancer (ctrl) (**Supplementary Table 2**) (**d**). (**e**–**g**) qPCR validation of miR-23b expression and miR-146a as positive control in joints pooled from 12 CIA mice or 6 naive DBA/1J mice (ctrl) (**e**); in kidney tissues pooled from 6 10-week-old MRL/*lpr* (Lpr), 10 40-week-old MRL/*lpr* or 6 40-week-old MRL control mice (**f**); or in spinal cords pooled from 6 EAE mice 14 d after immunization, 6 EAE mice 28 d after immunization or 6 naive control C57BL/6 mice (**g**). The relative miRNA expressions were normalized to the expression of RNU48 (**c**,**d**) or snoRNA202 (**e**–**g**). All data are means ± s.e.m. *$P < 0.05$, **$P < 0.01$, ***$P < 0.001$ (Student's *t* test), NS, no significant difference between the indicated groups or relative to the control group (**c**–**g**) in three independent experiments (**e**–**g**).

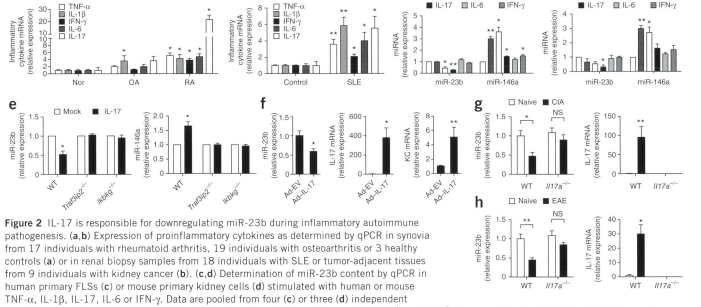

Figure 2 IL-17 is responsible for downregulating miR-23b during inflammatory autoimmune pathogenesis. (**a**,**b**) Expression of proinflammatory cytokines as determined by qPCR in synovia from 17 individuals with rheumatoid arthritis, 19 individuals with osteoarthritis or 3 healthy controls (**a**) or in renal biopsy samples from 18 individuals with SLE or tumor-adjacent tissues from 9 individuals with kidney cancer (**b**). (**c**,**d**) Determination of miR-23b content by qPCR in human primary FLSs (**c**) or mouse primary kidney cells (**d**) stimulated with human or mouse TNF-α, IL-1β, IL-17, IL-6 or IFN-γ. Data are pooled from four (**c**) or three (**d**) independent experiments. (**e**) Expression of miR-23b as determined by qPCR in wild-type, *Traf3ip2*$^{-/-}$ or *Ikbkg*$^{-/-}$ mouse embryonic fibroblasts stimulated with IL-17. Data are representative of three independent experiments. (**f**) Expression of miR-23b, IL-17 or KC mRNA as determined by qPCR in joints treated with adenovirus expressing IL-17 (Ad–IL-17) or empty virus (Ad-EV). $n = 4$ mice per group in three independent experiments. (**g**,**h**) Determination of miR-23b or IL-17 mRNA expression by qPCR in joints of wild-type or *Il17a*$^{-/-}$ mice 2 months after induction of CIA (**g**) or in spinal cord tissue from EAE mice two weeks after immunization (**h**). $N = 4$–5 mice per group in two independent experiments. Cytokine and chemokine expressions were normalized to the expression of the housekeeping gene *Rpl13a* in **a**, **b** and **f**–**h**. The relative miRNA expressions were normalized to the expression of RNU48 in **c** and of snoRNA202 in **d**–**h**. All data represent means ± s.e.m. $^*P < 0.05$, $^{**}P < 0.01$ (Student's *t* test), NS, no significant difference relative to the control group.

Supplementary Tables 1 and **2**). We found that miR-23b and miR-30a were commonly downregulated and that miR-146a and miR-214 were upregulated in all the autoimmune disease samples compared to their representative controls (**Fig. 1a**,**b** and **Supplementary Table 3**). Apart from miR-146a, the other three commonly regulated miRNAs that we found have not previously been reported to participate in the pathogenesis of autoimmune inflammatory diseases. Considering that the downregulation of miR-23b was much stronger than that of miR-30a in the humans and mouse models we studied and there have been few studies on downregulated miRNAs in the pathogenesis of inflammatory autoimmune diseases, we selected miR-23b for further investigation.

We confirmed the downregulation of miR-23b and the upregulation of miR-146a by quantitative real time PCR (qPCR) in a larger number of human samples, including synovial tissues from 17 individuals with rheumatoid arthritis or 22 controls (19 individuals with osteoarthritis and 3 individuals without arthritis) (**Fig. 1c** and **Supplementary Table 1**) and kidney tissues from 18 individuals with SLE or tumor-adjacent kidney tissues of 9 individuals with kidney cancer as relative controls (**Fig. 1d** and **Supplementary Table 2**), as well as mouse samples, including joint tissues of CIA mice compared to naive mice (**Fig. 1e**), kidney tissues of MRL/*lpr* mice compared to MRL control mice (naive mice on an MRL background) (**Fig. 1f**) and spinal cords of EAE mice compared to naive mice (**Fig. 1g**).

IL-17 is responsible for the downregulation of miR-23b

Chronic inflammation and elevated production of TNF-α and IL-1β are common features of several autoimmune diseases, both of which can regulate miRNA expression in cell culture systems[31,32]. Although the expression of miR-23b was markedly lower in the affected tissues from individuals with rheumatoid arthritis or SLE (**Fig. 1c**,**d**), the concentrations of inflammatory cytokines, including TNFα, IL-1β, IL-17, IL-6 and interferon γ (IFNγ), were markedly higher in those tissues compared to the respective control individuals (**Fig. 2a**,**b**). Linear correlation analyses of transcripts of miR-23b and the cytokines showed that miR-23b expression inversely correlated with amount of IL-17 in samples from patients with rheumatoid arthritis and their controls ($R^2 = 0.306$, $P < 0.001$) and in samples from patients with SLE and their controls ($R^2 = 0.211$, $P<0.05$), although the correlations were not strong (**Supplementary Fig. 1**). IL-17 downregulated the expression of miR-23b in human primary FLSs or in mouse primary kidney cells, whereas the other cytokines had a weaker effect or had no effect on miR-23b expression (**Fig. 2c**,**d**). IL-17 promotes the activation of nuclear factor of κ light polypeptide gene enhancer in B cells 1 (NF-κB) through the adaptor TRAF3-interacting protein 2 (Act1) and the IκB kinase (IKK) complex[33–35]. MiRNAs have been shown to be regulated by the cytokine-mediated NF-κB activation pathway[32,36]. We found that deficiency of Act1 (*Traf3ip2*$^{-/-}$) or IKK-γ (*Ikbkg*$^{-/-}$) blunted the IL-17–mediated regulation of miR-23b and miR-146a (**Fig. 2e**), suggesting that IL-17–mediated NF-κB activation is key for its regulation of miRNAs. Indeed, knockdown of p65 blocked the IL-17–mediated regulation of miR-23b and miR-146a (**Supplementary Fig. 2a**). We then performed chromatin immunoprecipitation (ChIP) assays and found that IL-17 stimulation led to the recruitment of NF-κB subunits, p50 and p65, to the miR-23b promoter (**Supplementary Fig. 2b**)[37]. Bioinformatic analyses revealed that there is a consensus NF-κB binding site in the miR-23b promoter (**Supplementary Fig. 2c**). In cells expressing a luciferase construct containing the wild-type miR-23b promoter, IL-17 markedly reduced luciferase activity, whereas mutation of the NF-κB binding sites in the promoter inhibited

IL-17–triggered suppression of reporter activity (**Supplementary Fig. 2d**), indicating that NF-κB binding to the promoter is crucial for the regulation of miR-23b expression by IL-17.

Although both TNF-α and IL-1β promote NF-κB activation and NF-κB is essential for miR-23b regulation, IL-17 more effectively downregulates miR-23b expression, and the degree of NF-κB activation did not correlate well with the amount of miR-23b downregulation in three different primary cell types (**Supplementary Fig. 3**), suggesting that NF-κB is not the only regulator of miR-23b and that other factors must contribute to the regulation of miR-23b. One potential factor might be IκB-ζ, which associates with and modulates NF-κB activity[38] and has been reported to be strongly induced by IL-17 (refs. 39,40). We found that upregulation of IκB-ζ was associated with miR-23b downregulation (**Supplementary Fig. 3**),

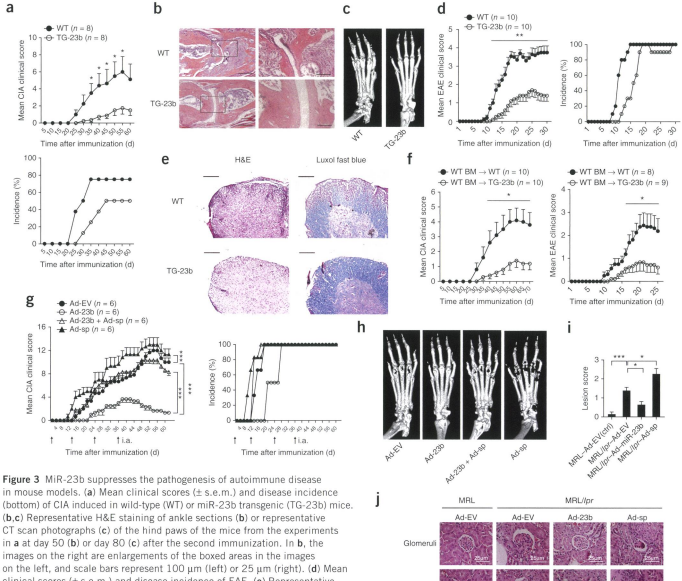

Figure 3 MiR-23b suppresses the pathogenesis of autoimmune disease in mouse models. (**a**) Mean clinical scores (± s.e.m.) and disease incidence (bottom) of CIA induced in wild-type (WT) or miR-23b transgenic (TG-23b) mice. (**b**,**c**) Representative H&E staining of ankle sections (**b**) or representative CT scan photographs (**c**) of the hind paws of the mice from the experiments in **a** at day 50 (**b**) or day 80 (**c**) after the second immunization. In **b**, the images on the right are enlargements of the boxed areas in the images on the left, and scale bars represent 100 μm (left) or 25 μm (right). (**d**) Mean clinical scores (± s.e.m.) and disease incidence of EAE. (**e**) Representative H&E staining or Luxol fast blue staining of spinal cord sections at day 16 after immunization from the mice in the experiments in **d**. Scale bars represent 100 μm. (**f**) Mean clinical scores (± s.e.m.) of CIA (left) or EAE (right) in WT or TG-23b mice reconstituted with WT bone marrow cells (WT BM). (**g**) Mean clinical scores (± s.e.m.) and disease incidence of CIA in DBA/1J mice treated with intra-articular (i.a.) injection of adenovirus control (Ad-EV), adenovirus encoding miR-23b (Ad-23b), adenovirus encoding miR-23b sponge (Ad-sp) or adenovirus encoding miR-23b and miR-23 sponge together (Ad-23b + Ad-sp) at the times indicated by the arrows. (**h**) Representative CT scan photographs of the hind paws at day 80 after the second immunization from the mice in the experiments in **g**. (**i**) The renal histological lesion scores of MRL/*lpr* mice intravenously injected with Ad-EV (MRL/*lpr*–Ad-EV), Ad-23b (MRL/*lpr*–Ad-23b) or Ad-sp (MRL/*lpr*–Ad-sp) every 3 weeks from 6–24 weeks of age. Control 24-week-old MRL mice injected with Ad-EV (MRL–Ad-EV) were used as controls. $n = 5$–6 mice per group. (**j**) Representative H&E staining of kidney sections of the treated mice in **i** at 24 weeks of age showing glomerular cell proliferation (top and middle) and perivascular mononuclear cell infiltration in the tubulointerstitium (bottom). All data represent means ± s.e.m. $^*P < 0.05$, $^{**}P < 0.01$, $^{***}P < 0.001$ (Student's *t* test in **a**,**d**,**f** and **i** or two-way analysis of variance in **g**) in two (**f**) or three (**a**,**d**,**g**,**i**) independent experiments.

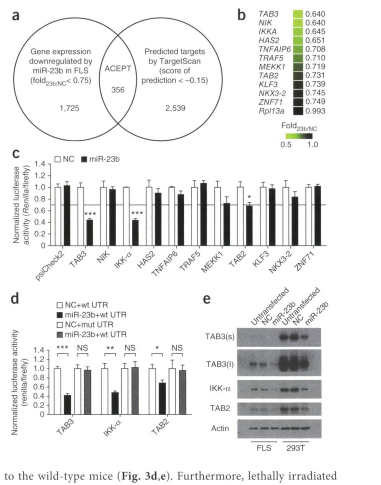

Figure 4 MiR-23b targets TAB2, TAB3 and IKK-α. (**a**) Total RNAs of FLSs transduced with the miR-23b mimic or control mimic (NC) were used for a microarray analysis (38,500 genes total). Transcripts of 1,725 genes were found to be downregulated by 25% by the miR-23b mimic. TargetScan predicted 2,539 potential targets of miR-23b. The overlapping 356 genes are defined as ACEPT genes. The ACEPT list is shown in **Supplementary Table 4**. Fold$_{23b/NC}$, Fold change of gene expression in FLSs transfected with miR-23b mimic compared to control mimic. (**b**) Eleven selected ACEPT genes that were related to the inflammatory response according to ingenuity pathway analysis (**Supplementary Fig. 5**). *Rpl13a* is shown as negative control. The gradually changing colors (green indicates downregulated, and black indicates no change) and the numbers indicate the gene expression in FLSs transduced with the miR-23b mimic compared to those transduced with the control mimic, as determined by microarray. (**c**,**d**) Luciferase activity determined in HEK293T cells that were first transfected with the indicated 3′ UTR reporter constructs (**c**) or with the indicated wild-type or point-mutated 3′ UTR reporter constructs (wt UTR or mut UTR) (**d**) and then transduced with miR-23b or control mimic. Data are representative of four independent experiments (means ± s.e.m.). $^{*}P < 0.05$, $^{**}P < 0.01$, $^{***}P < 0.001$ (Student's *t* test), NS, no significant difference relative to the control group or between the indicated groups. (**e**) Immunoblotting of endogenous TAB2, TAB3 and IKK-α expression in FLSs or HEK293T cells untransfected, transfected with the control mimic or with the miR-23b mimic. (s), short exposure; (l), long exposure. Data represent three independent experiments.

suggesting that IκB-ζ may be contributing to the regulation of miR-23b. Indeed, IL-17 stimulation led to the recruitment of IκB-ζ to the miR-23b promoter (**Supplementary Fig. 4a**), and siRNA-mediated gene knockdown of IκB-ζ blocked IL-17–mediated regulation of miR-23b (**Supplementary Fig. 4b**), confirming that IκB-ζ contributes to IL-17–mediated miR-23b regulation. Although other uncharacterized factors may also be involved in miR-23b regulation, IκB-ζ seemed to be specific for miR-23b regulation, as IκB-ζ did not affect IL-17–mediated regulation of miR-146a (**Supplementary Fig. 4b**,**c**). Consistent with the NF-κB–mediated suppression of the miR-23b promoter, IL-17 also inhibited the expression of primary miR-23b (pri-miR-23b) (**Supplementary Fig. 5**), suggesting that IL-17 mediates miR-23b regulation at the transcriptional level.

To determine the *in vivo* effect of IL-17 on miR-23b regulation, we injected adenovirus encoding mouse IL-17 into mouse joints. Consistent with the results in the primary cells, IL-17 repressed miR-23b expression in the mouse joints *in vivo* (**Fig. 2f**). Although miR-23b was repressed after the induction of CIA and EAE in wild-type mice that express IL-17, downregulation of miR-23b was considerably blocked in *Il17*-deficient mice (**Fig. 2g**,**h**), suggesting that IL-17 was responsible for miR-23b regulation during autoimmune pathogenesis.

MiR-23b suppresses autoimmune pathogenesis

To investigate its potential function during autoimmune pathogenesis, we generated miR-23b transgenic (TG-23b) mice (**Supplementary Fig. 6**). The transgenic mice were born normally with the expected Mendelian frequency and did not show any abnormality in body size and weight and in lymphocyte populations in age-matched mice (data not shown). Notably, the onset of CIA was delayed and the clinical score and incidence of CIA were lower in the transgenic mice compared to wild-type mice (**Fig. 3a**). H&E staining and micro computed tomography (micro-CT) confirmed reduced inflammatory infiltration and bone erosion in the transgenic mice compared to the wild-type mice (**Fig. 3b**,**c**). Similarly, the onset of EAE was delayed and the EAE clinical score and amounts of inflammatory infiltration and demyelination were substantially lower in the transgenic mice compared to the wild-type mice (**Fig. 3d**,**e**). Furthermore, lethally irradiated miR-23b transgenic mice reconstituted with wild-type bone marrow had delayed onset and much lower clinical scores of EAE and CIA as compared to irradiated wild-type recipient mice reconstituted with wild-type bone marrow (**Fig. 3f**), similar to those seen in miR-23b transgenic mice compared to WT mice (**Fig. 3a**,**d**). We also found that there was no significant difference in clinical scores of EAE or CIA between the *Rag1*-deficient mice transferred with splenocytes from miR-23b transgenic mice or wild-type control mice (data not shown). These data suggest that miR-23b expression in radio-resistant resident cells is crucial for its suppression of autoimmune pathogenesis.

Adenoviral-mediated, ectopic expression of miR-23b in mouse ankles markedly reduced CIA disease severity, incidence and bone erosion (**Fig. 3g**,**h** and **Supplementary Fig. 7**), similar to the results obtained from miR-23b transgenic mice (**Fig. 3a**). In contrast, administration of an adenovirus expressing a sponge of miR-23b that antagonizes miR-23b substantially enhanced disease severity and bone erosion during CIA (**Fig. 3g**,**h**), confirming the suppressive effect of miR-23b on CIA. In addition, in a spontaneous lupus nephritis model, adenoviral-mediated overexpression of miR-23b reduced and overexpression of the miR-23b sponge increased the severity of renal lesions, including the proliferation of glomerular cells and the infiltration of periglomerular, perivascular and interstitial mononuclear cells in MRL/*lpr* mice (**Fig. 3i**,**j**), suggesting that miR-23b also has a suppressive role in lupus nephritis.

We next sought to determine whether miR-23b inhibits inflammatory cytokine expression during autoimmune pathogenesis. The expression of several inflammatory genes was markedly suppressed in the joints or spinal cords of miR-23b transgenic mice

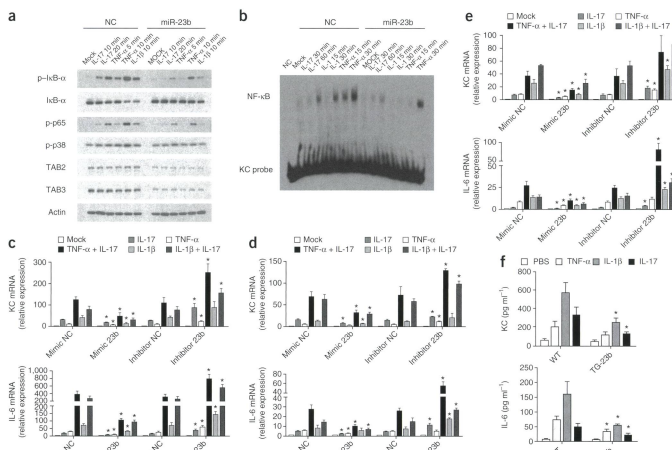

Figure 5 MiR-23b inhibits inflammatory cytokine-mediated signaling and gene expression. (**a**,**b**) Immunoblotting of whole-cell lysates (**a**) or electrophoretic mobility shift assay of nuclear extracts (**b**) from HeLa cells transfected with the miR-23b mimic or control mimic (NC) and then left untreated (Mock) or incubated with IL-17, TNF-α or IL-1β for the indicated times. The NF-κB binding site from the KC gene was used as a probe. Data represent four (**a**) or two (**b**) independent experiments. p- indicates the phosphorylated form of the protein. (**c**–**e**) The expression of KC or IL-6 mRNA determined by qPCR in primary FLSs (**c**), mouse primary kidney cells (**d**) or mouse primary astrocytes (**e**), which were transfected with the miR-23b mimic, miR-23b inhibitor or the relative controls (mimic NC and inhibitor NC) and then incubated with IL-17, TNF-α, IL-1β or a combination thereof. (**f**) The concentrations of KC or IL-6 determined by ELISA in serum from 8-week-old WT and TG-23b mice that were injected intravenously with the indicated cytokines or PBS. Data are representative of four (**c**) or three (**d**–**f**) independent experiments (means ± s.e.m.). $^{*}P < 0.05$ (Student's *t* test) relative to the control group.

compared to those of wild-type mice during CIA or EAE, respectively (**Supplementary Fig. 8a**,**b**). Similarly, adenoviral-mediated overexpression of miR-23b inhibited the expression of proinflammatory genes in MRL/*lpr* mice, whereas overexpression of the miR-23b sponge increased their expression (**Supplementary Fig. 8c**). These results suggest that miR-23b suppresses autoimmune pathogenesis, probably through the suppression of inflammatory cytokine expression.

MiR-23b targets multiple genes in proinflammatory signaling

To identify potential targets of miR-23b, we combined target prediction through TargetScan and microarray gene-expression analyses to look for gene transcripts downregulated by miR-23b overexpression. Using a combination of the two approaches, we identified 356 genes (**Fig. 4a** and **Supplementary Table 4**), which we defined as anti-correlated expressed predicted target (ACEPT) genes[41]. To assess the potential roles of the proteins encoded by these 356 genes in inflammatory signaling pathways, we predicted the biological functions and mapped biomolecular networks based on known pathways, gene ontology and interactions using ingenuity pathway analysis. Predicted genes targeted by miR-23b were associated with biological networks related to the inflammatory response and cell death or canonical pathways containing tumor necrosis factor receptor superfamily, member 1 (TNFR1) signaling and NF-κB signaling (**Supplementary Table 5**). As we found that miR-23b suppressed proinflammatory gene expression (**Supplementary Fig. 8**), we chose 11 inflammation-related genes that belong to the biological function network of inflammatory response and cell death to validate because they were ranked first and are functionally consistent with the suppressive function of miR-23b in autoimmune disease models (**Fig. 4b** and **Supplementary Fig. 9**). MiR-23b markedly repressed the reporter activity of the 3′ untranslated regions (UTRs) of three genes, encoding TAB3, IKK-α and TAB2, whereas reporter activity of constructs containing the 3′ UTRs of the other eight genes were either only slightly affected or were not affected by miR-23b (**Fig. 4c**). Mutation of the 3′ UTRs of the three repressed genes confirmed they are targets of miR-23b (**Fig. 4d** and **Supplementary Fig. 10**). Consistent with the reporter assays, the expressions of endogenous TAB3, IKK-α and

TAB2 protein were decreased in primary FLSs or HEK 293T cells by overexpression of the miR-23b mimic (**Fig. 4e**).

To avoid potentially significant genes from being excluded as a result of the 3′ UTR consideration only, we also used RNA22 to predict potential target sites of miR-23b in the 11 inflammation-related genes and found additional sites in the coding sequence (CDS) regions of mitogen-activated protein kinase kinase kinase 1 (MEKK1), mitogen-activated protein kinase kinase kinase 14 (NIK), hyaluronan synthase 2 (HAS2), Kruppel-like factor 3 (Klf3) and zinc finger protein 71 (ZNF71) (**Supplementary Fig. 11a**). However, a miR-23b mimic did not reduce the amounts of the five proteins encoded by their cloned CDS regions (**Supplementary Fig. 11b**), indicating that none of the five CDS regions was targeted by miR-23b.

MiR-23b suppresses inflammatory cytokine-mediated signaling

TAB2 and TAB3, two targets of miR-23b, are essential for signaling mediated by TNF-α or IL-1β[12]. We therefore determined whether miR-23b affects TNF-α– or IL-1β–mediated NF-κB activation.

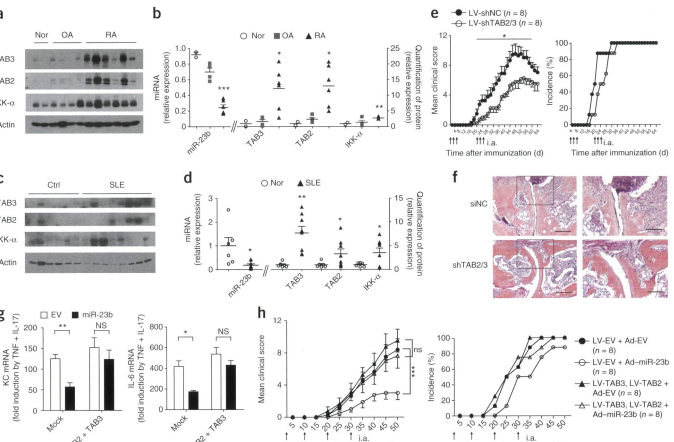

Figure 6 TAB2 and TAB3 are functional targets of miR-23b. (**a**–**d**) Immunoblotting (**a**,**c**) and quantification of the protein expression (**b**,**d**) of endogenous TAB3, TAB2 and IKK-α or expression of miR-23b in the same set of synovial samples from individuals with osteoarthritis or rheumatoid arthritis and healthy controls (**a**,**b**) or in kidney samples from individuals with SLE and controls (**c**,**d**). Protein expression was normalized to the expression of actin. (**e**) Mean clinical scores and disease incidence of CIA in DBA/1J mice injected intra-articularly with lentiviral vectors encoding shRNA directed against both TAB2 and TAB3 (LV-shTAB2/3) or nontargeting shRNA (LV-shNC) at the times indicated by the arrows. (**f**) Representative H&E staining of ankle sections at day 50 after the second immunization from the mice in the experiments in **e**. In **f**, the images on the right are enlargements of the boxed areas in the images on the left., and **s**cale bars represent 100 μm (left) or 50 μm (right). (**g**) Expression of KC or IL-6 mRNA determined by qPCR in FLSs transfected with constructs encoding TAB2 and TAB3 containing mutated miR-23b binding sites or empty construct and then infected with empty virus or adenovirus encoding miR-23b and stimulated with TNF-α plus IL-17. Data are representative of four independent experiments. (**h**) Mean clinical scores and disease incidence of CIA in DBA/1J mice after intra-articular injection of the indicated combination of adenoviruses encoding miR-23b (Ad–miR-23b) or control (Ad-EV) and lentiviruses encoding TAB2 (LV-TAB2) plus TAB3 (LV-TAB3) with mutated miR-23b binding sites or control lentivirus (LV-EV). The injection was done several times, as indicated by the arrows. Data represent three independent experiments (**a**,**c**,**e**,**h**) and are means ± s.e.m. $^*P < 0.05$, $^{**}P < 0.01$, $^{***}P < 0.001$ (Student's *t* test in **b**,**d**,**e** and **g** or two-way analysis of variance in **h**), NS, no significant difference relative to the control group or between the indicated groups (**b**,**d**,**e**,**g**,**h**). (**i**) Schematic model of the regulation and function of miR-23b in inflammatory autoimmune pathogenesis. NEMO, inhibitor of κ light polypeptide gene enhancer in B cells, kinase γ; TAB2/3, TAB2 or TAB3.

We confirmed that a synthetic miR-23b mimic or its inhibitor was active using a luciferase reporter assay, which we then used for further experiments (**Supplementary Fig. 12**). Overexpression of miR-23b suppressed both TNF-α– and IL-1β–induced NF-κB activation in HeLa cells (**Fig. 5a**,**b** and **Supplementary Fig. 13**). Because IL-17 is crucial for the pathogenesis of autoimmune diseases[43–45] and regulates miR-23b expression (**Fig. 2c**–**h**), we tested whether miR-23b affects IL-17–mediated signaling, and whether TAB2 and TAB3 are involved in IL-17–mediated signaling. MiR-23b suppressed TAB2 and TAB3 expression and IL-17–induced NF-κB activation (**Fig. 5a**,**b** and **Supplementary Fig. 13**). We then performed coimmunoprecipitation and found that TNF receptor-associated factor 6 (TRAF6) was associated with TAB2 and TAB3 in a manner that was dependent on IL-17 (**Supplementary Fig. 14a**). Given the redundant roles of TAB2 and TAB3 in TNF-α– and IL-1β–mediated signaling, we then knocked down both TAB2 and TAB3 and found that they were required for IL-17–induced NF-κB activation but not MAPK activation (**Supplementary Fig. 14b**). Knockdown of TGF-β activated kinase 1 (TAK1) also suppressed IL-17–mediated NF-κB activation but not MAPK activation (**Supplementary Fig. 14c**). Consistent with the function of the TAK1 complex (TAK1-TAB2-TAB3) in IL-17–mediated signaling, knockdown of TAB2 and TAB3 together but not individually markedly reduced IL-17–mediated induction of IL-6 and chemokine (C-X-C motif) ligand 1 (KC, also known as CXCL1), similar to the roles of TAB2 and TAB3 in TNF-α– or IL-1β–mediated gene induction (**Supplementary Fig. 14d**). In addition to TRAF6-dependent NF-κB activation, IL-17 also induces mRNA stability in inflammatory genes[46–48]. We found that miR-23b did not affect the IL-17–mediated mRNA stabilization of KC (**Supplementary Fig. 15**), suggesting that miR-23b specifically targets IL-17–induced NF-κB signaling. Our data show that NF-κB suppresses miR-23b expression and that miR-23b also inhibits NF-κB activation, suggesting there may be a feedback loop. Indeed, we found that the miR-23b mimic upregulated and the miR-23b inhibitor downregulated primary miR-23b expression both in the basal state and in an IL-17–dependent manner (**Supplementary Fig. 16**).

Next, we sought to determine whether miR-23b suppresses the induction of KC and IL-6 expression by TNF-α, IL-1β or IL-17 in physiologically relevant cell types. The miR-23b mimic inhibited and the miR-23b inhibitor enhanced the induction of KC and IL-6 in primary FLSs (**Fig. 5c**), mouse kidney cells (**Fig. 5d**) and mouse astrocytes (**Fig. 5e**). Consistent with the findings *in vitro*, TNF-α–, IL-1β– or IL-17–mediated induction of KC and IL-6 was lower *in vivo* in miR-23b transgenic mice as compared to wild-type mice (**Fig. 5f**).

TAB2 and TAB3 are functional targets of miR-23b *in vivo*

To determine whether TAB2 and TAB3 are functional targets of miR-23b *in vivo* during autoimmune pathogenesis, we investigated their expression in humans with rheumatoid arthritis or SLE. The expression of TAB2 and TAB3 were indeed markedly higher in synovial tissue from individuals with rheumatoid arthritis as compared to normal or osteoarthritis samples (**Fig. 6a**,**b**). The expression of IKK-α, another miR-23b target, was also higher in tissue from individuals with rheumatoid arthritis compared to the normal and osteoarthritis tissues (**Fig. 6a**,**b**). Expression of TAB2, TAB2 and IKK-α protein was also higher in kidney tissue from individuals with SLE compared to normal controls (**Fig. 6c**,**d**). Elevated expression of these proteins was associated with lower expression of miR-23b in both rheumatoid arthritis and SLE tissue (**Fig. 6b**,**d**). In mouse models of autoimmune disease, the amounts of TAB2, TAB3 and IKK-α were also higher in the joints of CIA mice, the kidneys of MRL/*lpr* mice and the spinal cords of EAE mice compared to the samples from the representative control mice (**Supplementary Fig. 17a**–**c**). Further, we found that adenoviral-mediated overexpression of IL-17 *in vivo* in mouse joints increased the expression of TAB2, TAB3 and IKK-α (**Supplementary Fig. 17d**). These results indicate TAB2, TAB3 and IKK-α may be targeted by miR-23b.

To investigate the potential pathological functions of TAB2 and TAB3, we used lentiviral vectors expressing shRNAs to silence the *Tab2* and *Tab3* genes. A panel of siRNAs targeting *Tab2* or *Tab3* (siTAB2 or siTAB3, respectively) was screened for effective gene silencing in mouse melanoma B16 cells (**Supplementary Fig. 18a**). We then chose sequences of siTAB2-4, siTAB2-5, siTAB3-1 and siTAB3-3 for further *in vivo* experiments. Administration of the combined lentiviruses reduced TAB2 and TAB3 protein expression in the joint tissues of mice (**Supplementary Fig. 18b**). Knockdown of TAB2 and TAB3 *in vivo* markedly reduced the severity of CIA (**Fig. 6e**), although the effect of TAB2 and TAB3 knockdown on CIA pathogenesis was weaker than that of miR-23b overexpression (**Fig. 3a**). This may be the result of residual expression of TAB2 and TAB3 or other potential targets of miR-23b. H&E staining also showed reduced lymphocyte infiltration and bone erosion (**Fig. 6f**).

To further show that TAB2 and TAB3 are functional targets of miR-23b in autoimmune pathogenesis, we transfected FLSs with constructs encoding TAB2 and TAB3 containing mutated miR-23b target sites. These vectors reversed the miR-23b–imposed inhibitory effect on IL-17– and TNF-α–mediated induction of KC and IL-6. (**Fig. 6g**). Subsequent injection of mice with lentiviruses encoding TAB2 or TAB3 containing mutated miR-23b target sites markedly reduced the miR-23b–mediated suppression of CIA (**Fig. 6h** and **Supplementary Fig. 19**), suggesting that TAB2 and TAB3 are key targets of miR-23b *in vivo* and contribute to the beneficial effects of miR-23b in mouse models of autoimmune disease.

DISCUSSION

MiRNA profilings performed to date have been on individual autoimmune diseases and focused mainly on peripheral blood cells[25–30]. Here we determined whether miRNAs are commonly regulated in local inflammatory lesions of multiple human autoimmune diseases, as well as their relevant mouse models, using miRNA microarrays. Apart from miR-146a, which was commonly elevated and has been well characterized previously[13,32,49], our study indentified three previously uncharacterized miRNAs (miR-23b, miR-30a and miR-214) that are commonly altered in the three autoimmune diseases studied. We further characterized miR-23b because it was markedly downregulated and there was a lack of information regarding downregulated miRNAs during autoimmune pathogenesis. Although both TNF-α and IL-1β were more potent than IL-17 at inducing miR-146a expression, IL-17 more potently suppressed miR-23b expression, suggesting that miRNAs are differentially regulated by different cytokines. The induction of IκB-ζ by IL-17 and its recruitment to the miR-23b promoter may account for the specific effects of IL-17 on miR-23b. Although we showed that IL-17 regulated miR-23b expression at the transcriptional level, we cannot exclude the possibility that miR-23b may also be regulated post-transcriptionally.

Although miR-23b regulates cell metabolism and cancer development[50,51], a role for miR-23b in autoimmune pathogenesis was previously unknown. Here we show that miR-23b suppresses the development and pathogenesis of multiple autoimmune diseases, consistent with its common downregulation. Although miR-23b has

been found to target glutaminase and regulate glutamine metabolism[51], we identified additional targets of miR-23b, including TAB2, TAB3 and IKK-α, that act in signaling cascades downstream of inflammatory cytokines. Whereas miR-23b overexpression downregulated these targets, TAB2, TAB3 and IKK-α were upregulated in human autoimmune diseases, as well as in the relevant mouse models, in which miR-23b was downregulated. Although TAB2 and TAB3 have been shown to be crucial for TNF-α– and IL-1β–mediated NF-κB activation, as well as MAPK activation, their involvement in IL-17–mediated signaling was previously unknown[35,42,52–56]. We found that TAB2 and TAB3 were specifically required for IL-17–mediated NF-κB activation but not MAPK activation. Our finding that miR-23b regulates inflammatory cytokine-mediated (TNF-α, IL-1β and IL-17) signaling suggests that miR-23b may have regulatory roles in other inflammatory diseases that involve these inflammatory cytokines, such as infectious diseases, septic shock and type 2 diabetes. We also found that miR-23b regulated lipopolysaccharide-mediated inflammatory responses and septic shock (S.Z. and Y.Q., unpublished data), suggesting that miR-23b inhibits inflammatory responses in multiple disease models.

Although previous studies have shown that several miRNAs, including miR-146a and miR-155, regulate autoimmune pathogenesis through their effects on T and B cells[13,14], the role of miRNAs in radio-resident cells during autoimmune pathogenesis is unclear. Our study found that miR-23b regulates autoimmunity through its effect on local resident cells by targeting proinflammatory cytokine-mediated signaling (**Fig. 6i**). Although miR-23b overexpression can inhibit NF-κB activation in immune cells (**Supplementary Fig. 20**), miR-23b expression in these cells may not be crucial for autoimmune pathogenesis because miR-23b has lower expression in lymphoid tissues than in stromal cells, and transgenic overexpression of miR-23b in radio-resistant cells was crucial for its suppression of autoimmune pathogenesis. As there has been no previous *in vivo* study of downregulated miRNAs during autoimmune pathogenesis, to the best of our knowledge, miR-23b is the first downregulated miRNA to be functionally characterized during the pathogenesis of autoimmune disease. Thus, miR-23b may be a common therapeutic target for inflammatory disease.

METHODS

Methods and any associated references are available in the online version of the paper.

Accession codes. Gene Expression Omnibus: GSE37276.

Note: Supplementary information is available in the online version of the paper.

ACKNOWLEDGMENTS

We thank R. Flavell (Yale University) for providing *Il17a*-deficient mice. This work is supported by grants from National Natural Science Foundation of China and 973 program (30930084, 2010CB529705, 91029708 and 30871298), Chinese Academy of Sciences (KSCX2-YW-R-146) and the Science and Technology Commission of Shanghai Municipality (10JC1416600) to Y.Q.; as well as National Natural Science Foundation of China (30971632 and 81025016), Chinese Ministry of Health (201202008) and the Program of the Shanghai Commission of Science and Technology (10JC1409300) to N.S.

AUTHOR CONTRIBUTIONS

S.Z. and Y.Q. designed the experiments and wrote the manuscript. S.Z. and W.P. conducted most of the experiments and analyzed the data. W.P., N.S. and J.B.H. edited the manuscript. X. Song and Y.L. helped with mouse experiments. X. Shao helped with molecular cloning. Y.S., Y.T. and D.L. provided technical support. H.W. provided *Il17a*$^{-/-}$ mice. W.L. performed Ingenuity Pathway Analyses. N.S. and D.H. provided clinical samples. Y.Q. and N.S. supervised the study.

COMPETING FINANCIAL INTERESTS

The authors declare no competing financial interests.

Published online at http://www.nature.com/doifinder/10.1038/nm.2815.
Reprints and permissions information is available online at http://www.nature.com/reprints/index.html.

1. Firestein, G.S. Evolving concepts of rheumatoid arthritis. *Nature* **423**, 356–361 (2003).
2. Compston, A. & Coles, A. Multiple sclerosis. *Lancet* **372**, 1502–1517 (2008).
3. Rahman, A. & Isenberg, D.A. Systemic lupus erythematosus. *N. Engl. J. Med.* **358**, 929–939 (2008).
4. Zhu, S. & Qian, Y. IL-17/IL-17 receptor system in autoimmune disease: mechanisms and therapeutic potential. *Clin. Sci. (Lond.)* **122**, 487–511 (2012).
5. Feldmann, M., Brennan, F.M. & Maini, R.N. Role of cytokines in rheumatoid arthritis. *Annu. Rev. Immunol.* **14**, 397–440 (1996).
6. Smolen, J.S., Steiner, G. & Aringer, M. Anti-cytokine therapy in systemic lupus erythematosus. *Lupus* **14**, 189–191 (2005).
7. Sospedra, M. & Martin, R. Immunology of multiple sclerosis. *Annu. Rev. Immunol.* **23**, 683–747 (2005).
8. Williams, R.O., Paleolog, E. & Feldmann, M. Cytokine inhibitors in rheumatoid arthritis and other autoimmune diseases. *Curr. Opin. Pharmacol.* **7**, 412–417 (2007).
9. Hueber, W. *et al.* Effects of AIN457, a fully human antibody to interleukin-17A, on psoriasis, rheumatoid arthritis, and uveitis. *Sci. Transl. Med.* **2**, 52ra72 (2010).
10. Lipsky, P.E. *et al.* Infliximab and methotrexate in the treatment of rheumatoid arthritis. Anti-Tumor Necrosis Factor Trial in Rheumatoid Arthritis with Concomitant Therapy Study Group. *N. Engl. J. Med.* **343**, 1594–1602 (2000).
11. Geyer, M. & Muller-Ladner, U. Actual status of antiinterleukin-1 therapies in rheumatic diseases. *Curr. Opin. Rheumatol.* **22**, 246–251 (2010).
12. Genovese, M.C. *et al.* LY2439821, a humanized anti–interleukin-17 monoclonal antibody, in the treatment of patients with rheumatoid arthritis: a phase I randomized, double-blind, placebo-controlled, proof-of-concept study. *Arthritis Rheum.* **62**, 929–939 (2010).
13. Lu, L.F. *et al.* Function of miR-146a in controlling T_{reg} cell–mediated regulation of Th1 responses. *Cell* **142**, 914–929 (2010).
14. O'Connell, R.M. *et al.* MicroRNA-155 promotes autoimmune inflammation by enhancing inflammatory T cell development. *Immunity* **33**, 607–619 (2010).
15. Du, C. *et al.* MicroRNA miR-326 regulates TH-17 differentiation and is associated with the pathogenesis of multiple sclerosis. *Nat. Immunol.* **10**, 1252–1259 (2009).
16. Stittrich, A.B. *et al.* The microRNA miR-182 is induced by IL-2 and promotes clonal expansion of activated helper T lymphocytes. *Nat. Immunol.* **11**, 1057–1062 (2010).
17. Xiao, C. *et al.* MiR-150 controls B cell differentiation by targeting the transcription factor c-Myb. *Cell* **131**, 146–159 (2007).
18. Rodriguez, A. *et al.* Requirement of bic/microRNA-155 for normal immune function. *Science* **316**, 608–611 (2007).
19. Thai, T.H. *et al.* Regulation of the germinal center response by microRNA-155. *Science* **316**, 604–608 (2007).
20. Johnnidis, J.B. *et al.* Regulation of progenitor cell proliferation and granulocyte function by microRNA-223. *Nature* **451**, 1125–1129 (2008).
21. Lu, L.F. *et al.* Foxp3-dependent microRNA155 confers competitive fitness to regulatory T cells by targeting SOCS1 protein. *Immunity* **30**, 80–91 (2009).
22. Xiao, C. *et al.* Lymphoproliferative disease and autoimmunity in mice with increased miR-17-92 expression in lymphocytes. *Nat. Immunol.* **9**, 405–414 (2008).
23. Ponomarev, E.D., Veremeyko, T., Barteneva, N., Krichevsky, A.M. & Weiner, H.L. MicroRNA-124 promotes microglia quiescence and suppresses EAE by deactivating macrophages via the C/EBP-α-PU.1 pathway. *Nat. Med.* **17**, 64–70 (2011).
24. O'Connell, R.M., Rao, D.S., Chaudhuri, A.A. & Baltimore, D. Physiological and pathological roles for microRNAs in the immune system. *Nat. Rev. Immunol.* **10**, 111–122 (2010).
25. Nakamachi, Y. *et al.* MicroRNA-124a is a key regulator of proliferation and monocyte chemoattractant protein 1 secretion in fibroblast-like synoviocytes from patients with rheumatoid arthritis. *Arthritis Rheum.* **60**, 1294–1304 (2009).
26. Junker, A. *et al.* MicroRNA profiling of multiple sclerosis lesions identifies modulators of the regulatory protein CD47. *Brain* **132**, 3342–3352 (2009).
27. Dai, Y. *et al.* Comprehensive analysis of microRNA expression patterns in renal biopsies of lupus nephritis patients. *Rheumatol. Int.* **29**, 749–754 (2009).
28. Pan, W. *et al.* MicroRNA-21 and microRNA-148a contribute to DNA hypomethylation in lupus CD4+ T cells by directly and indirectly targeting DNA methyltransferase 1. *J. Immunol.* **184**, 6773–6781 (2010).
29. Li, J. *et al.* Altered microRNA expression profile with miR-146a upregulation in CD4+ T cells from patients with rheumatoid arthritis. *Arthritis Res. Ther.* **12**, R81 (2010).
30. De Santis, G. *et al.* Altered miRNA expression in T regulatory cells in course of multiple sclerosis. *J. Neuroimmunol.* **226**, 165–171 (2010).

31. Tili, E. *et al.* Modulation of miR-155 and miR-125b levels following lipopolysaccharide/TNF-α stimulation and their possible roles in regulating the response to endotoxin shock. *J. Immunol.* **179**, 5082–5089 (2007).
32. Taganov, K.D., Boldin, M.P., Chang, K.J. & Baltimore, D. NF-κB-dependent induction of microRNA miR-146, an inhibitor targeted to signaling proteins of innate immune responses. *Proc. Natl. Acad. Sci. USA* **103**, 12481–12486 (2006).
33. Chang, S.H., Park, H. & Dong, C. Act1 adaptor protein is an immediate and essential signaling component of interleukin-17 receptor. *J. Biol. Chem.* **281**, 35603–35607 (2006).
34. Sønder, S.U. *et al.* IL-17-induced NF-κB activation via CIKS/Act1: physiologic significance and signaling mechanisms. *J. Biol. Chem.* **286**, 12881–12890 (2011).
35. Qian, Y. *et al.* The adaptor Act1 is required for interleukin 17-dependent signaling associated with autoimmune and inflammatory disease. *Nat. Immunol.* **8**, 247–256 (2007).
36. Ma, F. *et al.* The microRNA miR-29 controls innate and adaptive immune responses to intracellular bacterial infection by targeting interferon-γ. *Nat. Immunol.* **12**, 861–869 (2011).
37. Rodriguez, A., Griffiths-Jones, S., Ashurst, J.L. & Bradley, A. Identification of mammalian microRNA host genes and transcription units. *Genome Res.* **14**, 1902–1910 (2004).
38. Yamamoto, M. *et al.* Regulation of Toll/IL-1-receptor-mediated gene expression by the inducible nuclear protein IκBζ. *Nature* **430**, 218–222 (2004).
39. Shen, F., Ruddy, M.J., Plamondon, P. & Gaffen, S.L. Cytokines link osteoblasts and inflammation: microarray analysis of interleukin-17– and TNF-α–induced genes in bone cells. *J. Leukoc. Biol.* **77**, 388–399 (2005).
40. Kao, C.Y., Kim, C., Huang, F. & Wu, R. Requirements for two proximal NF-κB binding sites and IκB-ζ in IL-17A-induced human β-defensin 2 expression by conducting airway epithelium. *J. Biol. Chem.* **283**, 15309–15318 (2008).
41. Rossi, R.L. *et al.* Distinct microRNA signatures in human lymphocyte subsets and enforcement of the naive state in CD4+ T cells by the microRNA miR-125b. *Nat. Immunol.* **12**, 796–803 (2011).
42. Ishitani, T. *et al.* Role of the TAB2-related protein TAB3 in IL-1 and TNF signaling. *EMBO J.* **22**, 6277–6288 (2003).
43. Qian, Y., Kang, Z., Liu, C. & Li, X. IL-17 signaling in host defense and inflammatory diseases. *Cell. Mol. Immunol.* **7**, 328–333 (2010).
44. Onishi, R.M. & Gaffen, S.L. Interleukin-17 and its target genes: mechanisms of interleukin-17 function in disease. *Immunology* **129**, 311–321 (2010).
45. Iwakura, Y., Ishigame, H., Saijo, S. & Nakae, S. Functional specialization of interleukin-17 family members. *Immunity* **34**, 149–162 (2011).
46. Hartupee, J. *et al.* IL-17 signaling for mRNA stabilization does not require TNF receptor-associated factor 6. *J. Immunol.* **182**, 1660–1666 (2009).
47. Bulek, K. *et al.* The inducible kinase IKKi is required for IL-17–dependent signaling associated with neutrophilia and pulmonary inflammation. *Nat. Immunol.* **12**, 844–852 (2011).
48. Sun, D. *et al.* Treatment with IL-17 prolongs the half-life of chemokine CXCL1 mRNA via the adaptor TRAF5 and the splicing-regulatory factor SF2 (ASF). *Nat. Immunol.* **12**, 853–860 (2011).
49. Nakasa, T. *et al.* Expression of microRNA-146 in rheumatoid arthritis synovial tissue. *Arthritis Rheum.* **58**, 1284–1292 (2008).
50. Zhang, H. *et al.* Genome-wide functional screening of miR-23b as a pleiotropic modulator suppressing cancer metastasis. *Nat. Commun.* **2**, 554 (2011).
51. Gao, P. *et al.* c-Myc suppression of miR-23a/b enhances mitochondrial glutaminase expression and glutamine metabolism. *Nature* **458**, 762–765 (2009).
52. Zhu, S. *et al.* Modulation of experimental autoimmune encephalomyelitis through TRAF3-mediated suppression of interleukin 17 receptor signaling. *J. Exp. Med.* **207**, 2647–2662 (2010).
53. Kanayama, A. *et al.* TAB2 and TAB3 activate the NF-κB pathway through binding to polyubiquitin chains. *Mol. Cell* **15**, 535–548 (2004).
54. Liu, C. *et al.* Act1, a U-box E3 ubiquitin ligase for IL-17 signaling. *Sci. Signal.* **2**, ra63 (2009).
55. Shen, F. *et al.* IL-17 receptor signaling inhibits C/EBPβ by sequential phosphorylation of the regulatory 2 domain. *Sci. Signal.* **2**, ra8 (2009).
56. Shi, P. *et al.* Persistent stimulation with interleukin-17 desensitizes cells through SCFβ-TrCP–mediated degradation of Act1. *Sci. Signal.* **4**, ra73 (2011).

nature medicine

Silencing microRNA-134 produces neuroprotective and prolonged seizure-suppressive effects

Eva M Jimenez-Mateos[1], Tobias Engel[1], Paula Merino-Serrais[2], Ross C McKiernan[1], Katsuhiro Tanaka[1], Genshin Mouri[1], Takanori Sano[1], Colm O'Tuathaigh[3], John L Waddington[3], Suzanne Prenter[3], Norman Delanty[4], Michael A Farrell[5], Donncha F O'Brien[6], Ronán M Conroy[7], Raymond L Stallings[3,8], Javier DeFelipe[2] & David C Henshall[1]

Temporal lobe epilepsy is a common, chronic neurological disorder characterized by recurrent spontaneous seizures. MicroRNAs (miRNAs) are small, noncoding RNAs that regulate post-transcriptional expression of protein-coding mRNAs, which may have key roles in the pathogenesis of neurological disorders. In experimental models of prolonged, injurious seizures (status epilepticus) and in human epilepsy, we found upregulation of miR-134, a brain-specific, activity-regulated miRNA that has been implicated in the control of dendritic spine morphology. Silencing of miR-134 expression *in vivo* using antagomirs reduced hippocampal CA3 pyramidal neuron dendrite spine density by 21% and rendered mice refractory to seizures and hippocampal injury caused by status epilepticus. Depletion of miR-134 after status epilepticus in mice reduced the later occurrence of spontaneous seizures by over 90% and mitigated the attendant pathological features of temporal lobe epilepsy. Thus, silencing miR-134 exerts prolonged seizure-suppressant and neuroprotective actions; determining whether these are anticonvulsant effects or are truly antiepileptogenic effects requires additional experimentation.

Epilepsy is a serious, chronic neurological disorder characterized by recurrent spontaneous seizures that affects about 50 million people worldwide. Antiepileptic drugs typically control seizures in two-thirds of patients but probably do not alter the underlying pathophysiology[1]. The development of symptomatic epilepsy is thought to involve altered expression of ion channels, synaptic remodeling, inflammation, gliosis and neuronal death, among other factors[2–5]. However, few antiepileptogenic interventions targeting these processes have shown sufficient efficacy *in vivo*[1], and our understanding of the cell and molecular mechanisms of epileptogenesis is incomplete.

Evidence is emerging that miRNAs may be crucial to the pathogenesis of several neurological disorders[6,7], including epilepsy[8,9]. MiRNAs are a family of small (~22 nt), endogenously expressed noncoding RNAs that regulate mRNA translation by imperfect base-pairing interactions within the 3′ untranslated region[10,11]. Depending on the degree of sequence complementarity, miRNA binding, which occurs with the help of Argonaute proteins within the RNA-induced silencing complex (RISC), results in either cleavage of the target mRNA or a reduction in its translational efficiency[10,11].

MiR-134 is a brain-specific, activity-regulated miRNA that has been implicated in the control of neuronal microstructure[12,13]. Pyramidal cells are the most common neurons in the neocortex and hippocampus[2]. They are the major source of intrinsic excitatory cortical synapses, and their dendritic spines are the main postsynaptic target of excitatory synapses, with their spine size acting as an index of synaptic strength[14–16]. Spine remodeling occurs during learning and memory formation, as well as in the setting of neuropsychiatric disorders and pathological brain activity[17–21]. Spine collapse is mediated in part by the *N*-methyl-D-aspartate (NMDA)-receptor–dependent and calcium-dependent depolymerization of actin by cofilin[19,22,23]. LIM kinase-1 (Limk1) phosphorylates cofilin and inactivates the ability of cofilin to depolymerize actin, and loss of Limk1 results in abnormal spine morphology[24]. In hippocampal neurons, miR-134 targets *Limk1* mRNA, thereby preventing Limk1 protein translation[13]. Overexpression of miR-134 *in vitro* has been reported to reduce spine volume[13], whereas overexpression of miR-134 *in vivo* reduces total dendritic length[25] and abrogates long-term potentiation[26]. Mice haploinsufficient for the miRNA biogenesis component DiGeorge syndrome critical region gene 8 do not produce several mature miRNAs, including miR-134, and have lower hippocampal spine density compared to wild-type mice[27]. Spine loss may have divergent consequences according to context[28], promoting excitability[29] or uncoupling NMDA-receptor–driven currents in neurons and preventing excitotoxicity[30].

Here we investigated the role of miR-134 in epilepsy and explored the *in vivo* effect of inhibiting miR-134. We report that miR-134 is upregulated

[1]Department of Physiology and Medical Physics and Centre for the Study of Neurological Disorders, Royal College of Surgeons in Ireland, Dublin, Ireland. [2]Instituto Cajal (CSIC) and Laboratorio Cajal de Circuitos Corticales (Centro de Tecnología Biomédica), Universidad Politécnica de Madrid, Madrid, Spain. [3]Molecular and Cellular Therapeutics, Royal College of Surgeons in Ireland, Dublin, Ireland. [4]Department of Neurology, Beaumont Hospital, Dublin, Ireland. [5]Department of Pathology, Beaumont Hospital, Dublin, Ireland. [6]Department of Neurological Surgery, Beaumont Hospital, Dublin, Ireland. [7]Division of Population Health Sciences, Royal College of Surgeons in Ireland, Dublin, Ireland. [8]National Children's Research Centre, Our Lady's Children's Hospital, Dublin, Ireland. Correspondence should be addressed to D.C.H. (dhenshall@rcsi.ie).

Received 28 November 2011; accepted 15 May 2012; published online 10 June 2012; doi:10.1038/nm.2834

in experimental and human epilepsy and show that silencing miR-134 generates a seizure-refractory state and attenuates epileptic seizures and the pathophysiological features of temporal lobe epilepsy (TLE).

RESULTS

MiR-134 is regulated by status epilepticus and in epilepsy

We first investigated whether pathologic brain activity *in vivo* affects miR-134 levels. We triggered prolonged seizures (status epilepticus) in C57BL/6 mice by intra-amygdala microinjection of the glutamate receptor agonist kainic acid[31,32]. The resultant seizures caused neuronal damage mainly within the hippocampal CA3 subfield (**Fig. 1a**).

To identify the cell populations expressing miR-134 *in vivo*, we performed *in situ* hybridization on tissue sections from C57BL/6 control mice labeled with a probe specific for mature miR-134. We detected a strong signal in the soma of hippocampal pyramidal neurons and hilar interneurons, as well as in neurons in the neocortex and amygdala (**Fig. 1b** and **Supplementary Fig. 1**).

Real-time quantitative PCR (qPCR) analysis showed that status epilepticus resulted in an increase in mature miR-134 levels in the ipsilateral CA3 ($P = 0.016$) and CA1 ($P = 0.035$) subfields (**Fig. 1c**). The levels of mature miR-134 were not changed in the undamaged contralateral CA3 subfield (**Supplementary Fig. 2a**). Nonharmful, nonconvulsive seizures induced by a low dose of systemic kainic acid, a model of epileptic preconditioning[33] in which status epilepticus does not develop, did not alter miR-134 levels compared to vehicle controls in the CA3 ($P = 0.89$) or CA1 subfields ($P = 0.56$) ($n = 6$ mice per group; data not shown).

To determine whether miR-134 was functional, we measured its levels within the RISC, where targeting of miRNAs to mRNA occurs[34], in control mice and in mice after status epilepticus. We eluted Argonaute-2 from the CA3 subfield[35,36] and extracted miRNA. We detected a low level of miR-134 in the RISC in the controls, whereas the levels of Argonaute-2–bound miR-134 were higher ($P = 0.035$) in mice in which we induced status epilepticus (**Fig. 1d**). Protein concentrations of the miR-134 target, Limk1 (ref. 13), were lower ($P = 0.001$) in mice after status epilepticus than in the controls (**Fig. 1e**).

We next investigated whether miR-134 levels and the expression of Limk1 were altered in experimental epilepsy. Recurrent spontaneous

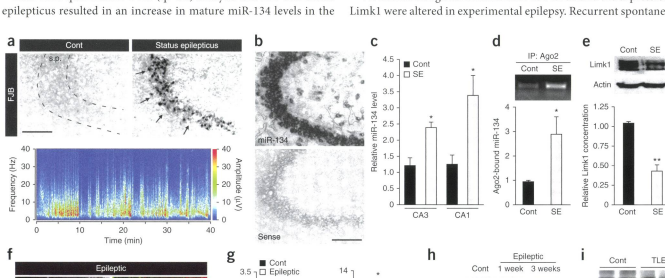

Figure 1 MiR-134 upregulation after status epilepticus and in epilepsy. (**a**) Photomicrographs show neuronal death (FJB) in the CA3 stratum pyramidale (s.p., within dashed lines in the top left image) 24 h after status epilepticus induced by intra-amygdala kainic acid compared to control (Cont) mouse. Arrows in the image on the top right point to damaged neurons. Below is a depiction of electrographic seizure frequency and amplitude during status epilepticus. Scale bar, 200 μm (**b**) *In situ* hybridization showing miR-134 in the soma of CA3 pyramidal neurons. Scale bar, 200 μm.'Sense' indicates the sense-labeled control section as a control for probe specificity. (**c**) Real-time qPCR measurement of miR-134 (normalized to RNU19) for the CA3 and CA1 24 h after status epilepticus (SE). $n = 5$ mice per group. $^*P < 0.05$ compared to Cont subfield by *t* test. (**d**) Argonaute-2 (Ago2)-immunoprecipitated (IP) miR-134 from control mice and mice 24 h after status epilepticus. $n = 3$ mice per group. $^*P < 0.05$ compared to Cont by *t* test. (**e**) Limk1 western blot and densitometry. Actin was used as the loading control. $n = 5$ mice per group. $^{**}P < 0.05$ compared to Cont by *t* test. (**f**) Photomicrographs showing loss of CA3 neurons (NeuN, arrows) and astrogliosis (glial fibrillary acidic protein, GFAP) in epileptic mice 14 d after status epilepticus (top) and a telemetry-recorded spontaneous seizure (bottom; denoted by arrows). Scale bar, 200 μm. (**g**) MiR-134 levels in the CA3 and CA1 subfields 1 and 3 weeks after status epilepticus. $n = 5$ mice per group. $^*P < 0.05$ compared to time-matched Cont by *t* test. (**h**) Western blot showing Limk1 concentrations 1 and 3 weeks after status epilepticus and densitometry. $n = 4$ mice per group. $^*P < 0.05$ compared to Cont by analysis of variance (ANOVA) followed by Bonferroni's *post hoc* test. (**i**) MiR-134 levels in surgically resected temporal lobe samples from individuals with TLE compared to autopsy controls (Cont). $n = 3$ samples per group. $^*P < 0.05$ compared to Cont by *t* test. Western blot (above) shows LIMK1 concentrations ($n = 1$ sample per lane). All data are mean ± s.e.m.

seizures emerge 3–4 d after status epilepticus in the model we used[31,33], and within 3 weeks, the mice show pathologic hallmarks of TLE, including neuron loss and astrogliosis (**Fig. 1f**). MiR-134 levels were elevated in the CA3 subfield 3 weeks after status epilepticus ($P = 0.049$) and 1 ($P = 0.003$) and 3 ($P = 0.008$) weeks after status epilepticus in the CA1 subfield compared to controls (**Fig. 1g**). Limk1 protein concentrations followed an opposite trend and were lower ($P = 0.028$) in epileptic mice than control mice (**Fig. 1h**). The concentrations of cAMP responsive element binding protein 1 (Creb1), another validated miR-134 target[26], were also lower in epileptic mice than control mice (**Supplementary Fig. 2b**).

We next analyzed surgically obtained temporal lobe material from individuals with pharmacoresistent TLE. We detected higher levels ($P = 0.029$) of mature miR-134 in the TLE specimens compared to autopsy control samples from people who died of causes unrelated to neurological disease (**Fig. 1i**). This difference was not an artifact of postmortem delay (**Supplementary Fig. 2c–e**). Protein concentrations of LIMK1 were lower ($P = 0.039$, t test) in individuals with TLE compared to the autopsy controls (**Fig. 1i**).

In vivo depletion of miR-134 using antagomirs

To explore the function of miR-134 *in vivo*, we injected mice with locked nucleic acid (LNA) 3′ cholesterol-conjugated oligonucleotides ('antagomirs')[36–39]. We injected antagomirs targeting miR-134 (Ant-134) (**Supplementary Fig. 3a**) or a nontargeting scrambled sequence (Scr) into the mouse ventricle (intracerebroventricularly, i.c.v.) (**Supplementary Fig. 3b**) and measured the miRNA levels 1, 4, 8 and 12 h later and then after 1, 3, 5 and 7 d and after 1 and 2 months. Knockdown of miR-134 was first evident 12 h after injection of 0.12 nmol Ant-134 (**Supplementary Fig. 4a–d**), and by 24 h after injection, the levels of miR-134 in the hippocampus of these mice were reduced by over 95% ($P = 0.005$) (**Fig. 2a**). This is similar to effects reported for antagomirs in other tissues[37]. Hippocampal levels of an unrelated miRNA, miR-19a, were not changed by injection of Ant-134 (**Fig. 2b**). Increasing the amount of Ant-134 injected to 1 nmol seemed to produce off-target knockdown of miRNAs (**Supplementary Fig. 4e,f**). The miR-134 levels began to recover by 7 d after Ant-134 injection, although they remained lower than the miR-134 levels in the mice injected with Scr at 1 month after injection ($P = 0.034$), which is consistent with other reports[37], and were no longer different from the levels in mice injected with Scr ($P = 0.469$) by 2 months after injection (**Fig. 2c**).

Brains from mice injected with the antagomirs had grossly normal anatomy (data not shown). We found no evidence of hippocampal neuronal death when we stained sections from the mice injected with antagomirs for Fluoro-Jade B (FJB), DNA fragmentation (terminal deoxynucleotidyl dUTP nick end labeling; TUNEL)[40] and the neuronal marker NeuN (**Fig. 2d,e** and data not shown).

To determine whether the reduction in the levels of miR-134 had any gross effects on mouse behavior, we performed ethological tests[41]. We injected mice with either Scr or Ant-134 and assessed them 24 h later. We found no differences in measures of animal exploratory activity including ambulatory counts, distance traveled or vertical counts between the two groups (**Fig. 2f**), suggesting that silencing of miR-134 does not alter normal exploratory activities.

MiR-134 antagomirs reduce pyramidal neuron spine density

Because *in vitro* and *in vivo* evidence supports a role for miR-134 in controlling dendritic spine morphology[13,25,27], we examined whether antagomirs caused changes to dendritic spines *in vivo*. We microinjected Lucifer yellow into individual CA3 pyramidal neurons in hippocampal slices from control mice 24 h after injection of 0.12 nmol Ant-134 or Scr and imaged them using confocal microscopy, as previously described[42,43] (**Fig. 3a,b**).

We analyzed 218 neurons in the Scr-injected mice ($n = 7$) and 181 neurons in the Ant-134–injected mice ($n = 7$). The structures of the basal dendritic trees were grossly normal in both groups, as were the distributions of spines (**Fig. 3c–e**). Dendrites from the Scr-injected mice had an average of 68 nodes (ramifications) compared to 72 nodes in the Ant-134–injected mice. The number of ramification points per μm was also similar in the two groups (0.0127 nodes per μm in the Scr-injected mice compared to 0.0131 nodes per μm in the Ant-134–injected mice). We then analyzed spine density, assessing a total length of 5,343.7 μm of dendrites in the Scr-injected mice (7,455 spines) and a similar length (5,477.5 μm) of dendrites in the Ant-134–injected mice (6,196 spines). Spine density in the Scr-injected mice was within the expected range[42] (**Fig. 3d–f**). Notably, spine density was 21% lower ($P = 0.037$) in Ant-134–injected mice than in the Scr-injected mice (**Fig. 3d–f**). Thus, injecting miR-134 antagomirs *in vivo* results in a reduction in spine density.

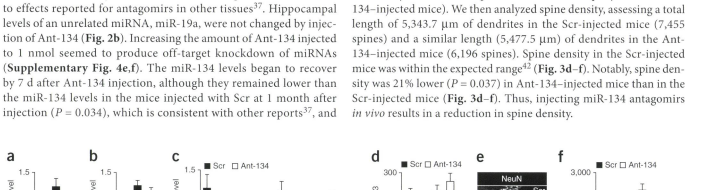

Figure 2 Antagomir-mediated silencing of miR-134 in mouse hippocampus. (**a**,**b**) Real-time qPCR measurement of miR-134 (**a**) and miR-19a (**b**) in mouse hippocampus 24 h after i.c.v. injection of Ant-134 or Scr. $n = 3$ mice per group. $^{***}P < 0.001$ compared to artificial cerebrospinal fluid (aCSF) and $^{###}P < 0.001$ compared to Scr by ANOVA followed by Bonferroni's *post hoc* test. (**c**) MiR-134 levels in hippocampus after injection of Ant-134 or Scr at 1 d, 3 d, 5 d, 7 d, 1 month and 2 months after injection. $n = 3$ or 4 mice per group. $^{*}P < 0.05$, $^{**}P < 0.01$ compared to Scr by ANOVA followed by Bonferroni's *post hoc* test. NS, not significant. (**d**) NeuN counts at two different levels of the dorsal hippocampus in mice 24 h after injection with either Scr or Ant-134. $n = 4$ mice per group. (**e**) NeuN staining of the CA3 subfield 24 h after injection of Scr or Ant-134. Scale bar, 200 μm. (**f**) Behavioral analysis of mice 24 h after injection with Scr or Ant-134. The graph shows indices of exploratory activity: total ambulatory counts; distance traveled (cm); and vertical counts. All data are mean ± s.e.m.

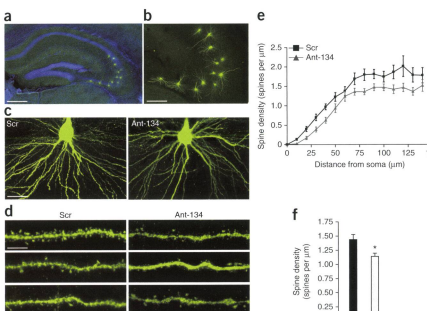

Figure 3 Antagomir silencing of miR-134 reduces hippocampal CA3 spine density *in vivo*. (**a**) Field view of a hippocampus showing Lucifer yellow–injected CA3 neurons (green) and nuclei (DAPI, blue). Scale bar, 500 μm. (**b**) Higher magnification of **a** showing the injected CA3 neurons. Scale bar, 100 μm. (**c**) Photomicrographs of the basal tree from Lucifer yellow–injected mice 24 h after injection with either Scr or Ant-134. Scale bar, 20 μm. (**d**) Representative images of individual dendrites from four mice injected with Scr (left) and four mice injected with Ant-134 (right). Scale bar, 12 μm. (**e**) Spine density as a function of the distance from the soma (by Sholl analysis) for Scr-injected and Ant-134–injected mice. (**f**) Spine density in Scr-injected and Ant-134–injected mice. $n = 7$ mice per group. $^*P < 0.05$ compared to Scr by *t* test. All data are mean ± s.e.m.

Silencing miR-134 reduces status epilepticus and neuronal death

To test the idea that antagomirs might influence pathologic brain activity *in vivo*, we compared seizures evoked by intra-amygdala microinjection of kainic acid in mice 24 h after injection with either Scr or Ant-134 (**Fig. 4** and **Supplementary Fig. 3c**). There was no difference in basal electroencephalography (EEG) measures between the two groups of mice (**Supplementary Fig. 5a**). Scr-injected mice experienced typical status epilepticus, comprising episodes of high-amplitude, high-frequency discharges (HAHFDs)[44] (**Fig. 4a–c**; compare **Fig. 4c** to **Fig. 1a**). An EEG analysis revealed that the duration of the HAHFDs ($P = 0.0051$), which are associated with damage-causing pathologic activity[45], and total EEG power ($P = 0.033$) were lower in Ant-134–injected mice compared to Scr-injected mice (**Fig. 4a–c**). This effect was qualitatively similar to the seizure suppression observed in mice given lorazepam 10 min before injection of kainic acid (compare **Fig. 4c** to **Supplementary Fig. 5b**).

MiR-134 levels were lower ($P = 0.0078$) in mice injected with Ant-134 before intra-amygdala injection of kainic acid compared to the mice injected with Scr (**Fig. 4d** and **Supplementary Fig. 6a**). Limk1 protein concentrations (**Fig. 4e**) and the concentrations of Creb1 (**Supplementary Fig. 6b**) were lower after status epilepticus in Scr-injected mice than in Ant-134–injected mice ($P = 0.018$), which had similar levels as nonseizure controls.

We next examined hippocampal damage in tissue sections from Scr-injected and Ant-134–injected mice. Scr-injected mice had typical CA3 lesions 24 h after status epilepticus, with extensive staining of neurons for FJB and TUNEL and a loss of NeuN staining (**Fig. 5a–f**). Mice injected with Ant-134 showed a marked

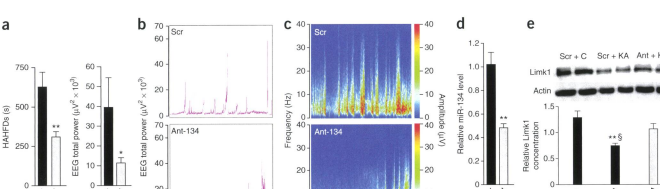

Figure 4 Antagomir silencing of miR-134 reduces seizure severity during status epilepticus. (**a**) Graphs show HAHFDs and total EEG power during status epilepticus in mice 24 h after injection with Scr or Ant-134. $n = 4$–8 mice per group. $^*P < 0.05$, $^{**}P < 0.01$ compared to Scr by *t* test. (**b**,**c**) Total EEG power (**b**) and the frequency and amplitude parameters (**c**) during status epilepticus in representative Scr-injected and Ant-134–injected mice covering the period between kainic acid injection and lorazepam administration. (**d**) MiR-134 levels in Scr- and Ant-134–injected mice 24 h after status epilepticus. $n = 4$ mice per group. $^{**}P < 0.01$ compared to Scr by *t* test. (**e**) Limk1 protein concentrations in Scr-injected mice without kainic-acid–induced status epilepticus (Scr + C) and after status epilepticus in mice given Scr (Scr + KA) or Ant-134 (Ant + KA). The graph shows Limk1 concentrations normalized to actin. $n = 4$ mice per group. $^{**}P < 0.01$ for Scr + KA compared to Scr + C; $^{\S}P < 0.05$ for Scr + KA compared to Ant + KA, by ANOVA with Bonferroni's *post hoc* test. All data are mean ± s.e.m.

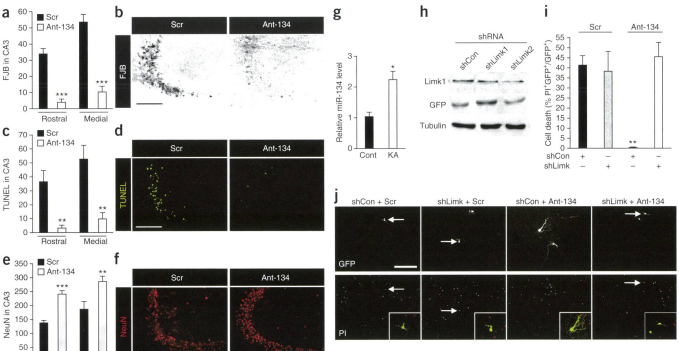

Figure 5 Antagomir silencing of miR-134 protects against status epilepticus *in vivo* and kainic acid toxicity *in vitro*. (**a**–**f**) *In vivo* studies. Graphs and representative photomicrographs from the dorsal hippocampus of mice 24 h after status epilepticus in mice treated beforehand with Scr or Ant-134 showing; FJB counts (**a**,**b**), TUNEL counts (**c**,**d**) and NeuN counts (**e**,**f**). $n = 4$–8 mice per group. $^{**}P < 0.01$, $^{***}P < 0.001$ compared to Scr by t test. Scale bars, 200 μm. (**g**–**j**) *In vitro* studies. (**g**) MiR-134 levels in primary hippocampal neurons 24 h after treatment with kainic acid. Data are from three independent experiments. $^{*}P < 0.05$ compared to Cont by t test. (**h**) Western blots showing Limk1 and GFP in SH-SY5Y cells transfected with control shRNA (shCon) or different shRNAs targeting Limk1 (shLimk1 and shLimk2). The shLimk2 reduced Limk1 concentrations by ~48% compared to shCon (average of two experiments). (**i**) Percentage of cell death induced by kainic acid treatment of hippocampal neurons (as the ratio of propidium iodide (PI)$^{+}$GFP^{+} neurons over total GFP^{+} neurons) and the effect of Scr or Ant-134 in neurons cotransfected with either shCon or shLimk2 (shLimk). Results are from $n = 4$ independent experiments per group. $^{**}P < 0.01$ for shCon + Ant-134 compared to other groups by ANOVA with Bonferroni's *post hoc* test. (**j**) Photomicrographs of hippocampal neurons in each condition. Arrows indicate dead cells positive for both GFP (green) and PI (red), and the insets (40× lens) emphasize these regions. Scale bar, 50 μm. All data are mean ± s.e.m.

reduction in FJB and TUNEL staining and less of a loss of NeuN staining after status epilepticus (**Fig. 5a**–**f**).

To specifically link the neuroprotective effects of antagomirs to miR-134 and Limk1, we treated cultures of primary hippocampal neurons from C57BL/6 mice with kainic acid to model excitotoxic injury. Treatment of hippocampal neurons with kainic acid increased miR-134 levels ($P = 0.019$) (**Fig. 5g**). Next, neurons were co-transfected with shRNAs that targeted Limk1 (**Fig. 5h**), and either Scr or Ant-134, and then treated 48 h later with kainic acid. Ant-134 prevented kainic-acid–induced neurotoxicty in hippocampal neurons co-transfected with a non-targeting shRNA, and this protective effect was blocked in neurons cotransfected with shRNA targeting Limk1 (**Fig. 5i**,**j**).

Silencing miR-134 reduces spontaneous recurrent seizures

Based on our findings so far, we hypothesized that silencing miR-134 might also affect epilepsy. To avoid a confounding influence of shortened status epilepticus duration or neuroprotection on epileptogenesis[40,46], we injected antagomirs 1 h after triggering status epilepticus with intra-amygdala kainic acid. An analysis of EEG measures confirmed that when we injected antagomirs 1 h after kainic acid injection, there was no difference in duration of HAHFDs during status epilepticus between the Ant-134–injected and Scr-injected groups (**Fig. 6a**). In addition, CA3 damage assessed 24 h after triggering status epilepticus was similar between the Ant-134–injected and Scr-injected mice (**Fig. 6b**,**c**).

We then equipped groups of mice with EEG telemetry units[31] and undertook continuous EEG recording for 2 weeks after status epilepticus. In agreement with the normal course of epilepsy in this model[31], mice injected with Scr after status epilepticus experienced the first spontaneous seizures on the third day, and all mice were epileptic by the fourth day after status epilepticus (**Fig. 6d**,**e** and **Supplementary Fig. 6c**). The median epileptic seizure count during 14 d of monitoring of Scr-injected mice was 25 (range 8–79), with 200 epileptic seizures recorded in total for all the Scr-injected mice over this time period (**Fig. 6d** and **Supplementary Fig. 6c**). In contrast, only 60% of mice injected with Ant-134 had had a spontaneous seizure by the eleventh day after status epilepticus (**Fig. 6d** and **Supplementary Fig. 6c**); one mouse had only a single seizure on day 14 and another had no seizures in the 14 d after status epilepticus (**Fig. 6d**). Ant-134–injected mice had a median epileptic seizure count of 2 during the 14-d recording period (range 0–7), with just 16 epileptic seizures recorded in total for these mice during the 2 week recording period ($P = 0.0001$, compared to the Scr-injected group by two-way ANOVA) (**Fig. 6e**). The total amount of time spent in seizures also differed between the two groups, with Scr-injected mice spending more time in seizures then Ant-134–injected mice ($P < 0.001$ by two-way ANOVA; **Supplementary Fig. 6c**). The durations of the individual epileptic seizures were similar between the groups (**Supplementary Fig. 6d**).

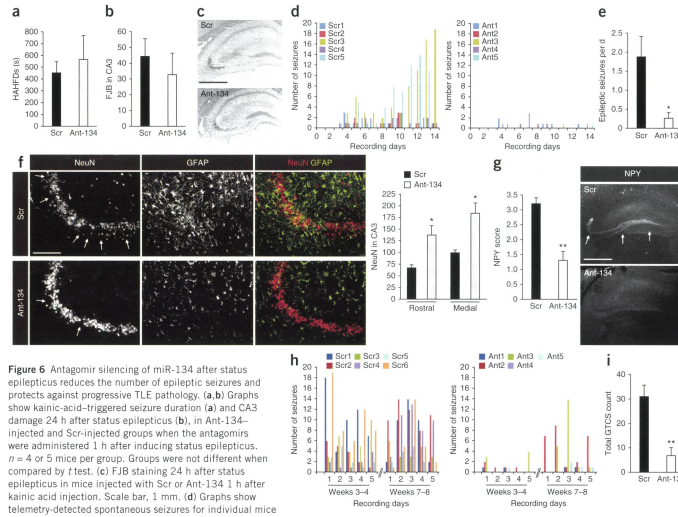

Figure 6 Antagomir silencing of miR-134 after status epilepticus reduces the number of epileptic seizures and protects against progressive TLE pathology. (**a**,**b**) Graphs show kainic-acid–triggered seizure duration (**a**) and CA3 damage 24 h after status epilepticus (**b**), in Ant-134–injected and Scr-injected groups when the antagomirs were administered 1 h after inducing status epilepticus. $n = 4$ or 5 mice per group. Groups were not different when compared by t test. (**c**) FJB staining 24 h after status epilepticus in mice injected with Scr or Ant-134 1 h after kainic acid injection. Scale bar, 1 mm. (**d**) Graphs show telemetry-detected spontaneous seizures for individual mice during the 2 weeks after status epilepticus for Scr-injected (left) and Ant-134–injected (right) mice. Scr1–Scr5, the five mice injected with Scr; Ant1–Ant5, the five mice injected with Ant-134. (**e**) Daily epileptic seizures in Scr-injected and Ant-134–injected mice. $n = 5$ mice per group. $^*P < 0.05$ compared to Scr by t test. (**f**) Hippocampal NeuN (arrows indicate areas of reduced NeuN staining) and GFAP (astrogliosis) staining in Scr-injected and Ant-134–injected mice after 2 weeks of epilepsy monitoring. The graph to the right shows NeuN counts in the dorsal hippocampus from the mice in each group. $^*P < 0.05$ compared to Scr group at rostral and $^*P < 0.05$ compared to Scr group at medial levels, by t test, $n = 5$ mice per group. Scale bar, 200 μm. (**g**) NPY scores in mice 14 d after status epilepticus (left) and representative NPY-stained sections from Scr-injected and Ant-134–injected mice (right). $^{**}P < 0.01$ compared to Scr by t test. Scale bar, 1 mm. $n = 5$ mice per group. (**h**) Graphs show the number of generalized tonic-clonic seizures (GTCS) each day for individual mice during two periods of 5 d of continuous video monitoring after status epilepticus for Scr-injected (left) and Ant-134–injected (right) mice. Scr1–Scr6, the six mice injected with Scr; Ant1–Ant5, the five mice injected with Ant-134. (**i**) Total GTCS counts averaged from the two monitoring periods. $n = 5$ or 6 mice per group. $^{**}P < 0.01$ compared to Scr by t test. All data are mean ± s.e.m.

Silencing miR-134 alters pathologic hallmarks of TLE

Progressive neuron loss, gliosis and rearrangement of mossy fibers are common pathological hallmarks of TLE[47,48]. We therefore examined whether Ant-134 altered the underlying pathology in the telemetry-equipped mice. Hippocampal CA3 neuron counts in the Ant-134–injected mice were higher than in the Scr-injected mice at the end of epilepsy monitoring, and astrogliosis was lower in the Ant-134–injected mice than in the Scr-injected mice (**Fig. 6f**). Neuropeptide Y (NPY) staining, an index of increasing reorganization of the hippocampus[33,49], in Scr-injected mice (**Fig. 6g**) was similar to the previously reported scores in epileptic mice[33], whereas the NPY scores in the Ant-134–injected mice were lower ($P = 0.008$) than in the Scr-injected mice (**Fig. 6g**).

To investigate whether the reduced epileptic seizure rates were the result of an antiepileptogenic effect or a prolonged anticonvulsant effect of Ant-134, we performed additional experiments. We first measured miR-134 levels in Ant-134–injected mice at the end of 14 d of telemetry recordings, which established that the miR-134 levels were ~55% of those in the Scr-injected mice (**Supplementary Fig. 7a**). Reducing miR-134 levels to ~55% of Scr in additional mice by injecting Ant-134 did not produce an anticonvulsant effect against kainic-acid–induced status epilepticus (**Supplementary Fig. 7b**,**c**). Likewise, mice subjected to kainic-acid–induced status epilepticus 14 d after i.c.v. injection with Ant-134, when levels of miR-134 are ~70% of those in Scr-injected mice (**Supplementary Fig. 7d**), were as sensitive to kainic-acid–induced status epilepticus as Scr-injected mice (**Supplementary Fig. 7e**–**h**), and mice were not protected against status epilepticus–induced hippocampal damage (**Supplementary Fig. 7i**,**j**).

Finally, longer-term video monitoring revealed that mice injected with Ant-134 after status epilepticus had fewer generalized tonic-clonic seizures and more seizure-free days at up to 2 months after

injection compared to Scr-injected mice, although the seizure rates did increase toward the rate of Scr-injected mice in three out of the 5 Ant-134–injected mice (**Fig. 6h,i** and **Supplementary Fig. 8**).

DISCUSSION

Our study shows that silencing miR-134 in mice using antagomirs suppresses evoked seizures, the occurrence of spontaneous seizures and the associated pathologic hallmarks of epilepsy. These are the first *in vivo* data, to our knowledge, to show that inhibition of a single mature miRNA can alter pathologic electrical activity in the brain, and they offer a new therapeutic target for the treatment of epilepsy.

An association between seizures and changes in miRNA expression has been suggested by recent profiling work[8,9,36,50] and by the phenotype of mice lacking Dicer[51], although our experiments are the first, to our knowledge, to link upregulation of miR-134 to evoked, harmful seizures and chronic epilepsy. Brief, nonharmful generalized seizures were insufficient to alter miR-134 expression. This suggests that *in vivo* regulation of miR-134 is not only a response to increased neuronal activity[13] but is also coupled to epileptic or pathogenic brain activity. Crucially, our miRNA silencing experiments support a role for miR-134 in facilitating pathologic neuronal activity *in vivo* because status epilepticus was potently suppressed in mice in which miR-134 was depleted by antagomirs. Notably, the seizure-suppressing effect of the antagomirs was nearly comparable to that of benzodiazepines[45,46,52]. Injecting antagomirs before status epilepticus also protected against seizure-induced hippocampal damage. This probably arises because of the resulting shortened seizure duration[46,52], but antagomirs also inhibited direct kainic acid toxicity *in vitro*. Our *in vitro* experiments also implicated Limk1 in the mechanism of protection, but rescuing Creb1 may also contribute[53], and our data are consistent with the neuroprotective effect of sirtuin 1, which negatively regulates miR-134 expression in brain[26].

Despite progress in understanding the pathogenesis of epilepsy, few studies targeting epileptogenic processes have shown sufficient efficacy at reducing the occurrence, course or severity of the disease[1,54]. A second major finding here was that silencing miR-134 after status epilepticus resulted in a substantial reduction in the number of epileptic seizures in mice. Epilepsy developed normally in Scr-injected mice[31], whereas spontaneous seizures seldom occurred in the Ant-134–injected mice. Thus, the effect of Ant-134 injection after status epilepticus was superior to that of neuroprotection by other means applied at the time of status epilepticus[40,55] and was comparable to or exceeded the performance of other experimental antiepileptogenic treatments[1]. Did the antagomirs interrupt epileptogenesis or simply prevent epileptic seizures from occurring as a result of a prolonged anticonvulsant effect, or did they work in a manner similar to antiepileptic drugs? We detected spontaneous seizures, albeit infrequently, in the mice treated with antagomirs, and the increase in seizure rates over extended monitoring in these mice supports the interpretation of a prolonged anticonvulsant or antiepileptic effect. Nevertheless, seizure rates in these mice never recovered to baseline, and seizure frequency 2 months after status epilepticus, a time when antagomir suppression of miR-134 was no longer occurring, was over 70% lower than baseline, so an antiepileptogenic effect is possible. Additional experiments examining seizure frequency at time points later than 2 months after antagomir administration will be required to distinguish between these possibilities.

The mechanism by which miR-134 antagomirs suppress seizures is unknown, but our study offers the possibility that the effect is through changes to dendritic spines. The finding that Ant-134 reduced hippocampal CA3 dendritic spine density *in vivo* was notable and contrasts with reports that spine size, not density, is controlled by miR-134 (ref. 13). Thus, a different phenotype results from miR-134 inhibition *in vivo*, which may be explained by the scale of miRNA suppression achieved, the distribution of the antagomir (somal compared to dendritic), the targets affected or the potency of LNA-modified antagomirs over 2′-O-methyl oligonucleotides[39]. Coincidently, a similar reduction in spine density was reported in mice lacking an miRNA biogenesis component in which the hippocampal levels of mature miR-134 were also reduced[27]. A key target of miR-134 is Limk1, which regulates dendritic spine dynamics[13]. Limk1 protein concentrations followed an opposite pattern as miR-134 expression, and miR-134 silencing prevented seizure-induced downregulation of Limk1, although other explanations for a decrease in spines are possible[15,56]. Could the reduction in spines account for the suppression of seizures? Dendritic spines are targets of excitatory axons in the brain[14,15]. Although spines have been suggested to operate as barriers against potentially harmful afferent input[28], our data are consistent with evidence showing that spine loss reduces excitatory responses[17,57] and transient spine reduction uncouples excitotoxic NMDA-mediated signaling[30]. The antagomirs seem to curtail pathologic activity in the brain without impairing tonic neuronal communication; an impairment would have been detected by the ethogram, and this result is consistent with reports that a ~20% reduction in the number of hippocampal pyramidal neuron spines does not alter basal neurotransmission[58]. Spine-localized synaptic signaling is also implicated in the pathogenesis of TLE[3], but whether a similar mechanism may account for the seizure-suppressive effects of miR-134 silencing is unknown. Loss of Limk1, which was countered with antagomirs, can result in increased hippocampal excitability[24]. However, other miR-134 targets with effects on excitability and seizure suppression are known, so we cannot exclude the involvement of these other targets in the effects we observed[26,53].

Although the therapeutic application of miR-134 antagomirs for status epilepticus is probably barred by a need for pretreatment, the longevity of the suppression after a single injection, consistent with antagomir data from mouse and primate experiments[37,39], suggests applications in refractory epilepsy or in disease modification in the wake of epilepsy-precipitating injuries. Alternate routes for antagomir delivery, such as an intranasal route, which has been considered for antiepileptic drug delivery[59], may avoid the blood-brain barrier exclusion of antagomirs *in vivo*[37] and may facilitate translation to the clinic for the treatment of epilepsy.

METHODS

Methods and any associated references are available in the online version of the paper.

Note: Supplementary information is available in the online version of the paper.

ACKNOWLEDGMENTS

We would like to thank J. Varley, J. Phillips and members of the Epilepsy Programme, Beaumont Hospital. We thank S. Miller-Delaney for assistance and N. Plesnila, J. Prehn and R. Simon for helpful suggestions on the manuscript. We thank the Brain and Tissue Bank for Developmental Disorders at the University of Maryland, Baltimore, Maryland. This work was supported by funding from Science Foundation Ireland awards 08/IN1/B1875 (D.C.H., E.M.J.-M., K.T., G.M. and T.S.), 11/TIDA/B1988 (D.C.H.) and 07/IN.1/B960 (J.W. and C.O.), US National Institute of Neurological Disorders and Stroke award R56 073714 (D.C.H.), an Irish Research Council for Science, Engineering and Technology postdoctoral fellowship (E.M.J.-M.), Irish Health Research Board grant PHD/2007/11 (R.C.M.) and the Spanish Ministry of Education, Science and Innovation grant SAF2009-09394 (J.D.).

AUTHOR CONTRIBUTIONS

E.M.J.-M. performed expression analyses, tissue culture, spine imaging, histology and epilepsy monitoring. T.E., K.T., G.M. and T.S. performed mouse modeling and telemetry. P.M.-S. and J.D. performed spine injections and data analysis. R.C.M. and S.P. performed expression studies. C.O. and J.L.W. conducted and analyzed the behavioral studies. N.D., D.F.O. and M.A.F. organized the human studies. R.M.C. performed statistical analyses. R.L.S. contributed to study design and analysis. D.C.H. and E.M.J.-M. conceived of the study, analyzed data and wrote the manuscript.

COMPETING FINANCIAL INTERESTS

The authors declare no competing financial interests.

Published online at http://www.nature.com/doifinder/10.1038/nm.2834. Reprints and permissions information is available online at http://www.nature.com/reprints/index.html.

1. Pitkänen, A. & Lukasiuk, K. Mechanisms of epileptogenesis and potential treatment targets. *Lancet Neurol.* **10**, 173–186 (2011).
2. DeFelipe, J. Chandelier cells and epilepsy. *Brain* **122**, 1807–1822 (1999).
3. McNamara, J.O., Huang, Y.Z. & Leonard, A.S. Molecular signaling mechanisms underlying epileptogenesis. *Sci. STKE* **2006**, re12 (2006).
4. Wetherington, J., Serrano, G. & Dingledine, R. Astrocytes in the epileptic brain. *Neuron* **58**, 168–178 (2008).
5. Vezzani, A., French, J., Bartfai, T. & Baram, T.Z. The role of inflammation in epilepsy. *Nat. Rev. Neurol.* **7**, 31–40 (2011).
6. Eacker, S.M., Dawson, T.M. & Dawson, V.L. Understanding microRNAs in neurodegeneration. *Nat. Rev. Neurosci.* **10**, 837–841 (2009).
7. Saugstad, J.A. MicroRNAs as effectors of brain function with roles in ischemia and injury, neuroprotection, and neurodegeneration. *J. Cereb. Blood Flow Metab.* **30**, 1564–1576 (2010).
8. Aronica, E. *et al.* Expression pattern of miR-146a, an inflammation-associated microRNA, in experimental and human temporal lobe epilepsy. *Eur. J. Neurosci.* **31**, 1100–1107 (2010).
9. Song, Y.J. *et al.* Temporal lobe epilepsy induces differential expression of hippocampal miRNAs including let-7e and miR-23a/b. *Brain Res.* **1387**, 134–140 (2011).
10. Ambros, V. The functions of animal microRNAs. *Nature* **431**, 350–355 (2004).
11. Bartel, D.P. MicroRNAs: genomics, biogenesis, mechanism, and function. *Cell* **116**, 281–297 (2004).
12. Lagos-Quintana, M. *et al.* Identification of tissue-specific microRNAs from mouse. *Curr. Biol.* **12**, 735–739 (2002).
13. Schratt, G.M. *et al.* A brain-specific microRNA regulates dendritic spine development. *Nature* **439**, 283–289 (2006).
14. Matsuzaki, M., Honkura, N., Ellis-Davies, G.C. & Kasai, H. Structural basis of long-term potentiation in single dendritic spines. *Nature* **429**, 761–766 (2004).
15. Zhou, Q., Homma, K.J. & Poo, M.M. Shrinkage of dendritic spines associated with long-term depression of hippocampal synapses. *Neuron* **44**, 749–757 (2004).
16. Noguchi, J., Matsuzaki, M., Ellis-Davies, G.C. & Kasai, H. Spine-neck geometry determines NMDA receptor-dependent Ca^{2+} signaling in dendrites. *Neuron* **46**, 609–622 (2005).
17. Müller, M., Gahwiler, B.H., Rietschin, L. & Thompson, S.M. Reversible loss of dendritic spines and altered excitability after chronic epilepsy in hippocampal slice cultures. *Proc. Natl. Acad. Sci. USA* **90**, 257–261 (1993).
18. Rensing, N. *et al. In vivo* imaging of dendritic spines during electrographic seizures. *Ann. Neurol.* **58**, 888–898 (2005).
19. Zeng, L.H. *et al.* Kainate seizures cause acute dendritic injury and actin depolymerization *in vivo*. *J. Neurosci.* **27**, 11604–11613 (2007).
20. Penzes, P., Cahill, M.E., Jones, K.A., VanLeeuwen, J.E. & Woolfrey, K.M. Dendritic spine pathology in neuropsychiatric disorders. *Nat. Neurosci.* **14**, 285–293 (2011).
21. Bhatt, D.H., Zhang, S. & Gan, W.B. Dendritic spine dynamics. *Annu. Rev. Physiol.* **71**, 261–282 (2009).
22. Halpain, S., Hipolito, A. & Saffer, L. Regulation of F-actin stability in dendritic spines by glutamate receptors and calcineurin. *J. Neurosci.* **18**, 9835–9844 (1998).
23. Saneyoshi, T., Fortin, D.A. & Soderling, T.R. Regulation of spine and synapse formation by activity-dependent intracellular signaling pathways. *Curr. Opin. Neurobiol.* **20**, 108–115 (2010).
24. Meng, Y. *et al.* Abnormal spine morphology and enhanced LTP in LIMK-1 knockout mice. *Neuron* **35**, 121–133 (2002).
25. Christensen, M., Larsen, L.A., Kauppinen, S. & Schratt, G. Recombinant adeno-associated virus-mediated microRNA delivery into the postnatal mouse brain reveals a role for miR-134 in dendritogenesis *in vivo*. *Front Neural Circuits* **3**, 16 (2010).
26. Gao, J. *et al.* A novel pathway regulates memory and plasticity via SIRT1 and miR-134. *Nature* **466**, 1105–1109 (2010).
27. Stark, K.L. *et al.* Altered brain microRNA biogenesis contributes to phenotypic deficits in a 22q11-deletion mouse model. *Nat. Genet.* **40**, 751–760 (2008).
28. Segal, M. Dendritic spines, synaptic plasticity and neuronal survival: activity shapes dendritic spines to enhance neuronal viability. *Eur. J. Neurosci.* **31**, 2178–2184 (2010).
29. Sierra-Paredes, G., Oreiro-García, T., Nunez-Rodriguez, A., Vazquez-Lopez, A. & Sierra-Marcuno, G. Seizures induced by *in vivo* latrunculin a and jasplakinolide microperfusion in the rat hippocampus. *J. Mol. Neurosci.* **28**, 151–160 (2006).
30. Meller, R. *et al.* Ubiquitin proteasome-mediated synaptic reorganization: a novel mechanism underlying rapid ischemic tolerance. *J. Neurosci.* **28**, 50–59 (2008).
31. Mouri, G. *et al.* Unilateral hippocampal CA3-predominant damage and short latency epileptogenesis after intra-amygdala microinjection of kainic acid in mice. *Brain Res.* **1213**, 140–151 (2008).
32. Murphy, B.M. *et al.* Contrasting patterns of Bim induction and neuroprotection in Bim-deficient mice between hippocampus and neocortex after status epilepticus. *Cell Death Differ.* **17**, 459–468 (2010).
33. Jimenez-Mateos, E.M., Mouri, G., Conroy, R.M. & Henshall, D.C. Epileptic tolerance is associated with enduring neuroprotection and uncoupling of the relationship between CA3 damage, neuropeptide Y rearrangement and spontaneous seizures following intra-amygdala kainic acid-induced status epilepticus in mice. *Neuroscience* **171**, 556–565 (2010).
34. Peters, L. & Meister, G. Argonaute proteins: mediators of RNA silencing. *Mol. Cell* **26**, 611–623 (2007).
35. Karginov, F.V. *et al.* A biochemical approach to identifying microRNA targets. *Proc. Natl. Acad. Sci. USA* **104**, 19291–19296 (2007).
36. Jimenez-Mateos, E.M. *et al.* MicroRNA expression profile after status epilepticus and hippocampal neuroprotection by targeting miR-132. *Am. J. Pathol.* **179**, 2519–2532 (2011).
37. Krützfeldt, J. *et al.* Silencing of microRNAs *in vivo* with 'antagomirs'. *Nature* **438**, 685–689 (2005).
38. Krützfeldt, J. *et al.* Specificity, duplex degradation and subcellular localization of antagomirs. *Nucleic Acids Res.* **35**, 2885–2892 (2007).
39. Elmén, J. *et al.* LNA-mediated microRNA silencing in non-human primates. *Nature* **452**, 896–899 (2008).
40. Engel, T. *et al.* Reduced hippocampal damage and epileptic seizures after status epilepticus in mice lacking proapoptotic Puma. *FASEB J.* **24**, 853–861 (2010).
41. O'Tuathaigh, C.M. *et al.* Phenotypic characterization of spatial cognition and social behavior in mice with 'knockout' of the schizophrenia risk gene neuregulin 1. *Neuroscience* **147**, 18–27 (2007).
42. Merino-Serrais, P., Knafo, S., Alonso-Nanclares, L., Fernaud-Espinosa, I. & Defelipe, J. Layer-specific alterations to CA1 dendritic spines in a mouse model of Alzheimer's disease. *Hippocampus* **21**, 1037–1044 (2011).
43. Ballesteros-Yáñez, I., Benavides-Piccione, R., Bourgeois, J.P., Changeux, J.P. & DeFelipe, J. Alterations of cortical pyramidal neurons in mice lacking high-affinity nicotinic receptors. *Proc. Natl. Acad. Sci. USA* **107**, 11567–11572 (2010).
44. Engel, T. *et al.* Loss of p53 results in protracted electrographic seizures and development of an aggravated epileptic phenotype following status epilepticus. *Cell Death Dis.* **1**, e79 (2010).
45. Shinoda, S. *et al.* Development of a model of seizure-induced hippocampal injury with features of programmed cell death in the BALB/c mouse. *J. Neurosci. Res.* **76**, 121–128 (2004).
46. Pitkänen, A., Kharatishvili, I., Narkilahti, S., Lukasiuk, K. & Nissinen, J. Administration of diazepam during status epilepticus reduces development and severity of epilepsy in rat. *Epilepsy Res.* **63**, 27–42 (2005).
47. Nairismägi, J. *et al.* Progression of brain damage after status epilepticus and its association with epileptogenesis: a quantitative MRI study in a rat model of temporal lobe epilepsy. *Epilepsia* **45**, 1024–1034 (2004).
48. Mathern, G.W., Babb, T.L. & Armstrong, D.L. Hippocampal sclerosis. in *Epilepsy: A Comprehensive Textbook* Vol. 13 (eds. Engel, J.J. & Pedley, T.A.) 133–155 (Lippincott-Raven Publishers, Philadelphia, 1997).
49. Cavazos, J.E., Golarai, G. & Sutula, T.P. Mossy fiber synaptic reorganization induced by kindling: time course of development, progression, and permanence. *J. Neurosci.* **11**, 2795–2803 (1991).
50. Hu, K. *et al.* Expression profile of microRNAs in rat hippocampus following lithium-pilocarpine-induced status epilepticus. *Neurosci. Lett.* **488**, 252–257 (2011).
51. Tao, J. *et al.* Deletion of astroglial dicer causes non-cell-autonomous neuronal dysfunction and degeneration. *J. Neurosci.* **31**, 8306–8319 (2011).
52. Araki, T., Simon, R.P., Taki, W., Lan, J.Q. & Henshall, D.C. Characterization of neuronal death induced by focally evoked limbic seizures in the C57BL/6 mouse. *J. Neurosci. Res.* **69**, 614–621 (2002).
53. Lee, B. *et al.* The CREB/CRE transcriptional pathway: protection against oxidative stress-mediated neuronal cell death. *J. Neurochem.* **108**, 1251–1265 (2009).
54. Brandt, C., Potschka, H., Loscher, W. & Ebert, U. N-methyl-D-aspartate receptor blockade after status epilepticus protects against limbic brain damage but not against epilepsy in kainate model of temporal lobe epilepsy. *Neuroscience* **118**, 727–740 (2003).
55. Jimenez-Mateos, E.M. *et al.* Hippocampal transcriptome after status epilepticus in mice rendered seizure damage-tolerant by epileptic preconditioning features suppressed calcium and neuronal excitability pathways. *Neurobiol. Dis.* **32**, 442–453 (2008).
56. Nägerl, U.V., Eberhorn, N., Cambridge, S.B. & Bonhoeffer, T. Bidirectional activity-dependent morphological plasticity in hippocampal neurons. *Neuron* **44**, 759–767 (2004).
57. Kim, C.H. & Lisman, J.E. A role of actin filament in synaptic transmission and long-term potentiation. *J. Neurosci.* **19**, 4314–4324 (1999).
58. Pavlowsky, A. *et al.* A postsynaptic signaling pathway that may account for the cognitive defect due to IL1RAPL1 mutation. *Curr. Biol.* **20**, 103–115 (2010).
59. Wermeling, D.P. Intranasal delivery of antiepileptic medications for treatment of seizures. *Neurotherapeutics* **6**, 352–358 (2009).

nature medicine

Matrix IGF-1 maintains bone mass by activation of mTOR in mesenchymal stem cells

Lingling Xian[1,2], Xiangwei Wu[1,2], Lijuan Pang[1,2], Michael Lou[1], Clifford J Rosen[3], Tao Qiu[1], Janet Crane[1,4], Frank Frassica[1], Liming Zhang[1], Juan Pablo Rodriguez[5], Xiaofeng Jia[6], Shoshana Yakar[7], Shouhong Xuan[8], Argiris Efstratiadis[8], Mei Wan[1] & Xu Cao[1]

Insulin-like growth factor 1 (IGF-1), the most abundant growth factor in the bone matrix, maintains bone mass in adulthood. We now report that IGF-1 released from the bone matrix during bone remodeling stimulates osteoblastic differentiation of recruited mesenchymal stem cells (MSCs) by activation of mammalian target of rapamycin (mTOR), thus maintaining proper bone microarchitecture and mass. Mice with knockout of the IGF-1 receptor (*Igf1r*) in their pre-osteoblastic cells showed lower bone mass and mineral deposition rates than wild-type mice. Further, MSCs from *Igf1r*$^{flox/flox}$ mice with *Igf1r* deleted by a Cre adenovirus *in vitro*, although recruited to the bone surface after implantation, were unable to differentiate into osteoblasts. We also found that the concentrations of IGF-1 in the bone matrix and marrow of aged rats were lower than in those of young rats and directly correlated with the age-related decrease in bone mass. Likewise, in age-related osteoporosis in humans, we found that bone marrow IGF-1 concentrations were 40% lower in individuals with osteoporosis than in individuals without osteoporosis. Notably, injection of IGF-1 plus IGF binding protein 3 (IGFBP3), but not injection of IGF-1 alone, increased the concentration of IGF-1 in the bone matrix and stimulated new bone formation in aged rats. Together, these results provide mechanistic insight into how IGF-1 maintains adult bone mass, while also providing a further rationale for its therapeutic targeting to treat age-related osteoporosis.

Bone mass peaks in mid or late adolescence, plateaus for several years and then inexorably declines to a point, usually in older individuals, during which there is increased skeletal fragility and, often times, establishment of osteoporosis[1–4]. Acquisition of peak bone mass (PBM) is thought to reduce the subsequent risk of bone fracture, whereas impaired acquisition of PBM or loss of bone during adolescence is associated with greater fracture risk. IGF-1 is a key factor in the endocrine regulation of body composition and is integral not only to the acquisition of PBM but also to the maintenance of bone mineral density (BMD)[5–9]. In particular, IGF-1 and several of its binding proteins positively correlate with bone mass and can act as independent predictors for the risk of osteoporosis and incident fractures[10–13].

The maintenance of adult bone mass is accomplished by skeletal remodeling[3,14]. This remodeling is precisely coordinated by the activities of osteoblasts and osteoclasts[15,16]. We have previously shown that in response to osteoclastic bone resorption, active transforming growth factor β 1 (TGF-β1) is released from the bone surface and recruits MSCs to bone-resorptive sites, where they undergo differentiation into mature osteoblasts, thus coupling bone resorption with bone formation[17]. However, the osteogenic nature of the microenvironment at bone-resorptive sites is not well known. IGF-1 is the most abundant growth factor that is deposited in the bone matrix[12,18–20] and has been implicated in the coupling process through its actions on MSC differentiation *in vitro*[21]. In this study, we found that the concentrations of IGF-1 in bone marrow and matrix were lower in aged rats than in young rats and were closely associated with the change in bone volume in these rats, whereas blood serum concentrations of IGF-1 remained relatively steady during aging. We also found that IGF-1 released from the bone matrix during bone resorption generates an osteogenic microenvironment and induces the differentiation of recruited MSCs for new bone formation. Notably, IGF-1 activates mTOR through the phosphoinositide-3-kinase (PI3K)–thymoma viral proto-oncogene 1 (Akt) pathway to induce differentiation of MSCs into osteoblasts. Thus, we postulate that a primary function of IGF-1 in the bone matrix is to maintain bone mass and skeletal homeostasis during bone remodeling.

RESULTS

Knockout of *Igf1r* impairs bone formation in adult mice

To understand the role of IGF-1 in the maintenance of bone mass during bone remodeling, we first examined whether knockout of IGF-1 type 1 receptor (*Igf1r*) in the osteoprogenitor cells committed

[1]Department of Orthopaedic Surgery, Johns Hopkins University School of Medicine, Baltimore, Maryland, USA. [2]School of Medicine, Shihezi University, Shihezi, Xinjiang, China. [3]Center for Clinical & Translational Research, Maine Medical Center Research Institute, Scarborough, Maine, USA. [4]Department of Pediatrics, Johns Hopkins University School of Medicine, Baltimore, Maryland, USA. [5]Laboratorio de Biología Celular, Instituto de Nutrición y Tecnología de los Alimentos (INTA), The University of Chile, Santiago, Chile. [6]Department of Biomedical Engineering, Johns Hopkins University School of Medicine, Baltimore, Maryland, USA. [7]Division of Endocrinology, Diabetes and Bone Diseases, Mount Sinai School of Medicine, New York, New York, USA. [8]Department of Genetics and Development, Columbia University, New York, New York, USA. Correspondence should be addressed to X.C. (xcao11@jhmi.edu).

Received 7 March; accepted 18 April; published online 24 June 2012; doi:10.1038/nm.2793

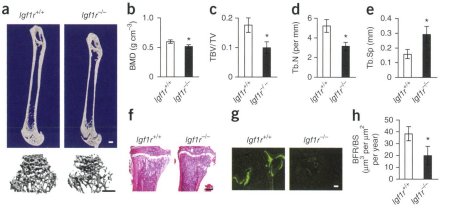

Figure 1 Low bone formation during bone remodeling in *Igf1r*$^{-/-}$ mice. (**a**) Representative micro-CT images of femora from a 3-month-old female *Igf1r*$^{-/-}$ mouse and a *Igf1r*$^{+/+}$ littermate. Scale bars, 1 mm. (**b**–**e**) Quantitative micro-CT analysis of the secondary spongiosa of proximal tibiae. Volumetric BMD (**b**), trabecular bone volume fraction (TBV/TV) (**c**), trabecular number (Tb.N) (**d**) and trabecular separation (Tb.Sp) (**e**) are shown. (**f**) H&E histological sections of tibiae from 3-month-old *Igf1r*$^{+/+}$ and *Igf1r*$^{-/-}$ mice. Scale bar, 1 mm. (**g**) Calcein double labeling of the metaphyseal trabecular bone at distal femora. Scale bar, 1 mm. (**h**) Bone formation rate per bone surface (BFR/BS). All data are mean ± s.e.m. $n = 10$. $^*P < 0.05$ by one-way analysis of variance (ANOVA) followed by *t* test.

lower in 3-month-old *Igf1r*$^{-/-}$ mice than in their *Igf1r*$^{+/+}$ littermates of the same age (**Fig. 1a**,**b**). In particular, *Igf1r*$^{-/-}$ mice had a significantly lower trabecular bone volume and thickness and a greater trabecular bone space relative to their *Igf1r*$^{+/+}$ littermates ($P < 0.05$) (**Fig. 1c**–**e**).

We found similar results in H&E-stained sections and in histomorphometric analyses (**Fig. 1f** and **Supplementary Fig. 2**). The trabecular bone deficiency in female *Igf1r*$^{-/-}$ mice was more substantial than that in their male *Igf1r*$^{-/-}$ littermates (**Supplementary Fig. 2**), probably as a result of the dependency of IGF-1 action on estrogen in bone[23]. An analysis of calcein double labeling showed a lower dynamic bone formation rate in *Igf1r*$^{-/-}$ mice than in *Igf1r*$^{+/+}$ mice (**Fig. 1g**,**h**). Notably, periosteal bone formation was not affected in *Igf1r*$^{-/-}$ mice (**Supplementary Fig. 2g**). The results suggest a crucial role of IGF-1 in maintaining bone homeostasis in adult mice.

to the osteoblast lineage would reduce bone mass in adult mice. To achieve such a cell type-specific knockout, we crossed floxed *Igf1r* mice with Osx-GFP::Cre mice (which express a GFP-Cre fusion protein under the direction of the *Osx1* promoter[22]) to generate conditional *Igf1r* knockout mice (called here *Igf1r*$^{-/-}$) (**Supplementary Fig. 1a**,**b**) that express GFP in *Igf1r*-deficient cells. For both genders, the sizes of the newborn *Igf1r*$^{-/-}$ mice were similar to those of their *Osx1-GFP::*Cre; *Igf1r*$^{+/+}$ control littermates (here referred to as *Igf1r*$^{+/+}$) (**Supplementary Fig. 1c**–**f**). BMD was

Igf1r$^{-/-}$ mice have fewer mature osteoblasts than wild type

To determine if the reduced BMD in the *Igf1r*$^{-/-}$ mice was the result of reduced numbers of osteoblasts, we next measured their numbers at different stages of differentiation by immunostaining femur sections of *Igf1r*$^{-/-}$ mice and their *Igf1r*$^{+/+}$ littermates. The numbers of runt related transcription factor 2 (Runx2)$^+$ and osterix-positive osteoprogenitors on the bone surfaces of *Igf1r*$^{-/-}$ mice were not significantly ($P > 0.05$) different from those in their *Igf1r*$^{+/+}$ littermates (**Fig. 2a**–**c**); however, the number of osteocalcin-positive mature osteoblasts on

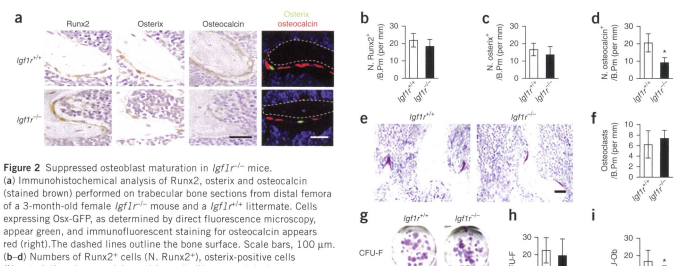

Figure 2 Suppressed osteoblast maturation in *Igf1r*$^{-/-}$ mice. (**a**) Immunohistochemical analysis of Runx2, osterix and osteocalcin (stained brown) performed on trabecular bone sections from distal femora of a 3-month-old female *Igf1r*$^{-/-}$ mouse and a *Igf1r*$^{+/+}$ littermate. Cells expressing Osx-GFP, as determined by direct fluorescence microscopy, appear green, and immunofluorescent staining for osteocalcin appears red (right).The dashed lines outline the bone surface. Scale bars, 100 μm. (**b**–**d**) Numbers of Runx2$^+$ cells (N. Runx2$^+$), osterix-positive cells (N. osterix$^+$) and osteocalcin-positive cells (N. osteocalcin$^+$) on the bone surface, measured as cells per millimeter of perimeter in sections (/B.Pm). All data are mean ± s.e.m. $n = 5$ mice. $^*P < 0.05$ by one-way ANOVA followed by *t* test. (**e**,**f**) Light micrographs of TRAP staining (dark purple) performed on trabecular bone sections from distal femora of mice. The number of osteoclasts on the bone surface (/B.Pm) was measured. All data are mean ± s.e.m. $n = 10$ mice. $^*P < 0.05$ by one-way ANOVA followed by *t* test. Scale bar, 100 μm. (**g**) CFU-F and CFU-Ob assays from harvested bone marrow of the mice, as indicated. Representative images of CFU-Fs stained with crystal violet (top) and representative images of CFU-Obs stained with Alizarin red (bottom). (**h**,**i**) Quantifications of the CFU-F and CFU-Ob assays. All data are the mean ± s.e.m. of triplicate cultures of bone marrow nucleated cells pooled from five individual mice. $^*P < 0.05$ by one-way ANOVA followed by *t* test.

the bone surfaces of *Igf1r*$^{-/-}$ mice was significantly lower than in their *Igf1r*$^{+/+}$ littermates ($P < 0.05$) (**Fig. 2a,d**).

Additionally, as the *Igf1r*$^{-/-}$ mice also express GFP, this allowed us to visualize endogenous cells with specific deletion of *Igf1r* in the pre-osteoblasts *in vivo*. The *Igf1r*-deficient osteoprogenitors were therefore GFP^{+} and were located primarily at the bone surface. However, *Igf1r*$^{-/-}$ mice had fewer osteocalcin-positive mature osteoblasts than *Igf1r*$^{+/+}$ mice (**Fig. 2a**). The number of tartrate-resistant acid phosphatase (TRAP)$^{+}$ mature osteoclasts in *Igf1r*$^{-/-}$ mice was not significantly different than that in their *Igf1r*$^{+/+}$ littermates ($P > 0.05$) (**Fig. 2e,f**). Colony-forming unit fibroblast (CFU-F) and colony-forming unit osteoblast (CFU-Ob) assays showed that the number of CFU-Fs in the *Igf1r*$^{-/-}$ mice was not significantly different than the number in their *Igf1r*$^{+/+}$ littermates ($P > 0.05$) (**Fig. 2g,h**); however, the number of CFU-Obs was lower in the *Igf1r*$^{-/-}$ mice than in their *Igf1r*$^{+/+}$ littermates ($P < 0.05$) (**Fig. 2g–i**). This finding further indicates that the lower number of mature osteoblasts on the bone surfaces of *Igf1r*$^{-/-}$ mice was probably the result of reduced differentiation of MSCs recruited to bone remodeling sites.

IGF-1 induces osteoblast differentiation through mTOR

We then sought to elucidate the signaling mechanism of IGF-1–induced osteogenic differentiation of MSCs by isolating mouse bone marrow cells and sorting them by flow cytometry. We defined MSCs as positive for stem cell antigen (Sca-1) and intergin β-1 (CD29) and negative for CD45 and CD11b, which represents the hematopoietic lineage, as previously reported[17]. Treatment with the PI3K inhibitor, LY294002 (10 μM), or the mTOR inhibitor, rapamycin (20 nM), impaired the MSC-mediated mineralization that was induced by IGF-1 but did not affect their cell growth or survival (**Fig. 3a**). In addition, IGF-1 stimulated the phosphorylation of the IGF-1 receptor (IGF1R), insulin receptor substrate 1 (IRS1), PI3K, Akt and mTOR in MSCs. Although treatment of the MSCs with LY294002 reduced the phosphorylation of PI3K, Akt and mTOR, treatment with rapamycin inhibited only the phosphorylation of mTOR (**Fig. 3b**), indicating that IGF-1 activates mTOR through the PI3K-Akt pathway in MSCs.

We also knocked down *Irs1* in MSCs with *Irs1*-targeting siRNA, which resulted in an inhibition in the IGF-1–induced (20 ng ml^{-1}, 15 min) phosphorylation of PI3K, Akt and mTOR (**Fig. 3c**), confirming that IRS1 mediates the IGF-1–induced activation of mTOR. Notably, rapamycin inhibited the IGF-1–induced expression of markers of osteoblast differentiation such as osterix (*Sp7*), *Runx2*, alkaline phosphatase (*Alp*), osteocalcin (*Bglap*), osteoglycin (*Ogn*) and osteoactivin (*Gpnmb*) (**Supplementary Fig. 3**).

To investigate the role of mTOR in IGF-1–induced MSC differentiation *in vivo*, we isolated MSCs from *Igf1r*$^{flox/flox}$ mice and deleted *Igf1r* in them using an adenovirus expressing Cre with GFP (Ad-Cre-GFP) or an adenovirus expressing GFP only (Ad-GFP) as a control. We transplanted Ad-Cre-GFP–treated MSCs (Ad-Cre-GFP MSCs) or Ad-GFP–treated MSCs (Ad-GFP MSCs) embedded in Matrigel underneath the renal capsules of immune-deficient *Rag2*$^{-/-}$ mice and injected each group of mice with rapamycin (3 mg per kg of body weight) or vehicle daily for 4 weeks. Ad-GFP MSCs underwent osteoblast differentiation and mineralization underneath the renal capsule, as shown by H&E staining, Alizarin red staining and immunohistology of osteocalcin staining (**Fig. 3d**). Similar to the results of the Ad-Cre-GFP MSCs, treatment with rapamycin inhibited the osteoblast differentiation and mineralization of Ad-GFP MSCs (**Fig. 3d**). Furthermore, we subcutaneously injected 6-week-old wild-type

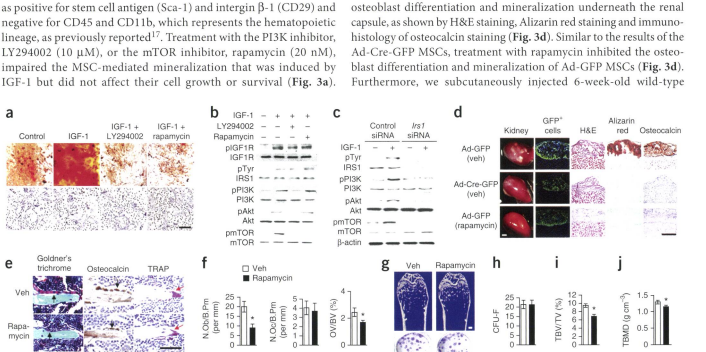

Figure 3 IGF-1 induces the osteoblastic differentiation of MSCs through the IRS-PI3K-Akt-mTOR pathway. (**a**) Alizarin red staining showing the osteoblastic differentiation of MSCs induced by IGF-1, as indicated (top). The number of live cells was determined by hematoxylin staining (bottom). Scale bar, 100 μm. (**b**) Western blot analysis of the IGF-1–induced phosphorylation of IGF1R (pIGF1R), phosphorylation of IRS1 at the tyrosine residue (pTyr), PI3K (pPI3K), Akt (pAkt) and mTOR (pmTOR) in MSCs treated with IGF-1 (20 ng ml^{-1}) or vehicle in the presence or absence of LY294002 (10 μM) or rapamycin (20 nM) for 15 min, as indicated. (**c**) Western blot analysis of the IGF-1–induced phosphorylation of IRS1, PI3K, Akt and mTOR in MSCs treated with IGF-1 after being transfected with *Irs1* siRNA or control siRNA. (**d**) IGF-1 induced the differentiation of MSCs underneath renal capsules. The renal sections were analyzed by direct GFP fluorescence visualization, H&E staining, Alizarin red staining or immunohistology for osteocalcin. Scale bars, 100 μm. Veh, vehicle. (**e–g**) Rapamycin impairs trabecular bone formation. (**e**) Representative images of mouse distal femora sections with Goldner's trichrome staining or staining for osteocalcin or TRAP. The black arrows indicate osteoblasts, and red arrows indicate osteoclasts. Scale bar, 100 μm. (**f,g**) Histomorphometric analysis of remodeling trabecular bone after treatment with rapamycin; shown are the number of osteoblasts (N.Ob) per bone perimeter, the number of osteoclasts (N.Oc) per bone perimeter, osteoid volume per bone volume (OV/BV; **f**) and representative micro-CT images of distal femora (**g**, top). Scale bar, 1 mm. (**g–j**) CFU-F assays (**g**(bottom),**h**), trabecular bone volume fraction (TBV/TV) (**i**) and the trabecular bone mineral density (TBMD) (**j**) are shown. All data are mean ± s.e.m. $n = 8$ mice. *$P < 0.05$ by one-way ANOVA followed by t test.

C57BL/6 mice with rapamycin daily (3 mg per kg body weight per day) for 4 weeks. The numbers of osteocalcin-positive osteoblasts on the bone surfaces of the C57BL/6 rapamycin-injected mice were significantly lower than in vehicle-injected littermates ($P < 0.05$), whereas the number of osteoclasts was the same in the two groups (**Fig. 3e,f**). In the rapamycin-injected group of C57BL/6 mice, we observed significantly less new bone formation and a lower trabecular bone mass compared to the vehicle-injected group by trichrome staining and a micro computed tomography (micro-CT) analysis. However, the number of CFU-Fs was not affected by introduction of rapamycin in either group (**Fig. 3e,g–j** and **Supplementary Table 1**). In summary, IGF-1 activates mTOR through the IRS1-PI3K-Akt pathway to regulate the osteoblast differentiation of MSCs for bone formation.

IGF-1 from bone matrix induces differentiation of MSCs

We know that recruited MSCs at bone-resorptive sites undergo differentiation and contribute to new bone formation, but the osteogenic nature of the microenvironment at bone-resorptive sites is not well known. We therefore examined the amount of phosphorylated IGF1R in the bone-resorption areas by co-staining for IGF1R and TRAP$^+$ osteoclasts in mouse femora. We found phosphorylated IGF1R primarily at the bone surfaces along bone-resorptive sites, as defined by the presence of mature TRAP$^+$ osteoclasts, whereas we found the IGF1R$^+$ cells to be evenly distributed in the bone marrow (**Fig. 4a**). This suggests that active IGF-1 is released during osteoclastic bone resorption. After bone marrow transplantation of Ad-Cre-GFP or Ad-GFP MSCs, we identified bone-marrow–transplanted GFP-labeled mouse MSCs on the bone surfaces by immunostaining with an antibody to GFP and quantified these cells. We found no significant difference in the number of GFP$^+$ cells on the bone surfaces of the group transplanted with Ad-Cre-GFP MSCs and the group transplanted with Ad-GFP MSCs at 2 weeks after bone marrow transplantation (**Fig. 4b,c**). There were significantly more GFP$^+$ MSCs embedded in the bone matrix of mice transplanted with Ad-GFP MSCs than in the bone matrix of the mice transplanted with Ad-Cre-GFP MSCs at 4 weeks after transplantation (**Fig. 4b,d**). We analyzed the survival rate of the transplanted GFP-labeled MSCs in the bone marrow of these mice by flow cytometry 2 weeks after transplantation, and the results indicate that deletion of *Igf1r* did not affect the survival rate of the MSCs in the bone marrow (**Supplementary Fig. 4**).

We reasoned that the IGF-1 released from the bone matrix comprises the osteogenic microenvironment for the induction of osteoblast differentiation. We cultured osteoclast precursors or mature osteoclasts from wild-type C57BL/6 mice with or without bone slices *in vitro* and collected the culture media to examine the effects on the osteoblastic differentiation of MSCs. Bone-resorption–conditioned media (BRCM) from mature osteoclasts containing bone slices had the highest capability to induce alkaline phosphatase (ALP) activity, a marker for osteoblast differentiation (**Fig. 4e**). We detected IGF-1 only in the BRCM from mature osteoclasts plus bone slices but not in any other conditioned media (**Fig. 4f**). We found that BRCM stimulated the phosphorylation of IGF1R, IRS1, PI3K, Akt and mTOR within 1 h after treatment (**Fig. 4g**). Furthermore, addition of an antibody specific for IGF-1 to the BRCM significantly inhibited the activity of ALP ($P < 0.05$), whereas treating the mature osteoclasts plus bone slices BRCM with noggin (an antagonist for bone morphogenetic protein) and other antibodies against IGF-II and PGDF had no effect or a minimal effect on ALP activity (**Fig. 4h**), suggesting that IGF-1 is the primary factor for the osteogenic microenvironment at bone-resorptive sites. Deletion of *Igf1r* in MSCs isolated from *Igf1r*$^{flox/flox}$ mice blocked the osteoblast differentiation induced by BRCM, as evident by both ALP staining and Alizarin red staining (**Fig. 4i,j**). Thus, IGF-1 released from the bone matrix induces the osteoblast differentiation of MSCs recruited by TGF-β1 in the process of coupling bone resorption with bone formation.

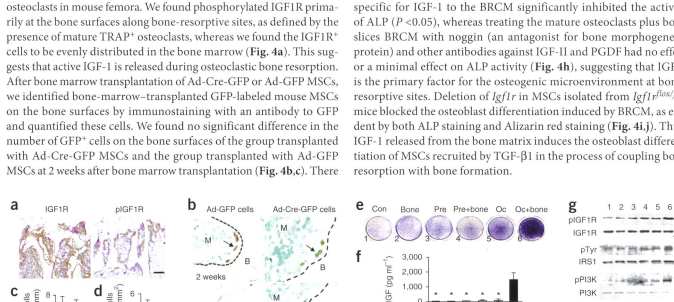

Figure 4 BRCM induces the osteogenic differentiation of MSCs. (**a**) Immunohistochemical analysis of the trabecular bone sections of mouse distal femora with antibodies to IGF1R (left) and pIGF1R (right). Scale bar, 200 μm. (**b**) Immunohistochemical analysis of femora sections of 3-month-old *Rag2*$^{-/c-}$ mice transplanted with GFP-labeled mouse MSCs (Ad-GFP cells or Ad-Cre-GFP cells) by antibody to GFP. Scale bar, 100 μm. B, bone; M, bone marrow. The arrows point to GFP$^+$ cells (stained brown), and the dashed lines indicate the bone surface. (**c**,**d**) Quantification of GFP$^+$ cells on the bone surface 2 weeks after transplantation (N. GFP$^+$/B.Pm) or in the bone matrix 4 weeks after transplantation (N. GFP$^+$/Bmx.Ar). $n = 5$ mice. $^*P < 0.05$ by one-way ANOVA followed by *t* test. (**e**) ALP staining for the differentiation potentials of MSCs cultured in various conditioned media, as indicated. Con, medium only (1); bone, bone slice only (2); pre, osteoclast precursor culture (3); pre+bone, osteoclast precursors cultured with bone slice (4); oc, osteoclast culture (5); oc+bone, osteoclasts cultured with bone (6). (**f**) ELISA analysis of IGF-1 concentrations in the BRCM. $n = 3$ repeats of each BRCM. $^*P < 0.05$ by one-way ANOVA followed by Dunnett's test compared to the oc+bone group. All data are mean ± s.e.m. (**g**) Western blot analysis of the effects of various conditioned media on the phosphorylation of IGF1R, IRS1, PI3K, Akt and mTOR in MSCs. (**h**) ALP staining for the differentiation potentials of MSCs cultured in BRCM with the addition of individual neutralizing antibodies (to Ig, PGDF, IGF-II or IGF-1) or noggin, as indicated. Con, conditioned media with no antibody. (**i**,**j**) ALP staining (**i**) and Alizarin red staining (**j**) for the effect of BRCM on the differentiation potentials of MSCs isolated from *Igf1r*$^{flox/flox}$ mice by infection with Ad-Cre-GFP or Ad-GFP (**j**, top). Western blot analysis of IGF1R in MSCs (**j**, bottom).

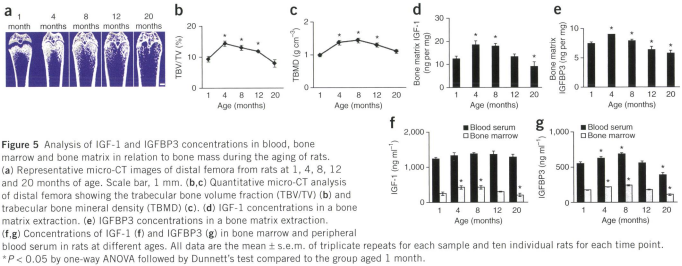

Figure 5 Analysis of IGF-1 and IGFBP3 concentrations in blood, bone marrow and bone matrix in relation to bone mass during the aging of rats. (**a**) Representative micro-CT images of distal femora from rats at 1, 4, 8, 12 and 20 months of age. Scale bar, 1 mm. (**b**,**c**) Quantitative micro-CT analysis of distal femora showing the trabecular bone volume fraction (TBV/TV) (**b**) and trabecular bone mineral density (TBMD) (**c**). (**d**) IGF-1 concentrations in a bone matrix extraction. (**e**) IGFBP3 concentrations in a bone matrix extraction. (**f**,**g**) Concentrations of IGF-1 (**f**) and IGFBP3 (**g**) in bone marrow and peripheral blood serum in rats at different ages. All data are the mean ± s.e.m. of triplicate repeats for each sample and ten individual rats for each time point. $^*P < 0.05$ by one-way ANOVA followed by Dunnett's test compared to the group aged 1 month.

Age-related bone loss is associated with bone matrix IGF-1

We assessed the concentrations of IGF-1 and IGFBP3 in the bone matrix and its potential correlation with the bone mass of wild-type rats at ages 1, 4, 8, 12 and 20 months. We found that the bone volume and bone mass in these rats increased steadily from 1 to 8 months after birth and then decreased continuously from 8 months of age onwards (**Fig. 5a–c**). We also observed PBM at 8 months of age. Notably, changes in the concentrations of IGF-1 and IGFBP3 in the bone matrix of the rats were well correlated with the changes in bone mass described above (**Fig. 5d,e**), and the number of osteoblasts decreased with higher age (**Supplementary Fig. 5a,b**). In contrast, the concentration of IGF-1 in the blood serum was much higher than that in bone marrow at all ages and did not decrease considerably with age ascension (**Fig. 5f**). However, blood sera IGFBP3 concentrations decreased in an age-dependent manner (**Fig. 5g**). Of note, in humans, IGF-1 and IGFBP3 concentrations in the bone martrix were also correlated with the changes in bone mass over aging[12]. Notably, we found that in individuals with osteoporosis with hip fractures, the concentration of IGF-1 in their bone marrow was 40% lower than in controls with normal bone mass (**Supplementary Fig. 5d** and **Supplementary Table 2**).

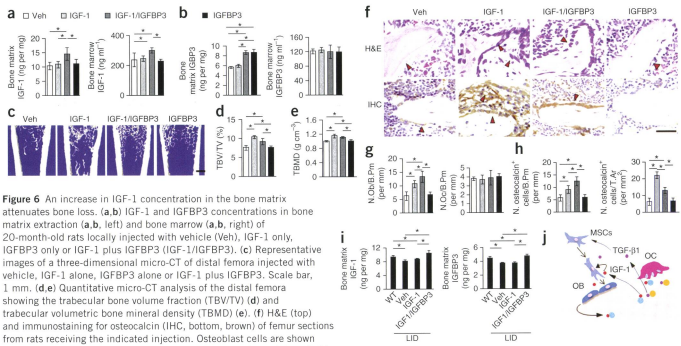

Figure 6 An increase in IGF-1 concentration in the bone matrix attenuates bone loss. (**a**,**b**) IGF-1 and IGFBP3 concentrations in bone matrix extraction (**a**,**b**, left) and bone marrow (**a**,**b**, right) of 20-month-old rats locally injected with vehicle (Veh), IGF-1 only, IGFBP3 only or IGF-1 plus IGFBP3 (IGF-1/IGFBP3). (**c**) Representative images of a three-dimensional micro-CT of distal femora injected with vehicle, IGF-1 alone, IGFBP3 alone or IGF-1 plus IGFBP3. Scale bar, 1 mm. (**d**,**e**) Quantitative micro-CT analysis of the distal femora showing the trabecular bone volume fraction (TBV/TV) (**d**) and trabecular volumetric bone mineral density (TBMD) (**e**). (**f**) H&E (top) and immunostaining for osteocalcin (IHC, bottom, brown) of femur sections from rats receiving the indicated injection. Osteoblast cells are shown with red arrowheads. Scale bar, 100 μm. (**g**) Number of osteoblasts (left) and osteoclasts (right) of remodeling trabecular bone quantified by histomorphometric analysis. (**h**) Quantification of osteocalcin-positive cells on the bone surface (left) and in the total tissue area (T.Ar, right). (**i**) Concentrations of IGF-1 (left) and IGFBP3 (right) in bone matrix extractions from LID mice or their wild-type littermates infused with vehicle, IGF-1 only or IGF-1 plus IGFBP3 by osmotic pumps. All data are mean ± s.e.m. $n = 10$ rats or mice. $^*P < 0.05$ by one-way ANOVA followed by Bonferroni test. (**j**) Schematic diagram of bone matrix IGF-1–induced osteoblast differentiation of MSCs during bone remodeling. TGF-β1 recruits MSCs to the bone-resorptive site in response to osteoclastic bone resorption, and IGF-1 released from the bone matrix comprises the osteogenic microenvironment for the differentiation of recruited MSCs. OB, osteoblast; OC, osteoclast.

To determine whether aging affects the potency of IGF1R activation on MSCs, we isolated bone marrow cells from rats at 1, 4 and 20 months of age for CFU-F assays. We picked a single colony and then expanded, cultured and treated it with IGF-1 (20 ng ml^{-1}) for 10 min. We found no remarkable differences in IGF1R activation in MSCs from young (1 month of age), adult (4 months of age) or old (20 months of age) rats by western blot analysis (**Supplementary Fig. 5e**). The correlation of bone matrix IGF-1 concentrations with bone mass quantifications suggests a crucial role for bone matrix IGF-1 in the maintenance of bone mass.

Administration of IGF-1 plus IGFBP3 attenuates bone loss

To assess whether IGFBP3 binds IGF-1 in the extracellular matrix and enhances its activity, we injected vehicle, IGF-1, IGFBP3 or IGF-1 plus IGFBP3 into the distal femur cavity of 20-month-old rats once a week for 4 weeks. We measured the concentrations of IGF-1 and IGFBP3 in the serum, bone marrow and bone matrix 10 d after the last injection. The concentrations of IGF-1 in the bone matrix and marrow were significantly higher in rats injected with IGF-1 plus IGFBP3 than in rats injected with IGF-1 only, IGFBP3 only or vehicle ($P < 0.05$) (**Fig. 6a**). The concentrations of IGFBP3 in the bone matrix were also higher in the rats injected with IGF-1 plus IGFBP3 and IGFBP3 only relative to the vehicle and IGF-1 only groups (**Fig. 6b**). Blood serum IGF-1 and IGFBP3 concentrations were the same in all injection groups (**Supplementary Fig. 5f**). This suggests that IGFBP3 could regulate IGF-1 deposition in the bone matrix and its lifespan in the bone marrow.

Of note, both bone volume and bone density were higher in rats injected with IGF-1 only or IGF-1 plus IGFBP3 than those injected with IGFBP3 only or vehicle (**Fig. 6c–e**). However, bone formation in the rats injected with IGF-1 only occurred in clusters that were structurally deficient of natural trabecular bone, whereas rats injected with IGF-1 plus IGFBP3 had improvements in bone mass and in bone microarchitecture (**Fig. 6c–f**). An analysis of contralateral control samples indicated that such changes in the trabecular bone are limited only to the injected femur (**Supplementary Fig. 5g–i**). H&E staining and immunohistology for osteocalcin in femur sections showed that a large number of osteoblast-like cells or osteocalcin-positive osteoblasts were scattered throughout the bone marrow in the rats injected with IGF-1 only (**Fig. 6c**). Notably, in the rats injected with IGF-1 plus IGFBP3, we found osteocalcin-positive osteoblasts primarily on the bone surface (**Fig. 6g,h**). We also found that osteoclast numbers did not change significantly between any of the injection groups.

These results indicate that IGFBP3 mediates the association of IGF-1 to the bone extracellular matrix for *de novo* bone formation at the bone surface. We therefore examined whether circulating IGF-1 and IGFBP3 can target and become immobilized in the bone matrix. We infused IGF-1, IGF-1 plus IGFBP3 or vehicle into the circulations of 4-week-old mice with liver-specific deletion of the IGF-1 gene (LID mice) using osmotic pumps for 4 weeks. Infusion of IGF-1 plus IGFBP3 led to significantly higher concentrations ($P < 0.05$) of both IGF-1 and IGFBP3 in the bone matrix of LID mice (**Fig. 6i**), as well as enhanced trabecular bone formation ($P < 0.05$), relative to LID mice infused with IGF-1 alone or with vehicle (**Supplementary Table 3**). Our results suggest that IGFBPs such as IGFBP3 facilitate the deposition of IGF-1 in the bone matrix for its function during bone remodeling.

DISCUSSION

Bone formation is an energy-consuming metabolic process in which there are major events of bone matrix synthesis and mineralization by osteoblasts. IGF-1 regulates new bone formation by acting more as a differentiation factor than as a mitogen for osteoblastic cells. We found that IGF-1 induced the osteoblast differentiation of MSCs through activation of the mTOR signaling pathway. Inhibition of mTOR activity with rapamycin blocked the IGF-1–induced osteoblast differentiation of MSCs, as well as their mineralization.

mTOR is crucial as a signaling molecule contributing to both the whole organ and to cellular energy metabolism in response to nutrient availability and environmental stimuli[24]. The mTOR pathway, when genetically downregulated, increases life span and stem cell homeostasis in evolutionarily diverse organisms such as mammals[24]. IGF-1 is also a key determinant of body size and lifespan in animals. Our results indicate that the regulation of osteoblast differentiation from MSCs in the bone remodeling unit by IGF-1 through mTOR may help explain the mechanism behind the regulation of body size and longevity by IGF-1(refs. 25,26). In addition, the mTOR complex has emerged as a key regulator of cell migration and chemotaxis[27], suggesting that IGF-1 may also facilitate the recruitment of MSCs in the coupling process during bone remodeling. In the coupling process, active IGF-1, released from the bone matrix during the resorptive phase, induces differentiation of MSCs that were recruited by TGF-β1, which was also released during the resorptive phase (**Fig. 6j**).

Although most efforts to prevent fracture in osteoporosis have been directed at inhibiting age-related bone loss, growing evidence suggests that bone mass maintenance during early adult life is a key contributor to bone strength during aging[12,28–31]. IGF-1 is the most abundant growth factor that is deposited in the bone matrix throughout the mammalian lifetime[32]. IGF-1 concentrations in the circulation and the bone matrix decline substantially with age in both men and women[33–35], probably as a result of a reduction in growth hormone secretion. Notably, a previous study reported that skeletal IGF-1 content in human bones also declines almost 60% between the ages of 20 and 60 years[36]. Circulating IGF-1 concentrations are much higher in rodents than in humans, and the circulating concentrations of IGF-II in humans are higher than those of IGF-1. Furthermore, IGF-1 concentrations in blood serum do not change with age in rats, whereas in humans they progressively decline with age to less than 100 ng ml^{-1} at around 60 years of age. However, despite these differences, it should be noted that the concentrations of IGF-1 in the bone matrix in both humans and rodents decrease with age.

In this study, we found that IGF-1 concentrations were significantly ($P < 0.05$) lower in the bone marrow of individuals with osteoporosis with low bone mass compared to individuals with osteoarthritis with normal bone mass. Although the subjects with osteoarthritis and those with osteoporosis were age matched, one limitation of our study was that we could not evaluate healthy aged controls. Despite this limitation and consistent with our findings, a previous clinical trial reported that individuals with a hip fracture that were treated with a complex of IGF-1 plus IGFBP3 had marked functional improvements and a blunting in femoral bone loss compared to vehicle-treated control subjects with osteoporosis after hip fracture[37]. Administration of IGF-1 alone has not been shown to enhance bone mass or improve functional outcomes in older individuals. Currently available clinical observations and our rodent results suggest that the essential pool of IGF-1 in the bone matrix may not be sufficiently available for new bone formation during the aging process. Therefore, modulation of IGF-1 deposition in the bone matrix could potentially be a therapeutic approach to delay or prevent osteoporosis.

METHODS

Methods and any associated references are available in the online version of the paper.

Note: Supplementary information is available in the online version of the paper.

ACKNOWLEDGMENTS

The project described was supported by grant AR 053973 (X.C.) from NIAMS/NIH. J.C. is supported by grant T32DK007751v from the US National Institutes of Health. The authors thank B.J. Canning (Asthma and Allergy Center, Johns Hopkins University) for providing guinea pig marrow cells.

AUTHOR CONTRIBUTIONS

L.X., X.W., M.L. and L.P. performed the majority of the experiments, analyzed data and prepared the manuscript. T.Q. maintained mice, collected tissue samples and helped with micro-CT analyses. L.P. helped with the *in vitro* transwell migration assay. J.P.R. finished the human sample detection. X.J. and L.Z. assisted with rat *in vivo* experiments. J.C., F.F., C.J.R., S.Y., S.X., A.E. and M.W. provided suggestions for the project and critically reviewed the manuscript. X.C. supervised the project and wrote most of the manuscript.

COMPETING FINANCIAL INTERESTS

The authors declare no competing financial interests.

Published online at http://www.nature.com/doifinder/10.1038/nm.2793.
Reprints and permissions information is available online at http://www.nature.com/reprints/index.html.

1. Rizzoli, R., Bianchi, M.L., Garabedian, M., McKay, H.A. & Moreno, L.A. Maximizing bone mineral mass gain during growth for the prevention of fractures in the adolescents and the elderly. *Bone* **46**, 294–305 (2010).
2. Schettler, A.E. & Gustafson, E.M. Osteoporosis prevention starts in adolescence. *J. Am. Acad. Nurse Pract.* **16**, 274–282 (2004).
3. Teitelbaum, S.L. Bone resorption by osteoclasts. *Science* **289**, 1504–1508 (2000).
4. Zaidi, M. Skeletal remodeling in health and disease. *Nat. Med.* **13**, 791–801 (2007).
5. Agnusdei, D. & Gentilella, R. GH and IGF-I as therapeutic agents for osteoporosis. *J. Endocrinol. Invest.* **28**, 32–36 (2005).
6. Belfiore, A., Frasca, F., Pandini, G., Sciacca, L. & Vigneri, R. Insulin receptor isoforms and insulin receptor/insulin-like growth factor receptor hybrids in physiology and disease. *Endocr. Rev.* **30**, 586–623 (2009).
7. Giustina, A., Mazziotti, G. & Canalis, E. Growth hormone, insulin-like growth factors, and the skeleton. *Endocr. Rev.* **29**, 535–559 (2008).
8. Yakar, S. & Rosen, C.J. From mouse to man: redefining the role of insulin-like growth factor-I in the acquisition of bone mass. *Exp. Biol. Med. (Maywood)* **228**, 245–252 (2003).
9. Yakar, S., Pennisi, P., Wu, Y., Zhao, H. & LeRoith, D. Clinical relevance of systemic and local IGF-I. *Endocr. Dev.* **9**, 11–16 (2005).
10. Amin, S. *et al.* High serum IGFBP-2 is predictive of increased bone turnover in aging men and women. *J. Bone Miner. Res.* **22**, 799–807 (2007).
11. Ohlsson, C. *et al.* The role of liver-derived insulin-like growth factor-I. *Endocr. Rev.* **30**, 494–535 (2009).
12. Seck, T. *et al.* Concentration of insulin-like growth factor (IGF)-I and -II in iliac crest bone matrix from pre- and postmenopausal women: relationship to age, menopause, bone turnover, bone volume, and circulating IGFs. *J. Clin. Endocrinol. Metab.* **83**, 2331–2337 (1998).
13. Yamaguchi, T. *et al.* Serum levels of insulin-like growth factor (IGF); IGF-binding proteins-3, -4, and -5; and their relationships to bone mineral density and the risk of vertebral fractures in postmenopausal women. *Calcif. Tissue Int.* **78**, 18–24 (2006).
14. Hill, P.A. Bone remodelling. *Br. J. Orthod.* **25**, 101–107 (1998).
15. Abe, E. *et al.* TSH is a negative regulator of skeletal remodeling. *Cell* **115**, 151–162 (2003).
16. Mundy, G.R. & Elefteriou, F. Boning up on ephrin signaling. *Cell* **126**, 441–443 (2006).
17. Tang, Y. *et al.* TGF-β1–induced migration of bone mesenchymal stem cells couples bone resorption with formation. *Nat. Med.* **15**, 757–765 (2009).
18. Bautista, C.M., Mohan, S. & Baylink, D.J. Insulin-like growth factors I and II are present in the skeletal tissues of ten vertebrates. *Metabolism* **39**, 96–100 (1990).
19. Canalis, E., Pash, J., Gabbitas, B., Rydziel, S. & Varghese, S. Growth factors regulate the synthesis of insulin-like growth factor-I in bone cell cultures. *Endocrinology* **133**, 33–38 (1993).
20. Pfeilschifter, J. *et al.* Parathyroid hormone increases the concentration of insulin-like growth factor-I and transforming growth factor β 1 in rat bone. *J. Clin. Invest.* **96**, 767–774 (1995).
21. Hayden, J.M., Mohan, S. & Baylink, D.J. The insulin-like growth factor system and the coupling of formation to resorption. *Bone* **17**, 93S–98S (1995).
22. Rodda, S.J. & McMahon, A.P. Distinct roles for Hedgehog and canonical Wnt signaling in specification, differentiation and maintenance of osteoblast progenitors. *Development* **133**, 3231–3244 (2006).
23. Callewaert, F., Sinnesael, M., Gielen, E., Boonen, S. & Vanderschueren, D. Skeletal sexual dimorphism: relative contribution of sex steroids, GH-IGF1, and mechanical loading. *J. Endocrinol.* **207**, 127–134 (2010).
24. Russell, R.C., Fang, C. & Guan, K.L. An emerging role for TOR signaling in mammalian tissue and stem cell physiology. *Development* **138**, 3343–3356 (2011).
25. Harrison, D.E. *et al.* Rapamycin fed late in life extends lifespan in genetically heterogeneous mice. *Nature* **460**, 392–395 (2009).
26. Selman, C. *et al.* Ribosomal protein S6 kinase 1 signaling regulates mammalian life span. *Science* **326**, 140–144 (2009).
27. Liu, L. & Parent, C.A. Review series: TOR kinase complexes and cell migration. *J. Cell Biol.* **194**, 815–824 (2011).
28. Blüher, M., Kahn, B.B. & Kahn, C.R. Extended longevity in mice lacking the insulin receptor in adipose tissue. *Science* **299**, 572–574 (2003).
29. Bonjour, J.P., Chevalley, T., Ferrari, S. & Rizzoli, R. The importance and relevance of peak bone mass in the prevalence of osteoporosis. *Salud Publica Mex.* **51** (suppl. 1), S5–S17 (2009).
30. Liu, J.M. *et al.* IGF-1 as an early marker for low bone mass or osteoporosis in premenopausal and postmenopausal women. *J. Bone Miner. Metab.* **26**, 159–164 (2008).
31. Ohlsson, C. *et al.* Older men with low serum IGF-1 have an increased risk of incident fractures: the MrOS Sweden study. *J. Bone Miner. Res.* **26**, 865–872 (2011).
32. Hauschka, P.V., Mavrakos, A.E., Iafrati, M.D., Doleman, S.E. & Klagsbrun, M. Growth factors in bone matrix. Isolation of multiple types by affinity chromatography on heparin-Sepharose. *J. Biol. Chem.* **261**, 12665–12674 (1986).
33. Lamberts, S.W., van den Beld, A.W. & van der Lely, A.J. The endocrinology of aging. *Science* **278**, 419–424 (1997).
34. Tatar, M., Bartke, A. & Antebi, A. The endocrine regulation of aging by insulin-like signals. *Science* **299**, 1346–1351 (2003).
35. Ziv, E. & Hu, D. Genetic variation in insulin/IGF-1 signaling pathways and longevity. *Ageing Res. Rev.* **10**, 201–204 (2011).
36. Mohan, S. & Baylink, D.J. Serum insulin-like growth factor binding protein (IGFBP)-4 and IGFBP-5 levels in aging and age-associated diseases. *Endocrine* **7**, 87–91 (1997).
37. Boonen, S. *et al.* Musculoskeletal effects of the recombinant human IGF-I/IGF binding protein-3 complex in osteoporotic patients with proximal femoral fracture: a double-blind, placebo-controlled pilot study. *J. Clin. Endocrinol. Metab.* **87**, 1593–1599 (2002).

nature medicine

A new isoform of steroid receptor coactivator-1 is crucial for pathogenic progression of endometriosis

Sang Jun Han[1], Shannon M Hawkins[2,3], Khurshida Begum[1], Sung Yun Jung[1,4], Ertug Kovanci[2,3], Jun Qin[1,4], John P Lydon[1], Francesco J DeMayo[1] & Bert W O'Malley[1]

Endometriosis is considered to be an estrogen-dependent inflammatory disease, but its etiology is unclear. Thus far, a mechanistic role for steroid receptor coactivators (SRCs) in the progression of endometriosis has not been elucidated. An SRC-1–null mouse model reveals that the mouse *SRC-1* gene has an essential role in endometriosis progression. Notably, a previously unidentified 70-kDa SRC-1 proteolytic isoform is highly elevated both in the endometriotic tissue of mice with surgically induced endometriosis and in endometriotic stromal cells biopsied from patients with endometriosis compared to normal endometrium. *Tnf*$^{-/-}$ and *Mmp9*$^{-/-}$ mice with surgically induced endometriosis showed that activation of tumor necrosis factor α (TNF-α)–induced matrix metallopeptidase 9 (MMP9) activity mediates formation of the 70-kDa SRC-1 C-terminal isoform in endometriotic mouse tissue. In contrast to full-length SRC-1, the endometriotic 70-kDa SRC-1 C-terminal fragment prevents TNF-α–mediated apoptosis in human endometrial epithelial cells and causes the epithelial-mesenchymal transition and the invasion of human endometrial cells that are hallmarks of progressive endometriosis. Collectively, the newly identified TNF-α–MMP9–SRC-1 isoform functional axis promotes pathogenic progression of endometriosis.

The defining feature of endometriosis is that endometrial tissues deposit to and grow in sites outside of the uterine cavity[1]. The pathogenesis of endometriosis remains under debate despite extensive research. Among the hypotheses are Sampson's retrograde menstruation theory, which proposes that endometrial cells are refluxed through the fallopian tubes during menstruation and then are implanted onto the peritoneum or pelvic organs. In addition to retrograde menstruation, however, other factors must be involved in the progression of endometriosis, as only 15% of all women of reproductive age have endometriosis even though retrograde menstruation is a common phenomenon.

Estrogen is considered to be one of the key modulators in the pathophysiology and/or pathogenesis of endometriosis because a considerable number of clinical reports have defined endometriosis as an estrogen-dependent disease[2,3]. The estrogen-dependent growth of endometriotic tissue is enhanced by high local estrogen concentrations that are mediated by aromatase[4]. Therefore, drugs that suppress estrogen production, such as gonadotropin-releasing hormone analogs and aromatase inhibitors, have been used in endometriosis treatments[5–7]. In addition to the elevation of local estrogen concentrations, the upregulation of the estrogen receptor β (ER-β) concentrations in endometriotic tissue is correlated with the progression of endometriosis[8]. The regulation of ER-β activity by selective estrogen receptor modulators has also been proffered as a potential treatment for endometriosis[9,10]. For example, treatment with ERB-041 (an ER-β–selective agonist) regressed ectopic lesion growth in mice with endometriosis[9]. Nevertheless, the role of ER-β in the estrogen-dependent progression of endometriosis has not been clearly elucidated.

Proinflammatory signaling also has an essential role in the progression of endometriosis because a number of cytokines in the peritoneal fluid of patients with endometriosis are actively involved in the pathogenesis and progression of the disorder[11,12]. Interference with the proinflammatory signaling in the peritoneal fluid has been used to suppress ectopic lesion growth. For example, treatment with a monoclonal antibody to tumor necrosis factor α (TNF-α) (c5N) in baboons with endometriosis substantially reduces the extent of endometriosis progression[13]. Nonsteroidal anti-inflammatory drugs, such as ibuprofen, also have been used for the treatment of endometriosis[14].

To advance their progression, endometriotic cells express aberrant, elevated concentrations of matrix metalloproteinases (MMPs) during their migration to, and implantation in, distinct anatomical sites[15]. Therefore, the inhibition of MMP activity by MMP inhibitor III may prevent the progression of endometriosis[16].

To precisely respond to external hormonal stimuli, SRCs dynamically modulate nuclear-receptor–mediated cellular processes in a tissue-selective manner. Accordingly, altered concentrations of SRCs and nuclear receptors in specific target tissues are frequently associated with human disease progression[17]. In endometriosis, lower full-length SRC-1 protein concentrations have been reported in endometriotic tissue compared to normal endometrium[18,19]. However, the role of SRC-1 in the progression of endometriosis has not been elucidated.

[1]Department of Molecular and Cellular Biology, Baylor College of Medicine, Houston, Texas, USA. [2]Department of Obstetrics, Baylor College of Medicine, Houston, Texas, USA. [3]Department of Gynecology, Baylor College of Medicine, Houston, Texas, USA. [4]Center for Molecular Discovery, Verna and Marrs McLean, Department of Biochemistry and Molecular Biology, Baylor College of Medicine, Houston, Texas, USA. Correspondence should be addressed to B.W.O. (berto@bcm.tmc.edu).

Received 23 December 2011; accepted 3 May 2012; published online 3 June 2012; doi:10.1038/nm.2826

Therefore, the object of this study was to investigate the functional role of the SRC-1 gene in the progression of endometriosis. Based on our results, we suggest that a newly identified SRC-1 isoform can be a new molecular target for therapy of this disease.

RESULTS

Endometriotic tissues contain a 70-kDa SRC-1 isoform

To investigate the role of SRCs in the progression of endometriosis, we used C57BL/6J mice with surgically induced endometriosis (SIE)[20] in parallel with primary human endometriotic stromal cells isolated from individuals who received a diagnosis of endometriosis. In our C57BL/6J mouse model, we successfully implanted endometrial fragments that eventually progressed to ectopic lesions in an estrogen-dependent manner in recipient C57BL/6J mice (**Supplementary Fig. 1a**,**b**). Next we determined the expression of cyclooxygenase-2 (COX-2) to validate the progression of endometriosis; COX-2 has been reported to be elevated in endometriotic endometrium compared to normal endometrium[21]. We found that endometriotic tissues of mice with SIE had higher COX-2 expression relative to the uterine tissue from sham-treated mice (**Supplementary Fig. 1c**). To investigate the expression profiles of SRCs in normal and endometriotic tissues, we divided the mice into two groups: sham treated, referring to the uterine tissue from ovariectomized mice that we treated with estradiol (E2) pellets and surgery but in which we did not implant an endometrial fragment; and endometriosis, referring to the ectopic and eutopic endometrium of ovariectomized mice with SIE in the presence of E2 pellets (**Fig. 1a**). We found that the uterine tissue of the sham-treated mice had a 160-kDa intact SRC-1 protein (**Fig. 1a**). However, the ectopic and eutopic endometrium of mice with SIE had lower amounts of full-length SRC-1 but higher amounts of a 70-kDa truncated form of SRC-1 compared to the sham-treated uterine tissue (**Fig. 1a**,**b**). To evaluate the nature of the 70-kDa fragment, we isolated uteri from ovariectomized SRC-1–null mice treated with E2 pellets. The uterine tissue from the SRC-1–null mice did not have intact full-length SRC-1 or the 70-kDa SRC-1 fragment (**Fig. 1c**). Therefore, the 70-kDa fragment was substantiated as an isoform of SRC-1. An immunostaining analysis revealed that SRC-1 isoform had similar endometrial-compartment–specific expression patterns (for example, in the luminal epithelium and stroma) as those of full-length SRC-1 in normal endometrium (**Fig. 1d**). However, we found that sham-treated uterine tissue primarily had an intact SRC-1 in the nuclei, but endometriotic tissue had the 70-kDa SRC-1 isoform in both the cytoplasm and the nuclei (**Fig. 1d**).

We then examined whether human endometriotic tissue also contained the 70-kDa SRC-1 isoform. We determined an SRC-1 expression profile in primary human endometrial stromal cells (HESCs) isolated from women without endometriosis ($n = 3$) and women with endometriosis ($n = 10$). We found that eight of ten primary HESCs from women with endometriosis had higher amounts of this 70-kDa truncated SRC-1 form compared to the primary HESCs of women without endometriosis (**Fig. 1e**,**f** and **Supplementary Fig. 2a**). Consistent with the findings in the SRC-1–null mice, SRC-1 knockdown in HESCs from women with endometriosis validated that the 70-kDa fragment is an SRC-1 isoform in humans (**Supplementary Fig. 2b**). We then examined whether an external hormone changed the amount of the 70-kDa SRC-1 isoform in human endometriotic stromal cells. We found that treatment with estrogen, progesterone or a combination of the two did not change the amount of the SRC-1 isoform in primary human endometriotic stromal cells in cell culture (**Supplementary Fig. 2d**–**h**). Primary human endometriotic stromal cells had variable

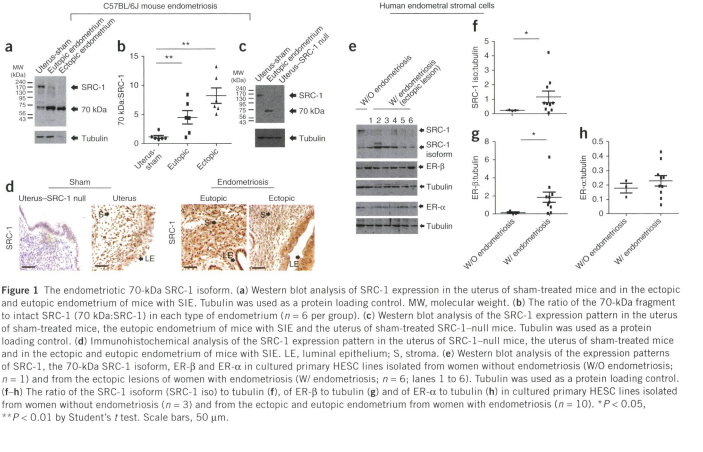

Figure 1 The endometriotic 70-kDa SRC-1 isoform. (**a**) Western blot analysis of SRC-1 expression in the uterus of sham-treated mice and in the ectopic and eutopic endometrium of mice with SIE. Tubulin was used as a protein loading control. MW, molecular weight. (**b**) The ratio of the 70-kDa fragment to intact SRC-1 (70 kDa:SRC-1) in each type of endometrium ($n = 6$ per group). (**c**) Western blot analysis of the SRC-1 expression pattern in the uterus of sham-treated mice, the eutopic endometrium of mice with SIE and the uterus of sham-treated SRC-1–null mice. Tubulin was used as a protein loading control. (**d**) Immunohistochemical analysis of the SRC-1 expression pattern in the uterus of SRC-1–null mice, the uterus of sham-treated mice and in the ectopic and eutopic endometrium of mice with SIE. LE, luminal epithelium; S, stroma. (**e**) Western blot analysis of the expression patterns of SRC-1, the 70-kDa SRC-1 isoform, ER-β and ER-α in cultured primary HESC lines isolated from women without endometriosis (W/O endometriosis; $n = 1$) and from the ectopic lesions of women with endometriosis (W/ endometriosis; $n = 6$; lanes 1 to 6). Tubulin was used as a protein loading control. (**f**–**h**) The ratio of the SRC-1 isoform (SRC-1 iso) to tubulin (**f**), of ER-β to tubulin (**g**) and of ER-α to tubulin (**h**) in cultured primary HESC lines isolated from women without endometriosis ($n = 3$) and from the ectopic and eutopic endometrium from women with endometriosis ($n = 10$). $^{*}P < 0.05$, $^{**}P < 0.01$ by Student's t test. Scale bars, 50 μm.

ratios of the SRC-1 isoform to full-length SRC-1 (**Fig. 1e** and **Supplementary Fig. 2a**). However, further examination of information about the subjects from which these cells came (**Supplementary Fig. 2c**) revealed that the differential ratio of the SRC-1 isoform to full-length SRC-1 was correlated with the site of biopsy. We detected the SRC-1 isoform predominantly in HESCs isolated from ectopic lesions of women with endometriosis (**Fig. 1e**). However, we found a low ratio of the SRC-1 isoform to full-length SRC-1 in the HESCs of the eutopic endometrium from these women (**Supplementary Fig. 2a**). Therefore, ectopic lesions had a higher SRC-1 processing activity compared to the eutopic endometrium. Also, the menstrual cycle did not affect the ratio of the SRC-1 isoform to full-length SRC-1.

In addition to the uterus, endometriosis affected the SRC-1 milieus of other organs of the abdominal cavity: the intestine and liver of mice with SIE had higher amounts of the endometriotic SRC-1 isoform compared to sham-treated mice (**Supplementary Fig. 2i**). We also found that the primary HESCs of women with endometriosis had higher expression of ER-β compared to normal primary HESCs, as has been described previously (**Fig. 1e,g** and **Supplementary Fig. 2a**)[22,23]. In contrast to ER-β, however, we found that the expression of ER-α was the same in HESCs of women with endometriosis as in HESCs of women without endometriosis (**Fig. 1e,h** and **Supplementary Fig. 2a**).

In addition to SRC-1, we found that endometriotic mouse tissue also had various altered forms of SRC-2 and SRC-3 (**Supplementary Fig. 3a,b**). However, only the ectopic lesions, and not the eutopic endometrium, had truncated forms of SRC-2 (110 kDa) and SRC-3 (85 kDa) in mice with SIE. In contrast to the SRC-1 isoform, we found that HESCs isolated from the ectopic lesions of women with endometriosis did not have the altered forms of SRC-2 and SRC-3 (**Supplementary Fig. 3c,d**). Collectively, these data reveal that mouse and human endometriotic tissues have the 70-kDa SRC-1 isoform but not the altered forms of SRC-2 and SRC-3.

Notably, we found that SRC-2–null and SRC-3–null ectopic lesions had a lower ectopic lesion volume compared to wild-type ectopic lesions in mice with SIE (**Supplementary Fig. 3e**). Therefore, the SRC-2 and SRC-3 genes might have a permissive or cooperative role with the SRC-1 isoform to modulate the growth of ectopic lesions in mice with SIE.

Mouse *SRC-1* modulates the progression of ectopic lesions

The finding of the endometriotic SRC-1 isoform raised the question of whether it is required for endometriosis to develop. To address this issue, we surgically induced endometriosis using SRC-1–null mice. We transplanted the endometrial tissue fragments generated from the uteri of SRC-1–null mice or congenic C57BL/6J mice into ovariectomized C57BL/6J recipient mice treated with E2 pellets to induce endometriosis. We found that the endometrial tissue fragments from C57BL/6J donors successfully developed into ectopic lesions (**Fig. 2a**). However, the deletion of the mouse *SRC-1* gene resulted in lower volumes of ectopic lesions by over 500% compared to the wild-type ectopic lesions (**Fig. 2a,b**). Therefore, the mouse *SRC-1* gene is an essential factor for the growth of ectopic lesions. To further validate the role of the mouse *SRC-1* gene in ectopic lesion growth in mice with

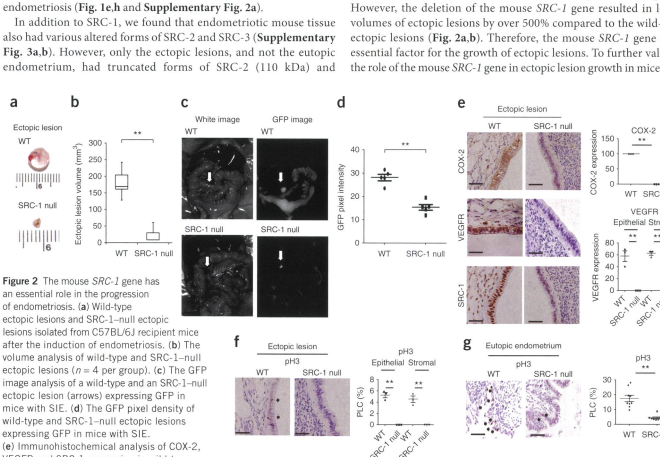

Figure 2 The mouse *SRC-1* gene has an essential role in the progression of endometriosis. (**a**) Wild-type ectopic lesions and SRC-1–null ectopic lesions isolated from C57BL/6J recipient mice after the induction of endometriosis. (**b**) The volume analysis of wild-type and SRC-1–null ectopic lesions ($n = 4$ per group). (**c**) The GFP image analysis of a wild-type and an SRC-1–null ectopic lesion (arrows) expressing GFP in mice with SIE. (**d**) The GFP pixel density of wild-type and SRC-1–null ectopic lesions expressing GFP in mice with SIE. (**e**) Immunohistochemical analysis of COX-2, VEGFR and SRC-1 expression in wild-type ectopic lesions and SRC-1–null ectopic lesions and the quantification of COX-2 and VEGFR expression in each type of ectopic lesion ($n = 3$ per group). (**f**,**g**) Immunohistochemical analysis of the expression of phosphorylated H3 (pH3, arrows) and activated caspase 3 (arrows) in wild-type and SRC-1–null ectopic lesions (**f**) or in wild-type and SRC-1–null eutopic endometrium (**g**) and a quantification of their expression in each type of ectopic lesion ($n = 3$ per group) and eutopic endometrium ($n = 9$ per group). PLC, percentage of labeled cells. $^{**}P < 0.01$ by Student's t test. Scale bars, 50 μm.

SIE, we used GFP transgenic mice (C57BL/6-Tg(CAG-GFP)10sb/J) that ubiquitously express GFP in all tissue types. To obtain SRC-1–null uterine tissue that expressed GFP, we generated bigenic SRC-1 null; GFP mice by crossing SRC-1–null mice with the GFP-expressing transgenic mice. We isolated the wild-type and SRC-1–null uterine fragments expressing GFP and then implanted them into ovariectomized C57BL/6J recipient mice treated with E2 pellets to induce endometriosis. After the progression of endometriosis, we detected ectopic lesions expressing GFP in the mesenteric membrane of recipient mice under a fluorescence dissecting microscope (**Fig. 2c**). The SRC-1–null ectopic lesions had a lower density of GFP compared to the wild-type ectopic lesions (**Fig. 2d**).

To further analyze the growth defects in the ectopic lesions stemming from SRC-1–null endometrial fragments, we determined the expression of COX-2 and of the vascular endothelial growth factor receptor (VEGFR) because endometriotic tissues have higher COX-2 and VEGFR expression relative to normal tissues[24,25]. We found that SRC-1–null ectopic lesions had lower expression of both endometriosis marker genes compared to wild-type ectopic lesions (**Fig. 2e**). In addition, an analysis of the concentration of phosphorylated histone H3 revealed that the SRC-1–null ectopic lesions also had lower proliferative activity relative to wild-type ectopic lesions (**Fig. 2f**). However, we found that SRC-1–null ectopic lesions had higher amounts of active caspase 3 compared to wild-type ectopic lesions (**Fig. 2f**). In addition to ectopic lesions, we found that the proliferative activity and apoptosis signaling were also lower and higher, respectively, in SRC-1–null eutopic endometrium compared to wild-type eutopic endometrium of mice with SIE (**Fig. 2g**). Collectively, these results suggest that the mouse *SRC-1* gene has a similar effect on both the ectopic and eutopic endometrium of mice with SIE.

The derivation of the 70-kDa isoform of SRC-1

We next attempted to discern the exact origin of the SRC-1 isoform in endometriotic tissue. A northern blot analysis with a probe against full-length mouse SRC-1 revealed that the SRC-1 mRNA expression patterns in the eutopic endometrium of mice with SIE were the same as those in the sham-treated uterine tissue (**Supplementary Fig. 4**). This result implied that the SRC-1 isoform is not an alternative RNA splicing variant but may be a post-translational and site-specific protease-mediated proteolytic cleavage product.

To identify the SRC-1 isoform, we used a heterologous mouse model of endometriosis with severe combined immune deficiency (SCID) mutant mice and immortalized human endometrial cells, as previously described[26]. We used immortalized human endometrial epithelial cells (IHEECs) obtained by stably transfecting the catalytic subunit (hTERT) of the human telomerase complex[27] and immortalized human endometrial stromal cell lines (IHESCs) generated by the transfection of hTERT using a retroviral system[28]. To determine whether the endometriotic SRC-1 isoform contained the N terminus or the C terminus, we modified human *SRC1* complementary DNA by adding a Flag tag on the N-terminal region and a MYC tag on the C-terminal region (resulting in a gene we refer to here as F-*SRC1*-M). Using this lentiviral vector containing the F-*SRC1*-M gene, we modified IHEECs and IHESCs to stably express the exogenous F-*SRC1*-M gene. To efficiently induce endometriosis in the SCID mouse model, we mixed and cultured recombinant IHESCs expressing F-SRC-1-M with recombinant IHEECs expressing F-SRC-1-M on Matrigel because paracrine communication between the stromal and epithelial compartments is a crucial factor for modulating endometrial function *in vivo*[29]. We then transplanted the mixed-cultured recombinant human endometrial cells into the pelvic cavities of ovariectomized SCID mice treated with E2 pellets (**Fig. 3a**). To precisely analyze the exogenous F-SRC-1-M processing pattern in ectopic lesions using antibodies to the Flag and MYC tags, we produced another type of ectopic lesion using the transplantation of mixed-cultured parental IHESCs and IHEECs into SCID mice because ectopic lesions that are developed from the parental human endometrial cells do not express F-SRC-1-M (**Fig. 3a**).

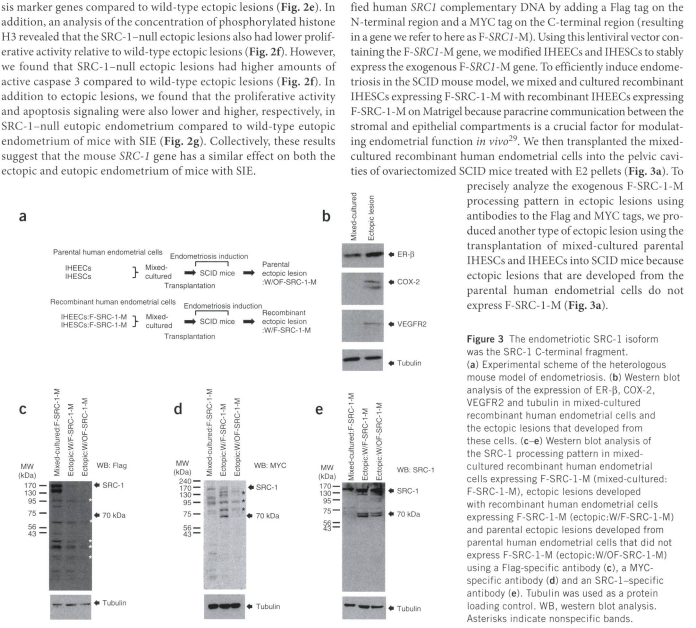

Figure 3 The endometriotic SRC-1 isoform was the SRC-1 C-terminal fragment. (**a**) Experimental scheme of the heterologous mouse model of endometriosis. (**b**) Western blot analysis of the expression of ER-β, COX-2, VEGFR2 and tubulin in mixed-cultured recombinant human endometrial cells and the ectopic lesions that developed from these cells. (**c**–**e**) Western blot analysis of the SRC-1 processing pattern in mixed-cultured recombinant human endometrial cells expressing F-SRC-1-M (mixed-cultured: F-SRC-1-M), ectopic lesions developed with recombinant human endometrial cells expressing F-SRC-1-M (ectopic:W/F-SRC-1-M) and parental ectopic lesions developed from parental human endometrial cells that did not express F-SRC-1-M (ectopic:W/OF-SRC-1-M) using a Flag-specific antibody (**c**), a MYC-specific antibody (**d**) and an SRC-1–specific antibody (**e**). Tubulin was used as a protein loading control. WB, western blot analysis. Asterisks indicate nonspecific bands.

We found that the ectopic lesions were well developed in ~80% of the SCID mice that we transplanted with mixed-cultured human endometrial cells (**Supplementary Fig. 5a–c**). Immunostaining with antibodies to vimentin (an endometrial stromal cell biomarker) and cytokeratin 18 (an endometrial epithelial cell biomarker) revealed that ectopic lesions successfully developed from mixed cultures of IHEECs and IHESCs (**Supplementary Fig. 5d–f**). In addition, we found that human ectopic lesions developed in SCID mice had higher expressions of several endometriosis marker genes (such as the ER-β, VEGFR2 and COX-2 genes) compared to the mixed-cultured human endometrial cells (**Fig. 3b**). Therefore, the mixed-cultured IHEECs and IHESCs successfully developed into typical ectopic lesions in SCID mice.

For the identification of the SRC-1 isoform present in the ectopic lesions that developed in the SCID mice, we conducted a western blot analysis with antibodies to the Flag or MYC peptides. We found that the antibody to Flag did not detect the 70-kDa SRC-1 isoform or any SRC-1 fragments of other sizes in recombinant ectopic lesions expressing F-SRC-1-M (**Fig. 3c**). In contrast to the antibody to Flag, however, the antibody to MYC recognized the 70-kDa protein in recombinant ectopic lesions expressing F-SRC-1-M but not in the control ectopic lesions expressing no F-SRC-1-M (**Fig. 3d**). We found that this 70-kDa fragment containing the MYC tag in recombinant ectopic lesions was also recognized by the antibody to SRC-1 that we used for the detection of the 70-kDa SRC-1 isoform in endometriotic mouse tissue (**Fig. 3e**). Therefore, the 70-kDa SRC-1 isoform in endometriotic tissues is a post-translational proteolytic C-terminal isoform of SRC-1.

The TNF-α–MMP9 axis generates endometriotic SRC-1 isoform

A protease cleavage site prediction program (http://pops.csse.monash.edu.au/pops-cgi/index.php) indicated that MMP9 can generate the 70-kDa SRC-1 C-terminal isoform from intact SRC-1 because SRC-1 has a potential MMP9 cleavage site at P790-M791. A gelatin zymography analysis revealed that the eutopic endometrium of mice with SIE and the primary HESCs from women with endometriosis had higher MMP9 activity compared to the endometrium of sham-treated mice and normal HESCs, respectively (**Fig. 4a,b**). In contrast to MMP9, however, both mouse and human endometriotic cells had very limited MMP2 activity (**Fig. 4a,b**). The inhibition of MMP9 activity by treatment with an inhibitor of MMP2 and MMP9 (MMP2/MMP9 inhibitor III) reduced the volume of the ectopic lesions in mice with SIE and did not produce the endometriotic 70-kDa SRC-1 C-terminal isoform in the eutopic endometrium (**Fig. 4c–e**). In addition to treatment with the MMP2/MMP9 inhibitor, the *Mmp9* gene also had an essential role in ectopic lesion growth because ectopic lesions in *Mmp9*$^{-/-}$ mice with SIE had a lower ectopic lesion volume compared to the wild-type ectopic lesions in congenic FVB/NJ mice (**Supplementary Fig. 6a**). In addition to the regression of ectopic lesion growth, we found that the eutopic endometrium of *Mmp9*$^{-/-}$ mice with SIE did not have the endometriotic SRC-1 isoform whereas eutopic endometrium of the congenic FVB/NJ mice with SIE did (**Supplementary Fig. 6b**). Collectively, these results suggested that MMP9 has an essential role in both ectopic lesion growth and the generation of the SRC-1 C-terminal isoform in the endometriotic tissue of mice with SIE.

How is MMP9 activity regulated in endometriotic tissues during the progression of endometriosis? Previous studies revealed

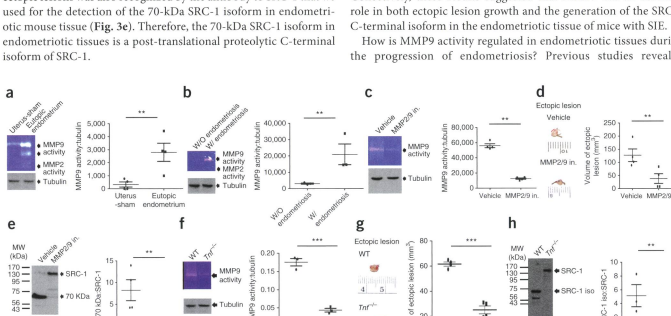

Figure 4 The TNF-α–MMP9 functional axis had an essential role in the progression of endometriosis and the formation of the endometriotic SRC-1 isoform in endometriotic tissue. (**a**) Gelatin zymography analysis of MMP9 and MMP2 activity in the uterus of sham-treated mice and in the eutopic endometrium of mice with SIE and the ratio of MMP9 activity to tubulin in each type of endometrium ($n = 4$ per group). (**b**) Gelatin zymography analysis of MMP9 and MMP2 activity in primary HESCs isolated from women without endometriosis (W/O endometriosis) and from women with endometriosis (W/ endometriosis) and the ratio of MMP9 activity to tubulin in each type of cell ($n = 3$ per group). (**c**) Gelatin zymography analysis of MMP9 activity in the eutopic endometrium of C57BL/6J mice with SIE treated with vehicle or MMP2/MMP9 inhibitor III (MMP2/9 in.) and the ratio of MMP9 activity to tubulin in each eutopic endometrium ($n = 4$ per group). (**d**) Ectopic lesions isolated from mice with SIE treated with vehicle or MMP2/MMP9 inhibitor III and a volume analysis of each isolated ectopic lesion ($n = 4$ per group). (**e**) Western blot analysis of the SRC-1 expression patterns in the eutopic endometrium of mice with SIE treated with vehicle or MMP2/MMP9 inhibitor III and the ratio of the 70-kDa SRC-1 isoform to intact SRC-1 in each type of endometrium. (**f**) Gelatin zymography analysis of MMP9 activity in the eutopic endometrium of *Tnf*$^{-/-}$ mice and congenic wild-type mice with SIE and the ratio of MMP9 activity to tubulin in each type of eutopic endometrium ($n = 3$ per group). (**g**) Ectopic lesions isolated from congenic wild-type mice and *Tnf*$^{-/-}$ mice with SIE and a volume analysis of each isolated ectopic lesion ($n = 4$ per group). (**h**) Western blot analysis of the expression patterns of SRC-1 in the eutopic endometrium of *Tnf*$^{-/-}$ mice and congenic wild-type mice with SIE and the ratio of the 70-kDa SRC-1 isoform to intact SRC-1 in each type of eutopic endometrium ($n = 3$ per group). $^{**}P < 0.01$, $^{***}P < 0.001$ by Student's t test.

that proinflammatory signaling is closely associated with tissue-remodeling pathways in inflammatory disease progression. For example, TNF-α induces the expression of invasion mediators, such as MMPs, to promote cell mobility[30]. In our mouse model, we also found that the eutopic and ectopic endometrium of mice with SIE had higher concentrations of TNF-α compared to normal endometrium (**Supplementary Fig. 6c**). Notably, gelatin zymography revealed that the eutopic endometrium of *Tnf*$^{-/-}$ mice with SIE had lower MMP9 activity than congenic wild-type mice with SIE (**Fig. 4f**). In addition to the lower MMP9 activity, we found that *Tnf*$^{-/-}$ mice with SIE had lower volumes of ectopic lesions than congenic wild-type mice with SIE (**Fig. 4g**). The eutopic endometrium of *Tnf*$^{-/-}$ mice with SIE did not have the SRC-1 isoform whereas the endometrium of wild-type mice with SIE did (**Fig. 4h**). Collectively, these results suggested that the induction of TNF-α signaling activates MMP9 to promote ectopic lesion growth and generate the SRC-1 C-terminal isoform in endometriotic tissue.

The above observation raised the issue of whether SRC-1 is a direct substrate for MMP9 in endometriotic tissue. To address this, we conducted *in vitro* MMP9 processing assays with the purified double-tagged F-SRC-1-M protein and activated recombinant MMP9 protein. The antibody to Flag revealed that recombinant MMP9 generated a 60-kDa N-terminal SRC-1 fragment *in vitro* (**Fig. 5a**). However, the human ectopic lesions that developed in SCID mice did not have this N-terminal SRC-1 fragment *in vivo* (**Fig. 3c**). In contrast to the antibody to Flag, MYC-specific antibody detected the 70-kDa SRC-1 C-terminal isoform (**Fig. 5b**). We found that this 70-kDa SRC-1 C-terminal fragment also was recognized by an SRC-1–specific antibody that has been used for the detection of SRC-1 isoforms in mouse endometriotic tissue (**Fig. 5c**). Therefore, MMP9 directly recognized SRC-1 and processed it to the 70-kDa SRC-1 C-terminal isoform *in vitro*. In contrast to MMP9, however, MMP2 did not produce the 70-kDa SRC-1 C-terminal isoform *in vitro* (**Supplementary Fig. 6d**).

The protease prediction program (http://pops.csse.monash.edu.au/pops-cgi/index.php) revealed that MMP9 can recognize the P790-M791 dipeptide in SRC-1 to process the 70-kDa SRC-1 C-terminal isoform. To confirm this prediction, we substituted Pro790 with alanine to generate an MMP9-cleavage–defective SRC-1 mutant (Pro790Ala) that had a Flag tag in the N-terminal region and a MYC tag in the C-terminal region. An *in vitro* MMP9 processing assay with the purified SRC-1 Pro790Ala mutant revealed that MMP9 also generated the same 60-kDa N-terminal SRC-1 fragment from the mutant as we found in wild-type SRC-1 (**Fig. 5d**). However, a western blot analysis with the MYC-specific antibody revealed that MMP9 did not generate the 70-kDa SRC-1 C-terminal isoform from the SRC-1 Pro790Ala mutant *in vitro* (**Fig. 5e**). The antibody to SRC-1 also did not recognize the 70-kDa fragment from the SRC-1 Pro790Ala mutant after incubation with MMP9 (**Fig. 5f**). These findings indicated that MMP9 cleaved SRC-1 at the P790-M791 site to produce the 70-kDa SRC-1 C-terminal isoform *in vitro*.

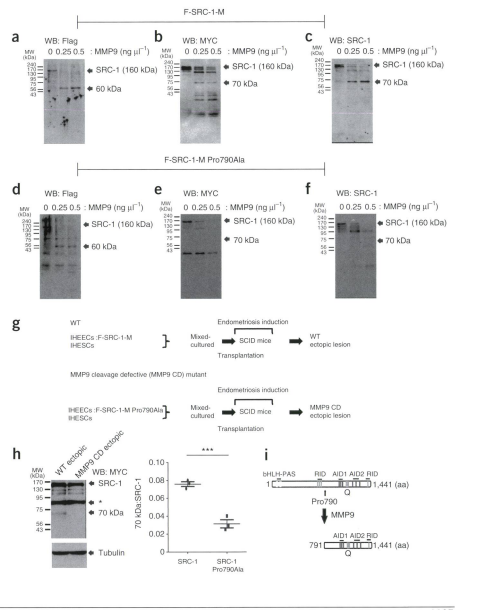

Figure 5 MMP9 directly cleaved human SRC-1 at P790-M791 *in vitro* and *in vivo*. (**a**–**c**) Western blot analysis of the resulting processed forms of SRC-1 by MMP9 with antibodies to Flag (**a**), MYC (**b**) or SRC-1 (**c**). (**d**–**f**). Western blot analysis of the resulting processed forms of the SRC-1 Pro790Ala mutant by MMP9 with antibodies to Flag (**d**), MYC (**e**) and SRC-1 (**f**). (**g**) Experimental scheme for the transplantation of recombinant IHEECs stably expressing wild-type F-SRC-1-M or the F-SRC-1-M Pro790Ala mutant into SCID mice to induce endometriosis. (**h**) Western blot analysis of SRC-1 expression pattern in ectopic lesions expressing F-SRC-1-M or the F-SRC-1-M Pro790Ala mutant with a MYC-specific antibody and the ratio of the 70-kDa SRC-1 isoform to intact SRC-1 in each ectopic lesion ($n = 3$ per group). Asterisks indicate nonspecific bands. (**i**) The processing pattern of SRC-1 to the endometriotic SRC-1 C-terminal isoform (amino acids 791–1,441) by MMP9 in endometriotic tissues. bHLH, basic helix-loop-helix; PAS, period circadian protein, aryl hydrocarbon receptor nuclear translocator protein and single-minded protein; RID, receptor interacting domain; AID, activation domain; Q, proline-rich domain; aa, amino acid. $^{***}P < 0.001$ by Student's *t* test.

The above observation raised the question of whether MMP9 also cleaves the P790-M791 site of SRC-1 to produce the SRC-1 C-terminal isoform in endometriotic tissue *in vivo*. To address this, we transplanted mixed cultures of recombinant IHEECs stably expressing the F-SRC-1-M Pro790Ala mutant and IHESCs into SCID mice to induce ectopic lesions (**Fig. 5g**). A western blot analysis with the MYC-specific antibody revealed that ectopic lesions did not generate the 70-kDa isoform from the F-SRC-1-M Pro790Ala mutant (**Fig. 5h**). Taken together, these results suggest that MMP9 cleaves at the P790-M791 site of SRC-1 to generate the 70-kDa SRC-1 C-terminal isoform in endometriotic tissue (**Fig. 5i**).

The 70-kDa SRC-1 isoform and endometriosis progression

What is the differential role of the SRC-1 C-terminal isoform compared to full-length SRC-1 in endometriotic tissue? To address this question, we generated IHEECs that stably expressed the SRC-1

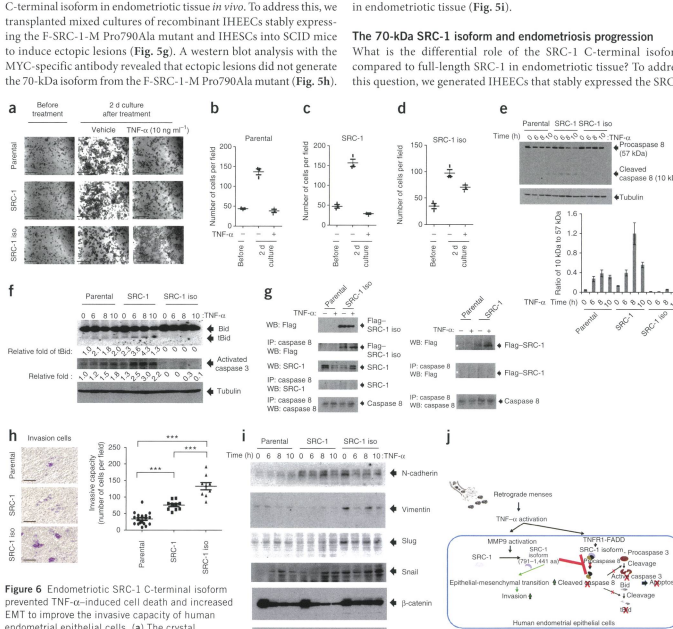

Figure 6 Endometriotic SRC-1 C-terminal isoform prevented TNF-α–induced cell death and increased EMT to improve the invasive capacity of human endometrial epithelial cells. (**a**) The crystal violet cell proliferation assay of parental IHEECs and recombinant IHEECs stably expressing full-length SRC-1 or the SRC-1 C-terminal isoform (SRC-1 iso) in the absence or presence of TNF-α. (**b**–**d**) The viable cell numbers of the parental IHEECs (**b**) and the recombinant IHEECs expressing full-length SRC-1 (**c**) or the SRC-1 isoform (**d**) per field at the indicated time points. (**e**) Western blot analysis of the expression of procaspase 8 (57 kDa) and its cleaved form (10 kDa) in parental IHEECs and recombinant IHEECs stably expressing full-length SRC-1 or the SRC-1 C-terminal isoform as a result of TNF-α treatment at the indicated time points and the ratio of the 10-kDa isoform to the 50-kDa isoform in each type of cell at the indicated time points ± s.d. (**f**) Western blot analysis of the expression of apoptosis markers (tBid and activated caspase 3) in parental IHEECs and recombinant IHEECs stably expressing full-length SRC-1 or the SRC-1 C-terminal isoform as a result of TNF-α treatment at the indicated time points. (**g**) Immunoprecipitation (IP) of caspase 8 with parental IHEECs or IHEECs stably expressing full-length SRC-1 (SRC-1) or the SRC-1 C-terminal isoform (SRC-1 iso) treated with vehicle or TNF-α. Western blot analysis of the amounts of the Flag-tagged SCR-1 (Flag–SRC-1) C-terminal isoform, SRC-1, Flag–SRC-1 and caspase 8 in immunoprecipitated pellets. Asterisks indicate nonspecific bands. (**h**) Transwell invasion assays of parental IHEECs and recombinant IHEECs stably expressing full-length SRC-1 or the SRC-1 C-terminal isoform and the average number of invasive cells per field at the indicated time points. (**i**) Western blot analysis of expression patterns of EMT markers (such as N-cadherin, vimentin, Slug, Snail, β-catenin and TCF8) in parental IHEECs and recombinant IHEECs stably expressing full-length SRC-1 or the SRC-1 C-terminal isoform as a result of TNF-α treatment at the indicated time points. (**j**) The TNF-α–MMP9–SRC-1 isoform functional axis in human endometriotic epithelial cells. TNFR1, tumor necrosis factor receptor superfamily, member 1a; FADD, Fas (TNFRSF6)-associated via death domain. ***$P < 0.001$ by Student's t test. Scale bars, 50 μm.

C-terminal isoform (amino acids 791–1,441) using a lentivirus-mediated gene transfer protocol (**Supplementary Fig. 7a**). An immunostaining analysis revealed that the SRC-1 C-terminal isoform was located in both the nuclear and cytoplasmic compartments of these IHEECs (**Supplementary Fig. 7b**).

In nuclear-receptor–mediated signaling, the SRC-1 C-terminal isoform interacted with ER-α, ER-β and progesterone receptor (**Supplementary Fig. 8a–c**) and activated ER-α–, ER-β– and progesterone-receptor–mediated gene transcription, as did full-length SRC-1 (**Supplementary Fig. 8d–g**).

The endometriosis-associated proinflammatory pelvic environment normally causes cell death, such that menstrual cell masses are cleared. Therefore, the evasion of TNF-α–induced cell death is an essential step for the development of stable ectopic lesions during the progression of endometriosis. We therefore investigated the role of the SRC-1 C-terminal isoform in the evasion of TNF-α–induced cell death. The parental IHEECs and two different recombinant IHEECs expressing full-length SRC-1 or the SRC-1 isoform grew well under vehicle treatment (**Fig. 6a**). However, treatment with 10 ng ml^{-1} of TNF-α for 2 d prevented the growth of parental (**Fig. 6a**,**b**) and recombinant IHEECs expressing full-length SRC-1 (**Fig. 6a**,**c**) compared to the vehicle treatment. In contrast, however, IHEECs expressing the SRC-1 C-terminal isoform did not have a substantial amount of TNF-α–induced growth inhibition compared to the parental IHEECs and those expressing full-length SRC-1 (**Fig. 6a**,**d**). Therefore, we concluded that the endometriotic SRC-1 C-terminal isoform prevented the TNF-α–induced growth inhibition of IHEECs.

The activation of the apoptosis pathway mediated by caspase 8, caspase 3 and truncated BH3 interacting-domain death agonist (tBid) has a key role in TNF-α–induced growth inhibition[31]. Therefore, we examined whether the expression of the endometriotic SRC-1 isoform inhibited TNF-α–induced apoptosis signaling in IHEECs. Consistent with previous observations, we found that TNF-α treatment led to higher amounts of cleaved caspase 8, tBid and activated caspase 3 in parental IHEECs as compared to parental IHEECs treated with vehicle (**Fig. 6e**,**f**). Notably, after treatment with TNF-α, the recombinant IHEECs expressing full-length SRC-1 had higher expression of these apoptosis markers relative to the parental IHEECs (**Fig. 6e**,**f**). In contrast, however, recombinant IHEECs expressing the SRC-1 C-terminal isoform did not have higher amounts of cleaved caspase 8, tBid and activated caspase 3 as a result of TNF-α treatment than the parental and recombinant IHEECs expressing full-length SRC-1 (**Fig. 6e**,**f**). To determine how the SRC-1 isoform inhibits TNF-α–induced apoptosis in IHEECs, we performed a coimmunoprecipitation assay. We found that the SRC-1 C-terminal isoform, but not full-length SRC-1 (F-SRC-1-M or endogenous SRC-1), interacted with procaspase 8 in IHEECs in both the absence and presence of TNF-α (**Fig. 6g**). Therefore, we concluded that the SRC-1 C-terminal isoform protected the IHEECs from TNF-α–induced apoptosis by interacting with procaspase 8 to prevent its activational processing.

In addition to the evasion of TNF-α–induced cell death, the extensive invasion of ectopic endometrium into target tissues (such as the ovary, uterus, intestine and bladder) is another essential step in the progression of endometriosis. We found that the recombinant IHEECs expressing full-length SRC-1 had higher invasive capacity than the parental IHEECs (**Fig. 6h**). However, we found that the invasive capacity of the IHEECs was more enhanced by the overexpression of the endometriotic SRC-1 C-terminal isoform compared to the overexpression of full-length SRC-1 (**Fig. 6h**).

The epithelial-mesenchymal transition (EMT) has a key role in metastasis and is characterized by the conversion of epithelial cancer cells to a more motile phenotype that facilitates invasion. We therefore investigated whether the endometriotic SRC-1 C-terminal isoform induced EMT in IHEECs to enhance the invasive capacity of these cells. We found that the recombinant IHEECs that overexpressed the endometriotic SRC-1 C-terminal isoform had higher expression of many of the acquired markers of EMT (N-cadherin, vimentin, Slug, Snail, β-catenin and transcription factor 8 (TCF8)) when compared to parental IHEECs and to IHEECs overexpressing full-length SRC-1 in the absence or presence of TNF-α treatment (**Fig. 6i**). Therefore, the SRC-1 isoform enhanced EMT to facilitate invasion by the ectopic endometrium during the progression of endometriosis.

In summary, to efficiently promote endometriosis, the activated TNF-α–MMP9 axis processes SRC-1 to its C-terminal isoform to protect the ectopic endometrium from a proinflammatory cytokine-mediated cell death, which is then accompanied by EMT and the enhancement of the invasive capacity of the ectopic endometrium (**Fig. 6j**).

DISCUSSION

Despite their well-known and essential role in estrogen- and progesterone-mediated cellular processes, the role of SRCs in the progression of endometriosis has not been well studied. Here we propose a new TNF-α–MMP9–SRC-1 isoform functional axis as a previously unknown pathogenic pathway for endometriosis. The SRC-1 isoform promotes endometriosis progression by causing EMT and the invasion of endometrial epithelial cells. An accompanying alteration of proinflammatory signaling is closely associated with inflammatory diseases and cancer progression because proinflammatory signaling changes the molecular properties of target cells[32,33]. For example, treatment with TNF-α changes the responsiveness to steroid hormones of uterine smooth muscle cells by suppressing the expression of SRC-1 and SRC-2 (ref. 34). In the present study, we found that TNF-α also changes the molecular properties of SRC-1 through proteolytic processing to a 70-kDa form that protects ectopic lesions from immune surveillance. Collectively, these results suggest that TNF-α signaling has an essential role in the initiation of endometriotic cellular processes. In addition to uterus, the TNF-α–induced inflammatory response to endometriosis can affect the SRC-1 milieus of other organs of the abdominal cavity, such as the intestine and liver. In this way, endometriosis can be accompanied by serious harmful systemic effects that are secondary to a widespread inflammatory response.

We found that MMP9, induced by TNF-α, is responsible for processing SRC-1 to the 70-kDa isoform. It was previously suggested that MMPs are secreted and then activated to remodel the mesothelial lining of the peritoneum and allow tissue invasion during the progression of endometriosis[35]. However, we detected the activities of both pro-MMP9 and processed MMP9 in the eutopic endometrium of mice with SIE. These data imply that the intracellular activation of MMP9 can occur within endometriotic tissue. Supporting our conclusion, the colocalization of trypsin-2 and MMP9 has been reported in intracellular pro-MMP9 processing, which causes full or partial activation of MMP9 activity in the intracellular vesicles of carcinoma cells[36]. Therefore, it is probable that intracellular MMP9 activation in endometriosis is performed by a specific TNF-α–induced protease to process SRC-1 for the progression of endometriosis. In addition to the proteolytic activity of MMP9, the nonproteolytic activity of MMP9 may be involved in the progression of endometriosis because nonproteolytic MMP9 activity is associated with cell migration[37].

Proinflammatory signaling is frequently associated with tissue-remodeling pathways in other inflammatory diseases and in cancer. For example, TNF-α–induced MMP9 activation is associated with the progression of various cancers[38]. Therefore, the TNF-α–MMP9 functional axis may have an essential role not only in endometriosis but also in other types of inflammatory diseases and cancer. Consequently, this functional axis should be considered a new molecular therapeutic target for the treatment of these diseases.

What is the pathobiological function of the anti-apoptotic processing mediated by the SRC-1 C-terminal isoform in human endometrial epithelial cells during the progression of endometriosis? The communication between the epithelial and stromal compartments has an essential role in endometrial function. Therefore, paracrine factors produced from stromal cells regulate cell-survival signaling in epithelial cells in the normal endometrium. In endometriosis, paracrine factors are also released from stromal cells to modulate cell-survival signaling in epithelial cells in the endometriotic ectopic endometrium[39]. In contrast to the eutopic endometrium, however, ectopic stromal cells lose the ability to regulate cell-survival signaling in ectopic epithelial cells[39]. Therefore, epithelial cells in ectopic lesions must acquire a new cell-survival system. In this context, epithelial cells in ectopic lesions activate the TNF-α–MMP9–SRC-1 isoform pathway in response to TNF-α during the progression of endometriosis. The activation of this pathway processes SRC-1 to the SRC-1 C-terminal isoform, protecting epithelial cells in ectopic lesions from TNF-α–induced cell death and, thus, promoting their survival. In this way, the activation of the TNF-α–MMP9–SRC-1 isoform pathway in ectopic lesions can compensate for the loss of paracrine survival signaling generated from ectopic stromal cells.

Endometriosis is known as an estrogen-dependent inflammatory disease. What is the role of the SRC-1 C-terminal isoform in the estrogen-dependent nature of endometriosis? Ectopic lesions require estrogen-dependent cellular processes for growth. However, ectopic lesions cannot use SRC-1 for estrogen-dependent gene regulation because full-length SRC-1 led to an increase in TNF-α–mediated cell death in IHEECs. For survival, SRC-1 must be processed to the SRC-1 C-terminal isoform in the epithelial cells of ectopic lesions to modulate estrogen-dependent cellular processes during activated proinflammatory signaling. In this way, the endometriosis-induced microenvironment actively changes the molecular properties of SRC-1 by proteolytic processing to prevent apoptosis but can still allow an estrogen-dependent progression of endometriosis.

We propose that this newly identified TNF-α–MMP9–SRC-1 C-terminal isoform functional axis is a new pathogenic pathway for the progression of endometriosis that has potential as a therapeutic target for endometriosis therapy. Indeed, anti-tumor necrosis factor therapy (etanercept) effectively reduces the development of endometriosis in an experimental rat model[40]. This observation further supports an essential role for the TNF-α–MMP9–SRC-1 C-terminal isoform functional axis in the progression of endometriosis.

METHODS

Methods and any associated references are available in the online version of the paper.

Note: Supplementary information is available in the online version of the paper.

ACKNOWLEDGMENTS

We thank C.J. Lockwood (Department of Obstetrics, Gynecology and Reproductive Science and Department of Genetics, Yale University School of Medicine) and T. Klonisch (Department of Human Anatomy and Cell Science, University of Manitoba) for providing immortalized human endometrial stromal and epithelial cells for this work. We thank M.J. Park for her technical support in animal experiments. We also thank the US National Institutes of Health–designated Diabetes and Endocrinology Research Center and the Proteomics Core in the Dan L. Duncan Cancer Center at Baylor College of Medicine for supporting this work. This work was supported by grants from the US National Institute of Diabetes and Digestive and Kidney Diseases (U54HD007495 and 5K12HD050128 to S.M.H., U54HD007495 to F.J.D., R01 HD08188 to B.W.O. and a U54HD007495 pilot grant to S.J.H.) and a grant from the US National Cancer Institute (R01 CA077030 to J.P.L.).

AUTHOR CONTRIBUTIONS

S.J.H. led the project and designed and performed most of experiments. K.B., S.Y.J. and J.Q. provided technical expertise. S.M.H. and E.K. provided primary normal HESCs and primary human endometriotic stromal cells. J.P.L. and F.J.D. provided intellectual inputs. B.W.O. supervised the entire project. S.J.H. and B.W.O. wrote the manuscript.

COMPETING FINANCIAL INTERESTS

The authors declare no competing financial interests.

Published online at http://www.nature.com/doifinder/10.1038/nm.2826.
Reprints and permissions information is available online at http://www.nature.com/reprints/index.html.

1. Bulun, S.E. Endometriosis. *N. Engl. J. Med.* **360**, 268–279 (2009).
2. Missmer, S.A. & Cramer, D.W. The epidemiology of endometriosis. *Obstet. Gynecol. Clin. North Am.* **30**, 1–19, vii (2003).
3. Meldrum, D.R. *et al.* "Medical oophorectomy" using a long-acting GNRH agonist—a possible new approach to the treatment of endometriosis. *J. Clin. Endocrinol. Metab.* **54**, 1081–1083 (1982).
4. Noble, L.S., Simpson, E.R., Johns, A. & Bulun, S.E. Aromatase expression in endometriosis. *J. Clin. Endocrinol. Metab.* **81**, 174–179 (1996).
5. Fedele, L., Bianchi, S., Zanconato, G., Tozzi, L. & Raffaelli, R. Gonadotropin-releasing hormone agonist treatment for endometriosis of the rectovaginal septum. *Am. J. Obstet. Gynecol.* **183**, 1462–1467 (2000).
6. Imai, A., Takagi, A. & Tamaya, T. Gonadotropin-releasing hormone analog repairs reduced endometrial cell apoptosis in endometriosis *in vitro*. *Am. J. Obstet. Gynecol.* **182**, 1142–1146 (2000).
7. Simsa, P. *et al.* Selective estrogen-receptor modulators and aromatase inhibitors: promising new medical therapies for endometriosis? *Womens Health (Lond. Engl.)* **3**, 617–628 (2007).
8. Fujimoto, J., Hirose, R., Sakaguchi, H. & Tamaya, T. Expression of oestrogen receptor-α and -β in ovarian endometriomata. *Mol. Hum. Reprod.* **5**, 742–747 (1999).
9. Harris, H.A., Bruner-Tran, K.L., Zhang, X., Osteen, K.G. & Lyttle, C.R. A selective estrogen receptor-β agonist causes lesion regression in an experimentally induced model of endometriosis. *Hum. Reprod.* **20**, 936–941 (2005).
10. Xiu-li, W., Wen-jun, C., Hui-hua, D., Su-ping, H. & Shi-long, F. ERB-041, a selective ER β agonist, inhibits iNOS production in LPS-activated peritoneal macrophages of endometriosis via suppression of NF-κB activation. *Mol. Immunol.* **46**, 2413–2418 (2009).
11. Bedaiwy, M.A. *et al.* Prediction of endometriosis with serum and peritoneal fluid markers: a prospective controlled trial. *Hum. Reprod.* **17**, 426–431 (2002).
12. Berkkanoglu, M. & Arici, A. Immunology and endometriosis. *Am. J. Reprod. Immunol.* **50**, 48–59 (2003).
13. Falconer, H. *et al.* Treatment with anti-TNF monoclonal antibody (c5N) reduces the extent of induced endometriosis in the baboon. *Hum. Reprod.* **21**, 1856–1862 (2006).
14. Efstathiou, J.A. *et al.* Nonsteroidal antiinflammatory drugs differentially suppress endometriosis in a murine model. *Fertil. Steril.* **83**, 171–181 (2005).
15. Osteen, K.G., Yeaman, G.R. & Bruner-Tran, K.L. Matrix metalloproteinases and endometriosis. *Semin. Reprod. Med.* **21**, 155–164 (2003).
16. Nap, A.W., Dunselman, G.A.J. & de Goeij, A.F.P.M. Evers, J.L.H. & Groothuis, P.G. Inhibiting MMP activity prevents the development of endometriosis in the chicken chorioallantoic membrane model. *Hum. Reprod.* **19**, 2180–2187 (2004).
17. Lonard, D.M., Lanz, R.B. & O'Malley, B.W. Nuclear receptor coregulators and human disease. *Endocr. Rev.* **28**, 575–587 (2007).
18. Suzuki, A. *et al.* Immunohistochemical detection of steroid receptor cofactors in ovarian endometriosis: involvement of down-regulated SRC-1 expression in the limited growth activity of the endometriotic epithelium. *Virchows Arch.* **456**, 433–441 (2010).
19. Kumagami, A., Ito, A., Yoshida-Komiya, H., Fujimori, K. & Sato, A. Expression patterns of the steroid receptor coactivator family in human ovarian endometriosis. *J. Obstet. Gynaecol. Res.* **37**, 1269–1276 (2011).
20. Fang, Z. *et al.* Intact progesterone receptors are essential to counteract the proliferative effect of estradiol in a genetically engineered mouse model of endometriosis. *Fertil. Steril.* **82**, 673–678 (2004).

21. Hirata, T. *et al.* Interleukin-17F increases the secretion of interleukin-8 and the expression of cyclooxygenase 2 in endometriosis. *Fertil. Steril.* **96**, 113–117 (2011).
22. Matsuzaki, S. *et al.* Expression of estrogen receptor α and β in peritoneal and ovarian endometriosis. *Fertil. Steril.* **75**, 1198–1205 (2001).
23. Bergqvist, A., Bruse, C., Carlberg, M. & Carlstrom, K. Interleukin 1β, interleukin-6, and tumor necrosis factor-α in endometriotic tissue and in endometrium. *Fertil. Steril.* **75**, 489–495 (2001).
24. Chishima, F. *et al.* Increased expression of cyclooxygenase-2 in local lesions of endometriosis patients. *Am. J. Reprod. Immunol.* **48**, 50–56 (2002).
25. Wang, H.B. *et al.* [Expression of vascular endothelial growth factor receptors in the ectopic and eutopic endometrium of women with endometriosis]. *Zhonghua Yi Xue Za Zhi* **85**, 1555–1559 (2005).
26. Banu, S.K., Starzinski-Powitz, A., Speights, V.O., Burghardt, R.C. & Arosh, J.A. Induction of peritoneal endometriosis in nude mice with use of human immortalized endometriosis epithelial and stromal cells: a potential experimental tool to study molecular pathogenesis of endometriosis in humans. *Fertil. Steril.* **91**, 2199–2209 (2009).
27. Hombach-Klonisch, S. *et al.* Regulation of functional steroid receptors and ligand-induced responses in telomerase-immortalized human endometrial epithelial cells. *J. Mol. Endocrinol.* **34**, 517–534 (2005).
28. Krikun, G. *et al.* A novel immortalized human endometrial stromal cell line with normal progestational response. *Endocrinology* **145**, 2291–2296 (2004).
29. Rubel, C.A., Jeong, J.W., Tsai, S.Y., Lydon, J.P. & Demayo, F.J. Epithelial-stromal interaction and progesterone receptors in the mouse uterus. *Semin. Reprod. Med.* **28**, 27–35 (2010).
30. Grund, E.M. *et al.* Tumor necrosis factor-α regulates inflammatory and mesenchymal responses via mitogen-activated protein kinase kinase, p38, and nuclear factor κB in human endometriotic epithelial cells. *Mol. Pharmacol.* **73**, 1394–1404 (2008).
31. Sanz, A.B., Santamaria, B., Ruiz-Ortega, M., Egido, J. & Ortiz, A. Mechanisms of renal apoptosis in health and disease. *J. Am. Soc. Nephrol.* **19**, 1634–1642 (2008).
32. Overton, C., Fernandez-Shaw, S., Hicks, B., Barlow, D. & Starkey, P. Peritoneal fluid cytokines and the relationship with endometriosis and pain. *Hum. Reprod.* **11**, 380–386 (1996).
33. Shakiba, K. & Falcone, T. Tumour necrosis factor-α blockers: potential limitations in the management of advanced endometriosis? A case report. *Hum. Reprod.* **21**, 2417–2420 (2006).
34. Leite, R.S., Brown, A.G. & Strauss Iii, J.F. Tumor necrosis factor-α suppresses the expression of steroid receptor coactivator-1 and -2: a possible mechanism contributing to changes in steroid hormone responsiveness. *FASEB J.* **18**, 1418–1420 (2004).
35. Pino, M. *et al.* Association between MMP1 and MMP9 activities and ICAM1 cleavage induced by tumor necrosis factor in stromal cell cultures from eutopic endometria of women with endometriosis. *Reproduction* **138**, 837–847 (2009).
36. Vilen, S.-T. *et al.* Intracellular co-localization of trypsin-2 and matrix metalloprotease-9: possible proteolytic cascade of trypsin-2, MMP-9 and enterokinase in carcinoma. *Exp. Cell Res.* **314**, 914–926 (2008).
37. Dufour, A., Zucker, S., Sampson, N.S., Kuscu, C. & Cao, J. Role of matrix metalloproteinase-9 (MMP-9) dimers in cell migration: design of inhibitory peptides. *J. Biol. Chem.* **285**, 35944–35956 (2010).
38. Scott, K.A. *et al.* TNF-α regulates epithelial expression of MMP-9 and integrin $\alpha_v\beta_6$ during tumour promotion. A role for TNF-α in keratinocyte migration? *Oncogene* **23**, 6954–6966 (2004).
39. Zhang, H. *et al.* Endometriotic stromal cells lose the ability to regulate cell-survival signaling in endometrial epithelial cells *in vitro*. *Mol. Hum. Reprod.* **15**, 653–663 (2009).
40. Islimye, M. *et al.* Regression of endometrial autografts in a rat model of endometriosis treated with etanercept. *Eur. J. Obstet. Gynecol. Reprod. Biol.* **159**, 184–189 (2011).

LETTERS

nature medicine

Activation of the epithelial Na^+ channel triggers prostaglandin E_2 release and production required for embryo implantation

Ye Chun Ruan[1,2,6], Jing Hui Guo[1,6], Xinmei Liu[3], Runju Zhang[3], Lai Ling Tsang[1], Jian Da Dong[1,2], Hui Chen[1], Mei Kuen Yu[1], Xiaohua Jiang[1,4], Xiao Hu Zhang[1], Kin Lam Fok[1], Yiu Wa Chung[1], Hefeng Huang[3], Wen Liang Zhou[2] & Hsiao Chang Chan[1,4,5]

Embryo implantation remains a poorly understood process. We demonstrate here that activation of the epithelial Na^+ channel (ENaC) in mouse endometrial epithelial cells by an embryo-released serine protease, trypsin, triggers Ca^{2+} influx that leads to prostaglandin E_2 (PGE_2) release, phosphorylation of the transcription factor CREB and upregulation of cyclooxygenase 2, the enzyme required for prostaglandin production and implantation[1–3]. We detected maximum ENaC activation, as indicated by ENaC cleavage[4], at the time of implantation in mice. Blocking or knocking down uterine ENaC in mice resulted in implantation failure. Furthermore, we found that uterine ENaC expression before *in vitro* fertilization (IVF) treatment is markedly lower in women with implantation failure as compared to those with successful pregnancy. These results indicate a previously undefined role of ENaC in regulating the PGE_2 production and release required for embryo implantation, defects that may be a cause of miscarriage and low success rates in IVF.

Embryo implantation, a rate-limiting step in human reproduction, is initiated by embryo attachment to endometrial epithelium followed by the so-called decidualization process in the stroma beneath the epithelium into large, round or polygonal decidual cells. The stromal decidualization is considered a maternal prerequisite for embryo implantation and successful pregnancy[5]. Ultrastructural studies of early stages of implantation have demonstrated a physical interaction between the embryo and endometrial epithelium[6,7] that is facilitated by the uterine 'closure' resulting from the removal of luminal fluid by transepithelial electrolyte and fluid reabsorption during the peri-implantation period[8,9]. It has long been observed in rodents that decidualization can be induced, in the absence of the embryo, by mechanical stimuli such as intraluminal injection of oil or air[10], or even scratching on the endometrium[11], resulting in pseudopregnancy. Notably, artificially stimulated decidualization in rodents cannot occur when the endometrial epithelium is destroyed or removed[12], suggesting the involvement of endometrial epithelium in decidualization. Clinical studies have shown that local injury to the endometrium (such as endometrial biopsy) promoted the implantation rate in women who had repeated implantation failure after IVF cycles[13]. Apart from physical signals, many different molecules have also been implicated as chemical signals for embryo implantation[14,15], among which serine proteases are abundantly found in the embryo-endometrium interface, released by the invading embryo and essential or implantation[14,16]. At the epithelium-stroma interface, prostaglandins, which are synthesized from the enzymatic conversion of phospholipase A_2 (PLA_2)-derived arachidonic acid by cyclooxygenases[1], have been shown to be essential decidualizing molecules[2,3]. However, it remains unclear how signals from the embryo (either physical or chemical) at the endometrial surface are converted into chemical signals such as prostaglandins, leading to decidualization in stromal cells that do not have direct contact with the embryo.

The amiloride-sensitive ENaC, encoded by *SCNN1* genes within the degenerin/ENaC superfamily[17], is localized in the apical membrane of a wide variety of epithelia, including endometrial epithelium[18]. We have previously observed upregulation of endometrial ENaC expression during the peri-implantation period in mice, and, given the well-established role of ENaC in electrolyte and water reabsorption[17], we have proposed that this ENaC upregulation is responsible for the disappearance of uterine fluid, or the closure of the uterine lumen, normally observed during this period[18]. Notably, ENaC has also been shown to be activated by mechanical force and serine proteases in various tissues[4,19,20]. In addition, both mechanical stimulation and serine proteases have been reported to promote prostaglandin release from esophageal and airway epithelial cells[21–23]. Therefore, we asked

[1]Epithelial Cell Biology Research Centre, School of Biomedical Sciences, Faculty of Medicine, The Chinese University of Hong Kong, Hong Kong. [2]School of Life Science, Sun Yat-sen University, Guangzhou, China. [3]Department of Reproductive Endocrinology, Key Laboratory of Reproductive Genetics of Ministry of Education of the People's Republic of China, Women's Hospital, Zhejiang University School of Medicine, Hangzhou, China. [4]Key Laboratory for Regenerative Medicine (Ji Nan University–The Chinese University of Hong Kong), Ministry of Education of the People's Republic of China, China . [5]Sichuan University–The Chinese University of Hong Kong Joint Laboratory for Reproductive Medicine, West China Second University Hospital, Chengdu, China. [6]These authors contributed equally to this work. Correspondence should be addressed to H.C.C. (hsiaocchan@cuhk.edu.hk), W.L.Z. (lszwl@yahoo.com.cn, lszwl@mail.sysu.edu.cn) or H.H. (huanghefg@hotmail.com).

Received 7 July 2011; accepted 10 April 2012; published online 24 June 2012; doi:10.1038/nm.2771

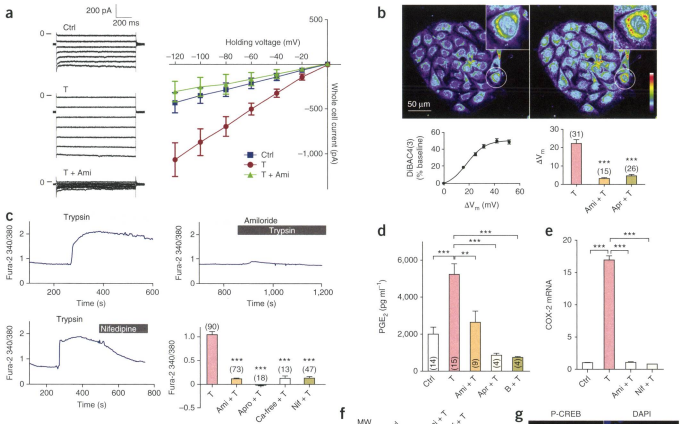

Figure 1 ENaC-mediated signal transduction events and PGE_2 release from mouse EECs. (**a**) Right, representative patch-clamp whole-cell currents elicited from −120 to 0 mV in an EEC before (Ctrl) and after trypsin with or without subsequent amiloride treatment. Left, corresponding current-voltage curves ($n = 4$). (**b**) Top, fluorescence photographs of EECs before (left) and after (right) treatment with trypsin. Color ranges from strongly hyperpolarized (purple) to strongly depolarized (red to white). The insets show higher-resolution images of the circled areas. Bottom left, calibration curve with measured changes in fluorescence intensity of DiBAC4(3) (% of baseline) as a function of membrane potential changes. Bottom right, summary of membrane potential changes (ΔV_m) elicited by trypsin, trypsin after pretreatment with amiloride or aprotinin. Number of measurements is shown in each column (***$P < 0.001$ compared to the trypsin-treated group). (**c**) Representative time-course changes in intracellular Ca^{2+} levels (indicated by 340/380 ratio of Fura-2) in EECs in response to trypsin in the presence of amiloride or nifedipine, with corresponding statistic analysis (***$P < 0.001$ compared to the trypsin-treated group). (**d**) Summary of trypsin-induced PGE_2 release from 3-d cultures of EECs (**$P < 0.01$, ***$P < 0.001$). (**e**) Quantitative PCR analysis of COX-2 mRNA levels in EECs under different conditions ($n = 4$, ***$P < 0.001$). (**f**) Western blot analysis of protein amounts of phosphorylated CREB (P-CREB). Data are presented as the ratio of P-CREB level to the level of β-tubulin ($n = 4$, *$P < 0.05$, **$P < 0.01$, ***$P < 0.001$). (**g**) Fluorescence labeling of P-CREB in EECs with DAPI-labeled nuclei (scale bars, 20 μm). T, trypsin (20 μg ml^{-1}); Ami, amiloride (10 μM); Apr, aprotinin (20 μg ml^{-1}); Nif, nifidipine (10 μM); B, BAPTA/AM (50 μM). Data are means ± s.e.m.

whether the activation of ENaC, which is sensitive to mechanical stimulation and proteases and whose expression is upregulated in the endometrium during peri-implantation, could trigger a sequence of events leading to the production and release of prostaglandins required for stromal decidualization and thus embryo implantation.

Using a primary culture of mouse endometrial epithelial cells (EECs) in conjunction with the patch-clamp technique, we observed that trypsin (20 μg ml^{-1}), a serine protease known to activate ENaC[24,25] and be released by invading embryos[16], induced an increase in inward whole-cell currents, which was abolished by subsequent addition of amiloride (10 μM), an ENaC inhibitor (**Fig. 1a**), indicating Na^+ influx. The immediate consequence of Na^+ influx upon ENaC activation would be membrane depolarization, and, indeed, trypsin (20 μg ml^{-1}) induced membrane depolarization (22.24 mV ± 2.2 mV) in EECs, which was abrogated by either amiloride (10 μM) or aprotinin (20 μg ml^{-1}), a protease inhibitor (**Fig. 1b**). Voltage-sensitive Ca^{2+} channel activities, which are known to be activated by membrane depolarization, have been suggested as a requirement for decidualization in mice[26]. Also, Ca^{2+} mobilization has been reported to facilitate cyclooxygenase-2 (COX-2)-dependent production of PGE_2 (ref. 27). We thus hypothesized that the serine protease–induced, ENaC-mediated membrane depolarization could result in Ca^{2+} mobilization leading to PGE_2 production or release. Addition of trypsin (20 μg ml^{-1}) induced sustained Ca^{2+} elevation in EECs,

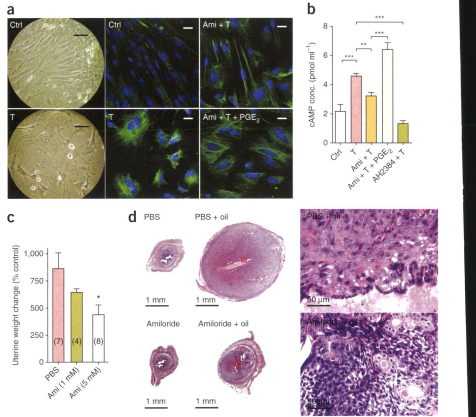

Figure 2 Involvement of ENaC in decidualization. (**a**) Bright-field photographs (scale bars, 50 μm) show the morphology of the cocultured stromal cells before (Ctrl) and after treatment with trypsin (T, 20 μg ml^{-1}). Fluorescence photographs (scale bars, 20 μm) show signal from fluorescently labeled antibody to desmin in the cocultured stromal cells before and after trypsin treatment, in the absence or presence of amiloride (Ami, 10 μM) or PGE_2 (10 μM). (**b**) Summary of intracellular cAMP concentration in cocultures in the presence or absence of trypsin, amiloride (Ami, 10 μM) or the EP4 receptor antagonist AH2384 (AH, 10 μM). $n = 6$, $^{**}P < 0.05$, $^{***}P < 0.001$. (**c**) Effect of amiloride on uterine weight change 3 d after oil-induced decidualization in pseudopregnant mice. Data are shown as percentage of controls without oil injection; the number of mice examined is shown in each column, $^{*}P < 0.05$. (**d**) H&E-stained micrographs showing uterine cross-sections from pseudopregnant mice 3 d after intrauterine injection of PBS, PBS with oil, amiloride (5 mM) or amiloride (5 mM) with oil. Higher-magnification micrographs show the framed areas. Data are means ± s.e.m.

which was inhibited by amiloride (10 μM) and aprotinin (20 μg ml^{-1}) (**Fig. 1c**). The trypsin-induced Ca^{2+} rise was largely lessened in Ca^{2+}-free solutions, suggesting Ca^{2+} influx through Ca^{2+} channels (**Fig. 1c**). Consistent with this notion, nifedipine (10 μM), a blocker of the voltage-dependent Ca^{2+} channel, abolished the trypsin-induced Ca^{2+} rise (**Fig. 1c**). We also detected L-type voltage-dependent Ca^{2+} channel mRNA expression and functional channel activities in EECs by the patch-clamp technique (**Supplementary Fig. 1**), indicating the involvement of L-type Ca^{2+} channel in the process. Using ELISA, we found that trypsin (20 μg ml^{-1}) could induce a nearly threefold increase, as compared to untreated controls, in PGE_2 release from the epithelial culture that could be attenuated by pretreatment with either amiloride (10 μM) or aprotinin (20 μg ml^{-1}) (**Fig. 1d**). Moreover, the trypsin-induced PGE_2 release from EECs was abolished by BAPTA/AM (50 μM), an intracellular calcium chelator (**Fig. 1d**), suggesting the involvement of Ca^{2+} in triggering PGE_2 release. Taken together, these results suggest that activation of ENaC by trypsin may result in membrane depolarization, which in turn leads to Ca^{2+} influx, resulting in PGE_2 release from EECs.

It has been suggested that continuous elevation of prostaglandin expression is required for decidualization[28]. Does ENaC also have a role in prostaglandin production during implantation, for example,

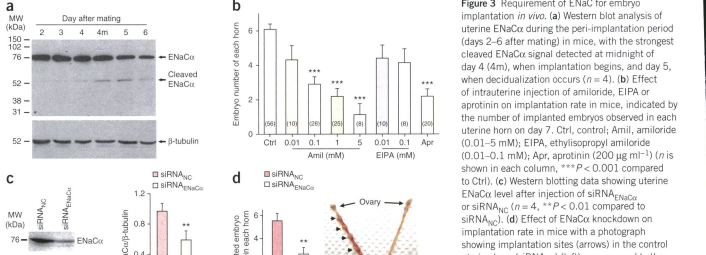

Figure 3 Requirement of ENaC for embryo implantation *in vivo*. (**a**) Western blot analysis of uterine ENaCα during the peri-implantation period (days 2–6 after mating) in mice, with the strongest cleaved ENaCα signal detected at midnight of day 4 (4m), when implantation begins, and day 5, when decidualization occurs ($n = 4$). (**b**) Effect of intrauterine injection of amiloride, EIPA or aprotinin on implantation rate in mice, indicated by the number of implanted embryos observed in each uterine horn on day 7. Ctrl, control; Amil, amiloride (0.01–5 mM); EIPA, ethylisopropyl amiloride (0.01–0.1 mM); Apr, aprotinin (200 μg ml^{-1}) (n is shown in each column, $^{***}P < 0.001$ compared to Ctrl). (**c**) Western blotting data showing uterine ENaCα level after injection of $siRNA_{ENaCα}$ or $siRNA_{NC}$ ($n = 4$, $^{**}P < 0.01$ compared to $siRNA_{NC}$). (**d**) Effect of ENaCα knockdown on implantation rate in mice with a photograph showing implantation sites (arrows) in the control uterine horn ($siRNA_{NC}$) (left) as compared to the $siRNA_{ENaCα}$-treated one (right) ($n = 18$, $^{**}P < 0.01$ compared to $siRNA_{NC}$). Data are means ± s.e.m.

by regulating the expression of COX-2, a key enzyme in prostaglandin synthesis? As shown by quantitative PCR (**Fig. 1e**), we found a significantly elevated mRNA level of COX-2 in EECs after a 15-min treatment with trypsin (20 μg ml^{-1}) that was abolished by pretreating the cells with either amiloride (10 μM) or nifidipine (10 μM). These results suggest that upregulation of COX-2 in EECs may be induced by ENaC activation–dependent Ca^{2+} influx. In this regard, transcription of COX-2 has been reported to be activated by the phosphorylation of cAMP/Ca^{2+} response element–binding protein (CREB), a transcription factor known to regulate prostaglandin production[29]. Indeed, western blot analysis showed that amounts of the phosphorylated form of CREB (P-CREB) were significantly increased in EECs 15 min after treatment with trypsin (20 μg ml^{-1}), which was attenuated by the pretreatment with amiloride (10 μM) or nifidipine (10 μM) (**Fig. 1f**). Immunofluorescence also showed an increased accumulation of P-CREB in the nuclei of cultured EECs after treatment with trypsin that was blocked by amiloride (**Fig. 1g**). These results suggest that ENaC activation may regulate transcriptional activities of COX-2.

Next, we tested whether the activation of endometrial ENaC by trypsin could indeed lead to stromal cell decidualization. We established an epithelial-stromal coculture and found that treatment of the coculture with trypsin (20 μg ml^{-1}, 4–6 h) induced substantial morphological changes of the stromal cells from elongated into polygonal and multinuclear cells (**Fig. 2a**), characteristic of decidual cells[30]. In addition, the expression of desmin, a reported marker of decidual cells[30], was upregulated in the trypsin-treated coculture, as indicated by immunostaining (**Fig. 2a**). Pretreatment with amiloride (10 μM) attenuated the effect of trypsin, whereas the inhibitory effect of amiloride could be reversed by adding PGE_2 (10 μM) to the coculture (**Fig. 2a**). As a decidualizing molecule[28], PGE_2 is believed to activate EP2 or EP4 receptors on stromal cells[31], which in turn leads to the accumulation of intracellular cAMP ($[cAMP]_i$)[32] and thus decidualization. We tested whether ENaC activation could lead to EP2 or EP4 receptor-mediated elevation of cAMP in EECs. We added trypsin (20 μg ml^{-1}, 20 min) to the EEC-stroma coculture and found elevated $[cAMP]_i$, which could be attenuated by pretreatment with amiloride (10 μM) (**Fig. 2b**). Consistent with the morphological result (**Fig. 2a**), adding PGE_2 could also reverse the inhibitory effect of amiloride on the trypsin-induced $[cAMP]_i$ in the coculture. Moreover, the EP4 receptor antagonist, AH2384 abolished the enhancing effect of trypsin on $[cAMP]_i$ in the coculture (**Fig. 2b**), confirming the involvement of the prostaglandin receptor in mediating the effect of ENaC activation on intracellular cAMP production. These results clearly demonstrated that the activation of ENaC by trypsin could lead to stromal decidualization involving PGE_2 and its receptor.

We further tested whether blocking ENaC could interfere with decidualization *in vivo* using a pseudopregnant mouse model with oil-induced decidualization[33]. Intrauterine injection of oil with PBS caused an ~8.5-fold higher uterine weight as compared to the weight in mice injected with PBS alone, suggesting successful induction of decidualization in these mice (**Fig. 2c,d**). Injection of amiloride (5 mM) with oil significantly ($P < 0.05$) reduced the uterine weight change, as well as the number of decidual cells (**Fig. 2c,d**). Both *in vitro* and *in vivo* results indicate a crucial role for ENaC in decidualization.

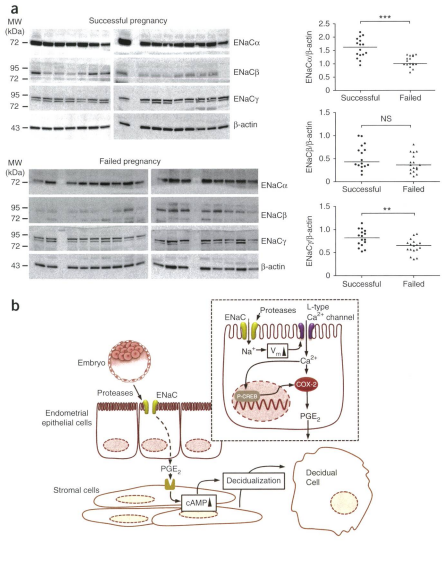

Figure 4 Abnormal ENaC expression in women with IVF failure and working model of ENaC in initiating decidualization. (**a**) Western blot analysis of protein levels of ENaC α, β and γ subunits from endometrial biopsy samples collected before the cycle of IVF and embryo transfer. Data are presented as the ratio of ENaC α, β and γ subunit levels to the level of β-actin. $n = 16$ (successful pregnancy) and 17 (failed pregnancy). $^{**}P < 0.01$; $^{***}P < 0.001$; NS, $P > 0.05$. Other parameters of the patients are not significantly different between the two groups, as shown in **Supplementary Table 2**. (**b**) Schematic drawing of ENaC involvement in decidualization. ENaC activation by serine proteases from the embryo causes epithelial cell membrane depolarization that activates L-type Ca^{2+} channel and Ca^{2+} influx leading to release of PGE_2 and phosphorylation of CREB that may upregulate the expression of COX-2. The endometrial epithelial released-PGE_2 in turn activates cAMP-related pathways in stromal cells, leading to stromal decidualization.

We next aimed to verify the involvement of ENaC in embryo implantation. We first tried to detect ENaC cleavage, an indication of ENaC activation[4], during the peri-implantation period in mouse uteri (days 2–6 after mating). By western blot analysis, we were able to clearly detect cleaved ENaCα (around 52 kDa) beginning approximately at midnight of day 4, when embryo implantation occurs in mice, and it persisted on day 5, when decidualization begins (**Fig. 3a**). We next tested whether interfering with ENaC function *in vivo* could impair implantation. Intrauterine injection with amiloride (100 μM–5 mM) induced a dose-dependent reduction in the number of implanted embryos in the amiloride-treated uterine horns compared with that in the vehicle-treated control horns (**Fig. 3b**). To exclude a possible non-specific effect of amiloride on the sodium-proton exchanger (NHE), we also applied ethyl isopropyl amiloride (EIPA), a specific blocker of NHE. Unlike amiloride injection, injection with EIPA (100 μM) showed no significant effect on implantation rate in mice (**Fig. 3b**). To confirm that serine proteases, which activate ENaC, are required for implantation, we also applied the protease inhibitor aprotinin to the pregnant mice. Similar to amiloride, aprotinin (200 μg ml^{-1}) also significantly reduced the number of implanted embryos (**Fig. 3b**). Together with the observed ENaC cleavage (or activation) at the time of implantation, the impaired implantation resulted from interfering with ENaC activation, either by protease inhibitor or ENaC blocker treatment, indicates that ENaC activation is required for embryo implantation.

The involvement of ENaC in implantation was further confirmed by knocking down ENaC *in vivo* in mice using siRNAs targeting ENaCα ($siRNA_{ENaCα}$) (**Fig. 3c**), and the results showed that the implanted embryo number counted on day 7 of pregnancy in ENaC-knockdown uterine horns (**Fig. 3d**), as well as the number of decidual cells (**Supplementary Fig. 2a**), was significantly lower compared to the control treated with negative control siRNAs ($siRNA_{NC}$), demonstrating the requirement of ENaC for implantation. The expression of three implantation markers, HoxA10, IgF2 and Lif, was also drastically reduced when ENaC was inhibited or knocked down (**Supplementary Fig. 2b**), suggesting that ENaC activation is a key upstream event during implantation.

Despite major improvements in assisted reproduction techniques (ARTs), the clinical pregnancy rate per embryo transfer in fresh ART cycles, or successful rate of IVF, remains at a low rate of 31% (ref. 34). Given that ENaC is required for embryo implantation, as we observed here in mice, alteration in ENaC expression or function may be a cause of implantation failure during IVF in humans. To test this, we examined the expression levels of the rate-limiting channel subunit ENaCα in a cohort of human endometrial samples obtained before IVF treatment and compared them between women with successful ($n = 16$) and failed ($n = 16$) pregnancy. The demographic and clinical data of the subjects showed no significant differences in age, ovarian hormonal profiles, endometrial thickness or oocyte quality between the two groups (**Supplementary Table 1**). However, the endometrial samples from women with failed pregnancy after IVF and embryo transfer showed a significantly lower average level of ENaCα subunit expression as compared to those from women with successful pregnancy ($P < 0.05$, **Supplementary Fig. 3**). In another cohort of samples from successful ($n = 16$) and failed ($n = 17$) pregnancy after IVF and embryo transfer, we examined the expression of all three ENaC subunits (α, β and γ). In addition to a significant difference observed for ENaCα ($P < 0.001$), the levels of ENaCγ, the subunit that has the protease activation site[35], were also significantly lower in the failed group than in the successful group ($P < 0.01$), whereas no significant difference observed for ENaCβ (**Fig. 4a**). These results, together with the results obtained from mice, suggest that ENaC activation is required for implantation and that abnormal ENaC expression could lead to implantation failure in humans.

We have demonstrated a crucial role for ENaC in signal transduction leading to stromal decidualization and thus embryo implantation, in addition to its previously reported role in regulating uterine fluid volume during the peri-implantation period[18]. As ENaC expression is subject to regulation by ovarian hormones[36], its normal expression pattern may be altered during IVF with ovarian overstimulation, which may contribute to the low pregnancy rate achieved through IVF. Thus, defects in ENaC, either in its expression or its function, may be one of the underlying mechanisms for spontaneous miscarriage and implantation failure during IVF. Of note, a recent study has reported that deregulation of SGK1, the serum- and glucocorticoid-inducible kinase and key regulator of ENaC, in the endometrium could interfere with embryo implantation[37], supporting a key role of ENaC in the process.

Taken together, the present results have revealed a previously unsuspected role of ENaC in regulating prostaglandin production and release required for embryo implantation (**Fig. 4b**). Given that ENaC is mechanosensitive[20], the presently demonstrated involvement of ENaC in decidualization also provides an explanation for the long-observed induction of decidualization by mechanical stimuli in animal models and improved implantation rate in women undergoing IVF after endometrial scratch[13]. The ability of ENaC to regulate PGE_2 production and release, as we showed here, may have far-reaching implications beyond embryo implantation or reproduction, as ENaC is widely distributed throughout the body and PGE_2 is a versatile regulator of many physiological functions and pathological processes[38].

METHODS

Methods and any associated references are available in the online version of the paper.

Note: Supplementary information is available in the online version of the paper.

ACKNOWLEDGMENTS

This work was supported in part by National 973 projects of China (2012CB944900, 2009CB522102, 2010CB945403), Natural Science Foundation of China (No. 30770817; No. 81161120006; No. 31071019), the Fundamental Research Funds for the Central Universities (Ji Nan University), the Focused Investment Scheme and Li Ka Shing Institute of Health Sciences of The Chinese University of Hong Kong, and the Morningside Foundation.

AUTHOR CONTRIBUTIONS

H.C.C. and Y.C.R.: conception and design; Y.C.R., J.H.G., X.L., R.Z., L.L.T., J.D.D., H.C., M.K.Y., X.L., X.H.Z., K.L.F. and Y.W.C.: experiments and/or data analysis; H.H.: clinical materials and consultancy; W.L.Z.: intellectual input and supervision; Y.C.R. and H.C.C.: article writing with contributions from other authors.

COMPETING FINANCIAL INTERESTS

The authors declare no competing financial interests.

Published online at http://www.nature.com/doifinder/10.1038/nm.2771.
Reprints and permissions information is available online at http://www.nature.com/reprints/index.html.

1. Ruan, Y.C., Zhou, W. & Chan, H.C. Regulation of smooth muscle contraction by the epithelium: role of prostaglandins. *Physiology (Bethesda)* **26**, 156–170 (2011).
2. Bonventre, J.V. *et al.* Reduced fertility and postischaemic brain injury in mice deficient in cytosolic phospholipase A2. *Nature* **390**, 622–625 (1997).
3. Lim, H. *et al.* Multiple female reproductive failures in cyclooxygenase 2-deficient mice. *Cell* **91**, 197–208 (1997).
4. Kleyman, T.R., Carattino, M.D. & Hughey, R.P. ENaC at the cutting edge: regulation of epithelial sodium channels by proteases. *J. Biol. Chem.* **284**, 20447–20451 (2009).
5. Ansell, J.D., Barlow, P.W. & McLaren, A. Binucleate and polyploid cells in the decidua of the mouse. *J. Embryol. Exp. Morphol.* **31**, 223–227 (1974).

6. Enders, A.C. & Schlafke, S. Comparative aspects of blastocyst-endometrial interactions at implantation. *Ciba Found. Symp.* **64**, 3–32 (1978).
7. Parkening, T.A. Apposition of uterine luminal epithelium during implantation in seriescent golden hamsters. *J. Gerontol.* **34**, 335–344 (1979).
8. Hedlund, K., Nilsson, O., Reinius, S. & Aman, G. Attachment reaction of the uterine luminal epithelium at implantation: light and electron microscopy of the hamster, guinea-pig, rabbit and mink. *J. Reprod. Fertil.* **29**, 131–132 (1972).
9. Martin, L., Finn, C.A. & Carter, J. Effects of progesterone and oestradiol-17 β on the luminal epithelium of the mouse uterus. *J. Reprod. Fertil.* **21**, 461–469 (1970).
10. Finn, C.A. Endocrine control of endometrial sensitivity during the induction of the decidual cell reaction in the mouse. *J. Endocrinol.* **36**, 239–248 (1966).
11. Lejeune, B., Lecocq, R., Lamy, F. & Leroy, F. Changes in the pattern of endometrial protein synthesis during decidualization in the rat. *J. Reprod. Fertil.* **66**, 519–523 (1982).
12. Lejeune, B., Van Hoeck, J. & Leroy, F. Transmitter role of the luminal uterine epithelium in the induction of decidualization in rats. *J. Reprod. Fertil.* **61**, 235–240 (1981).
13. Almog, B., Shalom-Paz, E., Dufort, D. & Tulandi, T. Promoting implantation by local injury to the endometrium. *Fertil. Steril.* **94**, 2026–2029 (2010).
14. Salamonsen, L.A. & Nie, G. Proteases at the endometrial-trophoblast interface: their role in implantation. *Rev. Endocr. Metab. Disord.* **3**, 133–143 (2002).
15. Salamonsen, L.A., Hannan, N.J. & Dimitriadis, E. Cytokines and chemokines during human embryo implantation: roles in implantation and early placentation. *Semin. Reprod. Med.* **25**, 437–444 (2007).
16. Sawada, H., Yamazaki, K. & Hoshi, M. Trypsin-like hatching protease from mouse embryos: evidence for the presence in culture medium and its enzymatic properties. *J. Exp. Zool.* **254**, 83–87 (1990).
17. Kellenberger, S. & Schild, L. Epithelial sodium channel/degenerin family of ion channels: a variety of functions for a shared structure. *Physiol. Rev.* **82**, 735–767 (2002).
18. Yang, J.Z. *et al.* Differential expression and localization of CFTR and ENaC in mouse endometrium during pre-implantation. *Cell Biol. Int.* **28**, 433–439 (2004).
19. Vallet, V., Chraibi, A., Gaeggeler, H.P., Horisberger, J.D. & Rossier, B.C. An epithelial serine protease activates the amiloride-sensitive sodium channel. *Nature* **389**, 607–610 (1997).
20. Fronius, M. & Clauss, W.G. Mechano-sensitivity of ENaC: may the (shear) force be with you. *Pflugers Arch.* **455**, 775–785 (2008).
21. Kawabe, A. *et al.* Production of prostaglandinE2 via bile acid is enhanced by trypsin and acid in normal human esophageal epithelial cells. *Life Sci.* **75**, 21–34 (2004).
22. Rastogi, P., Young, D.M. & McHowat, J. Tryptase activates calcium-independent phospholipase A2 and releases PGE2 in airway epithelial cells. *Am. J. Physiol. Lung Cell. Mol. Physiol.* **295**, L925–L932 (2008).
23. Orehek, J., Douglas, J.S. & Bouhuys, A. Contractile responses of the guinea-pig trachea *in vitro*: modification by prostaglandin synthesis–inhibiting drugs. *J. Pharmacol. Exp. Ther.* **194**, 554–564 (1975).
24. Donaldson, S.H. *et al.* Regulation of the epithelial sodium channel by serine proteases in human airways. *J. Biol. Chem.* **277**, 8338–8345 (2002).
25. Nesterov, V., Dahlmann, A., Bertog, M. & Korbmacher, C. Trypsin can activate the epithelial sodium channel (ENaC) in microdissected mouse distal nephron. *Am. J. Physiol. Renal Physiol.* **295**, F1052–F1062 (2008).
26. Sakoff, J.A. & Murdoch, R.N. The role of calcium in the artificially induced decidual cell reaction in pseudopregnant mice. *Biochem. Mol. Med.* **57**, 81–90 (1996).
27. Ruan, Y.C. *et al.* Regulation of smooth muscle contractility by the epithelium in rat vas deferens: role of ATP-induced release of PGE2. *J. Physiol. (Lond.)* **586**, 4843–4857 (2008).
28. Kennedy, T.G., Gillio-Meina, C. & Phang, S.H. Prostaglandins and the initiation of blastocyst implantation and decidualization. *Reproduction* **134**, 635–643 (2007).
29. Tsatsanis, C., Androulidaki, A., Venihaki, M. & Margioris, A.N. Signalling networks regulating cyclooxygenase-2. *Int. J. Biochem. Cell Biol.* **38**, 1654–1661 (2006).
30. Fouladi Nashta, A.A., Andreu, C.V., Nijjar, N., Heath, J.K. & Kimber, S.J. Role of leukemia inhibitor factor (LIF) in decidualisation of murine uterine stromal cells *in vitro*. *J. Endocrinol.* **181**, 477–492 (2004).
31. Pakrasi, P.L. & Jain, A.K. Cyclooxygenase-2 derived PGE2 and PGI2 play an important role via EP2 and PPARδ receptors in early steps of oil induced decidualization in mice. *Placenta* **29**, 523–530 (2008).
32. Yee, G.M. & Kennedy, T.G. Prostaglandin E2, cAMP and cAMP-dependent protein kinase isozymes during decidualization of rat endometrial stromal cells *in vitro*. *Prostaglandins* **46**, 117–138 (1993).
33. Dolphin, A.C. A short history of voltage-gated calcium channels. *Br. J. Pharmacol.* **147** (suppl. 1), S56–S62 (2006).
34. Toth, B. *et al.* Disorders of implantation—are there diagnostic and therapeutic options? *J. Reprod. Immunol.* **90**, 117–123 (2011).
35. Carattino, M.D., Hughey, R.P. & Kleyman, T.R. Proteolytic processing of the epithelial sodium channel gamma subunit has a dominant role in channel activation. *J. Biol. Chem.* **283**, 25290–25295 (2008).
36. Chan, L.N. *et al.* Distribution and regulation of ENaC subunit and CFTR mRNA expression in murine female reproductive tract. *J. Membr. Biol.* **185**, 165–176 (2002).
37. Salker, M.S. *et al.* Deregulation of the serum- and glucocorticoid-inducible kinase SGK1 in the endometrium causes reproductive failure. *Nat. Med.* **17**, 1509–1513 (2011).
38. Sugimoto, Y. & Narumiya, S. Prostaglandin E receptors. *J. Biol. Chem.* **282**, 11613–11617 (2007).

nature medicine

Autocrine activation of the MET receptor tyrosine kinase in acute myeloid leukemia

Alex Kentsis[1,2], Casie Reed[1,2], Kim L Rice[3], Takaomi Sanda[1,2], Scott J Rodig[4], Eleni Tholouli[5], Amanda Christie[1,2,6], Peter J M Valk[7], Ruud Delwel[7], Vu Ngo[8], Jeffery L Kutok[4], Suzanne E Dahlberg[9], Lisa A Moreau[1,2], Richard J Byers[5,10], James G Christensen[11], George Vande Woude[12], Jonathan D Licht[3], Andrew L Kung[1,2,6], Louis M Staudt[13] & A Thomas Look[1,2]

Although the treatment of acute myeloid leukemia (AML) has improved substantially in the past three decades, more than half of all patients develop disease that is refractory to intensive chemotherapy[1,2]. Functional genomics approaches offer a means to discover specific molecules mediating the aberrant growth and survival of cancer cells[3–8]. Thus, using a loss-of-function RNA interference genomic screen, we identified the aberrant expression of hepatocyte growth factor (HGF) as a crucial element in AML pathogenesis. We found HGF expression leading to autocrine activation of its receptor tyrosine kinase, MET, in nearly half of the AML cell lines and clinical samples we studied. Genetic depletion of HGF or MET potently inhibited the growth and survival of HGF-expressing AML cells. However, leukemic cells treated with the specific MET kinase inhibitor crizotinib developed resistance resulting from compensatory upregulation of HGF expression, leading to the restoration of MET signaling. In cases of AML where MET is coactivated with other tyrosine kinases, such as fibroblast growth factor receptor 1 (FGFR1)[9], concomitant inhibition of FGFR1 and MET blocked this compensatory HGF upregulation, resulting in sustained logarithmic cell killing both *in vitro* and in xenograft models *in vivo*. Our results show a widespread dependence of AML cells on autocrine activation of MET, as well as the key role of compensatory upregulation of HGF expression in maintaining leukemogenic signaling by this receptor. We anticipate that these findings will lead to the design of additional strategies to block adaptive cellular responses that drive compensatory ligand expression as an essential component of the targeted inhibition of oncogenic receptors in human cancers.

We used a doxycycline-inducible retroviral RNAi library of 5,087 barcoded shRNAs targeting 1,740 human genes to screen for functional pathway dependence in OCI-AML2 cells derived from a patient with complex-karyotype AML (**Supplementary Fig. 1a**)[10]. Among the 30 genes most substantially required for the proliferation and survival of OCI-AML2 cells but not cells from a variety of nonmyeloid hematologic malignancies was HGF, the ligand of the receptor tyrosine kinase MET (**Fig. 1a**)[11]. Targeting of *HGF* and downstream mediators of the MET signaling pathway, such as *STAT3* and *MAPK1*, with two independent shRNAs markedly suppressed the growth of AML cells but not of nonmyeloid hematologic cancer cells (**Supplementary Fig. 1b–d**).

In tests of the functional consequences of HGF expression in AML cell lines, we found that in four of seven AML cell lines, but not normal CD34$^+$ cells, expressed HGF was associated with MET activation (**Fig. 1b**). Given that normal CD34$^+$ cells do not express HGF, these data indicate that HGF expression by AML cells is aberrant, whereas expression of MET is lineage appropriate. Knockdown of *HGF* using two independent specific shRNAs inhibited the growth of OCI-AML2 cells (**Fig. 1c** and **Supplementary Fig. 2a**). This effect could be rescued with recombinant HGF protein (0.1 nM) or by the transduction of complementary DNA (cDNA) encoding *HGF* (**Fig. 1c**). OCI-AML2 cell growth was also inhibited by the addition of a neutralizing antibody against HGF (100 nM) to the culture medium (**Fig. 1c**). We also showed the requirement for HGF and MET signaling in three additional AML cell lines (HEL, SKNO-1 and KG-1) by depleting *HGF* and *MET* using specific shRNAs and inhibiting MET kinase signaling using the kinase inhibitor SU11274 (1 μM) (**Supplementary Figs. 3–5**). Inhibition of HGF and MET signaling led to a significant increase in the apoptosis of HGF-expressing cells (**Fig. 1d**) without

[1]Department of Pediatric Oncology, Dana-Farber Cancer Institute, Harvard Medical School, Boston, Massachusetts, USA. [2]Division of Hematology and Oncology, Children's Hospital Boston, Harvard Medical School, Boston, Massachusetts, USA. [3]Division of Hematology and Oncology, Northwestern University Feinberg School of Medicine, Chicago, Illinois, USA. [4]Department of Pathology, Brigham and Women's Hospital, Harvard Medical School, Boston, Massachusetts, USA. [5]Department of Haematology, Manchester Royal Infirmary, Central Manchester University Hospitals National Health Service Foundation Trust, and Manchester Academic Health Science Centre, Manchester, UK. [6]Lurie Family Imaging Center, Dana-Farber Cancer Institute, Boston, Massachusetts, USA. [7]Department of Hematology, Erasmus Medical Center, Rotterdam, The Netherlands. [8]Division of Hematopoietic Stem Cell and Leukemia Research, City of Hope National Medical Center, Duarte, California, USA. [9]Department of Biostatistics and Computational Biology, Dana-Farber Cancer Institute, Boston, Massachusetts, USA. [10]School of Cancer and Enabling Sciences, Faculty of Medical and Human Sciences, University of Manchester, Manchester, UK. [11]Department of Research Pharmacology, Pfizer Global Research and Development, La Jolla, California, USA. [12]Department of Molecular Oncology, Van Andel Research Institute, Grand Rapids, Michigan, USA. [13]Center for Cancer Research, National Cancer Institute, National Institutes of Health, Bethesda, Maryland, USA. Correspondence should be addressed to A.T.L. (thomas_look@dfci.harvard.edu).

Received 30 March 2011; accepted 30 April 2012; published online 10 June 2012; doi:10.1038/nm.2819

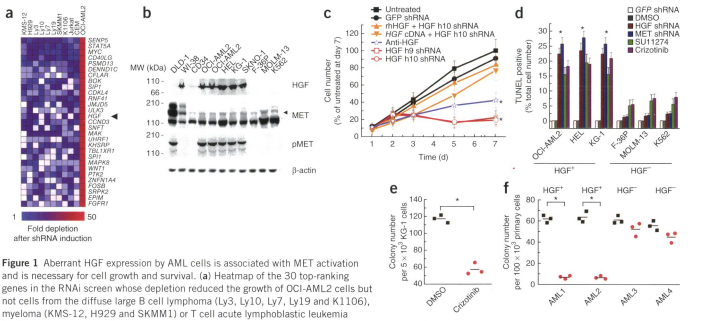

Figure 1 Aberrant HGF expression by AML cells is associated with MET activation and is necessary for cell growth and survival. (**a**) Heatmap of the 30 top-ranking genes in the RNAi screen whose depletion reduced the growth of OCI-AML2 cells but not cells from the diffuse large B cell lymphoma (Ly3, Ly10, Ly7, Ly19 and K1106), myeloma (KMS-12, H929 and SKMM1) or T cell acute lymphoblastic leukemia (Jurkat and CEM) lines. The relative cell depletion is indicated with a blue-to-red color gradient. The master myeloid transcription factor *SPI1* served as the internal positive control; *HGF* is indicated with an arrowhead. (**b**) Western blot analysis of lysates from colon carcinoma DLD-1 cells with *MET* amplification, WI-38 fibroblasts expressing HGF, normal human CD34$^+$ cells and seven AML cell lines; OCI-AML2 is duplicated. HGF is detected with an apparent mobility of 90 kDa, corresponding to its intracellular pro form, whereas MET is detected as both pro and mature forms in DLD-1 cells (180 and 140 kDa, respectively and predominantly as the mature form (140 kDa) in AML cells (arrowhead). pMET, phosphorylated MET. (**c**) The growth of OCI-AML2 cells is inhibited by the transduction of specific shRNAs targeting HGF (h9 and h10) or by treatment with a neutralizing antibody to HGF (anti-HGF) but not by transduction of control shRNA (GFP) or by concomitant rescue with *HGF* cDNA or recombinant human HGF (rhHGF). Measurements are normalized to the value for untreated cells at day 7 and are shown as means and s.d. of three biological replicates. $^*P < 0.05$ compared to untreated control by *t* test. (**d**) TUNEL analysis of AML cells that express HGF and activate MET (OCI-AML2, HEL and KG-1) compared to those that lack HGF expression (F-36P, MOLM-13 and K562) as a function of depletion of HGF or MET using RNAi, treatment with the MET kinase inhibitor SU11274 or crizotinib for 48 h. Transduction with *GFP* shRNA and treatment with DMSO served as controls. Values are means and s.d. of three biological replicates. $^*P < 0.05$ compared to DMSO or *GFP* shRNA control by *t* test. (**e**,**f**) Methylcellulose colony-forming assays of KG-1 cells (**e**) in the presence of DMSO control (black box) or crizotinib (red circle), and primary AML specimens (**f**) with aberrant HGF expression (AML1 and AML2) compared to those lacking HGF (AML3 and AML4). Individual data points and means (bars) of three biological replicates are shown. $^*P < 0.05$ compared to DMSO control by *t* test.

the induction of cell-cycle arrest (**Supplementary Fig. 3**). In addition, treatment with the specific MET kinase inhibitor crizotinib (100 nM) led to decreased colony formation of HGF-expressing primary AML samples (**Fig. 1e,f**). Taken together, our findings indicate that cell-autonomous production of HGF causes autocrine activation of MET and is necessary for the proliferation or survival of HGF-expressing AML cells.

To estimate the prevalence of aberrant HGF and MET signaling in patients with AML, we used immunohistochemistry to detect the coexpression of HGF and MET in bone marrow biopsy specimens from 138 adults with a broad spectrum of AML subtypes (**Fig. 2a–c** and **Supplementary Fig. 6a–e**). These proteins were expressed together in 58 (42%) of the patients (**Fig. 2c**), often in association with specific genetic abnormalities, including the *PML-RARA* and *AML1-ETO* (also known as *RUNX1-RUNX1T1*) translocations (**Supplementary Fig. 6f**). Using a capillary isoelectric focusing electrophoresis nano-immunoassay, which allows for precise quantification of differences in protein expression and phosphorylation, we observed expression of HGF and activation of MET in 5 (38%) of 13 viably frozen bone marrow aspirate specimens (**Supplementary Fig. 7**) and confirmed these results using flow cytometry (**Supplementary Fig. 8**). In the cohort we examined, there was no statistically significant difference in survival between patients with and without aberrant HGF expression (**Supplementary Fig. 6g**). An additional analysis of the gene expression profiles of primary blasts from 285 patients with AML using unsupervised clustering also revealed the high expression of HGF in a subset of patients with AML[12], including patients with the *PML-RARA* or *AML1-ETO* translocations (**Supplementary Fig. 9**).

Because HGF expression is associated with specific biologic subtypes of AML, we hypothesized that it might be induced by chimeric transcription factors that act in *trans* on the *HGF* locus to drive AML pathogenesis. Consistent with this concept, we did not detect any copy number changes (**Supplementary Fig. 10a,b**), mutations of the *HGF* promoter (**Supplementary Fig. 10c**) or allelic skewing of single nucleotide polymorphism expression (**Supplementary Fig. 10d**) in human AML cell lines with aberrant HGF expression. To test this predicted *trans*-acting mechanism directly, we transduced primary lineage-depleted mouse hematopoietic cells with fusion-protein–encoding retroviruses and monitored them for expression of HGF and activation of MET using nanoimmunoassays. Cells transduced with retroviruses encoding *PML-RARA*, *PLZF-RARA* (also known as *ZBTB16-RARA*) or *AML1-ETO* expressed HGF (**Fig. 2d** and **Supplementary Fig. 11**) and showed phosphorylation of MET (**Fig. 2e** and **Supplementary Fig. 11**). The transformed cells were sensitive to MET kinase inhibition in serial replating colony-formation assays (**Fig. 2f** and **Supplementary Fig. 11**) and showed downregulation of MET phosphorylation (**Fig. 2g** and **Supplementary Fig. 11**). Thus, distinct chimeric transcription factors can induce expression of HGF, leading to aberrant MET activation and functional dependence on HGF and MET signaling.

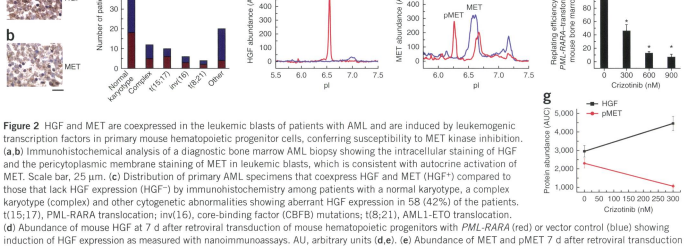

Figure 2 HGF and MET are coexpressed in the leukemic blasts of patients with AML and are induced by leukemogenic transcription factors in primary mouse hematopoietic progenitor cells, conferring susceptibility to MET kinase inhibition. (**a**,**b**) Immunohistochemical analysis of a diagnostic bone marrow AML biopsy showing the intracellular staining of HGF and the pericytoplasmic membrane staining of MET in leukemic blasts, which is consistent with autocrine activation of MET. Scale bar, 25 μm. (**c**) Distribution of primary AML specimens that coexpress HGF and MET (HGF^+) compared to those that lack HGF expression (HGF^-) by immunohistochemistry among patients with a normal karyotype, a complex karyotype (complex) and other cytogenetic abnormalities showing aberrant HGF expression in 58 (42%) of the patients. t(15;17), PML-RARA translocation; inv(16), core-binding factor (CBFB) mutations; t(8;21), AML1-ETO translocation. (**d**) Abundance of mouse HGF at 7 d after retroviral transduction of mouse hematopoietic progenitors with *PML-RARA* (red) or vector control (blue) showing induction of HGF expression as measured with nanoimmunoassays. AU, arbitrary units (**d**,**e**). (**e**) Abundance of MET and pMET 7 d after retroviral transduction of mouse hematopoietic progenitors with *PML-RARA* (red) or vector control (blue) showing activation of MET after induction of HGF expression. Equal protein loading was confirmed by the use of β_2-microglobulin as the loading control. (**f**) The colony replating efficiency of *PML-RARA*–transformed mouse hematopoietic progenitor cells as a function of increasing concentrations of crizotinib. Values are normalized to the number of colonies in mock-treated cells and plotted as means and s.d. of three biological replicates. $^*P < 0.05$ compared to DMSO-treated cells. AUC, area under the curve. (**g**) Abundance of HGF (black) and pMET (red) in *PML-RARA*–transformed mouse hematopoietic progenitor cells treated with varying concentrations of crizotinib showing inhibition of MET phosphorylation and upregulation of HGF.

To assess the potential of HGF and MET signaling as a therapeutic target, we investigated the sensitivity of HGF- and MET-dependent AML cell lines to chemical inhibition of the MET kinase using the specific MET and anaplastic lymphoma receptor tyrosine kinase (ALK) inhibitor crizotinib[13], which permits targeting of MET in AML because ALK is not expressed by hematopoietic cells or by any of the AML cell lines studied to date (**Supplementary Fig. 3b**). The growth of AML cell lines with aberrant HGF expression and MET activation was strongly inhibited by treatment with crizotinib (100 nM), whereas the growth of cell lines lacking HGF expression and MET activation was unaffected by crizotinib treatment (**Fig. 1d** and **Supplementary Fig. 4e**,**f**). However, HGF-expressing cells treated for more than 6 d with crizotinib seemed to regain their normal growth rate (**Fig. 3a** and **Supplementary Fig. 12a**,**b**).

Further experiments to determine the origin of the acquired resistance to crizotinib using quantitative nanoimmunoassays showed a profound inhibition of MET activation within 12 h of crizotinib treatment in OCI-AML2 cells (**Supplementary Fig. 13a**) that was associated with the induction of apoptosis (**Supplementary Fig. 14**). In addition, we observed a 13-fold upregulation of HGF in crizotinib-treated compared to vehicle-treated OCI-AML2 cells (**Supplementary Fig. 13b**), which occurred in concert with the recovery of the amount of phosphorylated MET after 10 d of treatment (**Supplementary Fig. 13a**), accounting for the restoration of pretreatment cell growth rates (**Fig. 3a**). This finding, confirmed in three different AML cell lines (**Supplementary Fig. 12c**), reflects an increased biallelic expression of *HGF* mRNA after crizotinib treatment (**Supplementary Fig. 15**). The recovery of MET phosphorylation corresponded with a recovery in the abundance of phosphorylated CRKL, phosphorylated signal transducer and activator of transcription 3 (STAT3) and phosphorylated mitogen-activated protein kinases 3/1 (ERK1/2) (**Supplementary Fig. 13d**–**f**), which are all associated with marked upregulation of HGF (**Supplementary Fig. 13b**). Depletion of HGF with a specific shRNA partially mitigated the compensatory upregulation of HGF in response to MET kinase inhibition, but this strategy was only partially successful in inhibiting leukemia growth *in vivo* because of the intrinsic variability in knockdown efficiency (**Supplementary Figs. 16** and **17**). Although the rapid development of crizotinib resistance was somewhat surprising to us, the selective pressure to maintain MET phosphorylation by upregulation of HGF reinforces our original conclusion that specific types of AML require aberrant HGF-mediated activation of MET signaling for sustained growth and survival.

As activation of MET can occur in AMLs that also harbor aberrant activation of other receptor tyrosine kinases, we reasoned that the combined inhibition of the signaling pathways that are coactivated with MET might be required to block the compensatory upregulation of HGF. In this study, we focused on the coactivation of FGFR1 with HGF and MET in KG-1 cells, which bear a *FGFR1OP2-FGFR1* chromosomal translocation and are derived from aggressive 8p11 myeloproliferative syndrome/stem cell leukemia[9]. After treating KG-1 cells with various concentrations of crizotinib and PD173074, a specific and potent inhibitor of the FGFR1 tyrosine kinase[14], we analyzed the effects using an isobologram analysis (**Supplementary Fig. 18a**). Nearly all dose combinations of PD173074 and crizotinib produced synergistic effects, as indicated by their low combination index values (**Supplementary Fig. 18a**). We found that the effect of PD173074 (20 nM) was mediated specifically by inhibition of FGFR1, as depletion of FGFR1 sensitized KG-1 cells to treatment with crizotinib (**Supplementary Fig. 19**).

Combination treatment of KG-1 cells with 100 nM crizotinib and 20 nM PD173074 (corresponding to their individual half-maximal inhibitory concentration (IC_{50}) values) prevented the compensatory upregulation of HGF (**Fig. 3b**), leading to sustained inhibition of MET phosphorylation (**Fig. 3c**) and sustained blockade of downstream signaling pathways (**Supplementary Fig. 18b**–**f**). This strategy also led to potent induction of apoptosis and logarithmic cell killing that was sustained for 14 d of treatment (**Fig. 3**). We confirmed the on-target effect of PD173074 by specifically depleting cells of FGFR1 by

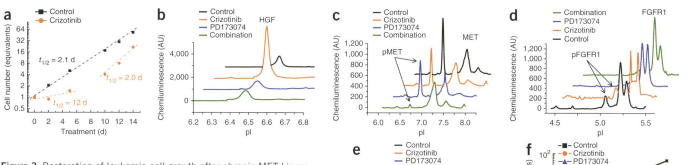

Figure 3 Restoration of leukemic cell growth after chronic MET kinase inhibitor treatment is a result of the compensatory upregulation of HGF and MET reactivation, which can be overcome by inhibiting the compensatory upregulation of HGF. (**a**) Kinetics of the growth of OCI-AML2 cells treated with crizotinib (in DMSO) or vehicle (DMSO) showing that acute crizotinib treatment leads to a significant reduction in AML cell growth (doubling time of 2.1 d compared to 12 d, respectively; $P < 0.05$), whereas with chronic treatment (10 d), the doubling time is 2.0 d. (**b**) Abundance of HGF in KG-1 cells treated for 10 d with DMSO (black), crizotinib (orange), PD173074 (blue) or a combination of crizotinib and PD173074 (green) as measured by quantitative nanoimmunoassay with β_2-microglobulin as the loading control (**Supplementary Fig. 16e**). (**c**) MET activation as assessed by the abundance of pMET in KG-1 cells treated for 10 d with the indicated drugs showing the maintenance of MET signaling in cells treated with crizotinib or PD173074 but not in cells exposed to the combination treatment. (**d**) FGFR1 activation as assessed by the abundance of phosphorylated FGFR1 (pFGFR1) in KG-1 cells treated for 10 d with the indicated drugs showing a lack of an effect of crizotinib on FGFR1 activity. (**e**) Induction of apoptosis as assessed by the abundance of cleaved caspase 3 (cCASP3) in KG-1 cells treated for 10 d showing substantially greater induction of apoptosis in cells treated with a combination of crizotinib and PD173074 compared to treatment with either drug alone. (**f**) Combined treatment of KG-1 cells with crizotinib and PD173074 leads to sustained logarithmic cell killing compared to treatment with either drug alone. Values are means and s.d. of three biological replicates. $^*P < 0.05$ compared to either drug alone by *t* test. AU, arbitrary units.

shRNA knockdown and showing that cells depleted of FGFR1, but not those transduced with the vector control, fail to upregulate HGF in response to chronic (≥10 d) crizotinib treatment (**Supplementary Fig. 19c**). Thus, FGFR1 activity is required for the compensatory upregulation of HGF in response to MET inhibition.

We then evaluated the simultaneous inhibition of MET and a blockade of compensatory HGF expression in KG-1 cells modified to express luciferase for bioluminescence imaging, which we engrafted into immunocompromised mice by tail vein injection. We treated the leukemic mice with vehicle control, crizotinib (50 mg per kg body weight) alone, PD173074 (25 mg per kg body weight) alone or a combination of the two agents by daily oral gavage 10 d after transplantation of the leukemia cells. Mice treated with the single drugs or the vehicle control continued to show exponentially growing leukemia, whereas mice treated with both crizotinib and PD173074 had significant regression in disease after 10 d of therapy, as measured by bioluminescence (**Fig. 4a**,**b**). We confirmed these results by flow cytometry, finding a near-complete ablation of CD45$^+$ human cells in the peripheral blood and bone marrow of mice treated with the combination of crizotinib and PD173074 but not in those treated with either drug alone or with the vehicle control (**Fig. 4c**,**d**). Although PD173074 alone had more potent effects on cell growth

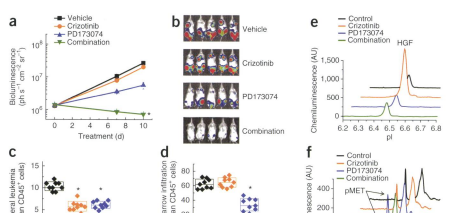

Figure 4 Combined inhibition of MET and FGFR1 blocks the compensatory upregulation of HGF, leading to sustained inhibition of MET in KG-1 cells and near-complete regression of AML *in vivo*. (**a**) Bioluminescence measurements of leukemic mice engrafted with luciferase-modified KG-1 cells and treated with vehicle control (black), crizotinib alone (orange), PD173074 alone (blue) or a combination of crizotinib and PD173074 (green) by daily oral gavage. Values are means and s.d. of each treatment group ($n = 9$ mice per group). $^*P < 0.05$ compared to all three other groups. (**b**) Bioluminescent photographs of representative mice from each treatment group (the blue-to-red color gradient indicates increasing bioluminescence intensities). (**c**,**d**) Scatter plots of the fraction of human CD45$^+$ KG-1 cells in the peripheral blood (**c**) and bone marrow (**d**) of mice after 10 d of treatment showing near-complete elimination of human AML cells in mice treated with the combination of crizotinib and PD173074. Boxes denote means and s.d. for each group ($n = 9$ mice per group). $^*P < 0.05$ compared to the vehicle-treated control group by *t* test. (**e**,**f**) Abundance of HGF (**e**) and pMET (**f**) in human CD45-selected KG-1 cells isolated from the bone marrow of mice after 10 d of treatment, as indicated, showing blockade of compensatory HGF upregulation in response to crizotinib treatment by the combined inhibition of MET and FGFR1 and the sustained inhibition of MET activation. AU, arbitrary units

than crizotinib alone, they were only modest at best, indicating that the striking therapeutic synergy of this combination stems primarily from the PD173074-induced blockade of compensatory HGF upregulation in response to crizotinib treatment (**Fig. 4e,f**).

We have identified aberrant HGF and MET signaling as a requisite pathway in the growth and survival of AML cells in nearly half of the primary clinical samples from a large group. In addition to *HGF*, our genome-wide shRNA screen identified a number of other genes as crucial factors in the biochemical processes that drive AML pathogenesis, which, with proper validation, could offer a functional taxonomy of AML cells, provide powerful insights into the pathophysiology of the disease and, ultimately, offer targets for improved therapy.

How does aberrant production of HGF contribute to the pathobiology of AML? We show here that dysregulated expression of this secreted growth factor, caused in part by the activity of distinct AML-associated transcription factors, leads to autocrine activation of the MET receptor and, in turn, to autocrine receptor tyrosine kinase signaling, as originally postulated on the basis of first-principle considerations[15]. Instead of direct mutational activation[16], we found that MET is activated in AML as a result of aberrant autocrine signaling by HGF, which seems to be dynamically controlled, as indicated by the upregulation of HGF in response to chronic MET kinase inhibition. Because constitutive activation of growth factor signaling pathways can have maladaptive cellular effects, such as cell-cycle arrest and senescence[17], these findings suggest that HGF deregulation and autocrine signaling provide a mechanism by which MET activity can be modulated to levels that optimize the fitness of AML cells, a property that may not be achieved by mutational activation of MET. In addition, *HGF* seems to be one of the most differentially expressed genes in the leukemia-initiating cells of AML as compared to normal hematopoietic stem cells[18], suggesting that aberrant HGF and MET signaling may contribute to the growth and survival of AML stem cells, thus strengthening the rationale for targeting this pathway.

Our study also raises the possibility that ligand-induced receptor activation may provide a general mechanism through which cancer cells can develop resistance to the therapeutic inhibition of receptor tyrosine kinase signaling. Autocrine signaling is widely prevalent in human cancers, affecting the epidermal GFR (EGFR), insulin-like GFR (IGFR), platelet-derived GFR (PDGFR), fibroblast GFR (FGFR), neurotrophic tyrosine kinase (TRK), EPH and TIE receptor families, many of which are currently being explored as therapeutic targets[19]. Indeed, ligand-dependent activation of receptor tyrosine kinases has been observed with other leukemogenic receptor tyrosine kinases, most notably the KIT oncogene and fms-related tyrosine kinase 3 (FLT3)[20]. Treatment with FLT3 kinase inhibitors leads to upregulation of the FLT3 ligand[21], which may be responsible, at least in part, for the diminished clinical efficacy of FLT3 inhibitors in patients with AML[22]. Autocrine or paracrine ligand-induced receptor activation will probably mitigate the effects of the targeted kinase inhibitors of these receptors in a manner that is analogous to the mechanisms by which HGF antagonizes inhibition of the MET kinase by crizotinib. Adaptive increases in ligand expression provide a means for cancer cell populations to re-establish the signal transduction pathways that existed before the onset of inhibitor treatment.

Clinical strategies will need to be developed to effectively overcome ligand-mediated resistance to targeted therapies. In the case of 8p11 stem cell leukemia involving *FGFR1* translocations, FGFR1 activity is required for the compensatory upregulation of HGF in response to MET inhibition. Combined inhibition of these coactivated pathways is highly synergistic as a result of the blockade of compensatory HGF upregulation, which leads to the sustained logarithmic cell killing that is required for clinically effective therapy.

METHODS

Methods and any associated references are available in the online version of the paper.

Note: Supplementary information is available in the online version of the paper.

ACKNOWLEDGMENTS

We thank A. Gutierrez, M. Mansour and E. Gjini for critical discussions and J. Gilbert for editorial advice. This research was supported by the US National Institutes of Health grant K08CA160660 (A.K.), the William Lawrence and Blanche Hughes Foundation (T.S.), the Samuel Waxman Cancer Research Foundation (J.D.L.), the V Foundation (A.T.L.) and the Intramural Research Program of the National Cancer Institute, Center for Cancer Research (L.M.S.).

AUTHOR CONTRIBUTIONS

A.K., C.R., K.L.R., T.S., A.C., E.T., V.N. and L.A.M. performed experiments. A.K., S.J.R., P.J.M.V., R.D., J.L.K., S.E.D., R.J.B., J.G.C., G.V.W., J.D.L., A.L.K., L.M.S. and A.T.L. analyzed data. A.K. and A.T.L. wrote the manuscript.

COMPETING FINANCIAL INTERESTS

The authors declare competing financial interests: details are available in the online version of the paper.

Published online at http://www.nature.com/doifinder/10.1038/nm.2819.
Reprints and permissions information is available online at http://www.nature.com/reprints/index.html.

1. Grimwade, D. *et al.* The predictive value of hierarchical cytogenetic classification in older adults with acute myeloid leukemia (AML): analysis of 1065 patients entered into the United Kingdom Medical Research Council AML11 trial. *Blood* **98**, 1312–1320 (2001).
2. Burnett, A., Wetzler, M. & Lowenberg, B. Therapeutic advances in acute myeloid leukemia. *J. Clin. Oncol.* **29**, 487–494 (2011).
3. Westbrook, T.F., Stegmeier, F. & Elledge, S.J. Dissecting cancer pathways and vulnerabilities with RNAi. *Cold Spring Harb. Symp. Quant. Biol.* **70**, 435–444 (2005).
4. Bernards, R., Brummelkamp, T.R. & Beijersbergen, R.L. shRNA libraries and their use in cancer genetics. *Nat. Methods* **3**, 701–706 (2006).
5. Ngo, V.N. *et al.* A loss-of-function RNA interference screen for molecular targets in cancer. *Nature* **441**, 106–110 (2006).
6. Whitehurst, A.W. *et al.* Synthetic lethal screen identification of chemosensitizer loci in cancer cells. *Nature* **446**, 815–819 (2007).
7. Turner, N.C. *et al.* A synthetic lethal siRNA screen identifying genes mediating sensitivity to a PARP inhibitor. *EMBO J.* **27**, 1368–1377 (2008).
8. Scholl, C. *et al.* Synthetic lethal interaction between oncogenic KRAS dependency and STK33 suppression in human cancer cells. *Cell* **137**, 821–834 (2009).
9. Gu, T.L. *et al.* Phosphotyrosine profiling identifies the KG-1 cell line as a model for the study of FGFR1 fusions in acute myeloid leukemia. *Blood* **108**, 4202–4204 (2006).
10. Wang, C., Curtis, J.E., Minden, M.D. & McCulloch, E.A. Expression of a retinoic acid receptor gene in myeloid leukemia cells. *Leukemia* **3**, 264–269 (1989).
11. Birchmeier, C., Birchmeier, W., Gherardi, E. & Vande Woude, G.F. MET, metastasis, motility, and more. *Nat. Rev. Mol. Cell Biol.* **4**, 915–925 (2003).
12. Valk, P.J. *et al.* Prognostically useful gene-expression profiles in acute myeloid leukemia. *N. Engl. J. Med.* **350**, 1617–1628 (2004).
13. Zou, H.Y. *et al.* An orally available small-molecule inhibitor of c-Met, PF-2341066, exhibits cytoreductive antitumor efficacy through antiproliferative and antiangiogenic mechanisms. *Cancer Res.* **67**, 4408–4417 (2007).
14. Mohammadi, M. *et al.* Crystal structure of an angiogenesis inhibitor bound to the FGF receptor tyrosine kinase domain. *EMBO J.* **17**, 5896–5904 (1998).
15. Sporn, M.B. & Todaro, G.J. Autocrine secretion and malignant transformation of cells. *N. Engl. J. Med.* **303**, 878–880 (1980).
16. Loriaux, M.M. *et al.* High-throughput sequence analysis of the tyrosine kinome in acute myeloid leukemia. *Blood* **111**, 4788–4796 (2008).
17. Haq, R. *et al.* Constitutive p38HOG mitogen-activated protein kinase activation induces permanent cell cycle arrest and senescence. *Cancer Res.* **62**, 5076–5082 (2002).
18. Majeti, R. *et al.* Dysregulated gene expression networks in human acute myelogenous leukemia stem cells. *Proc. Natl. Acad. Sci. USA* **106**, 3396–3401 (2009).
19. Robinson, D.R., Wu, Y.M. & Lin, S.F. The protein tyrosine kinase family of the human genome. *Oncogene* **19**, 5548–5557 (2000).
20. Zheng, R., Klang, K., Gorin, N.C. & Small, D. Lack of KIT or FMS internal tandem duplications but co-expression with ligands in AML. *Leuk. Res.* **28**, 121–126 (2004).
21. Zhou, J. *et al.* Enhanced activation of STAT pathways and overexpression of survivin confer resistance to FLT3 inhibitors and could be therapeutic targets in AML. *Blood* **113**, 4052–4062 (2009).
22. Sato, T. *et al.* FLT3 ligand impedes the efficacy of FLT3 inhibitors *in vitro* and *in vivo*. *Blood* **117**, 3286–3293 (2011).

nature medicine

Pharmacological targeting of the thrombomodulin–activated protein C pathway mitigates radiation toxicity

Hartmut Geiger[1,2,10], Snehalata A Pawar[3,10], Edward J Kerschen[4,10], Kalpana J Nattamai[1,10], Irene Hernandez[4], Hai Po H Liang[4], Jose Á Fernández[5], Jose A Cancelas[1], Marnie A Ryan[1], Olga Kustikova[6], Axel Schambach[6], Qiang Fu[3], Junru Wang[3], Louis M Fink[7], Karl-Uwe Petersen[8], Daohong Zhou[3], John H Griffin[5], Christopher Baum[6], Hartmut Weiler[4,10] & Martin Hauer-Jensen[3,9,10]

Tissue damage induced by ionizing radiation in the hematopoietic and gastrointestinal systems is the major cause of lethality in radiological emergency scenarios and underlies some deleterious side effects in patients undergoing radiation therapy[1,2]. The identification of target-specific interventions that confer radiomitigating activity is an unmet challenge. Here we identify the thrombomodulin (Thbd)–activated protein C (aPC) pathway as a new mechanism for the mitigation of total body irradiation (TBI)-induced mortality. Although the effects of the endogenous Thbd-aPC pathway were largely confined to the local microenvironment of Thbd-expressing cells, systemic administration of soluble Thbd or aPC could reproduce and augment the radioprotective effect of the endogenous Thbd-aPC pathway. Therapeutic administration of recombinant, soluble Thbd or aPC to lethally irradiated wild-type mice resulted in an accelerated recovery of hematopoietic progenitor activity in bone marrow and a mitigation of lethal TBI. Starting infusion of aPC as late as 24 h after exposure to radiation was sufficient to mitigate radiation-induced mortality in these mice. These findings suggest that pharmacologic augmentation of the activity of the Thbd-aPC pathway by recombinant Thbd or aPC might offer a rational approach to the mitigation of tissue injury and lethality caused by ionizing radiation.

TBI is associated with the dysfunction of radiosensitive organs[2–5]. To identify new genes and pathways protecting hematopoietic stem and progenitor cells (HSPCs) against radiation injury, we performed retroviral insertional mutagenesis screens in mice using a replication-deficient virus bearing a strong internal promoter expressing enhanced GFP (eGFP)[6] (**Supplementary Fig. 1a**). At weeks 4, 7 and 10 after the transfer of donor bone marrow cells transduced with the retrovirus, we exposed the recipient mice to a single dose of 3-Gy TBI, which resulted in three consecutive cycles of radiation-induced contraction and re-expansion of the hematopoietic system. In mice with a substantially augmented relative abundance of $eGFP^+$ cells in the peripheral blood or bone marrow[6] (**Supplementary Fig. 1b–e**), we used ligation-mediated PCR (LM-PCR)[6] to identify viral integration sites in the genomic DNA of their bone marrow cells. Among the loci targeted by integration, we identified genes known to have a role in the radioprotection of either hematopoietic or neuronal cells[2,7,8], such as *Puma* (also known as *Bbc3*; **Supplementary Fig. 2b–d**) and *c-Jun* (also known as *Jun*; data not shown). In the bone marrow cells of one mouse, designated animal 9 (**Fig. 1a** and **Supplementary Fig. 1b**), LM-PCR revealed integration of the retrovirus 31.6 kb upstream of the thrombomodulin (*Thbd*) gene (**Fig. 1b**). This integration event was associated with increased abundance of endogenous Thbd transcript and protein in radioselected $eGFP^+$ cells, whereas it had little effect on the expression of neighboring genes, such as the somatostatin receptor 4 gene (*Sstr4*) and the C-type lectin transmembrane receptor gene, *CD93* (**Fig. 1c,d**).

To ascertain whether augmented Thbd expression in HSPCs was sufficient to confer a competitive selection advantage to hematopoietic cells in response to TBI, we transduced HSPCs with lentiviral Thbd expression constructs and transplanted cells overexpressing Thbd into preconditioned C57BL/6-CD45.1 recipient mice (**Fig. 1e** and **Supplementary Fig. 3**). We administered one dose of 3-Gy TBI 4 weeks after this transplantation and analyzed the peripheral blood for $eGFP^+$ cell chimerism 3 weeks after TBI. Cells overexpressing Thbd were 1.5-fold enriched in the peripheral blood as compared to vector-only–transduced cells (**Fig. 1f,g**), indicating that elevated expression of Thbd in hematopoietic cells was sufficient to confer a selective advantage after radiation injury. However, HSPCs overexpressing Thbd were not protected from the effects of ionizing radiation *in vitro*, as determined by the survival, apoptosis and

[1]Division of Experimental Hematology and Cancer Biology, Cancer and Blood Diseases Institute, Cincinnati Children's Hospital Medical Center, University of Cincinnati, Cincinnati, Ohio, USA. [2]Department of Dermatology and Allergic Diseases, University of Ulm, Ulm, Germany. [3]Division of Radiation Health, College of Pharmacy, University of Arkansas for Medical Sciences, Little Rock, Arkansas, USA. [4]Blood Research Institute, Blood Center of Wisconsin and the Medical College of Wisconsin, Milwaukee, Wisconsin, USA. [5]Scripps Research Institute, La Jolla, California, USA. [6]Department of Experimental Hematology, Hannover Medical School, Hannover, Germany. [7]Desert Research Institute, Las Vegas, Nevada, USA. [8]PAION Deutschland GmbH, Aachen, Germany. [9]Surgical Service, Central Arkansas Veterans Healthcare System, Little Rock, Arkansas, USA. [10]These authors contributed equally to this work. Correspondence should be addressed to H.G. (hartmut.geiger@cchmc.org).

Received 3 January; accepted 24 April; published online 24 June 2012; doi:10.1038/nm.2813

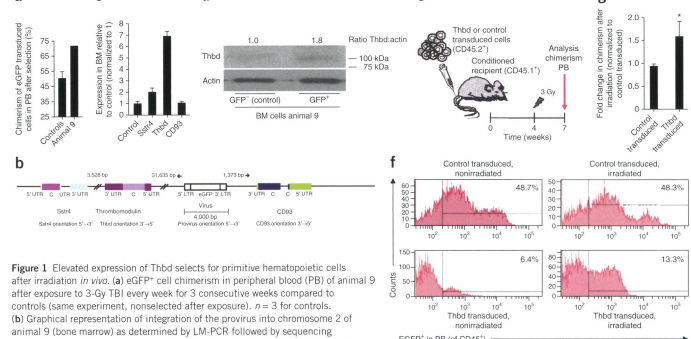

Figure 1 Elevated expression of Thbd selects for primitive hematopoietic cells after irradiation *in vivo*. (**a**) eGFP+ cell chimerism in peripheral blood (PB) of animal 9 after exposure to 3-Gy TBI every week for 3 consecutive weeks compared to controls (same experiment, nonselected after exposure). $n = 3$ for controls. (**b**) Graphical representation of integration of the provirus into chromosome 2 of animal 9 (bone marrow) as determined by LM-PCR followed by sequencing of the dominant integration product (see **Supplementary Table 1** for a list of all integration sites in animal 9). The numbers listed above the genes indicate the distances between the genes. C, coding region; UTR, untranslated region. (**c**) Transcriptional level of expression of Thbd and the two neighboring genes in bone marrow (BM) cells from animal 9, as determined by quantitative real-time RT-PCR. Expression was normalized to the level of expression of each of the gene measured (set to one) in a pool of control samples (bone marrow cells from C57BL/6 CD45.1 mice and mice 11 and 18, which were transplanted with transduced HSPCs but were not irradiated). (**d**) Expression of Thbd protein in the bone marrow of animal 9 compared to control mice (C57BL/6) as determined by western blot analysis. Actin served as a loading control. (**e**) Diagram of the experimental setup. Thbd was overexpressed in HSPCs by retroviral transduction, followed by transplantation and subsequent selection by irradiation. Recipient mice were preconditioned by irradiation with 11.75 Gy. Transplanted mice had a graft chimerism (CD45.2⁺ cells in peripheral blood) of higher than 90% 3 weeks after transplantation (data not shown). (**f**) Representative data showing the level of eGFP expression and selection among CD45.2⁺ cells in the peripheral blood of individual mice with and without irradiation in Thbd-transduced compared to control-transduced transplanted cells. (**g**) Quantification of the radioselection of Thbd-transduced hematopoietic cells in peripheral blood *in vivo* after irradiation relative to control (GFP)-transduced hematopoietic cells. $n = 3$ independent experiments with at least three recipients per single experiment. $^*P \leq 0.05$ (*t* test).

proliferation of these cells in response to irradiation (**Supplementary Fig. 4**). Therefore, the beneficial effects of Thbd on HSPCs *in vivo* must require additional cells or molecules.

Endogenous Thbd is a multifunctional cell-surface–associated receptor that regulates the activities of several physiological protease systems, including complement, fibrinolysis and blood coagulation[9]. Biochemically, Thbd functions as a high-affinity receptor for thrombin. The Thbd-thrombin complex activates thrombin activatable fibrinolysis inhibitor (TAFI) and also converts the plasma zymogen protein C into the natural anticoagulant aPC[10–12]. aPC inhibits blood coagulation through proteolysis of blood coagulation factors V and VIII, indirectly promotes the activity of the fibrinolytic system and exerts potent anti-inflammatory and cytoprotective effects on endothelial cells, neurons and various innate immune cell populations[13]. These latter effects are mediated by the interaction of aPC with signaling-competent receptors, such as the protease activated receptors Par1, Par2, and Par3, integrins and the endothelial protein C receptor (Epcr)[13,14].

In view of the beneficial effects of Thbd overexpression in HSPCs *in vivo*, we tested whether systemically-administered Thbd would have beneficial effects after radiation injury. Administration of recombinant soluble forms of THBD to baboons and humans is safe and has anticoagulant and antithrombotic activities[15–17]. Using an oxidation-resistant form of soluble, recombinant human THBD (Solulin, International Nonproprietary Name (INN) sothrombomodulin alpha; **Supplementary Fig. 5**), we found that administration up to 30 min after an 8.5-Gy or 9.5-Gy TBI resulted in significant ($P < 0.05$) radioprotection of wild-type mice compared to vehicle-treated controls, with a 40–80% survival benefit over vehicle-treated controls (**Fig. 2a,b**). Solulin has been shown to serve as a cofactor for the conversion of the plasma zymogen protein C into the natural anticoagulant aPC[10,16,18]. To determine whether the protective effects of soluble THBD could be related to activation of protein C, we investigated whether infusion of recombinant aPC could reproduce the radioprotective effect of soluble THBD. In independent experiments conducted in three different laboratories, administration of recombinant mouse aPC to C57BL/6 mice (at 5 μg per mouse intravenously (i.v.), equivalent to 0.4 mg per kg body weight) conferred a substantial survival benefit compared to vehicle-treated controls (**Fig. 2c,d**). We obtained similar data with genetically distinct CD2F1 mice (at 0.35 mg per kg body weight i.v. 30 min after TBI; data not shown), indicating that the effect of aPC was not dependent on a specific genetic background. In addition, after exposure to 10-Gy TBI, 40% of irradiated C57BL/6 mice survived after multiple injections of aPC (at 30 min, 1 h and 2 h after TBI) (**Fig. 2d**). Notably, even when the first injection of aPC was delayed until 24 h after TBI and a second injection of aPC was given at 48 h after TBI, we still observed significant radiomitigation (**Fig. 2e,f**).

The radiation doses used in our experiments resulted in death occurring 12–20 d after radiation exposure as a result of severe

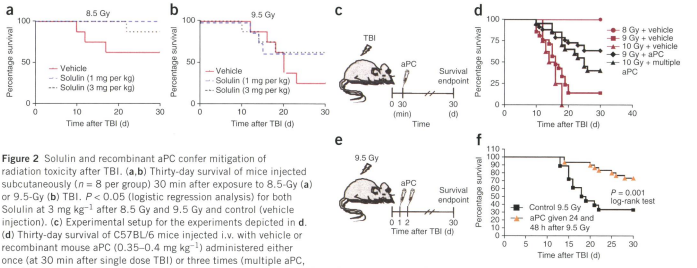

Figure 2 Solulin and recombinant aPC confer mitigation of radiation toxicity after TBI. (**a**,**b**) Thirty-day survival of mice injected subcutaneously ($n = 8$ per group) 30 min after exposure to 8.5-Gy (**a**) or 9.5-Gy (**b**) TBI. $P < 0.05$ (logistic regression analysis) for both Solulin at 3 mg kg^{-1} after 8.5 Gy and 9.5 Gy and control (vehicle injection). (**c**) Experimental setup for the experiments depicted in **d**. (**d**) Thirty-day survival of C57BL/6 mice injected i.v. with vehicle or recombinant mouse aPC (0.35–0.4 mg kg^{-1}) administered either once (at 30 min after single dose TBI) or three times (multiple aPC, administered at 30 min, 1 h and 2 h after TBI) or vehicle (PBS). $n = 8$ for 8 Gy + vehicle; $n = 33$ for 9 Gy + aPC; $n = 23$ for 9 Gy + vehicle; $n = 8$ for 10 Gy + vehicle; $n = 20$ for 10 Gy + multiple aPC. $P < 0.0001$ for 9 Gy + vehicle compared to 9 Gy + aPC; $P < 0.0001$ for 10 Gy + vehicle compared to 10 Gy + multiple aPC (log-rank (Mantel-Cox) test). (**e**) Depiction of experimental setup to test whether aPC given no earlier than 24 h after TBI can mitigate TBI toxicity. (**f**) Thirty-day survival of C57BL/6 mice injected with vehicle or mouse aPC at a dose of 5 μg per mouse through a single i.v. injection at 24 h and at 48 h after 9.5-Gy TBI (log-rank (Mantel-Cox) test); $n = 18$ vehicle-treated mice, $n = 30$ aPC-treated mice.

damage to bone marrow, suggesting that probable candidates for the relevant cellular targets of systemically administered Solulin and aPC in radiation mitigation include bone marrow hematopoietic cells and epithelial and/or endothelial structures of the bone marrow or gut. Administration of Solulin or aPC to lethally irradiated mice had no detectable effect on basic blood cell parameters at either day 3 or day 10 after radiation exposure (**Supplementary Fig. 6a** and data not shown), except for marginally elevated numbers of white blood cells in the bone marrow of mice treated with aPC at day 10 after radiation exposure (**Fig. 3a**,**b**). Hematopoietic progenitor cells (HPCs) in the bone marrow, determined either by flow cytometry ($Lin^-Sca1^+c\text{-}Kit^-$ cells; **Fig. 3c**) or functionally by colony-forming unit cell (CFU-C) assays (**Fig. 3d**), were almost undetectable at 3 d after irradiation (data not shown); however, at 10 d after irradiation, the number of these cells was substantially higher in aPC-treated mice than in vehicle-treated controls. The frequency of mice with more than ten CFU-C colonies per 5×10^4 bone marrow cells at day 10 after TBI was also substantially higher in the aPC-treated group than in controls (data not shown), and this frequency of CFU-C colonies correlated with the frequency of aPC-treated mice surviving exposure to lethal radiation doses (**Fig. 2d**,**f**). We obtained similar findings in lethally irradiated mice receiving Solulin (**Fig. 3e**,**f**), consistent with the notion that activation of protein C constitutes a relevant downstream effector of soluble THBD. Infusion of aPC did not alter biomarkers of radiation-induced gut injury, such as plasma citrulline concentrations and the integrity of the gut epithelial surface (**Supplementary Fig. 6c–e**), indicating that mitigation of radiation damage to the intestine probably did not substantially contribute to the efficacy of aPC.

To gain more insight into the molecular mechanisms of aPC action, we compared recombinant variants of aPC with respect to their radiomitigating activity. The mouse 5A aPC variant, which has full EPCR- and Par1-mediated cytoprotective function but only residual (~8%) anticoagulant activity[19,20], did not prevent radiation-induced mortality (**Fig. 3g**). In contrast, infusion of the Glu149Ala aPC variant (E149A aPC), which has augmented anticoagulant activity but deficient signaling activities (for example, only ~5% of normal anti-apoptotic activity)[21], conferred a significant ($P < 0.001$) survival benefit that was comparable to that of wild-type aPC (**Fig. 3g**). The biological activity of aPC that mediates radiomitigation is thus preserved in the E149A aPC variant but is compromised in the 5A aPC variant.

Both Par1 and Epcr are expressed on primitive bone marrow cells[22–25]. HSPCs lacking Par1 (ref. 26) or with greatly diminished expression of Epcr[27] were not impaired but, rather, were slightly favored compared to wild-type control HSPCs in competitive transplantation and radiation-injury experiments (**Supplementary Fig. 7a–c**). This result provides additional support for the notion that the radiomitigation activity of aPC does not involve Epcr- and Par1-dependent signaling on HSPCs, consistent with the failure of the signaling-selective 5A aPC variant to confer radioprotection.

Compared to the 5A aPC variant, the E149A aPC variant has increased anticoagulant effects and may also have increased coagulation-independent effects, such as in contributing to the degradation of cytotoxic histone-DNA complexes released from damaged cells[28]. However, inhibition of the cytotoxic histones 3 and 4 with the function-blocking BWA3 antibody under conditions shown previously to reduce mortality in sepsis[28,29] did not result in radioprotection (**Fig. 3h**). Similarly, inhibition of the intrinsic coagulation pathway with an antibody to factor XIa (14E11; ref. 30; **Fig. 3i**) or with low-molecular-weight heparin (data not shown) were both ineffective in conferring radioprotection. Biomarkers indicative of the activation state of the blood coagulation system in the peripheral blood (plasma thrombin-antithrombin complexes and the fibrin D dimer) were unaltered over a 24-h time window after exposure to lethal doses of radiation (**Supplementary Fig. 8**), suggesting that the radioprotective effect of the E149A aPC variant is not due to its antithrombotic actions. Although it is possible that optimized dosing with antibodies that block thrombosis or histone-induced inflammation might reveal some beneficial effect on radiation injury, it seems unlikely that these pathological mechanisms are the crucial targets of aPC in mediating the accelerated recovery of HPC activity and survival. The relevant targets of aPC therefore remain unknown and probably involve new functions associated with wild-type aPC and the E149A aPC variant[20,31].

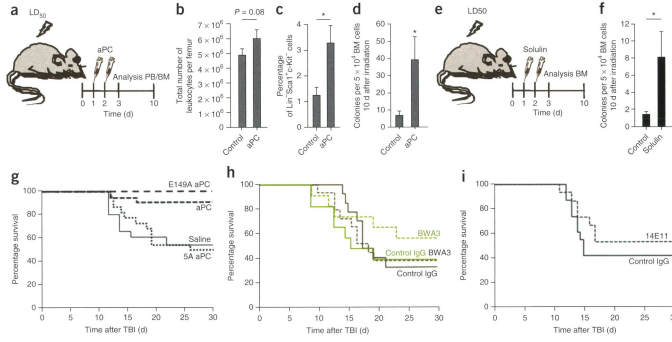

Figure 3 Mechanisms of the action of toxicity mitigation by soluble Thbd and aPC. (**a**) Experimental design for the data presented in **b**–**d**. (**b**) Total number of leukocytes per femur at 10 d after irradiation in irradiated and vehicle-treated control mice and in aPC-treated mice (*t* test). $n = 18$ for both vehicle-treated and aPC-treated mice. (**c**) Frequency of $Lin^{-}c\text{-}Kit^{+}$ cells in the bone marrow of the same mice 10 d after irradiation $^{*}P \leq 0.05$ by *t* test. $n = 18$ for both vehicle-treated and aPC-treated mice. (**d**) Frequency of colony-forming cells (CFCs) in bone marrow (BM) cells 10 d after irradiation. $^{*}P \leq 0.05$ by *t* test. $n = 18$ for vehicle-treated and aPC-treated mice. (**e**) Experimental design for the data presented in **f**. (**f**) Frequency of CFCs in bone marrow cells 10 d after irradiation and treatment with Solulin or vehicle control. $^{*}P \leq 0.05$ by *t* test. (**g**) Thirty-day survival of mice ($n = 15$ per group) irradiated with an LD_{50} dose receiving either 5 μg per mouse of the E149A aPC or 5A aPC variants or vehicle control through intravenous injection 30 min after TBI. $P < 0.001$ (Wilcoxon test) for E149A compared to saline, E149A compared to 5A, aPC compared to saline and aPC compared to 5A. (**h**) Thirty-day survival of mice given an LD_{50} dose of TBI and treated with the histone-blocking antibody BWA3 (30 mg kg^{-1} intraperitoneally) 0 h (black lines) or 16 h (green lines) after irradiation compared to injection of control isotype-matched, non-immune IgG. $n \geq 12$ per experimental group. (**i**) Thirty-day survival of mice given an LD_{50} dose of TBI and treated with an antibody to factor XIa (14E11) at 0 h after irradiation (30 mg kg^{-1} intraperitoneally) compared to injection of control antibody. $n \geq 16$ per experimental group.

Given the beneficial effects of THBD and aPC administration, the endogenous Thbd-aPC pathway might have a previously unrecognized role in mitigating the lethal consequences of radiation-induced bone marrow failure. In adult mice and humans, Thbd is expressed ubiquitously in endothelial cells of small blood vessels, except in certain brain microvascular beds, in which its expression is low[32]. Within the human hematopoietic system, THBD is expressed in a subpopulation of human dendritic cells, in monocytes and in a small subset of neutrophils[33,34]. Western blot analysis of bone marrow from radiation-exposed mice indicated the presence of Thbd protein in their bone marrow cells (**Fig. 1d**), and we detected Thbd transcripts in differentiated bone marrow cells and bone marrow hematopoietic progenitor and early hematopoietic progenitor cells (**Fig. 4a**), as well as in bone-marrow–derived $CD45^{-}Ter119^{-}CD31^{+}$ endothelial cells and in the $CD45^{-}Ter119^{-}CD31^{-}$ stromal cell compartment of bone marrow (**Fig. 4a**,**b**). An *in situ* survey of β-galactosidase expression in the femurs of $Thbd^{lacZ}$ knock-in mice indicated abundant Thbd expression within the endosteal region, as well as in femoral blood vessel endothelial cells supplying the bone marrow (**Fig. 4c**). Flow cytometry confirmed Thbd expression in $Ly\text{-}6G^{-}\ Gr1^{+}CD115^{+}$ bone marrow macrophages, as well as in B220- and CD19-positive B cell precursors (**Supplementary Fig. 9a** and data not shown). Thbd-expressing macrophages are distinct from two previously described macrophage populations with the surface phenotype $CD169^{+}CD115^{intermediate}F4/80^{+}Gr1^{-}$ or $CD11b^{+}Ly\text{-}6G^{+}F4/80^{+}$ that are involved in the maintenance of the hematopoietic niche (**Supplementary Fig. 9b**). Within the $CD45^{-}CD31^{+}$ endothelial cell population in bone marrow, we detected Thbd expression in $Sca1^{-}$ sinusoidal endothelium but not in $Sca1^{+}$ arterial endothelium (**Supplementary Fig. 9c**). This analysis of Thbd mRNA, Thbd antigen and *lacZ* reporter gene expression is consistent with the presence of Thbd on both hematopoietic and nonhematopoietic cells within the bone marrow.

We next investigated whether selective genetic disruption of protein C activation by endogenous $Thbd^{35-37}$ would modify survival after TBI. Mice with the genotype $Thbd^{Pro/lacZ}$ (ref. 36) carry only one functional Thbd allele, which encodes a Thbd variant (Thbd Pro) with severely reduced ability to activate protein C. These mice had increased sensitivity to TBI, such that the dose of radiation needed to elicit a 50% lethality shifted from ~8.75 Gy in wild-type mice to ~7.5 Gy in $Thbd^{Pro/lacZ}$ mice (**Fig. 4d**). $Thbd^{Pro/Pro}$ mice, which have a less severe Thbd deficiency than do $Thbd^{Pro/lacZ}$ mice, showed elevated sensitivity to TBI compared to wild-type mice (**Fig. 4e**). In contrast, aPC^{HI} transgenic mice, which have constitutively high plasma aPC concentrations caused by the expression of a human protein C variant that is efficiently activated by thrombin even in the absence of THBD[38], were protected from radiation-induced bone marrow failure to a similar extent as wild-type mice treated with recombinant aPC (**Fig. 4f**). Expression of the aPC^{HI} transgene also rescued the

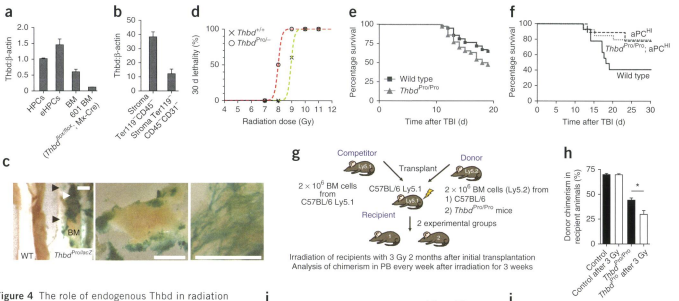

Figure 4 The role of endogenous Thbd in radiation protection. (**a**) Expression of Thbd relative to β-actin mRNA in the indicated hematopoietic cell populations. As a control for primer specificity, RNA from bone marrow (BM) cells from $Thbd^{flox/flox}$ mice crossed with Mx-Cre mice treated with polyinosinic-polycytidylic acid (pIC) to delete the Thbd allele in bone marrow cells (6Tr BM, deletion of up to 80% confirmed by PCR, data not shown) was used. $n \geq 3$ per experimental group. HPCs, $Lin^-Sca1^+c\text{-}Kit^+$ cells; eHPCs, $Lin^-Sca1^+c\text{-}Kit^+$ cells. (**b**) Expression of Thbd relative to β-actin mRNA in bone marrow stromal cells. Populations of cells containing endothelial cells ($CD45^-Ter119^-$) or not ($CD45^-Ter119^-CD31^-$) were used. $n \geq 3$ per experimental group. (**c**) Femoral bone marrow of $Thbd^{Pro/lacZ}$ mice stained *in situ* with a substrate for β-galactosidase. Blue staining indicates expression of the *lacZ* reporter gene controlled by the endogenous *Thbd* gene promoter. Staining was observed in the endothelium of the blood vessel on the outer surface of the bone or penetrating the bone (black arrowheads) and, in some vessels, within the bone marrow mass (left). Intense staining can be seen in a loose meshwork of cells located between the entire inner surface of the bone and the central bone marrow (white arrowhead). BM, bone marrow partially exposed by removal of the $lacZ^+$ layer. No staining was noted in wild-type (WT) controls processed in parallel. $LacZ^+$ clusters of cells are predominantly associated with the periphery of the marrow extruded from the bone cavity (middle). $LacZ^+$ endothelial cells seen in small blood vessels supplying the outer bone surface (right). Scale bars, 1 mm. (**d**) Thirty-day lethality of $Thbd^{+/+}$ and $Thbd^{Pro/-}$ mice ($n = 8$ per group) subjected to TBI with doses ranging from 7 Gy to 11 Gy. $P = 0.0001$ ($Thbd^{+/+}$ compared to $Thbd^{Pro/-}$ by logistic regression analysis). (**e**) Twenty-day survival of $Thbd^{Pro/Pro}$ mice irradiated with an LD_{50} dose of TBI. $n \geq 11$ per group. $P = 0.09$ for wild-type compared to $Thbd^{Pro/Pro}$ mice (log-rank (Mantel-Cox) test). (**f**) Thirty-day survival of mice treated with an LD_{50} dose of TBI. $n = 10$ for aPC^{HI}; $n = 15$ each for $Thbd^{Pro/Pro}$; aPC^{HI} and WT controls. $P < 0.05$ (log-rank (Mantel-Cox) test) for $Thbd^{Pro/Pro}$ compared to WT and for aPC^{HI} compared to WT. (**g**) Setup for competitive transplantation and radioselection experiments with bone marrow cells from $Thbd^{Pro/Pro}$ mice. (**h**) Donor chimerism in the peripheral blood (PB) of mice competitively transplanted according to the procedure in **g** 3 weeks after 3-Gy irradiation of recipients compared to C57BL/6 controls. $n = 4$ recipients per group. $^*P < 0.05$ by *t* test. (**i**) Setup for transplantation and radioselection experiments in which $Thbd^{Pro/Pro}$ and WT mice were reconstituted with WT bone marrow cells. (**j**) Thirty-day survival of WT and $Thbd^{Pro/Pro}$ recipients treated according to the procedure in **i**. $n = 20$ for WT recipients; $n = 9$ for $Thbd^{Pro/Pro}$ recipients. $P < 0.05$ (log-rank (Mantel-Cox) test) for $Thbd^{Pro/Pro}$ recipients compared to WT recipients.

increased radiation sensitivity of $Thbd^{Pro/Pro}$ mice (**Fig. 4f**), providing direct genetic evidence that the increased radiation sensitivity of Thbd-deficient mice is caused by inadequate activation of endogenous protein C.

We next performed competitive hematopoietic reconstitution experiments in which lethally irradiated wild-type recipients were transplanted with bone marrow from $Thbd^{Pro/Pro}$ and wild-type mice, followed by exposure to 3-Gy TBI given 8 weeks after transplantation (**Fig. 4g**). $Thbd^{Pro/Pro}$ cells showed less recovery than did wild-type cells (**Fig. 4h**). The initially lower contribution of $Thbd^{Pro/Pro}$ bone marrow cells to chimerism before irradiation might be caused by additional functions of Thbd in HSC biology that have not yet been investigated. In noncompetitive reconstitution experiments, we transplanted irradiated wild-type or $Thbd^{Pro/Pro}$ recipients with wild-type bone marrow, followed by a second exposure to a lethal dose (LD_{50}) of TBI (**Fig. 4i**). Transplantation into $Thbd^{Pro/Pro}$ recipients resulted in a significantly ($P < 0.05$) increased 30-d mortality rate compared to transplantation into wild-type recipients (**Fig. 4j**). Hence, endogenous Thbd expression on hematopoietic cells as well as on nonhematopoietic stroma cells confers protection against radiation, mirroring the protection conferred by forced Thbd overexpression in HSPCs or by therapeutic administration of soluble Thbd or aPC.

In summary, we have identified the Thbd-aPC pathway as a physiologically relevant mechanism that accelerates HSPC recovery in response to lethal TBI, resulting in substantial radiomitigation. Our data are consistent with a mechanism by which endogenous Thbd expressed on stromal endothelial or hematopoietic cells promotes protein C

activation and the release of aPC into the bone marrow microenvironment, leading to aPC-stimulated recovery from radiation-induced hematopoietic suppression. Based on the effect of Thbd deficiency on 30-d mortality (**Fig. 4j**), Thbd expression on stromal endothelial cells seems to make a more crucial contribution to overall survival than does Thbd expression in hematopoietic cells. Nevertheless, our findings also indicate that Thbd expression on HSPCs supports hematopoietic recovery after TBI in a cell-autonomous manner, with unknown effects on animal survival. Although the cellular and molecular mechanisms underlying the effect of soluble Thbd or aPC on the recovery of HSPC activity need to be studied in more detail, they are probably distinct from previously explored pathways involved in radioprotection, including those mediated by agonists of toll-like receptor 5 (ref. 39), inhibitors of cyclin-dependent kinase 4 and 6 (ref. 40) or various antioxidant compounds. Although the effects of endogenous aPC may remain largely confined to its site of formation, that is, the local microenvironment of Thbd-expressing cells, systemic administration of soluble Thbd or aPC can reproduce and augment the radioprotective effect of the endogenous protein C pathway.

Recombinant human aPC has undergone extensive clinical testing in patients, and recombinant soluble human THBD is currently being investigated for efficacy in antithrombotic therapy in humans. Our data encourage the further evaluation of these proteins for their radiomitigating activities. Moreover, these agents, possibly in combinations with other compounds targeting other pathways, may provide new medical countermeasures against radiation-induced pathologies.

METHODS

Methods and any associated references are available in the online version of the paper.

Note: Supplementary information is available in the online version of the paper.

ACKNOWLEDGMENTS

This work was supported by the US National Institutes of Health (grants CA71382 and AI67798 to M.H.-J., AI080557 to H.W., J.A.F. and H.G., HL31950 and HL052246 to J.H.G., HL44612 to H.W. and CA122023 and AI080421 to D.Z.), the Edward P. Evans Foundation (M.H.-J., D.Z. and H.G.), the Ziegler Family Chair for Research (H.W.) and the Veterans Administration. We thank J. Bailey and V. Summey from the Comprehensive Mouse and Cancer Core at Cincinnati Children's Hospital Medical Center (CCHMC) for their support and services. We are grateful to M. Monsteller (Temple University School of Medicine, Philadelphia, Pennsylvania, USA) for the BWA3 antibody, S.J. Kennel (University of Tennessee Graduate School of Medicine, Knoxville, Tennessee, USA) for the antibodies to Thbd (273-34A and 411-201B) and D. Gailani and A. Gruber (Vanderbilt University, Nashville, Tennessee, USA) for providing the 14E11 antibody.

AUTHOR CONTRIBUTIONS

H.G. and H.W. designed and performed experiments, and wrote the paper. S.A.P. collected, analyzed and summarized data. E.J.K., I.H., H.P.H.L., J.A.C. and M.A.R. performed experiments. K.J.N. performed experiments and wrote parts of the paper. J.A.F., A.S. and J.H.G. provided reagents and advised on experimental design. O.K., D.Z. and C.B. advised on experimental design and provided experimental expertise. Q.F. and J.W. performed *in vivo* studies. L.M.F. advised on experimental design and participated in writing the manuscript. K.-U.P. performed pharmacokinetics studies with Solulin and advised on experimental details. M.H.-J. designed experiments and wrote the paper.

COMPETING FINANCIAL INTERESTS

The authors declare competing financial interests: details are available in the online version of the paper.

Published online at http://www.nature.com/doifinder/10.1038/nm.2813.
Reprints and permissions information is available online at http://www.nature.com/reprints/index.html.

1. Mauch, P. *et al.* Hematopoietic stem cell compartment: acute and late effects of radiation therapy and chemotherapy. *Int. J. Radiat. Oncol. Biol. Phys.* **31**, 1319–1339 (1995).
2. Kirsch, D.G. *et al.* p53 controls radiation-induced gastrointestinal syndrome in mice independent of apoptosis. *Science* **327**, 593–596 (2010).
3. Schuller, B.W. *et al.* Selective irradiation of the vascular endothelium has no effect on the survival of murine intestinal crypt stem cells. *Proc. Natl. Acad. Sci. USA* **103**, 3787–3792 (2006).
4. Rotolo, J.A. *et al.* Regulation of ceramide synthase-mediated crypt epithelium apoptosis by DNA damage repair enzymes. *Cancer Res.* **70**, 957–967 (2010).
5. Paris, F. *et al.* Endothelial apoptosis as the primary lesion initiating intestinal radiation damage in mice. *Science* **293**, 293–297 (2001).
6. Kustikova, O.S. *et al.* Retroviral vector insertion sites associated with dominant hematopoietic clones mark "stemness" pathways. *Blood* **109**, 1897–1907 (2007).
7. Yu, H. *et al.* Deletion of Puma protects hematopoietic stem cells and confers long-term survival in response to high-dose gamma-irradiation. *Blood* **115**, 3472–3480 (2010).
8. Kanzawa, T. *et al.* Ionizing radiation induces apoptosis and inhibits neuronal differentiation in rat neural stem cells via the c-Jun NH_2-terminal kinase (JNK) pathway. *Oncogene* **25**, 3638–3648 (2006).
9. Weiler, H. & Isermann, B.H. Thrombomodulin. *J. Thromb. Haemost.* **1**, 1515–1524 (2003).
10. Wang, W., Nagashima, M., Schneider, M., Morser, J. & Nesheim, M. Elements of the primary structure of thrombomodulin required for efficient thrombin-activable fibrinolysis inhibitor activation. *J. Biol. Chem.* **275**, 22942–22947 (2000).
11. Esmon, N.L., Owen, W.G. & Esmon, C.T. Isolation of a membrane-bound cofactor for thrombin-catalyzed activation of protein C. *J. Biol. Chem.* **257**, 859–864 (1982).
12. Esmon, C.T., Esmon, N.L. & Harris, K.W. Complex formation between thrombin and thrombomodulin inhibits both thrombin-catalyzed fibrin formation and factor V activation. *J. Biol. Chem.* **257**, 7944–7947 (1982).
13. Mosnier, L.O., Zlokovic, B.V. & Griffin, J.H. The cytoprotective protein C pathway. *Blood* **109**, 3161–3172 (2007).
14. Weiler, H. Regulation of inflammation by the protein C system. *Crit. Care Med.* **38**, S18–S25 (2010).
15. Tanaka, K.A. *et al.* Soluble thrombomodulin is antithrombotic in the presence of neutralising antibodies to protein C and reduces circulating activated protein C levels in primates. *Br. J. Haematol.* **132**, 197–203 (2006).
16. van Iersel, T., Stroissnig, H., Giesen, P., Werner, J. & Wilhelm-Ogunbiyi, K. Phase I study of Solulin, a novel recombinant soluble human thrombomodulin analogue. *Thromb. Haemost.* **105**, 302–312 (2011).
17. Su, E.J. *et al.* The thrombomodulin analog Solulin promotes reperfusion and reduces infarct volume in a thrombotic stroke model. *J. Thromb. Haemost.* **9**, 1174–1182 (2011).
18. Foley, J.H., Rea, C.J., Petersen, K.U., Nesheim, M.E. & Sorensen, B. Solulin increases clot stability in whole blood from humans and dogs with hemophilia. *Blood* **119**, 3622–3628 (2012).
19. Mosnier, L.O., Yang, X.V. & Griffin, J.H. Activated protein C mutant with minimal anticoagulant activity, normal cytoprotective activity, and preservation of thrombin activable fibrinolysis inhibitor-dependent cytoprotective functions. *J. Biol. Chem.* **282**, 33022–33033 (2007).
20. Kerschen, E. *et al.* Activated protein C targets CD8$^+$ dendritic cells to reduce the mortality of endotoxemia in mice. *J. Clin. Invest.* **120**, 3167–3178 (2010).
21. Mosnier, L.O. *et al.* Hyperantithrombotic, noncytoprotective Glu149Ala-activated protein C mutant. *Blood* **113**, 5970–5978 (2009).
22. Ramalho-Santos, M., Yoon, S., Matsuzaki, Y., Mulligan, R.C. & Melton, D.A. "Stemness": transcriptional profiling of embryonic and adult stem cells. *Science* **298**, 597–600 (2002).
23. Kent, D.G. *et al.* Prospective isolation and molecular characterization of hematopoietic stem cells with durable self-renewal potential. *Blood* **113**, 6342–6350 (2009).
24. Balazs, A.B., Fabian, A.J., Esmon, C.T. & Mulligan, R.C. Endothelial protein C receptor (CD201) explicitly identifies hematopoietic stem cells in murine bone marrow. *Blood* **107**, 2317–2321 (2006).
25. Iwasaki, H., Arai, F., Kubota, Y., Dahl, M. & Suda, T. Endothelial protein C receptor-expressing hematopoietic stem cells reside in the perisinusoidal niche in fetal liver. *Blood* **116**, 544–553 (2010).
26. Darrow, A.L. *et al.* Biological consequences of thrombin receptor deficiency in mice. *Thromb. Haemost.* **76**, 860–869 (1996).
27. Iwaki, T., Cruz, D.T., Martin, J.A. & Castellino, F.J. A cardioprotective role for the endothelial protein C receptor in lipopolysaccharide-induced endotoxemia in the mouse. *Blood* **105**, 2364–2371 (2005).
28. Xu, J. *et al.* Extracellular histones are major mediators of death in sepsis. *Nat. Med.* **15**, 1318–1321 (2009).
29. Xu, J., Zhang, X., Monestier, M., Esmon, N.L. & Esmon, C.T. Extracellular histones are mediators of death through TLR2 and TLR4 in mouse fatal liver injury. *J. Immunol.* **187**, 2626–2631 (2011).
30. Luo, D. *et al.* Factor XI-deficient mice display reduced inflammation, coagulopathy, and bacterial growth during listeriosis. *Infect. Immun.* **80**, 91–99 (2012).
31. Kerschen, E.J. *et al.* Endotoxemia and sepsis mortality reduction by non-anticoagulant activated protein C. *J. Exp. Med.* **204**, 2439–2448 (2007).
32. Ismail, J.A. *et al.* Immunohistologic labeling of murine endothelium. *Cardiovasc. Pathol.* **12**, 82–90 (2003).

33. Conway, E.M., Nowakowski, B. & Steiner-Mosonyi, M. Human neutrophils synthesize thrombomodulin that does not promote thrombin-dependent protein C activation. *Blood* **80**, 1254–1263 (1992).
34. Yerkovich, S.T. *et al.* Allergen-enhanced thrombomodulin (blood dendritic cell antigen 3, CD141) expression on dendritic cells is associated with a T_H2-skewed immune response. *J. Allergy Clin. Immunol.* **123**, 209–216 (2009).
35. Weiler-Guettler, H. *et al.* A targeted point mutation in thrombomodulin generates viable mice with a prethrombotic state. *J. Clin. Invest.* **101**, 1983–1991 (1998).
36. Weiler, H. *et al.* Characterization of a mouse model for thrombomodulin deficiency. *Arterioscler. Thromb. Vasc. Biol.* **21**, 1531–1537 (2001).
37. Weiler-Guettler, H., Aird, W.C., Husain, M., Rayburn, H. & Rosenberg, R.D. Targeting of transgene expression to the vascular endothelium of mice by homologous recombination at the thrombomodulin locus. *Circ. Res.* **78**, 180–187 (1996).
38. Isermann, B. *et al.* Activated protein C protects against diabetic nephropathy by inhibiting endothelial and podocyte apoptosis. *Nat. Med.* **13**, 1349–1358 (2007).
39. Burdelya, L.G. *et al.* An agonist of toll-like receptor 5 has radioprotective activity in mouse and primate models. *Science* **320**, 226–230 (2008).
40. Johnson, S.M. *et al.* Mitigation of hematologic radiation toxicity in mice through pharmacological quiescence induced by CDK4/6 inhibition. *J. Clin. Invest.* **120**, 2528–2536 (2010).

nature medicine

Therapy of Pelizaeus-Merzbacher disease in mice by feeding a cholesterol-enriched diet

Gesine Saher[1], Fabian Rudolphi[1,3], Kristina Corthals[1,3], Torben Ruhwedel[1], Karl-Friedrich Schmidt[2], Siegrid Löwel[2], Payam Dibaj[1], Benoit Barrette[1], Wiebke Möbius[1] & Klaus-Armin Nave[1]

Duplication of *PLP1* (proteolipid protein gene 1) and the subsequent overexpression of the myelin protein PLP (also known as DM20) in oligodendrocytes is the most frequent cause of Pelizaeus-Merzbacher disease (PMD), a fatal leukodystrophy[1] without therapeutic options[2,3]. PLP binds cholesterol and is contained within membrane lipid raft microdomains[4]. Cholesterol availability is the rate-limiting factor of central nervous system myelin synthesis[5]. Transgenic mice with extra copies of the *Plp1* gene[6] are accurate models of PMD. Dysmyelination[6–8] followed by demyelination[9,10], secondary inflammation and axon damage contribute to the severe motor impairment in these mice[9,10]. The finding that in *Plp1*-transgenic oligodendrocytes, PLP and cholesterol accumulate in late endosomes and lysosomes (endo/lysosomes)[9,11–13], prompted us to further investigate the role of cholesterol in PMD. Here we show that cholesterol itself promotes normal PLP trafficking and that dietary cholesterol influences PMD pathology. In a preclinical trial, PMD mice were fed a cholesterol-enriched diet. This restored oligodendrocyte numbers and ameliorated intracellular PLP accumulation. Moreover, myelin content increased, inflammation and gliosis were reduced and motor defects improved. Even after onset of clinical symptoms, cholesterol treatment prevented disease progression. Dietary cholesterol did not reduce *Plp1* overexpression but facilitated incorporation of PLP into myelin membranes. These findings may have implications for therapeutic interventions in patients with PMD.

We have previously shown that mouse mutants lacking cholesterol synthesis in oligodendrocytes (*Fdft1*$^{flox/flox}$ × *Cnp1*$^{+/cre}$, termed cSQS knockout) express myelin protein genes, including *Plp1*, at a low level[5]. We therefore tested the potential application of an inhibitor of squalene synthase and cholesterol synthesis (squalestatin) for the downregulation of toxic *Plp1* overexpression in mice with increased *Plp1* gene dosage[6] (PLP-tg$^{72/72}$, *Plp1* transgenic line 72 containing three copies of the transgene, termed PMD mice hereafter, **Supplementary Table 1**). To protect PMD mice from the possible side effects of high-dose squalestatin treatment, we supplemented peripheral cholesterol levels with a high-cholesterol diet. We assumed that the CNS was shielded from cholesterol from the circulation by the blood-brain barrier (BBB)[14]. To our surprise, all mice of this pilot trial improved dramatically in comparison to the known PMD phenotype in mice (data not shown). This raised the possibility that the increase in circulating cholesterol by itself (or an indirect effect) ameliorates the leukodystrophy associated with PLP overexpression.

Next, we systematically compared PMD mice that received a cholesterol-enriched diet with littermates receiving normal chow. Serum cholesterol levels of PMD mice before treatment were not different from those of wild-type (WT) mice and increased in response to the cholesterol-enriched chow by about 10% as expected[15]. The cholesterol-rich diet had no effect on body weight (**Supplementary Fig. 1**).

In PMD mice injected with Evans blue dye (0.5 μg per g body weight intraperitoneally) to test the permeability of the BBB, the BBB was compromised already at 2 weeks of age (**Supplementary Fig. 2a**). Mice with a lower level of *Plp1* overexpression (PLP-tg$^{+/66}$, *Plp1* transgenic line 66 containing seven copies of the transgene)[6] lack such BBB opening (data not shown), in line with other studies[8,16]. In addition, cSQS knockout mouse mutants show normal BBB properties. On a cholesterol-enriched diet, cSQS mutant mice remain severely hypomyelinated[5]. Thus, we wanted to determine whether circulating cholesterol can cross the BBB in PMD mice. When tested 7 d after a single injection of BODIPY-cholesterol, fluorescence was readily detectable in the optic nerve from PMD mice (in contrast to WT controls) with a fiber-like pattern typical for myelinated axons (**Fig. 1a** and **Supplementary Fig. 2b**). Thus, in PMD mice peripheral cholesterol can pass the BBB, which is possibly perturbed by secondary inflammation[9,17].

Next, we wanted to determine whether dietary cholesterol supplementation can ameliorate existing pathology in PMD mice. We tested PMD mice (n = 15 or 16) that were put on a high-cholesterol diet at 6 weeks of age for a duration of 6 weeks, that is, after the onset of clinical signs as measured by decreased visual acuity (**Fig. 1b,c**). Visual acuity further declined in untreated PMD mice, whereas in PMD mice receiving cholesterol, visual acuity remained stable (**Fig. 1c** and **Supplementary Fig. 3**). PLP overexpression in PMD oligodendrocytes

[1]Department of Neurogenetics, Max Planck Institute of Experimental Medicine, Göttingen, Germany. [2]Bernstein Focus Neurotechnology and Johann-Friedrich-Blumenbach Institute of Zoology and Anthropology, Georg-August University, Göttingen, Germany. [3]These authors contributed equally to this work. Correspondence should be addressed to G.S. (saher@em.mpg.de) or K.-A.N. (nave@em.mpg.de).

Received 22 November 2011; accepted 15 May 2012; published online 17 June 2012; doi:10.1038/nm.2833

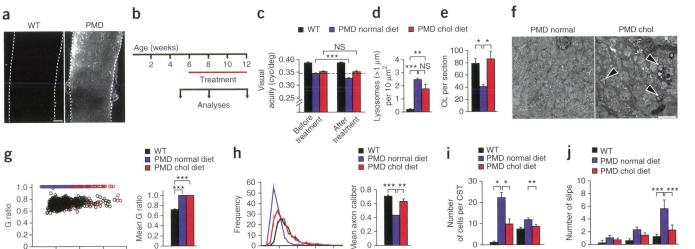

Figure 1 Cholesterol prevents the clinical deterioration of PMD mice. (**a**) BODIPY-cholesterol–derived fluorescence in the optic nerve of WT mice and PMD mice 7 d after intraperitoneal (i.p.) injection, as analyzed by two-photon microscopy. Scale bar, 50 μm. (**b**) Treatment scheme. PMD mice were given normal chow (control group) or cholesterol-enriched chow (treatment group) starting at 6 weeks of age with a 6-week duration. (**c**) Behavioral analysis using a virtual-reality optomotor system ($n = 9$ or 10). The dashed line marks the level of PMD mice on normal diet before treatment (cyc/deg, cycles per degree). (**d**) Quantification of large lysosomes (>1 μm in diameter) in the optic nerve ($n = 3$). (**e**) Number of oligodendrocytes (OL) per optic nerve cross section ($n = 3$). (**f**) Ultrastructural analysis of optic nerves revealing myelinated axons (arrowheads) in PMD mice on high-cholesterol diet (scale bar, 5 μm). (**g**) G-ratio analysis of optic nerve axons from WT and PMD mice ($n = 3$). (**h**) Axon caliber measurement of axon diameters of WT, PMD and cholesterol-fed PMD mice ($n = 3$). (**i**) Quantification of MAC3-positive microglia and GFAP-positive astrocytes in the corticospinal tract (CST) ($n = 3$–5 mice). (**j**) Beam tests, measuring the number of slips before the onset of treatment, after 3 weeks (during) and at the end of the trial (after) ($n = 9$ or 10 mice). Data are means ± s.e.m. $^*P < 0.05$; $^{**}P < 0.01$; $^{***}P < 0.001$, one-way (**d**–**i**) or two-way (**c**,**j**) analysis of variance (ANOVA) followed by Bonferroni test.

resulted in its accumulation in the Lamp1-positive endo/lysosomal compartment (**Supplementary Fig. 4**) in agreement with previous studies[11–13]. The high-cholesterol diet slightly decreased the abundance of large lysosomes (**Fig. 1d**). The number of oligodendrocytes, which is reduced in PMD optic nerves to about 50% of that in WT mice, was normalized (**Fig. 1e**), although improvement in myelination was only minimal (**Fig. 1f,g**). Notably, axon calibers in PMD mice increased to WT sizes after cholesterol treatment (**Fig. 1h**). Axonal loss was not observed in treated or untreated PMD mice at the end of this study (data not shown), in agreement with another study[9]. Secondary astrogliosis and microgliosis in the spinal cord were reduced by dietary cholesterol (**Fig. 1i**). This 6-week-long cholesterol treatment delayed the decline in motor coordination typically observed in PMD mice (**Fig. 1j**). Thus, despite persistent hypomyelination, cholesterol administration prevents the clinical deterioration in PMD mice, potentially by maintaining oligodendrocyte numbers, increasing axon calibers and

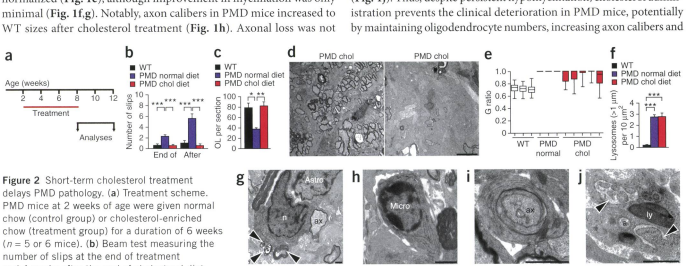

Figure 2 Short-term cholesterol treatment delays PMD pathology. (**a**) Treatment scheme. PMD mice at 2 weeks of age were given normal chow (control group) or cholesterol-enriched chow (treatment group) for a duration of 6 weeks ($n = 5$ or 6 mice). (**b**) Beam test measuring the number of slips at the end of treatment and 4 weeks after the end of cholesterol diet ($n = 5$–7 mice). (**c**) Number of oligodendrocytes per optic nerve cross-section from WT and PMD mice ($n = 3$–6). (**d**) Electron microscopic images of the optic nerve from two different PMD mice in the cholesterol group showing variability of myelination (scale bar, 5 μm). (**e**) Boxplot analysis of g-ratios of individual mice reflecting the variability of treatment benefit in PMD mice. (**f**) Quantification of lysosomes (>1 μm in diameter) in the optic nerve of WT and PMD mice ($n = 3$). (**g**–**j**) Electron microscopic images of optic nerves of cholesterol treated PMD mice show signs of ongoing pathology (**g**), such as oligodendrocytes (n, oligodendrocyte nucleus) with degenerating myelin profiles marked by arrowheads and a thin myelin sheath surrounding an axon (ax) (Astro, astrocyte), as well as microglia (Micro) with characteristic undulating long ER cisternae (**h**) and remyelinating profiles (**i**). (**j**) Oligodendrocytes containing dilated ER (a, autophagosome; ly, lysosome; scale bars, 1 μm). Data are means ± s.e.m. $^*P < 0.05$; $^{**}P < 0.01$; $^{***}P < 0.001$, one-way (**c**,**f**) or two-way (**b**) ANOVA followed by Bonferroni test.

reducing gliosis. The observation that not all defects were reverted may be due in part to the late onset and brevity of the treatment.

Next, we tested whether a similar treatment of PMD mice around the peak of myelination would be therapeutically more efficient (treatment from 2–8 weeks of age, analysis at 12 weeks of age) (**Fig. 2a**). In this treatment paradigm, motor performance did not overtly decline during the 4 weeks after cholesterol supplementation (**Fig. 2b**). Oligodendrocyte numbers were maintained (**Fig. 2c**). Ultrastructural analysis revealed a considerable number of myelinated axons; however, there was substantial interindividual variability (**Fig. 2d**,**e**). Large lysosomes were as frequent as in untreated PMD mice (**Fig. 2f**). Degenerating myelin profiles indicated ongoing demyelination, and signs of remyelination were also observed (**Fig. 2g**–**i**). Dilated endoplasmic reticulum (ER) was prominent in oligodendrocytes of untreated PMD mice, pointing to alterations also in this cellular compartment (**Fig. 2j** and see below). Thus, cholesterol treatment over the peak myelination period is advantageous.

Finally, we tested a combination of both early-onset and long-term treatment with cholesterol (2–12 weeks of age; $n = 7$–9; **Fig. 3a**). A high-cholesterol diet markedly increased the diameter of PMD optic nerves and normalized myelin content to near WT levels (**Fig. 3b**–**d**). Oligodendrocyte numbers and axon calibers also normalized (**Fig. 3e**,**f**). A high-cholesterol diet visibly reduced PLP abundance in the endo/lysosomal compartment and decreased the number of large lysosomes in PMD oligodendrocytes (**Fig. 3g**,**h** and **Supplementary Fig. 5**). Theoretically, *Plp1* overexpression and increased availability of cholesterol could elevate the amount of PLP in myelin membranes. However, by western blot analysis the amount of PLP in myelin purified from PMD mice was the same as in WT mice, irrespective of the diet (**Fig. 3i**). In the PMD spinal cord, the high-cholesterol diet normalized myelination and reduced reactive gliosis and T cell infiltration (**Supplementary Fig. 6**). All these changes correlated with an amelioration of the clinical score and improved the motor abilities of PMD mice close to WT levels (**Fig. 3j** and **Supplementary Video 1**). Already at 6 weeks of age, visual acuity was almost normal (data not shown). Unexpectedly, when PMD mice started the high-cholesterol diet only 1 week later (3–12 weeks, $n = 8$), visual acuity was comparable to that of PMD mice on a high-cholesterol diet from 6 to 12 weeks (**Fig. 1c**), and optic nerves were poorly myelinated. These findings underscore that the third week of life is crucial for myelination in the optic nerve of PMD mice. We note that at the age of 6 months PMD mice on a high-cholesterol diet appear healthy ($n = 14$, data not shown). Taken together, our results suggest that, for maximal amelioration of PMD pathology, treatment should begin early in life and continue into adulthood.

Oligodendrocyte-specific inactivation of cholesterol synthesis in *Plp1*-transgenic mice (cSQS knockout × PLP-tg$^{+/66}$) further aggravates pathology (**Supplementary Fig. 7** and **Supplementary Video 2**). We therefore asked whether cholesterol synthesis itself is affected in PMD oligodendrocytes and compared the expression of sterol-synthesizing enzymes by real-time RT-PCR in spinal cord from WT and PMD mice. The expression of *Hmgcr* (encoding the rate-limiting enzyme of cholesterol biosynthesis) and of *Fdft1* was strongly reduced in PMD mice on a normal diet as compared to WT mice (**Fig. 4a**). Notably, in brains of Niemann-Pick type C1 (NPC1) model mice, cholesterol synthesis is also downregulated[18,19]. PMD oligodendrocytes also have reduced expression of myelin genes as compared to WT mice[6,12]. We found reduced expression of *Mbp* (encoding myelin basic protein) in PMD spinal cord compared to WT spinal cord (for *Plp1*, this reduction is leveled out by the higher gene dosage), but no obvious oligodendrocyte loss (**Fig. 4a** and **Supplementary Fig. 6**). In cholesterol-fed PMD mice, we observed

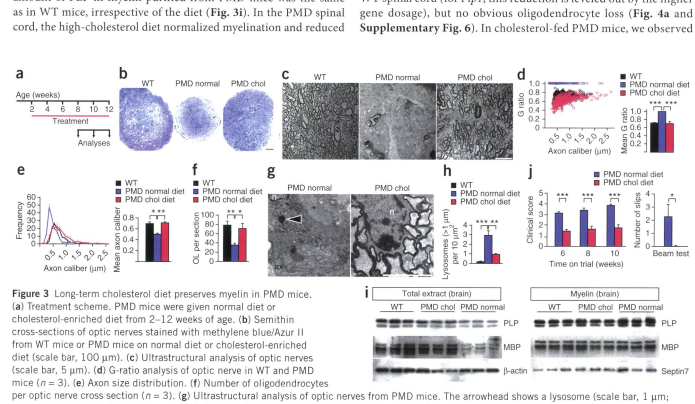

Figure 3 Long-term cholesterol diet preserves myelin in PMD mice. (**a**) Treatment scheme. PMD mice were given normal diet or cholesterol-enriched diet from 2–12 weeks of age. (**b**) Semithin cross-sections of optic nerves stained with methylene blue/Azur II from WT mice or PMD mice on normal diet or cholesterol-enriched diet (scale bar, 100 μm). (**c**) Ultrastructural analysis of optic nerves (scale bar, 5 μm). (**d**) G-ratio analysis of optic nerve in WT and PMD mice ($n = 3$). (**e**) Axon size distribution. (**f**) Number of oligodendrocytes per optic nerve cross section ($n = 3$). (**g**) Ultrastructural analysis of optic nerves from PMD mice. The arrowhead shows a lysosome (scale bar, 1 μm; ax, axon; n, nucleus, *, astrocyte process). (**h**) Quantification showing the abundance of large lysosomes in optic nerve (>1 μm in diameter; $n = 3$). (**i**) Western blot analysis of brain extracts and myelin-enriched fractions detecting the compact myelin proteins PLP and MBP. Loading controls are β-actin in extracts and Septin7 in myelin fractions. (**j**) Evaluation of the clinical score in mice. 1, normal; 2, mild tremor, mild ataxia; 3, strong tremor, strong ataxia; 4, seizures; 5, death ($n = 7$–9; unpaired Mann-Whitney test). Motor abilities of PMD mice after therapy assessed with a beam test (Student's *t* test, $n = 7$–9). Data are means ± s.e.m. $^*P < 0.05$; $^{**}P < 0.01$; $^{***}P < 0.001$, one-way ANOVA followed by Bonferroni test (**d**–**f**,**h**,**j**).

increased expression of *Mbp* and *Plp1* (**Fig. 4a**), probably reflecting ongoing myelination (compare to **Supplementary Fig. 6**). Thus, cholesterol treatment of PMD mice does not reduce *Plp1* overexpression, the primary cause of disease. Unexpectedly, cholesterol also increased transcription of genes for sterol-synthesizing enzymes (**Fig. 4a**). This finding was unexpected because it is thought that external cholesterol negatively feeds back on endogenous cholesterol biosynthesis[20] (see below).

To obtain insight into the mechanism by which additional cholesterol restores the integrity of *Plp1*-overexpressing oligodendrocytes, we cultured primary oligodendrocytes from WT and PMD mice (PMD oligodendrocytes). During differentiation, we supplemented the medium with cholesterol or zaragozic acid A , an inhibitor of squalene synthase and cholesterol biosynthesis (**Fig. 4b–h**). Compared to WT oligodendrocytes, PMD oligodendrocytes more often accumulated PLP in the cell soma, colocalizing with Lamp1 in endo/lysosomes. The addition of cholesterol decreased this intracellular PLP retention to the same level as found in WT oligodendrocytes (**Fig. 4c**).

Cholesterol promotes the differentiation of Schwann cells[21]. We found that cholesterol supplementation slightly enhanced the maturation of WT oligodendrocytes when we scored PLP-positive membrane sheaths (**Fig. 4d**). In turn, the inhibition of cholesterol synthesis reduced oligodendrocyte maturation by about 50% (**Fig. 4e**). Cholesterol availability may thus be limiting for the maturation of oligodendrocytes. In cultures of PMD oligodendrocytes, only 40% of cells matured compared to WT oligodendrocytes. This maturation almost doubled in the presence of extra cholesterol (**Fig. 4d**). Notably, the poor maturation of PMD oligodendrocytes was not further

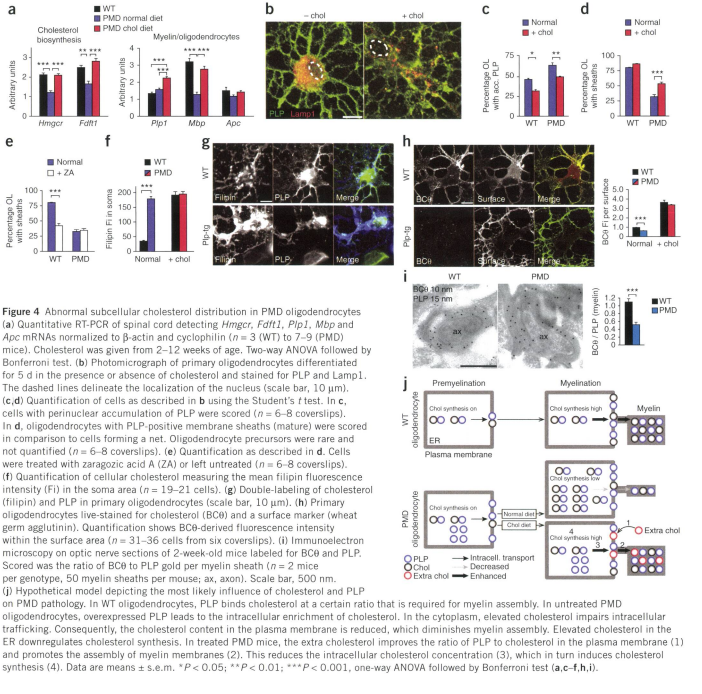

Figure 4 Abnormal subcellular cholesterol distribution in PMD oligodendrocytes (**a**) Quantitative RT-PCR of spinal cord detecting *Hmgcr*, *Fdft1*, *Plp1*, *Mbp* and *Apc* mRNAs normalized to β-actin and cyclophilin ($n = 3$ (WT) to 7–9 (PMD) mice). Cholesterol was given from 2–12 weeks of age. Two-way ANOVA followed by Bonferroni test. (**b**) Photomicrograph of primary oligodendrocytes differentiated for 5 d in the presence or absence of cholesterol and stained for PLP and Lamp1. The dashed lines delineate the localization of the nucleus (scale bar, 10 μm). (**c**,**d**) Quantification of cells as described in **b** using the Student's *t* test. In **c**, cells with perinuclear accumulation of PLP were scored ($n = 6$–8 coverslips). In **d**, oligodendrocytes with PLP-positive membrane sheaths (mature) were scored in comparison to cells forming a net. Oligodendrocyte precursors were rare and not quantified ($n = 6$–8 coverslips). (**e**) Quantification as described in **d**. Cells were treated with zaragozic acid A (ZA) or left untreated ($n = 6$–8 coverslips). (**f**) Quantification of cellular cholesterol measuring the mean filipin fluorescence intensity (Fi) in the soma area ($n = 19$–21 cells). (**g**) Double-labeling of cholesterol (filipin) and PLP in primary oligodendrocytes (scale bar, 10 μm). (**h**) Primary oligodendrocytes live-stained for cholesterol (BCθ) and a surface marker (wheat germ agglutinin). Quantification shows BCθ-derived fluorescence intensity within the surface area ($n = 31$–36 cells from six coverslips). (**i**) Immunoelectron microscopy on optic nerve sections of 2-week-old mice labeled for BCθ and PLP. Scored was the ratio of BCθ to PLP gold per myelin sheath ($n = 2$ mice per genotype, 50 myelin sheaths per mouse; ax, axon). Scale bar, 500 nm. (**j**) Hypothetical model depicting the most likely influence of cholesterol and PLP on PMD pathology. In WT oligodendrocytes, PLP binds cholesterol at a certain ratio that is required for myelin assembly. In untreated PMD oligodendrocytes, overexpressed PLP leads to the intracellular enrichment of cholesterol. In the cytoplasm, elevated cholesterol impairs intracellular trafficking. Consequently, the cholesterol content in the plasma membrane is reduced, which diminishes myelin assembly. Elevated cholesterol in the ER downregulates cholesterol synthesis. In treated PMD mice, the extra cholesterol improves the ratio of PLP to cholesterol in the plasma membrane (1) and promotes the assembly of myelin membranes (2). This reduces the intracellular cholesterol concentration (3), which in turn induces cholesterol synthesis (4). Data are means ± s.e.m. $^*P < 0.05$; $^{**}P < 0.01$; $^{***}P < 0.001$, one-way ANOVA followed by Bonferroni test (**a**,**c**–**f**,**h**,**i**).

impaired by zaragozic acid A (**Fig. 4e**). This underscores that cholesterol synthesis is perturbed in PMD oligodendrocytes, correlating with our *in vivo* data.

What causes the downregulation of cholesterol synthesis? PMD oligodendrocytes, grown in normal medium and labeled for cholesterol (using filipin, a fluorescent antibiotic that binds unesterified cholesterol), appeared cholesterol laden (**Fig. 4f,g**). Mean filipin-derived fluorescence intensity, which correlates with the cholesterol content[22], could barely be increased by cholesterol supplementation, in contrast to a six- to sevenfold increase seen in WT oligodendrocytes. Moreover, filipin fluorescence was barely seen in the soma of WT oligodendrocytes. In PMD oligodendrocytes, the strong intracellular filipin fluorescence was also found outside of endo/lysosomes (**Supplementary Fig. 8a**). When optic nerve sections from PMD mice at 2 weeks of age were stained for BCθ (ref. 23), a bacterial toxin that binds cholesterol, the ER of oligodendrocytes from PMD mice contained noticeably more BCθ-derived label compared to WT controls (**Supplementary Fig. 8b**). Thus, in the active phase of the disease, cholesterol abundance is increased in the ER, the cellular compartment that controls cellular cholesterol synthesis[20]. It is therefore plausible that cholesterol-laden PMD oligodendrocytes have downregulated cholesterol synthesis.

In what way could an elevated content of intracellular cholesterol affect myelin assembly? High cholesterol impairs intracellular trafficking[24–27], PLP overexpression in BHK cells prevents plasma membrane trafficking of a membrane lipid raft marker[13], possibly by elevation of intracellular cholesterol. In NPC1-null cells, the cholesterol content in the plasma membrane is decreased[28]. Thus, PMD oligodendrocytes may also suffer from intracellular trafficking defects and from reduced cholesterol content in the plasma membrane. Indeed, the plasma membrane of PMD oligodendrocytes showed reduced staining with BCθ to about 60% of WT levels (**Fig. 4h**). Moreover, the ratio of BCθ to PLP (quantified by immunoelectron microscopy) also revealed a similar reduction of cholesterol in myelin sheaths of PMD optic nerves (**Fig. 4i**). Notably, the staining density of PLP was similar in mutants and controls, in agreement with our biochemical data (**Fig. 3i**). The reduced association of PLP with membrane lipid rafts in PMD myelin further supports this notion[10].

Our data have revealed a previously unknown role of cholesterol in the clinical course of PMD (**Fig. 4j** contains a working model). PLP overexpression, when untreated, leads to increased intracellular concentration of this myelin protein and aberrant deposition in endo/lysosomes. As PLP associates with cholesterol, cholesterol abundance is also increased intracellularly. Elevated cholesterol in the ER seems to downregulate endogenous cholesterol synthesis. In the secretory pathways, excess cholesterol impairs vesicular transport. The resulting decreased amount of cholesterol in the plasma membrane seems too low for efficient myelin assembly[29]. We envision that the association of cholesterol with (increased) PLP in the ER inhibits PMD oligodendrocytes from downregulating cholesterol synthesis early enough to prevent the intracellular traffic jam that ultimately leads to impaired myelin assembly. This premature arrest of myelination in PMD mice[6–10] can be overcome by the administration of external cholesterol, presumably by improving the stoichiometry between PLP and cholesterol in the plasma membrane. Once bound to sufficient cholesterol, PLP is integrated into myelin membranes. This subsequently reduces the intracellular cholesterol and PLP concentration and allows for an increase of cell-autonomous cholesterol synthesis, which further promotes myelin membrane synthesis.

Together, our data suggest that dietary cholesterol does not cure PMD but has a striking potential to relieve oligodendrocytes from defects caused by Plp1 overexpression. This amelioration of disease in a mouse model of PMD has implications for therapeutic interventions in patients with PMD.

METHODS

Methods and any associated references are available in the online version of the paper.

Note: Supplementary information is available in the online version of the paper.

ACKNOWLEDGMENTS

We dedicate this work to the memory of Jim Garbern for his support of PMD research. We are grateful to A. Fahrenholz, T. Freerck, M. Schildmann, M. Matthes and A. Kanbach for technical support and thank J. Edgar for helpful comments on the manuscript. We thank M. Grebe (Umea University) for providing the BCθ expression construct and Pfizer for the generous gift of the squalestatin CP-340868. This work was funded by the PMD foundation and the Deutsche Forschungsgemeinschaft (SA2114/1-1) to G.S. K.-A.N. is supported by the EU-FP7 (Leukotreat, Ngidd), the Bundesministerium für Bildung und Forschung (BMBF; Leukonet) and a European Research Council (ERC) Advanced Grant. Support of the BMBF to S.L. and K.-F.S. is gratefully acknowledged (01GQ0810).

AUTHOR CONTRIBUTIONS

G.S. supervised the project, conducted experiments and wrote the manuscript; F.R., K.C. and T.R. conducted experiments, K.-F.S. and S.L. performed visual acuity measurements, P.D. conducted the two-photon microscopic analysis, B.B. implemented the beam test, W.M. supervised and contributed to electron microscopic studies, and K.-A.N. contributed to the discussion and the writing of the manuscript.

COMPETING FINANCIAL INTERESTS

The authors declare no competing financial interests.

Published online at http://www.nature.com/doifinder/10.1038/nm.2833.
Reprints and permissions information is available online at http://www.nature.com/reprints/index.html.

1. Seitelberger, F. Neuropathology and genetics of Pelizaeus-Merzbacher disease. *Brain Pathol.* **5**, 267–273 (1995).
2. Garbern, J.Y. Pelizaeus-Merzbacher disease: Genetic and cellular pathogenesis. *Cell Mol. Life Sci.* **64**, 50–65 (2007).
3. Woodward, K.J. The molecular and cellular defects underlying Pelizaeus-Merzbacher disease. *Expert Rev. Mol. Med.* **10**, e14 (2008).
4. Simons, M., Kramer, E.M., Thiele, C., Stoffel, W. & Trotter, J. Assembly of myelin by association of proteolipid protein with cholesterol- and galactosylceramide-rich membrane domains. *J. Cell Biol.* **151**, 143–154 (2000).
5. Saher, G. *et al.* High cholesterol level is essential for myelin membrane growth. *Nat. Neurosci.* **8**, 468–475 (2005).
6. Readhead, C., Schneider, A., Griffiths, I. & Nave, K.A. Premature arrest of myelin formation in transgenic mice with increased proteolipid protein gene dosage. *Neuron* **12**, 583–595 (1994).
7. Anderson, T.J. *et al.* Distinct phenotypes associated with increasing dosage of the PLP gene: implications for CMT1A due to PMP22 gene duplication. *Ann. NY Acad. Sci.* **883**, 234–246 (1999).
8. Anderson, T.J. *et al.* Late-onset neurodegeneration in mice with increased dosage of the proteolipid protein gene. *J. Comp. Neurol.* **394**, 506–519 (1998).
9. Edgar, J.M. *et al.* Demyelination and axonal preservation in a transgenic mouse model of Pelizaeus-Merzbacher disease. *EMBO Mol. Med.* **2**, 42–50 (2010).
10. Karim, S.A. *et al.* PLP/DM20 expression and turnover in a transgenic mouse model of Pelizaeus-Merzbacher disease. *Glia* **58**, 1727–1738 (2010).
11. Krämer, E.M., Schardt, A. & Nave, K.A. Membrane traffic in myelinating oligodendrocytes. *Microsc. Res. Tech.* **52**, 656–671 (2001).
12. Karim, S.A. *et al.* PLP overexpression perturbs myelin protein composition and myelination in a mouse model of Pelizaeus-Merzbacher disease. *Glia* **55**, 341–351 (2007).
13. Simons, M. *et al.* Overexpression of the myelin proteolipid protein leads to accumulation of cholesterol and proteolipid protein in endosomes/lysosomes: implications for Pelizaeus-Merzbacher disease. *J. Cell Biol.* **157**, 327–336 (2002).
14. Björkhem, I. & Meaney, S. Brain cholesterol: long secret life behind a barrier. *Arterioscler. Thromb. Vasc. Biol.* **24**, 806–815 (2004).
15. Alberti, S. *et al.* Hepatic cholesterol metabolism and resistance to dietary cholesterol in LXRbeta-deficient mice. *J. Clin. Invest.* **107**, 565–573 (2001).

16. Ip, C.W. *et al.* Origin of CD11b$^+$ macrophage-like cells in the CNS of PLP-overexpressing mice: low influx of haematogenous macrophages and unchanged blood-brain-barrier in the optic nerve. *Mol. Cell Neurosci.* **38**, 489–494 (2008).
17. Stolp, H.B. & Dziegielewska, K.M. Review: Role of developmental inflammation and blood-brain barrier dysfunction in neurodevelopmental and neurodegenerative diseases. *Neuropathol. Appl. Neurobiol.* **35**, 132–146 (2009).
18. Xie, C., Lund, E.G., Turley, S.D., Russell, D.W. & Dietschy, J.M. Quantitation of two pathways for cholesterol excretion from the brain in normal mice and mice with neurodegeneration. *J. Lipid Res.* **44**, 1780–1789 (2003).
19. Liu, B. *et al.* Reversal of defective lysosomal transport in NPC disease ameliorates liver dysfunction and neurodegeneration in the *Npc1*$^{-/-}$ mouse. *Proc. Natl. Acad. Sci. USA* **106**, 2377–2382 (2009).
20. Brown, M.S. & Goldstein, J.L. The SREBP pathway: regulation of cholesterol metabolism by proteolysis of a membrane-bound transcription factor. *Cell* **89**, 331–340 (1997).
21. Saher, G. *et al.* Cholesterol regulates the endoplasmic reticulum exit of the major membrane protein P0 required for peripheral myelin compaction. *J. Neurosci.* **29**, 6094–6104 (2009).
22. Qin, C., Nagao, T., Grosheva, I., Maxfield, F.R. & Pierini, L.M. Elevated plasma membrane cholesterol content alters macrophage signaling and function. *Arterioscler. Thromb. Vasc. Biol.* **26**, 372–378 (2006).
23. Shepard, L.A. *et al.* Identification of a membrane-spanning domain of the thiol-activated pore-forming toxin Clostridium perfringens perfringolysin O: an α-helical to β-sheet transition identified by fluorescence spectroscopy. *Biochemistry* **37**, 14563–14574 (1998).
24. Karten, B., Peake, K.B. & Vance, J.E. Mechanisms and consequences of impaired lipid trafficking in Niemann-Pick type C1–deficient mammalian cells. *Biochim. Biophys. Acta* **1791**, 659–670 (2009).
25. Otomo, T., Higaki, K., Nanba, E., Ozono, K. & Sakai, N. Lysosomal storage causes cellular dysfunction in mucolipidosis II skin fibroblasts. *J. Biol. Chem.* **286**, 35283–35290 (2011).
26. Tang, Y., Leao, I.C., Coleman, E.M., Broughton, R.S. & Hildreth, J.E. Deficiency of niemann-pick type C-1 protein impairs release of human immunodeficiency virus type 1 and results in Gag accumulation in late endosomal/lysosomal compartments. *J. Virol.* **83**, 7982–7995 (2009).
27. Sobo, K. *et al.* Late endosomal cholesterol accumulation leads to impaired intra-endosomal trafficking. *PLoS ONE* **2**, e851 (2007).
28. Hawes, C.M., Wiemer, H., Krueger, S.R. & Karten, B. Pre-synaptic defects of NPC1-deficient hippocampal neurons are not directly related to plasma membrane cholesterol. *J. Neurochem.* **114**, 311–322 (2010).
29. Bauer, N.G., Richter-Landsberg, C. & Ffrench-Constant, C. Role of the oligodendroglial cytoskeleton in differentiation and myelination. *Glia* **57**, 1691–1705 (2009).

nature medicine

Viral delivery of miR-196a ameliorates the SBMA phenotype via the silencing of CELF2

Yu Miyazaki[1], Hiroaki Adachi[1], Masahisa Katsuno[1], Makoto Minamiyama[1], Yue-Mei Jiang[1], Zhe Huang[1], Hideki Doi[1], Shinjiro Matsumoto[1], Naohide Kondo[1], Madoka Iida[1], Genki Tohnai[1], Fumiaki Tanaka[1], Shin-ichi Muramatsu[2] & Gen Sobue[1]

Spinal and bulbar muscular atrophy (SBMA) is an inherited neurodegenerative disorder caused by the expansion of the polyglutamine (polyQ) tract of the androgen receptor (AR-polyQ)[1,2]. Characteristics of SBMA include proximal muscular atrophy, weakness, contraction fasciculation and bulbar involvement[3]. MicroRNAs (miRNAs) are a diverse class of highly conserved small RNA molecules that function as crucial regulators of gene expression in animals and plants[4]. Recent functional studies have shown the potent activity of specific miRNAs as disease modifiers both *in vitro* and *in vivo*[5–8]. Thus, potential therapeutic approaches that target the miRNA processing pathway have recently attracted attention[9,10]. Here we describe a novel therapeutic approach using the adeno-associated virus (AAV) vector–mediated delivery of a specific miRNA for SBMA. We found that miR-196a enhanced the decay of the AR mRNA by silencing CUGBP, Elav-like family member 2 (CELF2). CELF2 directly acted on AR mRNA and enhanced the stability of AR mRNA. Furthermore, we found that the early intervention of miR-196a delivered by an AAV vector ameliorated the SBMA phenotypes in a mouse model. Our results establish the proof of principle that disease-specific miRNA delivery could be useful in neurodegenerative diseases.

A mouse model of SBMA has been developed[11], and several therapeutic approaches for SBMA have been presented using this mouse model[11–15]. Among these approaches, the reduction of mutant AR protein levels in male mice ameliorated disease manifestations, suggesting a potential therapy for SBMA. miRNAs guide the RNA-induced silencing complex to mRNAs that have a target sequence complementary to that of the miRNA. The interaction between the miRNA and the target can occur with an incomplete complementary sequence; thus, a single miRNA can modulate complex physiological functions or disease phenotypes by regulating widespread networks[16]. Over the last several years, an important role of miRNAs in the pathogenesis of neurodegenerative disorders has been reported[5–8,17,18].

In this study, we used a miRNA microarray analysis to compare the miRNA expression in the spinal cords of male transgenic SBMA model mice expressing full-length human AR with 97 glutamine residues (AR-97Q) and in male mice expressing wild-type human AR (AR-24Q)[11]. Of more than 500 miRNAs tested, miR-196a (accession number MIMAT_0000518), miR-196b (accession number MIMAT_0001081), miR-496 (accession number MIMAT_0003738), miR miR-323-3p (accession number MIMAT_0000551) and miR-29b* (accession number MIMAT_0004523) showed a greater than two-fold upregulation in the spinal cord of AR-97Q mice at an advanced disease stage relative to the AR-24Q mice (**Fig. 1a**).

To examine the effects of these five miRNAs on the expression levels of AR mRNA transcribed from the *AR* gene, we co-transfected synthetic miRNAs with vectors expressing human AR-24Q or AR-97Q into HEK293T cells. Among these five miRNAs, miR-196a and miR-196b downregulated the AR mRNA and protein (**Fig. 1b,c**), although the transgene used in both the *in vitro* and *in vivo* experiments lacked the DNA sequence that encodes the AR mRNA 3′ untranslated region (UTR) (**Supplementary Fig. 1**). To determine whether the decrease in the AR mRNA level was due to the enhancement of mRNA degradation or a decrease in mRNA synthesis, we assessed the turnover of AR mRNA using an RNA stability assay with actinomycin D. In the absence of miR-196a and miR-196b, the AR mRNA had a half-life of >1.5 h. The AR mRNA had a half-life of <0.5 h in the presence of miR-196a and miR-196b (**Fig. 1d**). These findings indicated that miR-196a and miR-196b enhanced the degradation of AR mRNA via an interaction with cofactors that were able to stabilize both the wild-type and mutant AR mRNAs.

To elucidate the molecular mechanisms by which miR-196a and miR-196b regulate the stability of AR mRNA, we analyzed their potential targets using the bioinformatics program TargetScan Release 6.0. Among the hundreds of mRNAs targeted by miR-196a and miR-196b, CELF2 mRNA has a common binding site for miR-196a and miR-196b that is broadly conserved among vertebrates (**Supplementary Fig. 2**). We found that CELF2 mRNA and protein levels were significantly reduced by treatment with miR-196a and miR-196b in HEK293T cells (**Fig. 1e**) and that CELF2 was required for AR mRNA stability

[1]Department of Neurology, Nagoya University Graduate School of Medicine, Nagoya, Japan. [2]Division of Neurology, Department of Medicine, Jichi Medical University, Tochigi, Japan. Correspondence should be addressed to G.S. (sobueg@med.nagoya-u.ac.jp).

Received 3 October 2011; accepted 18 April 2012; published online 3 June 2012; doi:10.1038/nm.2791

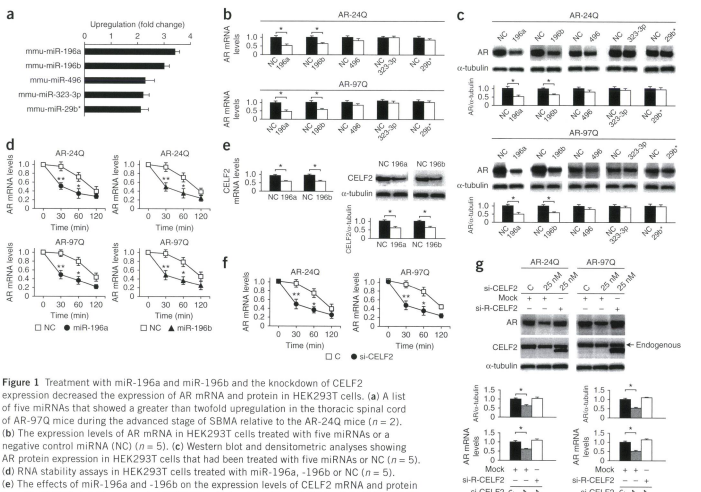

Figure 1 Treatment with miR-196a and miR-196b and the knockdown of CELF2 expression decreased the expression of AR mRNA and protein in HEK293T cells. (**a**) A list of five miRNAs that showed a greater than twofold upregulation in the thoracic spinal cord of AR-97Q mice during the advanced stage of SBMA relative to the AR-24Q mice ($n = 2$). (**b**) The expression levels of AR mRNA in HEK293T cells treated with five miRNAs or a negative control miRNA (NC) ($n = 5$). (**c**) Western blot and densitometric analyses showing AR protein expression in HEK293T cells that had been treated with five miRNAs or NC ($n = 5$). (**d**) RNA stability assays in HEK293T cells treated with miR-196a, -196b or NC ($n = 5$). (**e**) The effects of miR-196a and -196b on the expression levels of CELF2 mRNA and protein ($n = 5$). (**f**) RNA stability assays in HEK293T cells treated with a siRNA for CELF2 (si-SELF2) or a scrambled control siRNA (C) ($n = 5$). (**g**) The expression levels of AR mRNA and protein treated with si-CELF2 and the reversal of the effect by treatment with a DNA plasmid expressing siRNA-resistant-CELF2 (si-R-CELF2) ($n = 5$). All data are means ± s.e.m. $^*P < 0.05$ and $^{**}P < 0.01$. We analyzed the results by unpaired t tests in **b**, **c** and **e**; by two-way ANOVA followed by the Bonferroni test comparing HEK293T cells treated with miR-196a or miR-196b to cells treated with NC in **d**; by two-way ANOVA followed by the Bonferroni test comparing HEK293T cells treated with si-CELF2 to cells treated with control siRNA in **f**; and by the Dunnett test in **g**.

(**Fig. 1f**). The knockdown of CELF2 expression with specific small interfering RNAs (siRNAs) silenced CELF2 protein, accelerated the degradation of AR mRNA and led to a decrease in AR protein expression levels (**Fig. 1g**). These downregulating effects were reversed in rescue experiments using a DNA plasmid that expressed siRNA-resistant CELF2, thus confirming the interaction between CELF2 and AR mRNA (**Fig. 1g**). In contrast to the knockdown and rescue results, the overexpression of CELF2 increased the expression levels of AR mRNA and protein (**Fig. 2a**) and increased the stability of the AR mRNA (**Fig. 2b**). To determine the region of the AR mRNA that interacts with CELF2, we prepared several constructs of the mutated *AR* transgene that lacked the CAG repeats (AR-0Q) or the three triplet repeats of the CUGCUGCUG sequence (ΔCUG-AR-24Q and ΔCUG-AR-97Q), which is immediately proximal to the CAG repeats in exon 1 of the AR mRNA and is conserved in the endogenous human AR mRNA (**Fig. 2c**). Although the overexpression of CELF2 increased the expression levels of AR mRNA and protein transcribed from the mutated transgene lacking CAG repeats, the expression levels of AR mRNA and protein transcribed from the mutated transgene lacking the three triplet repeats of the CUGCUGCUG sequence were not increased relative to controls by CELF2 (**Fig. 2d**). In addition, immunoprecipitation-coupled quantitative real time-PCR (qRT-PCR) revealed the binding affinity of CELF2 to the three triplet repeats of the CUGCUGCUG sequence in exon 1 of the AR mRNA (**Fig. 2e**). On the basis of these findings, we concluded that miR-196a and miR-196b were able to decrease the expression levels of AR mRNA and protein by silencing CELF2, a protein that enhances the stability of AR mRNA through direct binding to the CUG triplet repeat sequence in exon 1 of the AR mRNA.

To examine the effects of CELF2 silencing on the motor impairment of SBMA mice, we constructed an *in vivo* delivery system based on an AAV vector that allowed for the simultaneous expression of enhanced green fluorescent protein (EGFP) and either miR-196a (AAV-miR-196a) or a nonspecific miRNA, miR-mock (AAV-miR-mock). We chose to use miR-196a instead of miR-196b because the expression of miR-196a was highly upregulated in the cytoplasm of the motor neurons of AR-97Q mice (**Supplementary Fig. 3**). A viral load of 10^{11} vector genomes (vg) of each of these constructs was injected into the skeletal muscle of the left quadriceps femoris of AR-97Q mice. The AAV vector can be transported efficiently in a retrograde manner from muscle to the motor neurons of the spinal cord[19,20] and can spread hematogenously[21,22]. Two weeks after AAV vector injection,

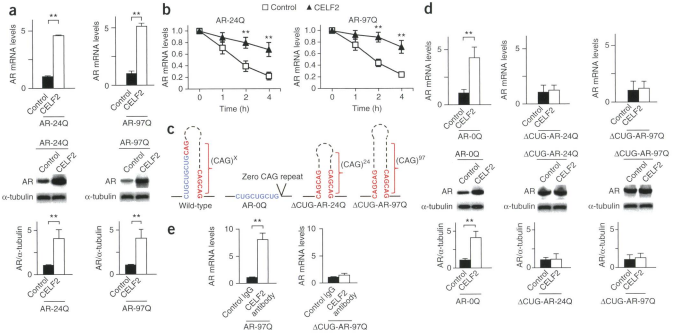

Figure 2 CELF2 recognizes the sequence CUGCUGCUG in exon 1 of the AR mRNA and increases the stability of the AR mRNA. (**a**) The expression levels of AR mRNA and protein in HEK293T cells treated with the DNA plasmid expressing human CELF2 (CELF2) or the original pcDNA3.1/HisC vector (control) ($n = 5$). (**b**) RNA stability assays in HEK293T cells treated with CELF2 or control ($n = 5$). (**c**) Schematic diagrams of the AR mRNA structure near the hairpin loop of the CAG repeats (red) transcribed from wild-type and mutated DNA plasmids. AR-0Q lacks the CAG repeats, and ΔCUG-AR-24Q and ΔCUG-AR-97Q lack the sequence CUGCUGCUG (blue) immediately adjacent to the CAG repeats. (**d**) AR mRNA and protein expression levels in HEK293T cells co-transfected with CELF2 and the mutated DNA plasmids expressing AR ($n = 5$). (**e**) The amount of AR-97Q and ΔCUG-AR-97Q mRNA binding to CELF2 that was immunoprecipitated using an antibody against CELF2 or a control immunoglobulin (IgG) ($n = 5$). All data are means ± s.e.m. $^{**}P < 0.01$ (we analyzed the results by unpaired *t* tests in **a**,**d** and **e** and by two-way ANOVA followed by the Bonferroni test comparing HEK293T cells treated with CELF2 to cells treated with control in **b**).

a widespread transduction of the viral particles throughout the brain, spinal cord and the skeletal muscle of the upper and lower limbs was observed (**Supplementary Fig. 4a**). There was no difference in the expression of EGFP between the left and right sides of the spinal cord (**Supplementary Fig. 4b**). The presence of the AAV vector in the motor neurons of infected mice was visually confirmed by the colocalization of EGFP and staining for choline acetyltransferase (ChAT), a motor neuron marker (**Supplementary Fig. 4c**). Because the widespread viral transduction throughout the entire body was also detected in mice in which virus was injected into a cardiac chamber (**Supplementary Fig. 4d**), we deduced that the viral particles injected into the hind limb skeletal muscle spread hematogenously throughout the entire body of the mouse. In addition to viral distribution, a tyrosine mutation of the adeno-associated viral capsid protein may contribute to the enhanced transgene expression levels delivered by AAV[23]. We then did an AAV vector injection into the quadriceps femoris of a 5-week-old mouse, before the onset of motor impairment in the SBMA mice (approximately 7 weeks of age), because transgene expression stabilizes approximately 2 weeks after vector delivery.

The disease progression in the AR-97Q mice treated with AAV-miR-196a (AR-97Q-miR-196a mice) was ameliorated compared with AAV-miR-mock-treated mice. The AR-97Q mice treated with AAV-miR-mock (AR-97Q-miR-mock mice) showed motor impairment, as assessed by the rotarod task, as early as 7 weeks after birth. By contrast, the AR-97Q-miR-196a mice showed an initial impairment at 13 weeks after birth but showed less deterioration than their AR-97Q-miR-mock counterparts ($P < 0.001$) (**Fig. 3a**). The locomotor cage activity of the AR-97Q-miR-mock mice was also markedly decreased at 7 weeks compared with that of the AR-97Q-miR-196a mice ($P < 0.001$), which showed decreased activity at 13 weeks of age (**Fig. 3b**). Moreover, the AR-97Q-miR-mock mice lost weight significantly earlier and more profoundly than the AR-97Q-miR-196a mice ($P < 0.001$) (**Fig. 3c**). Treatment with miR-196a significantly prolonged the survival of the AR-97Q-miR-196a mice ($P < 0.001$) compared with the AR-97Q-miR-mock mice (**Fig. 3d**). By 12 weeks of age, the AR-97Q-miR-mock mice showed obvious differences in body size, muscular atrophy and kyphosis compared with the AR-97Q-miR-196a mice (**Fig. 3e**). In addition, the AR-97Q-miR-mock mice showed motor weakness, as indicated by short steps and leg dragging, whereas the AR-97Q-miR-196a mice showed almost normal ambulation (**Fig. 3f**). Immunohistochemical examination of mouse tissues using 1C2 antibody, which specifically recognizes the expanded polyQ region in the mutant AR, showed a marked reduction in 1C2-positive nuclear accumulation in the anterior horn of the thoracic spinal cord and in the skeletal muscles of the right quadriceps femoris of the AR-97Q-miR-196a mice compared with those of the AR-97Q-miR-mock mice. Glial fibrillary acidic protein (GFAP)-specific antibody staining showed that the AAV vector–mediated delivery of miR-196a reduced reactive astrogliosis in the thoracic spinal anterior horn of the AR-97Q mice, thereby suggesting that miR-196a attenuated neurodegenerative changes. Histopathological examination of the skeletal muscle showed marked amelioration of neurogenic muscle atrophy in the AR-97Q-miR-196a mice compared with the AR-97Q-miR-mock mice (**Fig. 3g**). By quantitative assessment, we confirmed that AAV-miR-196a significantly reduced 1C2-positive nuclear accumulation in the anterior horn of the thoracic spinal cord ($P < 0.01$) and

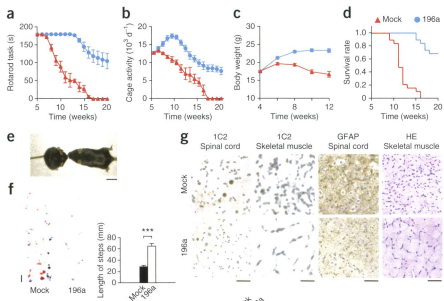

Figure 3 The effects of miR-196a on the phenotype of male AR-97Q mice. (**a**–**d**) A rotarod task (**a**), cage activity (**b**), body weight (**c**) and survival rate (Kaplan-Meier analysis and log-rank test) (**d**) of the AR-97Q-miR-mock (mock) or AR-97Q-miR-196a mice (196a) ($n = 19$ in each group). $P < 0.001$ for all data at each time after 8 weeks of age in **a**–**c**. (**e**,**f**) A representative photograph (**e**) and footprints (**f**) of a 12-week-old AR-97Q-miR-mock mouse (left) and an age-matched AR-97Q-miR-196a mouse (right). The front and hind paws are indicated in red and blue, respectively. Each column shows the average length of the steps taken by the hind paw ($n = 5$). Scale bars, 20 mm. (**g**) Immunohistochemical staining for the mutant AR using the 1C2 antibody of the thoracic spinal cord and skeletal muscle of the right quadriceps femoris; immunohistochemical staining with a GFAP-specific antibody of the thoracic spinal anterior horn; and hematoxylin and eosin (HE) staining of the skeletal muscle of the right quadriceps femoris. Scale bars, left to right: 50 μm, 10 μm, 50 μm, 20 μm. (**h**) Quantification of 1C2-positive cells in the thoracic spinal cord and skeletal muscle of the right quadriceps femoris ($n = 5$). (**i**) Western blot and densitometric analyses showing the levels of GFAP protein expression in the thoracic spinal cord ($n = 5$). (**j**) The mean size of the motor neurons of the thoracic spinal cord obtained from AR-97Q-miR-196a mice compared with that of AR-97Q-miR-mock mice ($n = 5$). Scale bar, 20 μm. All data are means ± s.e.m. $^*P < 0.05$, $^{**}P < 0.01$ and $^{***}P < 0.001$ (we analyzed the results by two-way ANOVA followed by the Bonferroni test comparing the mock to 196a in **a**–**c** and by unpaired t test in **f**, **h**–**j**).

in the skeletal muscle of the right quadriceps femoris ($P < 0.001$) of the AR-97Q-mice (**Fig. 3h**). Western blot analyses and quantification of the immunohistochemical signal intensities revealed that treatment with miR-196a downregulated the expression levels of GFAP (**Fig. 3i** and **Supplementary Fig. 5**). In addition, treatment with miR-196a significantly suppressed motor neuron shrinkage ($P < 0.001$) (**Fig. 3j**).

At 3 weeks after injection of a viral load of 10^{11} vg, we killed the mice and harvested the RNA and protein in the thoracic spinal cord for analysis. The AR-97Q-miR-196a mice showed high expression levels of miR-196a and low expression levels of CELF2 mRNA, mutant AR mRNA and the endogenous mouse AR mRNA in the thoracic spinal cord compared with AR-97Q-miR-mock mice (**Fig. 4a**). The mouse AR mRNA lacks a CUGCUGCUG tract; however, it has the CUGCUG sequence in its coding region that would interact with CELF2. Western blotting analyses of thoracic spinal cord lysates of the AR-97Q-miR-mock mice showed that the high-molecular-weight mutant AR protein complex was retained in the stacking gel and that a monomeric AR migrated as a band through the separating gel (**Fig. 4b**). Treatment with AAV-miR-196a notably reduced both the high-molecular-weight complex and the monomer of AR and CELF2 in the thoracic spinal cord (**Fig. 4b**). We observed the elevated expression levels of miR-196a achieved by AAV vector–mediated expression and the decreased expression levels of mutant AR mRNA in the thoracic spinal cord throughout the follow-up period of 15 weeks (**Fig. 4c**). Although we detected the effects of the miR-196a treatment in the skeletal muscle, we found that the increase in the levels of miR-196a expression and the downregulation of mutant AR mRNA and protein were more prominent in the spinal cord than in the skeletal muscle (**Supplementary Fig. 6**). The skeletal muscle of the right quadriceps femoris, contralateral to the site of the AAV vector injection, also showed treatment effects (**Supplementary Fig. 6**). AR-97Q-miR-196a mice showed no detectable reduction in the normal serum testosterone levels, which has been shown to directly affect the levels of AR expression (**Fig. 4d**)[11].

To address whether miR-196a-mediated treatment can be useful in the therapy of patients with SBMA, we examined the effects of miR-196a on AR mRNA and protein in fibroblasts obtained from patients with SBMA and from disease control subjects. Treatment with miR-196a downregulated both the AR and CELF2 mRNAs and proteins in the fibroblasts obtained from patients with SBMA (**Fig. 4e**) and disease control subjects (**Supplementary Fig. 7**). We also observed similar effects for AR mRNA and protein in fibroblasts treated with CELF2 siRNA (**Fig. 4f**). Taken together, these findings suggest that miR-196a-mediated treatment might be useful in the therapy of patients with SBMA. Furthermore, we measured the expression levels of miR-196a, miR-196b and CELF2 mRNA in the thoracic spinal cord of patients with SBMA. Both of the two miRNAs were upregulated and the CELF2 mRNA was downregulated in the thoracic spinal cord of patients with SBMA compared with those of disease control subjects (**Fig. 4g**). qRT-PCR revealed that the expression levels of CELF2 mRNA were lower in the thoracic spinal cord of AR-97Q mice than in AR-24Q mice (**Supplementary Fig. 8**), thereby confirming the correlations between the *in vivo* levels of the two miRNAs and CELF2 mRNA. We also showed the *in vivo* correlation between miR-196a and mutant AR mRNA levels and monitored the side effects of mice treated with AAV-miR-196a (**Supplementary Note**

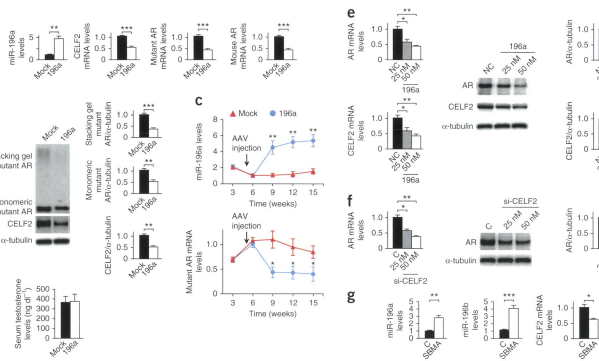

Figure 4 The effects of miR-196a on mutant AR expression in male AR-97Q mice and patients with SBMA. (**a**) The levels of miR-196a, CELF2 mRNA, mutant AR mRNA and the endogenous mouse AR mRNA expression in the thoracic spinal cord of AR-97Q-miR-mock (mock) and AR-97Q-miR-196a (196a) mice ($n = 5$). (**b**) Western blot and densitometric analyses showing the expression levels of mutant AR both in the stacking and separating gels as well as those of CELF2 ($n = 5$). (**c**) A temporal change in the levels of miR-196a and mutant AR mRNA expression in the thoracic spinal cord of AR-97Q-miR-mock and AR-97Q-miR-196a mice ($n = 3$ to 4). (**d**) The serum testosterone levels of AR-97Q-miR-mock and AR-97Q-miR-196a mice ($n = 5$). (**e**) The expression levels of mutant AR mRNA, CELF2 mRNAs and their proteins in the fibroblasts of patients with SBMA ($n = 5$). NC, a negative control miRNA. (**f**) The effects of CELF2 silencing on mutant AR mRNA and protein in the fibroblasts of patients with SBMA ($n = 5$). C, a scrambled control siRNA. (**g**) The expression levels of miR-196a, -196b and CELF2 mRNA in the thoracic spinal cord of patients with SBMA ($n = 3$). C, disease control subjects. All data are means ± s.e.m. $^*P < 0.05$, $^{**}P < 0.01$ and $^{***}P < 0.001$ (we analyzed the results by unpaired t tests in **a**,**b**,**d** and **g** and by two-way ANOVA followed by the Bonferroni test comparing the mock to 196a in **c**, and by the Dunnett test in **e**,**f**).

and **Supplementary Fig. 8**). In addition, we examined the post-translational effects of miR-196a in HEK293T and the effects of miR-196a on apoptosis in Neuro2a cells (**Supplementary Note** and **Supplementary Fig. 9**). We also showed the effects of miR-196a downregulation on mutant AR mRNA and protein in HEK293T cells (**Supplementary Note** and **Supplementary Fig. 10**).

In this study, we showed that miR-196a is upregulated in the spinal cord of a transgenic mouse model of SBMA during the symptomatic stage and that early intervention by the transduction of mice with miR-196a via an AAV vector can markedly ameliorate the motor impairment of SBMA mice. We further showed that miR-196a silences CELF2, which then directly acts on AR mRNA to affect its stability. Although polyQ models have been shown to have altered miRNA profiles[7,17] and miRNAs targeting of the polyQ disease gene have been proposed as disease modifiers [6,7], the miRNA-mediated therapeutic approach targeting a regulator of the disease transcript described in our study is conceptually novel and could be strategically applied to other polyQ-related diseases.

The upregulation of miR-196a has been reported in a wide variety of cancers[24,25] and has also been shown to be involved in differentiation[26,27] and the development of the immune system[28]. Hence, miR-196a has previously been proposed as a therapeutic target for these ailments. Similarly, the modulation of CELF2 has known implications for myotonic dystrophy[29] and several cancer types[30,31].

Our results show that the strong and continuous inhibition of the expression of CELF2 by the AAV vector–mediated delivery of miR-196a has a substantial effect on the SBMA phenotype. Although the reason for the natural upregulation of miR-196a in the spinal cord of SBMA mice and patients with SBMA is unknown, it may indicate a protective mechanism that is insufficient alone but sufficiently beneficial when amplified by AAV-mediated overexpression. However, whether similarly effective therapy would result from injections to an isolated skeletal muscle in patients with SBMA must be verified. The appropriate route and the required dose of AAV administration should be determined in future studies. Our findings indicate that the miRNA-mediated regulation of RNA metabolism is a logical target for the therapeutic intervention of SBMA and they suggest a new therapeutic approach using an AAV vector–mediated miRNA delivery system for the treatment of neurodegenerative disease.

METHODS

Methods and any associated references are available in the online version of the paper.

Note: Supplementary information is available in the online version of the paper.

ACKNOWLEDGMENTS

We are grateful to T. Cooper (Department of Pathology and Immunology, Baylor College of Medicine) for kindly providing the plasmid expressing human CELF2. We also thank N. Takino, H. Miyauchi and K. Ayabe (Division of Neurology, Department of Medicine, Jichi Medical University) for their help with the production of the AAV vectors and Y. Kondo and K. Shinjo (Division of Molecular Oncology, Aichi Cancer Center Research Institute) for expert technical support and helpful discussions. This work was supported by grants from the Ministry of Health,

Labor and Welfare; grants from the Ministry of Education, Culture, Sports, Science, and Technology of Japan; a Center-of-Excellence (COE) grant; a Grant-in-Aid for Scientific Research on Innovated Areas "Foundations of Synapse and Neurocircuit Pathology"; and the Core Research for Evolutional Science and Technology (CREST) program of the Japan Science and Technology Agency (JST).

AUTHOR CONTRIBUTIONS

Project planning was done by Y.M., H.A., M.K., F.T., S. Muramatsu and G.S.; experimental work was done by Y.M., H.A., M.K., M.M., Y.-M.J., Z.H., H.D., S. Matsumoto, N.K., M.I., G.T. and S. Muramatsu; data analysis was done by Y.M., H.A., M.K., F.T., S. Muramatsu and G.S.; the manuscript was written by Y.M., H.A., M.K., F.T., S. Muramatsu and G.S.

COMPETING FINANCIAL INTERESTS

The authors declare no competing financial interests.

Published online at http://www.nature.com/doifinder/10.1038/nm.2791.
Reprints and permissions information is available online at http://www.nature.com/reprints/index.html.

1. La Spada, A.R., Wilson, E.M., Lubahn, D.B., Harding, A.E. & Fischbeck, K.H. Androgen receptor gene mutations in X-linked spinal and bulbar muscular atrophy. *Nature* **352**, 77–79 (1991).
2. Kennedy, W.R., Alter, M. & Sung, J.H. Progressive proximal spinal and bulbar muscular atrophy of late onset: a sex-linked recessive trait. *Neurology* **50**, 583–593 (1998).
3. Sobue, G. *et al.* X-linked recessive bulbospinal neuronopathy. A clinicopathological study. *Brain* **112**, 209–232 (1989).
4. Kim, V.N., Han, J. & Siomi, M.C. Biogenesis of small RNAs in animals. *Nat. Rev. Mol. Cell Biol.* **10**, 126–139 (2009).
5. Kim, J. *et al.* A MicroRNA feedback circuit in midbrain dopamine neurons. *Science* **317**, 1220–1224 (2007).
6. Karres, J.S., Hilgers, V., Carrera, I., Treisman, J. & Cohen, S.M. The conserved microRNA miR-8 tunes atrophin levels to prevent neurodegeneration in *Drosophila*. *Cell* **131**, 136–145 (2007).
7. Lee, Y. *et al.* miR-19, miR-101 and miR-130 co-regulate ATXN1 levels to potentially modulate SCA1 pathogenesis. *Nat. Neurosci.* **11**, 1137–1139 (2008).
8. Williams, A.H. *et al.* MicroRNA-206 delays ALS progression and promotes regeneration of neuromuscular synapses in mice. *Science* **326**, 1549–1554 (2009).
9. Roshan, R., Ghosh, T., Scaria, V. & Pillai, B. MicroRNAs: novel therapeutic targets in neurodegenerative diseases. *Drug Discov. Today* **14**, 1123–1129 (2009).
10. Boudreau, R.L., Rodríguez-Lebrón, E. & Davidson, B.L. RNAi medicine for the brain: progresses and challenges. *Hum. Mol. Genet.* **20**, R21–R27 (2011).
11. Katsuno, M. *et al.* Testosterone reduction prevents phenotypic expression in a transgenic mouse model of spinal and bulbar muscular atrophy. *Neuron* **35**, 843–854 (2002).
12. Katsuno, M. *et al.* Leuprorelin rescues polyglutamine-dependent phenotypes in a transgenic mouse model of spinal and bulbar muscular atrophy. *Nat. Med.* **9**, 768–773 (2003).
13. Adachi, H. *et al.* Heat shock protein 70 chaperone overexpression ameliorates phenotypes of the spinal and bulbar muscular atrophy transgenic mouse model by reducing nuclear-localized mutant androgen receptor protein. *J. Neurosci.* **23**, 2203–2211 (2003).
14. Waza, M. *et al.* 17-AAG, an Hsp90 inhibitor, ameliorates polyglutamine-mediated motor neuron degeneration. *Nat. Med.* **11**, 1088–1095 (2005).
15. Tokui, K. *et al.* 17-DMAG ameliorates polyglutamine-mediated motor neuron degeneration through well-preserved proteasome function in an SBMA model mouse. *Hum. Mol. Genet.* **18**, 898–910 (2009).
16. Eacker, S.M., Dawson, T.M. & Dawson, V.L. Understanding microRNAs in neurodegeneration. *Nat. Rev. Neurosci.* **10**, 837–841 (2009).
17. Bilen, J., Liu, N., Burnett, B.G., Pittman, R.N. & Bonini, N.M. MicroRNA pathways modulate polyglutamine-induced neurodegeneration. *Mol. Cell* **24**, 157–163 (2006).
18. Schaefer, A. *et al.* Cerebellar neurodegeneration in the absence of microRNAs. *J. Exp. Med.* **204**, 1553–1558 (2007).
19. Kaspar, B.K. *et al.* Retrograde viral delivery of IGF-1 prolongs survival in a mouse ALS model. *Science* **301**, 839–842 (2003).
20. Towne, C. *et al.* Efficient transduction of non-human primate motor neurons after intramuscular delivery of recombinant AAV serotype 6. *Gene Ther.* **17**, 141–146 (2010).
21. Dominguez, E. *et al.* Intravenous scAAV9 delivery of a codon-optimized SMN1 sequence rescues SMA mice. *Hum. Mol. Genet.* **20**, 681–693 (2011).
22. Fu, H., Dirosario, J., Killedar, S., Zaraspe, K. & McCarty, D.M. Correction of neurological disease of mucopolysaccharidosis IIIB in adult mice by rAAV9 trans-blood-brain barrier gene delivery. *Mol. Ther.* **19**, 1025–1033 (2011).
23. Petrs-Silva, H. *et al.* Novel properties of tyrosine-mutant AAV2 vectors in the mouse retina. *Mol. Ther.* **19**, 293–301 (2011).
24. Hui, A.B. *et al.* Robust global micro-RNA profiling with formalin-fixed paraffin-embedded breast cancer tissues. *Lab. Invest.* **89**, 597–606 (2009).
25. Maru, D.M. *et al.* MicroRNA-196a is a potential marker of progression during Barrett's metaplasia-dysplasia-invasive adenocarcinoma sequence in esophagus. *Am. J. Pathol.* **174**, 1940–1948 (2009).
26. Yekta, S., Shih, I.H. & Bartel, D.P. MicroRNA-directed cleavage of HOXB8 mRNA. *Science* **304**, 594–596 (2004).
27. Hornstein, E. *et al.* The microRNA miR-196 acts upstream of Hoxb8 and Shh in limb development. *Nature* **438**, 671–674 (2005).
28. Pedersen, I.M. *et al.* Interferon modulation of cellular microRNAs as an antiviral mechanism. *Nature* **449**, 919–922 (2007).
29. Dhaenens, C.M. *et al.* Mis-splicing of *Tau* exon 10 in myotonic dystrophy type 1 is reproduced by overexpression of CELF2 but not by MBNL1 silencing. *Biochim. Biophys. Acta* **1812**, 732–742 (2011).
30. Natarajan, G. *et al.* CUGBP2 downregulation by prostaglandin E2 protects colon cancer cells from radiation-induced mitotic catastrophe. *Am. J. Physiol. Gastrointest. Liver Physiol.* **294**, G1235–G1244 (2008).
31. Subramaniam, D. *et al.* RNA binding protein CUGBP2/CELF2 mediates curcumin-induced mitotic catastrophe of pancreatic cancer cells. *PLoS ONE* **6**, e16958 (2011).

TECHNICAL REPORTS

nature medicine

Versatile robotic interface to evaluate, enable and train locomotion and balance after neuromotor disorders

Nadia Dominici[1,2,8], Urs Keller[3,8], Heike Vallery[3,4], Lucia Friedli[1,2], Rubia van den Brand[1,2], Michelle L Starkey[5,6], Pavel Musienko[1,2,7], Robert Riener[3,6] & Grégoire Courtine[1,2]

Central nervous system (CNS) disorders distinctly impair locomotor pattern generation and balance, but technical limitations prevent independent assessment and rehabilitation of these subfunctions. Here we introduce a versatile robotic interface to evaluate, enable and train pattern generation and balance independently during natural walking behaviors in rats. In evaluation mode, the robotic interface affords detailed assessments of pattern generation and dynamic equilibrium after spinal cord injury (SCI) and stroke. In enabling mode, the robot acts as a propulsive or postural neuroprosthesis that instantly promotes unexpected locomotor capacities including overground walking after complete SCI, stair climbing following partial SCI and precise paw placement shortly after stroke. In training mode, robot-enabled rehabilitation, epidural electrical stimulation and monoamine agonists reestablish weight-supported locomotion, coordinated steering and balance in rats with a paralyzing SCI. This new robotic technology and associated concepts have broad implications for both assessing and restoring motor functions after CNS disorders, both in animals and in humans.

Neuromotor disorders such as SCI and stroke lead to distinct impairments of motor pattern generation and balance[1,2]. Consequently, dissociating these subfunctions is essential for assessment and neurorehabilitation of gait. Conceptually, neurorehabilitation systems should act as a propulsive or postural neuroprosthesis that assists or perturbs propulsion, balance or the combination of both to varying degrees according to experimental purposes or patient-specific needs.

Existing systems designed to compensate for impaired propulsion and balance rely on passive spring support, counterweight mechanisms or force-controlled systems that generate vertical forces at the trunk level during treadmill-restricted stepping[3,4]. However, these approaches present several drawbacks. These current systems provide support only in the vertical direction, whereas well-balanced locomotion requires finely tuned trunk movements in virtually every direction[5]. Furthermore, the optic flow, which substantially modulates locomotion[6], is suppressed during treadmill-restricted stepping. Last, rehabilitation is restricted to stepping on a treadmill[7], a condition that markedly differs from the rich repertoire of natural locomotor tasks.

Robotic systems have been designed to overcome these limitations. The ZeroG[8] provides vertical support during overground walking using a lifting unit mounted on a rail-guided trolley. However, the rails constrain subjects along a fixed direction, and trunk support is restricted to the vertical direction. The NaviGaitor[9] allows translations in all directions by means of an overhead linear multiaxis system, but its massive structure leads to high inertia that prevents normal-paced movements.

Here we introduce a multidirectional trunk support system that solves these various issues. The robotic interface continuously and independently assists or perturbs propulsion and balance along four degrees of freedom while rats are progressing overground within a large workspace. Using various models of SCI and stroke, we document advanced capacities to evaluate, enable and train pattern generation and balance during walking under natural conditions encompassing a broad spectrum of locomotor behaviors.

RESULTS

Design and properties of the robotic interface

We developed a multidirectional support system that exploits three advanced robotic principles (**Supplementary Fig. 1**). (i) We designed a large serial robotic module consisting of three translational axes defining a Cartesian frame (x, y, z), as well as one rotational axis (φ, **Fig. 1a**). (ii) A parallel Delta linkage prevents tilting and allows measurement of the rat's position. (iii) To decouple the inertia of the massive robotic structure from the end effector, we fabricated a suspension system with a spring assembly that generates forces directed in each of the four degrees of freedom of the serial structure (**Fig. 1a**). This suspension system capitalizes on the high performance of series elastic actuators for the realization of transparently behaving haptic devices[10,11]. Together, this unique robotic arrangement allows real-time control of horizontal body translations (propulsion, lateral balance) and body-weight support (BWS) (balance) along four independent degrees of freedom that can be

[1]Neurology Department, University of Zurich, Zurich, Switzerland. [2]Center for Neuroprosthetics and Brain Mind Institute, School of Life Science, Swiss Federal Institute of Technology, Lausanne, Switzerland. [3]Sensory-Motor Systems Lab, Institute of Robotics and Intelligent Systems, Swiss Federal Institute of Technology, Zurich, Switzerland. [4]Department of Biomedical Engineering, Khalifa University, Abu Dhabi, United Arab Emirates. [5]Brain Research Institute, University of Zurich, Zurich, Switzerland. [6]Spinal Cord Injury Center, Balgrist University Hospital, University of Zurich, Switzerland. [7]Pavlov Institute of Physiology, St. Petersburg, Russia. [8]These authors contributed equally to this work. Correspondence should be addressed to G.C. (gregoire.courtine@epfl.ch).

Received 5 July 2011; accepted 7 March 2012; published online 31 May 2012; doi:10.1038/nm.2845

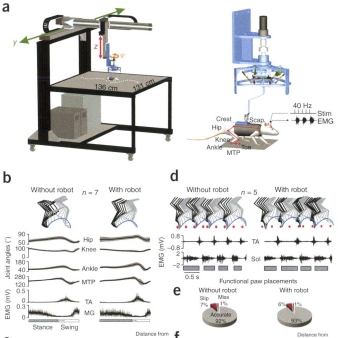

Figure 1 Design and transparency of the robotic interface in healthy rats. (**a**) Large and detailed view of the robotic interface. The actuated degrees of freedom are represented with distinct colored arrows. The rat is placed in a skin-like jacket attached to a back plate at the trunk level. EMG, electromyograph; MTP, metatarsophalange. (**b**) Stick diagram decomposition of hindlimb motion during stance (black) and swing (gray) together with limb endpoint trajectory, hindlimb joint angles and EMG activity of medial gastrocnemius (MG) and tibialis anterior (TA) muscles during locomotion along a straight runway without and with robotic support. (**c**) Principal component (PC) analysis was applied on all the measured variables ($n = 144$) from all the rats. Gait cycles are represented in the new three-dimensional (3D) space created by the three first PCs (explained variance, 39%). Least-squares spheres are traced to emphasize the overlap between gaits performed without and with robot. The bar graphs report the average ($n = 7$ rats) 3D distance between conditions (distance for each rat from mean of all gait cycles without robot) as well as 3D dispersion (gait variability). AU, arbitrary units. (**d**) The same representation is shown during locomotion along irregularly spaced rungs (red dots) with and without robotic support. Sol, soleus. (**e**) The pie charts show the percentage of steps that were accurately placed versus when the paw missed or slipped off the rung. (**f**) PC analysis of gait during locomotion along a ladder. Error bars, s.e.m.

continuously adjusted, that is, from stiff position control to high-fidelity, zero-force control (**Supplementary Video 1**).

To demonstrate the transparency of the robot, we compared the kinematics and muscle activity underlying locomotion of healthy rats ($n = 7$) walking along a straight runway with and without the robot (**Fig. 1b** and **Supplementary Fig. 2**). Despite detailed analyses (**Supplementary Fig. 3**), we did not detect significant differences between these conditions ($P > 0.3$, **Fig. 1c**), indicating that the massive robot did not interfere with gait. We confirmed these results during walking on a horizontal ladder ($n = 5$) (**Fig. 1d**). Even in such challenging conditions, precise paw placement ($P > 0.4$, **Fig. 1e**) and gait features were virtually unaffected by the robotic interface ($P > 0.3$, **Fig. 1f**).

Evaluation of motor pattern generation and balance

We first aimed to document advanced robot-assisted capabilities to assess motor pattern generation and balance. We embodied these control schemes under the term 'evaluation mode'. Most BWS systems rely on passive spring mechanisms, which provide a support against gravity that is proportional to the subject's vertical position. Although special kinematic configurations can achieve position-independent, constant force support[3], these passive systems do not compensate for rapid movements. Our robotic system can apply well-controlled, arbitrary vertical force profiles capable of emulating spring-like conditions or a reduced gravitational environment. We exploited this advanced functionality to compare the effect of spring-like versus constant-force BWS conditions on locomotor pattern generation in rats with complete SCI ($n = 5$, **Fig. 2**). To enable stepping, we applied a combination of epidural electrical stimulation and monoamine agonists[1] (**Fig. 2a**,**b**). We tuned the spring constant to an optimal value for facilitating stepping[1] and maintained the exact same amount of support during constant-force conditions. Compared to spring-like BWS, the constant-force BWS markedly improved the quality and consistency ($P < 0.01$, **Fig. 2b**,**c**) of gait features (**Supplementary Fig. 4**) and promoted locomotor patterns that converged toward those of healthy rats ($P < 0.01$, **Fig. 2c** and **Supplementary Video 2**).

The human[12] and rat[1,13] lumbosacral spinal cord can interpret weight-bearing information during stepping. We evaluated whether weight-bearing input also determines gait quality in rats with complete SCI ($n = 4$). Decreasing the level of constant-force BWS resulted in graded adjustments in hindlimb kinematics, forces and muscle activity ($P < 0.01$; **Supplementary Fig. 5b**–**e**), which confirmed the ability of lumbosacral circuitries to transform weight-bearing information into specific locomotor patterns (**Supplementary Video 2**). However, we found an inverted U-shaped relationship ($R^2 = 0.87$, **Supplementary Fig. 5c**) between gait quality and the level of BWS. These findings emphasize the importance of optimal constant-force support conditions to enable and train locomotion in subjects with gait disorders.

A unilateral cortical stroke has limited impact on basic locomotion in rats, but behavioral observations have suggested deficits in balance control[14]. To demonstrate impairment of equilibrium after stroke, we exploited the capacity of the robot to superimpose any force at any time and in any actuated degree of freedom onto the zero-force control mode. Specifically, we applied a sudden triangular force profile (2.5 N, **Fig. 2d**,**e**) in the mediolateral direction (y axis, pushing rightward) for 1 s while rats were progressing freely along a straight runway. Shortly after a left-sided stroke (6 d), the rats failed to compensate for the perturbation. They showed ample rightward deviations ($P < 0.002$, **Fig. 2e**,**f**) and frequently fell off the runway (56% ± 39%, mean ± s.d.). After 1 month of recovery, the rats responded to the perturbation with a controlled co-activation of extensor and flexor muscles (**Fig. 2g**,**h**), followed by a prolonged activity of contralesional extensor muscles (360% ± 80%, $P < 0.001$, **Fig. 2g**,**h**). This muscle synergy stabilized the trunk and hindlimb (**Fig. 2e**,**f**) and produced substantial mediolateral forces ($P < 0.001$, 0.60 ± 0.07 N at 6 d versus 1.54 ± 0.18 N at 30 d post-lesion) that restored the locomotor trajectory (**Supplementary Video 3**). Collectively, these results demonstrate that the evaluation mode of the robotic interface provides heuristic conditions to assess motor pattern generation and balance in neuromotor disorders.

Robot-enabled motor control after neuromotor disorders

We next sought to use the robotic interface as a propulsive or postural neuroprosthesis that provides adjustable assistance to propel the body forward and to restore postural orientation and stability. We hypoth-

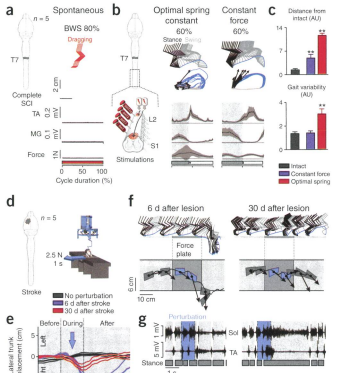

Figure 2 The robotic interface affords detailed assessment of pattern generation and balance. (**a**,**b**) Rats received a complete SCI. Hindlimb locomotion is shown without (paralysis) (**a**) and with (**b**) electrical and pharmacological stimulations. Stick diagram decomposition of hindlimb motion with spring-like versus constant-force BWS is shown together with successive limb endpoint trajectories ($n = 10$ steps), activity of TA and MG muscles and vertical ground reaction forces. The vectors indicate the direction and intensity of foot velocity at swing onset. (**c**) The bar graphs report the average distance from intact rats as well as gait variability computed through PC analysis. (**d**) Scheme showing lateral (rightward) postural perturbation (1 s) applied during runway locomotion in rats with a left-sided cortical stroke. (**e**) Averaged ($n = 5$ rats) lateral trunk displacements 1 s before, during and 2 s after perturbation. (**f**) Stick diagram decomposition of hindlimb motion and trunk positioning. Arrows indicate the intensity (velocity) and direction of trunk motion. Blue, during perturbation. (**g**) EMG activity of Sol and TA muscles during a representative trial at 6 d and 30 d post-lesion. (**h**) Plots illustrating coordination (density distribution) between Sol and TA muscles without perturbation and during perturbation at 6 d and 30 d after lesion (all trials and rats, scale is the same for all the plots). Error bars, s.e.m. $^{**}P < 0.01$ compared to all other nonmarked conditions.

esized that this so-called 'enabling mode' would uncover unexpected locomotor capacities that are dissimulated by impairments in propulsion, balance or both.

Electrical and pharmacological stimulations enable locomotion in rats with complete SCI (**Supplementary Fig. 6a**,**b**), but the rats fail to produce the necessary forces to propel their bodies forward overground. Instead, they show tonic activity in extensor muscles, behaviorally apparent as standing (**Supplementary Fig. 6c**). To compensate for the lack of propulsion, we configured the robot to act as a propulsive neuroprosthesis that moved the rats forward (x axis, 13 cm s^{-1}) while providing constant-force vertical support (60% ± 10% of BWS). After we initiated the robotic guidance, the rats smoothly transitioned from quiet standing to continuous locomotion (**Supplementary Fig. 6d**). Rhythmic movements arrested instantly when the propulsive neuroprosthesis stopped translating the rat forward (**Supplementary Video 4**).

Rats with unilateral cortical stroke show significant impairments in contralesional paw placement when crossing a horizontal ladder[14] (**Fig. 3**). These deficits have been attributed to the loss of visuomotor control, which heavily relies on the damaged motor cortex[15]. We tested the hypothesis that impaired equilibrium maintenance (**Fig. 2d–h**) may also contribute to the alteration of skilled locomotion after a cortical stroke. We configured the robotic interface to act as a postural neuroprosthesis. In this enabling mode, the robot provided a constant-force support in the vertical direction (z axis, 27% ± 4% of BWS) and stiff support in the lateral directions (y and rotational axes). The robotic postural neuroprosthesis instantly improved the rats' ability to position their contra-

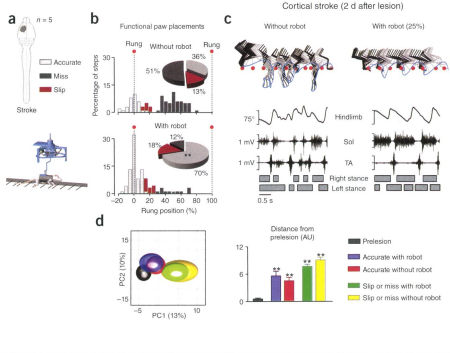

Figure 3 The robotic postural neuroprosthesis enables skilled motor control after cortical stroke. (**a**) Schemes depicting the stroke lesion and testing paradigm. Rats were evaluated during walking along a ladder with irregularly-spaced rungs. (**b**) The relative positioning of the contralesional hindpaw with respect to two successive rung positions (red dots) was evaluated over all the trials from all the rats without and with constant-force robot support. The number of occurrences per 5% bin is reported together with the percentage of accurate, slipped and missed placements, which are color coded as in **a**. (**c**) Stick diagram decomposition of hindlimb motion during a trial along the ladder with and without robot. Hindlimb oscillations and EMG activity of TA and Sol muscles are shown at the bottom. (**d**) PC analysis (explained variance, 28%). Accurate steps are dissociated from missed steps to emphasize that the robot increased the percentage of accurate steps but had no influences on locomotor strategy *per se*. The bar graph reports the average ($n = 5$ rats) 3D distance from prelesion trials. $^{**}P < 0.01$ compared to all prelesion conditions. Error bars, s.e.m.

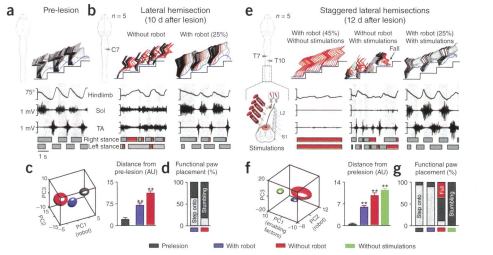

lesional hindpaws accurately onto the irregularly spaced rungs of the ladder ($P < 0.002$, **Fig. 3b,c** and **Supplementary Video 5**). Statistical analyses showed that the robot significantly decreased the number of misses and slips ($P < 0.01$, **Fig. 3d**), which correlated with improved postural stability ($P < 0.01$, **Supplementary Fig. 7c**).

We next assessed the capacity of the robotic postural neuroprosthesis to enable motor control in rats with a lateral C7 hemisection ($n = 5$). Ten days after lesion, the rats dragged the ipsilesional hindlimb during locomotion (**Supplementary Fig. 8a**), especially during climbing on a staircase (**Fig. 4**). Without robotic support, they stumbled against and rarely stepped onto the staircase (**Fig. 4b,d**). The robotic postural neuroprosthesis instantly enabled coordinated plantar stepping, both during horizontal walking (32% ± 4% of BWS; **Supplementary Fig. 8a,b**) and climbing on a staircase (28% ± 3% of BWS; **Fig. 4b,c**). The robotic support restored trunk orientation and stability ($P < 0.001$, **Supplementary Fig. 9b,c**), which correlated with near-normal hindlimb kinematics (**Supplementary Figs. 8** and **9**) and accurate positioning of the ipsilesional paw onto the staircase ($P < 0.001$, **Fig. 4d** and **Supplementary Video 6**).

We then investigated whether the robotic postural neuroprosthesis could enable motor control shortly after a more severe SCI consisting of two lateral hemisections placed on opposite sides and at different spinal levels (T7 and T10, **Fig. 4e**). This SCI completely interrupted direct supraspinal input, thus leading to permanent hindlimb paralysis[16] (**Fig. 4e**). To enable locomotion as early as 12 d after SCI, we applied electrical and pharmacological stimulations. Without robotic support, the rats showed rhythmic hindlimb movements, but they failed to perform plantar steps (91% ± 7% of dragging, **Supplementary Fig. 8e**) and often fell laterally during walking (**Fig. 4e**). With the robotic postural neuroprosthesis, all the tested rats ($n = 5$) showed bilateral weight-bearing plantar steps (**Fig. 4e** and **Supplementary Video 7**). Despite the interruption of direct supraspinal pathways, the rats immediately regained the ability to accurately position both hindpaws onto the staircase ($P < 0.001$, **Fig. 4**). The otherwise paralyzed rats showed gait patterns that were nearly indistinguishable from those of healthy rats, both during horizontal locomotion (**Supplementary Fig. 8e–h**) and stair climbing (**Fig. 4e–g**). For both tasks, improvement of hindlimb locomotion correlated with robot-enabled recovery of trunk position and stability (**Supplementary**

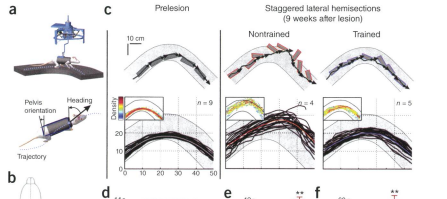

Figure 4 The robotic postural neuroprosthesis enables coordinated locomotion on a staircase after moderate and severe SCI. (**a**) Representative stick diagram decomposition of hindlimb motion during climbing on a staircase before lesion. The plots show hindlimb oscillations and EMG activity of MG and TA muscles. (**b**) Climbing on a staircase without and with constant-force robotic support 10 d after a C7 lateral hemisection. (**c**) PC analysis was applied on all gaits and rats. (**d**) Percentage of steps accurately positioned onto the staircase. (**e**) Locomotion on a staircase without and with constant-force robotic support 12 d after staggered hemisections. Locomotion is shown without (spontaneous) and with electrical and pharmacological stimulations. (**f**) PC analysis. (**g**) Percentage of steps accurately positioned onto the staircase. Error bars, s.e.m. $^{**}P < 0.01$ compared to the prelesion condition.

Figure 5 Training enabled by the robotic postural neuroprosthesis restores equilibrated steering in rats with a severe SCI. (**a**) Schemes depicting experimental testing paradigm and conventions to compute body angles. Rats were positioned quadrupedally in the robotic interface, which provided constant-force vertical support while delivering zero force in all the other directions. The rats walked along a 90°-curved runway. Trunk orientation was measured as the angle between the pelvis and the orientation of the upper body velocity vector, termed heading, which also defined the locomotor trajectory. (**b**) Schemes depicting the SCI, as well as the electrical and pharmacological stimulations for enabling locomotor states. (**c**) Successive positions of the trunk at swing onset, locomotor trajectory and velocity (arrow's length) of trunk motion as well as direction of upper body motion (arrow) during a representative trial performed before the lesion and at 60 d after lesion for a nontrained and a trained rat. The bottom plots show the superimposed locomotor trajectories extracted from all the trials of all the rats. The density distribution of locomotor trajectories (all trials and rats) is shown in the top left corner of each plot. (**d**) Averaged (all rats, ± s.d.) distance between locomotor trajectories and the optimal trajectory computed from all the prelesion trials ($n = 9$ rats). The shaded area indicates the progression along the curved section of the runway. (**e**) Averaged distance between each locomotor trajectory and the optimal trajectory. (**f**) Maximum deviation of the pelvis segment with respect to the heading vector. Error bars, s.e.m. $^{**}P < 0.01$ from all the other nonmarked conditions.

Fig. 10b,c). Together, these findings demonstrate that the enabling mode of the robotic interface instantly restored advanced locomotor capacities across a wide range of natural walking behaviors in moderate to severe neuromotor disorders.

Robot-enabled training after a paralyzing SCI

Finally, we exploited the enabling mode of the robotic interface to enhance functional capacities with repeated practice, a control scheme that we termed 'training mode'. We subjected rats ($n = 5$) with staggered hemisection SCIs to 30-min locomotor training sessions every other day for 8 weeks (see Online Methods). The robotic postural neuroprosthesis provided support against gravity (z axis), but did not deliver forces in the other directions (x, y and φ axes, **Supplementary Fig. 2**). Locomotion was enabled by electrical and pharmacological stimulations (**Fig. 5**). At 9 weeks after lesion, nontrained rats showed weight-bearing steps but failed to control body inertia and balance during robot-assisted locomotion along a curved runway ($P < 0.001$, **Fig. 5c–e**). In contrast, trained rats were capable of steering curves (**Fig. 5c–f**) while maintaining equilibrated trunk movements ($P < 0.001$, **Fig. 5c,f** and **Supplementary Video 8**). These results reveal that the training mode of the robotic interface markedly improved locomotor capacities in rats with paralyzing SCI.

DISCUSSION

We have introduced an advanced robotic interface to evaluate, enable and train motor pattern generation and balance across a variety of natural walking behaviors in rats with neuromotor impairments. To hide the inertia of the massive robotic structure, we developed a multidirectional elastic decoupling system that allowed high-fidelity force control. This robotic interface effectively solves the main issues associated with existing rodent and human support systems, such as unidirectional trunk support, high inertia and treadmill-restricted stepping. We validated our methods and concepts in rats with various SCIs and stroke. We expect that similar multidirectional trunk support systems will substantially improve gait rehabilitation in humans with neuromotor disorders.

Evaluation of locomotor function in animals often relies on visual scoring systems[17] or single-variable analyses[14] that not only lack objectivity but also fail to capture the multidimensional correlative structures of locomotor control strategies[18]. Here we combined robotically assisted evaluation tools with sophisticated neurobiomechanical and statistical analyses. Together, these paradigms provide the means for assessing the control of, and the interactions between, gait and balance with refinement and objectivity. Future animal and human studies can exploit these analytical tools to evaluate whether and, to a certain extent, how a given therapeutic intervention can enhance specific features of functional recovery in neuromotor disorders.

When acting as a postural or propulsive neuroprosthesis, the robotic interface instantly enabled advanced locomotor capacities in rats with SCI or stroke. We systematically found correlations between robotically restored multidirectional trunk balance and improved hindlimb motor control. These immediate functional improvements emphasize the importance of expanding currently available trunk support systems, which are exclusively unidirectional, to multiple dimensions. Likewise, robotic exoskeletons that provide multidirectional support against gravity enable enhanced upper limb recovery in stroke survivors[19] and improved locomotion in humans with partial SCI[20]. These results demonstrate that the concept of robotically enabled motor control has broad implications to enhance functional recovery after CNS disorders.

Our robotic postural neuroprosthesis not only provided multidirectional trunk support but also restored limb and trunk orientation. Consequently, the flow of stretch- and load-related afferent input from hip and ankle joints, which has an essential role in coordinating locomotion[21], came closer to a normal range. We surmise that the recovery of crucial sensory feedback and its task-specific modulation substantially contributed to reestablishing gait control. For example, the robotic postural neuroprosthesis enabled enhanced hip extension during stair climbing compared to horizontal locomotion. This afferent information appeared sufficient to mediate increased step height and accurate paw placement onto the staircase. Similarly, side-dependent modulation of load- and stretch-sensitive receptors from ankle and trunk muscles during curve walking resulted in the production of asymmetric force patterns that maintained equilibrated steering. These sensorimotor processes were improved with training. Together, these findings confirm and expand current views on the ability of sensory information to act as a source of control for locomotion after the loss of supraspinal influences[1,12]. In this respect, our interface could be equipped with robotic legs attached to the hindlimbs[3] to ensure appropriate task-specific sensory feedback during rehabilitation[22].

There is evidence suggesting that gait rehabilitation should be conducted overground[23] across multiple walking paradigms[7], with adequate support conditions[23–25], enabling systems[1,12,19,22,24], task-specific sensory cues[1,12] and active patient cooperation[20,22], but these concepts remain fragmented. Our versatile propulsive and postural neuroprosthetic interface crystallizes these views into a unified therapeutic tool to evaluate and restore locomotor function after CNS disorders, both in animals and in humans.

METHODS

Methods and any associated references are available in the online version of the paper.

Note: Supplementary information is available in the online version of the paper.

ACKNOWLEDGMENTS

We would like to acknowledge the excellent technical help provided by J. Heutschi, N. Wenger, M. Hirlimann, Q. Barraud and S. Duis for data collection and care of the rats, as well as A.S. Tafreshi for the design of the user interface to control the robotic system and A. Brunschweiler, A. Rotta and M. Fritschi for the realization of the suspension system. This work was supported by the National Centers of Competence in Research "Neural Plasticity and Repair" and "Robotics" of the Swiss National Science Foundation, the European Research Council (ERC 261247, "Walk Again"), European Community's Seventh Framework Programme (CP-IP 258654, NeuWALK), the Christopher and Dana Reeve Foundation and the Swiss National Science Foundation (subside 310030_130850).

AUTHOR CONTRIBUTIONS

U.K., H.V., R.R. and G.C. conceived of and designed the robotic interface. P.M., M.L.S. and G.C. performed the surgeries. N.D. and G.C. conceived of the experiments, analyzed the data and prepared the figures with the help of the other authors. N.D., L.R., R.v.d.B. trained the rats and collected the data. G.C. wrote the manuscript, and all the authors contributed to its editing. G.C. supervised all aspects of the work.

COMPETING FINANCIAL INTERESTS

The authors declare no competing financial interests.

Published online at http://www.nature.com/doifinder/10.1038/nm.2811.
Reprints and permissions information is available online at http://www.nature.com/reprints/index.html.

1. Courtine, G. *et al.* Transformation of nonfunctional spinal circuits into functional states after the loss of brain input. *Nat. Neurosci.* **12**, 1333–1342 (2009).
2. Harkema, S.J. *et al.* Human lumbosacral spinal cord interprets loading during stepping. *J. Neurophysiol.* **77**, 797–811 (1997).
3. Nessler, J.A. *et al.* A robotic device for studying rodent locomotion after spinal cord injury. *IEEE Trans. Neural. Syst. Rehabil. Eng.* **13**, 497–506 (2005).
4. Frey, M. *et al.* A novel mechatronic body weight support system. *IEEE Trans. Neural. Syst. Rehabil. Eng.* **14**, 311–321 (2006).
5. Winter, D.A., MacKinnon, C.D., Ruder, G.K. & Wieman, C. An integrated EMG/biomechanical model of upper body balance and posture during human gait. *Prog. Brain Res.* **97**, 359–367 (1993).

6. Warren, W.H. Jr., Kay, B.A., Zosh, W.D., Duchon, A.P. & Sahuc, S. Optic flow is used to control human walking. *Nat. Neurosci.* **4**, 213–216 (2001).
7. Musselman, K., Brunton, K., Lam, T. & Yang, J. Spinal cord injury functional ambulation profile: a new measure of walking ability. *Neurorehabil. Neural Repair* **25**, 285–293 (2011).
8. Hidler, J. *et al.* ZeroG: overground gait and balance training system. *J. Rehabil. Res. Dev.* **48**, 287–298 (2011).
9. Shetty, D., Fast, A. & Campana, C.A. Ambulatory suspension and rehabilitation apparatus. US patent 7462138 (2008).
10. Pratt, G.A. *et al.* Stiffness Isn't Everything, in *International Symposium on Experimental Robotics* http://citeseerx.ist.psu.edu/viewdoc/summary?doi=10.1.1.26.3136 (1995).
11. Vallery, H. *et al.* Compliant actuation of rehabilitation robots—benefits and limitations of series elastic actuators. *IEEE Robot. Autom. Mag.* **15**, 60–69 (2008).
12. Harkema, S. *et al.* Effect of epidural stimulation of the lumbosacral spinal cord on voluntary movement, standing, and assisted stepping after motor complete paraplegia: a case study. *Lancet* **377**, 1938–1947 (2011).
13. Timoszyk, W.K. *et al.* Hindlimb loading determines stepping quantity and quality following spinal cord transection. *Brain Res.* **1050**, 180–189 (2005).
14. Zörner, B. *et al.* Profiling locomotor recovery: comprehensive quantification of impairments after CNS damage in rodents. *Nat. Methods* **7**, 701–708 (2010).
15. Drew, T., Andujar, J.E., Lajoie, K. & Yakovenko, S. Cortical mechanisms involved in visuomotor coordination during precision walking. *Brain Res. Rev.* **57**, 199–211 (2008).
16. Courtine, G. *et al.* Recovery of supraspinal control of stepping via indirect propriospinal relay connections after spinal cord injury. *Nat. Med.* **14**, 69–74 (2008).
17. Basso, D.M. *et al.* MASCIS evaluation of open field locomotor scores: effects of experience and teamwork on reliability. Multicenter Animal Spinal Cord Injury Study. *J. Neurotrauma* **13**, 343–359 (1996).
18. Musienko, P. *et al.* Controlling specific locomotor behaviors through multidimensional monoaminergic modulation of spinal circuitries. *J. Neurosci.* **31**, 9264–9278 (2011).
19. Kwakkel, G., Kollen, B.J. & Krebs, H.I. Effects of robot-assisted therapy on upper limb recovery after stroke: a systematic review. *Neurorehabil. Neural Repair* **22**, 111–121 (2008).
20. Duschau-Wicke, A., Caprez, A. & Riener, R. Patient-cooperative control increases active participation of individuals with SCI during robot-aided gait training. *J. Neuroeng. Rehabil.* **7**, 43 (2010).
21. Pearson, K.G. Generating the walking gait: role of sensory feedback. *Prog. Brain Res.* **143**, 123–129 (2004).
22. Edgerton, V.R. & Roy, R.R. Robotic training and spinal cord plasticity. *Brain Res. Bull.* **78**, 4–12 (2009).
23. Wessels, M., Lucas, C., Eriks, I. & de Groot, S. Body weight-supported gait training for restoration of walking in people with an incomplete spinal cord injury: a systematic review. *J. Rehabil. Med.* **42**, 513–519 (2010).
24. Reinkensmeyer, D.J. *et al.* Tools for understanding and optimizing robotic gait training. *J. Rehabil. Res. Dev.* **43**, 657–670 (2006).
25. Ada, L., Dean, C.M., Vargas, J. & Ennis, S. Mechanically assisted walking with body weight support results in more independent walking than assisted overground walking in non-ambulatory patients early after stroke: a systematic review. *J. Physiother.* **56**, 153–161 (2010).

nature medicine

Versatile robotic interface to evaluate, enable and train locomotion and balance after neuromotor disorders

Nadia Dominici[1,2,8], Urs Keller[3,8], Heike Vallery[3,4], Lucia Friedli[1,2], Rubia van den Brand[1,2], Michelle L Starkey[5,6], Pavel Musienko[1,2,7], Robert Riener[3,6] & Grégoire Courtine[1,2]

Central nervous system (CNS) disorders distinctly impair locomotor pattern generation and balance, but technical limitations prevent independent assessment and rehabilitation of these subfunctions. Here we introduce a versatile robotic interface to evaluate, enable and train pattern generation and balance independently during natural walking behaviors in rats. In evaluation mode, the robotic interface affords detailed assessments of pattern generation and dynamic equilibrium after spinal cord injury (SCI) and stroke. In enabling mode, the robot acts as a propulsive or postural neuroprosthesis that instantly promotes unexpected locomotor capacities including overground walking after complete SCI, stair climbing following partial SCI and precise paw placement shortly after stroke. In training mode, robot-enabled rehabilitation, epidural electrical stimulation and monoamine agonists reestablish weight-supported locomotion, coordinated steering and balance in rats with a paralyzing SCI. This new robotic technology and associated concepts have broad implications for both assessing and restoring motor functions after CNS disorders, both in animals and in humans.

Neuromotor disorders such as SCI and stroke lead to distinct impairments of motor pattern generation and balance[1,2]. Consequently, dissociating these subfunctions is essential for assessment and neurorehabilitation of gait. Conceptually, neurorehabilitation systems should act as a propulsive or postural neuroprosthesis that assists or perturbs propulsion, balance or the combination of both to varying degrees according to experimental purposes or patient-specific needs.

Existing systems designed to compensate for impaired propulsion and balance rely on passive spring support, counterweight mechanisms or force-controlled systems that generate vertical forces at the trunk level during treadmill-restricted stepping[3,4]. However, these approaches present several drawbacks. These current systems provide support only in the vertical direction, whereas well-balanced locomotion requires finely tuned trunk movements in virtually every direction[5]. Furthermore, the optic flow, which substantially modulates locomotion[6], is suppressed during treadmill-restricted stepping. Last, rehabilitation is restricted to stepping on a treadmill[7], a condition that markedly differs from the rich repertoire of natural locomotor tasks.

Robotic systems have been designed to overcome these limitations. The ZeroG[8] provides vertical support during overground walking using a lifting unit mounted on a rail-guided trolley. However, the rails constrain subjects along a fixed direction, and trunk support is restricted to the vertical direction. The NaviGaitor[9] allows translations in all directions by means of an overhead linear multiaxis system, but its massive structure leads to high inertia that prevents normal-paced movements.

Here we introduce a multidirectional trunk support system that solves these various issues. The robotic interface continuously and independently assists or perturbs propulsion and balance along four degrees of freedom while rats are progressing overground within a large workspace. Using various models of SCI and stroke, we document advanced capacities to evaluate, enable and train pattern generation and balance during walking under natural conditions encompassing a broad spectrum of locomotor behaviors.

RESULTS

Design and properties of the robotic interface

We developed a multidirectional support system that exploits three advanced robotic principles (**Supplementary Fig. 1**). (i) We designed a large serial robotic module consisting of three translational axes defining a Cartesian frame (x, y, z), as well as one rotational axis (φ, **Fig. 1a**). (ii) A parallel Delta linkage prevents tilting and allows measurement of the rat's position. (iii) To decouple the inertia of the massive robotic structure from the end effector, we fabricated a suspension system with a spring assembly that generates forces directed in each of the four degrees of freedom of the serial structure (**Fig. 1a**). This suspension system capitalizes on the high performance of series elastic actuators for the realization of transparently behaving haptic devices[10,11]. Together, this unique robotic arrangement allows real-time control of horizontal body translations (propulsion, lateral balance) and body-weight support (BWS) (balance) along four independent degrees of freedom that can be

[1]Neurology Department, University of Zurich, Zurich, Switzerland. [2]Center for Neuroprosthetics and Brain Mind Institute, School of Life Science, Swiss Federal Institute of Technology, Lausanne, Switzerland. [3]Sensory-Motor Systems Lab, Institute of Robotics and Intelligent Systems, Swiss Federal Institute of Technology, Zurich, Switzerland. [4]Department of Biomedical Engineering, Khalifa University, Abu Dhabi, United Arab Emirates. [5]Brain Research Institute, University of Zurich, Zurich, Switzerland. [6]Spinal Cord Injury Center, Balgrist University Hospital, University of Zurich, Switzerland. [7]Pavlov Institute of Physiology, St. Petersburg, Russia. [8]These authors contributed equally to this work. Correspondence should be addressed to G.C. (gregoire.courtine@epfl.ch).

Received 5 July 2011; accepted 7 March 2012; published online 31 May 2012; doi:10.1038/nm.2845

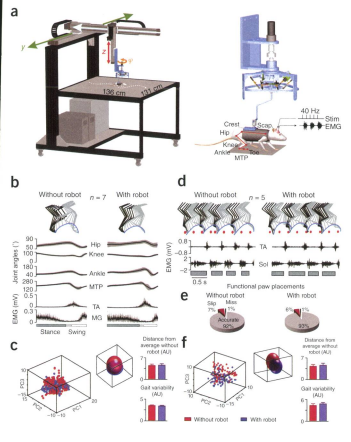

Figure 1 Design and transparency of the robotic interface in healthy rats. (**a**) Large and detailed view of the robotic interface. The actuated degrees of freedom are represented with distinct colored arrows. The rat is placed in a skin-like jacket attached to a back plate at the trunk level. EMG, electromyograph; MTP, metatarsophalange. (**b**) Stick diagram decomposition of hindlimb motion during stance (black) and swing (gray) together with limb endpoint trajectory, hindlimb joint angles and EMG activity of medial gastrocnemius (MG) and tibialis anterior (TA) muscles during locomotion along a straight runway without and with robotic support. (**c**) Principal component (PC) analysis was applied on all the measured variables ($n = 144$) from all the rats. Gait cycles are represented in the new three-dimensional (3D) space created by the three first PCs (explained variance, 39%). Least-squares spheres are traced to emphasize the overlap between gaits performed without and with robot. The bar graphs report the average ($n = 7$ rats) 3D distance between conditions (distance for each rat from mean of all gait cycles without robot) as well as 3D dispersion (gait variability). AU, arbitrary units. (**d**) The same representation is shown during locomotion along irregularly spaced rungs (red dots) with and without robotic support. Sol, soleus. (**e**) The pie charts show the percentage of steps that were accurately placed versus when the paw missed or slipped off the rung. (**f**) PC analysis of gait during locomotion along a ladder. Error bars, s.e.m.

continuously adjusted, that is, from stiff position control to high-fidelity, zero-force control (**Supplementary Video 1**).

To demonstrate the transparency of the robot, we compared the kinematics and muscle activity underlying locomotion of healthy rats ($n = 7$) walking along a straight runway with and without the robot (**Fig. 1b** and **Supplementary Fig. 2**). Despite detailed analyses (**Supplementary Fig. 3**), we did not detect significant differences between these conditions ($P > 0.3$, **Fig. 1c**), indicating that the massive robot did not interfere with gait. We confirmed these results during walking on a horizontal ladder ($n = 5$) (**Fig. 1d**). Even in such challenging conditions, precise paw placement ($P > 0.4$, **Fig. 1e**) and gait features were virtually unaffected by the robotic interface ($P > 0.3$, **Fig. 1f**).

Evaluation of motor pattern generation and balance

We first aimed to document advanced robot-assisted capabilities to assess motor pattern generation and balance. We embodied these control schemes under the term 'evaluation mode.' Most BWS systems rely on passive spring mechanisms, which provide a support against gravity that is proportional to the subject's vertical position. Although special kinematic configurations can achieve position-independent, constant force support[3], these passive systems do not compensate for rapid movements. Our robotic system can apply well-controlled, arbitrary vertical force profiles capable of emulating spring-like conditions or a reduced gravitational environment. We exploited this advanced functionality to compare the effect of spring-like versus constant-force BWS conditions on locomotor pattern generation in rats with complete SCI ($n = 5$, **Fig. 2**). To enable stepping, we applied a combination of epidural electrical stimulation and monoamine agonists[1] (**Fig. 2a,b**). We tuned the spring constant to an optimal value for facilitating stepping[1] and maintained the exact same amount of support during constant-force conditions. Compared to spring-like BWS, the constant-force BWS markedly improved the quality and consistency ($P < 0.01$, **Fig. 2b,c**) of gait features (**Supplementary Fig. 4**) and promoted locomotor patterns that converged toward those of healthy rats ($P < 0.01$, **Fig. 2c** and **Supplementary Video 2**).

The human[12] and rat[1,13] lumbosacral spinal cord can interpret weight-bearing information during stepping. We evaluated whether weight-bearing input also determines gait quality in rats with complete SCI ($n = 4$). Decreasing the level of constant-force BWS resulted in graded adjustments in hindlimb kinematics, forces and muscle activity ($P < 0.01$; **Supplementary Fig. 5b–e**), which confirmed the ability of lumbosacral circuitries to transform weight-bearing information into specific locomotor patterns (**Supplementary Video 2**). However, we found an inverted U-shaped relationship ($R^2 = 0.87$, **Supplementary Fig. 5c**) between gait quality and the level of BWS. These findings emphasize the importance of optimal constant-force support conditions to enable and train locomotion in subjects with gait disorders.

A unilateral cortical stroke has limited impact on basic locomotion in rats, but behavioral observations have suggested deficits in balance control[14]. To demonstrate impairment of equilibrium after stroke, we exploited the capacity of the robot to superimpose any force at any time and in any actuated degree of freedom onto the zero-force control mode. Specifically, we applied a sudden triangular force profile (2.5 N, **Fig. 2d,e**) in the mediolateral direction (y axis, pushing rightward) for 1 s while rats were progressing freely along a straight runway. Shortly after a left-sided stroke (6 d), the rats failed to compensate for the perturbation. They showed ample rightward deviations ($P < 0.002$, **Fig. 2e,f**) and frequently fell off the runway (56% ± 39%, mean ± s.d.). After 1 month of recovery, the rats responded to the perturbation with a controlled co-activation of extensor and flexor muscles (**Fig. 2g,h**), followed by a prolonged activity of contralesional extensor muscles (360% ± 80%, $P < 0.001$, **Fig. 2g,h**). This muscle synergy stabilized the trunk and hindlimb (**Fig. 2e,f**) and produced substantial mediolateral forces ($P < 0.001$, 0.60 ± 0.07 N at 6 d versus 1.54 ± 0.18 N at 30 d post-lesion) that restored the locomotor trajectory (**Supplementary Video 3**). Collectively, these results demonstrate that the evaluation mode of the robotic interface provides heuristic conditions to assess motor pattern generation and balance in neuromotor disorders.

Robot-enabled motor control after neuromotor disorders

We next sought to use the robotic interface as a propulsive or postural neuroprosthesis that provides adjustable assistance to propel the body forward and to restore postural orientation and stability. We hypoth-

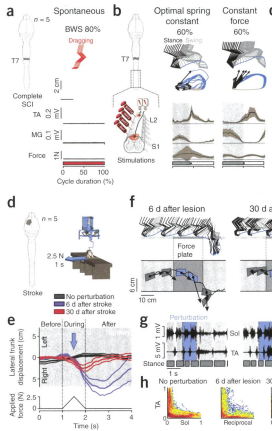

Figure 2 The robotic interface affords detailed assessment of pattern generation and balance. (**a**,**b**) Rats received a complete SCI. Hindlimb locomotion is shown without (paralysis) (**a**) and with (**b**) electrical and pharmacological stimulations. Stick diagram decomposition of hindlimb motion with spring-like versus constant-force BWS is shown together with successive limb endpoint trajectories ($n = 10$ steps), activity of TA and MG muscles and vertical ground reaction forces. The vectors indicate the direction and intensity of foot velocity at swing onset. (**c**) The bar graphs report the average distance from intact rats as well as gait variability computed through PC analysis. (**d**) Scheme showing lateral (rightward) postural perturbation (1 s) applied during runway locomotion in rats with a left-sided cortical stroke. (**e**) Averaged ($n = 5$ rats) lateral trunk displacements 1 s before, during and 2 s after perturbation. (**f**) Stick diagram decomposition of hindlimb motion and trunk positioning. Arrows indicate the intensity (velocity) and direction of trunk motion. Blue, during perturbation. (**g**) EMG activity of Sol and TA muscles during a representative trial at 6 d and 30 d post-lesion. (**h**) Plots illustrating coordination (density distribution) between Sol and TA muscles without perturbation and during perturbation at 6 d and 30 d after lesion (all trials and rats, scale is the same for all the plots). Error bars, s.e.m. $^{**}P < 0.01$ compared to all other nonmarked conditions.

esized that this so-called 'enabling mode' would uncover unexpected locomotor capacities that are dissimulated by impairments in propulsion, balance or both.

Electrical and pharmacological stimulations enable locomotion in rats with complete SCI (**Supplementary Fig. 6a**,**b**), but the rats fail to produce the necessary forces to propel their bodies forward overground. Instead, they show tonic activity in extensor muscles, behaviorally apparent as standing (**Supplementary Fig. 6c**). To compensate for the lack of propulsion, we configured the robot to act as a propulsive neuroprosthesis that moved the rats forward (x axis, 13 cm s^{-1}) while providing constant-force vertical support (60% ± 10% of BWS). After we initiated the robotic guidance, the rats smoothly transitioned from quiet standing to continuous locomotion (**Supplementary Fig. 6d**). Rhythmic movements arrested instantly when the propulsive neuroprosthesis stopped translating the rat forward (**Supplementary Video 4**).

Rats with unilateral cortical stroke show significant impairments in contralesional paw placement when crossing a horizontal ladder[14] (**Fig. 3**). These deficits have been attributed to the loss of visuomotor control, which heavily relies on the damaged motor cortex[15]. We tested the hypothesis that impaired equilibrium maintenance (**Fig. 2d–h**) may also contribute to the alteration of skilled locomotion after a cortical stroke. We configured the robotic interface to act as a postural neuroprosthesis. In this enabling mode, the robot provided a constant-force support in the vertical direction (z axis, 27% ± 4% of BWS) and stiff support in the lateral directions (y and rotational axes). The robotic postural neuroprosthesis instantly improved the rats' ability to position their contra-

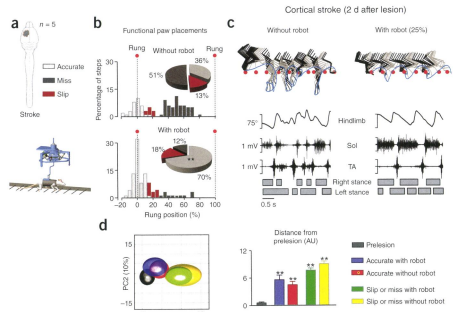

Figure 3 The robotic postural neuroprosthesis enables skilled motor control after cortical stroke. (**a**) Schemes depicting the stroke lesion and testing paradigm. Rats were evaluated during walking along a ladder with irregularly-spaced rungs. (**b**) The relative positioning of the contralesional hindpaw with respect to two successive rung positions (red dots) was evaluated over all the trials from all the rats without and with constant-force robot support. The number of occurrences per 5% bin is reported together with the percentage of accurate, slipped and missed placements, which are color coded as in **a**. (**c**) Stick diagram decomposition of hindlimb motion during a trial along the ladder with and without robot. Hindlimb oscillations and EMG activity of TA and Sol muscles are shown at the bottom. (**d**) PC analysis (explained variance, 28%). Accurate steps are dissociated from missed steps to emphasize that the robot increased the percentage of accurate steps but had no influences on locomotor strategy *per se*. The bar graph reports the average ($n = 5$ rats) 3D distance from prelesion trials. $^{**}P < 0.01$ compared to all prelesion conditions. Error bars, s.e.m.

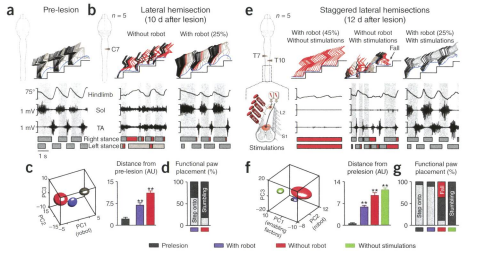

Figure 4 The robotic postural neuroprosthesis enables coordinated locomotion on a staircase after moderate and severe SCI. (**a**) Representative stick diagram decomposition of hindlimb motion during climbing on a staircase before lesion. The plots show hindlimb oscillations and EMG activity of MG and TA muscles. (**b**) Climbing on a staircase without and with constant-force robotic support 10 d after a C7 lateral hemisection. (**c**) PC analysis was applied on all gaits and rats. (**d**) Percentage of steps accurately positioned onto the staircase. (**e**) Locomotion on a staircase without and with constant-force robotic support 12 d after staggered hemisections. Locomotion is shown without (spontaneous) and with electrical and pharmacological stimulations. (**f**) PC analysis. (**g**) Percentage of steps accurately positioned onto the staircase. Error bars, s.e.m. $^{**}P < 0.01$ compared to the prelesion condition.

lesional hindpaws accurately onto the irregularly spaced rungs of the ladder ($P < 0.002$, **Fig. 3b,c** and **Supplementary Video 5**). Statistical analyses showed that the robot significantly decreased the number of misses and slips ($P < 0.01$, **Fig. 3d**), which correlated with improved postural stability ($P < 0.01$, **Supplementary Fig. 7c**).

We next assessed the capacity of the robotic postural neuroprosthesis to enable motor control in rats with a lateral C7 hemisection ($n = 5$). Ten days after lesion, the rats dragged the ipsilesional hindlimb during locomotion (**Supplementary Fig. 8a**), especially during climbing on a staircase (**Fig. 4**). Without robotic support, they stumbled against and rarely stepped onto the staircase (**Fig. 4b,d**). The robotic postural neuroprosthesis instantly enabled coordinated plantar stepping, both during horizontal walking (32% ± 4% of BWS; **Supplementary Fig. 8a,b**) and climbing on a staircase (28% ± 3% of BWS; **Fig. 4b,c**). The robotic support restored trunk orientation and stability ($P < 0.001$, **Supplementary Fig. 9b,c**), which correlated with near-normal hindlimb kinematics (**Supplementary Figs. 8** and **9**) and accurate positioning of the ipsilesional paw onto the staircase ($P < 0.001$, **Fig. 4d** and **Supplementary Video 6**).

We then investigated whether the robotic postural neuroprosthesis could enable motor control shortly after a more severe SCI consisting of two lateral hemisections placed on opposite sides and at different spinal levels (T7 and T10, **Fig. 4e**). This SCI completely interrupted direct supraspinal input, thus leading to permanent hindlimb paralysis[16] (**Fig. 4e**). To enable locomotion as early as 12 d after SCI, we applied electrical and pharmacological stimulations. Without robotic support, the rats showed rhythmic hindlimb movements, but they failed to perform plantar steps (91% ± 7% of dragging, **Supplementary Fig. 8e**) and often fell laterally during walking (**Fig. 4e**). With the robotic postural neuroprosthesis, all the tested rats ($n = 5$) showed bilateral weight-bearing plantar steps (**Fig. 4e** and **Supplementary Video 7**). Despite the interruption of direct supraspinal pathways, the rats immediately regained the ability to accurately position both hindpaws onto the staircase ($P < 0.001$, **Fig. 4**). The otherwise paralyzed rats showed gait patterns that were nearly indistinguishable from those of healthy rats, both during horizontal locomotion (**Supplementary Fig. 8e–h**) and stair climbing (**Fig. 4e–g**). For both tasks, improvement of hindlimb locomotion correlated with robot-enabled recovery of trunk position and stability (**Supplementary**

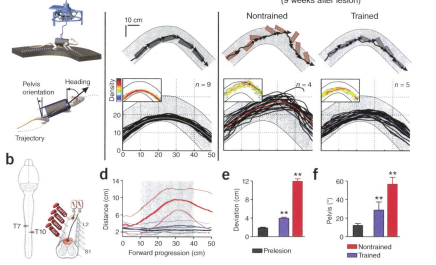

Figure 5 Training enabled by the robotic postural neuroprosthesis restores equilibrated steering in rats with a severe SCI. (**a**) Schemes depicting experimental testing paradigm and conventions to compute body angles. Rats were positioned quadrupedally in the robotic interface, which provided constant-force vertical support while delivering zero force in all the other directions. The rats walked along a 90°-curved runway. Trunk orientation was measured as the angle between the pelvis and the orientation of the upper body velocity vector, termed heading, which also defined the locomotor trajectory. (**b**) Schemes depicting the SCI, as well as the electrical and pharmacological stimulations for enabling locomotor states. (**c**) Successive positions of the trunk at swing onset, locomotor trajectory and velocity (arrow's length) of trunk motion as well as direction of upper body motion (arrow) during a representative trial performed before the lesion and at 60 d after lesion for a nontrained and a trained rat. The bottom plots show the superimposed locomotor trajectories extracted from all the trials of all the rats. The density distribution of locomotor trajectories (all trials and rats) is shown in the top left corner of each plot. (**d**) Averaged (all rats, ± s.d.) distance between locomotor trajectories and the optimal trajectory computed from all the prelesion trials ($n = 9$ rats). The shaded area indicates the progression along the curved section of the runway. (**e**) Averaged distance between each locomotor trajectory and the optimal trajectory. (**f**) Maximum deviation of the pelvis segment with respect to the heading vector. Error bars, s.e.m. $^{**}P < 0.01$ from all the other nonmarked conditions.

Fig. 10b,c). Together, these findings demonstrate that the enabling mode of the robotic interface instantly restored advanced locomotor capacities across a wide range of natural walking behaviors in moderate to severe neuromotor disorders.

Robot-enabled training after a paralyzing SCI

Finally, we exploited the enabling mode of the robotic interface to enhance functional capacities with repeated practice, a control scheme that we termed 'training mode'. We subjected rats ($n = 5$) with staggered hemisection SCIs to 30-min locomotor training sessions every other day for 8 weeks (see Online Methods). The robotic postural neuroprosthesis provided support against gravity (z axis), but did not deliver forces in the other directions (x, y and φ axes, **Supplementary Fig. 2**). Locomotion was enabled by electrical and pharmacological stimulations (**Fig. 5**). At 9 weeks after lesion, nontrained rats showed weight-bearing steps but failed to control body inertia and balance during robot-assisted locomotion along a curved runway ($P < 0.001$, **Fig. 5c–e**). In contrast, trained rats were capable of steering curves (**Fig. 5c–f**) while maintaining equilibrated trunk movements ($P < 0.001$, **Fig. 5c,f** and **Supplementary Video 8**). These results reveal that the training mode of the robotic interface markedly improved locomotor capacities in rats with paralyzing SCI.

DISCUSSION

We have introduced an advanced robotic interface to evaluate, enable and train motor pattern generation and balance across a variety of natural walking behaviors in rats with neuromotor impairments. To hide the inertia of the massive robotic structure, we developed a multidirectional elastic decoupling system that allowed high-fidelity force control. This robotic interface effectively solves the main issues associated with existing rodent and human support systems, such as unidirectional trunk support, high inertia and treadmill-restricted stepping. We validated our methods and concepts in rats with various SCIs and stroke. We expect that similar multidirectional trunk support systems will substantially improve gait rehabilitation in humans with neuromotor disorders.

Evaluation of locomotor function in animals often relies on visual scoring systems[17] or single-variable analyses[14] that not only lack objectivity but also fail to capture the multidimensional correlative structures of locomotor control strategies[18]. Here we combined robotically assisted evaluation tools with sophisticated neurobiomechanical and statistical analyses. Together, these paradigms provide the means for assessing the control of, and the interactions between, gait and balance with refinement and objectivity. Future animal and human studies can exploit these analytical tools to evaluate whether and, to a certain extent, how a given therapeutic intervention can enhance specific features of functional recovery in neuromotor disorders.

When acting as a postural or propulsive neuroprosthesis, the robotic interface instantly enabled advanced locomotor capacities in rats with SCI or stroke. We systematically found correlations between robotically restored multidirectional trunk balance and improved hindlimb motor control. These immediate functional improvements emphasize the importance of expanding currently available trunk support systems, which are exclusively unidirectional, to multiple dimensions. Likewise, robotic exoskeletons that provide multidirectional support against gravity enable enhanced upper limb recovery in stroke survivors[19] and improved locomotion in humans with partial SCI[20]. These results demonstrate that the concept of robotically enabled motor control has broad implications to enhance functional recovery after CNS disorders.

Our robotic postural neuroprosthesis not only provided multidirectional trunk support but also restored limb and trunk orientation. Consequently, the flow of stretch- and load-related afferent input from hip and ankle joints, which has an essential role in coordinating locomotion[21], came closer to a normal range. We surmise that the recovery of crucial sensory feedback and its task-specific modulation substantially contributed to reestablishing gait control. For example, the robotic postural neuroprosthesis enabled enhanced hip extension during stair climbing compared to horizontal locomotion. This afferent information appeared sufficient to mediate increased step height and accurate paw placement onto the staircase. Similarly, side-dependent modulation of load- and stretch-sensitive receptors from ankle and trunk muscles during curve walking resulted in the production of asymmetric force patterns that maintained equilibrated steering. These sensorimotor processes were improved with training. Together, these findings confirm and expand current views on the ability of sensory information to act as a source of control for locomotion after the loss of supraspinal influences[1,12]. In this respect, our interface could be equipped with robotic legs attached to the hindlimbs[3] to ensure appropriate task-specific sensory feedback during rehabilitation[22].

There is evidence suggesting that gait rehabilitation should be conducted overground[23] across multiple walking paradigms[7], with adequate support conditions[23–25], enabling systems[1,12,19,22,24], task-specific sensory cues[1,12] and active patient cooperation[20,22], but these concepts remain fragmented. Our versatile propulsive and postural neuroprosthetic interface crystallizes these views into a unified therapeutic tool to evaluate and restore locomotor function after CNS disorders, both in animals and in humans.

METHODS

Methods and any associated references are available in the online version of the paper.

Note: Supplementary information is available in the online version of the paper.

ACKNOWLEDGMENTS

We would like to acknowledge the excellent technical help provided by J. Heutschi, N. Wenger, M. Hürlimann, Q. Barraud and S. Duis for data collection and care of the rats, as well as A.S. Taflreshi for the design of the user interface to control the robotic system and A. Brunschweiler, A. Rotta and M. Fritschi for the realization of the suspension system. This work was supported by the National Centers of Competence in Research "Neural Plasticity and Repair" and "Robotics" of the Swiss National Science Foundation, the European Research Council (ERC 261247, "Walk Again"), European Community's Seventh Framework Programme (CP-IP 258654, NeuWALK), the Christopher and Dana Reeve Foundation and the Swiss National Science Foundation (subside 310030_130850).

AUTHOR CONTRIBUTIONS

U.K., H.V., R.R. and G.C. conceived of and designed the robotic interface. P.M., M.L.S. and G.C. performed the surgeries. N.D. and G.C. conceived of the experiments, analyzed the data and prepared the figures with the help of the other authors. N.D., L.F., R.v.d.B. trained the rats and collected the data. G.C. wrote the manuscript, and all the authors contributed to its editing. G.C. supervised all aspects of the work.

COMPETING FINANCIAL INTERESTS

The authors declare no competing financial interests.

Published online at http://www.nature.com/doifinder/10.1038/nm.2811.
Reprints and permissions information is available online at http://www.nature.com/reprints/index.html.

1. Courtine, G. *et al.* Transformation of nonfunctional spinal circuits into functional states after the loss of brain input. *Nat. Neurosci.* **12**, 1333–1342 (2009).
2. Harkema, S.J. *et al.* Human lumbosacral spinal cord interprets loading during stepping. *J. Neurophysiol.* **77**, 797–811 (1997).
3. Nessler, J.A. *et al.* A robotic device for studying rodent locomotion after spinal cord injury. *IEEE Trans. Neural. Syst. Rehabil. Eng.* **13**, 497–506 (2005).
4. Frey, M. *et al.* A novel mechatronic body weight support system. *IEEE Trans. Neural. Syst. Rehabil. Eng.* **14**, 311–321 (2006).
5. Winter, D.A., MacKinnon, C.D., Ruder, G.K. & Wieman, C. An integrated EMG/biomechanical model of upper body balance and posture during human gait. *Prog. Brain Res.* **97**, 359–367 (1993).

6. Warren, W.H. Jr., Kay, B.A., Zosh, W.D., Duchon, A.P. & Sahuc, S. Optic flow is used to control human walking. *Nat. Neurosci.* **4**, 213–216 (2001).
7. Musselman, K., Brunton, K., Lam, T. & Yang, J. Spinal cord injury functional ambulation profile: a new measure of walking ability. *Neurorehabil. Neural Repair* **25**, 285–293 (2011).
8. Hidler, J. *et al.* ZeroG: overground gait and balance training system. *J. Rehabil. Res. Dev.* **48**, 287–298 (2011).
9. Shetty, D., Fast, A. & Campana, C.A. Ambulatory suspension and rehabilitation apparatus. US patent 7462138 (2008).
10. Pratt, G.A. *et al.* Stiffness Isn't Everything. in *International Symposium on Experimental Robotics* http://citeseerx.ist.psu.edu/viewdoc/summary?doi=10.1.1.26.3136 (1995).
11. Vallery, H. *et al.* Compliant actuation of rehabilitation robots—benefits and limitations of series elastic actuators. *IEEE Robot. Autom. Mag.* **15**, 60–69 (2008).
12. Harkema, S. *et al.* Effect of epidural stimulation of the lumbosacral spinal cord on voluntary movement, standing, and assisted stepping after motor complete paraplegia: a case study. *Lancet* **377**, 1938–1947 (2011).
13. Timoszyk, W.K. *et al.* Hindlimb loading determines stepping quantity and quality following spinal cord transection. *Brain Res.* **1050**, 180–189 (2005).
14. Zörner, B. *et al.* Profiling locomotor recovery: comprehensive quantification of impairments after CNS damage in rodents. *Nat. Methods* **7**, 701–708 (2010).
15. Drew, T., Andujar, J.E., Lajoie, K. & Yakovenko, S. Cortical mechanisms involved in visuomotor coordination during precision walking. *Brain Res. Rev.* **57**, 199–211 (2008).
16. Courtine, G. *et al.* Recovery of supraspinal control of stepping via indirect propriospinal relay connections after spinal cord injury. *Nat. Med.* **14**, 69–74 (2008).
17. Basso, D.M. *et al.* MASCIS evaluation of open field locomotor scores: effects of experience and teamwork on reliability. Multicenter Animal Spinal Cord Injury Study. *J. Neurotrauma* **13**, 343–359 (1996).
18. Musienko, P. *et al.* Controlling specific locomotor behaviors through multidimensional monoaminergic modulation of spinal circuitries. *J. Neurosci.* **31**, 9264–9278 (2011).
19. Kwakkel, G., Kollen, B.J. & Krebs, H.I. Effects of robot-assisted therapy on upper limb recovery after stroke: a systematic review. *Neurorehabil. Neural Repair* **22**, 111–121 (2008).
20. Duschau-Wicke, A., Caprez, A. & Riener, R. Patient-cooperative control increases active participation of individuals with SCI during robot-aided gait training. *J. Neuroeng. Rehabil.* **7**, 43 (2010).
21. Pearson, K.G. Generating the walking gait: role of sensory feedback. *Prog. Brain Res.* **143**, 123–129 (2004).
22. Edgerton, V.R. & Roy, R.R. Robotic training and spinal cord plasticity. *Brain Res. Bull.* **78**, 4–12 (2009).
23. Wessels, M., Lucas, C., Eriks, I. & de Groot, S. Body weight–supported gait training for restoration of walking in people with an incomplete spinal cord injury: a systematic review. *J. Rehabil. Med.* **42**, 513–519 (2010).
24. Reinkensmeyer, D.J. *et al.* Tools for understanding and optimizing robotic gait training. *J. Rehabil. Res. Dev.* **43**, 657–670 (2006).
25. Ada, L., Dean, C.M., Vargas, J. & Ennis, S. Mechanically assisted walking with body weight support results in more independent walking than assisted overground walking in non-ambulatory patients early after stroke: a systematic review. *J. Physiother.* **56**, 153–161 (2010).

a nature conference

Nature Genetics and the Wellcome Trust present:

The Genomics of Common Diseases 2012

Nature Genetics in association with the Wellcome Trust is pleased to announce the sixth annual Genomics of Common Diseases meeting, which will address the following topics across a range of common diseases: exome and whole genome sequencing, clinical and targeted sequencing, regulatory and functional genomics, cancer genomics, clinical translation and pharmacogenetics, statistical analyses of sequencing datasets, population and evolutionary genetics and infectious disease and host genetics.

September 19-22, 2012
Bolger Center, Potomac, MD, USA

KEYNOTE SPEAKERS

Thomas Hudson (Ontario Institute for Cancer Research, Canada)
Neil Risch (University of California, San Francisco, USA)
Sarah Tishkoff (University of Pennsylvania School of Medicine, USA)

SPEAKERS

Antonis Antoniou
Les Biesecker
John Blangero
Mary Carrington
Stephen Chanock
Paul de Bakker
Claire Fraser-Liggett
Manolis Kellis
Patricia Munroe
Benjamin Neale
Alkes Price
Jonathan Pritchard
Dan Roden
Nicholas Schork
Christine Seidman
Jay Shendure
Adam Siepel
Pamela Sklar
Nicole Soranzo
Shamil Sunyaev
Cisca Wijmenga
Ramnik Xavier

ORGANIZERS:

Orli Bahcall (*Nature Genetics*, USA)
Aravinda Chakravarti (Johns Hopkins University School of Medicine, USA)
Peter Donnelly (University of Oxford, UK)
Michael Dunn (Wellcome Trust, UK)
Michel Georges (University of Liège, Belgium)
Terri Manolio (National Human Genome Research Institute, National Institutes of Health, USA)
Mark McCarthy (University of Oxford, UK)
Nazneen Rahman (Institute of Cancer Research, UK)
Mary Relling (St. Jude Children's Research Hospital, USA)

For more information and to register visit:

www.nature.com/natureconferences/gcd2012

Abstract submission deadline- June 28, 2012

nature genetics

wellcome trust

a **nature** conference

Nature Immunology and HudsonAlpha Institute for Biotechnology present:

HudsonAlpha - Nature Conference on Immunogenomics

The first HudsonAlpha - Nature Conference on Immunogenomics will bring together four areas to shape this emerging field: scientists in genomics and genetics, immunology, bioinformatics and methodology, and clinical research. We expect our invited talks to cover a range of topics: large-scale immune sequencing projects of the repertoire of T- and B-cell diversity, and clinical implications; epigenetics and the immune system; developmental lineage of immune cells; genetic and environmental contributions to autoimmunity; drug development for autoimmune conditions; pharmacogenomics and the immune response; gene regulation and cell-type identity and high-resolution transcriptome analyses.

October 1-3, 2012
The Jackson Center, Huntsville, AL, USA

KEYNOTE SPEAKERS

Daniel Kastner (National Institute of Arthritis and Musculoskeletal and Skin Diseases, National Institutes of Health, USA)
Stephen Quake (Stanford University, USA)
Ugur Sahin (Translational Oncology at the University Medical Center of the Johannes Gutenberg University Mainz, Germany)

SPEAKERS

Christophe Benoist
S. Louis Bridges, Jr.
Christopher Glass
Jian Han
Robert Holt
John O'Shea
Robert Plenge
Harlan Robins
Ellen Rothenberg
Harinder Singh
Casey Weaver
Wenzhong Xiao

ORGANIZERS:

S. Louis Bridges, Jr (University of Alabama Birmingham, USA)
Laurie Dempsey (*Nature Immunology*, USA)
Chris Gunter (HudsonAlpha Institute for Biotechnology, USA)
Jian Han (HudsonAlpha Institute for Biotechnology / iCubate / iRepertoire, USA)
Robert Holt (Michael Smith Genome Sciences Centre, BC Cancer Agency, Canada)
Robert Plenge (Harvard Medical School / Brigham & Women's Hospital, USA)
Ellen Rothenberg (California Institute of Technology, USA)

Abstract submission deadline: July 13, 2012
Early registration deadline: August 3, 2012

For more information and to register visit:
www.nature.com/natureconferences/haig2012

nature immunology

HUDSONALPHA
INSTITUTE FOR BIOTECHNOLOGY

NM225039E

nature reprint collection

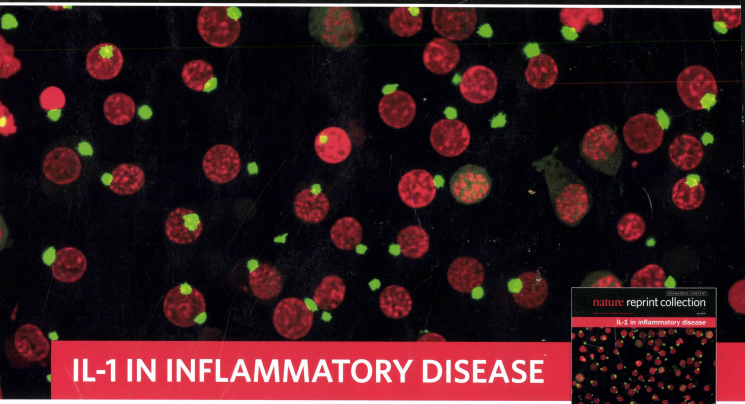

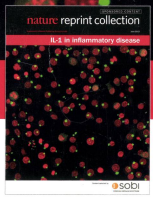

IL-1 IN INFLAMMATORY DISEASE

The proinflammatory cytokine IL-1 is activated by the inflammasome and has central roles not only in how we respond to infection but also in the pathogenesis of numerous inflammatory diseases, from gout to rheumatoid arthritis to diabetes mellitus.

Increased understanding of innate immunity over the past two decades has revealed IL-1's involvement in immunopathogenesis, and has led to the development and application of therapeutic approaches targeting this cytokine in several diseases, as discussed in the articles comprising this Nature Reprint collection.

Access the collection FREE online until June 2013.
www.nature.com/reprintcollections/interleukin-1

Produced with support from: sobi SWEDISH ORPHAN BIOVITRUM

nature REVIEWS RHEUMATOLOGY

nature publishing group npg